©Copyright 2021
Tyler D. Blanton

Advances to Three-Particle Quantization Conditions: Hadron Scattering Amplitudes from Lattice QCD

Tyler D. Blanton

A dissertation
submitted in partial fulfillment of the
requirements for the degree of

Doctor of Philosophy

University of Washington

2021

Reading Committee:

Stephen R. Sharpe, Chair

Silas R. Beane

Andreas Karch

Program Authorized to Offer Degree:

Department of Physics

University of Washington

Abstract

Advances to Three-Particle Quantization Conditions:
Hadron Scattering Amplitudes from Lattice QCD

Tyler D. Blanton

Chair of the Supervisory Committee:
Professor Stephen R. Sharpe
Department of Physics

The strong nuclear force is responsible for the vast majority of particles in nature; hundreds of hadrons with distinct masses and quantum numbers have been detected, and experimentalists are constantly searching for new hadron resonances and analyzing resonance decays to test the predictions of the Standard Model (e.g. by measuring the value of a CP-violating phase). While the formalism of quantum chromodynamics (QCD) appears to accurately describe the strong interaction, using it to extract theoretical predictions of hadronic properties has proven exceedingly difficult due to the nonperturbative nature of low-energy QCD. Lattice QCD (LQCD) is the state-of-the-art approach for computing physical observables using first-principles QCD, utilizing stochastic techniques to estimate the path-integral expressions for correlation functions in a latticized Euclidean spacetime. With the computational and algorithmic advances over the past few decades, LQCD can now be used to calculate many observables (e.g. hadron masses) to percent-level precision. However, LQCD simulations cannot directly calculate scattering amplitudes, due to both the necessary use of a finite volume and the need to analytically continue from Euclidean to Minkowski space, and thus a separate formalism is required. To bridge the gap between LQCD results and hadron spectroscopy, one needs some form of quantization condition (QC): a mathematical relation

used to extract physical scattering amplitudes of light hadrons from finite-volume energy spectra calculated with LQCD.

In this thesis, we present several theoretical and practical developments in the field of three-particle QCs (QC3s). We derive three significant advances to the theoretical formalism of QC3s within a generic relativistic effective field theory (RFT) framework. First, we perform an alternative derivation of the original QC3 for three identical scalars by using time-ordered perturbation theory (TOPT), which we find significantly simplifies the argument and thus renders the TOPT approach more amenable to generalization. We then demonstrate this point by using TOPT to derive a QC3 for the more complicated case of three nondegenerate scalars. Lastly, we use results from the TOPT approach to demonstrate the equivalence between the RFT QC3 for identical scalars and that of the finite-volume unitarity (FVU) approach.

We also present three numerical applications of QC3s to systems of three identical scalars. We detail the first QC3 study to include levels in nontrivial irreducible representations (irreps) of the cubic group and with nonzero d-wave two-particle interactions. Next, we perform an exploratory investigation of bound states and resonances by solving two- and three-particle QCs in various scenarios. Finally, we present the first ever extraction of $3\pi^+$ scattering information from LQCD data.

TABLE OF CONTENTS

LIST OF FIGURES

LIST OF TABLES

GLOSSARY

CMF: Center-of-momentum frame.

FV: Finite volume.

FVU: Finite-volume unitarity — a relativistic approach to QC3s based on S-matrix unitarity.

LQCD: Lattice quantum chromodynamics — the modern computational approach to first-principles QCD.

NREFT: Nonrelativistic effective field theory — a nonrelativistic approach to QC3s.

QC: Quantization condition — a mathematical relation between hadron scattering amplitudes and finite-volume energy spectra from LQCD. Plural: QCs.

QC2: Two-particle quantization condition. Plural: QC2s.

QC3: Three-particle quantization condition. Plural: QC3s.

QCD: Quantum chromodynamics — the QFT of the strong nuclear force.

QED: Quantum electrodynamics — the QFT of the electromagnetic force.

QFT: Quantum field theory.

RFT: Relativistic effective field theory — a diagram-based relativistic approach to QC3s, and the one that is chiefly used throughout this thesis.

TOPT: Time-ordered perturbation theory — an alternative to the standard perturbative method of Feynman diagrams.

ACKNOWLEDGMENTS

I would like to thank my advisor Steve Sharpe for his endless patience and constant support throughout our research together. He always encouraged me to pursue my own ideas, giving me room to fail and try again without fear of being judged or forced to give up. He also introduced me to several people in the field, including our collaborators Fernando Romero-López, Max Hansen, Raul Briceño, Drew Hanlon, Ben Hörz, and Colin Morningstar; each of them has contributed to part of the work presented in this thesis, and I am thankful for their help. I also want to thank my friends Sam, Bryce, Mike, Nick, and Paul for useful physics discussions. Lastly, thank you to all of my friends and family for always being there for me these past five years—I would not be where I am today without you.

Part I

INTRODUCTION

Chapter 1

BACKGROUND

1.1 History of the Standard Model[1]

The Standard Model is the modern theory of particle physics, with its formalism encapsulating three of the four known fundamental forces (gravity being the exception). With many of its predictions agreeing with experimental results to incredible accuracy, the Standard Model is one of the greatest theoretical achievements in all of science, and its current form represents the culmination of several decades of research.

The first major building block of the Standard Model to be assembled was quantum electrodynamics (QED), a quantum field theory (QFT) description of electromagnetism developed throughout the 1930s and 1940s. By that time, quantum mechanics and the particle theory of light were already well established after surviving the intense scrutiny of experimental testing, but several questions about its mathematical formalism were still unanswered. One such question was why all electrons are identical, as in quantum mechanics they are treated as separate quantities that just happen to have the same quantum numbers. There was also the issue of reconciling special relativity with quantum mechanics, as its governing formula (the Schrödinger equation) treats space and time very differently.

QED was developed to answer these and other questions. Instead of electrons being treated as different objects that just happen to be identical, in QED they are treated as local excitations in a single quantum field permeating all of spacetime. Interactions between such excitations are in turn mediated by excitations in another quantum field—the photon

[1]For more thorough accounts, see e.g. Refs. [2, 3].

field.

A useful feature of QED is the fact that at the low energy scales of our everyday world, each interaction with the photon field carries a small coupling constant (an indicator of interaction strength) of $\alpha_{EM} \approx \frac{1}{137}$, making the perturbation theory approach of Feynman diagrams an efficient method for calculating physical quantities from first principles. The most impressive example of the analytical power of QED is its prediction for the magnetic dipole moment of the electron, as rigorous experimental measurement has made it the most accurately verified prediction in the history of physics [4].

The second piece of the puzzle to be added to the Standard Model was the weak nuclear force—the mechanism responsible for the radioactive decay of atoms. Some of the basic features of the weak interaction like neutrino production in beta decay had been known about since 1930 [5], but it still took over a decade after the construction of QED before Glashow came up with a partial framework for combining QED with the quantum theory of the weak force in 1961. His theory featured three massless spin-1 bosons called $W^{\pm}$ and Z as the weak-force mediators [6], but it was clear that this was not the complete story. Forces with massless mediators should be able to act over long ranges, yet weak decays only occur at the length scale of atomic nuclei. This led many physicists to hypothesize that the $W^{\pm}$ and Z bosons were not only massive, but that they should be roughly 100 times heavier than the proton and neutron. In the following years, the mass-generating Higgs mechanism was formulated and eventually incorporated into the theory by Weinberg and Salam in 1967 [7, 8], marking the completion of the electroweak sector of the Standard Model. Since the newly introduced weak interactions are also described by small coupling constants $\alpha_W \sim 10^{-6}$ at low energies, the same perturbative techniques from QED could be applied to weak and electroweak processes. This allowed theorists to make more precise predictions for the $W^{\pm}$ and Z masses, well before they were detected experimentally in 1983 [9].

The final ingredient of the Standard Model to be developed was a QFT formulation

of the strong force holding atomic nuclei together. In the 1930s, Yukawa proposed that nucleons were attracted to each other via the exchange of strong-force mediators called mesons. This prediction was confirmed by experiment with the discovery of the pion in 1947[2] [10]. However, throughout the late 1940s and 1950s, dozens of other hadrons (strongly-interacting particles) were discovered in proton and electron collisions, and many began questioning whether all hadrons in this "particle zoo" were truly fundamental. In 1963, Gell-Mann and Zweig independently proposed that hadrons are composed of smaller spin-$\frac{1}{2}$ particles called quarks [11, 12]. A couple of years later, it was noted that for quarks to be antisymmetric under interchange, they must have an additional quantum number called color charge [13]. When the dust finally settled, the formalism that had been developed was QCD—a non-Abelian SU(3) gauge theory, with massless spin-1 bosons called gluons mediating the strong interaction between quarks.

The most notable property of QCD is that the strength of its interactions varies *inversely* with the energy scale being probed. This property is called asymptotic freedom, referring to the fact that the theory becomes free in the extreme high-energy/short-distance or ultraviolet (UV) limit. Conversely, in the low-energy/long-distance or infrared (IR) regime, the strong interactions are... well, strong. An important consequence is that quarks and antiquarks cannot appear in isolation, as the energy required to separate a quark from an antiquark (e.g. in a meson) grows linearly with the distance between them, and eventually it becomes energetically cheaper to create a new quark and antiquark from the vacuum and pair off the particles into two colorless (singlet) mesons. This explanation of color confinement has been confirmed by many lattice QCD calculations, and is the reason why individual quarks have never been observed experimentally—only hadrons.

Moreover, in this IR regime, the strong coupling constant is $\alpha_S \sim 1$ and QCD is non-

[2]The pion was technically first observed along with the muon in 1937 during studies of cosmic rays, but it took ten years for the physics community to properly understand the full picture and confidently identify the pion as Yukawa's meson.

perturbative, meaning the diagrammatic approach of the electroweak theory is not possible. The nonperturbative nature of low-energy QCD makes it much harder to study analytically; we discuss this in detail in the next section.

1.2 QCD formalism

Here we provide the complete mathematical formalism of QCD.[3] The results of this subsection are not used elsewhere in the thesis; we only include them for the sake of completeness and to introduce general aspects of QFT in a concrete setting.

The Standard Model description of the strong nuclear force is completely characterized by the QCD action

$$S_{\text{QCD}}[\psi, \overline{\psi}, A_\mu] = \int d^4x \; \mathcal{L}_{\text{QCD}}[\psi(x), \overline{\psi}(x), A_\mu(x)] \,, \tag{1.1}$$

where the integral is over all spacetime coordinates $x = (t, \mathbf{x}) \in \mathbb{R}^{1,3}$, and

$$\mathcal{L}_{\text{QCD}} = \mathcal{L}_q + \mathcal{L}_{\text{YM}} \tag{1.2}$$

is the QCD Lagrangian density, with

$$\mathcal{L}_q = \overline{\psi}_{i,f} \left(i\gamma^\mu D_{\mu,ij} - m_f \delta_{ij} \right) \psi_{j,f} \tag{1.3}$$

containing all contributions from quarks and their interactions with gluons, and

$$\mathcal{L}_{\text{YM}} = -\frac{1}{4} G^a_{\mu\nu} G^{a\mu\nu} \tag{1.4}$$

the gluon-only Yang-Mills contribution. Here $\mu, \nu \in \{0, 1, 2, 3\}$ are Lorentz indices, $i, j \in \{\text{red}, \text{green}, \text{blue}\}$ are color indices, $f \in \{\text{up}, \text{down}, \text{strange}, \text{charm}, \text{bottom}, \text{top}\}$ is a quark flavor index,[4] $a \in \{1, 2, \ldots, 8\}$ indexes the 8 generators of the gauge group SU(3), and we

[3] Throughout this thesis, we use natural units with $\hbar = c = 1$.

[4] Often only the lightest few flavors are necessary in practice, as any quark masses heavier than the energy of a given system have suppressed contributions to the physics.

use the convention that repeated indices are summed.

Each quark field $\psi_{i,f}(x)$ is a four-component Dirac spinor (Dirac indices suppressed) in the fundamental **3** representation of SU(3) and describes a quark with mass m_f, while its antiquark counterpart $\overline{\psi}_{i,f}(x) = \psi^\dagger_{i,f}(x)\gamma^0$ lives in the anti-fundamental $\overline{\mathbf{3}}$ representation. As for the remaining quantities: γ^μ is a 4×4 Dirac matrix satisfying the Clifford algebra $\{\gamma^\mu, \gamma^\nu\} = 2g^{\mu\nu}$, our Minkowski metric convention is $g_{\mu\nu} = \text{diag}(+,-,-,-)$,

$$D_{\mu,ij} = \partial_\mu \delta_{ij} - i g_S A^a_\mu T^a_{ij} \tag{1.5}$$

is the gauge covariant derivative, and

$$G^a_{\mu\nu} = \partial_\mu A^a_\nu - \partial_\nu A^a_\mu + g_S f^{abc} A^b_\mu A^c_\nu \tag{1.6}$$

is the gauge covariant gluon field strength tensor $G_{\mu\nu} = T^a G^a_{\mu\nu}$, where T^a is a generator of the SU(3) gauge group, f^{abc} is a structure constant of the group defined by

$$[T^a, T^b] = f^{abc} T^c \,, \tag{1.7}$$

$A^a_\mu(x)$ is a gluon field, and g_S is the strong coupling constant.

Using the path-integral formulation of QFT, we can write an expression for any correlation function involving strongly interacting states in terms of the QCD action. For example, an arbitrary two-point correlator[5] $\langle \mathcal{O}_f(x) | \mathcal{O}_i(0) \rangle$ can be written

$$\langle \mathcal{O}_f(x) | \mathcal{O}_i(0) \rangle = \langle 0 | \, \mathrm{T} \, \widehat{\mathcal{O}}_f(x) \widehat{\mathcal{O}}^\dagger_i(0) \, | 0 \rangle \tag{1.8}$$

$$= \frac{\int \mathcal{D}\psi \mathcal{D}\overline{\psi} \mathcal{D}A_\mu \; e^{iS_{\text{QCD}}[\psi, \overline{\psi}, A_\mu]} \, \mathcal{O}_f(x) \mathcal{O}^\dagger_i(0)}{\int \mathcal{D}\psi \mathcal{D}\overline{\psi} \mathcal{D}A_\mu \; e^{iS_{\text{QCD}}[\psi, \overline{\psi}, A_\mu]}} \,. \tag{1.9}$$

Here $|0\rangle$ is the (strongly interacting) vacuum state, T denotes time ordering, the integrations are over all field configurations, and $\widehat{\mathcal{O}}^\dagger_i(0)$ and $\widehat{\mathcal{O}}^\dagger_f(x)$ are operators creating some initial and final strongly interacting states $|\mathcal{O}_i(0)\rangle = \widehat{\mathcal{O}}^\dagger_i(0) \, |0\rangle$ and $|\mathcal{O}_f(x)\rangle = \widehat{\mathcal{O}}^\dagger_f(x) \, |0\rangle$, respectively.

[5] We can always choose the initial spacetime coordinate to be at the origin since Minkowski spacetime $\mathbb{R}^{1,3}$ is invariant under global translations.

Note that the right-hand side of Eq. (1.9) only involves classical objects; $\mathcal{O}_i^\dagger(0)$, $\mathcal{O}_f(x)$, and the fields $[\psi, \overline{\psi}, A_\mu]$ are all just vectors of numbers.[6]

In practice, it is often more convenient to work with Fourier transforms of such a correlator:

$$\widetilde{C}(t, \mathbf{P}) \equiv \int d^3x \; e^{-i\mathbf{P}\cdot\mathbf{x}} \langle 0|\mathrm{T}\, \widehat{\mathcal{O}}_f(t, \mathbf{x}) \widehat{\mathcal{O}}_i^\dagger(0, \mathbf{0})|0\rangle \;, \tag{1.10}$$

$$C(E, \mathbf{P}) \equiv \int d^4x \; e^{i(Ex^0 - \mathbf{P}\cdot\mathbf{x})} \langle 0|\mathrm{T}\, \widehat{\mathcal{O}}_f(x) \widehat{\mathcal{O}}_i^\dagger(0)|0\rangle \;. \tag{1.11}$$

The latter form is what we will be primarily using in later sections, but for now we restrict our attention to the original time-position space correlator $\langle \mathcal{O}_f(x)|\mathcal{O}_i(0)\rangle$.

Eq. (1.9) may seem promising, but it has several issues that render it impractical as a calculational method. For starters, it is still currently unknown whether such a path integral is mathematically well-defined. Even if it is, one would have to carry out an uncountably infinite number of integrals (one for each field at each point in spacetime), and it is not at all clear how or if such a calculation could be done analytically.

It should be noted that these path-integral issues are not specific to QCD; they arise in all QFTs, including the electroweak part of the Standard Model. However, if one is only interested in the IR regime, electroweak correlators can be approximated using perturbation theory ($\alpha_{EM} \approx \frac{1}{137}$, $\alpha_W \sim 10^{-6}$), with the dominant terms in the perturbative expansion being given by the simplest Feynman diagrams describing the process in question. Thus one can calculate any electroweak correlator to a high degree[7] of precision by summing over increasingly complicated Feynman diagrams.

QCD, on the other hand, is nonperturbative in the IR ($\alpha_S \equiv \frac{g_S^2}{4\pi} \sim 1$), meaning a diagrammatic approach is out of the question in this regime. To calculate correlators of

[6] These numbers are complex for bosonic fields like A_μ, and Grassmann-valued for fermionic fields like ψ and $\overline{\psi}$.

[7] The perturbative expansion is known to be an asymptotic series though, so perturbation theory cannot be applied to arbitrarily high orders.

strongly interacting matter, one must deal with the path integral directly.

1.3 Lattice QCD

Lattice QCD (LQCD) is the state-of-the-art method for computing correlators from first-principles QCD. In LQCD, several alterations are made to the original problem in order to render the path integral tractable. First, Minkowski time is Wick-rotated to Euclidean time $t \to -i\tau$, which sends $x \to x_E$ and $e^{iS_{\rm QCD}} \to e^{-S^E_{\rm QCD}}$, with $S^E_{\rm QCD}$ a real quantity. Performing this rotation allows one to write

$$\langle \mathcal{O}_f(x_E)|\mathcal{O}_i(0)\rangle = \int \mathcal{D}\psi\mathcal{D}\overline{\psi}\mathcal{D}A_\mu \; P[\psi,\overline{\psi},A_\mu]\,\mathcal{O}_f(x_E)\mathcal{O}_i^\dagger(0)\,, \tag{1.12}$$

where

$$P[\psi,\overline{\psi},A_\mu] \equiv \frac{1}{Z}e^{-S^E_{\rm QCD}[\psi,\overline{\psi},A_\mu]}\,, \qquad Z \equiv \int \mathcal{D}\psi\mathcal{D}\overline{\psi}\mathcal{D}A_\mu \; e^{-S^E_{\rm QCD}[\psi,\overline{\psi},A_\mu]} \tag{1.13}$$

is a normalized probability distribution functional of the field configurations $[\psi,\overline{\psi},A_\mu]$. Expressing the correlator in this way will ultimately allow the use of Monte Carlo integration techniques to estimate the value of the path integral as an average over stochastically generated field configurations, but first the number of degrees of freedom must be reduced to something finite.

The next step in the construction of LQCD is to approximate the path integral as a finite-dimensional integral by putting the (now Euclidean) spacetime on a lattice. In the most common approach, spacetime is discretized uniformly with a lattice spacing a and is restricted to have finite extent; space is replaced by a cubic box of side length $L = N_x a$ for some integer N_x, and Euclidean time is restricted to some integer number N_τ of values between zero and $T = N_\tau a$.[8] The boundary conditions of this latticized spacetime are typically chosen to be periodic or antiperiodic depending on the symmetries of the physical

[8] Typical lattice parameters in simulations are $a \sim 0.05$–0.1 fm and $N_x, N_\tau \sim 100$.

system of interest. With this setup, the total number of points in the spacetime volume—and equivalently the number of integrals for each field—is a finite number $N_V = N_x^3 N_\tau$. In practice though, N_V is far too large for direct integration to be viable, and one must resort to Monte Carlo methods using an appropriate lattice analogs of Eqs. (1.12) and (1.13).

Although latticizing spacetime is certainly beneficial in rendering the path integral tractable, it is not without its share of downsides. One issue is that LQCD requires one to define a discretized form of the (Euclidean) QCD action, and while there are several reasonable choices one can make, it is impossible to define a discretized action with all of the same symmetries as the continuum action.[9]

In any case, for given QCD inputs (quark masses m_f, coupling constant g_S) and lattice specifications (a, N_x, N_τ, discretized action), one can use Monte Carlo techniques to calculate the corresponding lattice correlator. By repeating this computation with several different[10] lattice spacings a while holding the box size $L = N_x a$ fixed, one can extrapolate $a \to 0$ to obtain the continuum finite-volume (FV) correlator for that particular L.

1.4 FV correlators and the FV spectrum

By taking the FV analog of Eq. (1.10) in Euclidean time and inserting a complete set of FV states with appropriate quantum numbers, one can derive the useful result

$$\widetilde{C}_L(T, \mathbf{P}) = \sum_{n=0}^{\infty} \frac{c_{\mathbf{P},n}}{2E_{\mathbf{P},n}} e^{-E_{\mathbf{P},n}|T|}\,, \tag{1.14}$$

where each $c_{\mathbf{P},n} > 0$ is a real constant involving matrix elements between the operators and the vacuum, and $E_{\mathbf{P},n} > 0$ is the n-th energy level in the FV spectrum (relative to the vacuum) for a given momentum $\mathbf{P}$, with $n = 0$ denoting the ground state. This expression

[9] The most famous example of this fact is the Nielson-Ninomaya theorem, which states that (under some assumptions) it is impossible to define a discretized QCD action that gives an LQCD theory with chiral symmetry and no fermion doublers [14].

[10] Alternatively, one can just use a single lattice spacing if it is small enough that discretization errors are within the accepted tolerance.

shows that for large Euclidean time $T = N_\tau a$, the lowest energies in the FV spectrum dominate, allowing them to be extracted through various methods [15–17].

From Eq. (1.14), one can Fourier transform to Euclidean energy and then Wick rotate back to Minkowski energy to obtain

$$C_L(E, \mathbf{P}) = \sum_{n=0}^{\infty} \frac{i c_{\mathbf{P},n}}{E^2 - E_{\mathbf{P},n}^2} = \sum_{n=0}^{\infty} \frac{i c_{\mathbf{P},n}}{(E + E_{\mathbf{P},n})(E - E_{\mathbf{P},n})}\,, \tag{1.15}$$

where E is a Minkowski energy. This result plays a key role in the quantization conditions we discuss throughout this thesis, as it shows that the FV two-point correlator $C_L(E, \mathbf{P})$ has simple poles at energies in the FV spectrum $\{E_{\mathbf{P},n}\}_{n=0}^{\infty}$, and that the residues of these poles lie on the positive imaginary axis. Thus if one wishes to extract infinite-volume scattering amplitudes from LQCD simulations, then it is enough to find an expression for $C_L(E, \mathbf{P})$ in terms of such amplitudes, as the analytic structure of the FV correlator can then be utilized to make contact with the FV spectrum, which can in turn be computed via LQCD. This is the general strategy of all quantization conditions we discuss in Chapters 3–8 below.

1.5 Effective field theory

Quarks are certainly necessary for describing the *internal* structure of nucleons (protons/neutrons) and other hadrons, but they are inconvenient building blocks for describing low-energy interactions *between* hadrons, as they never appear in isolation due to color confinement. Thus it makes more sense to use the hadrons themselves as the building blocks, while at even lower energy (longer length) scales it may be more natural to use atoms or even molecules. This concept of using different degrees of freedom depending on the energy/length scale of the theory being probed is the core idea behind effective field theories (EFTs).

An EFT is an approximation of an underlying QFT, with the constituent fields of the EFT chosen to correspond with the appropriate degrees of freedom at a specified energy scale Λ. Instead of using the QCD Lagrangian to analyze hadron interactions with quark

and gluon fields, one can define an EFT Lagrangian purely in terms of hadron fields.

To construct an interacting EFT, one must first identify the relevant degrees of freedom (quantum fields) and symmetries of the theory. In order for the EFT to include all of the physics of the underlying full theory, every field interaction term that is consistent with the symmetries must appear in the EFT Lagrangian along with an associated low-energy constant (LEC) describing the relative strength of the interaction as a function of Λ [18]. These LECs are unknowns in the theory that can only be determined by fitting to experimental data or deriving them from the underlying theory, e.g. via LQCD calculations.

EFTs will therefore generally have an infinite number of interaction terms and unknown LECs.[11] In such theories, one can write the EFT Lagrangian as an expansion in powers of Λ^{-1}, allowing perturbative diagrammatic techniques to be utilized for calculations.[12] For example, the two-point correlator $C(E, \mathbf{P})$ in Eq. (1.11) can be expressed as an infinite sum of all Feynman diagrams between the initial and final states $|\mathcal{O}_i\rangle$ and $|\mathcal{O}_f\rangle$ with total 4-momentum $P^\mu = (E, \mathbf{P})$. If one were to determine the LECs of the leading-order terms in the EFT Lagrangian (e.g. by fitting to experiment), then one could approximate $C(E, \mathbf{P})$ by summing the most significant diagrams. However, this approach becomes increasingly challenging as one goes to higher orders in perturbation theory and more LECs need to be determined. In this thesis, we are not interested in such pursuits, and it suffices to simply write the correlator as a sum of all diagrams without any knowledge of the LECs.

---

[11] All but a small handful of these LECs will be irrelevant/nonrenormalizable and vanish in the $\Lambda \to \infty$ limit, but for any finite Λ, each LEC describing an interaction that respects the symmetries of the theory will generally be nonzero.

[12] The most notable example of this is chiral perturbation theory, a hadronic EFT in which the small masses of the up and down (and sometimes strange) quarks relative to typical QCD energy scales ($\Lambda \sim 300$ MeV) are treated as perturbations breaking the chiral symmetry of the massless theory.

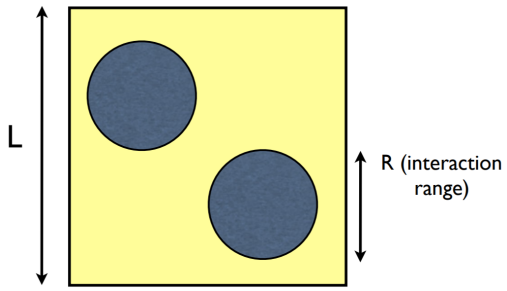

Figure 1.1: Qualitative visualization of how the relative sizes of the box size L and interaction range $R = \Lambda^{-1}$ determine the significance of FV effects. In this image, $L/R = \Lambda L \approx 2.5$, which is a borderline case; the two particles can both fit in the box and have some room to move around without interacting with each other, but they fill enough of the box that interactions will be frequent.

1.6 Finite-volume EFT

The continuum limit $a \to 0$ of LQCD correlators is relatively straightforward to take, but the same is not true of the infinite-volume limit $L \to \infty$, especially when it comes to hadron scattering. To relate finite-volume correlators and energy spectra to infinite-volume scattering amplitudes, an entirely new formalism is necessary—the formalism of quantization conditions and finite-volume EFT.

Restricting a field theory to a finite spatial volume leads to several effects of varying importance. The relative size of these effects is based on the relationship between the box size L and the natural length (inverse energy) scale or interaction range Λ^{-1} of the theory.[13] If $\Lambda L \lesssim 1$, then each particle fills most of the box and finite-volume effects dominate the physics. Conversely, if $\Lambda L \gg 1$, then particles have plenty of space to move around and interact within the box, and finite-volume effects are relatively small; see Fig. 1.1. These statements are, however, purely qualitative; to understand how FV effects can be tracked more rigorously, let us again consider the FV two-point correlation function $C_L(E, \mathbf{P})$, assuming periodic spatial boundary conditions.

[13]For example, the energy scale of an EFT with a single field with mass m is generally $\Lambda \sim m$.

Being in finite volume does not prevent us from expressing the correlator as an infinite sum of Feynman diagrams, but it does alter how we interpret momenta and loops in the diagrams. Just as a guitar string can only vibrate at certain discrete frequencies determined by the length of the string, a de Broglie wave that is forced to satisfy the periodic boundary conditions of the box can only describe particles with certain discrete spatial momenta: $\mathbf{p} = \frac{2\pi}{L}\mathbf{n}$ with $\mathbf{n} \in \mathbb{Z}^3$. All spatial momenta appearing in the diagrams (including the total momentum $\mathbf{P}$) must lie in this finite-volume set.

This change is most noticeable in loops—whenever one would normally integrate over all spatial momenta (up to some UV cutoff), in finite volume we must instead perform a discrete sum over all momenta in the FV set (again up to some UV cutoff). Thus in order to track the effects of evaluating the correlator in finite volume, we must analyze sum-integral differences of the form

$$\left[\frac{1}{L^3}\sum_{\mathbf{p}}^{\text{UV}} - \int^{\text{UV}} \frac{d\mathbf{p}}{(2\pi)^3}\right] f(E, \mathbf{P}, L; \mathbf{p})\,, \tag{1.16}$$

where f is some generic function. This type of difference has a very nice property that follows from the Poisson summation formula: if f is a smooth function of $\mathbf{p}$ within the domain of integration, then the sum-integral difference is exponentially suppressed[14] in the box size L. If not, i.e. if f has one or more singularities within the integration domain, then the difference will generally scale as some inverse power of L. Throughout this thesis, we assume all exponentially suppressed FV effects to be negligible[15] compared to the power-law terms, which we track to all orders.

---

[14] Technically, the summation formula just guarantees that the difference falls faster than any finite power of L^{-1}; any time we refer to "exponentially suppressed" FV effects, this is what we really mean.

[15] All examples in the below chapters satisfy $\Lambda L > 4$, so that the sizes of the exponentially suppressed terms are roughly $e^{-\Lambda L} < 2\%$.

Chapter 2

HADRON SPECTROSCOPY FROM LQCD

As mentioned in Section 1.1, hundreds of hadrons have been detected experimentally, each with a unique set of quantum numbers, and with masses ranging from 135 MeV (π^0) to over 5.8 GeV (Σ_b^+). With the countless number of different interactions between hadrons and other particles in the Standard Model, hadron spectroscopy is the largest playground we have for improving our understanding of particle physics.

2.1 Scattering basics

In order to properly discuss hadron spectroscopy, let us first recall some basic scattering theory. Given an initial N_i-particle state $|i\rangle = |p_1 \dots p_{N_i}\rangle$, the probability of observing it in the distant future[1] in a final N_f-particle state $|f\rangle = |p'_1 \dots p'_{N_f}\rangle$ is

$$\text{Prob}(i \to f) = |\langle f|S|i\rangle|^2 , \tag{2.1}$$

$$\langle f|S|i\rangle = \delta_{fi} + i(2\pi)^4 \delta^4(P^f - P^i) \langle f|T|i\rangle , \qquad S^\dagger S = \mathbf{1} , \tag{2.2}$$

where S is the (unitary) scattering matrix of the theory with nontrivial part T, and $P^i \equiv \sum_{j=1}^{N_i} p_j$ and $P^f \equiv \sum_{n=1}^{N_f} p'_n$ are the total initial and final 4-momenta, respectively. The nontrivial piece of this S-matrix element defines the scattering amplitude for the process:

$$\mathcal{M}_{i\to f} \equiv \langle f|T|i\rangle . \tag{2.3}$$

Amplitudes like $\mathcal{M}_{i\to f}$ are complex, Lorentz-invariant functions of the external 4-momenta, and are closely related to the two-point correlation functions $C(E, \mathbf{P})$ discussed in the pre-

[1] By this, we are assuming the states are asymptotic and taking them to be infinitely separated in time.

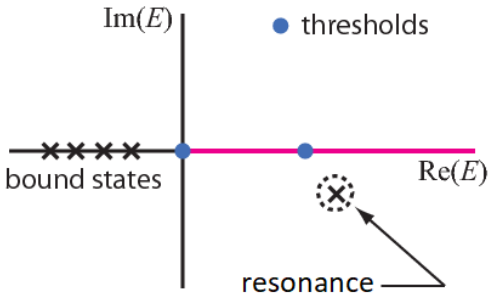

Figure 2.1: Sample analytic structure of a scattering amplitude $\mathcal{M}_{i\to f}$. Black crosses denote poles, whereas blue circles denote branch points. The imaginary axis is shown at the first threshold energy merely for convenience; it does not represent $\mathrm{Re}(E) = 0$.

vious chapter; in particular, both can be expressed as a sum of Feynman diagrams between the initial and final states, and their analytic structures have the same general features.[2]

In QFTs, a pole in a scattering amplitude (or more generally in the S-matrix) as a function of the center-of-momentum-frame (CMF) energy E corresponds to a physical particle or resonance. A pole on the real energy axis corresponds to a stable bound state with mass $M = E$, while a pole with a nonzero imaginary part $E = M - i\Gamma/2$ corresponds to an unstable resonance with mass M, decay width $\Gamma > 0$, and lifetime $1/\Gamma$. Amplitudes also have branch points on the real axis at threshold energies where new inelastic processes or "channels" become energetically accessible; see Fig. 2.1.

2.2 Stable hadrons vs. resonances

Although most light hadrons can be described as standard quark-antiquark ($q\overline{q}$) mesons or three-quark (qqq) baryons, many heavier states cannot be placed in either category. Some resonances like the $a_0(980)$ and[3] $f_0(980)$ are hypothesized to have tetraquark ($qq\overline{q}\overline{q}$) components [19], while others like the $P_c^+(4450)$ are conjectured to be pentaquark ($qqqq\overline{q}$) states

[2]The difference is that a correlator includes additional interpolating fields coupling to the vacuum that create/annihilate the initial/final states, with a (generally off-shell) scattering amplitude between them.

[3]The numbers in parentheses are the approximate resonance masses in MeV.

[20]. Perhaps most intriguing are the numerous X, Y, and Z resonances involving charm and bottom quarks that have been observed over the past couple decades, as they were not expected and do not seem to obey the standard quark-model classification scheme [21]. Such curiosities continue to serve as strong motivators for pushing forward the field of hadron spectroscopy.

The zoo of strong-interaction states provides ample opportunities for testing Standard Model predictions against experiment and potentially make new discoveries, but making these predictions requires one to perform nonperturbative QCD calculations in order to properly describe the hadronic physics. As we discussed in Sections 1.3–1.4, lattice QCD can be used to evaluate FV correlation functions and (consequently) FV spectra of hadronic systems. By using this method to obtain the FV ground-state energy from an appropriate FV correlator for multiple box sizes L and then extrapolating $L \to \infty$, it is possible to extract masses of *stable* hadrons in QCD for a given set of inputs—namely, the quark masses m_f and the strong coupling constant g_s.[4]

This procedure has been successfully implemented for several cases, with the details of the calculations evolving over time. Early calculations used isosymmetric LQCD in the quenched approximation (no dynamical quarks) and were able to roughly approximate the masses of many hadrons (e.g. pions and nucleons), but the errors were relatively large, and the exact isospin symmetry made it impossible to distinguish particles within a multiplet; for example, the neutron and proton were degenerate. As algorithmic efficiency and computing power improved, non-isosymmetric LQCD with dynamical quarks soon became viable, and calculations have become much more precise; in 2015, the first *ab initio* calculation of the proton-neutron mass difference was performed [22]. For a more thorough review of light hadron masses from LQCD, see Ref. [23].

---

[4]Note that this program can also be used in reverse; the LQCD inputs m_f and g_s can be determined (at a given energy scale) by forcing LQCD predictions to match well-known experimental masses of stable hadrons such as the pion.

While the above program is certainly useful, it is only applicable for hadrons that are stable in QCD. The vast majority of QCD states are unstable resonances with very short lifetimes ($\Gamma \sim 100$ MeV or $1/\Gamma \sim 10^{-24}$ s), and their properties are significantly more difficult to extract. The issue is that resonances are not asymptotic states; they merely manifest as complex poles in scattering amplitudes of particles which *are* stable under the strong interaction, such as pions, kaons, and nucleons. Thus in order to study a resonance analytically, one must extract a scattering amplitude involving states of stable hadrons that couple to the resonance (e.g. decay channels). Some examples of resonances and their dominant decay channels are the rho $\rho(770) \to \pi\pi$, the omega $\omega(782) \to \pi\pi\pi$, and the Roper resonance $N(1440) \to N\pi, N\pi\pi$.

2.3 Two-hadron scattering & the Lüscher method

Lüscher was the first to devise a strategy for determining scattering amplitudes from LQCD data [24, 25]. The so-called "Lüscher method" is to derive a nonperturbative relation between the FV spectrum of an appropriate FV correlator to infinite-volume scattering amplitudes, and then to constrain the amplitudes by inputting multiple energies in the FV spectrum computed with LQCD. Mathematical relations between FV spectra and infinite-volume scattering amplitudes are now commonly referred to as quantization conditions (QCs).

The original derivation by Lüscher was for a particular two-particle scattering case and involved transforming the QFT problem into a quantum mechanics problem, but in the following years several alternative derivations of and generalizations to two-particle QCs (QC2s) were developed. Notable advances included extensions to moving frames, arbitrary spins, multiple two-particle channels, and noncubic volumes. In addition to these numerous theoretical advances, QC2s have also been successfully applied to LQCD data to study several resonances, including the $\rho(770)$ and $\sigma/f_0(500)$ from $\pi\pi$ scattering and the D_{s0}^* from DK scattering. For a detailed review of QC2s (as well as other methods) and their

implementations with regards to resonances, see Ref. [26].

2.3.1 Summary of QC2 derivation in the RFT approach

In the paper generalizing the QC2 to moving frames (Ref. [27]), the authors introduced a derivation strategy that has since become a staple of many modern three-particle QCs. We summarize their approach here, with a few minor alterations made to better match the three-particle derivations presented later.

The derivation of Ref. [27] is rooted in a generic relativistic effective field theory (RFT) comprised of a single species of scalar field; for concreteness, let us call this field π^+. Their starting point is the (Minkowski) two-point FV correlator

$$C_L(E, \mathbf{P}) = \int_L d^4x \; e^{i(Ex^0 - \mathbf{p}\cdot\mathbf{x})} \langle 0|\mathrm{T}\sigma(x)\sigma^\dagger(0)|0\rangle \;, \tag{2.4}$$

where $P^\mu = (E, \mathbf{P})$ is the fixed total 4-momentum of the system and $\sigma^\dagger(x)$ is an interpolating operator creating a state that couples to the two-particle state of interest $\pi^+\pi^+$. The end goal is a quantitative relationship between the infinite-volume 2→2 scattering amplitude $\mathcal{M}_2 \equiv \mathcal{M}_{\pi^+\pi^+\to\pi^+\pi^+}$ and the FV spectrum of the theory, with all power-law FV effects accounted for.

The first step is to expand C_L as an infinite sum of Feynman diagrams and collect all sections which are two-particle irreducible (2PI) into FV amputated 2→2 Bethe-Salpeter kernels $B_{2,L}$, generalized endcaps A'_L and A_L, and $C_L^{(0)}$ which contains all diagrams that are completely 2PI. The result is a skeleton expansion for C_L, consisting of only these 2PI quantities and two-particle sections between them (see Figure 2.2). By analyzing the kinematics of the various diagrams that contribute to $B_{2,L}$ (or the other 2PI quantities), one can show that if the CMF energy $E^* \equiv \sqrt{E^2 - \mathbf{P}^2}$ is below the next inelastic threshold, then all terms which appear in $B_{2,L}$ (and $C_L^{(0)}, A'_L, A_L$) are smooth functions of the internal 4-momenta, including all summands associated with discrete sums over spatial momenta in the FV set.

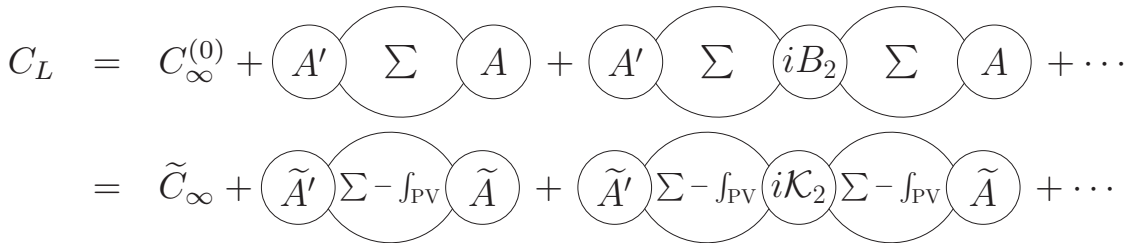

Figure 2.2: Skeleton expansion of the 2→2 FV correlator C_L. In the first line, we have already replaced all FV 2PI quantities with their infinite-volume limits. The sum-integral differences in the second line correspond to insertions of F, and effectively project adjacent quantities on shell.

From Eq. (3.2), it follows that $B_{2,L}$ is equal to $B_2 \equiv B_{2,\infty}$ up to exponentially suppressed FV corrections, and thus the Bethe-Salpeter kernels (and the endcaps) can be treated as infinite-volume quantities; we are free to replace $B_{2,L} \to B_2$, $C_L^{(0)} \to C_\infty^{(0)}$, $A'_L \to A' \equiv A'_\infty$, $A_L \to A \equiv A_\infty$.

The next step is to project these (generally off-shell) infinite-volume kernels onto the physical shell. This is accomplished by decomposing the kernels into partial waves or spherical harmonics, rewriting discrete FV sums over two-particle sections between adjacent 2PI kernels as $\sum = [\sum - \text{PV}\int] + \text{PV}\int$ with some appropriate principal value (PV) prescription,[5] and collecting all adjacent PV$\int$ terms and B_2 kernels into new $\mathcal{K}_2$ kernels (the other 2PI quantities change in a similar way: $A' \to \widetilde{A}'$, $A \to \widetilde{A}$, $C_\infty^{(0)} \to \widetilde{C}_\infty$). Each K-matrix $\mathcal{K}_2$ is effectively projected on shell by adjacent instances of the two-particle kinematic quantity F associated with a single $[\sum - \text{PV}\int]$ contribution.[6] $\mathcal{K}_2$ is related to the physical amplitude $\mathcal{M}_2$ via a simple algebraic relation involving the difference between the PV and $i\epsilon$ prescriptions.

[5] Using a PV prescription is actually not required in this case; Ref. [27] uses the standard $i\epsilon$ prescription, and this would give the physical $\mathcal{M}_2$ amplitudes directly instead of $\mathcal{K}_2$ kernels. However, a PV prescription *is* required for the three-particle case, so we include it here to simplify the later discussion.

[6] Ref. [27] calls the Bethe-Salpeter kernel K (we call it B_2). Our F is also defined with an extra symmetry factor of 1/2, and it contains an extra phase space factor compared to theirs since we use different integration prescriptions.

The final expression for the FV correlator is

$$C_L = \widetilde{C}_\infty + \widetilde{A}' i F \frac{1}{1 - i\mathcal{K}_2 i F} \widetilde{A}\,, \tag{2.5}$$

where each quantity in the second term on the right-hand side is an infinite-dimensional matrix with angular momentum indices ℓ, m. For a given $\mathbf{P}$, if the energy E lies in the FV spectrum $\{E_{\mathbf{P},n}\}_{n=0}^{\infty}$, then C_L necessarily has a pole; i.e., the following quantization condition must hold:

$$\det\left[F^{-1}(E, \mathbf{P}, L) + \mathcal{K}_2(E^*)\right] = 0\,. \tag{2.6}$$

We stress that $F(E, \mathbf{P}, L)$ contains all power-law FV dependence, and that it is a well-defined kinematic quantity that one can evaluate directly. $\mathcal{K}_2(E^*)$, on the other hand, is an infinite-volume amplitude that is on shell and Lorentz invariant (which is why it only depends on the CMF energy E^*), and is related to the physical amplitude by $\mathcal{M}_2^{-1}(E^*) = \mathcal{K}_2^{-1}(E^*) + \widetilde{\rho}(E^*)$, with $\widetilde{\rho}(E^*)$ a simple phase space factor. Thus one can fit (a parameterization of) $\mathcal{K}_2(E^*)$ by attempting to match the energies E which satisfy the two-particle quantization condition Eq. (2.6) for a given FV momentum $\mathbf{P}$ (and box size L) to the energies in the FV spectrum $\{E_{\mathbf{P},n}\}_{n=0}^{\infty}$.

2.4 Three-hadron scattering

While one- and two-hadron states are certainly prevalent in the QCD spectrum, the vast majority of resonances couple to states with three or more hadrons, e.g. the omega $\omega(782) \to \pi\pi\pi$ and the Roper resonance $N(1440) \to N\pi, N\pi\pi$ mentioned above.

Applying the Lüscher method to three-particle scattering amounts to deriving and implementing three-particle quantization conditions (QC3s), the natural analogs of QC2s. The first QC3 was derived by Hansen and Sharpe in 2014 using the same type of RFT approach discussed in the previous section [28, 29]. In 2017, two other QC3 strategies appeared: the nonrelativistic EFT (NREFT) approach by Hammer et al. [30, 31], and the relativistic finite-

volume unitarity (FVU) approach by Mai and Döring [32]. The NREFT method boasts the simplest formalism, but its neglect of relativistic effects limits its physical applicability. The FVU approach is rooted in the constraints that S-matrix unitarity places on FV scattering amplitudes and is manifestly relativistic like the RFT method, but the latter has always been more developed; e.g., to date the FVU method can still only accommodate s-wave dimer interactions, whereas the RFT method has always allowed for all partial waves and is the only approach to be further generalized, e.g. to include 2→3 processes.

While the RFT, FVU, and NREFT approaches are currently the only three known methods for deriving QC3s relating scattering amplitudes to FV spectra, there is also a very different method that does not connect to FV spectra at all. This "potential method" is favored by the HALQCD collaboration—in it, one associates a nonrelativistic inter-hadron potential with a quantity obtained from a correlation function of spatially separated hadron operators, and then one solves the Schrödinger equation with that potential to obtain scattering information [33].

In this thesis, our focus is on developments within the RFT approach to QC3s, and we do not discuss the other methods for studying three-hadron scattering in any detail.

2.4.1 Overview of original QC3 derivation

The original QC3 derivation by Hansen and Sharpe in Ref. [28] (hereafter referred to as "HS1") uses the RFT framework and follows a strategy that is very similar to that of the QC2 derivation in Section 2.3.1. The result is a similar-looking quantization condition:

$$\det\left[F_3^{-1}(E,\mathbf{P},L)+\mathcal{K}_{\mathrm{df},3}(E^*)\right]=0\,, \tag{2.7}$$

where $F_3(E,\mathbf{P},L)$ contains all FV dependence as well as contributions involving $\mathcal{K}_2$, and $\mathcal{K}_{\mathrm{df},3}(E^*)$ is an on-shell, Lorentz-invariant, infinite-volume 3→3 amplitude. Determining the physical 3→3 amplitude $\mathcal{M}_3$ from these K-matrices is not as simple as it was for the

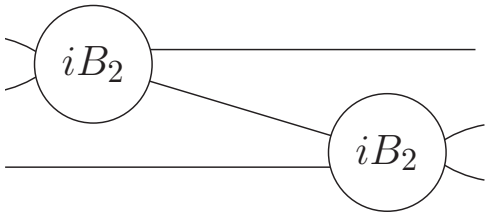

Figure 2.3: Feynman diagram of a switch state between two B_2 kernels. The propagators at the bottom left and top right are the spectators, as they merely spectate the 2→2 interactions within the B_2 kernels. The 4-momentum flowing through the center propagator is fixed by the spectator momenta, and thus can be forced to go on shell and diverge.

two-particle case, but it is possible via nested integral equations [29].

There are several aspects of the HS1 derivation that are unique to the three-particle case. Perhaps most notable is the new diagram topology called a "switch state," which refers to a three-particle section between B_2 kernels with different particles "spectating" the 2→2 interactions (see Figure 2.3). Switch states introduce new divergence concerns and have to be treated carefully; the "df" in $\mathcal{K}_{\text{df},3}$ stands for divergence-free, as $\mathcal{K}_{\text{df},3}$ has singular switch-state contributions explicitly removed. Another concern is that 2→2 kernels need to be evaluated below threshold, requiring one to use K-matrices with a carefully defined PV prescription and UV cutoff in order to avoid introducing cusps.

In addition to these issues that are inherent to 3→3 scattering, the HS1 derivation spends significant effort dealing with the energy integrals associated with loops in Feynman diagrams, organizing the diagrams into several different categories and handling them one at a time. HS1 also goes to great lengths to symmetrize $\mathcal{K}_{\text{df},3}$, as most diagrams are asymmetric under particle interchange. As a result, $\mathcal{K}_{\text{df},3}$ is only defined constructively in HS1; it does not have a closed-form expression.

In Chapter 3, we present an alternative derivation to that of HS1. The primary difference is that instead of dealing with Feynman diagrams and energy integrals, we work with diagrams in time-ordered perturbation theory (TOPT) where all individual 4-momenta are

on shell and no energy integrals are necessary. We are able to obtain simple closed-form expressions for all major quantities by using building blocks which are asymmetric under particle interchange (including an asymmetric K-matrix), and we show that our asymmetric QC3 is equivalent to the symmetric QC3, Eq. (2.7).

2.4.2 QC3 developments within the RFT approach

The original QC3 derivation of HS1 made several simplifying assumptions:

1. All particles were scalar (spinless).
2. All particles were identical.
3. The Lagrangian was assumed to have a G-parity-like global $\mathbb{Z}_2$ symmetry (e.g. no $2\to3$ transitions were allowed).
4. Two-particle subchannels were assumed to not have any resonances or bound states.

With all of these restrictions, the practical scope of the original QC3 is rather limited; it can only be applied to simple processes like $3\pi^+ \to 3\pi^+$ or $3K^+ \to 3K^+$, and even then only for energies up to the next inelastic threshold. In order to study more interesting phenomena like the Roper resonance, one needs more general QC3s that have some of these assumptions removed.

Lifting these restrictions of the RFT approach has therefore become one of the main goals within the QC3 community, and significant progress has been made in the past few years. Some of these developments include the incorporation of $2\to3$ transitions [34], resonant subprocesses [35, 36], multiple isospin channels [37], and relations between FV matrix elements and infinite-volume decay amplitudes [38].

Given the complicated nature of the derivation in the standard RFT method, an alternative line of argument is desirable for simplifying the generalization to more complicated

systems. This is the focus of the the theoretical work we present in Part II. In Chapter 3, we perform an alternate derivation of the original QC3 using time-ordered perturbation theory (TOPT), which we find significantly simplifies the argument. We then demonstrate the utility of this TOPT approach by using it to derive a QC3 for the more complicated case of three nondegenerate scalars in Chapter 4. Lastly, in Chapter 5 we use the results of Chapter 3 to demonstrate the equivalence between the RFT and FVU QC3s for identical scalars.

In addition to the many theoretical developments to QC3s over the past few years, there have also been a number of numerical QC3 implementations. The first was performed in 2018 for three identical scalars in the RFT approach for the simple case of the so-called isotropic approximation [39], and shortly after there were also implementations in the NREFT [40] and FVU [41] approaches. All of these studies were purely investigative though; the first fit to actual LQCD results for the $3\pi^+$ FV spectrum did not occur until the following year. For a recent review on two- and three-hadron QCs including various implementations, see Ref. [42].

In Part III, we present additional numerical applications of QC3s to systems of three identical scalars. In Chapter 6, we detail the first QC3 study to include levels in nontrivial irreducible representations (irreps) of the cubic group and with nonzero d-wave two-particle interactions. In Chapter 7, we present an exploratory investigation of bound states and resonances by solving two- and three-particle QCs. Lastly, we present the first ever extraction of $3\pi^+$ scattering information from LQCD data in Chapter 8.

In Chapter 9, we summarize and briefly discuss ongoing and future work. We also include six Appendices A–F, one for each of Chapters 3–8.

Part II

THEORETICAL FORMALISM

In the following three chapters, we present three major developments to the theoretical formalism of three-particle quantization conditions. Each chapter and its corresponding appendix is taken from a different research publication: Chapter 3 and Appendix A are from Ref. [43]; Chapter 4 and Appendix B are from Ref. [44]; and Chapter 5 and Appendix C are from Ref. [45].

Chapter 3

ALTERNATIVE DERIVATION OF THE RELATIVISTIC THREE-PARTICLE QUANTIZATION CONDITION[1]

3.1 Introduction

One of the present frontiers of lattice QCD (LQCD) is the study of systems containing three or more particles. The aims include the determination of the three-nucleon interaction and the study of resonances decaying to three or more particles. Advances have been made both in the ability to calculate multiple finite-volume energy levels using numerical simulations, and in the theoretical formalism needed to interpret the results. Examples of the successful combination of these methods are in Refs. [1, 41, 46–54].[2]

A key output of the theoretical formalism is a quantization condition, an equation whose solutions give the finite-volume three-particle energy levels in terms of infinite-volume scattering quantities. The latter quantities are then related to infinite-volume scattering amplitudes in a second step that involves solving integral equations. Our aim in this work is to provide a simplified method for deriving the quantization condition in a generic relativistic effective field theory (RFT). Our hope is that our new method will simplify the generalization of the quantization condition to systems not heretofore studied, for example to three nondegenerate particles and to more than three particles, as well as allow the unification of the different approaches used to develop the three-particle formalism (to be described below).

The two-particle quantization condition has been known for decades and is now a standard tool in LQCD [24, 25, 27, 56–63]. (See Ref. [26] for a review.) The three-particle formalism

[1]This chapter and Appendix A are taken directly from Ref. [43].

[2]For related applications in lattice simulations of ϕ^4 theory see Ref. [55].

has been developed more recently, using three main approaches:[3]

1. The RFT approach, which is the most general and also the most complicated. This formalism was derived in Refs. [28, 29] for the case of identical scalar particles with a $\mathbb{Z}_2$, G-parity-like, symmetry. We refer to these papers in the following as HS1 and HS2, respectively. The formalism has been subsequently generalized to allow $2 \leftrightarrow 3$ transitions [34], K matrix poles [35, 36], and nonidentical but degenerate particles [37]. The numerical implementation of the formalism has been studied in Refs. [36, 39, 76], and recently applied to extract the $3\pi^+$ interaction [51] using results for the $3\pi^+$ spectrum from Ref. [1].

2. The nonrelativistic effective field theory (NREFT) approach of Refs. [30, 31, 40, 77]. Here the derivation is much simpler, but to date the formalism has been developed only for two-particle interactions restricted to the s-wave.

3. The "finite-volume unitarity" (FVU) approach of Refs. [32, 41, 52, 53]. This is a relativistic formalism that is based on general forms for the three-particle scattering amplitude developed in Refs. [78, 79] that incorporate s-channel unitarity. As for the NREFT approach, it has to date been developed only for s-wave two-particle interactions. It has been applied to the $3\pi^+$ spectrum from LQCD in Refs. [52, 53].

Our aim, as already noted, is to simplify the RFT derivation given in HS1 and HS2. As a side benefit, our result provides a further check on the original formalism, adding to the checks provided in Refs. [68, 80–82].

The derivation of HS1 and HS2 uses TOPT to identify the loop integrals that lead to power-law finite-volume effects, but the main analysis is based on a skeleton expansion

[3] See also the foundational work of Ref. [64], the threshold expansions of Refs. [65–69], and the alternative approaches in Refs. [70–73]. For recent reviews, see Refs. [74, 75].

using Feynman diagrams. The strategy is, crudely speaking, to convert loop sums into integrals plus a volume-dependent remainder at every opportunity. This leads to complicated intermediate expressions involving kernels that are not symmetric under interchanges of external momenta, and are given by implicit, constructive definitions. Considerable effort is then required to rewrite the final quantization condition in terms of a symmetric three-particle K matrix (called $\mathcal{K}_{\text{df},3}$). Our alternative approach uses TOPT throughout,[4] converts fewer sums into integrals, and does not aim for full symmetrization in the initial quantization condition. This allows for a simpler derivation that is completely explicit. A second step then leads to the HS1 form of the quantization condition in terms of $\mathcal{K}_{\text{df},3}$. We stress that, despite the differences, many technical steps in our approach are based closely on the developments and technical results of HS1 and HS2.

We close the introduction with a summary of our approach, which also serves to describe the organization of the paper. The new derivation of the quantization condition is presented in Sec. 4.4, and is broken into several steps. We begin in Sec. 3.2.1 with a recap of the essentials of TOPT, and then, in Sec. 3.2.2, explain how the three-particle correlation function can be written in terms of two- and three-particle irreducible TOPT amplitudes. This is the analog in TOPT of the Feynman-diagram-based skeleton expansion used in HS1. The advantage of the TOPT approach is that the result, given in Eq. (3.24), is a simple geometric series that is straightforward to derive. The next step, described in Sec. 3.2.3, is to rewrite the expression for the correlator in terms of on-shell quantities. This is achieved by the results in Eqs. (3.52) and (3.57), which introduce two finite-volume quantities $\widetilde{G}$ and $\widetilde{F}$ that are closely related to the G and F appearing in HS1. Using these results, the form for the correlator can be reorganized into a geometric series involving on-shell, infinite-volume

[4] Aside from an initial use of Feynman diagrams to analyze self-energy diagrams, as described in Appendix A.1. We note that extension of the derivation of HS1 to theories without the $\mathbb{Z}_2$ symmetry, given in Ref. [34], makes more extensive use of TOPT, and we use several results concerning TOPT from that work.

kernels, Eq. (3.75). As described in Sec. 3.2.4, this immediately leads to our new form of the quantization condition, Eq. (3.81). While simple in form, this has the disadvantage of involving an asymmetric three-particle K matrix ($\widetilde{\mathcal{K}}_{\mathrm{df},3}^{(u,u)}$). The next sections of this work show how the quantization condition can be rewritten in terms of a symmetrized three-particle K matrix using relatively simple algebraic steps, with the final result, presented in Eq. (3.115), having exactly the same form as that of HS1. A spin-off from this analysis is that we obtain an explicit expression for the symmetric three-particle K matrix of HS1, $\mathcal{K}_{\mathrm{df},3}$, in terms of TOPT amplitudes connected by a sequence of integral operators.

Although these final symmetrization steps are straightforward, we take a somewhat indirect path to obtain them. This involves first, in Sec. 3.3, using the TOPT methodology to determine an expression for an asymmetric finite-volume three-particle scattering amplitude, $\widetilde{\mathcal{M}}_{3,L}^{(u,u)}$, in terms of $\widetilde{\mathcal{K}}_{\mathrm{df},3}^{(u,u)}$, Eq. (3.86); second, in Sec. 3.4.1, comparing that to the result for the similar amplitude $\mathcal{M}_{3,L}^{(u,u)}$ introduced in HS2; third, in Sec. 3.4.2, asymmetrizing the HS1 result so that it is written in terms of an asymmetric amplitude $\mathcal{K}_{\mathrm{df},3}^{(u,u)}$, and using this to show that the HS1 quantization condition can be recast in exactly the same form as our new version; and, finally, in Sec. 3.4.3, reversing the algebraic steps to show that our quantization condition can be rewritten in symmetric HS1 form. We close the paper with a summary and outlook.

We include several appendices collecting technical results. Appendix A.1 concerns TOPT. Appendix A.2 describes the relation of three- and two-particle finite-volume amplitudes, and gives details on the pole prescription that we use. Appendix A.3 explains a set of complicated though straightforward matrix manipulations that are needed in the main text. Appendix A.4 derives the asymmetrization identities needed in the main text. Appendix A.5 derives the relation between $\widetilde{\mathcal{K}}_{\mathrm{df},3}^{(u,u)}$ and $\mathcal{M}_3$. Appendix A.6 gives details of the steps needed to relate $\widetilde{\mathcal{K}}_{\mathrm{df},3}^{(u,u)}$ and $\mathcal{K}_{\mathrm{df},3}^{(u,u)}$. We also include Appendix A.7 in which we briefly describe a variant of our approach that leads to a slightly different form of the quantization condition,

and which may be advantageous when considering generalizations.

In a companion paper [45], we show that our new form of the quantization condition can be written in terms of the R matrix of Refs. [78, 79]. The provides a generalization of the FVU quantization condition to all two-particle partial waves.

3.2 Derivation of the new form of the quantization condition

We work in a generic relativistic effective field theory (RFT) of identical scalar particles with physical mass m in 3+1-dimensional Minkowski spacetime. We assume the Lagrangian has a G-parity-like $\mathbb{Z}_2$ symmetry so that only even-legged vertices are allowed. This is exactly the same setup as in HS1. Our aim is to derive an expression—the quantization condition—that determines the energy levels when this theory is considered in a finite spatial box. Following HS1, we choose a cubic volume of side length L, with periodic boundary conditions.

The tool we use is the finite-volume (FV) correlation function for fixed total four-momentum $P^\mu = (E, \mathbf{P})$:

$$C_{3,L}(E, \mathbf{P}) \equiv \int_L d^4x \; e^{i(Ex^0 - \mathbf{P}\cdot\mathbf{x})} \, \langle 0|\mathrm{T}\sigma(x)\sigma^\dagger(0)|0\rangle \;, \tag{3.1}$$

where $\mathbf{P} = \frac{2\pi}{L}\mathbf{n}_P$ with $\mathbf{n}_P \in \mathbb{Z}^3$, the integral is over $x^0 \in \mathbb{R}$ and $\mathbf{x} \in [0, L)^3$, $|0\rangle$ is the true vacuum state of the interacting theory, and $\sigma(x)$ is an interpolating field coupling to three-particle states. Throughout this paper, we assume the kinematic constraint $m < E^* < 5m$, where $E^* = \sqrt{E^2 - \mathbf{P}^2}$ is the total energy in the overall center-of-mass (CM) frame. This constraint ensures that only three-particle states may go entirely on shell, a restriction that is crucial to our derivation (as well as that of HS1).

For fixed $\mathbf{P}$, the correlator $C_{3,L}(E, \mathbf{P})$ will have poles in E at the energies of the FV states that have the quantum numbers of $\sigma^\dagger$, namely all states with odd particle number. By deriving an expression for the pole positions, we will obtain the desired FV quantization condition.

The derivation in HS1 involves summing over all Feynman diagrams contributing to $C_{3,L}(E, \mathbf{P})$. The expressions for each diagram differ from those in infinite volume only by the replacement of spatial loop integrals with sums over discrete spatial momenta, $\mathbf{k} \in \frac{2\pi}{L}\mathbb{Z}^3$. One of the key initial steps in the derivation is to note that some spatial-momentum sums have negligible dependence on L and can therefore be replaced with (infinite-volume) integrals. More precisely, if a summand/integrand $f(\mathbf{k})$ is smooth over the integration domain, with the derivatives scaling as appropriate powers of m, then, from the Poisson summation formula, the sum-integral difference is exponentially suppressed in mL:[5]

$$\frac{1}{L^3}\sum_{\mathbf{k}}^{\mathrm{UV}} f(\mathbf{k}) = \int^{\mathrm{UV}} \frac{d^3k}{(2\pi)^3} f(\mathbf{k}) + \mathcal{O}(e^{-mL})\,. \tag{3.2}$$

Here we have included an ultraviolet (UV) cutoff, the nature of which is unimportant as the sum-integral difference is an infrared effect. We assume throughout that mL is large enough that $\mathcal{O}(e^{-mL})$ terms can be safely neglected. An immediate consequence of this assumption is that the difference between a FV quantity and its infinite-volume analog is only non-negligible if the quantity contains a singularity in the spatial-momentum summand.

The next key step in HS1 is to utilize certain results from TOPT as a tool for identifying which Feynman diagrams can possess singularities and which cannot, as this greatly restricts the classes of Feynman diagrams that need to be considered to capture all significant FV contributions. However, this is the full extent to which TOPT is applied in HS1; actual time-ordered diagrams are never used.

3.2.1 TOPT basics

We begin the derivation proper by a brief recapitulation of the essential features of TOPT. A good source for the derivation of these results is Ref. [83]; further discussion in a context closely related to that considered here is given in Appendix B of Ref. [34]. The main subtlety

[5] Or, more precisely, falls faster than any power of mL.

in applying TOPT concerns the use of renormalized propagators, and we discuss this technical point in Appendix A.1.

In TOPT, one rewrites each Feynman diagram contributing to $C_{3,L}$ as a sum of all time orderings of the vertices, with each ordering corresponding to a unique time-ordered diagram. Each propagator in the diagram is associated with an on-shell four-momentum $p^\mu = (\omega_p, \mathbf{p})$, with positive energy $\omega_p \equiv \sqrt{\mathbf{p}^2 + m^2}$, and gives rise to a factor of $1/(2\omega_p)$. Spatial momentum is conserved at vertices, but energy is not. Each "cut" between consecutive vertices gives a kinematic factor

$$iK_t \equiv \frac{i}{E_t - \sum\limits_{p_{\text{on}} \in \mathcal{P}_t} \omega_p + i\epsilon}\,, \tag{3.3}$$

where $\mathcal{P}_t$ is the set of spatial momenta passing through the cut at time t, and

$$E_t \equiv \begin{cases} +E & \text{if } \; t_\sigma > t > t_{\sigma^\dagger} \\ -E & \text{if } \; t_{\sigma^\dagger} > t > t_\sigma \\ 0 & \text{otherwise,} \end{cases} \tag{3.4}$$

with $t_{\sigma^\dagger}$ and t_σ denoting the times at which $\sigma^\dagger$ and σ occur in the diagram, respectively.[6] The factor of $i\epsilon$ has no impact in finite volume, and can be set to zero in that case. When evaluating vertices with derivatives (which are present with arbitrary order in the generic RFT), the corresponding momenta are placed on shell. Symmetry factors are included as for Feynman diagrams. Finally, all spatial momenta are summed/integrated with the standard measure.

As discussed in Appendix A.1, by using an appropriate on-shell renormalization scheme and restricting to our kinematic regime in which only three particles can go on shell simultaneously, all self-energy diagrams can be absorbed into changes in the vertices, and it is the

[6] The precise values of the times are irrelevant to the value of the diagram; they are being used here only to label the ordering of vertices.

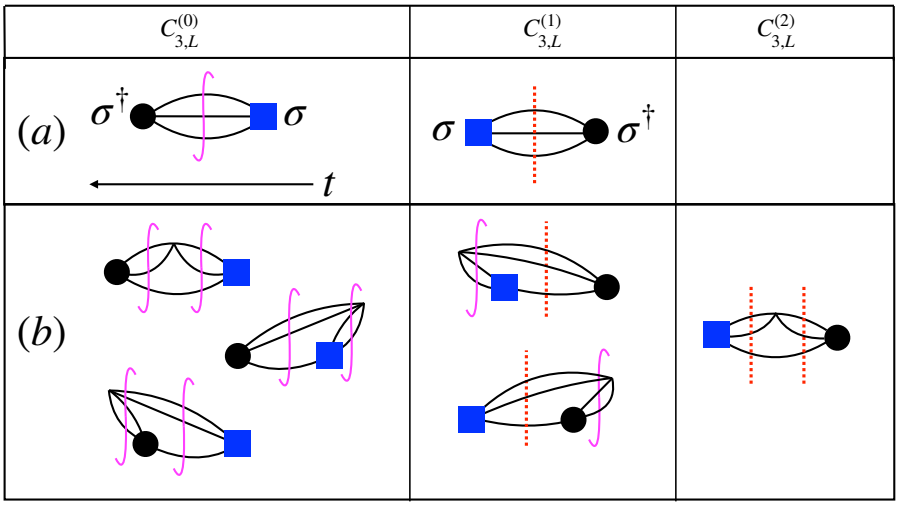

Figure 3.1: Examples of time orderings in diagrams contributing to $C_{3,L}$. Time flows from right to left, with the black circle (blue square) representing $\sigma^\dagger$ (σ). Relevant cuts are shown by vertical (red) dashed lines, while irrelevant cuts are shown by solid (magenta) integral signs. The factors associated with these cuts are described in the text. Vertical columns divide contributions according to the number of relevant cuts. Horizontal rows contain the time orderings of (a) the leading-order Feynman diagram and (b) a Feynman diagram with a single four-point vertex.

physical mass that enters into the factors of ω_p.

Given these rules, the only singularities in diagrams are due to the kinematic factors K_t; by assumption, the vertices are polynomials in momenta and thus nonsingular. Furthermore, within our range of E^*, the only singularities occur if $E_t = +E$ and $|\mathcal{P}_t| = 3$, i.e., if the cut at time t contains three lines and comes after $t_{\sigma^\dagger}$ and before t_σ. We shall refer to such cuts as "relevant three-particle cuts" or simply "relevant cuts."[7] The remaining cuts, which we refer to as "irrelevant," occur if either (i) $E_t = +E$ with $|\mathcal{P}_t| \neq 3$, or (ii) $E_t \in \{-E, 0\}$. Since $|\mathcal{P}_t|$ is necessarily odd for all cuts through $C_{3,L}$, case (i) corresponds to having either a single

[7] A potential second type of relevant cut, arising from a single dressed propagator, is discussed in Appendix A.1, and shown to be absent.

particle in the cut, leading to a singularity at $E^* = m$, or at least five particles, for which singularities occur for $E^* \geq 5m$. Both of these possibilities lie outside our kinematic range. For case (ii), there are no singularities because the denominator of K_t is negative definite. Examples of relevant and irrelevant cuts are shown for simple diagrams in Fig. 3.1.

Given this classification, irrelevant cuts yield a smooth K_t, and we can use Eq. (3.2) to take the infinite-volume limits of all spatial-momentum sums involving the cut, i.e. to replace the sums with integrals. This was the key result from TOPT that HS1 used to identify which Feynman diagrams contained singularities, but here we continue working with time-ordered diagrams.

Later in this work (in Sec. 3.3) we will consider scattering amplitudes, i.e. amputated correlation functions, both in finite and infinite volume. The corresponding Feynman diagrams can also be broken up into time-ordered components using TOPT. The rules are the same as above, except that the operators creating incoming (destroying outgoing) particles are always placed at the earliest (latest) time. In addition, there are no $1/(2\omega)$ factors for the external propagators; the first cut occurs after the first vertex, and the last cut before the final vertex. In general such an amplitude is off shell. The on-shell amplitude, whose absolute square is related to the scattering cross section, is obtained by choosing the initial and final spatial momenta such that the initial- and final-state energies both sum to E. In this on-shell limit, the result for the amplitude is identical to that given by the expression obtained using Feynman diagrams, and, in particular, is Lorentz invariant.

3.2.2 Expansion of $C_{3,L}(E, \mathbf{P})$ in relevant cuts

Our strategy is to organize the (renormalized) time-ordered diagrams that contribute to $C_{3,L}(E, \mathbf{P})$ by the number of relevant three-particle cuts they contain,

$$C_{3,L}(E, \mathbf{P}) = \sum_{n=0}^{\infty} C_{3,L}^{(n)}(E, \mathbf{P}) \,, \tag{3.5}$$

where $C_{3,L}^{(n)}(E,\mathbf{P})$ is the sum of all diagrams containing exactly n relevant cuts. Examples of this organization are shown in Fig. 3.1.

The $n = 0$ term $C_{3,L}^{(0)}(E,\mathbf{P})$ denotes the sum of all diagrams with no such cuts. Since all cuts in each diagram give smooth iK_t contributions, we can use Eq. (3.2) to replace all discrete momentum sums with integrals and take the infinite-volume limit:

$$C_{3,L}^{(0)}(E,\mathbf{P}) = C_{3,\infty}^{(0)}(E,\mathbf{P}) + \mathcal{O}(e^{-mL})\,. \tag{3.6}$$

From now on we will no longer track terms that are exponentially suppressed in mL.

For diagrams with at least one relevant cut, the expressions factorize into a form with a right-hand "endcap," followed by some (possibly zero) number of $3 \to 3$ segments, followed by a left-hand endcap. These pieces are separated by relevant cuts. This factorization can be seen in the examples in the $C_{3,L}^{(1)}$ and $C_{3,L}^{(2)}$ columns of Fig. 3.1. A more extensive example for $C_{3,L}^{(4)}$ is shown in Fig. 3.2, which shows that there are two types of nontrivial $3 \to 3$ segments: one in which two particles interact with the third particle spectating, and the other in which all three particles interact. We label these $\overline{\mathcal{B}}_{2,L}$ and $\mathcal{B}_3$ respectively, while the left (right) endcaps are denoted $\widehat{A}'$ ($\widehat{A}$).[8] Before presenting the general expression for $C_{3,L}$, we first give the definitions of these four segments.

Contributing segments

We begin with the left endcap $\widehat{A}'$. It is given by the sum of all time-ordered diagrams that contain σ, are three-particle irreducible in the s-channel (3PIs),[9] and begin with an amputated three-particle cut. The amputation removes the factors of $1/(2\omega)$ from each line,

[8] The "hat" on these quantities is used to distinguish them from similar, but different, endcaps denoted A' and A in HS1. Similarly, we label the intermediate segments with a calligraphic $\mathcal{B}$, in order to distinguish them from the Bethe-Salpeter kernels B_2 and B_3 used in HS1.

[9] Our definition of 3PIs includes, in principle, the possibility of a cut through a single propagator that is carrying the full momentum $\mathbf{P}$. However, as explained in Appendix A.1, in our kinematic regime all such single propagators can be collapsed into vertices, so the issue does not arise.

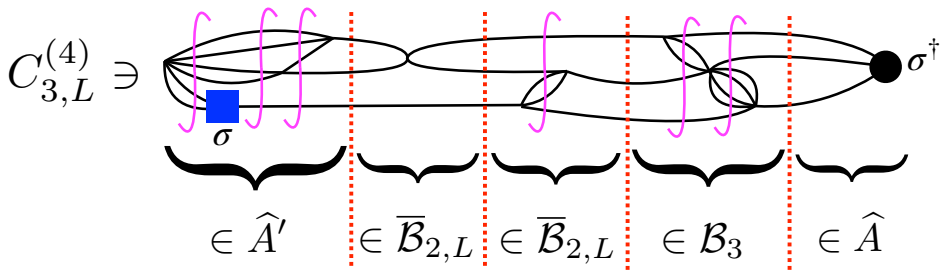

Figure 3.2: Example of a contribution to $C^{(4)}_{3,L}$. Notation is as in Fig. 3.1. The names for the different types of segment are indicated by the underbraces.

as well as the energy denominator of the relevant cut. These factors will be added back when we join the segments. For fixed E and $\mathbf{P}$, $\widehat{A}'$ depends on the spatial momenta of two of the particles in the relevant cut, usually denoted $\mathbf{k}$ and $\mathbf{a}$. The momentum of the third, usually denoted $\mathbf{b}_{ka}$, or simply $\mathbf{b}$ for short, is given by $\mathbf{b}_{ka} = \mathbf{P} - \mathbf{k} - \mathbf{a}$. We define $\widehat{A}'(\mathbf{k}, \mathbf{a})$ to include all distinct attachments of momentum labels to the external lines. This is exactly what would result were we to define this as an amplitude with three single-particle creation operators and included all Wick contractions. This implies that it is fully symmetric[10]

$$\widehat{A}'(\mathbf{k}, \mathbf{a}) = \widehat{A}'(\mathbf{a}, \mathbf{b}) = \widehat{A}'(\mathbf{b}, \mathbf{k}) = \widehat{A}'(\mathbf{a}, \mathbf{k}) = \widehat{A}'(\mathbf{b}, \mathbf{a}) = \widehat{A}'(\mathbf{k}, \mathbf{b})\,. \tag{3.7}$$

It turns out to be convenient to multiply the sum of all diagrams by a factor of 1/3, as this will cancel a labeling degeneracy that we describe below. This factor can be intuitively understood as placing this inherently symmetric object on the same footing as the inherently asymmetric segment $\overline{\mathcal{B}}_{2,L}$ to be defined below. Examples of diagrams contributing to this endcap are shown in Fig. 3.3.

The right endcap $\widehat{A}$ is defined as the sum of all amputated 3PIs TOPT diagrams con-

[10] A reader making a detailed comparison with HS1 will observe that the endcaps used initially in that work are asymmetric, and considerable effort is needed at a later stage to symmetrize them. One of the advantages of the TOPT approach is that we do not need to use asymmetric quantities at this stage, with the exception of $\overline{\mathcal{B}}_{2,L}$.

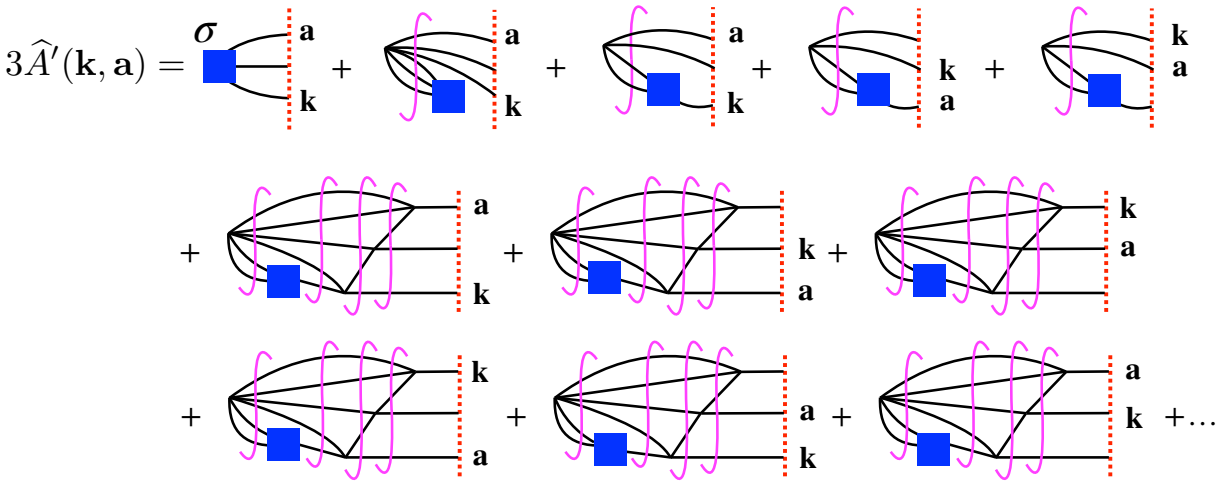

Figure 3.3: Examples of contributions to the left endcap $\widehat{A}'(\mathbf{k},\mathbf{a})$, with notation as in Fig. 3.1. When evaluating these diagrams, the external lines (those that end at the relevant cut) are amputated, with the factors of $1/(2\omega)$ dropped, and the energy denominator is also not included. The factor of 3 on the left-hand side is discussed in the text. The vertices in the diagram can represent interactions with or without derivatives, but in all cases are fully symmetric. The number of relabelings of a diagram depends on its intrinsic symmetry under interchange of the external particles. For the first two diagrams, which are symmetric under external particle interchange, there is only one labeling. For the next diagram, which is symmetric under interchange of the upper two particles, there are three labelings, as shown. The final diagram, shown on the second and third lines, is completely asymmetric, and all six relabelings must be included.

taining a $\sigma^\dagger$ and ending with an amputated three-particle cut, multiplied by 1/3. Diagrammatically, it is simply the horizontal "reflection" of $\widehat{A}'$. It is fully symmetric.

The fully connected $3 \to 3$ segment $i\mathcal{B}_3(\mathbf{k}',\mathbf{a}';\mathbf{k},\mathbf{a})$ (with fixed E and $\mathbf{P}$ implicit) is defined as the sum of all amputated, connected, 3PIs TOPT diagrams beginning and ending at a relevant cut.[11] All momentum assignments are included, and it is multiplied by 1/3

[11]The factor of i is included to match the standard definition of a scattering amplitude, and follows the notation of HS1.

for each cut, i.e. by 1/9 in total. It is fully symmetric separately for both initial and final momenta,

$$\mathcal{B}_3(\mathbf{k}',\mathbf{a}';\mathbf{k},\mathbf{a}) = \mathcal{B}_3(\mathbf{a}',\mathbf{k}';\mathbf{k},\mathbf{a}) = \mathcal{B}_3(\mathbf{k}',\mathbf{a}';\mathbf{a},\mathbf{b}) = \cdots . \tag{3.8}$$

The final segment is $i\overline{\mathcal{B}}_{2,L}$, in which only two of the particles are connected—the "interacting pair"—while the third spectates. This segment is intrinsically asymmetric, and we choose the spectator momentum to be $\mathbf{k} = \mathbf{k}'$,

$$\begin{aligned} i\overline{\mathcal{B}}_{2,L}(E,\mathbf{P};\mathbf{k}',\mathbf{a}';\mathbf{k},\mathbf{a}) &\equiv \delta_{k'k} 2\omega_k L^3 i\mathcal{B}_2(E_{2,k},\mathbf{P}_{2,k};\mathbf{a}';\mathbf{a}) , \\ E_{2,k} \equiv E - \omega_k , &\quad \mathbf{P}_{2,k} \equiv \mathbf{P} - \mathbf{k} , \end{aligned} \tag{3.9}$$

where $\delta_{k'k} = \delta^3_{\mathbf{k}',\mathbf{k}}$ is the three-dimensional Kronecker delta. Here $\mathcal{B}_2$ is the sum over all amputated TOPT diagrams describing connected $2 \to 2$ scattering that are 2PI in the s channel, which we denote as 2PIs diagrams. Note that the four-momentum flowing through $\mathcal{B}_2$ is $(E_{2,k},\mathbf{P}_{2,k})$, since the spectator four-momentum $k^\mu = (\omega_k,\mathbf{k})$ is subtracted from the total. We also include an L in the subscript to emphasize the presence of an explicit factor of L^3. Examples of diagrams contributing to $\mathcal{B}_2$ are shown in Fig. 3.4. It is symmetric under separate interchange of the momenta within initial and final pairs, i.e.

$$\begin{aligned} \mathcal{B}_2(E_2,\mathbf{P}_2;\mathbf{a}';\mathbf{a}) = \mathcal{B}_2(E_2,\mathbf{P}_2;\mathbf{b}';\mathbf{a}) = \mathcal{B}_2(E_2,\mathbf{P}_2;\mathbf{a}';\mathbf{b}) = \mathcal{B}_2(E_2,\mathbf{P}_2;\mathbf{b}';\mathbf{b}) , \\ \mathbf{b}' = \mathbf{P}_2 - \mathbf{a}' , \quad \mathbf{b} = \mathbf{P}_2 - \mathbf{a} . \end{aligned} \tag{3.10}$$

It is defined without any overall factors (unlike $\mathcal{B}_3$).

The factor of $2\omega_k L^3$ in the numerator of Eq. (3.9) is needed because the cuts on both sides of $\mathcal{B}_2$ include a spectator propagator, so one must be canceled. This is explained in greater detail below.

For the quantities $\widehat{A}'$, $\widehat{A}$, $\mathcal{B}_3$, and $\mathcal{B}_2$, we can proceed as for $C^{(0)}_{3,L}$ and take the infinite-volume limit, since they contain no relevant cuts in our kinematic region. The lack of such cuts is by construction for the 3PIs quantities $\widehat{A}'$, $\widehat{A}$, and $\mathcal{B}_3$. For $\mathcal{B}_2$, the lack of relevant

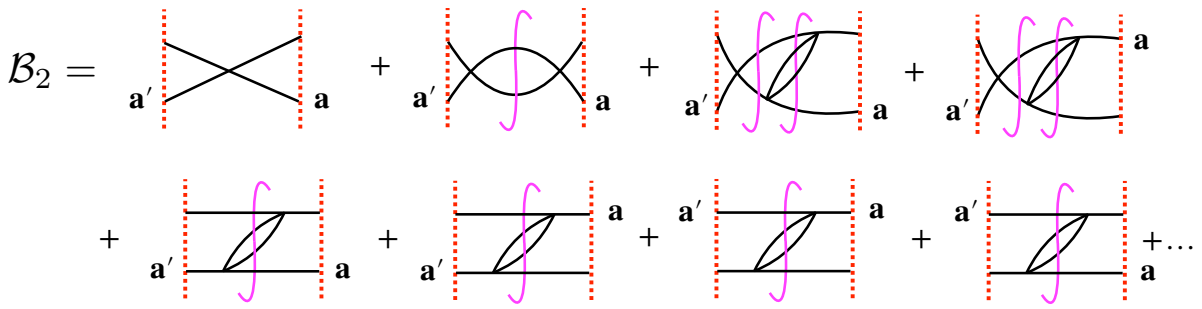

Figure 3.4: Examples of contributions to $i\mathcal{B}_2(E_2, \mathbf{P}_2; \mathbf{a}'; \mathbf{a})$, with notation as in Figs. 3.1 and 3.3. (In this and following figures we do not keep track of factors of i.) The number of relabelings of a diagram depends on its intrinsic symmetry under interchange of the external particles. For the first two diagrams, which are symmetric under external particle interchange, there is only one labeling. The next diagram is symmetric on the left, but not on the right, and so there are two relabelings, as shown. The final diagram is asymmetric under interchange of both initial and final particles, and thus there are four relabelings, as shown.

three-particle cuts in $\overline{\mathcal{B}}_{2,L}$ implies that $\mathcal{B}_2$ can have no on-shell two particle cuts, since its CM energy E_2^* cannot exceed $4m$. Because of the absence of relevant cuts, $\widehat{A}'$, $\widehat{A}$, $\mathcal{B}_3$, and $\mathcal{B}_2$ are all real in our kinematic range. As discussed in Appendix A.1, we implicitly use a diagram by diagram regularization and renormalization scheme, so that all quantities are UV finite.

Evaluating $C_{3,L}(E, \mathbf{P})$

With the 3PIs segments in hand, we can now proceed toward a general expression for the correlator. To write this compactly, we introduce a matrix notation, in which the indices are the two summed finite-volume momenta at each cut, $\{ka\} \equiv \{\mathbf{k}, \mathbf{a}\}$. Thus $\widehat{A}'$ becomes a row

vector, $\mathcal{B}_3$ and $\overline{\mathcal{B}}_{2,L}$ become matrices, and $\widehat{A}$ becomes a column vector:

$$\begin{aligned} \widehat{A}'_{k'a'} &\equiv \widehat{A}'(\mathbf{k}',\mathbf{a}')\,, \qquad & [\mathcal{B}_3]_{k'a';ka} &\equiv \mathcal{B}_3(\mathbf{k}',\mathbf{a}';\mathbf{k},\mathbf{a})\,, \\ \widehat{A}_{ka} &\equiv \widehat{A}(\mathbf{k},\mathbf{a})\,, \qquad & \left[\overline{\mathcal{B}}_{2,L}\right]_{k'a';ka} &\equiv \overline{\mathcal{B}}_{2,L}(E,\mathbf{P};\mathbf{k}',\mathbf{a}';\mathbf{k},\mathbf{a})\,. \end{aligned} \tag{3.11}$$

The sum of contributions containing exactly one relevant cut can then be written

$$C_{3,L}^{(1)}(E,\mathbf{P}) = \sum_{\mathbf{k}',\mathbf{a}'}^{\mathrm{UV}} \sum_{\mathbf{k},\mathbf{a}}^{\mathrm{UV}} \widehat{A}'_{k'a'} 3i [D_F]_{k'a';ka} \widehat{A}_{ka}\,, \tag{3.12}$$

$$= \widehat{A}'\, 3i D_F \widehat{A}\,, \tag{3.13}$$

where in the second line we have left matrix indices implicit. The matrix associated with the relevant cut is

$$[D_F]_{k'a';ka} \equiv \frac{1}{2!}\delta_{k'k}\delta_{a'a} D_{ka}\,, \tag{3.14}$$

$$D_{ka} \equiv \frac{1}{2\omega_k L^3} \frac{1}{2\omega_b (E-\omega_k-\omega_a-\omega_b)} \frac{1}{2\omega_a L^3} = D_{ak}\,. \tag{3.15}$$

The reason for the subscript F will become clear below.

The various terms in Eq. (3.13) are chosen so that the correct TOPT expression for $C_{3,L}^{(1)}$ is obtained when sewing $\widehat{A}'$ and $\widehat{A}$ together. In particular, D_{ka} plays three roles. First, it puts back in the propagator factors that have been removed when amputating $\widehat{A}'$ and $\widehat{A}$. Second, it contains the two factors of $1/L^3$ that are the standard measure associated with the sums over the loop momenta $\mathbf{k}$ and $\mathbf{a}$. Third, it includes the energy denominator from the kinematic factor K_t.

The numerical factors of 3 [multiplying D_F in Eq. (3.13)] and 1/2! (in the definition of D_F), are needed to account for symmetry factors and labeling degeneracy. Recalling that $\widehat{A}'$ and $\widehat{A}$ each come with a factor of 1/3 included by hand, the product of these factors is $N_S = (1/3)\times(3/2!)\times(1/3) = 1/3!$. If one is considering contributions to $\widehat{A}'$ and $\widehat{A}$ that both correspond to completely asymmetric underlying diagrams with 3! possible labelings (as in the example shown in the last two lines of Fig. 3.3), then the $(3!)^2$ terms in the product

overcount the number of diagrams contributing to $C_{3,L}^{(1)}$ by a factor of 3!. This is canceled by N_S. If instead the contributions to both $\widehat{A}'$ and $\widehat{A}$ are completely symmetric (as in the first two examples in Fig. 3.3), then there is only one diagram that appears in the product, but it needs a symmetry factor of 1/3! that is provided N_S. Cases of intermediate symmetry work similarly.

For reasons that will become clear shortly, it is useful to rewrite Eq. (3.13) as

$$C_{3,L}^{(1)} = \widehat{A}'\, i(D_F + D_G)\widehat{A}\,, \tag{3.16}$$

$$[D_G]_{k'a';ka} \equiv \delta_{k'a}\delta_{ka'} D_{ka}\,. \tag{3.17}$$

The new matrix D_G differs from D_F in the manner in which the momenta are contracted, and also because it lacks the factor of 1/2!. When adjacent to a symmetric quantity (on either side) one can replace D_G with $2D_F$, because the corresponding momentum indices k and a can be freely interchanged, and because $D_{ka} = D_{ak}$. Given this substitution, the equivalence of Eqs. (3.13) and (3.16) is immediate.

We now move on to the contributions with two relevant cuts. These can involve either a $\mathcal{B}_3$ or a $\overline{\mathcal{B}}_2$ between the endcaps. For the former, using exactly the same arguments as just described, one finds that

$$C_{3,L}^{(2)} \ni \widehat{A}'\, 3iD_F i\mathcal{B}_3\, 3iD_F\widehat{A} = \widehat{A}'\, i(D_F + D_G)i\mathcal{B}_3 i(D_F + D_G)\widehat{A}\,. \tag{3.18}$$

For the latter, it turns out that the same form holds

$$C_{3,L}^{(2)} \ni \widehat{A}'\, 3iD_F i\overline{\mathcal{B}}_{2,L} 3iD_F\widehat{A} = \widehat{A}'\, i(D_F + D_G)i\overline{\mathcal{B}}_{2,L} i(D_F + D_G)\widehat{A}\,, \tag{3.19}$$

where the second result follows from the first because both D_F's are adjacent to a symmetric endcap. To understand why Eq. (3.19) gives the correct contribution to $C_{3,L}^{(2)}$, consider the diagram shown in the final column of Fig. 3.1. The $2\omega_k L^3$ in $\overline{\mathcal{B}}_{2,L}$, Eq. (3.9), cancels that in one of the D_F's, so that there is only one such factor in the overall diagram, as appropriate for the spectator line. Using the first form in Eq. (3.19), the numerical factors combine to

give $N'_S = (1/3) \times (3/2!) \times (3/2!) \times (1/3) = 1/(2!)^2$, which is the correct symmetry factor for the diagram as a whole. For completely asymmetric contributions to $\widehat{A}'$, $\overline{\mathcal{B}}_{2,L}$, and $\widehat{A}$, N'_S serves to cancel the labeling degeneracy. For cases with intermediate symmetry, N'_S provides a mix of the needed symmetry factors and cancellation of labeling degeneracies. The total result with two relevant cuts can thus be written

$$C^{(2)}_{3,L} = \widehat{A}'\, i(D_F + D_G) i(\overline{\mathcal{B}}_{2,L} + \mathcal{B}_3) i(D_F + D_G) \widehat{A}\,. \tag{3.20}$$

Generalizing to more cuts is straightforward if only $\mathcal{B}_3$ segments appear, for they can be connected together with factors of $3iD_F$ or, equivalently, $i(D_F + D_G)$. A complication arises, however, when one has adjacent factors of $\overline{\mathcal{B}}_{2,L}$, as occurs in the example shown in Fig. 3.2. In such cases the manner in which indices are contracted matters due to the asymmetry of $\overline{\mathcal{B}}_{2,L}$. In Fig. 3.2, the intermediate matrix must be a D_G, because the spectator line is switched. If there is no such switch then the intermediate matrix must be a D_F. This distinction is illustrated in Fig. 3.5. The relative factor of 2! between D_F and D_G is also needed to obtain the correct overall symmetry factor. One way to understand this is to note that there are two ways to join a spectator to the interacting pair, compared to only a single way of joining the spectators. The conclusion of this discussion is that factors of $\overline{\mathcal{B}}_{2,L}$ *must be joined by* $i(D_F + D_G)$, with no freedom to change to any other form. This is why in the cases above where there was such freedom, we rewrote the result in terms of the combination $D_F + D_G$.

We thus conclude that the result for $n \geq 1$ relevant cuts can be written

$$C^{(n)}_{3,L} = \widehat{A}'\, i(D_F + D_G) \left[i(\overline{\mathcal{B}}_{2,L} + \mathcal{B}_3) i(D_F + D_G) \right]^{n-1} \widehat{A}\,. \tag{3.21}$$

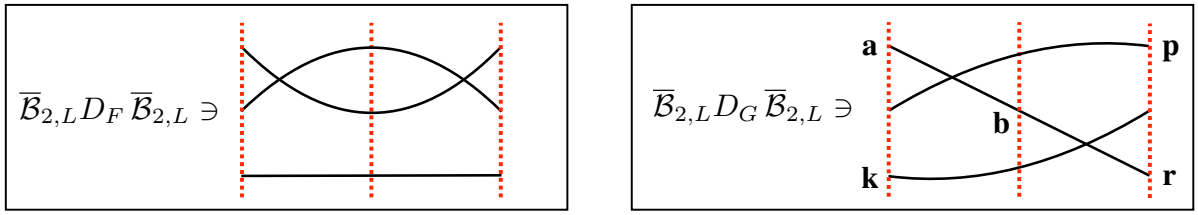

Figure 3.5: Example of the difference between D_F and D_G when connecting two $\overline{\mathcal{B}}_{2,L}$ segments. Notation as in Fig. 3.1. In this simple example, the extra factor of $1/2!$ contained in the definition of D_F is needed to give the symmetry factor associated with the closed loop that crosses the central cut in the left-hand diagram. Momentum labels are discussed in the text in Sec. 3.2.3.

The full correlator is then given by a geometric series

$$C_{3,L}(E,\mathbf{P}) = \sum_{n=0}^{\infty} C_{3,L}^{(n)}(E,\mathbf{P}) \tag{3.22}$$

$$= C_{3,L}^{(0)}(E,\mathbf{P}) + \sum_{n=1}^{\infty} \widehat{A}'\, i(D_F+D_G)\left[i(\overline{\mathcal{B}}_{2,L}+\mathcal{B}_3)i(D_F+D_G)\right]^{n-1} \widehat{A} \tag{3.23}$$

$$= C_{3,\infty}^{(0)}(E,\mathbf{P}) + \widehat{A}'\, i(D_F+D_G)\frac{1}{1-i(\overline{\mathcal{B}}_{2,L}+\mathcal{B}_3)i(D_F+D_G)}\widehat{A}\,. \tag{3.24}$$

We have obtained a closed-form expression for $C_{3,L}(E,\mathbf{P})$ in which the building blocks are infinite-volume "TOPT amplitudes"—$\widehat{A}'$, $\mathcal{B}_3$, $\mathcal{B}_2$ (contained in $\overline{\mathcal{B}}_{2,L}$), and $\widehat{A}$. Volume dependence enters through the fact that momenta are summed over the set of FV values, and through the explicit factors of L^3 associated with the sums and contained in $\overline{\mathcal{B}}_{2,L}$. The simplicity of the result and the straightforward manner of its derivation are two of the main advantages of using the TOPT approach.

3.2.3 On-shell projection

At this stage our expression for $C_{3,L}$ is built from infinite-volume quantities, but these are, in general, off shell. To obtain a useful quantization condition we need to rewrite $C_{3,L}$ in terms of fully on-shell quantities, which in turn can be related to physical amplitudes. By fully

on-shell, we mean that the incoming and outgoing four-momenta are both individually on shell and sum to the total four-momentum $P^\mu = (E, \mathbf{P})$. Within TOPT the first condition is automatically satisfied, as is the conservation of spatial momenta, so the issue to address is that, in general, the three particles at a relevant cut do not satisfy $\omega_k + \omega_a + \omega_b = E$. We stress that for the TOPT amplitudes $\mathcal{B}_3$ and $\overline{\mathcal{B}}_{2,L}$, one must separately consider on-shellness for the incoming and outgoing momenta—these amplitudes can, for example, be on shell on one side but off shell on the other.

The method we use in this subsection is to expand the amplitudes about their on-shell points. For fixed E and $\mathbf{P}$, these expansions are made in the spatial momenta of the external particles. This necessarily involves consideration of external momenta that do not lie in the discrete set allowed for finite volumes. Although such external momenta do not enter into the expression for $C_{3,L}$, Eq. (3.24), the TOPT amplitudes are well defined for all external momenta. This is because all internal loops have been converted to infinite-volume integrals, so changes in external momenta can be propagated through the diagrams into small changes in loop momenta. Since the integrands are nonsingular by construction, the dependence on external momenta is smooth. This result was used in HS1 and HS2 in the context of Feynman amplitudes.

We separately analyze cuts involving D_G and D_F, which we refer to as "G cuts" and "F cuts," respectively, and then apply the results to $C_{3,L}(E, \mathbf{P})$.

G cuts

To evaluate Eq. (3.24), we must repeatedly consider quantities of the form[12]

$$\begin{aligned} [X' D_G X]_{ka;pr} &= [X']_{ka;k'a'} \, [D_G]_{k'a';p'r'} \, [X]_{p'r';pr} \ , \\ X' \in \{\widehat{A}', \overline{\mathcal{B}}_{2,L}, \mathcal{B}_3\} \, , &\quad X \in \{\widehat{A}, \overline{\mathcal{B}}_{2,L}, \mathcal{B}_3\} \, . \end{aligned} \tag{3.25}$$

[12]If $X' = \widehat{A}'$ or $X = \widehat{A}$ then the corresponding outer momentum labels are absent.

Our aim is to rewrite these in terms of a part in which the right-hand momenta of X' (with indices $k'a'$) and the left-hand momenta of X (with indices $p'r'$) are both on shell, plus a residue that does not have a pole in E. In the following we refer to the momenta that we will set on shell as the "inside" momenta, while those that are left off shell (here ka and pr) as the "outside" momenta.

We consider in detail the case where $X' = X = \overline{\mathcal{B}}_{2,L}$, from which the results for other choices can easily be deduced. Writing this out, we have

$$\left[\overline{\mathcal{B}}_{2,L} D_G \, \overline{\mathcal{B}}_{2,L}\right]_{ka;pr} = \left[\overline{\mathcal{B}}_{2,L}\right]_{ka;k'a'} [D_G]_{k'a';p'r'} \left[\overline{\mathcal{B}}_{2,L}\right]_{p'r';pr} \tag{3.26}$$

$$= \mathcal{B}_2(E_{2,k}, \mathbf{P}_{2,k}; \mathbf{a}; \mathbf{p}) \frac{1}{2\omega_{b_{kp}}(E - \omega_k - \omega_p - \omega_{b_{kp}})} \times \mathcal{B}_2(E_{2,p}, \mathbf{P}_{2,p}; \mathbf{k}; \mathbf{r}) \,, \tag{3.27}$$

where in the first line repeated indices are summed. The choice of momentum labels is illustrated in the right-hand diagram of Fig. 3.5.

Our aim in the following is to expand the two factors of $\mathcal{B}_2$ about the points at which their internal momenta are on shell. Consider first the left-hand $\mathcal{B}_2$. Its internal (right-hand) momenta are $\mathbf{p}$ and $\mathbf{b}_{pk} = \mathbf{P} - \mathbf{k} - \mathbf{p} \equiv \mathbf{b}$. We wish to adjust $\mathbf{p}$ (which also changes $\mathbf{b}$ since $\mathbf{P}$ is fixed) until $\omega_p + \omega_b = E_{2,k}$. The way we do so is adapted from the approach used in Sec. IVB of HS1. We first change variables to those in the center-of-mass frame (CMF) of the scattered pair. Since the four-momentum of the pair is $(\omega_p + \omega_b, \mathbf{P}_{2,k})$, the boost to this frame has parameters

$$\beta_k = \frac{|\mathbf{P}_{2,k}|}{\omega_p + \omega_b} \,, \quad \gamma_k = \frac{\omega_p + \omega_b}{2\omega_p^*} \,, \quad 4\omega_p^{*2} = (\omega_p + \omega_b)^2 - \mathbf{P}_{2,k}^2 \,, \tag{3.28}$$

such that $(\omega_p, \mathbf{p})$ is boosted to $(\omega_p^*, \mathbf{p}_k^*)$, with

$$p_{k\|}^* = \gamma_k(p_\| - \beta_k \omega_p) \,, \quad \mathbf{p}_{k\perp}^* = \mathbf{p}_\perp \,, \tag{3.29}$$

where parallel and perpendicular components are relative to $\mathbf{P}_{2,k}$. Similarly, $(\omega_b, \mathbf{b})$ is boosted

to $(\omega_p^*, -\mathbf{p}_k^*)$. Here the subscripts "$k$" are a reminder that the boost depends on $\mathbf{k}$. This boost differs from that used in HS1, because here all particles are on shell while energy is not conserved, whereas in HS1 the particle with momentum $\mathbf{b}$ is off shell and energy is conserved. The boost used here has the advantage that it is well defined for all choices of $\mathbf{k}$, since $|\beta_k| < 1$. We refer to it below as the "Wu boost."[13] We also stress that $\mathbf{p}_k^*$ completely fixes $\mathbf{p}$ since it determines $E_{2,k}^* = 2\omega_p^*$, from which, for given $\mathbf{P}_{2,k}$, one obtains $\omega_p + \omega_b$ and thus the inverse boost. Thus we can change variables[14] in $\mathcal{B}_2$ from $\mathbf{p}$ to $\mathbf{p}_k^* = p_k^* \widehat{\mathbf{p}}_k^*$:

$$\mathcal{B}_2(E_{2,k}, \mathbf{P}_{2,k}; \mathbf{a}; \mathbf{p}) \equiv \mathcal{B}_2^*(E_{2,k}, \mathbf{P}_{2,k}; \mathbf{a}; \mathbf{p}_k^*)\,, \tag{3.30}$$

where the asterisk on $\mathcal{B}_2^*$ simply indicates the same function expressed in terms of the new variables.

The next step is to decompose the angular dependence of $\mathcal{B}_2^*$ into spherical harmonics,

$$\mathcal{B}_2^*(E_{2,k}, \mathbf{P}_{2,k}; \mathbf{a}; \mathbf{p}_k^*) \equiv \mathcal{B}_2^*(E_{2,k}, \mathbf{P}_{2,k}; \mathbf{a}; p_k^*)_{\ell m} \sqrt{4\pi} Y_{\ell m}(\widehat{\mathbf{p}}_k^*)\,, \tag{3.31}$$

where there is an implicit summation on angular-momentum indices, and the factor of $\sqrt{4\pi}$ follows the conventions of HS1. We use real spherical harmonics throughout to avoid an overabundance of asterisks. Since we expect $\mathcal{B}_2$ to be nonsingular in our kinematic regime, the coefficients $\mathcal{B}_2^*(E_{2,k}, \mathbf{P}_{2,k}; \mathbf{a}; p_k^*)_{\ell m}$ should be smooth functions of p_k^*. Indeed, if we can Taylor-expand $\mathcal{B}_2^*(E_{2,k}, \mathbf{P}_{2,k}; \mathbf{a}; \mathbf{p}_k^*)$ about $\mathbf{p}_k^* = 0$, it follows that, in order to avoid singularities at $p_k^* = 0$ from the spherical harmonics or the absolute value, we can pull out a factor of $p_k^{*\ell}$ from $\mathcal{B}_2^*$,

$$\mathcal{B}_2^*(E_{2,k}, \mathbf{P}_{2,k}; \mathbf{a}; p_k^*)_{\ell m} \equiv \mathcal{B}_2^{**}(E_{2,k}, \mathbf{P}_{2,k}; \mathbf{a}; p_k^{*2})_{\ell m} p_k^{*\ell}\,, \tag{3.32}$$

---

[13] We learned of this boost from J.-J. Wu, who used it in the context of the Hamiltonian effective field theory description of finite-volume effects [84].

[14] The fact that $\mathcal{B}_2$ is not Lorentz invariant presents no obstruction to this change of variables.

where $\mathcal{B}_2^{**}$ is a smooth function of p_k^{*2}. Thus we can rewrite the expansion as

$$\mathcal{B}_2(E_{2,k}, \mathbf{P}_{2,k}; \mathbf{a}; \mathbf{p}) = \mathcal{B}_2^{**}(E_{2,k}, \mathbf{P}_{2,k}; \mathbf{a}; p_k^{*2})_{\ell m} \mathcal{Y}_{\ell m}(\mathbf{p}_k^*)\,, \quad \mathcal{Y}_{\ell m}(\mathbf{p}_k^*) \equiv \sqrt{4\pi} Y_{\ell m}(\hat{\mathbf{p}}_k^*) p_k^{*\ell}\,. \tag{3.33}$$

The $\mathcal{Y}_{\ell m}$ are simply the harmonic polynomials, rescaled by $\sqrt{4\pi}$.

The final step is to set the amplitude on shell (on its right-hand side) by adjusting p_k^{*2}. If we set[15]

$$p_k^{*2} = q_{2,k}^{*2} \equiv E_{2,k}^{*2}/4 - m^2\,, \quad \text{where} \quad E_{2,k}^{*2} = E_{2,k}^2 - \mathbf{P}_{2,k}^2\,, \tag{3.34}$$

then we achieve the desired result:

$$\begin{aligned} p_k^{*2} = q_{2,k}^{*2} \quad &\Rightarrow \quad 4\omega_p^{*2} = E_{2,k}^{*2} \quad \Rightarrow \quad (\omega_p + \omega_b)^2 - \mathbf{P}_{2,k}^2 = E_{2,k}^2 - \mathbf{P}_{2,k}^2 \\ &\Rightarrow \quad E_{2,k} = \omega_p + \omega_b \quad \Rightarrow \quad E = \omega_k + \omega_p + \omega_b\,. \end{aligned} \tag{3.35}$$

We note that as $|\mathbf{k}|$ increases, $q_{2,k}^{*2}$ becomes negative, so that enforcing the on-shell condition of Eq. (3.34) requires an extrapolation of $\mathcal{B}_2$ below the two-particle threshold. In other words, even though $\mathbf{k}$ is such that, for the given values of E and $\mathbf{P}$, the other two particles cannot go on shell, we still must include a contribution from the TOPT amplitudes extrapolated below threshold. This feature is common to all three-particle quantization conditions [64]. However, we do not expect the three-particle levels to be sensitive to amplitudes far below threshold. To avoid this region, we introduce a function $H(\mathbf{k})$ that cuts off the sum over $\mathbf{k}$ (and depends implicitly on E and $\mathbf{P}$). At this stage, the details of this function do not matter, aside from four properties: (i) it must equal unity for all values of $\mathbf{k}$ for which an on-shell three-particle state is kinematically allowed, (ii) it must remain unity for a finite distance of $\mathcal{O}(m)$ below threshold, (iii) it must be smooth in $\mathbf{k}$, and (iv) it must vanish for large $|\mathbf{k}|$. The first property ensures that the pole terms that can lead to power-law FV dependence are fully incorporated into the analysis. The second ensures that exponentially suppressed volume terms are suppressed by $\exp(-\delta L)$ with $\delta = \mathcal{O}(m)$. The third property

[15] The definitions of $q_{2,k}^*$ and $E_{2,k}^*$ are the same as in HS1, and the on-shellness conditions also match.

is needed to avoid introducing unwanted power-law dependence, as we will see shortly. The final property truncates the sum over $\mathbf{k}$, which is essential to turn the quantization condition into a practical tool. Functions with these properties can be constructed easily from the example given in HS1. We stress that the quantization condition that we derive is valid for any cutoff function satisfying these properties, up to exponentially suppressed corrections. In other words, we do not lose control of power-law volume dependence when we add the cutoff function by hand.

We now write $\mathcal{B}_2$ in terms of an on-shell part and a residue

$$\mathcal{B}_2(E_{2,k}, \mathbf{P}_{2,k}; \mathbf{a}; \mathbf{p}) = \mathcal{B}_2^{**}(E_{2,k}, \mathbf{P}_{2,k}; \mathbf{a}; q_{2,k}^{*2})_{\ell m} \mathcal{Y}_{\ell m}(\mathbf{p}_k^*) H(\mathbf{k}) + \delta\mathcal{B}_2(E_{2,k}, \mathbf{P}_{2,k}; \mathbf{a}; \mathbf{p}) \,, \quad (3.36)$$

where the residue is

$$\begin{aligned}\delta\mathcal{B}_2(E_{2,k}, \mathbf{P}_{2,k}; \mathbf{a}; \mathbf{p}) = \left[\mathcal{B}_2^{**}(E_{2,k}, \mathbf{P}_{2,k}; \mathbf{a}; p_k^{*2})_{\ell m} - \mathcal{B}_2^{**}(E_{2,k}, \mathbf{P}_{2,k}; \mathbf{a}; q_{2,k}^{*2})_{\ell m}\right] \mathcal{Y}_{\ell m}(\mathbf{p}_k^*) H(\mathbf{k}) \\ + \mathcal{B}_2(E_{2,k}, \mathbf{P}_{2,k}; \mathbf{a}; \mathbf{p})[1 - H(\mathbf{k})] \,. \quad (3.37)\end{aligned}$$

The key point here is that $\delta\mathcal{B}_2$ cancels the pole in the energy denominator in Eq. (3.27). For the first term, the smoothness of $\mathcal{B}_{2;\ell m}^{**}$ implies that

$$\begin{aligned}&\mathcal{B}_2^{**}(E_{2,k}, \mathbf{P}_{2,k}; \mathbf{a}; p_k^{*2})_{\ell m} - \mathcal{B}_2^{**}(E_{2,k}, \mathbf{P}_{2,k}; \mathbf{a}; q_{2,k}^{*2})_{\ell m} \\ &\qquad \propto p_k^{*2} - q_{2,k}^{*2} = -\frac{1}{4}(E - \omega_k + \omega_p + \omega_b)(E - \omega_k - \omega_p - \omega_b) \,,\end{aligned} \quad (3.38)$$

which explicitly cancels the pole. For the second term in $\delta\mathcal{B}_2$, the factor of $1 - H(\mathbf{k})$ vanishes for all choices of $\mathbf{k}$ for which on-shell kinematics are possible, and in a finite neighborhood thereof, so that the pole is avoided. Thus the total summand involving $\delta\mathcal{B}_2$ is finite and smooth, allowing loop sums involving momenta crossing the cut to be converted to integrals, as discussed further below.

Our final step for the left-hand amplitude is to rewrite it in terms of $\mathcal{B}_{2;\ell m}^{*}$, i.e. the angular

components of the on-shell amplitude. Then Eq. (3.36) becomes

$$\mathcal{B}_2(E_{2,k},\mathbf{P}_{2,k};\mathbf{a};\mathbf{p}) = \mathcal{B}_2^*(E_{2,k},\mathbf{P}_{2,k};\mathbf{a};q_{2,k}^*)_{\ell m}\frac{\mathcal{Y}_{\ell m}(\mathbf{p}_k^*)}{q_{2,k}^{*\ell}}H(\mathbf{k}) + \delta\mathcal{B}_2(E_{2,k},\mathbf{P}_{2,k};\mathbf{a};\mathbf{p})\,. \tag{3.39}$$

The construction makes clear that the apparent pole at $q_{2,k}^* = 0$ is canceled by the behavior of $\mathcal{B}_{2;\ell m}^*$ near threshold.

We now make an analogous decomposition of the right-hand $\mathcal{B}_2$. The steps are the same with the roles of $\mathbf{k}$ and $\mathbf{p}$ interchanged. We thus find

$$\mathcal{B}_2(E_{2,p},\mathbf{P}_{2,p};\mathbf{k};\mathbf{r}) = H(\mathbf{p})\frac{\mathcal{Y}_{\ell m}(\mathbf{k}_p^*)}{q_{2,p}^{*\ell}}\mathcal{B}_2^*(E_{2,p},\mathbf{P}_{2,p};q_{2,p}^*;\mathbf{r})_{\ell m} + \mathcal{O}(E-\omega_k-\omega_p-\omega_b)\,. \tag{3.40}$$

Here we have set the left-hand momenta on shell.

We also find it convenient to rewrite the pole in the relativistic form used in Refs. [34, 36, 76]

$$\frac{1}{2\omega_b(E-\omega_k-\omega_p-\omega_b)} = \frac{1}{b^2-m^2}\left[1+\mathcal{O}(E-\omega_k-\omega_p-\omega_b)\right]\,, \tag{3.41}$$

where b here is the four-vector

$$b = (E-\omega_k-\omega_p, \mathbf{P}-\mathbf{k}-\mathbf{p}) = (\omega_b,\mathbf{b}) + (E-\omega_k-\omega_p-\omega_b,\mathbf{0})\,. \tag{3.42}$$

This step is not essential, and we could proceed with the derivation with the form of the pole used in HS1.

Inserting the results from Eqs. (3.39), (3.40), and (3.41) into Eq. (3.27), we find the pole part

$$\mathcal{B}_2^*(E_{2,k},\mathbf{P}_{2,k};\mathbf{a};q_{2,k}^*)_{\ell m}G^b_{k\ell m;p\ell' m'}\mathcal{B}_2^*(E_{2,p},\mathbf{P}_{2,p};q_{2,p}^*;\mathbf{r})_{\ell' m'}\,, \tag{3.43}$$

where the "switch matrix" G^b is[16]

$$G^b_{k\ell m;p\ell' m'} = \frac{\mathcal{Y}_{\ell m}(\mathbf{p}_k^*)}{q_{2,k}^{*\ell}}\frac{H(\mathbf{k})H(\mathbf{p})}{b^2-m^2}\frac{\mathcal{Y}_{\ell' m'}(\mathbf{k}_p^*)}{q_{2,p}^{*\ell'}}\,. \tag{3.44}$$

[16]This is the same as the object G^b appearing in HS1, except that we use the relativistic form of the pole and the Wu boost.

Equation (3.43) has achieved our goal of pulling out a term in which the inner indices are set on shell. Whenever the index set $\{k\ell m\}$ appears instead of, say, $\{ka\}$, this indicates that an on-shell projection has been carried out following the procedure explained above.

To package the final result in a way that generalizes to other choices of X' and X in Eq. (3.25), we reintroduce the factors of $2\omega L^3$ that cancel if $X' = X = \overline{\mathcal{B}}_{2,L}$ but do not cancel in general:[17]

$$\left[\overline{\mathcal{B}}_{2,L}\right]_{ka;k'\ell m} = 2\omega_k L^3 \delta_{kk'} \mathcal{B}_2^*(E_{2,k}, \mathbf{P}_{2,k}; \mathbf{a}; q_{2,k}^*)_{\ell m} \tag{3.45}$$

$$\left[\overline{\mathcal{B}}_{2,L}\right]_{p'\ell'm';pr} = 2\omega_p L^3 \delta_{p'p} \mathcal{B}_2^*(E_{2,p}, \mathbf{P}_{2,p}; q_{2,p}^*; \mathbf{r})_{\ell' m'} \tag{3.46}$$

$$\widetilde{G}_{k\ell m;p\ell'm'} = \frac{1}{2\omega_k L^3} G^b_{k\ell m;p\ell'm'} \frac{1}{2\omega_p L^3} \,. \tag{3.47}$$

Using these matrices we have

$$\left[\overline{\mathcal{B}}_{2,L} D_G \overline{\mathcal{B}}_{2,L}\right]_{ka;pr} = \left[\overline{\mathcal{B}}_{2,L} \left(\widetilde{G} + \delta\widetilde{G}\right) \overline{\mathcal{B}}_{2,L}\right]_{ka;pr} \,. \tag{3.48}$$

where the $\widetilde{G}$ term contains the pole, while $\delta\widetilde{G}$ is simply the sum of all nonsingular contributions. We will not need an explicit form for $\delta\widetilde{G}$. Equation (3.48) gives the result in a convenient, but highly compact, notation. It should always be kept in mind that any object adjacent to a factor of $\widetilde{G}$ is projected on shell. The $\delta\widetilde{G}$ contribution, however, does not include an on-shell projection. The result (3.48) is shown diagrammatically in the upper panel of Fig. 3.6, where the $\delta\widetilde{G}$ term is seen to sew together the two $\mathcal{B}_2$'s into an enlarged, infinite-volume amplitude.

The analysis proceeds similarly if we replace one or both of the $\overline{\mathcal{B}}_{2,L}$'s with one of the

[17] Here $\widetilde{G}$ is related to the matrix G of HS1 by $\widetilde{G}_{k\ell m;p\ell'm'} = (2\omega_k L^3)^{-1} G_{k\ell m;p\ell'm'}$, except that we use the relativistic form of the pole and the Wu boost. In fact, at this stage we could change to using the boost of HS1 (and, if desired, the nonrelativistic form of the pole) in $\widetilde{G}$. This only leads to a change in $\delta\widetilde{G}$. For completeness, we note that our $\widetilde{G}$ differs from the similar quantity of the same name used in Refs. [36, 39, 76]: our version contains an extra factor of $1/L^3$.

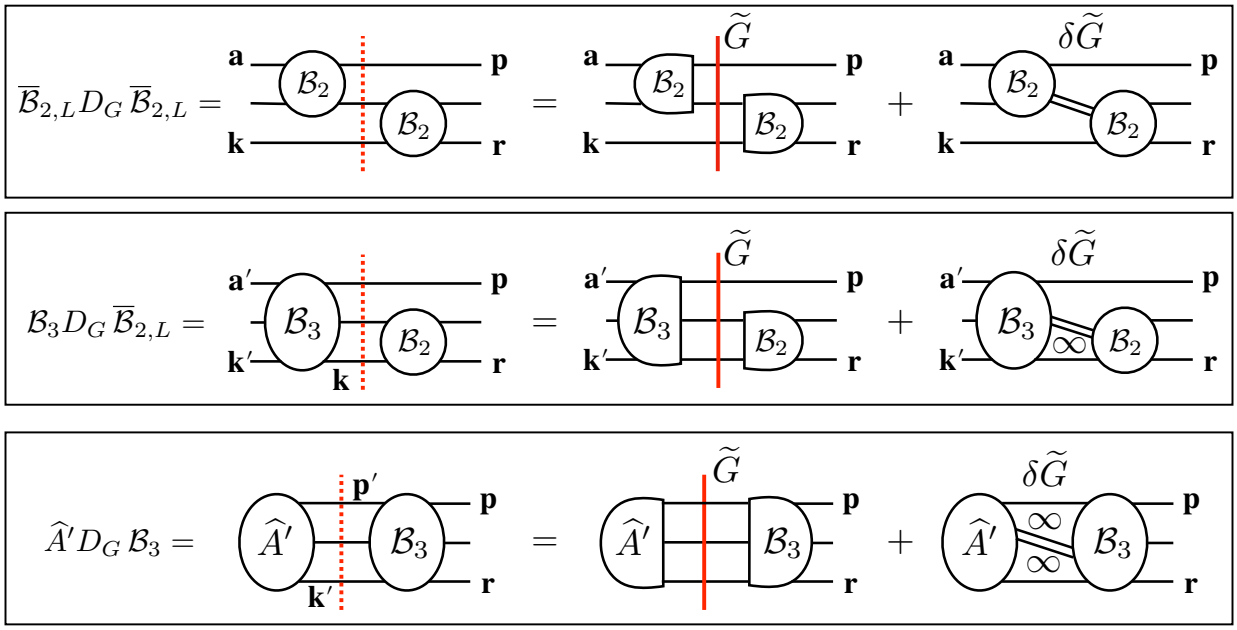

Figure 3.6: Diagrammatic illustration of on-shell projection for G cuts, specifically of the results Eq. (3.48) [upper panel], Eq. (3.49) [middle panel], and Eq. (3.52) with $X' = \widehat{A}'$ and $X = \mathcal{B}_3$ [lower panel]. The relevant cut corresponding to D_G is shown by the dashed (red) vertical line, while the insertion of the matrix $\widetilde{G}$ is shown by the solid (red) vertical line. Rounded ends of kernels are off shell, while straightened ends are on shell. The angled double solid line connecting amplitudes indicates that the pole in the energy denominator has been canceled. A loop containing "∞" is integrated, while other loops are summed.

other TOPT amplitudes. As an example, consider

$$\left[\mathcal{B}_3 D_G \overline{\mathcal{B}}_{2,L}\right]_{k'a';pr} = [\mathcal{B}_3]_{k'a';ka} \, [D_G]_{ka;p'r'} \left[\overline{\mathcal{B}}_{2,L}\right]_{p'r';pr} , \tag{3.49}$$

which is illustrated in the middle panel of Fig. 3.6. For notational convenience we have interchanged the dummy indices $\{ka\}$ and $\{k'a'\}$ compared to earlier. The differences from the analysis above are (i) that $\mathbf{k} \neq \mathbf{k}'$, so that the on-shell projection for $\mathcal{B}_3$ involves a boost determined by the inner momentum (here $\mathbf{k}$); (ii) the $1/(2\omega_k L^3)$ factor in D_G is not canceled; (iii) $\mathbf{k}$ is summed in the final result—with $1/(2\omega_k L^3)$ providing the correct measure factor;

and (iv) in the finite $\delta\widetilde{G}$ term, the sum over $\mathbf{k}$ can be converted to an integral, since the pole has been canceled, and this attaches a $\mathcal{B}_2$ to the $\mathcal{B}_3$ to create an enlarged infinite-volume amplitude. This step relies also on the smoothness of $H(\mathbf{k})$. This last point implies that we should view $\delta\widetilde{G}$ as an operator that acts differently depending on the adjacent kernels, and in particular implies integration over all internal loops that cross the original cut.

To give an explicit expression we need to define the version of $\mathcal{B}_3$ after on-shell projection on the right,

$$[\mathcal{B}_3]_{k'a';k\ell m} \equiv \mathcal{B}_3^*(\mathbf{k}', \mathbf{a}'; \mathbf{k}, a_k^* = q_{2,k}^*)_{\ell m} \frac{\mathcal{Y}_{\ell m}(\mathbf{a}_k^*)}{q_{2,k}^{*\ell}} , \tag{3.50}$$

using which we have

$$\Big[\mathcal{B}_3 D_G \overline{\mathcal{B}}_{2,L}\Big]_{k'a';pr} = \Big[\mathcal{B}_3(\widetilde{G} + \delta\widetilde{G})\overline{\mathcal{B}}_{2,L}\Big]_{k'a';pr} , \tag{3.51}$$

i.e. a result of exactly the same form as when $X' = X = \overline{\mathcal{B}}_{2,L}$.

The other cases follow analogously, and we do not discuss them in detail. Dropping external indices, the general result is simply

$$X' D_G X = X'(\widetilde{G} + \delta\widetilde{G})X . \tag{3.52}$$

The only new feature that enters if both X' and X are symmetric kernels is that both factors of $1/(2\omega L^3)$ are uncanceled, so both internal momenta end up summed (for the $\widetilde{G}$ term) or integrated (for the $\delta\widetilde{G}$ term). This is illustrated for $X' = \widehat{A}'$ and $X = \mathcal{B}_3$ in the lower panel of Fig. 3.6.

F cuts

Next, we wish to derive an analogous result for $X' D_F X$. One option is to split up the on- and off-shell contributions exactly as for D_G; we refer to this as the "$\widetilde{\Sigma}_F$ approach," as the analog to $\widetilde{G}$ that arises is a sum over spatial momenta. Although the $\widetilde{\Sigma}_F$ approach is perfectly valid and well defined, we relegate its details to Appendix A.7, as there is a more

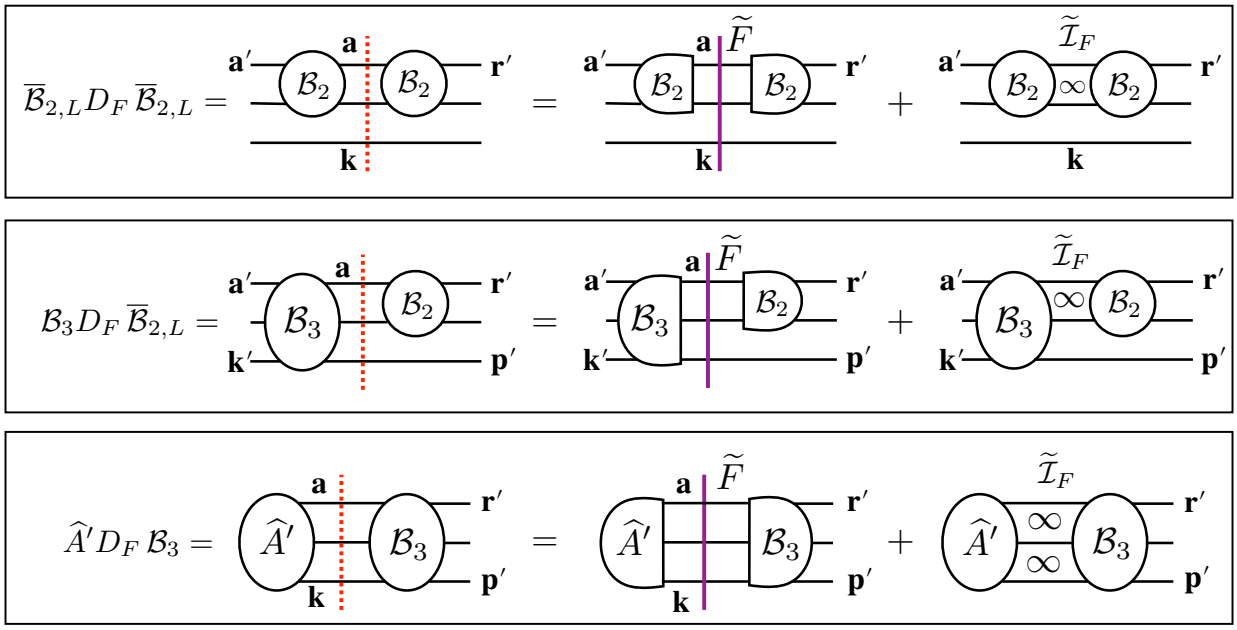

Figure 3.7: Diagrammatic illustrations of on-shell projection for F cuts. Notation as in Fig. 3.6 except that the insertion of the matrix $\widetilde{F}$ is shown by the solid (purple) vertical line. The integral over the momentum $\mathbf{a}$ (the upper loop) requires a pole prescription, for which we use a generalized PV prescription. Momentum labels are matched to the discussion in the text.

standard method—following essentially the same approach as in HS1—that we now discuss. We shall refer to the standard method as the "$\widetilde{F}$ approach," for reasons that will soon be apparent.

The results we obtain are illustrated in Fig. 3.7. As the figures show, an essential difference between the G and F cuts is that, for the latter, at least one of the momenta crossing the cut is part of an internal loop. This feature is exemplified by the explicit expression for $X' = X = \overline{\mathcal{B}}_{2,L}$,

$$\left[\overline{\mathcal{B}}_{2,L} D_F \overline{\mathcal{B}}_{2,L}\right]_{ka';pr'} = \delta_{kp} 2\omega_k L^3 \sum_{\mathbf{a}} \left[\frac{1}{2\omega_a L^3} \mathcal{B}_2(E_{2,k}, \mathbf{P}_{2,k}; \mathbf{a}'; \mathbf{a}) \times \frac{1}{2\omega_{b_{ka}}(E - \omega_k - \omega_a - \omega_{b_{ka}})} \mathcal{B}_2(E_{2,k}, \mathbf{P}_{2,k}; \mathbf{a}; \mathbf{r}') \right], \tag{3.53}$$

which is shown diagrammatically in the upper panel in Fig. 3.7. The $\mathbf{a}$ loop is always present, and, in the $\widetilde{F}$ approach, is treated first. The method is that introduced in Ref. [27] and extended in HS1: one replaces the sum in Eq. (3.53) using the identity $\sum = [\sum - \mathrm{PV}\int] + \mathrm{PV}\int$. Here PV indicates that we are using a generalized principal-value (PV) pole prescription, in the class introduced in Ref. [36]. The sum-integral difference projects the inner momenta of the adjacent amplitudes on shell, as shown by the identity derived in Appendix A of HS1.[18] Using this identity, we find, in our example,

$$\left[\overline{\mathcal{B}}_{2,L} D_F \, \overline{\mathcal{B}}_{2,L}\right]_{ka';pr'} = \left[\overline{\mathcal{B}}_{2,L}\right]_{ka';k'\ell m} \widetilde{F}_{k'\ell m;p'\ell' m'} \left[\overline{\mathcal{B}}_{2,L}\right]_{p'\ell' m';pr'} + \left[\overline{\mathcal{B}}_{2,L} \widetilde{\mathcal{I}}_F \overline{\mathcal{B}}_{2,L}\right]_{ka';pr'} , \quad (3.54)$$

where the partially on-shell amplitudes are defined in Eqs. (3.45) and (3.46), $\widetilde{F}$ is a matrix acting in the on-shell index space[19]

$$\widetilde{F}_{k\ell m;p\ell' m'} \equiv \delta_{kp} H(\mathbf{k}) \left[\frac{1}{L^3} \sum_{\mathbf{a}}^{\mathrm{UV}} - \mathrm{PV} \int_{\mathbf{a}}^{\mathrm{UV}}\right] \frac{\mathcal{Y}_{\ell m}(\mathbf{a}_k^*)}{q_{2,k}^{*\ell}} \frac{L^3 D_{ka}}{2!} \frac{\mathcal{Y}_{\ell' m'}(\mathbf{a}_k^*)}{q_{2,k}^{*\ell'}} , \quad (3.55)$$

with $\int_{\mathbf{a}} \equiv \int d^3a/(2\pi)^3$, and the action of the integral operator $\widetilde{\mathcal{I}}_F$ is

$$\begin{aligned}\left[\overline{\mathcal{B}}_{2,L} \widetilde{\mathcal{I}}_F \overline{\mathcal{B}}_{2,L}\right]_{ka';pr'} \equiv \sum_{\mathbf{k}',\mathbf{p}',\mathbf{r}} \left\{H(\mathbf{k})\, \mathrm{PV} \int_{\mathbf{a}}^{\mathrm{UV}} + [1 - H(\mathbf{k})] \int_{\mathbf{a}}^{\mathrm{UV}}\right\} \Bigg\{ \left[\overline{\mathcal{B}}_{2,L}\right]_{ka';k'a} \\ \times \frac{L^3 D_{k'a} \delta_{k'p'} \delta_{ar}}{2!} \left[\overline{\mathcal{B}}_{2,L}\right]_{p'r;pr'} \Bigg\} .\end{aligned} \quad (3.56)$$

The integral operator ties together the two factors of $\mathcal{B}_2$, as shown in the figure. Note that the overall factor of L^3 cancels that in the $1/(2\omega_a L^3)$ contained in D_{ka}.

One subtle feature of Eqs. (C.9) and (3.56) is the appearance of factors of $H(\mathbf{k})$. As for the G cuts, these are introduced so as to cut off the sum over $\mathbf{k}$. The identity (3.54) is valid

[18] Strictly speaking, the argument given in HS1 must be slightly modified to use the boost introduced above, but the essence is unchanged.

[19] Here $\widetilde{F}$ is related to the matrix F of HS1 by $\widetilde{F}_{k\ell m;p\ell' m'} = (2\omega_k L^3)^{-1} F_{k\ell m;p\ell' m'}$. The fact that we use a different boost in the on-shell projection only changes the sum-integral difference by exponentially suppressed terms. This is true also if the pole in D_{ka} is changed to the relativistic form used for $\widetilde{G}$, and for changes in the UV regulator. Our $\widetilde{F}$ differs from the quantity of the same name used in Refs. [36, 39, 76] by having an additional factor of $1/L^3$.

for any choice of $H(\mathbf{k})$ satisfying the properties enumerated earlier. In particular, the second integral on the right-hand side of Eq. (3.56) originates as a sum over $\mathbf{a}$, but can be converted to an integral because the overall $1 - H(\mathbf{k})$ cancels the pole in D_{ka}.[20]

The results for other choices of X' and X take the same form, and are illustrated in the middle and lower panels of Fig. 3.7. The only new feature occurs when both X' and X are symmetric amplitudes. In this case the sum over $\mathbf{k}$ is not resolved by Kronecker deltas, and remains as an internal loop. Here we can use the result that the PV integral over $\mathbf{a}$ leads to a smooth function of $\mathbf{k}$, despite the pole in the integrand. This is shown for the standard PV prescription in Appendix B of HS1, and holds also for the generalizations of Ref. [36]. Because of this result, and the smoothness of the TOPT amplitudes, the sum over $\mathbf{k}$ in the $\widetilde{\mathcal{I}}_F$ term can be replaced by an integral, as exemplified by the last term in the lower panel in the figure. Thus, as for $\delta\widetilde{G}$, the integral operator $\widetilde{\mathcal{I}}_F$ acts in a manner that depends on the adjacent amplitudes.

In summary, the general result (with matrix indices implicit) is

$$X' D_F \, X = X' \left(\widetilde{F} + \widetilde{\mathcal{I}}_F \right) X \,, \tag{3.57}$$

where any amplitude adjacent to $\widetilde{F}$ is placed on shell with indices $\{k\ell m\}$.

[20] Note also that, despite appearances, the $H(\mathbf{k})$ dependence of the two integrals in Eq. (3.56) *do not cancel*, because they are defined with different pole prescriptions: PV for the first integral, while no prescription is needed for the second (since the pole is avoided). This is equivalent to using the $i\epsilon$ prescription for the second integral.

Application to $C_{3,L}(E,\mathbf{P})$

We can use the results Eqs. (3.52) and (3.57) to rewrite our expression for the three-particle correlator, Eq. (3.24), so as to isolate on-shell contributions,

$$C_{3,L} - C^{(0)}_{3,\infty} = \widehat{A}'\, i(\widetilde{F}+\widetilde{G}+\widetilde{\mathcal{I}}_F+\delta\widetilde{G})\frac{1}{1-i(\overline{\mathcal{B}}_{2,L}+\mathcal{B}_3)i(\widetilde{F}+\widetilde{G}+\widetilde{\mathcal{I}}_F+\delta\widetilde{G}\,)}\widehat{A} \tag{3.58}$$

$$= \delta C_{3,\infty} + \widetilde{A}'^{(u)} i(\widetilde{F}+\widetilde{G}\,)\frac{1}{1-i\widetilde{\mathcal{K}}^{(u,u)}_{\mathrm{df},23,L} i(\widetilde{F}+\widetilde{G}\,)}\widetilde{A}^{(u)}\,, \tag{3.59}$$

where

$$i\widetilde{\mathcal{K}}^{(u,u)}_{\mathrm{df},23,L} \equiv \frac{1}{1-i(\overline{\mathcal{B}}_{2,L}+\mathcal{B}_3)i(\widetilde{\mathcal{I}}_F+\delta\widetilde{G}\,)} i(\overline{\mathcal{B}}_{2,L}+\mathcal{B}_3)\,, \tag{3.60}$$

$$\widetilde{A}'^{(u)} \equiv \widehat{A}'\frac{1}{1-i(\widetilde{\mathcal{I}}_F+\delta\widetilde{G})i(\overline{\mathcal{B}}_{2,L}+\mathcal{B}_3)}\,, \tag{3.61}$$

$$\widetilde{A}^{(u)} \equiv \frac{1}{1-i(\overline{\mathcal{B}}_{2,L}+\mathcal{B}_3)i(\widetilde{\mathcal{I}}_F+\delta\widetilde{G})}\widehat{A}\,, \tag{3.62}$$

$$\delta C_{3,\infty} \equiv \widehat{A}'\, i(\widetilde{\mathcal{I}}_F+\delta\widetilde{G})\frac{1}{1-i(\overline{\mathcal{B}}_{2,L}+\mathcal{B}_3)i(\widetilde{\mathcal{I}}_F+\delta\widetilde{G})}\widehat{A}\,. \tag{3.63}$$

Since $\widetilde{A}'^{(u)}$, $\widetilde{\mathcal{K}}^{(u,u)}_{\mathrm{df},23,L}$, and $\widetilde{A}^{(u)}$ all appear adjacent to $\widetilde{F}+\widetilde{G}$, they are all projected into the on-shell $\{k\ell m\}$ index space. We will refer them as "on-shell kernels."

Various aspects of these results deserve further explanation. The first is our use of tildes. We have added these in order to distinguish the kernels from quantities in HS1 that have similar names, but different definitions.

The second new feature is the appearance of superscripts (u) and (u,u). This notation, borrowed from HS1, indicates asymmetric quantities.[21] The asymmetry here arises from the presence of the asymmetric amplitude $\overline{\mathcal{B}}_{2,L}$. When we expand out the geometric series in Eqs. (3.60)-(3.62), the external amplitude can either be a $\overline{\mathcal{B}}_{2,L}$ or a symmetric amplitude.

[21] An important caveat, however, is that the precise nature of the asymmetry here differs from that in HS1. We discuss this further below.

For example, we can rewrite Eq. (3.62) as

$$\widetilde{A}^{(u)} = \widehat{A} + i(\overline{\mathcal{B}}_{2,L} + \mathcal{B}_3)i(\widetilde{\mathcal{I}}_F + \delta\widetilde{G})\frac{1}{1 - i(\overline{\mathcal{B}}_{2,L} + \mathcal{B}_3)i(\widetilde{\mathcal{I}}_F + \delta\widetilde{G})}\widehat{A}\,. \tag{3.64}$$

The presence of the $\overline{\mathcal{B}}_{2,L}$ in the second term on the right-hand side implies that this is an asymmetric quantity, since $\mathbf{k}$ is always associated with the spectator momentum when connecting to $\overline{\mathcal{B}}_{2,L}$.

The third new aspect is the subscript "df, 23" on $\widetilde{\mathcal{K}}^{(u,u)}_{\mathrm{df},23,L}$, as well as the use of the name $\mathcal{K}$. To explain these features, we expand the geometric series in Eq. (3.60), leading to the contributions shown diagrammatically in Fig. 3.8. These are exactly the set of diagrams that give rise, in TOPT, to the $2 \to 2$ amplitude (with a spectator) combined with the $3 \to 3$ amplitude, except that we have replaced the relevant cuts with integral operators. This is similar to what one does when defining a K matrix, namely removing the imaginary parts that arise from unitary cuts. In particular, since all the integrals that appear either use a PV prescription or avoid the pole, $\widetilde{\mathcal{K}}^{(u,u)}_{\mathrm{df},23,L}$ is real. Because of this similarity, we refer to it as a K matrix, and, indeed, the connection to standard K matrices can, in part, be made more precise, as we show below. We use the subscript "23" to indicate that it contains amplitudes for both two- and three-particle scattering. Finally, "df" stands for "divergence free," which is to say that, by construction, it contains no singularities due to three-particle cuts. This use of "df" is taken over from HS1.

The final issue concerns the volume dependence of the kernels. We find that $\widetilde{A}'^{(u)}$, $\widetilde{A}^{(u)}$, and $\delta C_{3,\infty}$ are infinite-volume quantities, and that $\widetilde{\mathcal{K}}^{(u,u)}_{\mathrm{df},23,L}$ can be simply related to infinite-volume quantities, both results holding up to exponentially suppressed corrections. These results, derived in the next subsection, will allow us to make all L dependence explicit.

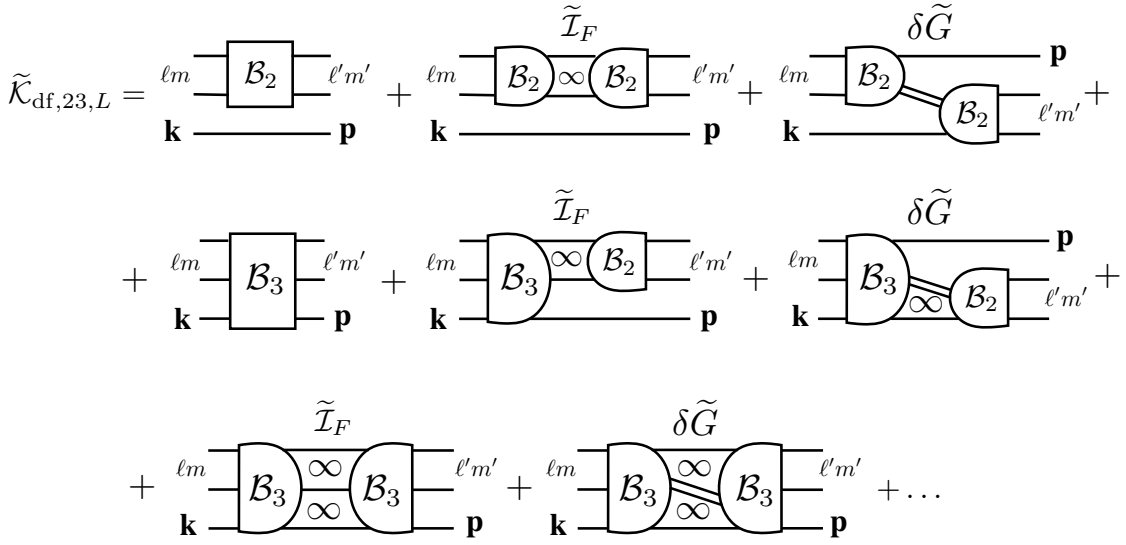

Figure 3.8: Diagrams contributing to $[\widetilde{\mathcal{K}}^{(u,u)}_{\mathrm{df},23,L}]_{k\ell m;p\ell' m'}$. Notation as in Figs. 3.6 and 3.7. Factors of i are implicit.

Volume (in)dependence of kernels

The most complicated of the kernels is $\widetilde{\mathcal{K}}^{(u,u)}_{\mathrm{df},23,L}$, and we address this first. As is clear from Fig. 3.8, the $2 \to 2$ part of $\widetilde{\mathcal{K}}^{(u,u)}_{\mathrm{df},23,L}$ is given by the geometric series

$$i\overline{\mathcal{K}}_{2,L} \equiv i\overline{\mathcal{B}}_{2,L} \frac{1}{1 - i\widetilde{\mathcal{I}}_F i\overline{\mathcal{B}}_{2,L}} = i\overline{\mathcal{B}}_{2,L} + i\overline{\mathcal{B}}_{2,L}\, i\widetilde{\mathcal{I}}_F\, i\overline{\mathcal{B}}_{2,L} + \cdots . \tag{3.65}$$

The off-shell version of this quantity, i.e. with indices $\{ka, pr\}$, will be a key building block in the final expression. The factors of $2\omega_k L^3$ cancel in pairs, leaving a single overall factor of this type, allowing us to write

$$\left[\overline{\mathcal{K}}_{2,L}\right]_{ka;pr} = 2\omega_k L^3 \left[\mathcal{K}_2\right]_{ka;pr} , \tag{3.66}$$

$$\left[\mathcal{K}_2\right]_{ka;pr} \equiv \delta_{kp} \mathcal{K}_2(E_{2,k}, \mathbf{P}_{2,k}; \mathbf{a}; \mathbf{r}) , \tag{3.67}$$

where $\mathcal{K}_2(E_2, \mathbf{P}_2; \mathbf{a}; \mathbf{r})$ is the infinite-volume $2 \to 2$ quantity obtained by sewing together any number of $\mathcal{B}_2$ kernels with the two-particle version of $\widetilde{\mathcal{I}}_F$. As the name suggests, it is related to a two-particle K matrix. Indeed, we show in Appendix A.2 that the on-shell restriction is given by

$$\left[\overline{\mathcal{K}}_{2,L}\right]_{k\ell m;p\ell' m'} = 2\omega_k L^3 \left[\mathcal{K}_2\right]_{k\ell m;p\ell' m'} , \tag{3.68}$$

$$\left[\mathcal{K}_2\right]_{k\ell m;p\ell' m'} = \delta_{kp}\delta_{\ell\ell'}\delta_{mm'}\mathcal{K}_2^{(\ell)}(q_{2,k}^*) , \tag{3.69}$$

where $\mathcal{K}_2^{(\ell)}$ is the ℓth partial-wave amplitude in the two-particle CMF, with $q_{2,k}^*$ the magnitude of the momentum of each particle. $\mathcal{K}_2^{(\ell)}$ has a known relation to the corresponding partial wave of the scattering amplitude, $\mathcal{M}_2^{(\ell)}$, given in Eq. (A.5). $\mathcal{K}_2$ becomes the standard K matrix if we use the standard PV scheme and set $H(\mathbf{k}) = 1$ for all $\mathbf{k}$.

Returning to $\widetilde{\mathcal{K}}_{\mathrm{df},23,L}^{(u,u)}$, we now reorder the terms in the geometric series (3.60) by first summing subsets of diagrams involving sequences of $\overline{\mathcal{B}}_{2,L}$'s and $\widetilde{\mathcal{I}}_F$'s into $\overline{\mathcal{K}}_{2,L}$'s. This is illustrated in the first panel of Fig. 3.9. We next sum sequences of the resulting $\overline{\mathcal{K}}_{2,L}$'s connected by factors of $\delta\widetilde{G}$, leading to the $3 \to 3$ quantity

$$i\widetilde{\mathcal{D}}_{3,L}^{(u,u)} \equiv i\overline{\mathcal{K}}_{2,L} i\delta\widetilde{G} i\overline{\mathcal{K}}_{2,L} \frac{1}{1 - i\delta\widetilde{G} i\overline{\mathcal{K}}_{2,L}} , \tag{3.70}$$

as shown in the lower panel of Fig. 3.9. Factors of $2\omega L^3$ cancel except for an inverse such factor for every internal loop, which would be absorbed if we could convert each loop sum into an integral. This requires, however, that the summand is smooth. Here we face a new issue: while the (double-line) connectors between adjacent $\mathcal{K}_2$'s are nonsingular, $\mathcal{K}_2$ itself can have singularities as a function of the loop momentum. For example, in the second contribution to $\widetilde{\mathcal{D}}_{3,L}^{(u,u)}$ shown in the figure, the four-momentum $(E_{2,a'}, \mathbf{P}_{2,a'})$ passing through the lower $\mathcal{K}_2$ clearly depends on the loop momentum $\mathbf{a}'$. We know that the on-shell $\mathcal{K}_2$ has poles for real momenta whenever there is a nearby narrow resonance, and, following the arguments of Ref. [35], we expect this to extend to the off-shell K matrix that enters here. There can also

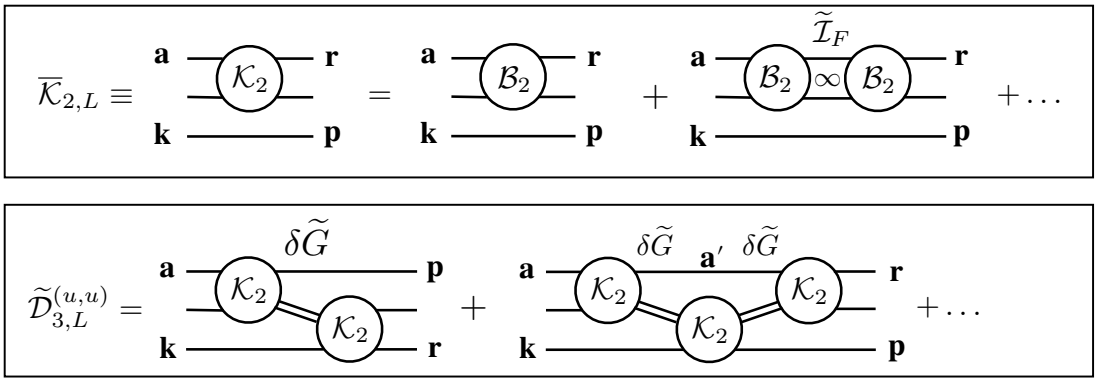

Figure 3.9: Diagrams contributing to $\overline{\mathcal{K}}_{2,L}$ and $\mathcal{D}_{3,L}^{(u,u)}$. Notation as in Figs. 3.6 and 3.7. Factors of i are implicit.

be subthreshold poles in $\mathcal{K}_2$, given our particular definition [39]. Thus there is, in general, a barrier to converting the sum into an integral, and, for this reason, the derivation of HS1 works only assuming the absence of singularities in $\mathcal{K}_2$. However, it has subsequently been understood that by generalizing the definition of the PV prescription, one can define a class of two-particle K matrices, and that by adjusting the parameters of the prescription, one can find definitions that are nonsingular for any given physical scattering amplitude [36]. We assume henceforth that such a prescription has been used, and thus that $\widetilde{\mathcal{D}}_{3,L}^{(u,u)}$ is an infinite-volume quantity.

To combine these ingredients we use algebraic manipulations that recur frequently in this

work, and which we derive in Appendix A.3. These lead to

$$i\widetilde{\mathcal{K}}_{\mathrm{df},23,L}^{(u,u)} = i\overline{\mathcal{K}}_{2,L} + i\widetilde{\mathcal{K}}_{\mathrm{df},3}^{(u,u)}\,, \tag{3.71}$$

$$\begin{aligned} i\widetilde{\mathcal{K}}_{\mathrm{df},3}^{(u,u)} \equiv{}& i\widetilde{\mathcal{D}}_{3,L}^{(u,u)} + \left(1 + i\widetilde{\mathcal{D}}_{23,L}^{(u,u)} i\widetilde{\mathcal{I}}_{FG}\right) \\ &\times i\mathcal{B}_3 \frac{1}{1 - \left(i\widetilde{\mathcal{I}}_{FG} + i\widetilde{\mathcal{I}}_{FG} i\widetilde{\mathcal{D}}_{23,L}^{(u,u)} i\widetilde{\mathcal{I}}_{FG}\right) i\mathcal{B}_3} \left(1 + i\widetilde{\mathcal{I}}_{FG} i\widetilde{\mathcal{D}}_{23,L}^{(u,u)}\right)\,, \end{aligned} \tag{3.72}$$

$$\widetilde{\mathcal{I}}_{FG} \equiv \widetilde{\mathcal{I}}_F + \delta\widetilde{G}\,, \tag{3.73}$$

$$i\widetilde{\mathcal{D}}_{23,L}^{(u,u)} \equiv i\overline{\mathcal{K}}_{2,L} + i\widetilde{\mathcal{D}}_{3,L}^{(u,u)} = i\overline{\mathcal{K}}_{2,L} \frac{1}{1 - i\delta\widetilde{G} i\overline{\mathcal{K}}_{2,L}}\,. \tag{3.74}$$

In $\widetilde{\mathcal{K}}_{\mathrm{df},3}^{(u,u)}$, there is an additional loop sum associated with each factor of $\widetilde{\mathcal{I}}_{FG}$ adjacent to a $\widetilde{\mathcal{D}}_{23,L}^{(u,u)}$, with the summand including a factor of $\mathcal{K}_2$. Using our generalized PV prescription, all such sums can be converted to integrals, and this absorbs all remaining factors of $2\omega L^3$. Thus $\widetilde{\mathcal{K}}_{\mathrm{df},3}^{(u,u)}$ is an infinite-volume quantity.

Using similar expansions for $\widetilde{A}^{\prime(u)}$, $\widetilde{A}^{(u)}$, and $\delta C_{3,\infty}$, we find that the factors of L^3 in $\overline{\mathcal{B}}_{2,L}$, $\widetilde{\mathcal{I}}_F$, and $\delta\widetilde{G}$ either cancel or can be used to convert sums into integrals, again assuming a PV prescription such that $\mathcal{K}_2$ is smooth. Thus these three kernels are also infinite-volume quantities.

Summary

We close this subsection by taking stock of what has been achieved. We started from the closed-form expression for the three-particle correlator, Eq. (3.24), which is composed of infinite-volume amplitudes, but has the disadvantage that these amplitudes are off shell. After some technical effort, which involved generalizing results from HS1 so that they applied to TOPT amplitudes, we obtained two simple equations, (3.52) and (3.57), that allow the correlator to be expressed in terms of on-shell kernels, as shown explicitly in Eq. (3.59). In a final step, we determined the volume (in)dependence of these kernels. These steps lead to

the following result for the correlation function,

$$C_{3,L}(E,\mathbf{P}) = \widetilde{C}_{3,\infty}(E,\mathbf{P}) + \widetilde{A}'^{(u)} i(\widetilde{F}+\widetilde{G}) \frac{1}{1 - i\left(2\omega L^3 \mathcal{K}_2 + \widetilde{\mathcal{K}}_{\mathrm{df},3}^{(u,u)}\right) i(\widetilde{F}+\widetilde{G})} \widetilde{A}^{(u)} \,, \tag{3.75}$$

where contributions with no L dependence are collected into[22]

$$\widetilde{C}_{3,\infty} \equiv C_{3,\infty}^{(0)} + \delta C_{3,\infty} \,, \tag{3.76}$$

and we have introduced the diagonal matrix

$$\left[2\omega L^3\right]_{k\ell m;p\ell' m'} = \delta_{kp}\delta_{\ell\ell'}\delta_{mm'}\, 2\omega_k L^3 \,. \tag{3.77}$$

All L dependence is now explicit, entering through the quantities $\widetilde{F}$, $\widetilde{G}$, and $2\omega L^3$.

Our result can be compared to Eq. (250) of HS1, rewritten to match our notation:

$$C_{3,L} = C_{3,\infty} + A' i F_3 \frac{1}{1 - i\mathcal{K}_{\mathrm{df},3} i F_3} A \,, \tag{3.78}$$

$$F_3 = \widetilde{F}\left[\frac{1}{3} - \frac{1}{1/(2\omega L^3 \mathcal{K}_2) + \widetilde{F} + \widetilde{G}}\,\widetilde{F}\right] . \tag{3.79}$$

This shows the trade-off that we have made: by using an asymmetric form of the three-particle K matrix, our final expression is simpler, containing only the combination $\widetilde{F}+\widetilde{G}$ and no factors of 1/3. Another gain is that we have explicit expressions for all quantities in terms of the underlying TOPT amplitudes, in contrast to HS1, where the definitions of the kernels are constructive and not explicit.

3.2.4 New form of the quantization condition

To make contact with the FV energy spectrum of the theory, we exploit the fact that $C_{3,L}(E,\mathbf{P})$ has a simple pole whenever E lies in the FV spectrum. Since $\widetilde{C}_{3,\infty}, \widetilde{A}'^{(u)}, \widetilde{A}^{(u)}$ are all smooth infinite-volume quantities, any singularity in $C_{3,L}$ must arise from the quan-

[22] Our notation (with the subscript ∞) is slightly misleading because $\widetilde{C}_{3,\infty}$ is not the complete infinite-volume limit of $C_{3,L}$, since the other term on the right-hand side of Eq. (3.75), which contains all the volume dependence, has a nonvanishing infinite-volume limit.

tity lying between $\widetilde{A}'^{(u)}$ and $\widetilde{A}^{(u)}$ in Eq. (3.75). This quantity is a matrix in the $\{k\ell m\}$ index space, and must have a diverging eigenvalue for $C_{3,L}$ to have a pole. Equivalently, the determinant of its inverse should vanish,

$$\det\left[\widetilde{F}+\widetilde{G}\right]^{-1}\det\left[1-i\left(2\omega L^3\mathcal{K}_2+\widetilde{\mathcal{K}}_{\mathrm{df},3}^{(u,u)}\right)i(\widetilde{F}+\widetilde{G})\right]=0\,. \tag{3.80}$$

The energies where $\det[\widetilde{F}+\widetilde{G}]^{-1}=0$ are the free three-particle energies where $E=\omega_k+\omega_a+\omega_{b_{ka}}$ for some choice of FV momenta $\mathbf{k},\mathbf{a}\in\frac{2\pi}{L}\mathbb{Z}^3$. For general $\mathcal{K}_2$ and $\widetilde{\mathcal{K}}_{\mathrm{df},3}^{(u,u)}$, we expect that the product of the two determinants will not vanish at these energies, because the second determinant will diverge.[23] Physically this corresponds to the fact that a general interaction will shift all FV energies from their free values. We therefore conclude that for a given $\mathbf{P}$, an energy E can only be in the finite-volume spectrum of the interacting theory if

$$\det\left[1+\left(2\omega L^3\mathcal{K}_2+\widetilde{\mathcal{K}}_{\mathrm{df},3}^{(u,u)}\right)(\widetilde{F}+\widetilde{G})\right]=0\,. \tag{3.81}$$

This is our alternate form of the three-particle quantization condition.

This result has a superficially similar form to that from HS1, which follows from Eq. (3.78),

$$\det\left[1+\mathcal{K}_{\mathrm{df},3}F_3\right]=0\,, \tag{3.82}$$

but many of the details are different. For example, in Eq. (3.81), the infinite-volume K matrices appear together and separate from the FV quantities $\widetilde{F}$ and $\widetilde{G}$, whereas F_3 in Eq. (3.82) is a relatively complicated function of $\mathcal{K}_2$, $\widetilde{F}$, and $\widetilde{G}$. We return to the relation between the two approaches in Sec. 3.4.

3.3 TOPT expression for $\mathcal{M}_{3,L}$

In order to understand the relation between quantization conditions, we need to first extend the developments of the previous section from the correlator $C_{3,L}$ to the finite-volume $3\to3$

[23] As is well known from numerical investigations, if one truncates the partial-wave expansions of $\mathcal{K}_2$ and $\widetilde{\mathcal{K}}_{\mathrm{df},3}^{(u,u)}$, then there will be solutions to the quantization condition at free energies [36, 39, 76].

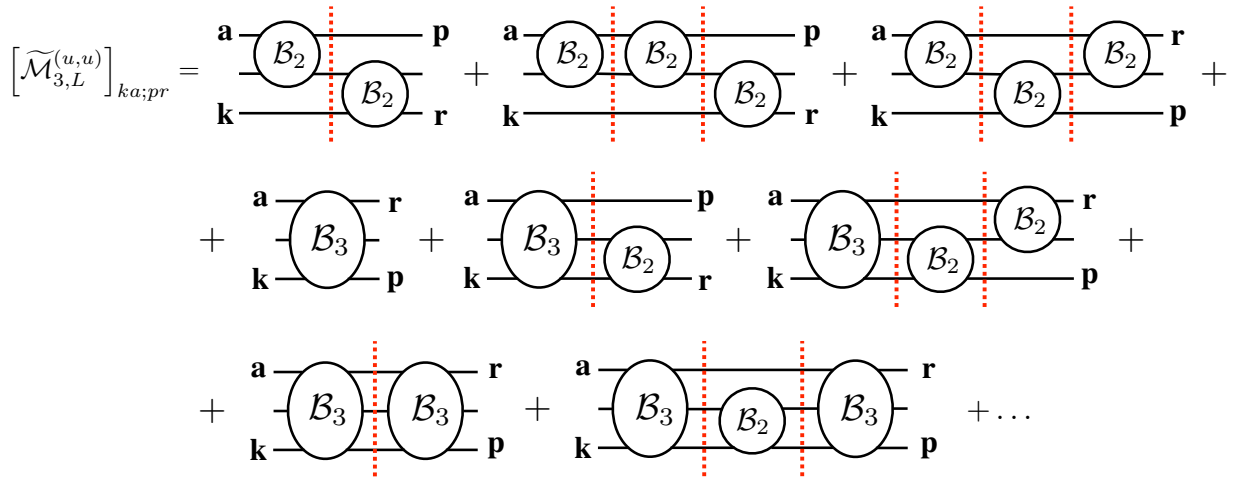

Figure 3.10: Diagrams contributing to $\mathcal{M}_{3,L}^{(u,u)}$ in TOPT. Notation as in Fig. 3.1. The asymmetric feature of this amplitude is that the momenta $\mathbf{k}$ and $\mathbf{p}$ are always assigned to a spectator line, if one is present.

amplitude $\mathcal{M}_{3,L}$. This extension also allows us to determine the infinite-volume relation between our asymmetric K matrix $\widetilde{\mathcal{K}}_{\text{df},3}^{(u,u)}$ and the full $3 \to 3$ amplitude $\mathcal{M}_3$. This latter relation is somewhat off the main line of development of this paper, so we relegate it to Appendix A.5.

$\mathcal{M}_{3,L}$ is defined as the amputated, connected, $3 \to 3$ finite-volume amplitude. It is in general off shell, and thus a matrix in $\{ka\}$ space. It is simpler to begin by considering an asymmetric version of the amplitude, $\widetilde{\mathcal{M}}_{3,L}^{(u,u)}$, defined so that, if there is an external factor of $\overline{\mathcal{B}}_{2,L}$, the spectator propagator is always labeled with one of the external momenta (typically called $\mathbf{k}$ or $\mathbf{p}$). This definition is illustrated in Fig. 3.10.[24] As we have seen several times above, results are simplified if we combine the asymmetric three-particle amplitude with the corresponding two-particle quantity, here $\overline{\mathcal{M}}_{2,L}$. (This is defined in Eq. (A.1), and is

[24]We include a tilde on $\widetilde{\mathcal{M}}_{3,L}^{(u,u)}$ since it is different from the similar quantity $\mathcal{M}_{3,L}^{(u,u)}$ defined in HS2, with the latter having an asymmetry based on the Feynman skeleton expansion. We stress, however, that the symmetrized version $\mathcal{M}_{3,L}$ is the same as in HS2 (when evaluated on shell).

simply $\mathcal{M}_{2,L}$ packaged with an inverse spectator propagator.) The TOPT result for this combination is a geometric series,

$$i\left(\overline{\mathcal{M}}_{2,L}+\widetilde{\mathcal{M}}^{(u,u)}_{3,L}\right)=\frac{1}{1-i(\overline{\mathcal{B}}_{2,L}+\mathcal{B}_3)i(D_F+D_G)}i(\overline{\mathcal{B}}_{2,L}+\mathcal{B}_3)\,. \tag{3.83}$$

To obtain the full $\mathcal{M}_{3,L}$ we symmetrize by summing over the different attachments of the external momenta

$$[\mathcal{M}_{3,L}]_{ka;k'a'}=\sum_{x\in P}\sum_{x'\in P'}\left[\widetilde{\mathcal{M}}^{(u,u)}_{3,L}\right]_{x;x'}\,,\qquad P=\{ka,ab,bk\}\,,\quad P'=\{k'a',a'b',b'k'\}\,. \tag{3.84}$$

Only three terms are needed on both sides (rather than the 3! one might have expected) because $\mathcal{B}_2$ is symmetric under $a\leftrightarrow b$ interchange. No overall factor of $1/9$ is needed because this factor is built into $\mathcal{B}_3$—see the discussion above Eq. (3.8).

The remaining steps are essentially a repeat of those we used for $C_{3,L}$. We find that Eq. (3.59) is replaced by[25]

$$i\left(\overline{\mathcal{M}}_{2,L}+\widetilde{\mathcal{M}}^{(u,u)}_{3,L}\right)=i\widetilde{\mathcal{K}}^{(u,u)}_{\mathrm{df},23,L}\frac{1}{1-i(\widetilde{F}+\widetilde{G})\,i\widetilde{\mathcal{K}}^{(u,u)}_{\mathrm{df},23,L}}\,, \tag{3.85}$$

Using the algebraic result (A.22), as well as the decomposition of $\widetilde{\mathcal{K}}^{(u,u)}_{\mathrm{df},23,L}$, Eq. (3.71), and the result for $\overline{\mathcal{M}}_{2,L}$, Eq. (A.3), we can extract the expression for $\widetilde{\mathcal{M}}^{(u,u)}_{3,L}$:

$$i\widetilde{\mathcal{M}}^{(u,u)}_{3,L}=i\mathcal{D}^{(u,u)}_{L}+i\widetilde{\mathcal{M}}^{(u,u)}_{\mathrm{df},3,L} \tag{3.86}$$

where

$$i\mathcal{D}^{(u,u)}_{L}\equiv i\overline{\mathcal{M}}_{2,L}i\widetilde{G}i\overline{\mathcal{M}}_{2,L}\frac{1}{1-i\widetilde{G}i\overline{\mathcal{M}}_{2,L}}\,, \tag{3.87}$$

$$i\widetilde{\mathcal{M}}^{(u,u)}_{\mathrm{df},3,L}\equiv\left[1+i\mathcal{D}^{(u,u)}_{23,L}i(\widetilde{F}+\widetilde{G})\right]i\widetilde{\mathcal{T}}^{(u,u)}_{L}\left[1+i(\widetilde{F}+\widetilde{G})i\mathcal{D}^{(u,u)}_{23,L}\right]\,, \tag{3.88}$$

[25]Strictly speaking, this way of writing the result only holds if all quantities are on shell, so that all matrices are square. Indeed, we have only considered above the on-shell form of $\widetilde{\mathcal{K}}^{(u,u)}_{\mathrm{df},23,L}$. However, its definition, given in Eqs. (3.71) and (3.72), can be extended off shell. The same is true for the result here, if one expands out the geometric series and evaluates it term by term, and also for Eq. (3.86). These extensions are convenient, but not essential for the following discussion.

with

$$i\widetilde{\mathcal{T}}_L^{(u,u)} \equiv i\widetilde{\mathcal{K}}_{\mathrm{df},3}^{(u,u)} \frac{1}{1-\left[1+i(\widetilde{F}+\widetilde{G})i\mathcal{D}_{23,L}^{(u,u)}\right] i(\widetilde{F}+\widetilde{G})i\widetilde{\mathcal{K}}_{\mathrm{df},3}^{(u,u)}}\,, \tag{3.89}$$

$$i\mathcal{D}_{23,L}^{(u,u)} \equiv i\overline{\mathcal{M}}_{2,L} + i\mathcal{D}_L^{(u,u)} = i\overline{\mathcal{M}}_{2,L}\frac{1}{1-i\widetilde{G}i\overline{\mathcal{M}}_{2,L}}\,. \tag{3.90}$$

Here $\mathcal{D}_L^{(u,u)}$ is the same as the quantity of the same name appearing in HS2, since the asymmetry arises from the external $\overline{\mathcal{M}}_{2,L}$, which is the same in both approaches.[26] These results can also be expressed in terms of $\overline{\mathcal{K}}_{2,L}$ instead of $\overline{\mathcal{M}}_{2,L}$,

$$i\widetilde{\mathcal{M}}_{\mathrm{df},3,L}^{(u,u)} = \frac{1}{1-i\overline{\mathcal{K}}_{2,L}i(\widetilde{F}+\widetilde{G})}i\widetilde{\mathcal{K}}_{\mathrm{df},3}^{(u,u)}\frac{1}{1-i(\widetilde{F}+\widetilde{G})\frac{1}{1-i\overline{\mathcal{K}}_{2,L}i(\widetilde{F}+\widetilde{G})}i\widetilde{\mathcal{K}}_{\mathrm{df},3}^{(u,u)}}\frac{1}{1-i(\widetilde{F}+\widetilde{G})i\overline{\mathcal{K}}_{2,L}}\,, \tag{3.91}$$

$$i\mathcal{D}_{23,L}^{(u,u)} = \frac{1}{1-i\overline{\mathcal{K}}_{2,L}i(\widetilde{F}+\widetilde{G})}i\overline{\mathcal{K}}_{2,L}\,. \tag{3.92}$$

These forms are used in our companion paper [45].

The results (3.86)-(3.90) make all volume dependence of $\widetilde{\mathcal{M}}_{3,L}^{(u,u)}$ explicit: it enters through $\widetilde{F}$, $\widetilde{G}$, and $\overline{\mathcal{M}}_{2,L}$. We also note that this result holds both for the off-shell amplitude and its on-shell limit.

We end this subsection with a side remark. As was pointed out in HS2, the quantization condition can be obtained from the off-shell $\widetilde{\mathcal{M}}_{3,L}^{(u,u)}$ instead of $C_{3,L}$, since the former is an (amputated) three-particle correlator. This is made particularly clear by the fact that, by comparing Eqs. (3.24) and (3.83), we can explicitly relate the two quantities:

$$C_{3,L} - C_{3,\infty}^{(0)} = \widehat{A}'i(D_F+D_G)\widehat{A} + \widehat{A}'i(D_F+D_G)i\left(\overline{\mathcal{M}}_{2,L} + \widetilde{\mathcal{M}}_{3,L}^{(u,u)}\right)i(D_F+D_G)\widehat{A}\,. \tag{3.93}$$

[26] This equality holds only on shell, which is all that we require in the following subsection.

3.4 Relation to quantization condition of HS1

In this section we show that our new quantization condition, Eq. (3.81), can be rewritten in the HS1 form of Eq. (3.82), and that the two approaches therefore lead to equivalent results. We refer to this transformation as the "symmetrization" of the quantization condition, since the HS1 form is written in terms of a symmetric three-particle K matrix. As a side benefit, we obtain the algebraic relation between our asymmetric amplitude $\widetilde{\mathcal{K}}_{\mathrm{df},3}^{(u,u)}$ and the symmetric quantity of HS1, $\mathcal{K}_{\mathrm{df},3}$.

3.4.1 Recap of result for $\mathcal{M}_{3,L}^{(u,u)}$ from HS2

The connection to the HS1 QC is provided by studying the result for $\mathcal{M}_{3,L}^{(u,u)}$, the asymmetric finite-volume three-particle amplitude introduced in HS2. This is defined as for our $\widetilde{\mathcal{M}}_{3,L}^{(u,u)}$, except that its asymmetry is based on the skeleton expansion in terms of 2PIs and 3PIs Bethe-Salpeter (B-S) kernels built from Feynman diagrams. Specifically, if the external legs connect to a 2PIs B-S kernel, then the spectator propagator associated with that kernel is connected to the spectator momentum of $\mathcal{M}_{3,L}^{(u,u)}$. This is the analog of our definition of $\widetilde{\mathcal{M}}_{3,L}^{(u,u)}$ (see Fig. 3.10) except that we use an expansion in terms of TOPT amplitudes, and for us $\mathcal{B}_2$ plays the role of the 2PIs B-S kernel. Since $\mathcal{B}_2$ contains only a subset of the time orderings that contribute to the 2PIs B-S kernel, more contributions are symmetrized in $\widetilde{\mathcal{M}}_{3,L}^{(u,u)}$ than in $\mathcal{M}_{3,L}^{(u,u)}$. We stress, however, that, after complete symmetrization, both objects lead to the same amplitude, $\mathcal{M}_{3,L}$. This is an example of the fact that there are many different ways to define asymmetric amplitudes, all of which symmetrize to the same quantity.

The result for $\mathcal{M}_{3,L}^{(u,u)}$ is given in Eq. (67) of HS2. Converting the expressions to our

notation, we have

$$i\mathcal{M}_{3,L}^{(u,u)} = i\mathcal{D}_{L}^{(u,u)} + \Big(\mathcal{L}_{L}^{(u)}\Big)\Big(i\mathcal{K}_{\rm df,3}\Big)\frac{1}{1-\Big(iF_3\Big)\Big(i\mathcal{K}_{\rm df,3}\Big)}\Big(\mathcal{R}_{L}^{(u)}\Big)\,, \tag{3.94}$$

where

$$\Big(\mathcal{L}_{L}^{(u)}\Big) = \Big(1\ 0\Big) + i\mathcal{D}_{23,L}^{(u,u)} i\widetilde{F}\Big(1\ 1\Big)\,, \tag{3.95}$$

$$\Big(i\mathcal{K}_{\rm df,3}\Big) = \begin{pmatrix} i\mathcal{K}_{\rm df,3}^{(u,u)} & i\mathcal{K}_{\rm df,3}^{(u,s+\tilde{s})} \\ i\mathcal{K}_{\rm df,3}^{(s+\tilde{s},u)} & i\mathcal{K}_{\rm df,3}^{(s+\tilde{s},s+\tilde{s})} \end{pmatrix}\,, \tag{3.96}$$

$$\Big(iF_3\Big) = \begin{pmatrix} 1 \\ 1 \end{pmatrix} iF_3\Big(1\ 1\Big) = \begin{pmatrix} 1 \\ 1 \end{pmatrix} [1/3 + i\widetilde{F}\mathcal{D}_{23,L}^{(u,u)}] i\widetilde{F}\Big(1\ 1\Big)\,, \tag{3.97}$$

$$\Big(\mathcal{R}_{L}^{(u)}\Big) = \begin{pmatrix} 1 \\ 0 \end{pmatrix} + \begin{pmatrix} 1 \\ 1 \end{pmatrix} i\widetilde{F} i\mathcal{D}_{23,L}^{(u,u)}\,. \tag{3.98}$$

Here $\mathcal{D}_{L}^{(u,u)}$ and $\mathcal{D}_{23,L}^{(u,u)}$, defined in Eqs. (5.11) and (3.90), respectively, are the same as in our result for $\widetilde{\mathcal{M}}_{3,L}^{(u,u)}$, Eq. (3.86). We note that the expression for F_3 given on the right-hand side of Eq. (3.97) is an alternative way of writing the earlier form, Eq. (6.28).

The quantities in round braces in Eqs. (3.94)-(3.98) live in a two-dimensional space: $(\mathcal{L}_{L}^{(u)})$ being a row vector, $(i\mathcal{K}_{\rm df,3})$ and (iF_3) being matrices, and $(\mathcal{R}_{L}^{(u)})$ being a column vector. The 1 in the denominator of Eq. (3.94 indicates the identity matrix in this space. The indices in this space are (u) and $(s+\tilde{s})$, as exemplified by the expression for $(i\mathcal{K}_{\rm df,3})$ in Eq. (3.96). These indices were introduced in HS1 to denote the different ways in which the spectator-momentum label is attached to diagrams. The precise definition is given in Appendix A.4.1. As an example of this matrix notation, the symmetrized $\mathcal{K}_{\rm df,3}$ (which is differentiated from the matrix version by the absence of surrounding parentheses) is given by

$$i\mathcal{K}_{\rm df,3} \equiv \Big(1\ 1\Big)\Big(i\mathcal{K}_{\rm df,3}\Big)\begin{pmatrix} 1 \\ 1 \end{pmatrix} = i\mathcal{K}_{\rm df,3}^{(u,u)} + i\mathcal{K}_{\rm df,3}^{(u,s+\tilde{s})} + i\mathcal{K}_{\rm df,3}^{(s+\tilde{s},u)} + i\mathcal{K}_{\rm df,3}^{(s+\tilde{s},s+\tilde{s})}\,. \tag{3.99}$$

This is the quantity that appears in the quantization condition of HS1, Eq. (3.78).

A noteworthy feature of the result (3.94) is that $\mathcal{M}_{3,L}^{(u,u)}$ is not given in terms only of the symmetrized $\mathcal{K}_{\rm df,3}$. This is because of the (1 0) term in $(\mathcal{L}_L^{(u)})$, and the corresponding term in $(\mathcal{R}_L^{(u)})$, which project onto asymmetric components of $(\mathcal{K}_{\rm df,3})$. If one symmetrizes, and considers $\mathcal{M}_{3,L}$, then it is possible to write the result in terms of the symmetric $\mathcal{K}_{\rm df,3}$, as shown by Eq. (68) of HS2.

The dependence of $\mathcal{M}_{3,L}^{(u,u)}$ brings up a potential conflict. On the one hand, we expect that we can obtain the HS1 quantization condition from $\mathcal{M}_{3,L}^{(u,u)}$, since any three-particle correlation function should have poles at the spectral energies. We know that the resulting quantization condition, Eq. (3.78), contains the symmetric $\mathcal{K}_{\rm df,3}$. On the other hand, $\mathcal{M}_{3,L}^{(u,u)}$ depends also on asymmetric components of $\mathcal{K}_{\rm df,3}$, as just noted. The resolution is that the central portion of the second term on the right-hand side of Eq. (3.94) can be rewritten as

$$\begin{aligned}\Big(i\mathcal{K}_{\rm df,3}\Big)\frac{1}{1-\Big(iF_3\Big)\Big(i\mathcal{K}_{\rm df,3}\Big)} &= \Big(i\mathcal{K}_{\rm df,3}\Big)+\Big(i\mathcal{K}_{\rm df,3}\Big)\frac{1}{1-\Big(iF_3\Big)\Big(i\mathcal{K}_{\rm df,3}\Big)}\Big(iF_3\Big)\Big(i\mathcal{K}_{\rm df,3}\Big) \qquad (3.100)\\ &= \Big(i\mathcal{K}_{\rm df,3}\Big)+\Big(i\mathcal{K}_{\rm df,3}\Big)\begin{pmatrix}1\\1\end{pmatrix}\frac{1}{1-iF_3i\mathcal{K}_{\rm df,3}}iF_3\begin{pmatrix}1&1\end{pmatrix}\Big(i\mathcal{K}_{\rm df,3}\Big)\,. \qquad (3.101)\end{aligned}$$

This shows that the geometric series leading to the poles does contain the symmetric $\mathcal{K}_{\rm df,3}$.

One final technical point needs to be mentioned. In HS1 and HS2, the versions of $\widetilde{F}$ and $\widetilde{G}$ differ from those used here in three ways: (i) they use a different boost to the interacting pair CMF (which only changes $\widetilde{G}$); (ii) $\widetilde{F}$ uses the original PV prescription rather than the generalized one used here; and (iii) $\widetilde{G}$ is defined with the nonrelativistic energy denominator. However, the derivations of HS1 and HS2 go through essentially unchanged if one uses our versions of $\widetilde{F}$ and $\widetilde{G}$, and, in particular, the expressions given in Eqs. (3.94)-(3.98) remain valid.

3.4.2 *Asymmetrizing* $\mathcal{M}_{3,L}^{(u,u)}$

The expressions for $\widetilde{\mathcal{M}}_{3,L}^{(u,u)}$ and $\mathcal{M}_{3,L}^{(u,u)}$, given in Eqs. (3.86) and (3.94), have a similar structure, but differ in many details. In this subsection we bring the almost symmetric result for $\mathcal{M}_{3,L}^{(u,u)}$ into an asymmetric form similar to that of $\widetilde{\mathcal{M}}_{3,L}^{(u,u)}$.

In Appendix A.4 we derive the following three "asymmetrization" identities (valid up to exponentially suppressed corrections, and for both the Wu boost and the boost of HS1)

$$X^{(u)}\,\widetilde{F}\,(1\ 1) = X^{(u)}(\widetilde{F}+\widetilde{G}-\overrightarrow{\mathcal{I}}_G)\,(1\ 0) \tag{3.102}$$

$$\begin{pmatrix}1\\1\end{pmatrix}\widetilde{F}X^{(u)} = \begin{pmatrix}1\\0\end{pmatrix}(\widetilde{F}+\widetilde{G}-\overleftarrow{\mathcal{I}}_G)X^{(u)}\,, \tag{3.103}$$

$$\begin{pmatrix}1\\1\end{pmatrix}\frac{\widetilde{F}}{3}\,(1\ 1) = \begin{pmatrix}1\\0\end{pmatrix}(\widetilde{F}+\widetilde{G}+\otimes_G)\,(1\ 0)\ . \tag{3.104}$$

where $X^{(u)}$ is a generic asymmetric amplitude, e.g. $\overline{\mathcal{M}}_{2,L}$ or $\mathcal{D}_{23,L}^{(u,u)}$, and there is an implicit matrix of amplitudes such as $(\mathcal{K}_{\mathrm{df},3})$ on the right of Eq. (3.102), on the left of Eq. (3.103), and on both sides of Eq. (3.104). The integral operators $\overrightarrow{\mathcal{I}}_G$, $\overleftarrow{\mathcal{I}}_G$, and $\otimes_G$ are defined in the appendix. The first two are similar to $\widetilde{\mathcal{I}}_F$, but their action is directional, as indicated by the arrows. The effect of all three operators is to sew together the adjacent amplitudes leading to new infinite-volume quantities.

Using the three identities, we can rewrite the expression for $\mathcal{M}_{3,L}^{(u,u)}$, Eq. (3.94), solely in terms of $\mathcal{K}_{\mathrm{df},3}^{(u,u)}$:

$$i\mathcal{M}_{\mathrm{df},3,L}^{(u,u)} \equiv i\mathcal{M}_{3,L}^{(u,u)} - i\mathcal{D}_{L}^{(u,u)} \tag{3.105}$$

$$= \left[1+i\mathcal{D}_{23,L}^{(u,u)}i(\widetilde{F}+\widetilde{G}-\overrightarrow{\mathcal{I}}_G)\right]i\mathcal{T}_{L}^{(u,u)}\left[1+i(\widetilde{F}+\widetilde{G}-\overleftarrow{\mathcal{I}}_G)i\mathcal{D}_{23,L}^{(u,u)}\right], \tag{3.106}$$

$$i\mathcal{T}_{L}^{(u,u)} = i\mathcal{K}_{\mathrm{df},3}^{(u,u)}\frac{1}{1-\left[i(\widetilde{F}+\widetilde{G}+\otimes_G)+i(\widetilde{F}+\widetilde{G}-\overleftarrow{\mathcal{I}}_G)i\mathcal{D}_{23,L}^{(u,u)}i(\widetilde{F}+\widetilde{G}-\overrightarrow{\mathcal{I}}_G)\right]i\mathcal{K}_{\mathrm{df},3}^{(u,u)}}\,. \tag{3.107}$$

In Appendix A.6, we show that this result can be reorganized into

$$i\mathcal{M}^{(u,u)}_{\mathrm{df},3,L} = \left[1 + i\mathcal{D}^{(u,u)}_{23,L} i(\widetilde{F}+\widetilde{G})\right] i\mathcal{K}'^{(u,u)}_{\mathrm{df},3} \times \frac{1}{1 - \left[1 + i(\widetilde{F}+\widetilde{G}) i\mathcal{D}^{(u,u)}_{23,L}\right] i(\widetilde{F}+\widetilde{G}) i\mathcal{K}'^{(u,u)}_{\mathrm{df},3}} \left[1 + i(\widetilde{F}+\widetilde{G}) i\mathcal{D}^{(u,u)}_{23,L}\right] , \tag{3.108}$$

where the primed version of the HS1 asymmetric amplitude is

$$i\mathcal{K}'^{(u,u)}_{\mathrm{df},3} \equiv \left(1 - i\overline{\mathcal{K}}_2 i\overrightarrow{\mathcal{I}}_G\right) i\mathcal{K}^{(u,u)}_{\mathrm{df},3} \frac{1}{1 - \left[i \otimes_G + i\overleftarrow{\mathcal{I}}_G i\overline{\mathcal{K}}_2 i\overrightarrow{\mathcal{I}}_G\right] i\mathcal{K}^{(u,u)}_{\mathrm{df},3}} \left(1 - i\overleftarrow{\mathcal{I}}_G i\overline{\mathcal{K}}_2\right) . \tag{3.109}$$

We observe that the form of Eq. (3.108) is identical to that of the result for $\widetilde{\mathcal{M}}^{(u,u)}_{3,L}$, Eq. (3.88), with $\mathcal{K}'^{(u,u)}_{\mathrm{df},3}$ playing the role of $\widetilde{\mathcal{K}}^{(u,u)}_{\mathrm{df},3}$.

An interesting implication of this result is that the HS1 quantization condition can be rewritten in the form derived here, Eq. (3.81), but with $\widetilde{\mathcal{K}}^{(u,u)}_{\mathrm{df},3}$ replaced by $\mathcal{K}'^{(u,u)}_{\mathrm{df},3}$:

$$\det\left[1 + \left(2\omega L^3 \mathcal{K}_2 + \mathcal{K}'^{(u,u)}_{\mathrm{df},3}\right)(\widetilde{F}+\widetilde{G})\right] = 0 . \tag{3.110}$$

To show this, we use the result, noted above, that the quantization condition can be derived from the poles in $\mathcal{M}^{(u,u)}_{3,L}$. To obtain an expression for $\mathcal{M}^{(u,u)}_{3,L}$, we start from Eq. (3.108), and reverse the steps leading from Eq. (3.85) to Eq. (3.88), obtaining

$$i\left(\overline{\mathcal{M}}_{2,L} + \mathcal{M}^{(u,u)}_{3,L}\right) = i(2\omega L^3 \mathcal{K}_2 + \mathcal{K}'^{(u,u)}_{\mathrm{df},3}) \frac{1}{1 - i(\widetilde{F}+\widetilde{G})\, i(2\omega L^3 \mathcal{K}_2 + \mathcal{K}'^{(u,u)}_{\mathrm{df},3})} , \tag{3.111}$$

the denominator of which leads immediately to the quantization condition Eq. (3.110).

We now have two quantization conditions of exactly the same form, Eqs. (3.81) and (3.110), but containing different asymmetric three-particle K matrices, $\widetilde{\mathcal{K}}^{(u,u)}_{\mathrm{df},3}$ and $\mathcal{K}'^{(u,u)}_{\mathrm{df},3}$ respectively. This does not, however, imply that these two K matrices are the same. One way of seeing this is to note that asymmetrization is not unique: there are many ways to divide a symmetric amplitude into asymmetric components. This is because, for a given asymmetric diagram (in either the Feynman or TOPT approach), one can choose to assign it directly to the asymmetric amplitude, or to first symmetrize and then assign. When using

the identities (3.102)-(3.104), the left-hand sides involve only the symmetric part of $\mathcal{K}_{\mathrm{df},3}$, while the right-hand sides involve only the (u) parts. Since the latter are ambiguous, the identity must be satisfied for all possible choices of asymmetric amplitude. In other words, the operators appearing on the right-hand sides, e.g. $\widetilde{F} + \widetilde{G} - \overrightarrow{\mathcal{I}}_G$, must have (an infinite number of) zero modes. These observations do not impact the derivation just given, in which we *choose* a particular asymmetrization. However, they imply that we could have made another choice, in which case the resulting $\mathcal{K}'^{(u,u)}_{\mathrm{df},3}$ would have been different while the form of the resulting quantization condition, Eq. (3.110), would have been unchanged.

3.4.3 Symmetric form of the new quantization condition

Having understood how asymmetrization turns the HS1 quantization condition into our new form, we now follow the inverse path and bring our quantization condition into HS1 form.

What we need to do is to rewrite our result for $\widetilde{\mathcal{M}}^{(u,u)}_{\mathrm{df},3,L}$, Eq. (3.88), in the form given in Eq. (3.106), for then we can use the asymmetrization identities in reverse and obtain the HS2 form, Eq. (3.94). In order to follow these steps we must first invert Eq. (3.109). We can do so by discretizing momentum space so that all relations are matrix equations. Then we obtain

$$i\widetilde{\mathcal{K}}'^{(u,u)}_{\mathrm{df},3} = i\widetilde{\mathcal{Z}}^{(u,u)} \frac{1}{1 + \left[i \otimes_G + i\overleftarrow{\mathcal{I}}_G i\overline{\mathcal{K}}_2 i\overrightarrow{\mathcal{I}}_G\right] i\widetilde{\mathcal{Z}}^{(u,u)}}\,, \tag{3.112}$$

$$i\widetilde{\mathcal{Z}}^{(u,u)} \equiv \frac{1}{1 - i\overline{\mathcal{K}}_2 i\overrightarrow{\mathcal{I}}_G} i\widetilde{\mathcal{K}}^{(u,u)}_{\mathrm{df},3} \frac{1}{1 - i\overleftarrow{\mathcal{I}}_G \overline{\mathcal{K}}_2}\,. \tag{3.113}$$

The next step is to obtain the other components of this new version of the K matrix, namely $\widetilde{\mathcal{K}}'^{(s+\bar{s},u)}_{\mathrm{df},3}$, etc. This is done using relations from HS1, which are recalled in Appendix A.4. Then the steps above lead to the analog of Eq. (3.94),

$$i\widetilde{\mathcal{M}}^{(u,u)}_{\mathrm{df},3,L} = \left(\mathcal{L}^{(u)}_L\right)\left(i\widetilde{\mathcal{K}}'_{\mathrm{df},3}\right) \frac{1}{1 - \left(iF_3\right)\left(i\widetilde{\mathcal{K}}'_{\mathrm{df},3}\right)} \left(\mathcal{R}^{(u)}_L\right), \tag{3.114}$$

with $(\mathcal{L}^{(u)}_L)$, (F_3), and $(\mathcal{R}^{(u)}_L)$ unchanged from above. Finally, we can use the arguments at

the end of Sec. 3.4.1 to determine the quantization condition from $\widetilde{\mathcal{M}}_{\mathrm{df},3,L}^{(u,u)}$, obtaining

$$\det\left[1+\widetilde{\mathcal{K}}'_{\mathrm{df},3}F_3\right]\,, \tag{3.115}$$

where the symmetrized K matrix is

$$\widetilde{\mathcal{K}}'_{\mathrm{df},3}=\widetilde{\mathcal{K}}'^{(u+s+\tilde{s},u+s+\tilde{s})}_{\mathrm{df},3}\,. \tag{3.116}$$

Thus we find that the symmetrized version of our new quantization condition is of exactly the same form as that of HS1.

We now argue that the symmetrized K matrix obtained here and that of HS1 are the same, i.e.[27]

$$\widetilde{\mathcal{K}}'_{\mathrm{df},3}=\mathcal{K}_{\mathrm{df},3}\,. \tag{3.117}$$

To do so, we use the result from HS2 that, by symmetrizing the infinite-volume limit of Eq. (3.94), the full $\mathcal{M}_3$ can be written in terms of integral equations containing $\mathcal{K}_{\mathrm{df},3}$ alone—the asymmetric form $\mathcal{K}_{\mathrm{df},3}^{(u,u)}$ is not needed, unlike for $\mathcal{M}_{\mathrm{df},3}^{(u,u)}$. Similarly, by symmetrizing the infinite-volume limit of Eq. (3.114), $\mathcal{M}_3$ is given by *exactly the same expression* in terms of $\widetilde{\mathcal{K}}'_{\mathrm{df},3}$. Now we assume that this relation is invertible and one-to-one. If so, the two symmetrized K matrices must be equal. Another way of stating this claim is that we are effectively assuming that there are no redundant parts of the symmetrized K matrices, which we view as plausible given the explicit construction presented here. This is in contrast to the asymmetrized K matrices, which we know are ambiguous.

The equality of $\widetilde{\mathcal{K}}'_{\mathrm{df},3}$ and $\mathcal{K}_{\mathrm{df},3}$ is also consistent with the quantization condition having the same form in both cases. However, this is not a sufficient argument to demonstrate equality of the K matrices, since the asymmetric form of the quantization conditions also agree, and yet we know that the asymmetric K matrices differ.

---

[27] We stress that this result will hold only if the same choice of boost in $\widetilde{G}$ and cutoff function $H(\mathbf{k})$ is used in both cases.

The result (D.77) connects the Feynman-diagram-based method of HS1/HS2 and the TOPT approach followed here. It also provides an explicit expression for $\mathcal{K}_{\mathrm{df},3}$ that goes beyond the constructive definition given in HS1.

We close by emphasizing two points. First, we stress that the steps leading to the result (3.114) for $\widetilde{\mathcal{M}}^{(u,u)}_{\mathrm{df},3,L}$ do not depend on the derivations of HS1 and HS2. While we have made use of results from these works as motivation for the logical progression of our approach, in the end the steps needed are simply algebraic. Second, although the symmetric K matrices are the same, this does not mean that $\mathcal{M}^{(u,u)}_{3,L}$ and $\widetilde{\mathcal{M}}^{(u,u)}_{3,L}$ are the same, because they depend also on $\mathcal{K}^{(u,u)}_{\mathrm{df},3}$ and $\widetilde{\mathcal{K}}^{(u,u)}_{\mathrm{df},3}$, respectively, and these differ. This is an important consistency check, as we know that $\mathcal{M}^{(u,u)}_{3,L}$ and $\widetilde{\mathcal{M}}^{(u,u)}_{3,L}$ are in fact different.

3.5 Conclusions

In this paper we provide a more direct and explicit path to the relativistic, model-independent, three-particle quantization condition of HS1 [28]. Although it is reassuring to check the result of the complicated and lengthy derivation of HS1, this is not our fundamental motivation. Instead, we expect that our method will simplify the generalization to nondegenerate particles, and hope to present results for this shortly. This is a complementary generalization to that achieved recently in Ref. [37], which considers degenerate, but potentially distinguishable, spinless particles. We expect it to be profitable to combine the two approaches.

As part of our derivation, we have shown that the three-particle quantization condition can be written in a simpler form in terms of asymmetric amplitudes [see Eqs. (3.81) and (3.110)]. We do not necessarily propose this as a practical alternative to the HS1 form, because the asymmetric amplitudes will require, at any order in the threshold expansion of Refs. [39, 76], a larger number of parameters for a general description than the symmetric form appearing in the HS1 quantization condition.[28] The parametrizations must therefore be

[28]This can be seen explicitly in chiral perturbation theory from the leading-order result for $\mathcal{K}^{(u,u)}_{\mathrm{df},3}$.

redundant, a result that is presumably related to the ambiguity in defining an asymmetric amplitude. However, we do expect that the new, asymmetric form of the quantization condition has theoretical implications. Indeed, in a companion paper we show that it allows one to derive a form of the quantization condition in terms of the R matrix of Refs. [78, 79] and thus obtain a generalization of the result of the FVU approach to all partial waves [45].

A more distant goal of our approach is to allow the generalization to more than three particles. In this regard we note that the complications associated with the possibility of on-shell intermediate states in three-particle scattering, which led in HS1 to the introduction of the divergence-free three-particle K matrix, $\mathcal{K}_{\text{df},3}$, are dealt with very simply and automatically in the TOPT approach used here. This gives us some hope that the additional complications that arise with more than three particles will be manageable. In this regard, the alternative approach for dealing with F cuts that is sketched in Appendix A.7 may be helpful as it does not require a choice of PV prescription.

An issue that we have commented on only peripherally in the text is whether the various three-particle K matrices that we have considered are Lorentz invariant. This is not relevant to the derivation, but is important for practical applications, since invariance restricts the number of terms that contribute. We summarize the status here. First, we stress that all the quantization conditions presented here—both the original HS1 form and our asymmetric form, and for both choices of boost—hold for all kinematically allowed choices of $P^\mu = (E, \mathbf{P})$. In particular they hold for choices of P^μ for which the three particles are relativistic, which is why we call the quantization conditions relativistic. This is, however, a separate issue from the relativistic invariance of the K matrices. Here the status is that, if we define $\widetilde{G}$ using the boost of HS1 and the relativistic form of the pole (which is possible for both the HS1 K matrices and the new TOPT versions introduced here), then the original symmetric $\mathcal{K}_{\text{df},3}$ and the asymmetric version $\mathcal{K}'^{(u,u)}_{\text{df},3}$ are both Lorentz invariant.[29] These appear, respectively,

[29]The latter result follows because $\mathcal{K}'^{(u,u)}_{\text{df},3}$ is related to the Lorentz invariant quantity $\mathcal{M}_3^{(u,u)}$ by integral

in the original HS1 quantization condition, Eq. (3.82), and the asymmetric form found here, Eq. (3.110). On the other hand, the asymmetric K matrix $\widetilde{\mathcal{K}}^{(u,u)}_{\mathrm{df},3}$ appearing in the TOPT version of the asymmetric quantization condition, Eq. (3.81), is not invariant (see Appendix A.5). However, the symmetrized quantity $\widetilde{\mathcal{K}}'_{\mathrm{df},3}$ is invariant, since it equals $\mathcal{K}_{\mathrm{df},3}$.

equations of the same form as given in Appendix A.5, which are boost invariant.

Chapter 4

RELATIVISTIC THREE-PARTICLE QUANTIZATION CONDITION FOR NONDEGENERATE SCALARS[1]

4.1 Introduction

The theoretical formalism needed to study three-particle interactions using lattice QCD (LQCD) has advanced considerably in recent years [28–32, 34–37, 41, 43, 45, 64, 77]. In addition, the formalism has been shown to be a practical tool in simple systems [39–41, 76], and applied to LQCD results for the $3\pi^+$ [1, 52, 53, 85, 86] and $3K^-$ systems [87], as well as to the ϕ^4 theory [55, 88]. For recent reviews, see Refs. [74, 75].[2]

The relativistic formalism has so far only been developed for degenerate scalars.[3] Within the generic relativistic effective field theory (RFT) approach, which we adopt here, the initial development was for identical scalars with a G-parity-like $\mathbb{Z}_2$ symmetry [28, 29], with the extension to theories without the $\mathbb{Z}_2$ symmetry presented in Ref. [34], and that to nonidentical but degenerate scalars (e.g. three pions with all allowed total isospins) given in Ref. [37]. An additional generalization to allow the inclusion of poles in the two-particle K matrices was given in Refs. [35, 36]. Alternative approaches have been developed using either nonrelativistic effective field theory (NREFT) [30, 31], or the application to finite volume of a unitary representation of the three-particle scattering amplitude [32, 41]. Both approaches have so far only considered identical scalars, and also only s-wave two-particle interactions. Recently,

[1] This chapter and Appendix B are taken directly from Ref. [44].

[2] For alternative approaches, see Refs. [70–73, 89, 90].

[3] The only nondegenerate three-particle formalism of which we are aware is the very recent Ref. [91], in which the DDK system is studied using the nonrelativistic effective field theory approach of Refs. [30, 31], and assuming only s-wave two-particle interactions.

the RFT and finite-volume unitarity approaches have been shown to be equivalent [45].

In this work we generalize the RFT approach to nondegenerate scalar particles. We derive three forms of the three-particle quantization condition, Eqs. (4.36), (7.33), and (6.1), each with associated integral equations relating the intermediate K matrices to the three-particle scattering amplitude, $\mathcal{M}_3$.

The first form is derived using the simplified method, based on time-ordered perturbation theory (TOPT), that we introduced recently in Ref. [43], a reference henceforth referred to as BS1. The quantization condition involves the nondegenerate generalization of the asymmetric three-particle K matrix used in BS1, and for this reason we refer to it as "asymmetric." This generalization is a three-dimensional flavor matrix of K matrices, denoted $\widehat{\mathcal{K}}_{\text{df},3}$. A significant disadvantage of this approach is that the K matrices are not Lorentz invariant (although the formalism is valid for relativistic kinematics).

The second form of the quantization condition resolves this shortcoming, as it involves a flavor matrix of Lorentz-invariant K matrices. Its derivation follows the original RFT works [28, 29] in using Feynman diagrams, but, compared to those works, rearranges the order in which the diagrams are analyzed, and the manner in which finite- and infinite-volume quantities are related. The guiding principle is to mirror, at every step, the form of the TOPT analysis, so that the algebraic simplifications in the latter approach carry over. For this reason the resulting quantization condition is also asymmetric. This leads to the major disadvantage of the resulting formalism (shared with the TOPT form), namely that it depends on *nine* intermediate three-particle K matrices, collected in the matrix denoted $\widehat{\mathcal{K}}'_{\text{df},3}$, which are distinguished by the choice of spectator flavors for incoming and outgoing particles.

This disadvantage is resolved by the final form of the quantization condition. By algebraic manipulations that generalize the (anti)symmetrization procedure introduced in BS1, we are able to take the second form of the quantization condition and reexpress it in terms

of a *single*, symmetrized Lorentz-invariant three-particle K matrix, $\widetilde{\mathcal{K}}_{\mathrm{df},3}$. The resulting "symmetric" quantization condition, given in Eq. (6.1), provides the natural generalization of that derived in Ref. [28] for identical particles, and indeed the two have very similar forms. We expect that this final form will be the most useful in practice. Given a technical assumption, it is also possible to obtain this final form by applying the same symmetrization procedure to the TOPT form of the quantization condition. In this way one can avoid the intermediate step involving Feynman diagrams.

We stress that no truncation of the two-particle angular momenta is needed in any of the derivations. The only approximation made is to drop terms that are exponentially suppressed in the box size L.

Our main focus in this work is the presentation of a theoretical framework that will be straightforward to generalize to all three-particle systems of interest, e.g. those involving multiple three-particle channels, and "$2+1$" systems involving two identical particles plus a third that is different (e.g. $N\pi\pi$). The applications of the specific results we present here to QCD are relatively limited. They require each particle to carry a different combination of flavors in such a way that there is only one allowed three-particle state, e.g. the $D_s^+ D^0 \pi^-$ and $D_s^+ D^0 D^+$ systems. We do not discuss here the practical implementation of the new formalism, which we expect to involve a straightforward generalization of previous implementations of the RFT approach [1, 36, 39, 76, 86].

The derivation we present here is lengthy, and the logic and necessity of the various steps may be difficult to follow. Thus we provide, in a brief first section, a road map to the derivation, which also serves to present the organization of the paper. We only note here that conclusions and directions for future work are presented in Sec. 8.6.

4.2 Summary of the steps of the derivation

Here we provide a summary of the approach that we follow in this work, which also serves to provide a "recipe" for future generalizations.

1. Choose the desired three-particle state of interest, e.g. $3\pi^+$, $D_s^+ D^0 \pi^-$, $K^+\pi^+\pi^0$, ... Consider a finite-volume correlator $C_{3,L}(E, \mathbf{P})$ with operators coupling to this state, restricting the overall 4-momentum $P^\mu = (E, \mathbf{P})$ so that only said state is kinematically allowed to go on shell. This is discussed in Sec. 4.3.

2. Working in a generic relativistic effective field theory describing the interactions of the particles under consideration, express $C_{3,L}$ as an infinite sum of diagrams in TOPT. Organize them by number of "relevant" cuts—sections consisting of the three-particle state of interest—while taking the infinite-volume limit of all sections involving "ir-relevant" cuts. The result is a simple geometric series for the correlator involving off-shell generalized infinite-volume kernels. Project the kernels on shell to rewrite $C_{3,L}$ in terms of on-shell two and three-particle K-matrices, here $\mathcal{K}_2$ and $\widehat{\mathcal{K}}_{\text{df},3}$, and known finite-volume kinematic quantities associated with the relevant cuts.

   These steps are presented here in Sec. 4.4, with some details relegated to Appendix C.1, and are mostly a straightforward generalization of the analysis of BS1 for identical particles.

3. At this point one obtains a quantization condition relating the finite-volume energy spectrum to the K matrices, here given in Eq. (4.36). It will, however, involve a K matrix that is asymmetric under particle interchange and is not Lorentz invariant.

4. A shortcut is now available, based on an assumption explained in Sec. 4.8.6. This uses symmetrization identities, introduced in Sec. 4.8, to rewrite the quantization condition

in terms of a symmetric, three-particle K matrix (denoted here $\widetilde{\mathcal{K}}_{\text{df},3}$). Here this form of the quantization condition is given in Eq. (6.1). The K matrix obtained in this way is also Lorentz invariant.

Two appendices fill in steps in the derivation of Sec. 4.8. Appendix B.3 derives the symmetrization identities, while Appendix B.4 gives further details of the steps needed to derive the quantization condition.

5. The K matrices can be related to the physical scattering amplitudes $\mathcal{M}_2$ and $\mathcal{M}_3$ via nested integral equations. How this is done is explained in detail for the asymmetric, non-Lorentz-invariant K matrix $\widehat{\mathcal{K}}_{\text{df},3}$ in Sec. 4.5. For the final form of the quantization condition the integral equations are sketched briefly in Sec. 4.8.5.

Although the assumption mentioned in step 4 is plausible, it has not been demonstrated. An alternative approach to obtain the final quantization condition without assumptions replaces TOPT with a method using Feynman diagrams. While more complicated than the TOPT approach, it is simpler and more explicit than the original method of Ref. [28]. This new method is presented in Sec. 4.6 and mirrors steps 2-5 of the TOPT recipe, with details of the derivation given in the associated Appendix B.2. It involves an asymmetric but Lorentz-invariant K matrix, here $\widehat{\mathcal{K}}'_{\text{df},3}$, and leads to an intermediate, asymmetric form of the quantization condition, here Eq. (7.33). This is then converted into the symmetric form using the same symmetrization identities as for the TOPT result, as explained in Sec. 4.8. Both $\widehat{\mathcal{K}}'_{\text{df},3}$ and its symmetrized version can be related to the physical amplitude $\mathcal{M}_3$ via integral equations, as shown in Secs. 4.7 and 4.8.5, respectively.

4.3 Setup and overview

For the derivations presented below we work in the following theoretical setup. Our theory has three real scalar fields, ϕ_i, $i = 1, 2, 3$, with the Lagrangian having the most general

Lorentz-invariant form that is symmetric under $\phi_i \to -\phi_i$ for each field separately. We describe the fields as having different "flavors," although the associated symmetry is $\mathbb{Z}_2$ rather than the usual $U(1)$. We label the physical masses of the particles m_i, and assume, without loss of generality, the ordering $m_1 \leq m_2 \leq m_3$. We determine the quantization condition from the poles in the correlator

$$C_{3,L}(E,\mathbf{P}) \equiv \int_L d^4x \; e^{i(Ex^0 - \mathbf{P}\cdot\mathbf{x})} \langle 0|\mathrm{T}\sigma_{123}(x)\sigma_{123}^\dagger(0)|0\rangle \,, \tag{4.1}$$

where $\sigma_{123}^\dagger \sim \phi_1\phi_2\phi_3$ is an operator that creates states having an odd number of each of the flavors. We do not need to specify the spatial form of the operator, except to note that we allow the three fields to be spatially separated in such a way that no rotational quantum numbers are excluded. The theory lives in a cubic spatial box of length L, as indicated by the subscript on the integral sign, and periodic boundary conditions are assumed. The total four-momentum flowing through the correlator is $(E,\mathbf{P})$, with $\mathbf{P}$ lying in the finite-volume set, $\mathbf{P} \in (2\pi/L)\mathbb{Z}^3$. In the overall center of mass frame (CMF), the energy is $E^* = \sqrt{E^2 - \mathbf{P}^2}$.

To ensure that the only intermediate states that can go completely on shell are those consisting of exactly three particles (one of each flavor), we impose the following restriction:

$$0 < E^* < 3m_1 + m_2 + m_3 \,. \tag{4.2}$$

Here we are using the mass ordering assumed above, such that the lowest-energy on-shell five-particle state involves the addition of two particles of flavor 1. Because of the $\mathbb{Z}_2^3$ symmetry, there are no possible single-particle intermediate states, so the lower bound on E^* is lower than in the identical-particle case (where $m < E^* < 5m$).

In the first derivation below, we follow the same strategy as in BS1. We begin by considering all Feynman diagrams contributing to $C_{3,L}$ and then, after an initial analysis dealing with self-energy diagrams (discussed in Appendix A of BS1 and carrying over essentially unchanged to the present analysis), convert to time-ordered diagrams. The rules for such diagrams are summarized in Sec. IIA of BS1. We only note here that the factor associated

with a propagator of flavor i and momentum $\mathbf{p}_i$ is $1/(2\omega_{p_i})$, where $\omega_{p_i} = \sqrt{\mathbf{p}_i^2 + m_i^2}$, with m_i the physical (not bare) mass.

Given the kinematic restriction (4.2), the only singular behavior in TOPT diagrams arises from energy denominators for intermediate states ("cuts") containing three particles, and thus having the form $1/(E - \omega_{p_1} - \omega_{p_2} - \omega_{p_3})$. We refer to these intermediate states as "relevant cuts." All other ("irrelevant") cuts lead to sums over internal momenta (which lie in the finite-volume set) with nonsingular summands, which can therefore be replaced by integrals, up to exponentially suppressed corrections, which are typically of the form $\sim \exp(-m_i L)$. We assume throughout this work that such corrections can be neglected.

In the second derivation below, we work entirely with Feynman diagrams. As in Ref. [28], we do begin by using TOPT to justify that power-law volume effects come only from three-particle intermediate states, but the actual analysis does not use TOPT.

We close this overview by discussing the generality of the results that we derive. The consideration of a theory with a $\mathbb{Z}_2^3$ symmetry is convenient—reducing the number of diagrams that contribute to the skeleton expansion of the correlator $C_{3,L}$—but not necessary. Once the dust of the derivations has settled, it becomes clear that the only necessary criterion is for there to be a range of E^* in which the only allowed on-shell intermediate state consists of one of each flavor of particle. Thus, for example, the derivation applies also to the $D^s D^0 \pi^-$ system, since the quark compositions, $(c\bar{s})(c\bar{u})(d\bar{u})$, constrain the flavor such that there are no other intermediate states until one reaches the $D^0 D^0 K^0$ threshold. Our formalism is valid in this case for $0 < E^* < 2M(D_0) + M(K_0) = 4224\,\text{MeV}$. In practice, of course, aside from the possibility of bound states, the lower limit of interest is $E^* \approx M(D^s) + M(D^0) + M(\pi^-) = 3973\,\text{MeV}$, so there is a small kinematic range of applicability. Other similar examples are discussed in the conclusions.

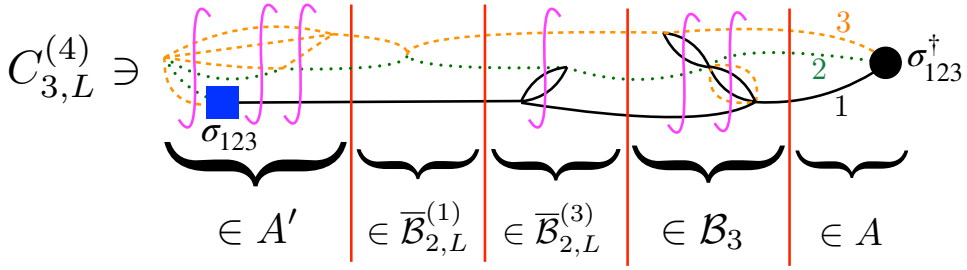

Figure 4.1: Example of a contribution to the correlator $C_{3,L}$ in TOPT, illustrating the segments that appear. The solid (red) vertical lines indicate relevant (three-particle) cuts, which are associated with factors of D. Time runs from right to left. Cuts that cannot go on shell are indicated by the (magenta) integral signs. The three flavors are denoted, respectively, by (black) solid lines, (green) dotted lines, and (orange) dashed lines. We note that all vertices, which arise from the generic EFT, contain an even number of each flavor of particle. We also stress that vertices are allowed to lie outside of the time interval bracketed by $\sigma_{123}(t)$ and $\sigma_{123}^\dagger(0)$, an example being the six-point vertex at the left of the diagram.

4.4 Derivation of quantization condition using TOPT

In this section we derive the three-particle quantization condition for nondegenerate scalars using the TOPT-based approach of BS1.

An example of the TOPT diagrams contributing to $C_{3,L}$ is shown in Fig. 4.1. As in BS1, we can divide the diagrams into segments separated by relevant cuts. A simplification compared to BS1 is that we do not need to keep track of symmetry or relabeling factors.

The four types of segment that appear (all illustrated in the figure) are:[4]

$$\begin{aligned} \text{left endcap:} &\quad A'(\{\mathbf{p}\})\,, \\ \text{right endcap:} &\quad A(\{\mathbf{k}\})\,, \\ \text{3PIs kernel:} &\quad i\mathcal{B}_3(\{\mathbf{p}\};\{\mathbf{k}\})\,, \\ \text{2PIs kernels:} &\quad i\overline{\mathcal{B}}^{(i)}_{2,L}(\{\mathbf{p}\};\{\mathbf{k}\}) = 2\omega_{p_i}L^3\delta_{\mathbf{p}_i\mathbf{k}_i}i\mathcal{B}^{(i)}_2(\mathbf{p}_j,\mathbf{p}_k;\mathbf{k}_j,\mathbf{k}_k)\,. \end{aligned} \tag{4.3}$$

Here we are using the notation

$$\{\mathbf{p}\} \equiv \{\mathbf{p}_1,\mathbf{p}_2,\mathbf{p}_3\}\,, \quad \{\mathbf{k}\} \equiv \{\mathbf{k}_1,\mathbf{k}_2,\mathbf{k}_3\}\,, \quad \text{etc.} \tag{4.4}$$

for sets of three spatial momenta. The subscript on each momentum indicates the flavor of the particle, as do the superscripts on $\overline{\mathcal{B}}^{(i)}_{2,L}$ and $\mathcal{B}^{(i)}_2$. Where we use the triplet of flavor labels, i, j, and k, they are assumed to be in cyclic order. The quantities A', A, $\mathcal{B}_3$, and $\mathcal{B}_2$ can all be evaluated in infinite volume, i.e. with momentum sums replaced by integrals. Since, by construction, $\mathcal{B}_3$ has no three-particle cuts, it is three-particle irreducible in the s channel (3PIs). Similarly, the two-to-two kernels $\mathcal{B}^{(i)}_2$ are 2PIs. Finally, we note that all kernels depend implicitly on the input energy E.

There are several changes in these kernels compared to those needed for identical particles in BS1. First, there are three types of two-particle kernels, $\overline{\mathcal{B}}^{(i)}_{2,L}$, corresponding to the three choices of flavor i of the spectator particle. Second, the kernel $\mathcal{B}_3$ is defined here without any overall factor, whereas the quantity of the same name in BS1 (but which applies to identical particles) is defined to include a factor of 1/9. Third, the endcaps A' and A here have no overall factor, while in BS1 the corresponding quantities (denoted $\widehat{A}'$ and $\widehat{A}$) include a factor of 1/3. Finally, we use a redundant labeling for the allowed discrete choices of momenta, listing all three, as in Eq. (4.4), although they are constrained to sum to $\mathbf{P}$. This is a notational convenience, and avoids picking out arbitrarily one of the momenta. Although the

[4] We make one notational change compared to BS1, namely removing the hats on A' and A. This allows us to reintroduce hats below as a notation for the matrix forms of the various kernels.

kernels are infinite-volume quantities, defined for all external momenta, within the correlator the momenta are in the finite-volume set. Thus we treat the sets $\{\mathbf{p}\}$, $\{\mathbf{k}\}$, etc. as matrix indices, with A' a row vector, $\overline{\mathcal{B}}_{2,L}^{(i)}$ and $\mathcal{B}_3$ matrices, and A a column vector. In the following, these indices are implicitly summed, subject to the above-mentioned constraint.

The correlator can be written as a sum over terms containing different numbers of relevant cuts. Between each cut one can have either the kernel $\mathcal{B}_3$ or one of the $\overline{\mathcal{B}}_{2,L}^{(i)}$. This leads immediately to the geometric series

$$C_{3,L} = C_{3,L}^{(0)} + A' i D \sum_{n=0}^{\infty} \left[(i\overline{\mathcal{B}}_{2,L}^{(1)} + i\overline{\mathcal{B}}_{2,L}^{(2)} + i\overline{\mathcal{B}}_{2,L}^{(3)} + i\mathcal{B}_3) i D \right]^n A \tag{4.5}$$

$$= C_{3,\infty}^{(0)} + A' i D \frac{1}{1 - (i\overline{\mathcal{B}}_{2,L}^{(1)} + i\overline{\mathcal{B}}_{2,L}^{(2)} + i\overline{\mathcal{B}}_{2,L}^{(3)} + i\mathcal{B}_3) i D} A \,. \tag{4.6}$$

Here $C_{3,L}^{(0)}$ is the contribution with no relevant cuts, which can be converted into an infinite-volume quantity up to exponentially-suppressed corrections. The matrix D is associated with relevant cuts and is given by

$$D(\{\mathbf{p}\};\{\mathbf{k}\}) = \mathbb{1}_{\mathbf{p},\mathbf{k}} \frac{1}{L^6} \frac{1}{8\omega_{p_1}\omega_{p_2}\omega_{p_3}} \frac{1}{E - \omega_{p_1} - \omega_{p_2} - \omega_{p_3}} \,, \tag{4.7}$$

where

$$\mathbb{1}_{\mathbf{p},\mathbf{k}} \equiv \delta_{\mathbf{p}_1\mathbf{k}_1}\delta_{\mathbf{p}_2\mathbf{k}_2}\delta_{\mathbf{p}_3\mathbf{k}_3} \,. \tag{4.8}$$

The third Kronecker delta is redundant and could be dropped—we include it to emphasize the symmetry of the expression. The simplicity of the result in Eq. (4.5) shows the advantage of the TOPT approach.

At this stage, the TOPT kernels are, in general, off shell, i.e. $E \neq \omega_{p_1} + \omega_{p_2} + \omega_{p_3}$ for each intermediate cut. The next step is to include an on-shell projection. The procedure for doing so in the degenerate case is described in detail in BS1, following the analysis of Ref. [28]. The only changes needed here are kinematical, and are explained below. The nature of the on-shell projection depends on the form of the kernels adjacent to factors of D.

In particular, between two-particle kernels with the same spectator flavor, i.e. $\overline{\mathcal{B}}^{(i)}_{2,L} D \overline{\mathcal{B}}^{(i)}_{2,L}$, are relevant cuts with a common spectator particle[5] ("F cuts"), while if the flavors differ, as in $\overline{\mathcal{B}}^{(1)}_{2,L} D \overline{\mathcal{B}}^{(2)}_{2,L}$, the relevant cuts all have the spectator particle switch between the kernels ("G cuts"). Between two- and three-particle kernels, or between a pair of three-particle kernels, one can use either type of cut, or a linear combination thereof, and we use this freedom to give a compact expression for subsequent results. In particular, we find it convenient to add an additional layer of matrix indices, corresponding to the flavor of the spectator particle. This allows us to rewrite Eq. (4.6) as

$$C_{3,L} - C^{(0)}_{3,\infty} = \widehat{A}' i\widehat{D} \frac{1}{1 - i\widehat{\mathcal{B}} i\widehat{D}} \widehat{A} \,, \tag{4.9}$$

where

$$\widehat{A}' \equiv \frac{A'}{3} \langle 1| \,, \tag{4.10}$$

$$\widehat{A} \equiv \frac{A}{3} |1\rangle \,, \tag{4.11}$$

$$\widehat{\mathcal{B}} \equiv \widehat{\overline{\mathcal{B}}}_{2,L} + |1\rangle \frac{\mathcal{B}_3}{9} \langle 1| \,, \tag{4.12}$$

$$\widehat{D} \equiv |1\rangle D \langle 1| \,, \tag{4.13}$$

with

$$\widehat{\overline{\mathcal{B}}}_{2,L} \equiv \mathrm{diag}(\overline{\mathcal{B}}^{(1)}_{2,L}, \overline{\mathcal{B}}^{(2)}_{2,L}, \overline{\mathcal{B}}^{(3)}_{2,L}) \,, \tag{4.14}$$

and the (unnormalized) vector $\langle 1|$ given by

$$\langle 1| \equiv (1,\ 1,\ 1) \,, \qquad |1\rangle \equiv \langle 1|^T \,. \tag{4.15}$$

We stress that all quantities still have implicit momentum indices as well as the explicit flavor indices.

---

[5] Note that there are no diagrams in $\overline{\mathcal{B}}^{(i)}_{2,L} D \overline{\mathcal{B}}^{(i)}_{2,L}$ where the spectator particle switches between the kernels, as this would require two of the three particles in the relevant cut to have the same flavor i.

The extra flavor matrix structure allows us to implement different cuts depending on the nature of the adjacent kernels. Specifically, on-shell projection is effected by rewriting $\widehat{D}$ as

$$\widehat{D} = \widehat{F}_G + \widehat{\delta F}_G \,, \tag{4.16}$$

$$\widehat{F}_G = \begin{pmatrix} \widetilde{F}^{(1)} & \widetilde{G}^{(12)} P_L & P_L \widetilde{G}^{(13)} \\ P_L \widetilde{G}^{(21)} & \widetilde{F}^{(2)} & \widetilde{G}^{(23)} P_L \\ \widetilde{G}^{(31)} P_L & P_L \widetilde{G}^{(32)} & \widetilde{F}^{(3)} \end{pmatrix} , \tag{4.17}$$

$$\widehat{\delta F}_G = \begin{pmatrix} \widetilde{I}_F^{(1)} & \delta\widetilde{G}^{(12)} & \delta\widetilde{G}^{(13)} \\ \delta\widetilde{G}^{(21)} & \widetilde{I}_F^{(2)} & \delta\widetilde{G}^{(23)} \\ \delta\widetilde{G}^{(31)} & \delta\widetilde{G}^{(32)} & \widetilde{I}_F^{(3)} \end{pmatrix} , \tag{4.18}$$

where the objects in $\widehat{F}_G$ project adjacent kernels on shell, while those in $\widehat{\delta F}_G$ are integral operators that sew together adjacent kernels into new infinite-volume quantities. The notation for these objects is the same as in BS1, except that here there are superscripts indicating the flavors of the spectator particles. In particular,

$$\begin{aligned} \left[\widetilde{F}^{(i)}\right]_{p_i \ell' m'; k_i \ell m} = \delta_{\mathbf{p}_i \mathbf{k}_i} \frac{H^{(i)}(\mathbf{p}_i)}{2\omega_{p_i} L^3} \left[\frac{1}{L^3} \sum_{\mathbf{p}_j}^{\text{UV}} - \text{PV} \int^{\text{UV}} \frac{d^3 p_j}{(2\pi)^3} \right] \Bigg\{ \frac{\mathcal{Y}_{\ell' m'}(\mathbf{p}_j^{*(p_i)})}{q_{2,p_i}^{*\ell'}} \\ \times \frac{1}{4\omega_{p_j}\omega_{p_k}(E - \omega_{p_1} - \omega_{p_2} - \omega_{p_3})} \frac{\mathcal{Y}_{\ell m}(\mathbf{p}_j^{*(p_i)})}{q_{2,p_i}^{*\ell}} \Bigg\} \end{aligned} \tag{4.19}$$

is a generalized Lüscher zeta function, and

$$\left[\widetilde{G}^{(ij)}\right]_{p_i \ell' m'; k_j \ell m} = \frac{1}{2\omega_{p_i} L^3} \frac{\mathcal{Y}_{\ell' m'}(\mathbf{k}_j^{*(p_i)})}{q_{2,p_i}^{*\ell'}} \frac{H^{(i)}(\mathbf{p}_i) H^{(j)}(\mathbf{k}_j)}{b_{ij}^2 - m_k^2} \frac{\mathcal{Y}_{\ell m}(\mathbf{p}_i^{*(k_j)})}{q_{2,k_j}^{*\ell}} \frac{1}{2\omega_{k_j} L^3} \tag{4.20}$$

is a generalized switch factor,[6] with the four-vector b_{ij} given by

$$b_{ij} = (E - \omega_{p_i} - \omega_{k_j}, \mathbf{P} - \mathbf{p}_i - \mathbf{k}_j) \,. \tag{4.21}$$

---

[6]Here we are using the relativistic form of the energy denominator, which is an allowed choice, as explained in BS1, and is needed when we construct the fully Lorentz-invariant form of three-particle K matrix below. For $\widetilde{F}^{(i)}$ we keep the nonrelativistic form of the denominator for notational brevity; the change to the relativistic form only changes $\widetilde{F}^{(i)}$ by exponentially suppressed contributions.

The parity operators are a new feature here and are given by

$$[P_L]_{p_i\ell' m';k_i\ell m} = \delta_{p_i\ell' m';k_i\ell m}(-1)^\ell \,. \tag{4.22}$$

The integral operators $\widetilde{I}_F^{(i)}$ and $\delta\widetilde{G}^{(ij)}$ are then defined by the difference $\widehat{D} - \widehat{F}_G$, and explicit forms are not needed. The discussion of their general properties in BS1 remains valid here, and we do not repeat it.

We now explain the notation in Eqs. (C.9) and (C.10). We begin with the matrix indices on both $\widetilde{F}^{(i)}$ and $\widetilde{G}^{(ij)}$, which are of similar form to those used in all previous RFT quantization conditions. A key property of $\widetilde{F}^{(i)}$ and $\widetilde{G}^{(ij)}$ is that they project adjacent kernels—here the elements of $\widehat{\mathcal{B}}$, $\widehat{A}'$, and $\widehat{A}$—on shell. This projection changes the matrix indices from $\{\mathbf{k}\}$ to $\{k_i\ell m\}$, with the latter denoting an on-shell, three-particle state. The new feature for nondegenerate particles is that there are three choices of indices, labeled by $i = 1-3$. Here i is the flavor of the particle chosen as the "spectator," and k_i is shorthand for its momentum, $\mathbf{k}_i$, which is drawn from the finite-volume set. The remaining two ("nonspectator") particles, whose flavors are denoted j and k, are then boosted to their center-of-mass frame (CMF), in which the kernel is decomposed into spherical harmonics. Denoting a generic on-shell kernel by $X(\{\mathbf{k}\})$—this could, for example, be $B_3(\{\mathbf{p}\};\{\mathbf{k}\})$, with the $\{\mathbf{p}\}$ index left implicit, and with $\{\mathbf{k}\}$ restricted so that the three particles are on shell for the given E and $\mathbf{P}$—this decomposition is

$$X(\{\mathbf{k}\}) = \sum_{\ell m} X(\{\mathbf{k}\})_{k_i\ell m}\sqrt{4\pi}Y_{\ell m}(\widehat{\mathbf{k}}_j^{*(k_i)}) \,. \tag{4.23}$$

Here $\widehat{\mathbf{k}}_j^{*(k_i)}$ is the unit vector in the direction of $\mathbf{k}_j^{*(k_i)}$, which itself is the spatial part of the four-vector obtained by boosting $(\omega_{k_j}, \mathbf{k}_j)$ into the CMF of the nonspectator pair. Details of the boost are discussed in Appendix C.1; we stress that, for an on-shell quantity, the two boosts discussed there are equivalent. In Eq. (4.23), we must specify which flavor from the pair is used to define the harmonic decomposition. This is because $\mathbf{k}_j^{*(k_i)} = -\mathbf{k}_k^{*(k_i)}$,

implying that $Y_{\ell m}(\widehat{\mathbf{k}}_j^{*(k_i)}) = (-1)^\ell Y_{\ell m}(\widehat{\mathbf{k}}_k^{*(k_i)})$. Since both even and odd waves are present for nondegenerate particles, the decompositions with respect to flavors j and k differ. Our convention for the decomposition of kernels is that it is done relative to the direction of the particle whose flavor follows cyclically after that of the spectator.

Returning to the definition of $\widetilde{F}^{(i)}$, Eq. (C.9), we note that the spectator flavor is chosen to be i for both incoming (right-hand) and outgoing (left-hand) indices. We follow the convention just described in choosing the flavor used for spherical harmonic decompositions, namely that j follows cyclically after i. Note that, even though $\mathbf{p}_j$ is a dummy variable, this choice has content because it specifies which mass to use when calculating ω_{p_j}. The third momentum, needed to determine ω_{p_k}, is then given by $\mathbf{p}_k = \mathbf{P} - \mathbf{p}_i - \mathbf{p}_j$. The boosted momentum $\mathbf{p}_j^{*(p_i)}$ is defined in the same way as $\mathbf{k}_j^{*(k_i)}$. Here the three particles are in general off shell, so that the two boosts discussed in Appendix C.1 differ. However, as discussed in BS1, the difference leads only to exponentially suppressed shifts in $\widetilde{F}^{(i)}$. The harmonic polynomials are defined by

$$\mathcal{Y}_{\ell m}(\mathbf{a}) = \sqrt{4\pi} Y_{\ell m}(\hat{\mathbf{a}}) |\mathbf{a}|^\ell \,, \tag{4.24}$$

with the spherical harmonics chosen to be in the real basis. The quantity q_{2,p_i}^* is given by

$$4q_{2,p_i}^{*2} = \frac{\lambda(\sigma_i, m_j^2, m_k^2)}{\sigma_i} \,, \tag{4.25}$$

$$\sigma_i = (E - \omega_{p_i})^2 - (\mathbf{P} - \mathbf{p}_i)^2 \,, \tag{4.26}$$

where $\lambda(a,b,c) = a^2 + b^2 + c^2 - 2ab - 2ac - 2bc$ is the standard triangle function. q_{2,p_i}^* is the magnitude of the spatial momenta of each of the interacting pair for fully on-shell kinematics, i.e. if $E = \sum_i \omega_{p_i}$. This requires that the momenta of the pair not lie in the finite-volume set. The superscript UV on the sum and integral in $\widetilde{F}^{(i)}$ indicate an ultraviolet regularization, the nature of which affects $\widetilde{F}^{(i)}$ only at the level of exponentially suppressed terms. The sum over $\mathbf{p}_j$ runs over the finite-volume set, while the integral is defined by the generalized

principal-value (PV) pole prescription introduced in Ref. [36].

Turning now to $\widetilde{G}^{(ij)}$, Eq. (C.10), here the incoming and outgoing spectator indices differ, the former being j and the latter i. In this case the harmonic decompositions are done using a different convention from that used above, so as to conform, in the degenerate limit, with the definitions used in previous RFT works. On the outgoing side, with spectator flavor i, the decomposition is done relative to the direction of the particle of flavor j in the pair CMF, as indicated by the argument of $\mathcal{Y}_{\ell' m'}$ in Eq. (C.10) being $\mathbf{k}_j^{*(p_i)}$. Similarly, with the incoming flavor j, the decomposition is done relative to the direction of the particle of flavor i. In one of these two cases, the ordering is not cyclic, and thus there is a mismatch between the convention used for $\widetilde{G}^{(ij)}$ and the adjacent kernels. The factors of P_L correct this mismatch, as described in more detail shortly. To define the arguments of the harmonic polynomials in $\widetilde{G}^{(ij)}$, we must, at this stage, use the Wu boost, which is one of the two boosts discussed in Appendix C.1.

Both $\widetilde{F}^{(i)}$ and $\widetilde{G}^{(ij)}$ contain the cutoff functions $H^{(i)}(\mathbf{p}_i)$. These are smooth functions whose role is to cut off the sums over spectator momenta in the region where the three particles lie far below threshold. They are generalizations to nondegenerate kinematics of the cutoff function introduced for identical particles in Ref. [28], and their technical properties are discussed in Appendix C.1. We stress two features of these functions. First, their introduction (discussed in detail in BS1) is an intrinsic part of the derivation, and not an ad hoc feature. Second, they introduce a scheme dependence into intermediate quantities that appear in the quantization condition that is derived below, specifically into $\mathcal{K}_2$ and $\widehat{\mathcal{K}}_{\mathrm{df},3}$. This scheme dependence cancels, however, in the spectrum that is predicted by the quantization condition, and in the relation of these intermediate quantities to the three-particle scattering amplitude, $\mathcal{M}_3$.

There are two particularly notable features of these definitions in which they differ from the forms used in BS1 and previous RFT works. The first is that $\widetilde{F}^{(i)}$ does not contain the

symmetry factor 1/2! that is present in the quantity $\widetilde{F}$ defined in BS1. This change arises simply because we are considering nonidentical particles.

The second feature is the presence of the parity matrices P_L. As indicated by Eq. (4.22), these matrices are diagonal in the $\{k_i \ell m\}$ indices—with the flavor i determined by the position in the flavor matrix—and simply give a minus sign for odd values of angular momentum. As announced above, the factors P_L are needed to account for mismatches in the momenta used to decompose into spherical harmonics as part of the on-shell projection. We show how this works by considering two examples. First, consider the following subsequence contained in $C_{3,L}$,

$$\overline{\mathcal{B}}^{(3)}_{2,L} D \overline{\mathcal{B}}^{(1)}_{2,L} D \overline{\mathcal{B}}^{(1)}_{2,L} D \overline{\mathcal{B}}^{(3)}_{2,L} \,. \tag{4.27}$$

Among the terms that arise after inserting the decomposition of Eq. (4.16) is

$$\overline{\mathcal{B}}^{(3)}_{2,L} \widetilde{G}^{(31)} P_L \overline{\mathcal{B}}^{(1)}_{2,L} \widetilde{F}^{(1)} \overline{\mathcal{B}}^{(1)}_{2,L} P_L \widetilde{G}^{(13)} \overline{\mathcal{B}}^{(3)}_{2,L} \,. \tag{4.28}$$

The leftmost P_L is needed because the leftmost $\overline{\mathcal{B}}^{(1)}_{2,L}$ is projected on shell on its left-hand side using $\mathbf{p}_3$ to determine the harmonic decomposition (since this decomposition arises from $\widetilde{G}^{(31)}$), while the right-hand projection is done using $\mathbf{p}_2$ for the harmonic decomposition (since flavor 2 follows cyclically after flavor 1). The P_L converts the left-hand decomposition into that for flavor 2, so that both decompositions match. A mirrored explanation holds for the right-hand factor of P_L.

For the second example we begin with the subsequence

$$\left[\widehat{\mathcal{B}}\widehat{D}\widehat{\mathcal{B}} = \widehat{\mathcal{B}}(\widehat{F}_G + \widehat{\delta F}_G)\widehat{\mathcal{B}}\right]_{ij} \,, \tag{4.29}$$

and pick out the $\mathcal{B}_3$ parts of both $\widehat{\mathcal{B}}$s and the $\widehat{F}_G$ part of $\widehat{D}$. Since $\mathcal{B}_3$ is distributed equally among all elements of $\widehat{\mathcal{B}}$, there are, for a given choice i and j, nine contributions to this quantity, one from each of the elements of $\widehat{F}_G$. We focus on the contribution containing

$\widetilde{G}^{(12)}$. This is given by

$$\tfrac{1}{9}\,[\mathcal{B}_3]_{;p_1\ell'm'}\,\widetilde{G}^{(12)}_{p_1\ell'm';k_2\ell m}(-1)^{\ell}\tfrac{1}{9}\,[\mathcal{B}_3]_{k_2\ell m;}\ , \tag{4.30}$$

where for the sake of clarity, we have shown only the "internal" indices of the $\mathcal{B}_3$s. What we need to explain is why the factor of $(-1)^\ell$, which arises from the P_L on the right of $\widetilde{G}^{(12)}$ in $\widehat{D}$, is needed. To see this we note that, according to the definition of $\widetilde{G}^{(12)}$ given above, the decomposition into spherical harmonics with indices ℓm is done relative to the momentum of the flavor 1 particle (with the flavor 2 being the spectator). By contrast, the harmonic decomposition of the right-hand $\mathcal{B}_3$, which also has spectator flavor 2, is done relative to the momentum of the particle of flavor 3 (using the cyclic convention). This mismatch is corrected by the $(-1)^\ell$. There is no such mismatch for the left-hand $\mathcal{B}_3$, since with a flavor 1 spectator, the harmonics $\ell'm'$ are defined relative to the flavor 2 momentum both in the $\mathcal{B}_3$ and in $\widetilde{G}^{(12)}$. All other factors of P_L in $\widehat{F}_G$ can be understood in a similar fashion. This example also affords an example of the difference between the TOPT approach of BS1 and the original derivation of Ref. [28]. In the latter, the three-particle cut between two $\mathcal{B}_3$ kernels is expressed entirely in terms of $\widetilde{F}$, whereas in the TOPT approach there are both $\widetilde{F}$ and $\widetilde{G}$ contributions. Both are legitimate expressions, but only the latter leads to simple all-orders expressions for $C_{3,L}$.

As a side note, we observe that the matrix $\widehat{F}_G$ is symmetric under the interchange of all indices (i.e. flavor and $\{k\ell m\}$). This is because $[\widetilde{G}^{(ij)}]^{\rm Tr} = [\widetilde{G}^{(ji)}]$, i.e.

$$\left[\widetilde{G}^{(ij)}\right]_{p_i\ell'm';k_j\ell m} = \left[\widetilde{G}^{(ji)}\right]_{k_j\ell m;p_i\ell'm'}\ , \tag{4.31}$$

and because $\widetilde{F}^{(i)}$ is symmetric in its indices. Since $\widehat{D}$ is manifestly symmetric, this implies that $\widehat{\delta F}_G$ is symmetric. By construction, $\widehat{\mathcal{B}}$ is also symmetric.

We now insert the decomposition of Eq. (4.16) into our result for the correlator, Eq. (4.9).

After some rearrangement, this leads to

$$C_{3,L} - C_{3,\infty}^{(0)} = \widehat{A}'_F i\widehat{F}_G \frac{1}{1 - i\widehat{\mathcal{K}}_{\mathrm{df},23,L} i\widehat{F}_G} \widehat{A}_F \,, \tag{4.32}$$

where the new endcaps are

$$\widehat{A}_F = \frac{1}{1 - i\widehat{\mathcal{B}}\, i\widehat{\delta F}_G} \widehat{A} \,, \tag{4.33}$$

$$\widehat{A}'_F = \widehat{A}' \frac{1}{1 - i\widehat{\delta F}_G\, i\widehat{\mathcal{B}}} \,, \tag{4.34}$$

while[7]

$$i\widehat{\mathcal{K}}_{\mathrm{df},23,L} = i\widehat{\mathcal{B}} \frac{1}{1 - i\widehat{\delta F}_G\, i\widehat{\mathcal{B}}} \,. \tag{4.35}$$

Although these three definitions work both off and on shell, in Eq. (4.32) these quantities always appear adjacent to factors of $\widehat{F}_G$, and are thus always projected on shell. In the following we consider only the on-shell forms.

From the result for the correlator, Eq. (4.32), we can read off the quantization condition

$$\det\left[1 + \widehat{\mathcal{K}}_{\mathrm{df},23,L} \widehat{F}_G\right] = 0 \,. \tag{4.36}$$

This has a similar form to that for identical particles obtained in BS1, a similarity that is made clearer if one replaces $\widehat{F}_G$ with the equivalent $\widehat{F} + \widehat{G}$. Here, however, the determinant runs over both the on-shell indices and the additional 3 flavor dimensions. It is important to keep in mind that, in this expression, different decompositions of the on-shell momenta are being used for the different indices of the matrices $\widehat{\mathcal{K}}_{\mathrm{df},23,L}$ and $\widehat{F}_G$. If the index is i, then the momentum of the corresponding flavor is the spectator.[8] We also note that, at this stage, we can change the boost used in defining $\widetilde{G}^{(ij)}$ to that used in Ref. [28] (referred to below as

[7] When evaluating the terms in the geometric series in Eq. (4.34) one must do the integrals associated with the integral operators contained in $\widehat{\delta F}_G$. Those in $\widetilde{I}_F^{(i)}$ involve a PV prescription, and must be done first, leaving the integrals implicit in the $\delta\widetilde{G}^{(ij)}$ for second. The latter do not require a pole prescription.

[8] This implies that, in general, the number of values of $\mathbf{k}_i$ that lie below the cutoff depends on i.

the HS boost), since this change can be absorbed by a shift in the integral operators $\delta\widetilde{G}^{(ij)}$.

In order to make the content of the quantization condition clearer, it is useful to unpack $\widehat{\mathcal{K}}_{\mathrm{df},23,L}$. As the name suggests,[9] this contains both two- and three-particle K matrices—real functions of the kinematic variables that are devoid of unitary cuts. The subscript "df" stands for "divergence-free," and indicates the absence of singularities related to exchanging a particle between two pairs. This name is inherited from the Feynman-diagram approach of Refs. [28, 29]; within the TOPT framework the absence of such divergences follows from their factorization into $\widehat{F}_G$. To pull out the part containing only two-particle K matrices, we set $\mathcal{B}_3$ and the $\delta G^{(ij)}$ to zero, leaving

$$\widehat{\mathcal{K}}_{\mathrm{df},23,L}\Big|_{\mathcal{B}_3=\delta G^{(ij)}=0} = \mathrm{diag}\left(\overline{\mathcal{K}}_{2,L}^{(1)}, \overline{\mathcal{K}}_{2,L}^{(2)}, \overline{\mathcal{K}}_{2,L}^{(3)}\right) \equiv \widehat{\overline{\mathcal{K}}}_{2,L}\,, \tag{4.37}$$

where

$$i\overline{\mathcal{K}}_{2,L}^{(i)} = i\overline{\mathcal{B}}_{2,L}^{(i)} \frac{1}{1 - i\widetilde{I}_F^{(i)} i\overline{\mathcal{B}}_{2,L}^{(i)}}\,. \tag{4.38}$$

As shown in Appendix B of BS1, $\overline{\mathcal{K}}_{2,L}^{(i)}$ can be written

$$\left[\overline{\mathcal{K}}_{2,L}^{(i)}\right]_{p_i\ell' m';k_i\ell m} = 2\omega_{k_i} L^3 \delta_{\mathbf{p}_i\mathbf{k}_i}\delta_{\ell'\ell}\delta_{m'm}\mathcal{K}_{2,\ell}^{(i)}(q_{2,k_i}^*)\,, \tag{4.39}$$

where $\mathcal{K}_{2,\ell}^{(i)}$ is the ℓth partial wave of the infinite-volume two-particle K matrix involving scattering of flavors j and k. These K matrices depend on the details of the PV pole prescription, as described explicitly in BS1. In general, all partial waves are nonzero, unlike for identical particles, where only even waves are present.

The remainder of $\widehat{\mathcal{K}}_{\mathrm{df},23,L}$ involves all three particles, either through alternating factors of $\overline{\mathcal{K}}_{2,L}^{(i)}$ and $\delta G^{(ij)}$, or through factors of $\mathcal{B}_3$. We call it $\widehat{\mathcal{K}}_{\mathrm{df},3}$, and stress that all entries of this flavor matrix are nonzero. An explicit expression can be given, but is not illuminating.

---

[9] In BS1, we added tildes to quantities that were composed of TOPT (rather than Feynman-diagram-based) kernels, but here we drop the tildes to lighten the notation (given the presence of hats). Kernels defined in terms of Feynman diagrams, to be discussed below, are denoted by primes.

Thus we simply define it by

$$\widehat{\mathcal{K}}_{\mathrm{df},23,L} = \widehat{\overline{\mathcal{K}}}_{2,L} + \widehat{\mathcal{K}}_{\mathrm{df},3} \,. \tag{4.40}$$

An important property of $\widehat{\mathcal{K}}_{\mathrm{df},3}$ is that, for all of its elements, one can take the $L \to \infty$ limit, up to exponentially suppressed corrections. As explained in BS1, this holds only if one chooses the PV scheme such that there are no poles in any of the $\mathcal{K}_{2,\ell}^{(i)}$ in the kinematic region of interest. This is possible with the generalized PV prescription of Ref. [36].[10] We also note that $\widehat{\mathcal{K}}_{\mathrm{df},3}$ is a symmetric matrix.

The elements of the matrix $\widehat{\mathcal{K}}_{\mathrm{df},3}$ have a similar status to the asymmetric quantity $\widetilde{\mathcal{K}}_{\mathrm{df},3}^{(u,u)}$ entering the alternate form of the RFT quantization condition derived in BS1. It is for this reason that we refer to $\widehat{\mathcal{K}}_{\mathrm{df},3}$ as an asymmetric (or, perhaps better, "unsymmetrized") K matrix, and the quantization condition itself as asymmetric. The nine flavor elements of $\widehat{\mathcal{K}}_{\mathrm{df},3}$ are distinguished by the nature of the external two-particle interaction for both initial and final states—the ij'th element has incoming spectator flavor j and outgoing spectator flavor i.[11] By contrast, the full three-particle scattering amplitude $\mathcal{M}_3$, discussed in the next section, is obtained by summing over all choices of initial and final spectators. This raises the question of whether the quantization condition can be written in terms of a similarly summed K matrix. This would be the analog of rewriting the alternate form of the quantization condition in terms of a symmetrized $\widetilde{\mathcal{K}}_{\mathrm{df},3}$, which is achieved in BS1, and leads to the original form obtained in Ref. [28]. This is achieved below in Sec. 4.8.

[10] We note that the freedom to treat each value of ℓ differently in this prescription extends also to allowing different prescriptions for each spectator flavor.

[11] Note that, because of the factor of $\mathcal{B}_3/9$ in the matrix $\widehat{\mathcal{B}}$ [see Eq. (4.12)], the external TOPT kernel can also be $\mathcal{B}_3$, which is symmetric.

4.5 *Relation of $\widehat{\mathcal{K}}_{\mathrm{df},3}$ to $\mathcal{M}_3$*

All three-particle formalisms require a second step, in which the three-particle K matrix that enters the quantization condition is related by integral equations to the physical three-particle scattering amplitude $\mathcal{M}_3$. This is necessary because the intermediate K matrix, despite being an infinite-volume quantity, is not physical, since it depends on the cutoff function and PV prescription. In this section we derive the form of the integral equations, using the method of Ref. [29]. This begins by considering the finite-volume scattering amplitude, $\mathcal{M}_{3,L}$, expressing it in terms of $\widehat{\mathcal{K}}_{\mathrm{df},3}$, and taking an appropriate $L \to \infty$ limit in order to obtain an expression for $\mathcal{M}_3$.

As for $\widehat{\mathcal{K}}_{\mathrm{df},23,L}$, simpler expressions are obtained by using a combination of two- and three-particle amplitudes, specifically

$$\mathcal{M}_{23,L} = \overline{\mathcal{M}}_{2,L}^{(1)} + \overline{\mathcal{M}}_{2,L}^{(2)} + \overline{\mathcal{M}}_{2,L}^{(3)} + \mathcal{M}_{3,L}\,, \tag{4.41}$$

where $\overline{\mathcal{M}}_{2,L}^{(i)}$ corresponds to the scattering of flavors j and k with i spectating. It is given by

$$i\overline{\mathcal{M}}_{2,L}^{(i)} = i\overline{\mathcal{K}}_{2,L}^{(i)} \frac{1}{1 - i\widetilde{F}^{(i)} i\overline{\mathcal{K}}_{2,L}^{(i)}}\,, \tag{4.42}$$

which is the nondegenerate generalization of Eq. (B3) from BS1.

The diagrams contributing to the off-shell $\mathcal{M}_{23,L}$ in TOPT are shown in Fig. 4.2 and lead to

$$i\mathcal{M}_{23,L}^{\mathrm{off}} = i(\overline{\mathcal{B}}_{2,L}^{(1)} + \overline{\mathcal{B}}_{2,L}^{(2)} + \overline{\mathcal{B}}_{2,L}^{(3)} + \mathcal{B}_3) \sum_{n=0}^{\infty} \left[iDi(\overline{\mathcal{B}}_{2,L}^{(1)} + \overline{\mathcal{B}}_{2,L}^{(2)} + \overline{\mathcal{B}}_{2,L}^{(3)} + \mathcal{B}_3) \right]^n . \tag{4.43}$$

This can be written compactly in matrix notation

$$\mathcal{M}_{23,L}^{\mathrm{off}} = \langle 1 |\, \widehat{\mathcal{M}}_{23,L}^{\mathrm{off}} \,| 1 \rangle\,, \tag{4.44}$$

with

$$i\widehat{\mathcal{M}}_{23,L}^{\mathrm{off}} = i\widehat{\mathcal{B}} \frac{1}{1 - i\widehat{D} i\widehat{\mathcal{B}}}\,. \tag{4.45}$$

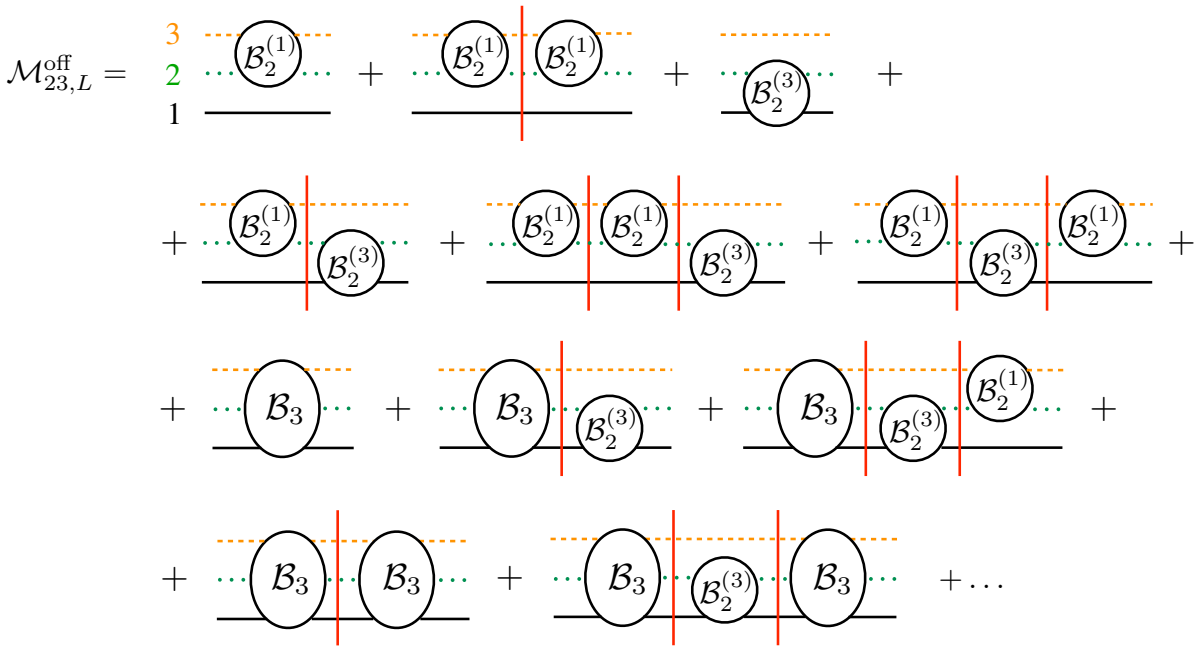

Figure 4.2: Contributions to the combined two- and three-particle finite-volume scattering amplitude $\mathcal{M}_{23,L}$ in TOPT. Notation as in Fig. 4.1. The absence of diagrams involving the two-particle kernel $\mathcal{B}_2^{(2)}$ is for representational simplicity—such diagrams are contained in the ellipsis.

The nine flavor elements of $\widehat{\mathcal{M}}^{\text{off}}_{23,L}$ are the analogs of the asymmetric amplitude $\overline{\mathcal{M}}_{2,L}+\widetilde{\mathcal{M}}^{(u,u)}_{3,L}$ appearing in the degenerate case analyzed in BS1. As for $\widehat{\mathcal{K}}_{\text{df},3}$, they correspond to the different choices of the initial and final spectator flavors. Summing over the different choices, as in Eq. (4.44), gives $\mathcal{M}^{\text{off}}_{23,L}$.

The next step is to consider the on-shell amplitude, and insert the decomposition Eq. (4.16). After some rearrangement this leads to the simple result (using the notation that the amplitude is on shell unless there is an explicit superscript "off")

$$i\widehat{\mathcal{M}}_{23,L} = i\widehat{\mathcal{K}}_{\text{df},23,L}\frac{1}{1 - i\widehat{F}_G i\widehat{\mathcal{K}}_{\text{df},23,L}}\,, \tag{4.46}$$

with $\widehat{\mathcal{K}}_{\mathrm{df},23,L}$ given in Eq. (4.35). The key point here is that the same two- and three-particle K matrices enter as in the quantization condition. We stress again that different on-shell projections are used for different flavor indices. This means that the elements of the matrix cannot be combined as in Eq. (4.44), to give an on-shell $\mathcal{M}_{23,L}$. Indeed, even if we multiply by spherical harmonics to convert the ℓm indices back into momenta, the elements of $\widehat{\mathcal{M}}_{23,L}$ cannot be combined for finite L, since the on-shell projection moves some momenta out of the finite-volume set. Such a combination is possible only in the infinite-volume limit, which, however, is all that we require below.

We next unpack the result (4.46) in order to extract a result for the three-particle amplitude itself. First, we package the finite-volume two-particle amplitudes into matrix form

$$\widehat{\overline{\mathcal{M}}}_{2,L} \equiv \mathrm{diag}(\overline{\mathcal{M}}_{2,L}^{(1)}, \overline{\mathcal{M}}_{2,L}^{(2)}, \overline{\mathcal{M}}_{2,L}^{(3)}) \,. \tag{4.47}$$

Next, we separate $\widehat{F}_G$, given in Eq. (4.17), into its $\widetilde{F}$ and $\widetilde{G}$ parts:

$$\widehat{F}_G = \widehat{F} + \widehat{G} \,, \tag{4.48}$$

with the diagonal terms contained in

$$\widehat{F} = \mathrm{diag}(\widetilde{F}^{(1)}, \widetilde{F}^{(2)}, \widetilde{F}^{(3)}) \,, \tag{4.49}$$

and the off-diagonal terms contained in $\widehat{G}$. Then Eq. (4.42) becomes

$$i\widehat{\overline{\mathcal{M}}}_{2,L} = i\widehat{\overline{\mathcal{K}}}_{2,L} \frac{1}{1 - i\widehat{F} i\widehat{\overline{\mathcal{K}}}_{2,L}} \,. \tag{4.50}$$

The matrix version of $\mathcal{M}_{3,L}$ is given by

$$\widehat{\mathcal{M}}_{3,L} \equiv \widehat{\mathcal{M}}_{23,L} - \widehat{\overline{\mathcal{M}}}_{2,L} \,, \tag{4.51}$$

and is related schematically to the full scattering amplitude by $\mathcal{M}_{3,L} = \langle 1 | \, \widehat{\mathcal{M}}_{3,L} \, | 1 \rangle$. As noted above, this equation only makes sense in the infinite-volume limit, after multiplying by appropriate spherical harmonics and summing over angular-momentum indices.

With this setup, the algebraic steps needed to obtain an expression for $\widehat{\mathcal{M}}_{3,L}$ are identical to those in BS1 (and given explicitly in Appendix C of that work). We find

$$i\widehat{\mathcal{M}}_{3,L} = i\widehat{\mathcal{D}}_L + i\widehat{\mathcal{M}}_{\mathrm{df},3,L}\,, \tag{4.52}$$

$$i\widehat{\mathcal{D}}_L = i\widehat{\overline{\mathcal{M}}}_{2,L} i\widehat{G} i\widehat{\overline{\mathcal{M}}}_{2,L} \frac{1}{1 - i\widehat{G} i\widehat{\overline{\mathcal{M}}}_{2,L}}\,, \tag{4.53}$$

$$i\widehat{\mathcal{M}}_{\mathrm{df},3,L} = \left[1 + i\widehat{\mathcal{D}}_{23,L} i\widehat{F}_G\right] i\widehat{\mathcal{K}}_{\mathrm{df},3} \frac{1}{1 - [1 + i\widehat{F}_G i\widehat{\mathcal{D}}_{23,L}] i\widehat{F}_G i\widehat{\mathcal{K}}_{\mathrm{df},3}} \left[1 + i\widehat{F}_G i\widehat{\mathcal{D}}_{23,L}\right]\,, \tag{4.54}$$

$$i\widehat{\mathcal{D}}_{23,L} = i\widehat{\overline{\mathcal{M}}}_{2,L} + i\widehat{\mathcal{D}}_L = i\widehat{\overline{\mathcal{M}}}_{2,L} \frac{1}{1 - i\widehat{G} i\widehat{\overline{\mathcal{M}}}_{2,L}}\,. \tag{4.55}$$

In the appropriate $L \to \infty$ limit [29] these results become integral equations for $\widehat{\mathcal{M}}_3$. We do not give these explicitly, since their form is almost identical to those arising in the Feynman diagram derivation, and we present the latter in full detail in Sec. 4.7 below.

It is worth understanding the source of the various terms contributing to $\widehat{\mathcal{M}}_{3,L}$ in Eqs. (4.52)-(4.55). $\widehat{D}_L$ is the contribution to three-particle scattering arising from repeated two-particle interactions, connected by the switch factors in $\widehat{G}$, arising from the diagrams on the second line of Fig. 4.2. The off-diagonal nature of $\widehat{G}$ enforces the switching of spectators, and the matrix structure ensures that all possible switches occur. Up to kinematical factors, $\overline{\mathcal{M}}_{2,L}^{(i)}$ goes over in the infinite-volume limit to the Lorentz-invariant two-particle scattering amplitude involving flavors j and k, $\mathcal{M}_2^{(i)}$ (see Appendix E of BS1). It follows that, if the relativistic form of $\widetilde{G}$ is used, the elements of $\widetilde{\mathcal{D}}_L^{(u,u)}$ are Lorentz invariant.[12]

The remaining part of $\widehat{\mathcal{M}}_{3,L}$ is denoted $\widehat{\mathcal{M}}_{\mathrm{df},3,L}$, where the subscript df indicates the "divergence-free" nature of this object, since the poles corresponding to on-shell one-particle exchange are contained in $\widehat{\mathcal{D}}^{(u,u)}$. $\widehat{\mathcal{M}}_{\mathrm{df},3,L}$ contains the contributions to three-particle scattering that involve the three-particle K matrix, $\widehat{\mathcal{K}}_{\mathrm{df},3}$. In words, the external factors in square braces correspond to repeated two-particle interactions with switches, prior to a gen-

[12] Strictly speaking, since all quantities in the quantization conditions carry indices $\{\mathbf{k}, \ell, m\}$, one must first multiply by the appropriate spherical harmonics in order to obtain a quantity whose Lorentz transformation properties can be studied. See Refs. [28] and BS1 for more details.

uine quasilocal three-particle interaction due to an element of $\widehat{\mathcal{K}}_{\mathrm{df},3}$, after which the middle section of Eq. (4.54) corresponds to repeated two-particle interactions prior to another three-particle interaction, etc. This is all a natural and simple generalization of the interpretation of the corresponding expression for identical particles.

We see from the result (4.54) that the elements of $\widehat{\mathcal{K}}_{\mathrm{df},3}$ are not Lorentz invariant. This is because, when $L \to \infty$, the set of integral equations that this matrix equation goes over to connects it to $\widehat{\mathcal{M}}_{\mathrm{df},3}$, whose elements are not Lorentz invariant because they are defined in TOPT. As noted in the introduction, the lack of Lorentz invariance of $\widehat{\mathcal{K}}_{\mathrm{df},3}$ is expected in the TOPT approach. This leads to complications when implementing the formalism in practice, and in the next section we explain how this problem can be resolved.

We close this section by emphasizing that we can use the expression (4.46) for $\widehat{\mathcal{M}}_{23,L}$ as an alternative vehicle for deriving the quantization condition. This possibility was first noted in Ref. [29] in the context of identical particles. The point is that $\mathcal{M}_{23,L}$ is a type of finite-volume correlator, so its poles determine the spectrum. Indeed, from the form of the denominator in Eq. (4.46) we immediately obtain the quantization condition obtained in the previous section, Eq. (4.36). One might be concerned that, since $\mathcal{M}_{23,L}$ contains $\widehat{\overline{\mathcal{M}}}_{2,L}$, there will also be poles at the positions where the latter quantity diverges. This occurs at energies of a free spectator combined with a two-particle finite-volume state, and these energies are not in the three-particle spectrum. It turns out, however, that these spurious poles cancel in $\mathcal{M}_{23,L}$, as can be seen by writing it as

$$\widehat{\mathcal{M}}_{23,L} = \widehat{\mathcal{D}}_{23,L} + \widehat{\mathcal{M}}_{\mathrm{df},3,L}\,, \tag{4.56}$$

and noting, from Eq. (4.55), that $\widehat{\mathcal{D}}_{23,L}$ remains finite when $\widehat{\overline{\mathcal{M}}}_{2,L}$ diverges. We stress that the quantization condition arising from the poles in $\widehat{\mathcal{M}}_{\mathrm{df},3,L}$ is indeed Eq. (4.36). This can be most easily seen by rewriting Eq. (4.54) using

$$1 + i\widehat{F}_G i\widehat{\mathcal{D}}_{23,L} = \left(1 + \widehat{F}_G \widehat{\overline{\mathcal{K}}}_{2,L}\right)^{-1}, \tag{4.57}$$

from which it follows that

$$i\widehat{\mathcal{M}}_{\mathrm{df},3,L} = \left[1 + i\widehat{\mathcal{D}}_{23,L} i\widehat{F}_G\right] i\widehat{\mathcal{K}}_{\mathrm{df},3} \frac{1}{1 + \widehat{F}_G \widehat{\mathcal{K}}_{\mathrm{df},23,L}} \,. \tag{4.58}$$

4.6 Quantization condition with Lorentz-invariant $\mathcal{K}_{\mathrm{df},3}$

In this section we derive the following alternate form for the quantization condition for nondegenerate scalars,

$$\det\left[1 + \widehat{\mathcal{K}}'_{\mathrm{df},23,L} \widehat{F}_G\right] = 0 \,, \tag{4.59}$$

where

$$\widehat{\mathcal{K}}'_{\mathrm{df},23,L} = \widehat{\overline{\mathcal{K}}}_{2,L} + \widehat{\mathcal{K}}'_{\mathrm{df},3} \,. \tag{4.60}$$

Here $\widehat{\overline{\mathcal{K}}}_{2,L}$ the same as above [see Eq. (4.37)], but now $\widehat{\mathcal{K}}'_{\mathrm{df},3}$ is a (matrix of) Lorentz-invariant three-particle K matrices that differs from $\widehat{\mathcal{K}}_{\mathrm{df},3}$. In this way, we obtain a fully Lorentz-invariant formalism: one that not only is valid for relativistic kinematics, but in which the elements of $\widehat{\mathcal{K}}'_{\mathrm{df},3}$ are Lorentz scalars. This is important for practical implementations, which typically use multiple values of $\mathbf{P}$, and thus require the relationship between $\widehat{\mathcal{K}}'_{\mathrm{df},3}$ in different Lorentz frames.

A striking feature of this result is that the quantization condition (7.33) has exactly the same form as that derived above using TOPT, Eq. (4.36), differing only in the K matrix that enters. This redundancy is of the same nature as that found in the identical-particle case in BS1, where two identical forms of the quantization condition were established, both involving asymmetric K matrices, one of which is Lorentz invariant while the other is not. This was understood as being due to the intrinsic ambiguity in the definition of an asymmetric object, since the only constraint is that by combining terms one ends up with the correct symmetrized quantity. An analogous understanding applies here: it is only by summing over the different choices of flavors of the external spectators for, say, the elements of $\widehat{\mathcal{M}}_{3,L}$ that

one obtains the physical amplitude, and thus there is some freedom in the definition of the individual elements. The same holds for the K matrices. Examples of this ambiguity will be seen in the subsequent discussion.

In BS1, we obtained the form of the quantization condition containing the Lorentz-invariant asymmetric K matrix by starting from the result derived using Feynman diagrams in Ref. [28]. Here there is no such result, so we must begin *de novo*. Our strategy is to reorganize the original Feynman-diagram-based approach of Ref. [28] into a form that mirrors the TOPT result at every step, so that, after setting up the calculation, we can simply carry over the algebra of the TOPT approach described above. In addition, we derive the quantization condition using the Feynman diagram version of the finite-volume amplitude $\widehat{\mathcal{M}}_{23,L}$, rather than the correlator $C_{3,L}$. As shown in the previous section, this leads to the same quantization condition, but avoids the need to deal with endcaps.

The starting point is the finite-volume three-particle amplitude with external spectators having flavors i and j. We refer to such amplitudes as "asymmetric," as it is only after summing the nine combinations of $\{i, j\}$ that we obtain the full amplitude. In the previous section we considered the asymmetric amplitude $[\widehat{\mathcal{M}}_{3,L}]_{ij}$, with its asymmetry defined using TOPT diagrams. Here we define the asymmetry using Feynman diagrams, leading to a different asymmetric amplitude $[\widehat{\mathcal{M}}'^{\text{off}}_{3,L}]_{ij}(\{p\};\{k\})$, where $\{p\} \equiv \{p_1, p_2, p_3\}$, etc. are sets of three four-momenta, and we are using the notation that a prime denotes quantities defined using Feynman diagrams. The external three-momenta are drawn from the finite-volume set, but at this stage the external energies are arbitrary, so that the four-momenta are in general off shell. Momentum conservation implies that the four-momenta satisfy $\sum_i p_i = P = \sum_j k_j$.

As explained in Ref. [28], when using Feynman diagrams, the amplitudes are given by a

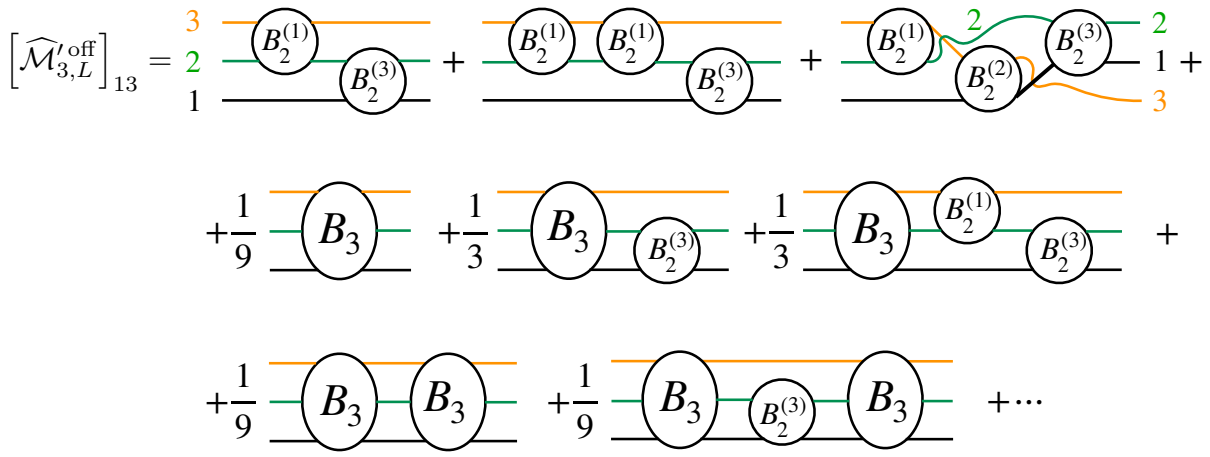

Figure 4.3: Contributions to $[\widehat{\mathcal{M}}'^{\,\mathrm{off}}_{3,L}]_{13}$ in the Feynman-diagram skeleton expansion. $B_2^{(i)}$ and B_3 are Bethe-Salpeter kernels, and solid lines represent fully dressed propagators. Unlike in earlier figures, all propagators are shown by solid lines, with the flavors now distinguished only by colors and explicit labels. External propagators are amputated.

skeleton expansion in terms of the Bethe-Salpeter kernels[13]

$$B_2^{(i)}(p_j, p_k; k_j, k_k) \quad \text{and} \quad B_3(\{p\}; \{k\})\,. \tag{4.61}$$

These are, respectively, the 2PIs and 3PIs two- and three-particle kernels, with the former having flavor i as the spectator, and with flavor labels $\{i, j, k\}$ ordered cyclically. In the skeleton expansion the kernels can be evaluated in infinite volume. In contrast to the TOPT kernels given in Eq. (4.3), $B_2^{(i)}$ and B_3 depend on four-momenta that are, in general, off shell. They are connected by fully dressed, relativistic propagators, normalized to unity at the single-particle pole, whose spatial momenta must be summed over the finite-volume set, while the energy is integrated as usual. External propagators are amputated. For a given quantity, the set of skeleton diagrams that contributes is exactly the same as in the expansion

[13] At the risk of confusion, we use the same letter for these kernels as for the corresponding TOPT objects, but without the calligraphic font.

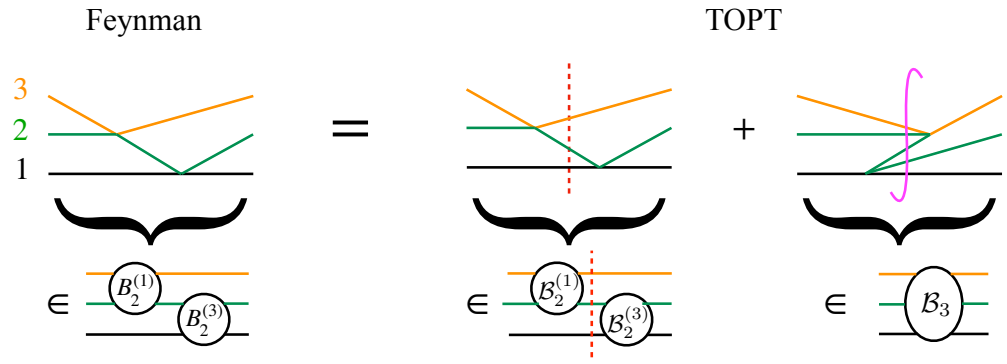

Figure 4.4: Example of how a Feynman diagram, which is assigned to one term in the corresponding skeleton expansion, breaks up into several (in this case two) TOPT diagrams, which are in turn assigned to several (here two) terms in the TOPT skeleton expansion. As discussed in the text, this implies that the asymmetric TOPT amplitudes $[\widehat{\mathcal{M}}_{3,L}]_{ij}$ are not Lorentz invariant. Notation is as in Figs. 4.1, 4.2 and 4.3, except that all propagators are shown by solid lines.

in TOPT kernels (see, e.g., Fig. 4.2), except that there is no time ordering. As a concrete example, we show diagrams that contribute to $[\widehat{\mathcal{M}}'^{\rm off}_{3,L}]_{13}$ in Fig. 4.3. This amplitude is defined so that, if there is a two-particle Bethe-Salpeter kernel on the left (right) end, it must be a $B_2^{(1)}$ ($B_2^{(3)}$). In addition, for each end with a B_3 kernel the contribution is multiplied by 1/3. The latter factors ensure that, when the flavor indices are summed, the contribution to the total amplitude has the correct weight.

To make clear that the elements of $\widehat{\mathcal{M}}'_{3,L}$ differ from those of the TOPT version, $\widehat{\mathcal{M}}_{3,L}$, we consider in Fig. 4.4 the simplest contribution to the first diagram in Fig. 4.3. In TOPT, it breaks into two diagrams, one of which contributes to $[\widehat{\mathcal{M}}_{3,L}]_{13}$, and the other of which is split equally between all elements of $\widehat{\mathcal{M}}_{3,L}$ (since it contributes to $\mathcal{B}_3$). Thus only 1/9th of the diagram is included in $[\widehat{\mathcal{M}}_{3,L}]_{13}$. This also shows that the latter quantity is not Lorentz invariant, since it is only by adding the two TOPT diagrams with equal weight that one regains an invariant quantity. On the other hand, each of the elements of $\widehat{\mathcal{M}}'^{\rm off}_{3,L}$ is Lorentz

invariant, simply because it is composed of Feynman diagrams.

We now begin the analysis of the elements of $\widehat{\mathcal{M}}_{3,L}^{\prime\,\mathrm{off}}$. Our approach quickly diverges from that in Refs. [28, 29], so that we cannot make a step-by-step comparison, but will rather emphasize global similarities and differences. We present an overview of the derivation in the main text, and describe the details in Appendix B.2.

In both approaches, the first step when analyzing a given diagram is to do the energy integrals for all independent momenta, i.e. those not constrained by four-momentum conservation. The difference from Refs. [28, 29] is that here we do such integrals for all diagrams before proceeding to the second step, rather than analyzing subsets of diagrams completely and then combining. As explained in Appendix B.2, the results of the energy integrals are diagrams in which two of the three particles in all cuts are on shell, i.e. with momenta $p_i^{\mathrm{on}} = (\omega_{p_i}, \mathbf{p}_i)$, while the momentum of the third particle remains, in general, off shell. The momentum configuration is then specified in the same way as in the TOPT analysis, namely with the (redundant) set of three finite-volume momenta $\{\mathbf{k}\}$. In order to present the result in a compact form, we need to introduce operators that specify which pair of momenta in the kernels are placed on shell. We call these $\overleftarrow{O}^{(i)}$ and $\overrightarrow{O}^{(i)}$, where the flavor label i indicates that the particles of the other two flavors are set on shell, and the arrow indicates whether the operator acts on the kernels immediately to the left or right, respectively. With this

notation, we find

$$\widehat{\mathcal{M}}'^{\text{off}}_{3,L} = \widehat{\mathcal{M}}'^{\text{off}}_{23,L} - \widehat{\overline{\mathcal{M}}}'^{\text{off}}_{2,L} \,, \tag{4.62}$$

$$i\widehat{\mathcal{M}}'^{\text{off}}_{23,L} = \widehat{\overrightarrow{O}} i\widehat{B} \frac{1}{1 - i\widehat{D}' i\widehat{B}} \widehat{\overleftarrow{O}} \,, \tag{4.63}$$

$$\widehat{\overrightarrow{O}} = \text{diag}\left(\overrightarrow{O}^{(3)}, \overrightarrow{O}^{(1)}, \overrightarrow{O}^{(2)}\right) \,, \tag{4.64}$$

$$\widehat{\overleftarrow{O}} = \text{diag}\left(\overleftarrow{O}^{(3)}, \overleftarrow{O}^{(1)}, \overleftarrow{O}^{(2)}\right) \,, \tag{4.65}$$

$$[\widehat{B}]_{i'i} = \tfrac{1}{9} B_3 + \delta B_3^{(i'i)} + \delta_{i'i} \left[\overline{B}^{(i)}_{2,L} + \overline{\delta B}^{(i)}_{2,L}\right] \,, \tag{4.66}$$

$$\widehat{D'} = \mathbb{1}_{\mathbf{p},\mathbf{k}} \begin{pmatrix} D'^{(3)} & D'^{(3)} & D'^{(2)} \\ D'^{(3)} & D'^{(1)} & D'^{(1)} \\ D'^{(2)} & D'^{(1)} & D'^{(2)} \end{pmatrix} \,, \tag{4.67}$$

$$D'^{(i)} = \overleftarrow{O}^{(i)} \frac{1}{4\omega_{p_j}\omega_{p_k} L^6} \frac{Z_i(p_i^2)}{p_i^2 - m_i^2} \overrightarrow{O}^{(i)} \,. \tag{4.68}$$

We observe that, with this result, we have succeeded in obtaining an expression for the finite-volume amplitude that is similar to the initial matrix form obtained with TOPT, Eq. (4.45).

There are many features of this rather elaborate result that require explanation. We first discuss the effect of the on-shell projectors that are contained in the $D'^{(i)}$ and also appear as external factors in $\widehat{\mathcal{M}}'^{\text{off}}_{23,L}$. When we expand out the geometric series in Eqs. (4.63), the kernels in $\widehat{B}$ are always projected on both sides, and thus we need only define the projected kernels. For B_3 and δB_3 all combinations of projectors can occur, and their action is exemplified by

$$\left[\overrightarrow{O}^{(1)} B_3 \overleftarrow{O}^{(3)}\right](\{\mathbf{p}\};\{\mathbf{k}\}) = B_3(p_1, p_2^{\text{on}}, p_3^{\text{on}}; k_1^{\text{on}}, k_2^{\text{on}}, k_3) \,. \tag{4.69}$$

For the two-particle kernels, the possible projections are restricted.[14] To explain this, we focus on $\overline{B}^{(1)}_{2,L}$. Due to the forms of $\widehat{\overrightarrow{O}}$, $\widehat{\overleftarrow{O}}$, and $\widehat{D'}$, the projection operators acting on $\overline{B}^{(1)}_{2,L}$

[14] In order that all appearances of $B_2^{(i)}$ have projectors on both sides, we have, in Eq. (4.63), placed projectors on both ends of the expression. Strictly speaking this means that $\widehat{\mathcal{M}}'^{\text{off}}_{3,L}$ has external momenta that are only partly off shell, differing from the original definition given above where all momenta can be off shell. Since we only consider the former quantity in the following, we have kept the same notation.

are either $\overrightarrow{O}^{(3)}$ or $\overrightarrow{O}^{(2)}$ on the left, and either $\overleftarrow{O}^{(3)}$ or $\overleftarrow{O}^{(2)}$ on the right. Thus the spectator, with flavor 1, is always on shell, whereas the second on-shell flavor is either 2 or 3. The definitions that we need are thus

$$\left[\overrightarrow{O}^{(3)}\overline{B}_{2,L}^{(1)}\overleftarrow{O}^{(3)}\right](\{\mathbf{p}\};\{\mathbf{k}\}) = \delta_{\mathbf{p}_1\mathbf{k}_1} 2\omega_{p_1} L^3 B_2(p_2^{\rm on}, p_3; k_2^{\rm on}, k_3)\,, \tag{4.70}$$

$$\left[\overrightarrow{O}^{(3)}\overline{B}_{2,L}^{(1)}\overleftarrow{O}^{(2)}\right](\{\mathbf{p}\};\{\mathbf{k}\}) = \delta_{\mathbf{p}_1\mathbf{k}_1} 2\omega_{p_1} L^3 B_2(p_2^{\rm on}, p_3; k_2, k_3^{\rm on})\,, \tag{4.71}$$

$$\left[\overrightarrow{O}^{(2)}\overline{B}_{2,L}^{(1)}\overleftarrow{O}^{(3)}\right](\{\mathbf{p}\};\{\mathbf{k}\}) = \delta_{\mathbf{p}_1\mathbf{k}_1} 2\omega_{p_1} L^3 B_2(p_2, p_3^{\rm on}; k_2^{\rm on}, k_3)\,, \tag{4.72}$$

$$\left[\overrightarrow{O}^{(2)}\overline{B}_{2,L}^{(1)}\overleftarrow{O}^{(2)}\right](\{\mathbf{p}\};\{\mathbf{k}\}) = \delta_{\mathbf{p}_1\mathbf{k}_1} 2\omega_{p_1} L^3 B_2(p_2, p_3^{\rm on}; k_2, k_3^{\rm on})\,. \tag{4.73}$$

The generalization to other elements of $\overline{B}_{2,L}^{(i)}$ and $\overline{\delta B}_{2,L}^{(i)}$ is straightforward. We stress that it is only because of the presence of the projection operators that we obtain a quantity that depends on three-momenta alone.

Next we give the definition of $\widehat{\overline{\mathcal{M}}}_{2,L}^{\prime\,\rm off}$. This is a diagonal matrix obtained by keeping the disconnected terms in $\widehat{\mathcal{M}}_{23,L}^{\prime\,\rm off}$, i.e. those obtained by keeping only the $\overline{B}_{2,L}^{(i)} + \overline{\delta B}_{2,L}^{(i)}$ parts of $\widehat{B}$ and the diagonal part of $\widehat{D}'$. Thus one particle spectates for the entire diagram. The projection rules embedded in the definitions imply that this particle is on shell, and that, if it has flavor i, then the second on-shell particle (which is one of the interacting pair) has the flavor that follows i cyclically. The sum of all the diagrams contributing to $[\widehat{\overline{\mathcal{M}}}_{2,L}^{\prime\,\rm off}]_{ii}$ is simply a rearrangement of the complete set of Feynman diagrams that describe the interactions of particles with flavors j and k. Additionally, the factors of $2\omega_{p_i}L^3$ cancel in pairs, leaving a single overall such factor. Thus we find that $\widehat{\overline{\mathcal{M}}}_{2,L}^{\prime\,\rm off}$ has the same form as $\widehat{\overline{\mathcal{M}}}_{2,L}$, Eq. (4.47), except that one each of the incoming and outgoing scattered particles are off shell. The reason that $\widehat{\overline{\mathcal{M}}}_{2,L}^{\prime\,\rm off}$ is added to $\widehat{\mathcal{M}}_{3,L}^{\prime}$ is the same as in the TOPT analysis: it leads to a quantity, $\widehat{\mathcal{M}}_{23,L}^{\prime\,\rm off}$, that has a simple expression, here Eq. (4.63).

One difference between the structure of the results here and those obtained in TOPT is the presence of the shifts δB_3 and δB_2 in the kernels. As shown in Appendix B.2, these

arise from off-shell contributions to the energy integrals. They are associated with particular elements of $\widehat{B}$, and are not distributed equally like B_3 [see Eq. (4.66)]. This structure is needed to ensure that $\widehat{\mathcal{M}}'^{\rm off}_{3,L}$ is unchanged, and thus, in particular, remains Lorentz invariant. We do not have explicit, all-orders expressions for δB_3 and δB_2, but this does not hinder the derivation.

Finally we discuss the form of $\widehat{D}'$, Eq. (4.67). This is the analog in the present derivation of the matrix $\widehat{D}$ defined in Eq. (4.13). The difference here is that the elements of the matrix differ, due to the presence of on-shell projectors and the Feynman propagator for the off-shell particle. The flavor structure of $\widehat{D}'$ reflects that which appears in the second stage of the TOPT derivation, namely the decomposition of $\widehat{D}$ given in Eqs. (4.16)–(4.18). It turns out that this decomposition must be introduced at the first stage in the Feynman approach. The final difference is the presence here of the wavefunction renormalization factor Z_i multiplying the pole. As noted above, this equals unity on shell, $Z_i(m_i^2) = 1$. In the TOPT analysis, the corresponding factor is absorbed into the kernels in a preparatory stage, as explained in Appendix A of BS1.[15]

We now turn to the second step in the analysis of the Feynman skeleton expansion. In this step, we project the three-particle state fully on shell using the $\{k_i \ell m\}$ variables described above. Since we have set up the intermediate states with two on-shell particles, the on-shell projection involves adjusting momenta so that the third is placed on shell. This is very similar to the procedure in the TOPT analysis, where we have to adjust momenta so that the three already-on-shell particles have total energy E. Indeed, as explained in BS1, the on-shell projection in the TOPT case can be done by a small variation of the method of Ref. [28] used in the Feynman-diagram analysis. In particular, near the pole in $D'^{(i)}$ [Eq. (4.68)], we

[15]The same approach could be used here, but is not necessary, as we can account for the presence of Z_i in the next step in the analysis.

have

$$p_i^2 - m_i^2 \xrightarrow{p_i^0 \to \omega_{p_i}} 2\omega_{p_i}(E - \omega_{p_1} - \omega_{p_2} - \omega_{p_3}) + \mathcal{O}\left[(E - \omega_{p_1} - \omega_{p_2} - \omega_{p_3})^2\right] , \tag{4.74}$$

so that the kinematic factor in $D'^{(i)}$ has the same residue at the pole as that in D [Eq. (8.8)]. This allows us to mirror the decomposition of $\widehat{D}$, Eqs. (4.16)–(4.18), and write

$$\widehat{D}' = \widehat{F}_G + \widehat{\delta F'}_G \, , \tag{4.75}$$

with $\widehat{F}_G$ exactly as in Eq. (4.17) above (with a technical restriction described below). The residue matrix $\widehat{\delta F'}_G$ differs from that in the TOPT analysis due to both the presence of the Z_i in Eq. (4.68) and the fact that the off-shellness of the kernels is different. The former factor can be dealt with by writing it as $1 + [Z_i(p_i^2) - 1]$, with the second term canceling the pole (since Z_i is an analytic function near $p_i^2 - m_i^2$) and thus only contributing to a shift in the residue matrix $\widehat{\delta F'}_G$. The difference in this matrix is not important, however, as it does not impact the subsequent algebraic manipulations.

The technical restriction on $\widehat{F}_G$ is that, in order for the final quantization condition to contain a Lorentz-invariant three-particle K matrix, we must, in the expression for $\widetilde{G}^{(ij)}$, boost to the pair CMF using the original boost of Ref. [28] rather than that introduced in BS1. This point is explained in detail in Appendix C.1.

To fully justify Eq. (4.75), we need to explain how the on-shell projection operators contained in $D'^{(i)}$, Eq. (4.68), lead to the factors of P_L in $\widehat{F}_G$, Eq. (4.17). First we note that, when the kernels $B_2^{(i)}$ and B_3 are set fully on shell, we must choose a convention for the variables $\{k_i \ell m\}$ that are used. We follow the convention of the TOPT analysis: if the flavor index is i, then the spectator has flavor i and the spherical harmonics are defined relative to the direction of the momentum of the particle of flavor j (in the pair CMF), where j follows cyclically after i. We note that projectors in $\widehat{D}'$ are set up so that the spectator is always on shell. For example, the first row of $\widehat{D}'$ has projectors $\overleftarrow{O}^{(3)}$ and $\overleftarrow{O}^{(2)}$, both of which set flavor 1 on shell, while the third row contains $\overleftarrow{O}^{(2)}$ and $\overleftarrow{O}^{(1)}$, both of which set

flavor 3 on shell. What does not always match, however, is the flavor of the particle that determines the spherical harmonic decomposition. We discuss this by considering the first row of $\widehat{D'}$ and focusing on the left-hand harmonic indices. Considering the first row again, the first element, $D'^{(3)}$, will be replaced after projection with $\widetilde{F}^{(1)}$, in which the harmonics are determined relative to flavor 2, which matches the convention of the element $[\widehat{B}]_{x1}$ on the left (with x an arbitrary flavor). The same is true for the second element, also $D'^{(3)}$, which will be replaced with $\widetilde{G}^{(12)}$, for which the harmonics of the left index are also determined relative to flavor 2. However, the third element, $D'^{(2)}$, is replaced by $\widetilde{G}^{(13)}$, for which the harmonics are determined by the particle of flavor 3, which does not match that used for $[\widehat{B}]_{x1}$. Indeed, the associated projector, $\overleftarrow{O}^{(2)}$, sets flavor 3 on shell first so as to match the projection enforced by $\widetilde{G}^{(13)}$. The end result is that the projection applied to $[\widehat{B}]_{x1}$ conflicts with the convention defined above. In order to bring them into agreement, a factor of $(-1)^\ell$ is needed, and this is provided by the P_L multiplying $\widetilde{G}^{(13)}$ on the left in the $[\widehat{F}_G]_{13}$. A similar analysis explains all other appearances of P_L in $\widehat{F}_G$.

Given the decomposition of Eq. (4.75), the remaining steps are algebraically identical to those of the previous section. In particular, if we set the elements of $\widehat{\mathcal{M}}'_{23,L}$ fully on shell using the same convention as just described for the kernels, then we obtain

$$i\widehat{\mathcal{M}}'_{23,L} = i\widehat{\mathcal{K}}'_{\mathrm{df},23,L}\frac{1}{1 - i\widehat{F}_G i\widehat{\mathcal{K}}'_{\mathrm{df},23,L}}\,, \tag{4.76}$$

with

$$i\widehat{\mathcal{K}}'_{\mathrm{df},23,L} = i\widehat{B}\frac{1}{1 - i\widehat{\delta F'}_G\, i\widehat{B}}\,, \tag{4.77}$$

where we are implicitly setting the external coordinates of $\widehat{B}$ on shell. These are identical in form to Eqs. (4.46) and (4.35), respectively. From Eq. (4.76) we immediately obtain the claimed form of the quantization condition, Eq. (7.33). In this way we have achieved our goal of recasting the analysis of the Feynman-diagram-based skeleton expansion in a form

that mirrors that of the TOPT approach.

4.7 *Relation of* $\widehat{\mathcal{K}}'_{\mathrm{df},3}$ *to* $\mathcal{M}_3$

In this section we derive the relationship of $\widehat{\mathcal{K}}'_{\mathrm{df},3}$ to the physical infinite-volume amplitude, $\mathcal{M}_3$. Unlike for the TOPT case discussed above, we do so here in complete detail. The utility of this result is twofold: first, it will be needed in any application of the formalism derived in this paper that aims to predict $\mathcal{M}_3$ from the finite-volume spectrum; second, it allows us to demonstrate that, expressed in the appropriate basis, the elements of $\widehat{\mathcal{K}}'_{\mathrm{df},3}$ are Lorentz invariant.

The method we use follows that first introduced in Ref. [29], and extended to the TOPT-based analysis in Appendix E of BS1. Since we have reformulated the Feynman-diagram-based approach to mirror that using TOPT, many of the results from BS1 can be taken over almost unchanged. The main change is the need to take care of the additional flavor indices.

As in the TOPT analysis, we first pull out the divergence-free finite-volume amplitude using

$$\widehat{\mathcal{M}}'_{23,L} = \widehat{\mathcal{D}}_{23,L} + \widehat{\mathcal{M}}'_{\mathrm{df},3,L}\,. \tag{4.78}$$

This has the same form as Eq. (4.46), and includes the same quantity $\widehat{\mathcal{D}}_{23,L}$—the difference is the presence of primes on the other two objects. No primes are needed on $\widehat{\mathcal{D}}_{23,L}$ because, as can be seen from its definition in Eq. (4.55), it depends only on the on-shell two-particle scattering amplitude, and this is the same whether calculated using TOPT or Feynman diagrams.

Starting from the result for $\widehat{\mathcal{M}}'_{23,L}$ given in Eq. (4.76), we then use the same algebraic steps used above to obtain Eq. (4.54). These are given explicitly in BS1, and lead to

$$i\widehat{\mathcal{M}}'_{\mathrm{df},3,L} = \left[1 + i\widehat{\mathcal{D}}_{23,L} i\widehat{F}_G\right] i\widehat{\mathcal{K}}'_{\mathrm{df},3} \frac{1}{1 - [1 + i\widehat{F}_G i\widehat{\mathcal{D}}_{23,L}] i\widehat{F}_G i\widehat{\mathcal{K}}'_{\mathrm{df},3}} \left[1 + i\widehat{F}_G i\widehat{\mathcal{D}}_{23,L}\right]. \tag{4.79}$$

We now take the $L \to \infty$ limit of $\widehat{\mathcal{M}}'_{\mathrm{df},3,L}$, using the $i\epsilon$ prescription of Ref. [29]. This means that sums over spectator momenta with the singular summands contained in $\widehat{F}_G$ go over to integrals with the poles shifted by the usual $i\epsilon$ prescription. Specifically, since all sums come with associated factors of $(2\omega L^3)^{-1}$, the integrals that result come with Lorentz-invariant measure

$$\sum_{\mathbf{k}} \frac{1}{2\omega_k L^3} \xrightarrow{L\to\infty} \int \frac{d^3k}{2\omega_k (2\pi)^3} \equiv \int_{\mathbf{k}} . \tag{4.80}$$

The sums over flavor and angular momentum indices remain.

Taking the limit in this way, the elements of $\widehat{\mathcal{M}}'_{\mathrm{df},3,L}$ go over to functions of momenta,

$$\left[\left[\widehat{\mathcal{M}}'_{\mathrm{df},3,L}\right]_{ij}\right]_{p_i \ell' m'; k_j \ell m} \xrightarrow{L\to\infty} \left[\widehat{\mathcal{M}}'_{\mathrm{df},3}\right]_{ij} (\mathbf{p}_i, \mathbf{k}_j)_{\ell' m'; \ell m} . \tag{4.81}$$

Here we have made all matrix indices explicit, including the spectator-flavor indices i and j, and used a nested structure because the choice of spectator momenta depends on the flavor indices. An analogous limit holds for the elements of $\widehat{\mathcal{D}}_{23,L}$, which go over to elements of $\widehat{\mathcal{D}}_{23}$. For the elements of the K matrix $\widehat{\mathcal{K}}'_{\mathrm{df},3}$, which are already infinite-volume quantities, one simply replaces discrete momenta with their continuous counterparts, leading to a form like the right-hand side of Eq. (4.81). We also need the limit

$$\left[\left[\widehat{\mathcal{M}}_{2,L}\right]_{ij}\right]_{p_i \ell' m'; k_j \ell m} \xrightarrow{L\to\infty} \left[\widehat{\mathcal{M}}_2\right]_{ij} (\mathbf{p}_i, \mathbf{k}_j)_{\ell' m'; \ell m} \equiv \delta_{ij} \overline{\delta}(\mathbf{p}_i - \mathbf{k}_i) \delta_{\ell' \ell} \delta_{m' m} \mathcal{M}^{(i)}_{2,\ell}(q^*_{2,k_i}) , \tag{4.82}$$

where $\mathcal{M}^{(i)}_{2,\ell}$ is the ℓth partial wave two-particle scattering amplitude for flavors j and k, and

$$\overline{\delta}(\mathbf{p} - \mathbf{k}) \equiv 2\omega_k (2\pi)^3 \delta^3(\mathbf{p} - \mathbf{k}) . \tag{4.83}$$

To obtain smooth limits of the elements of $\widehat{F}_G$, we need to introduce the diagonal matrix $\widehat{2\omega}$ with elements

$$\left[\left[\widehat{2\omega}\right]_{ij}\right]_{p_i \ell' m'; k_j \ell m} = \delta_{ij} \delta_{\mathbf{p}_i \mathbf{k}_j} \delta_{\ell' \ell} \delta_{m' m} 2\omega_{k_j} , \tag{4.84}$$

in terms of which

$$\widehat{2\omega}L^3\widehat{F}_G\widehat{2\omega}L^3 \xrightarrow{L\to\infty} \widehat{F}_G^\infty \equiv \widehat{F}^\infty + \widehat{G}^\infty \,. \tag{4.85}$$

The nonvanishing elements of the diagonal matrix $\widehat{F}^\infty$ are

$$\left[\widehat{F}^\infty\right]_{ii}(\mathbf{p}_i,\mathbf{k}_i)_{\ell' m';\ell m} = \overline{\delta}(\mathbf{p}_i-\mathbf{k}_i)\delta_{\ell'\ell}\delta_{m' m}\widetilde{\rho}^{(i)}_{\mathrm{PV},\ell}(q^*_{2,k_i}) \tag{4.86}$$

with $\widetilde{\rho}^{(i)}_{\mathrm{PV},\ell}$ a modified phase-space factor, defined by the nondegenerate generalization of Eq. (B6) of BS1. The nonvanishing elements of the off-diagonal matrix $\widehat{G}^\infty$ are

$$\left[\widehat{G}^\infty\right]_{ij}(\mathbf{p}_i,\mathbf{k}_j)_{\ell' m';\ell m} = \frac{\mathcal{Y}_{\ell' m'}(\mathbf{k}_j^{*(p_i)})}{q^{*\ell'}_{2,p_i}}\frac{H^{(i)}(\mathbf{p}_i)H^{(j)}(\mathbf{k}_j)}{b_{ij}^2-m_k^2+i\epsilon}\frac{\mathcal{Y}_{\ell m}(\mathbf{p}_i^{*(k_j)})}{q^{*\ell}_{2,k_j}} \,. \tag{4.87}$$

with $i\neq j$ and $b_{ij}=P-p_i^{\mathrm{on}}-k_j^{\mathrm{on}}$.

With this notation in hand, we can now take the $L\to\infty$ limit of Eq. (4.79). We write the results in a compact notation in which all indices, namely $\{j\mathbf{k}_j\ell m\}$, are implicit, and in which internal indices are implicitly either summed (for $\{j\ell m\}$) or integrated (for $\{\mathbf{k}_j\}$), the latter with measure (4.80). First we note that the limit of $\widehat{\mathcal{D}}_{23,L}$ satisfies

$$\widehat{\mathcal{D}}_{23} = \widehat{\overline{\mathcal{M}}}_2 - \widehat{\overline{\mathcal{M}}}_2\widehat{G}^\infty\widehat{\mathcal{D}}_{23} \,, \tag{4.88}$$

which is a set of coupled integral equations. The core geometric series in the center of the expression (4.79) becomes an integral equation for a new matrix quantity that we denote $\widehat{\mathcal{T}}'$, and which has the same implicit dependencies as $\widehat{\mathcal{M}}'_{\mathrm{df},3}$ and $\widehat{\mathcal{K}}'_{\mathrm{df},3}$,

$$\widehat{\mathcal{T}}' = \widehat{\mathcal{K}}'_{\mathrm{df},3} - \widehat{\mathcal{K}}'_{\mathrm{df},3}\left[1-\widehat{F}_G^\infty\widehat{\mathcal{D}}_{23}\right]i\widehat{F}_G^\infty\widehat{\mathcal{T}}' \,. \tag{4.89}$$

Combining these ingredients we have

$$\widehat{\mathcal{M}}'_{\mathrm{df},3} = \left(1-\widehat{\mathcal{D}}_{23}\widehat{F}_G^\infty\right)\widehat{\mathcal{T}}'\left(1-\widehat{F}_G^\infty\widehat{\mathcal{D}}_{23}\right) , \tag{4.90}$$

in which integral operators are applied to both sides of $\widehat{\mathcal{T}}'$. Here 1 is the identity operator in the full matrix space.

To reconstruct the full asymmetric scattering amplitude, we must add back in the part that contains the divergences,

$$\widehat{\mathcal{M}}'_3 = \lim_{L\to\infty} \widehat{\mathcal{M}}'_{3,L} = \widehat{\mathcal{M}}'_{\mathrm{df},3} + \widehat{\mathcal{D}}\,, \tag{4.91}$$

$$\widehat{\mathcal{D}} = \lim_{L\to\infty} \widehat{\mathcal{D}}_L = \widehat{\mathcal{D}}_{23} - \widehat{\overline{\mathcal{M}}}_2\,, \tag{4.92}$$

where $\widehat{\mathcal{D}}_L$ is defined in Eq. (4.53). To combine the elements of $\widehat{\mathcal{M}}'_3$ into the full scattering amplitude $\mathcal{M}_3$, we need first to convert all elements of this matrix to the same kinematic variables, namely those of Eq. (4.4). This is done by multiplying by the appropriate spherical harmonics and summing over angular momentum indices:

$$\left[\widehat{\mathcal{M}}'_3\right]_{i'i}(\{\mathbf{p}\};\{\mathbf{k}\}) = \sum_{\ell',m',\ell,m} \sqrt{4\pi} Y_{\ell' m'}(\widehat{\mathbf{p}}^{*(p_{i'})}_{j'}) \left\{\left[\widehat{\mathcal{M}}'_3\right]_{i'i}(\mathbf{p}_{i'},\mathbf{k}_i)_{\ell' m';\ell m}\right\} \sqrt{4\pi} Y_{\ell m}(\widehat{\mathbf{k}}^{*(k_i)}_{j}) \,. \tag{4.93}$$

Here j (j') is the flavor that follows i (i') in cyclic order. We have changed variables on the left-hand side to those in the original frame, and abused notation by using the same name for the resulting matrix as that on the right-hand side. The two quantities are distinguished by their argument. We obtain the full scattering amplitude by summing the elements of the resulting matrix

$$\mathcal{M}_3(\{\mathbf{p}\};\{\mathbf{k}\}) = \langle 1|\, \widehat{\mathcal{M}}'_3(\{\mathbf{p}\};\{\mathbf{k}\})\, |1\rangle \ . \tag{4.94}$$

We note that no prime is needed for $\mathcal{M}_3$ since one obtains the same result whether decomposing into TOPT or Feynman diagrams. We recall that this result holds for the fully on-shell amplitude.

We now return to the issue of the Lorentz invariance of $\widehat{\mathcal{K}}'_{\mathrm{df},3}$. The arguments we give are an elaboration of those first described in Ref. [34]. By construction, all elements of the flavor matrix $\widehat{\mathcal{M}}'_3$ are Lorentz invariant, since they are defined as sums of Feynman diagrams. This holds only when the amplitude is combined with spherical harmonics, as in Eq. (4.93). What we need, however, are the transformation properties of amplitudes expressed in the $\{\mathbf{k}_i \ell m\}$

basis, since this is what enters relations such as Eq. (4.90). The amplitudes in this basis are not invariant under rotations, since they depend on an arbitrary choice of quantization axis (conventionally the z axis). Instead, they transform under rotations by multiplication by appropriate Wigner D matrices, due to the standard result

$$Y_{\ell m}(R\hat{n}) = \sum_{m'} \mathcal{D}^{(\ell)}_{mm'}(R) Y_{\ell m'}(\hat{n})\,. \tag{4.95}$$

This rather trivial dependence also leads to a dependence on boosts, as follows. Consider a momentum configuration $\{\mathbf{k}\}$ and choose $\mathbf{k}_1$ to be the spectator momentum. To define the coordinates $\{\mathbf{k}_1 \ell m\}$ we must boost to the 23 pair CMF and then decompose into harmonics. Now imagine that we first do an overall boost of the initial configuration, leading to momenta $\{\mathbf{k}'\}$. This time the spectator momentum is $\mathbf{k}'_1$. When we boost to the CMF of the 23 pair, we end up in the same frame as before, except for an overall rotation. This is simply because a product of two boosts can be written as a single boost combined with a rotation. This implies that the elements of $\widehat{\mathcal{M}}'_3$ in the $\{\mathbf{k}_i \ell m\}$ basis will transform with Wigner matrices that depend on the choice of flavor index and on the spectator momentum. In the following, we refer to these transformation properties in as "standard." Any flavor matrix in the $\{\mathbf{k}\ell m\}$ basis that has standard transformation properties will yield a Lorentz-invariant amplitude when combined with harmonics as in Eq. (4.90).

We now argue that the standard transformation properties of $\widehat{\mathcal{M}}'_3$ are reproduced by Eqs. (4.90) and (4.91) if the elements of $\widehat{\mathcal{K}}'_{\text{df},3}$ themselves transform in the standard way. First we note that the elements of $\widehat{\overline{\mathcal{M}}}_2$ have standard transformation properties since the underlying amplitude $\mathcal{M}_2$ and the quantity $\overline{\delta}(\mathbf{p}-\mathbf{k})$ are both Lorentz invariant. Next we argue that the elements of $\widehat{D}_{23}$, given by Eq. (4.88), transform in the standard way. Iteratively expanding this equation yields an alternating series of factors of $\widehat{\overline{\mathcal{M}}}_2$ and $\widehat{G}^{\infty}$. From Eq. (4.87), we see that all quantities in $\widehat{G}^{\infty}$ are Lorentz invariant (q^*_{2,p_i}, b^2_{ij}, $|\mathbf{k}^{*(p_i)}_j|$, etc. and the cutoff functions) except for the directions of $\mathbf{k}^{*(p_i)}_j$ and $\mathbf{p}^{*(k_j)}_i$. These vectors

will, in general, be rotated if an overall boost is first applied, due to the above-discussed properties of successive boosts. This rotation of the vectors leads to a multiplication of the corresponding ℓm indices by appropriate Wigner D matrices. However, these D matrices cancel those arising from the standard transformation of the adjacent elements of $\widehat{\mathcal{M}}_2$. The key point here is that the same rotation appears for contracted indices, since the same boost to the pair CMF is used. Due to this cancellation, only the external Wigner D matrices survive—those associated with the external indices of the factors of $\widehat{\mathcal{M}}_2$ on the ends of the chain. Thus $\widehat{D}_{23}$ indeed has standard transformation properties.

The remainder of the argument follows in a similar way. The only additional result that we need is the transformation property of the $\widehat{F}^{\infty}$ part of $\widehat{F}_G^{\infty}$. From Eq. (4.86), we see that the elements of $\widehat{F}^{\infty}$ are, in fact, invariant under rotations and boosts. This implies that Wigner D matrices arising from amplitudes on the two sides of each element of $\widehat{F}^{\infty}$ cancel. Together with the result for $\widehat{G}^{\infty}$ discussed above, this implies that any sequence of amplitudes with standard transformation properties alternating with factors of $\widehat{F}_G^{\infty}$ will itself have standard transformation properties. Thus, using Eq. (4.89), if $\widehat{\mathcal{K}}'_{\mathrm{df},3}$ has standard transformations, it follows that $\widehat{\mathcal{T}}'$ does as well, and, using Eq. (4.90), the same holds for $\widehat{\mathcal{M}}'_{\mathrm{df},3}$. Finally, using Eqs. (4.91) and (4.92), and the standard transformation properties of $\widehat{\mathcal{D}}_{23}$ and $\widehat{\mathcal{M}}_2$, we find that $\widehat{\mathcal{M}}'_3$ transforms in the standard way, which is the desired result.

To complete the discussion we need to show that, if $\widehat{\mathcal{K}}'_{\mathrm{df},3}$ does not transform in the standard way, then neither does $\widehat{\mathcal{M}}'_3$. This seems highly plausible, since the above-described cancellation of Wigner D matrices would no longer occur. Another way of making this argument is to invert the relationship between $\widehat{\mathcal{M}}'_3$ and $\widehat{\mathcal{K}}'_{\mathrm{df},3}$, i.e. to determine the latter from the former. This can be done, for example, by first inverting Eq. (4.79) in finite volume, and then taking the $L \to \infty$ limit. This leads to an expression involving inverses of integral operators. By expanding out the inverses in geometric series, the relationship one obtains always involves sums of products of the amplitudes $\widehat{\mathcal{M}}'_{\mathrm{df},3}$ and $\widehat{D}_{23}$ alternating

with factors of $\widehat{F}_G^{\infty}$, and these preserve standard transformation properties. Thus we claim that $\widehat{\mathcal{K}}'_{\mathrm{df},3}$ does transform in the standard way, and therefore that, when it is combined with harmonics as in Eq. (4.93), its elements will be Lorentz invariant.

4.8 Symmetric form of the quantization condition

In this section we describe the derivation of our third and final form of the quantization condition, Eq. (6.1). This is written in terms of a single Lorentz-invariant three-particle K matrix, $\widetilde{\mathcal{K}}_{\mathrm{df},3}$, which has no flavor indices, and which we thus call symmetric. To obtain the new form we follow steps analogous to those used in BS1 to connect the asymmetric and symmetric forms of the quantization condition for identical particles, with suitable generalizations for nondegenerate particles. In addition, we provide the integral equations relating $\mathcal{M}_3$ to $\widetilde{\mathcal{K}}_{\mathrm{df},3}$, Eq. (4.122).

4.8.1 Symmetrization operators

$\widetilde{\mathcal{K}}_{\mathrm{df},3}$ is obtained by symmetrizing a modified version of $\widehat{\mathcal{K}}'_{\mathrm{df},3}$. We have already encountered symmetrization when constructing $\mathcal{M}_3$ in Eq. (4.94), but here we give more details, and introduce some helpful notation. In particular, we define the symmetrization operators $\overrightarrow{\mathcal{S}}$ and $\overleftarrow{\mathcal{S}}$, which play a central role in the final step of the derivation.

The symmetrization operators act on vectors in flavor space, e.g. the row vector $X_j = [\widehat{\mathcal{K}}'_{\mathrm{df},3}]_{ij}$ with i fixed. In our notation, the index j plays two roles. First, it labels the element of the vector, and in general the three elements are different. Second, it determines the coordinates that are used to describe the on-shell amplitude, with the jth element using coordinates $\{k_j \ell m\}$. Symmetrization acts on the underlying elements, but not on the coordinates, and so these two roles of the index must be decoupled. Here we use $X_j(\{\mathbf{k}\})$ to describe the underlying element, which depends on the on-shell momenta $\{\mathbf{k}\}$, and make

coordinates explicit,

$$\mathbf{X} = (X_1(\{\mathbf{k}\})_{k_1\ell m}, X_2(\{\mathbf{k}\})_{k_2\ell m}, X_3(\{\mathbf{k}\})_{k_3\ell m}) \ . \tag{4.96}$$

We recall that the relation between an underlying infinite-volume on-shell quantity $X(\{\mathbf{k}\})$ and its expression in terms of coordinates $\{k_j\ell m\}$ is given by Eq. (4.23). An example of this notation is the expression for the underlying quantity $X_2(\{\mathbf{k}\})$ in terms of the coordinates $\{k_1\ell m\}$,

$$X_2(\{\mathbf{k}\}) = \sum_{\ell m} X_2(\{\mathbf{k}\})_{k_1\ell m}\sqrt{4\pi}Y_{\ell m}(\widehat{\mathbf{k}}_2^{*(k_1)}) \, . \tag{4.97}$$

The left-acting symmetrization operator is defined by

$$\mathbf{X}\overleftarrow{\mathcal{S}} \equiv (X_\Sigma(\{\mathbf{k}\})_{k_1\ell m}, X_\Sigma(\{\mathbf{k}\})_{k_2\ell m}, X_\Sigma(\{\mathbf{k}\})_{k_3\ell m}) \ , \tag{4.98}$$

$$X_\Sigma(\{\mathbf{k}\}) = X_1(\{\mathbf{k}\}) + X_2(\{\mathbf{k}\}) + X_3(\{\mathbf{k}\}) \, . \tag{4.99}$$

The key point is that the same underlying element appears in all positions, but is expressed in terms of different coordinates. The right-acting operator $\overrightarrow{\mathcal{S}}$ is defined analogously for column vectors. We stress that this definition relies on the fact that the underlying elements are infinite-volume functions, defined for all $\{\mathbf{k}\}$, rather than finite-volume objects defined only for momenta in the finite-volume set.

4.8.2 Symmetrization identities

In BS1, three "asymmetrization" identities [Eqs. (102)-(104) of that work] were derived and used to convert the symmetric, identical-particle quantization condition of Ref. [28] into an asymmetric form. Here we use a generalization of these identities to move in the other direction, from the asymmetric to the symmetric form. Thus we refer to them in this work as symmetrization identities.

These identities apply when factors of $\widehat{F}_G$ lie between two matrix amplitudes, e.g. $\widehat{\mathcal{D}}_{23,L}$ and $\widehat{\mathcal{K}}'_{\mathrm{df},3}$. To simplify the presentation, and without loss of generality, we consider the case

where $\widehat{F}_G$ lies between a row vector $\mathbf{X}$ and a column vector $\mathbf{Z}$. The identities are then

$$\mathbf{X}\widehat{F}_G\mathbf{Z} = \mathbf{X}\widehat{F}\overrightarrow{\mathcal{S}}\mathbf{Z} + \mathbf{X}\overrightarrow{\widehat{\mathcal{I}}}_G\mathbf{Z}\,, \tag{4.100}$$

$$= \mathbf{X}\overleftarrow{\mathcal{S}}\widehat{F}\mathbf{Z} + \mathbf{X}\overleftarrow{\widehat{\mathcal{I}}}_G\mathbf{Z}\,, \tag{4.101}$$

$$= \tfrac{1}{3}\mathbf{X}\overleftarrow{\mathcal{S}}\widehat{F}\overrightarrow{\mathcal{S}}\mathbf{Z} + \mathbf{X}\widehat{\mathcal{I}}_{FG}\mathbf{Z}\,. \tag{4.102}$$

As usual, these hold up to exponentially suppressed corrections. The key aspect of these results is that the $\widehat{G}$ contribution to $\widehat{F}_G = \widehat{F} + \widehat{G}$ on the left-hand side can be replaced by one or more symmetrization operators on the right-hand sides, aside from integral operators $\overrightarrow{\widehat{\mathcal{I}}}_G$, $\overleftarrow{\widehat{\mathcal{I}}}_G$, and $\widehat{\mathcal{I}}_{FG}$, which sew together the two vectors into an extended infinite-volume quantity.

The derivation of these identities is sketched in Appendix B.3. We also provide there the definitions of the integral operators.

4.8.3 Applying the symmetrization identities

We wish to apply the identities to the result obtained above for $\widehat{\mathcal{M}}'_{\mathrm{df},3,L}$, Eq. (4.79). The nontrivial aspect of the resulting manipulations is dealing with the integral operators on the right-hand sides of the identities, namely $\overrightarrow{\widehat{\mathcal{I}}}_G$, $\overleftarrow{\widehat{\mathcal{I}}}_G$, and $\widehat{\mathcal{I}}_{FG}$. The steps that we follow mirror the approach taken in BS1 [see Eqs. (105)-(107) and (112)-(113) of that work], although in that work we were using the identities to asymmetrize a symmetric form, while here we are working in the opposite direction.

We begin by introducing an intermediate "decorated" K matrix given by

$$i\widehat{\mathcal{K}}''_{\mathrm{df},3} = i\widehat{\mathcal{Z}}\frac{1}{1 + \left[-i\widehat{\mathcal{I}}_{FG} + i\overleftarrow{\widehat{\mathcal{I}}}_G i\widehat{\mathcal{K}}_{2,L} i\overrightarrow{\widehat{\mathcal{I}}}_G\right] i\widehat{\mathcal{Z}}}\,, \tag{4.103}$$

where

$$i\widehat{\mathcal{Z}} \equiv \frac{1}{1 - i\widehat{\mathcal{K}}_{2,L} i\overrightarrow{\widehat{\mathcal{I}}}_G} i\widehat{\mathcal{K}}'_{\mathrm{df},3} \frac{1}{1 - i\overleftarrow{\widehat{\mathcal{I}}}_G i\widehat{\mathcal{K}}_{2,L}}\,. \tag{4.104}$$

We stress that, although these equations are written in terms of finite-volume matrices, they are equivalent to infinite-volume integral equations, up to exponentially suppressed corrections. This is because the decorations themselves involve integral operators, and because we have chosen a generalized PV prescription such that the two-particle K matrix $\mathcal{K}_2$ has no poles.

We now rewrite $\widehat{\mathcal{M}}'_{\mathrm{df},3}$ in terms of $\widehat{\mathcal{K}}''_{\mathrm{df},3}$. Using the steps sketched in Appendix B.4, we find

$$i\widehat{\mathcal{M}}'_{\mathrm{df},3,L} = \left[1 + i\widehat{\mathcal{D}}_{23,L} i(\widehat{F}_G - \overrightarrow{\widehat{\mathcal{I}}}_G)\right] i\widehat{\mathcal{T}}_L \left[1 + i(\widehat{F}_G - \overleftarrow{\widehat{\mathcal{I}}}_G) i\widehat{\mathcal{D}}_{23,L}\right] , \tag{4.105}$$

where

$$i\widehat{\mathcal{T}}_L = i\widehat{\mathcal{K}}''_{\mathrm{df},3} \frac{1}{1 - \left[i(\widehat{F}_G - \widehat{\mathcal{I}}_{FG}) + i(\widehat{F}_G - \overleftarrow{\widehat{\mathcal{I}}}_G) i\widehat{\mathcal{D}}_{23,L} i(\widehat{F}_G - \overrightarrow{\widehat{\mathcal{I}}}_G)\right] i\widehat{\mathcal{K}}''_{\mathrm{df},3}} . \tag{4.106}$$

Using the symmetrization identities (4.100)-(4.102), these can be rewritten as

$$i\widehat{\mathcal{M}}'_{\mathrm{df},3,L} = \left[1 + i\widehat{\mathcal{D}}_{23,L} i\widehat{F} \overrightarrow{\mathcal{S}}\right] i\widehat{\mathcal{T}}_L \left[1 + \overleftarrow{\mathcal{S}} i\widehat{F} i\widehat{\mathcal{D}}_{23,L}\right] , \tag{4.107}$$

where

$$i\widehat{\mathcal{T}}_L = i\widehat{\mathcal{K}}''_{\mathrm{df},3} \frac{1}{1 - \left[\frac{1}{3}\overleftarrow{\mathcal{S}} i\widehat{F} \overrightarrow{\mathcal{S}} + \overleftarrow{\widehat{\mathcal{S}}} i\widehat{F} i\widehat{\mathcal{D}}_{23,L} i\widehat{F} \overrightarrow{\widehat{\mathcal{S}}}\right] i\widehat{\mathcal{K}}''_{\mathrm{df},3}} . \tag{4.108}$$

Expanding out the geometric series we see that, except at the ends, $\widehat{\mathcal{K}}''_{\mathrm{df},3}$ is sandwiched between two symmetrization operators, and thus fully symmetrized.

4.8.4 Quantization condition

We recall from above that the quantization condition can be obtained from the poles in $\widehat{\mathcal{M}}'_{\mathrm{df},3,L}$. Looking at Eq. (4.107), we see that poles can only arise from the factors of $\widehat{F}$, $\widehat{\mathcal{D}}_{23,L}$, or $\widehat{\mathcal{T}}_L$. The former only has poles at free energies, which cannot be present in the interacting spectrum, and must cancel in the full expression. Poles arising from $\widehat{\mathcal{D}}_{23,L}$ do

not depend on $\widetilde{\mathcal{K}}_{\mathrm{df},3}$, and thus also must either be absent or cancel, since all finite-volume energies must have some dependence on the three-particle interaction. Thus the only source that remains is $\widehat{\mathcal{T}}_L$. To determine its poles, we rewrite Eq. (4.108) as

$$i\widehat{\mathcal{T}}_L = i\widehat{\mathcal{K}}''_{\mathrm{df},3} + i\widehat{\mathcal{K}}''_{\mathrm{df},3}\overleftarrow{\mathcal{S}}\frac{1}{1 - i\widehat{F}_3 i\widehat{\widetilde{\mathcal{K}}}_{\mathrm{df},3}} i\widehat{F}_3\overrightarrow{\mathcal{S}}\, i\widehat{\mathcal{K}}''_{\mathrm{df},3}\,. \tag{4.109}$$

where

$$\widehat{F}_3 = \tfrac{1}{3}\widehat{F} - \widehat{F}\widehat{\mathcal{D}}_{23,L}\widehat{F}\,, \tag{4.110}$$

and

$$\widehat{\widetilde{\mathcal{K}}}_{\mathrm{df},3} = \overrightarrow{\mathcal{S}}\,\widehat{\mathcal{K}}''_{\mathrm{df},3}\overleftarrow{\mathcal{S}}\,. \tag{4.111}$$

Since poles can only arise from the second term in Eq. (4.109), we obtain our third and final form for the quantization condition,

$$\det\left(1 + \widehat{F}_3\widehat{\widetilde{\mathcal{K}}}_{\mathrm{df},3}\right) = 0\,. \tag{4.112}$$

We refer to this as the symmetric form of the quantization condition.

Comparing to the quantization condition for identical particles derived in Ref. [28], we see that the nondegenerate result has the same form, but with an additional layer of matrix indices. This is what one might have naively expected, but, as we have shown, it is nontrivial to obtain this generalization. A key property of the matrix $\widehat{\widetilde{\mathcal{K}}}_{\mathrm{df},3}$ is that *it contains the same underlying K matrix in each element*, due to the presence of symmetrization operators on both sides of $\widehat{\mathcal{K}}''_{\mathrm{df},3}$ in Eq. (4.111). The underlying K matrix is

$$\widetilde{\mathcal{K}}_{\mathrm{df},3}(\{\mathbf{p}\};\{\mathbf{k}\}) = \sum_{i,j}[\widehat{\mathcal{K}}''_{\mathrm{df},3}]_{ij}(\{\mathbf{p}\};\{\mathbf{k}\})\,, \tag{4.113}$$

where, on the right-hand side, each element of $\widehat{\mathcal{K}}''_{\mathrm{df},3}$ has been converted from the $\{k\ell m\}$ basis to the momentum basis, using the appropriate generalization of Eq. (4.23), and then summed. The difference between the elements of the matrix $\widehat{\widetilde{\mathcal{K}}}_{\mathrm{df},3}$ arises only because $\widetilde{\mathcal{K}}_{\mathrm{df},3}$

is expressed in different coordinates,

$$\left[\widehat{\widetilde{\mathcal{K}}}_{\mathrm{df},3}\right]_{ij} = \widetilde{\mathcal{K}}_{\mathrm{df},3}(\{\mathbf{p}\};\{\mathbf{k}\})_{p_i\ell' m';k_j\ell m}\,, \tag{4.114}$$

We stress that the complicated nature of the relation between $\widetilde{\mathcal{K}}_{\mathrm{df},3}$ (which appears in our final quantization condition) and the elements of $\widehat{\mathcal{K}}'_{\mathrm{df},3}$ [which appear in the previous form, Eq. (7.33)] is not a practical concern, because we are simply replacing one set of unknown quantities with another. In fact, as already stressed above, the final form of the condition, Eq. (6.1) has the great advantage of requiring the parametrization of only a single K matrix, rather than nine.

The form of $\widehat{F}_3$, Eq. (4.110), is also the same as that in Ref. [28], although here the matrix structure has more content. In particular, the entries of the diagonal flavor matrix $\widehat{F}$ are different, as they correspond to a different choice of spectator flavor. Similarly, the factors of $\widehat{G}$ contained in $\widehat{\mathcal{D}}_{23,L}$ have a nontrivial matrix structure. Since this matrix version of $\widehat{F}_3$ is a quantity not previously considered, we note that it can be written as

$$\widehat{F}_3 = \tfrac{1}{3}\widehat{F} - \widehat{F}\frac{1}{\widehat{\widetilde{\mathcal{K}}}_{2,L}^{-1} + \widehat{F}_G}\widehat{F} \tag{4.115}$$

$$= \widehat{F}\left[-\frac{2}{3} + \frac{1}{1 + (1 + \widehat{\widetilde{\mathcal{K}}}_{2,L}\widehat{G})^{-1}\widehat{\widetilde{\mathcal{K}}}_{2,L}\widehat{F}}\right], \tag{4.116}$$

which are generalizations of forms that have been used for identical particles.

4.8.5 Relating $\widetilde{\mathcal{K}}_{\mathrm{df},3}$ to $\mathcal{M}_3$

The final ingredient in the symmetrized form of the formalism for nondegenerate particles is to relate $\widetilde{\mathcal{K}}_{\mathrm{df},3}$ to $\mathcal{M}_3$. The approach we take has already described in detail in Sec. 4.7, so here we provide only a summary.

We begin by noting that $\widehat{\mathcal{M}}'_{\mathrm{df},3,L}$ cannot be written in terms of $\widetilde{\mathcal{K}}_{\mathrm{df},3}$ alone, because the "1" terms in square brackets in Eq. (4.107) do not involve symmetrization operators. However,

since $\mathcal{M}_3$ is itself symmetrized [as in Eq. (4.94)], it can be written in terms of a symmetrized version of $\widehat{\mathcal{M}}'_{\mathrm{df},3,L}$ which itself *can* be written solely in terms of $\widetilde{\mathcal{K}}_{\mathrm{df},3}$. To explain this it is useful to introduce a matrix version of $\mathcal{M}_3$, whose elements are

$$\left[\widehat{\mathcal{M}}_3\right]_{ij} \equiv \mathcal{M}_3(\mathbf{p}_i;\mathbf{k}_j)_{\ell'm';\ell m}\,. \tag{4.117}$$

In other words, all elements are given by the same underlying quantity, but expressed in different coordinates. Equations (4.91)-(4.94) can then be rewritten as

$$\widehat{\mathcal{M}}_3 = \lim_{L\to\infty}\left(\overrightarrow{\mathcal{S}}\,\widehat{\mathcal{M}}'_{\mathrm{df},3,L}\,\overleftarrow{\mathcal{S}}\right) + \overrightarrow{\mathcal{S}}\,\widehat{\mathcal{D}}\,\overleftarrow{\mathcal{S}}\,, \tag{4.118}$$

where $\mathcal{D}$ is defined in Eq. (4.92), and the infinite-volume limit is taken using the $i\epsilon$ pole prescription. Here we are using the fact that the symmetrization operators work equally well on infinite-volume quantities. Using the properties

$$\overrightarrow{\mathcal{S}}\,\overrightarrow{\mathcal{S}} = 3\,\overrightarrow{\mathcal{S}}\,, \qquad \overleftarrow{\mathcal{S}}\,\overleftarrow{\mathcal{S}} = 3\,\overleftarrow{\mathcal{S}}\,, \tag{4.119}$$

we obtain

$$\overrightarrow{\mathcal{S}}\,\widehat{\mathcal{M}}'_{\mathrm{df},3,L}\,\overleftarrow{\mathcal{S}} = \overrightarrow{\mathcal{S}}\left[\tfrac{1}{3} + i\widehat{\mathcal{D}}_{23,L} i\widehat{F}\right]\widehat{\widetilde{\mathcal{K}}}_{\mathrm{df},3}\frac{1}{1 - i\widehat{F}_3 i\widehat{\widetilde{\mathcal{K}}}_{\mathrm{df},3}}\left[\tfrac{1}{3} + i\widehat{F} i\widehat{\mathcal{D}}_{23,L}\right]\overleftarrow{\mathcal{S}}\,, \tag{4.120}$$

which indeed depends only on the symmetrized $\widetilde{\mathcal{K}}_{\mathrm{df},3}$.

These results can be written as integral equations using results from Sec. 4.7. The equation for $\widehat{\mathcal{D}}_{23} = \lim_{L\to\infty}\widehat{\mathcal{D}}_{23,L}$ is unchanged, Eq. (4.88); from this and the result for $\widehat{\mathcal{M}}_2$, Eq. (4.82), we obtain $\widehat{\mathcal{D}} = \widehat{\mathcal{D}}_{23} - \widehat{\mathcal{M}}_2$. The central geometric series in Eq. (4.120) is solved by the integral equation

$$\widehat{\widetilde{\mathcal{T}}} = \widehat{\widetilde{\mathcal{K}}}_{\mathrm{df},3} - \widehat{\widetilde{\mathcal{K}}}_{\mathrm{df},3}\left[\tfrac{1}{3} - \widehat{F}^{\infty}\widehat{\mathcal{D}}_{23}\right]\widehat{F}^{\infty}\widehat{\widetilde{\mathcal{T}}}\,, \tag{4.121}$$

which is the symmetric version of the equation for $\widehat{\mathcal{T}}'$, Eq. (4.89) Despite its matrix form, this is an integral equation for a single function $\widetilde{\mathcal{T}}(\{\mathbf{p}\};\{\mathbf{k}\})$ which is packaged into the matrix $\widehat{\widetilde{\mathcal{T}}}$ in the same manner as in Eq. (4.117). We next apply integral operators to $\widehat{\widetilde{\mathcal{T}}}$, combine

with $\widehat{\mathcal{D}}$, and symmetrize to obtain the final result

$$\widehat{\mathcal{M}}_3 = \overrightarrow{\mathcal{S}} \left\{ \left[\tfrac{1}{3} - \widehat{\mathcal{D}}_{23}\widehat{F}^{\infty}\right] \widehat{\tilde{\mathcal{T}}} \left[\tfrac{1}{3} - \widehat{F}^{\infty}\widehat{\mathcal{D}}_{23}\right] + \widehat{\mathcal{D}} \right\} \overleftarrow{\mathcal{S}} \,. \tag{4.122}$$

Again, the matrix form is somewhat deceptive, as one needs only to calculate a single element of $\widehat{\mathcal{M}}_3$, since all elements contain the same function expressed in different coordinates.

4.8.6 Symmetrizing the TOPT quantization condition

The steps we have taken to obtain the symmetrized quantization condition starting from the result for $\widehat{\mathcal{M}}'_{\mathrm{df},3,L}$, Eq. (4.79), can also be applied to the TOPT result for $\widehat{\mathcal{M}}_{\mathrm{df},3,L}$, Eq. (4.54). Since these two equations have the same form, differing only by the version of $\widehat{\mathcal{K}}_{\mathrm{df},3}$ that enters, the final results of the symmetrization process will also have the same form. In particular, we obtain a TOPT-based quantization condition having the form of Eq. (6.1), and an equation for $\widehat{\mathcal{M}}_3$ having the same form as Eq. (4.122), except in both cases we are starting from $\widehat{\mathcal{K}}_{\mathrm{df},3}$ rather than $\widehat{\mathcal{K}}'_{\mathrm{df},3}$.

We now argue, however, that these new forms of the final results are actually *exactly the same*.[16] In other words, although we start with different versions of $\widehat{\mathcal{K}}_{\mathrm{df},3}$ in the two cases, one Lorentz invariant and the other not, we claim that, after the manipulations involved in symmetrization, the final resulting symmetrized quantity $\widehat{\tilde{\mathcal{K}}}_{\mathrm{df},3}$ is the same. Our argument for this is the same as that we used for identical particles in BS1. The key point is that, after symmetrization, one ends with an equation for the same quantity, $\widehat{\mathcal{M}}_3$, in both cases. This is because symmetrization corresponds to summing all diagrams that contribute, and this results in the full scattering amplitude irrespective of whether one uses TOPT or Feynman diagrams. If we assume that the relation between $\mathcal{M}_3$ and $\widetilde{\mathcal{K}}_{\mathrm{df},3}$ given by Eqs. (4.121) and (4.122) is invertible, then it must be that the symmetrized K matrix is the same for both TOPT and Feynman approaches. In more physical terms, the assumption is that any changes

[16] This only holds if the HS boost is used in the TOPT approach.

to the K matrix (which is simply a short-distance three-particle interaction) will lead to a change in the full scattering amplitude.

If we accept this argument, then we can obtain the symmetrized form of the quantization condition and the relation between $\widetilde{\mathcal{K}}_{\mathrm{df},3}$ and $\mathcal{M}_3$ *without using the Feynman-diagram approach as an intermediate step.*

4.9 Summary and Outlook

In this paper we have generalized the relativistic three-particle quantization condition, and the relation of the intermediate three-particle K matrix to $\mathcal{M}_3$, to the case of nondegenerate particles. We have derived three versions of the quantization condition: two asymmetric forms—Eqs. (4.36) and (7.33)—each involving a flavor matrix composed of nine three-particle K matrices, and a symmetric form—Eq. (6.1)—involving only a single K matrix. The latter two versions of the quantization condition involve Lorentz-invariant K matrices. These three quantization conditions are the generalizations of those for identical particles obtained in BS1 (the first two) and Ref. [28] (the final form).

The main new feature that arises for nondegenerate particles is the need to introduce an additional flavor index on the matrices, at least at intermediate steps. This corresponds to the different choices for the flavor of the external spectator particles. Even though the symmetric form of the quantization condition involves a K matrix, $\widetilde{\mathcal{K}}_{\mathrm{df},3}$, that has been symmetrized with respect to these indices, the quantization condition must still be written in terms of flavor matrices because of the different kinematical factors arising from the different choices of spectator flavor. Aside from this extra layer of indices, the form of the quantization conditions is essentially unchanged from those for identical particles.

The path that we have taken to derive the final, symmetric, form of the quantization condition has been rather lengthy and indirect. We first use TOPT, where the derivation is relatively straightforward, but involves an asymmetric and Lorentz-noninvariant K matrix.

Then we revert to a Feynman-diagram expansion of the amplitudes, and develop a new all-orders approach that yields expressions that mirror those from TOPT, and leads to a quantization condition that involves a K matrix that is Lorentz invariant, although still asymmetric. Finally, we use symmetrization identities to obtain a quantization condition involving a K matrix that is both Lorentz invariant and symmetric. A natural question is whether there is a shorter path to the final result, especially since, as already noted, it has a very similar form to that derived in Ref. [28] for identical particles. For example, could one not simply generalize every step in the derivation of Ref. [28]? We think that this is almost certainly possible, but have not followed that path as the derivation of Ref. [28] is itself very lengthy and does not lead to explicit expressions for the K matrices and other quantities. The approach followed here is explicit at every stage, so that, for example, we have given a chain of expressions relating $\widetilde{\mathcal{K}}_{\mathrm{df},3}$ back to the Feynman or TOPT Bethe-Salpeter amplitudes. Now that we have done the groundwork, we expect that the present approach can be simply generalized to other cases of interest.

Furthermore, as discussed in Sec. 4.8.6, if the relation between $\mathcal{M}_3$ and $\widetilde{\mathcal{K}}_{\mathrm{df},3}$ is invertible, then we can derive the final form of the quantization condition without the need for the intermediate step involving Feynman diagrams. Instead, we need only symmetrize the expressions that result from the TOPT approach. Although we have not demonstrated the necessary invertibility, we think that this is a physically reasonable assumption. Thus, although here we have provided the longer path to the final result, in which no assumptions are needed, we think that the shorter, two-step path can be used for future generalizations.

The theory that we consider in our derivations, which has a $\mathbb{Z}_2$ symmetry for each of the real scalar fields, is somewhat artificial, and has no direct application in QCD. It is clear from the derivations, however, that all that matters for the validity of the final results is that the kinematic constraints are such that the only on-shell intermediate state consists of one particle of each flavor. One example, already discussed in Sec. 4.3, is the $D_s^+ D^0 \pi^-$

system, which is chosen such that each of the three particles has a different total flavor. Here the $U(1)$ flavor symmetries are playing a similar role to the $\mathbb{Z}_2$ symmetries in our standard theory. Another example is the $D_s^+ D^0 D^+$ system, and similar examples can be constructed containing B mesons.

Since there are few direct applications, and also because this paper is quite lengthy, we have reserved discussion of issues related to practical implementation, as well as various cross checks, for a follow-up article. For example, a threshold expansion of $\widetilde{\mathcal{K}}_{\mathrm{df},3}$ needs to be developed, along the lines of Ref. [76]. Also of interest is the degenerate limit of our formalism, which can be related to the recently developed generalization of the symmetric quantization condition of Ref. [28] to three pions of arbitrary isospin in isosymmetric QCD [37]. The $I = 0$ case can be described by both formalisms, because this only has contributions from $\pi^+\pi^0\pi^-$ intermediate states, with no mixing with the $3\pi^0$ state. Another issue we aim to address is the relation between the degenerate limit of our formalism and the results for identical particles obtained in Ref. [28] and BS1.

We also intend, in this follow-up work, to present the generalization of the formalism that will allow application to systems of greater phenomenological interest. A simple extension is to "2+1" systems like $K^+\pi^+\pi^+$, with two identical particles and a third that is different. Cases with multiple three-particle channels are also of interest, for example $\pi^+\pi^-\pi^0 \leftrightarrow 3\pi^0$ with $m_u \neq m_d$, and the $D_s^+ D^0\pi^- \leftrightarrow D^0 D^0 K^0$ system mentioned above. Another "2+1" system of great interest is $N\pi\pi$, given its relevance to the Roper resonance, but in this case one needs also to include the $N\pi$ channel, requiring a combination of the methods introduced here and those of Refs. [34, 36]. We also note that the quantization condition for the DDK system has recently been determined in the s-wave approximation using NREFT [91].

As already observed, we expect that the symmetric form of the quantization condition, Eq. (6.1), will be most useful for practical applications, since it requires parametrizing only a single three-particle K matrix. Nevertheless, the asymmetric, Lorentz-invariant form,

Eq. (7.33), may be useful in order to determine the relation to the finite-volume unitarity (FVU) approach to deriving the quantization condition [32, 41]. In the case of identical particles, we have recently shown that the asymmetric RFT quantization condition, when written in terms of the R matrix introduced in Refs. [78, 79] (an alternate version of the three-particle K matrix), is equivalent to the FVU quantization condition [45]. We expect that this equivalence can be extended to the nondegenerate case, where the R matrix is extended to a flavor matrix.

Chapter 5

EQUIVALENCE OF RELATIVISTIC THREE-PARTICLE QUANTIZATION CONDITIONS[1]

5.1 Introduction

The study of resonant three-particle systems using lattice QCD (LQCD) is becoming feasible, due to advances in the underlying theoretical formalism [28–32, 34–37, 41, 43, 64, 77] and its practical application [39–41, 76], as well as in algorithmic and computational methods necessary to extract three-particle spectra (see, for example, the recent results presented in Refs. [1, 53, 54]).[2] The present frontier is the application to the $3\pi^+$ system [51–53]. For recent reviews, see Refs. [74, 75].

One of the key steps in the formalism is the derivation of three-particle quantization conditions, equations whose solutions give the finite-volume spectrum of three-particle states as functions of infinite-volume two- and three-particle K matrices. These K matrices can then be related to two- and three-particle scattering amplitudes by solving integral equations. Three different approaches have been followed to obtain the quantization conditions.

The first is based on an all-orders diagrammatic analysis in a generic relativistic field theory, and is usually denoted the RFT approach. It was initially developed for identical scalar particles with a G-parity-like $\mathbb{Z}_2$ symmetry [28, 29], and subsequently extended to allow $2 \to 3$ processes [34], the inclusion of poles in the two-particle K matrix [35, 36], and nonidentical but degenerate scalars [37]. In all cases, the formalism allows arbitrary interactions in two-particle subsystems (which we henceforth refer to as "dimers"). In a

[1] This chapter and Appendix C are taken directly from Ref. [45].

[2] For related applications to lattice ϕ^4 theories see Ref. [55]. For alternative approaches see Refs. [70–73].

companion paper [43], henceforth referred to as BS1, we have presented an alternative, simpler, derivation of the RFT quantization condition in the presence of the $\mathbb{Z}_2$ symmetry, including an alternative form of the quantization condition itself. This new form, which depends on an unsymmetrized three-particle K matrix, will play a crucial role in the present work.

The second approach uses nonrelativistic effective field theory (NREFT), allowing a much simplified derivation of the quantization condition [30, 31]. The formalism has so far only been developed for identical scalars with s-wave dimers and no $2 \to 3$ transitions.

The third approach, developed in Refs. [32, 41], is based on a unitary parametrization of the three-particle scattering amplitude, $\mathcal{M}_3$, in terms of a K-matrix-like real quantity called the R matrix (and denoted $\mathcal{R}^{(u,u)}$ below) [78, 79]. Following Ref. [74], we call this method the "finite-volume unitarity" (FVU) approach. It leads to a quantization condition that incorporates relativistic effects, and has so far only been developed for scalars with s-wave dimers and no $2 \to 3$ transitions.

A natural question is whether there are relations between the approaches, particularly between the two relativistic approaches (RFT and FVU). In addition, as stressed in Ref. [74], it is not clear in the FVU approach whether all sources of power-law volume dependence have been accounted for. Thus an alternative derivation of the FVU result would be welcome.

The relationship between approaches was first addressed in Ref. [31], where it was shown that the nonrelativistic limit of the RFT quantization condition of Ref. [28], restricted to s-wave dimers, reproduced the NREFT result, aside from certain technical differences. The agreement also required that the quantities describing three-particle interactions in the two approaches were restricted to their simplest, momentum-independent form. This agreement was reproduced in Ref. [74] using a simplified method. In addition, Ref. [74] showed that, when restricted to s-wave dimers, and assuming a constant three-particle interaction, the RFT quantization condition could be manipulated into a form that agreed with that from

the FVU approach (again aside from certain technical differences).

Our aim here is to extend these results to general two- and three-particle interactions. In particular, we are able to derive the FVU form of the quantization condition starting from the RFT result, and thus to generalize the FVU approach to dimers in all partial waves. The key inputs here are, first, the new form of the RFT quantization condition that we obtained in BS1, and, second, a generalization we derive here of the relation between the K matrix of the RFT approach and the R matrix obtained in Ref. [92]. Our final result, given in Eq. (5.45), is a form of the quantization condition given explicitly in terms of $\mathcal{R}^{(u,u)}$.

This article is organized as follows. In the following section we summarize the relativistic quantization conditions obtained previously, in both the RFT approach (Sec. 5.2.1) and the FVU approach (Sec. 5.2.2). Additionally, in Sec. 5.2.1 we rewrite the new form of the quantization condition from BS1 in an alternate form. In Sec. 5.3 we derive the infinite-volume relationship between asymmetric forms of the three-particle K matrix and the R matrix, $\mathcal{R}^{(u,u)}$. Using these, in Sec. 5.4 we rewrite the RFT quantization condition (in its asymmetric form) in terms of $\mathcal{R}^{(u,u)}$, thus obtaining the general form of the FVU quantization condition. In a concluding section, Sec. 5.5, we briefly compare the advantages of the different forms of the quantization condition for practical applications. Appendix C.1 summarizes notation and definitions, while Appendix C.2 discusses subtleties concerning infinite-volume limits.

5.2 Recap of prior forms of the relativistic quantization condition

5.2.1 Results in the RFT approach

The RFT quantization condition of Ref. [28] is given by

$$\det\left[1 + \mathcal{K}_{\mathrm{df},3} F_3\right] = 0\,, \tag{5.1}$$

where $\mathcal{K}_{\mathrm{df},3}$ and F_3 are matrices in the space of on-shell three-particle states, with F_3 containing the two-particle K matrix as well as known kinematical factors,

$$F_3 = \widetilde{F}\left[\frac{1}{3} - \frac{1}{\widetilde{H}}\widetilde{F}\right], \qquad \widetilde{H} = 1/\overline{\mathcal{K}}_{2,L} + \widetilde{F} + \widetilde{G}\,, \tag{5.2}$$

while $\mathcal{K}_{\mathrm{df},3}$ is a three-particle K matrix. The notation here is that of BS1, which differs somewhat from that of Ref. [28]. We summarize the relevant definitions in Appendix C.1, and only note here that $\overline{\mathcal{K}}_{2,L}$ contains the two-particle K matrix, while $\widetilde{F}$ and $\widetilde{G}$ are known kinematic functions. All three quantities depend on the box size L, with the dependence of $\overline{\mathcal{K}}_{2,L}$ being of a simple kinematic nature [see Eq. (C.2)] while $\widetilde{F}$ and $\widetilde{G}$ contain the nontrivial volume dependence. A key property of $\mathcal{K}_{\mathrm{df},3}$ is that it is symmetric under particle exchange, separately for both the initial and final three-particle states. Thus it has the same symmetry properties as the three-particle scattering amplitude $\mathcal{M}_3$.

In BS1 we show that the quantization condition of Eq. (5.1) is equivalent to a form written in terms of the asymmetric K matrix $\mathcal{K}_{\mathrm{df},3}^{(u,u)}$. Here the right (left) superscript "u" indicates that one of the three incoming (outgoing) momenta is being singled out as being the "spectator" in cases where the initial interaction involves only two particles. The precise definition of $\mathcal{K}_{\mathrm{df},3}^{(u,u)}$ is given constructively in Ref. [28], but is not important here. In fact, to write the asymmetrized quantization condition in a simple form, one must use a new version of the asymmetric K matrix, denoted $\mathcal{K}_{\mathrm{df},3}^{\prime(u,u)}$, which is obtained from $\mathcal{K}_{\mathrm{df},3}^{(u,u)}$ by solving an integral equation containing $\mathcal{K}_2$ and given explicitly in BS1. Then the new form of the RFT quantization condition is

$$\det\left[1 + \left(\overline{\mathcal{K}}_{2,L} + \mathcal{K}_{\mathrm{df},3}^{\prime(u,u)}\right)\left(\widetilde{F} + \widetilde{G}\right)\right] = 0\,. \tag{5.3}$$

We stress that no information is lost in the transition from $\mathcal{K}_{\mathrm{df},3}^{(u,u)}$ to $\mathcal{K}_{\mathrm{df},3}^{\prime(u,u)}$, since we do not have an explicit form for either. In practical applications of the quantization condition, both must be parametrized. They are both related to $\mathcal{M}_3$ by (different) integral equations, and both are Lorentz invariant if the relativistic form of $\widetilde{G}$ is used.

It turns out to be useful to rewrite the asymmetrized quantization condition as follows:[3]

$$\det\left[\widetilde{H} - X^{(u,u)}\right] = 0\,, \tag{5.4}$$

$$X^{(u,u)} = \overline{\mathcal{K}}_{2,L}^{-1} - \left[\overline{\mathcal{K}}_{2,L} + \mathcal{K}_{\mathrm{df},3}^{\prime(u,u)}\right]^{-1} \tag{5.5}$$

$$= \overline{\mathcal{K}}_{2,L}^{-1}\mathcal{K}_{\mathrm{df},3}^{\prime(u,u)}\overline{\mathcal{K}}_{2,L}^{-1}\frac{1}{1 + \mathcal{K}_{\mathrm{df},3}^{\prime(u,u)}\overline{\mathcal{K}}_{2,L}^{-1}}\,. \tag{5.6}$$

We return below to the issue of whether $X^{(u,u)}$ is an infinite-volume object, i.e. whether the matrix products in its definition can be replaced by integrals.

BS1 also presents an alternative *ab initio* derivation of the asymmetric form of the quantization condition,

$$\det\left[1 + \left(\overline{\mathcal{K}}_{2,L} + \widetilde{\mathcal{K}}_{\mathrm{df},3}^{(u,u)}\right)\left(\widetilde{F} + \widetilde{G}\right)\right] = 0\,. \tag{5.7}$$

This differs from Eq. (5.3) only in the three-particle K matrix that enters: here it is $\widetilde{\mathcal{K}}_{\mathrm{df},3}^{(u,u)}$, while $\mathcal{K}_{\mathrm{df},3}^{\prime(u,u)}$ appears in Eq. (5.3).[4] These two asymmetric K matrices are similar, but differ in their detailed definitions. $\widetilde{\mathcal{K}}_{\mathrm{df},3}^{(u,u)}$ is defined using an asymmetry based on diagrams in time-ordered perturbation theory, while that for $\mathcal{K}_{\mathrm{df},3}^{\prime(u,u)}$ is based on Feynman perturbation theory, together with additional complications.[5] As discussed in BS1, the fact that the same form of the quantization condition can hold with *different* asymmetric K matrices is a reflection of an intrinsic ambiguity in the definition of asymmetric quantities. We return to this point below. Finally, we note that Eq. (5.7) can also be manipulated into the form of Eq. (5.4), with $X^{(u,u)}$ now given by Eq. (5.6) with $\mathcal{K}_{\mathrm{df},3}^{\prime(u,u)}$ replaced by $\widetilde{\mathcal{K}}_{\mathrm{df},3}^{(u,u)}$.

---

[3] To obtain this form, we are assuming that $\det[\overline{\mathcal{K}}_{2,L} + \mathcal{K}_{\mathrm{df},3}^{\prime(u,u)}] \neq 0$, which we expect to be true in general.

[4] Another technical difference is that the BS1 derivation defines $\widetilde{G}$ using a different boost to the dimer center-of-mass frame than that used in Ref. [28]. However, the derivation of Eq. (5.3) goes through using either boost. The equations in the remainder of the paper also hold using either boost—although one must use the same choice throughout.

[5] One implication of this difference is that $\widetilde{\mathcal{K}}_{\mathrm{df},3}^{(u,u)}$ is not Lorentz invariant (irrespective of the choice of $\widetilde{G}$), because it is defined in a frame-dependent way in terms of the diagrams of time-ordered perturbation theory.

5.2.2 The FVU quantization condition

The FVU form of the quantization condition has been written explicitly so far only when the particles in the dimer interact in the s wave. The original forms given in Refs. [32, 41] are quite complicated, but it is shown in Ref. [74] that the FVU quantization condition can be rewritten as

$$\det\left[\widetilde{H}_s - (2\omega L^3)^{-1}\widetilde{C}_s^{(u,u)}(2\omega L^3)^{-1}\right] = 0\,, \tag{5.8}$$

where ω is the on-shell single-particle energy (defined in Appendix C.1), $\widetilde{H}_s$ is the s-wave restriction of $\widetilde{H}$ (i.e. with ℓ and m set to zero on both sides), and $\widetilde{C}_s^{(u,u)}(\mathbf{k},\mathbf{p})$ is a smooth, real function of the spectator momenta. Using the definition of $\mathcal{R}^{(u,u)}$ given in Refs. [41, 92] together with results from Ref. [74], one can show that $\widetilde{C}_s^{(u,u)} = \mathcal{R}_s^{(u,u)}$, with $\mathcal{R}_s^{(u,u)}$ the s-wave restriction of $\widetilde{\mathcal{R}}^{(u,u)}$. We have added the "$(u,u)$" superscript (which is absent in the original FVU works and in Ref. [74]) in order to emphasize that this is an intrinsically asymmetric object, since it parametrizes the smooth part of the dimer-particle contact interaction.

In writing the result (5.8) in terms of $\widetilde{F}$ and $\widetilde{G}$, we are implicitly assuming that we are using the smooth cutoff function that is built into the approach of Ref. [28]. The introduction of this cutoff function is essential in that work (and in the alternative approach of BS1) in order to argue that all power-law volume dependence is accounted for. By contrast, in the FVU approach, a hard cutoff is introduced by hand. There is, however, no technical reason not to use the smooth cutoff in the FVU approach, and we assume henceforth that this has been done.

Aside from this technical issue, Eqs. (5.4) and (5.8) are clearly very similar, and suggest a relation between the s-wave restriction of $X^{(u,u)}$ and $\mathcal{R}_s^{(u,u)}$. In the following sections we will make this concrete, using a variant of the relationship between $\mathcal{K}_{\mathrm{df},3}^{(u,u)}$ and the matrix $\mathcal{R}$ introduced in Ref. [92].

5.3 The $\mathcal{R}^{(u,u)}$ matrix and its relation to $\mathcal{K}'^{(u,u)}_{\text{df},3}$ and $\widetilde{\mathcal{K}}^{(u,u)}_{\text{df},3}$

One of the results of the RFT approach is an integral equation relating $\mathcal{K}_{\text{df},3}$ to the physical three-particle scattering amplitude $\mathcal{M}_3$ [29]. This provides a representation of $\mathcal{M}_3$ in terms of a real function that is devoid of s-channel unitary cuts (up to the five-particle threshold) and of on-shell singularities. An important check on this result was the demonstration, in Ref. [93], that it provided a representation of $\mathcal{M}_3$ that satisfied the constraints of s-channel unitarity.[6] A similar, but different, parametrization of $\mathcal{M}_3$, in terms of a real K-matrix-like asymmetric[7] amplitude $\mathcal{R}^{(u,u)}$, had previously been suggested in the context of amplitude analyses of experimental results for resonances that decay to three particles [78, 79]. This parametrization was developed in order to satisfy s-channel unitarity. In Ref. [92], it was shown that these two parametrizations are equivalent, and the relationship between $\mathcal{K}_{\text{df},3}$ and $\mathcal{R}^{(u,u)}$ was derived.

Here we need to extend the analysis of Ref. [92] to relate the asymmetric RFT amplitudes $\mathcal{K}'^{(u,u)}_{\text{df},3}$ and $\widetilde{\mathcal{K}}^{(u,u)}_{\text{df},3}$ to the FVU amplitude $\mathcal{R}^{(u,u)}$. This brings to light two technical issues that were overlooked in Ref. [92], although it turns out that they do not impact the final conclusion of that work. We will describe these in the course of our discussion.

The desired relationships are determined by equating expressions for asymmetric forms of the three-particle scattering amplitude. We use two such amplitudes: $\mathcal{M}_3^{(u,u)}$ defined in Ref. [29] in the context of a Feynman diagram analysis, and $\widetilde{\mathcal{M}}_3^{(u,u)}$ defined in BS1 in an analysis using time-ordered perturbation theory (TOPT). We present the results for these quantities in turn, and then compare them to the corresponding expressions in terms of $\mathcal{R}^{(u,u)}$.

---

[6] This demonstration remains valid when $\widetilde{G}$ is defined with the boost used in BS1.

[7] As with $\widetilde{C}_s^{(u,u)}$, we have added the superscript (u,u), which is not present in the original works, to emphasize the asymmetry of $\mathcal{R}^{(u,u)}$.

5.3.1 *Expression for* $\mathcal{M}_3^{(u,u)}$

$\mathcal{M}_3^{(u,u)}$ is defined in Ref. [29] using a skeleton expansion in terms of Bethe-Salpeter kernels. The external particles can be directly connected to either two- or three-particle kernels. The asymmetry arises because two-particle kernels are connected to the external momenta such that the spectator momentum is always associated with the noninteracting propagator. The connection to the three-particle kernel does not lead to asymmetry, since this kernel is symmetric.

In Ref. [29], an expression for $\mathcal{M}_3^{(u,u)}$ is obtained that depends on both $\mathcal{K}_{\text{df},3}^{(u,u)}$ and $\mathcal{K}_{\text{df},3}$. In particular, it does not depend solely on the symmetric form $\mathcal{K}_{\text{df},3}$ alone. This brings up the first technical issue alluded to above. In the analysis of Ref. [92], a different expression for $\mathcal{M}_3^{(u,u)}$ is used that is given wholly in terms of $\mathcal{K}_{\text{df},3}$ [see Eqs. (20) and (21) of [92], in which $\mathcal{M}_3^{(u,u)}$ is called $\mathcal{A}$]. This is, in fact, not the correct expression for $\mathcal{M}_3^{(u,u)}$, but rather describes a related (and implicitly defined) quantity, in which a certain subclass of diagrams has has been symmetrized. This change does not impact the final results of Ref. [92] because both the correct and incorrect expressions for $\mathcal{M}_3^{(u,u)}$ symmetrize to the same quantity, $\mathcal{M}_3$, and this is all that is required for the derivation.

Here we use the correct expression for $\mathcal{M}_3^{(u,u)}$. To determine this, we start from the finite-volume version of the amplitude, $\mathcal{M}_{3,L}^{(u,u)}$ (also defined in Ref. [29]), which goes over to $\mathcal{M}_3^{(u,u)}$ in the appropriate $L \to \infty$ limit. It was shown in BS1 how to asymmetrize the result for $\mathcal{M}_{3,L}^{(u,u)}$ given in Ref. [29] so as to write it solely in terms of $\mathcal{K}_{\text{df},3}^{(u,u)}$. After further manipulation this is rewritten in BS1 in terms of $\mathcal{K}_{\text{df},3}^{\prime(u,u)}$,

$$\mathcal{M}_{\text{df},3,L}^{(u,u)} = \mathcal{M}_{3,L}^{(u,u)} - \mathcal{D}_L^{(u,u)} \tag{5.9}$$

$$= \frac{1}{1+\overline{\mathcal{K}}_{2,L}(\widetilde{F}+\widetilde{G})}\mathcal{K}_{\text{df},3}^{\prime(u,u)}\frac{1}{1+(\widetilde{F}+\widetilde{G})\frac{1}{1+\overline{\mathcal{K}}_{2,L}(\widetilde{F}+\widetilde{G})}\mathcal{K}_{\text{df},3}^{\prime(u,u)}}\frac{1}{1+(\widetilde{F}+\widetilde{G})\overline{\mathcal{K}}_{2,L}}\,. \tag{5.10}$$

Here we have switched to using the divergence-free form of the three-particle amplitude, whose difference from the original form is given by the multiple two-particle scattering con-

tribution

$$\mathcal{D}_L^{(u,u)} = -\overline{\mathcal{M}}_{2,L}\widetilde{G}\overline{\mathcal{M}}_{2,L}\frac{1}{1+\widetilde{G}\overline{\mathcal{M}}_{2,L}}\,, \tag{5.11}$$

where $\mathcal{M}_{2,L}$ is defined in Eq. (C.12).

Taking the infinite-volume limit of Eq. (5.10) using the $i\epsilon$ prescription described in Ref. [29], we obtain

$$\mathcal{M}_{\mathrm{df},3}^{(u,u)} = \mathcal{L}\,\mathcal{K}_{\mathrm{df},3}^{\prime(u,u)}\frac{1}{1+(\widetilde{\rho}_{\mathrm{PV}}+G^{\infty})\,\mathcal{L}\,\mathcal{K}_{\mathrm{df},3}^{\prime(u,u)}}\,\mathcal{L}^T\,, \tag{5.12}$$

$$\mathcal{L} = \frac{1}{1+\overline{\mathcal{K}}_2(\widetilde{\rho}_{\mathrm{PV}}+G^{\infty})}\,, \tag{5.13}$$

$$\mathcal{L}^T = \frac{1}{1+(\widetilde{\rho}_{\mathrm{PV}}+G^{\infty})\overline{\mathcal{K}}_2}\,. \tag{5.14}$$

This is written in a highly compact notation, adapted from that of Ref. [92], which we now explain. All quantities depend implicitly on initial and final on-shell variables, each in the $\{\mathbf{k},\ell,m\}$ space. For example, $\mathcal{K}_{\mathrm{df},3}^{\prime(u,u)}$ is given explicitly by

$$\mathcal{K}_{\mathrm{df},3}^{\prime(u,u)}(\mathbf{k},\mathbf{p})_{\ell m;\ell' m'} = \lim_{L\to\infty}\left[\mathcal{K}_{\mathrm{df},3}^{\prime(u,u)}\right]_{k\ell m;p\ell' m'}\,, \tag{5.15}$$

with $\mathcal{M}_{\mathrm{df},3}^{(u,u)}$ defined similarly. The explicit forms for the other quantities are

$$\overline{\mathcal{K}}_2(\mathbf{k},\mathbf{p})_{\ell m;\ell' m'} = \lim_{L\to\infty}\left[\overline{\mathcal{K}}_{2,L}\right]_{k\ell m;p\ell' m'} = \overline{\delta}(\mathbf{k}-\mathbf{p})\delta_{\ell\ell'}\delta_{mm'}\,\mathcal{K}_2^{(\ell)}(q_{2,k}^*)\,, \tag{5.16}$$

$$\widetilde{\rho}_{\mathrm{PV}}(\mathbf{k},\mathbf{p})_{\ell m;\ell' m'} = \overline{\delta}(\mathbf{k}-\mathbf{p})\delta_{\ell\ell'}\delta_{mm'}\,\widetilde{\rho}_{\mathrm{PV}}^{(\ell)}(q_{2,k}^{*2})\,, \tag{5.17}$$

$$G^{\infty}(\mathbf{k},\mathbf{p})_{\ell m;\ell' m'} = \frac{\mathcal{Y}_{\ell m}(\mathbf{p}_k^*)}{q_{2,k}^{*\ell}}\frac{H(\mathbf{k})H(\mathbf{p})}{b_{pk}^2-m^2+i\epsilon}\frac{\mathcal{Y}_{\ell' m'}(\mathbf{k}_p^*)}{q_{2,p}^{*\ell'}}\,, \tag{5.18}$$

where

$$\overline{\delta}(\mathbf{k}-\mathbf{p}) = 2\omega_k(2\pi)^3\delta^3(\mathbf{k}-\mathbf{p})\,, \tag{5.19}$$

and $\mathcal{K}_2^{(\ell)}$, $\widetilde{\rho}_{\mathrm{PV}}^{(\ell)}$, and the kinematic variables are defined in Appendix C.1. The products appearing in Eqs. (5.12)-(5.14) should be viewed as matrix products in the on-shell index space. Angular momentum indices are summed as usual, while the spectator momenta

(which are now continuous variables) are integrated with the Lorentz-invariant measure[8] $\int_{\mathbf{r}} \equiv \int d^3r/(2\omega_r[2\pi]^3)$. Thus

$$[XZ]\,(\mathbf{k},\mathbf{p})_{\ell m;\ell' m'} \equiv \sum_{\ell'' m''} \int_{\mathbf{r}} X(\mathbf{k},\mathbf{r})_{\ell m;\ell'' m''} Z(\mathbf{r},\mathbf{p})_{\ell'' m'';\ell' m'}\,, \tag{5.20}$$

where $X, Z \in \{\overline{\mathcal{K}}_2, \widetilde{\rho}_{\mathrm{PV}}, G^{\infty}, \mathcal{K}_{\mathrm{df},3}^{\prime(u,u)}\}$. Finally, the inverses in Eqs. (5.12)-(5.14), which are well defined as matrix inverses for finite L, become integral equations in the infinite-volume limit. Thus, for example, $\mathcal{L}$ satisfies

$$\mathcal{L} = 1 - \overline{\mathcal{K}}_2(\widetilde{\rho}_{\mathrm{PV}} + G^{\infty})\mathcal{L}\,. \tag{5.21}$$

Further details on how the infinite-volume limit of $\mathcal{M}_{\mathrm{df},3,L}^{(u,u)}$ leads to Eq. (5.12) are provided in Appendix C.2. In addition, we describe there how the inverses of $\overline{\mathcal{K}}_2$, $\mathcal{K}_{\mathrm{df},3}^{\prime(u,u)}$, and related quantities are defined, since these are needed below.

5.3.2 Expression for $\widetilde{\mathcal{M}}_3^{(u,u)}$

An alternative version of the asymmetric scattering amplitude is introduced in BS1 and denoted $\widetilde{\mathcal{M}}_3^{(u,u)}$. Its asymmetry is defined in terms of two- and three-particle irreducible TOPT amplitudes, which differ from the corresponding Bethe-Salpeter kernels. Thus it differs from $\mathcal{M}_3^{(u,u)}$, although both symmetrize to the physical scattering amplitude $\mathcal{M}_3$.

The expression for $\widetilde{\mathcal{M}}_3^{(u,u)}$ (given in Appendix E of BS1) is identical to that for $\mathcal{M}_3^{(u,u)}$, Eq. (5.12), except with $\mathcal{K}_{\mathrm{df},3}^{\prime(u,u)}$ replaced by $\widetilde{\mathcal{K}}_{\mathrm{df},3}^{(u,u)}$:

$$\widetilde{\mathcal{M}}_{\mathrm{df},3}^{(u,u)} = \mathcal{L}\,\widetilde{\mathcal{K}}_{\mathrm{df},3}^{(u,u)} \frac{1}{1 + (\widetilde{\rho}_{\mathrm{PV}} + G^{\infty})\,\mathcal{L}\,\widetilde{\mathcal{K}}_{\mathrm{df},3}^{(u,u)}} \mathcal{L}^T\,. \tag{5.22}$$

Here $\widetilde{\mathcal{K}}_{\mathrm{df},3}^{(u,u)}$ is the asymmetric K matrix appearing in Eq. (5.7), the new form of the RFT quantization condition obtained in BS1.

---

[8] This differs from the notation of BS1, where the $1/(2\omega_r)$ factor is not included in the definition of $\int_{\mathbf{r}}$.

5.3.3 *Result for asymmetric amplitudes in terms of* $\mathcal{R}^{(u,u)}$

We now recall the expression for the asymmetric scattering amplitude in terms of the R matrix [78, 79]. For reasons that will become clear shortly, we give the amplitude a different name from those discussed earlier, calling it $\mathcal{M}_{\mathrm{df},3}^{\mathcal{R},(u,u)}$. We use the form given in Eqs. (15)-(19) of Ref. [92], which, converted into our notation, becomes[9]

$$\mathcal{M}_{\mathrm{df},3}^{\mathcal{R},(u,u)} = \widetilde{\mathcal{L}}\,\mathcal{R}^{(u,u)}\frac{1}{1-\widetilde{\mathcal{L}}\,\mathcal{R}^{(u,u)}}\widetilde{\mathcal{L}}\,, \tag{5.23}$$

$$\widetilde{\mathcal{L}} = \overline{\mathcal{M}}_2\frac{1}{1+G^{\infty}\overline{\mathcal{M}}_2} = \frac{1}{1+\overline{\mathcal{M}}_2 G^{\infty}}\overline{\mathcal{M}}_2\,, \tag{5.24}$$

where

$$\overline{\mathcal{M}}_2(\mathbf{k},\mathbf{p})_{\ell m;\ell' m'} = \overline{\delta}(\mathbf{k}-\mathbf{p})\delta_{\ell\ell'}\delta_{mm'}\,\mathcal{M}_2^{(\ell)}(q_{2,k}^*)\,, \tag{5.25}$$

with $\mathcal{M}_2^{(\ell)}$ being the ℓth partial wave of the two-particle scattering amplitude. Using the result

$$\overline{\mathcal{M}}_2 = \overline{\mathcal{K}}_2\frac{1}{1+\widetilde{\rho}_{\mathrm{PV}}\overline{\mathcal{K}}_2}\,, \tag{5.26}$$

which follows from Eq. (C.6), we find

$$\widetilde{\mathcal{L}} = \frac{1}{1+\overline{\mathcal{K}}_2(\widetilde{\rho}_{\mathrm{PV}}+G^{\infty})}\overline{\mathcal{K}}_2 = \overline{\mathcal{K}}_2\frac{1}{1+(\widetilde{\rho}_{\mathrm{PV}}+G^{\infty})\overline{\mathcal{K}}_2}\,. \tag{5.27}$$

Before comparing to the earlier expressions (5.12) and (5.22), we discuss the second technical issue alluded to above. This issue is whether $\mathcal{M}_{\mathrm{df},3}^{\mathcal{R},(u,u)}$ should be equated to $\mathcal{M}_{\mathrm{df},3}^{(u,u)}$ or to $\widetilde{\mathcal{M}}_{\mathrm{df},3}^{(u,u)}$. All three amplitudes symmetrize to the same quantity, $\mathcal{M}_{\mathrm{df},3}$, but this does not guarantee equivalence before symmetrization. Furthermore, as we have already noted, the analysis of Ref. [92] uses a different, partially symmetrized version of $\mathcal{M}_{\mathrm{df},3}^{(u,u)}$ (which also

[9] In the original works that introduce this form [78, 79], a different choice of G^{∞} was used than that we use here, Eq. (C.10). In particular, the cutoff function $H(\mathbf{k})$ was replaced with a hard cutoff, and barrier factors were not included. However, as noted in Ref. [92], the derivation of s-channel unitarity—which is the essential property of this form—goes through for all choices of G^{∞} that have the same residues of the on-shell poles, which is the case for the choices used here.

symmetrizes to $\mathcal{M}_{\mathrm{df},3}$). In Ref. [92], it is implicitly assumed that this last version of the asymmetric amplitude is equal to $\mathcal{M}_{\mathrm{df},3}^{\mathcal{R},(u,u)}$. However, since the R-matrix parametrization is not obtained using Feynman or TOPT diagrams, but rather is a form constructed solely to satisfy s-channel unitarity, we see no *fundamental* way of connecting it to any of the diagram-based definitions. We also see no sense in which either $\mathcal{M}_{\mathrm{df},3}^{(u,u)}$ or $\widetilde{\mathcal{M}}_{\mathrm{df},3}^{(u,u)}$ (or the partially symmetrized version of the former) is better suited to an R-matrix parametrization.

We propose that the resolution to this conundrum is that $\mathcal{R}^{(u,u)}$ is intrinsically ambiguous, and that, with suitable choices of this quantity, we can equate $\mathcal{M}_{\mathrm{df},3}^{\mathcal{R},(u,u)}$ to either $\mathcal{M}_{\mathrm{df},3}^{(u,u)}$ or $\widetilde{\mathcal{M}}_{\mathrm{df},3}^{(u,u)}$ (or to the partially symmetrized version of the former, as done in Ref. [92]). To say it differently, we propose that the parametrization of $\mathcal{M}_3$ in terms of $\mathcal{R}^{(u,u)}$ involves a redundancy, such that a family of choices of $\mathcal{R}^{(u,u)}$ leads to the same physical scattering amplitude. We stress that we are not suggesting that any ambiguity arises in the relation between $\mathcal{R}^{(u,u)}$ and $\mathcal{M}_{\mathrm{df},3}^{\mathcal{R},(u,u)}$—for a given choice of the latter quantity (including its sub-threshold continuation), we expect that $\mathcal{R}^{(u,u)}$ is uniquely determined. The ambiguity arises in the definition of $\mathcal{M}_{\mathrm{df},3}^{\mathcal{R},(u,u)}$ itself.[10] The relations derived below demonstrate *a posteriori* the validity of our proposal, because they show that the expressions given above for both $\mathcal{M}_{\mathrm{df},3}^{(u,u)}$ and $\widetilde{\mathcal{M}}_{\mathrm{df},3}^{(u,u)}$ can be rewritten exactly in the R-matrix form.

5.3.4 Combining results

Returning to the main line of argument, we note that the external integral operators in the two expressions, Eqs. (5.12) and (5.23), are related by

$$\widetilde{\mathcal{L}} = \mathcal{L}\,\overline{\mathcal{K}}_2 = \overline{\mathcal{K}}_2\,\mathcal{L}^T\,. \tag{5.28}$$

[10] A potentially confusing point is that, in Ref. [92], the amplitude $\mathcal{M}_{\mathrm{df},3}^{\mathcal{R},(u,u)}$ is called $\mathcal{A}_{\mathbf{p}'\mathbf{p}}$, with no explicit indication that it is an asymmetric quantity. We stress that $\mathcal{A}_{\mathbf{p}'\mathbf{p}}$ is asymmetric, and is related to $\mathcal{M}_3$ by the symmetrization procedure of Eq. (7) of Ref. [92].

Thus, Eq. (5.23) can be rewritten as[11]

$$\mathcal{M}_{\rm df,3}^{\mathcal{R},(u,u)} = \mathcal{L}\,\overline{\mathcal{K}}_2\,\mathcal{R}^{(u,u)}\frac{1}{1-\mathcal{L}\,\overline{\mathcal{K}}_2\,\mathcal{R}^{(u,u)}}\overline{\mathcal{K}}_2\,\mathcal{L}^T \tag{5.29}$$

$$= \mathcal{L}\frac{1}{\overline{\mathcal{K}}_2^{-1}[\mathcal{R}^{(u,u)}]^{-1}\overline{\mathcal{K}}_2^{-1}-\overline{\mathcal{K}}_2^{-1}\mathcal{L}}\mathcal{L}^T\,. \tag{5.30}$$

Comparing this to a slightly rewritten version of Eq. (5.12)

$$\mathcal{M}_{\rm df,3}^{(u,u)} = \mathcal{L}\frac{1}{\left[\mathcal{K}_{\rm df,3}^{\prime(u,u)}\right]^{-1}+(\widetilde{\rho}_{\rm PV}+G^{\infty})\mathcal{L}}\mathcal{L}^T\,, \tag{5.31}$$

we observe that these expressions match if and only if

$$\left[\mathcal{K}_{\rm df,3}^{\prime(u,u)}\right]^{-1} = \overline{\mathcal{K}}_2^{-1}\left[\mathcal{R}^{(u,u)}\right]^{-1}\overline{\mathcal{K}}_2^{-1}-\left(\overline{\mathcal{K}}_2^{-1}+\widetilde{\rho}_{\rm PV}+G^{\infty}\right)\mathcal{L} \tag{5.32}$$

$$= \overline{\mathcal{K}}_2^{-1}\left[\mathcal{R}^{(u,u)}\right]^{-1}\overline{\mathcal{K}}_2^{-1}-\overline{\mathcal{K}}_2^{-1}\,, \tag{5.33}$$

where the second step follows from Eq. (5.13). This can be rewritten as

$$\mathcal{K}_{\rm df,3}^{\prime(u,u)} = \overline{\mathcal{K}}_2\mathcal{R}^{(u,u)}\overline{\mathcal{K}}_2\frac{1}{1-\mathcal{R}^{(u,u)}\overline{\mathcal{K}}_2}\,, \tag{5.34}$$

or, equivalently, as an integral equation

$$\mathcal{K}_{\rm df,3}^{\prime(u,u)} = \overline{\mathcal{K}}_2\mathcal{R}^{(u,u)}\overline{\mathcal{K}}_2+\overline{\mathcal{K}}_2\mathcal{R}^{(u,u)}\mathcal{K}_{\rm df,3}^{\prime(u,u)}\,. \tag{5.35}$$

The inverse relation can also be given, as discussed below. Reversing the algebraic steps, we conclude that, if $\mathcal{K}_{\rm df,3}^{\prime(u,u)}$ and $\mathcal{R}^{(u,u)}$ are related in this manner, then $\mathcal{M}_{\rm df,3}^{(u,u)}$ can be written in the R-matrix form of Eq. (5.23).

We can follow exactly the same steps if we equate the result for $\widetilde{\mathcal{M}}_{\rm df,3}^{(u,u)}$, Eq. (5.22), to $\mathcal{M}_{\rm df,3}^{\mathcal{R},(u,u)}$. Thus, with a *different* choice of $\mathcal{R}^{(u,u)}$, we have

$$\widetilde{\mathcal{K}}_{\rm df,3}^{(u,u)} = \overline{\mathcal{K}}_2\mathcal{R}^{(u,u)}\overline{\mathcal{K}}_2\frac{1}{1-\mathcal{R}^{(u,u)}\overline{\mathcal{K}}_2}\,. \tag{5.36}$$

The relations (5.34) and (5.36) are simpler than that between (a third choice of) $\mathcal{R}^{(u,u)}$

[11]The inverses appearing in this section and the next are defined in Appendix C.2.

and $\mathcal{K}_{\mathrm{df},3}$ obtained in Ref. [92]. This is perhaps to be expected as both are asymmetric quantities. We note that the new relations are consistent with the fact that both the R and K matrices are purely real. The appearance of factors of $\overline{\mathcal{K}}_2$ "wrapping" $\mathcal{R}^{(u,u)}$ is a result of the choice in the R-matrix approach of pulling out the dimer scattering amplitude as an explicit external factor—see Fig. 2(a) of Ref. [92].

A technical point concerns the integrals over intermediate momenta that are implicit in Eqs. (5.34) and (5.36). Expanding the geometric series, there are terms of the form $\ldots \mathcal{R}^{(u,u)}\overline{\mathcal{K}}_2\mathcal{R}^{(u,u)}\ldots$, which lead to an integral over the spectator-momentum associated with $\mathcal{K}_2^{(\ell)}$. If there are narrow resonances in a given channel, then $\mathcal{K}_2^{(\ell)}$ can have poles on the real axis, and one must specify how to do the integrals. These can be dealt with either by using a pole prescription or by generalizing the principal value (PV) prescription used to define $\mathcal{K}_2^{(\ell)}$, which can move the poles out of the relevant kinematic range [36]. We prefer the latter approach, as this generalized PV prescription is needed to derive the quantization condition of Eq. (5.4) in the case where $\mathcal{K}_2^{(\ell)}$ has poles.

In fact, although $\mathcal{K}_2^{(\ell)}$ and $\mathcal{K}_{\mathrm{df},3}^{\prime(u,u)}$ both depend on the choice of PV prescription, it turns out that all choices of $\mathcal{R}^{(u,u)}$ are prescription independent. The key fact here is that the combination $\overline{\mathcal{K}}_{2,L}^{-1} + \widetilde{F}$ is, by construction, independent of the prescription. This in turn implies that $\widetilde{\mathcal{L}}$ is also prescription independent, since it can be written

$$\widetilde{\mathcal{L}} = \lim_{L\to\infty} \frac{1}{\overline{\mathcal{K}}_{2,L}^{-1} + \widetilde{F} + \widetilde{G}}\,. \tag{5.37}$$

Finally, using Eq. (5.23) and the fact that $\mathcal{M}_{\mathrm{df},3}^{\mathcal{R},(u,u)}$ is prescription independent (which follows from the prescription independence of $\mathcal{M}_3$ and $\mathcal{D}^{(u,u)}$), we see that $\mathcal{R}^{(u,u)}$ must also be independent of the PV prescription. In this sense, $\mathcal{R}^{(u,u)}$ is a "more physical" quantity than $\mathcal{K}_{\mathrm{df},3}^{\prime(u,u)}$ or $\widetilde{\mathcal{K}}_{\mathrm{df},3}^{(u,u)}$. We note, however, that $\mathcal{R}^{(u,u)}$ does depend on the cutoff function, since that dependence enters through G^∞ and is not canceled.

5.4 *Expressing the quantization condition in terms of* $\mathcal{R}^{(u,u)}$

We are now ready to combine the results obtained above to rewrite the quantization condition in terms of $\mathcal{R}^{(u,u)}$. For definiteness, we first consider the choice of $\mathcal{R}^{(u,u)}$ that is related to $\mathcal{K}_{\text{df},3}^{\prime(u,u)}$ by Eq. (5.34), and thus consider the form of the quantization condition containing the latter quantity, Eq. (5.4). We discuss the other choices of $\mathcal{R}^{(u,u)}$ subsequently.

We start from Eq. (5.33), from which follows

$$\left[\mathcal{R}^{(u,u)}\right]^{-1} = \overline{\mathcal{K}}_2 + \overline{\mathcal{K}}_2 \left[\mathcal{K}_{\text{df},3}^{\prime(u,u)}\right]^{-1} \overline{\mathcal{K}}_2 \,. \tag{5.38}$$

This can be rewritten as

$$\mathcal{R}^{(u,u)} = \overline{\mathcal{K}}_2^{-1} - \left[\overline{\mathcal{K}}_2 + \mathcal{K}_{\text{df},3}^{\prime(u,u)}\right]^{-1} \tag{5.39}$$

$$= \overline{\mathcal{K}}_2^{-1} \mathcal{K}_{\text{df},3}^{\prime(u,u)} \overline{\mathcal{K}}_2^{-1} \frac{1}{1 + \mathcal{K}_{\text{df},3}^{\prime(u,u)} \overline{\mathcal{K}}_2^{-1}} \,. \tag{5.40}$$

The key observation is that the quantity $X^{(u,u)}$ appearing in the quantization condition, Eq. (5.6), satisfies

$$\lim_{L\to\infty} (2\omega L^3) X^{(u,u)} (2\omega L^3) = \mathcal{R}^{(u,u)} \,, \tag{5.41}$$

where the factors of $(2\omega L^3)$ arise from Eq. (C.19). It follows that, if the finite-volume corrections to this result are exponentially suppressed, i.e. if

$$\left[(2\omega L^3) X^{(u,u)} (2\omega L^3)\right]_{k\ell m; p\ell' m'} = \left[\mathcal{R}^{(u,u)}\right]_{k\ell m; p\ell' m'} + \mathcal{O}(e^{-mL}) \,, \tag{5.42}$$

then the quantization condition (5.4) can be rewritten as

$$\det\left[\widetilde{H} - (2\omega L^3)^{-1} \mathcal{R}^{(u,u)} (2\omega L^3)^{-1}\right] = 0 \,. \tag{5.43}$$

Here $\mathcal{R}^{(u,u)}$ is the matrix form of the infinite-volume amplitude, obtained in the usual way

$$\left[\mathcal{R}^{(u,u)}\right]_{k\ell m; p\ell' m'} \equiv \mathcal{R}^{(u,u)}(\mathbf{k}, \mathbf{p})_{\ell m; \ell' m'} \,, \qquad \{\mathbf{k}, \mathbf{p}\} \in (2\pi/L)\mathbb{Z}^3 \,, \tag{5.44}$$

i.e. by restricting the momenta to the finite-volume set.

To discuss the validity of Eq. (5.42), we consider the definition of $X^{(u,u)}$, Eq. (5.6). Expanding out the geometric series, we find terms of the form $\ldots \mathcal{K}_{\mathrm{df},3}^{\prime(u,u)} \overline{\mathcal{K}}_{2,L}^{-1} \mathcal{K}_{\mathrm{df},3}^{\prime(u,u)} \ldots$. As shown in Eq. (C.20) this goes over to $\ldots \mathcal{K}_{\mathrm{df},3}^{\prime(u,u)} \overline{\mathcal{K}}_{2}^{-1} \mathcal{K}_{\mathrm{df},3}^{\prime(u,u)} \ldots$ in the infinite-volume limit, with the intermediate momentum sums over spectator momenta converted to integrals. However, if $\mathcal{K}_2^{(\ell)}$ has zeros within the kinematic range of interest (which ranges up to the four pion threshold for two-particle scattering), then the difference between sum and integral over the resulting poles in $\mathcal{K}_2^{-1}$ will lead to power-law corrections to Eq. (5.42), which would invalidate the quantization condition (5.43). Zeros in $\mathcal{K}_2^{(\ell)}$ (along the real $q_{2,k}^{*2}$ axis) occur when the phase shift passes through $n\pi$ with $n \in \mathbb{Z}$ and have no particular physical significance. Excluding such cases would be a major restriction on the applicability of Eq. (5.43).

In fact, we do not think that such cases need to be excluded. The point is that we expect $\mathcal{R}^{(u,u)}$ to be finite in the vicinity of positions where $\mathcal{K}_2^{(\ell)}$ (and thus $\mathcal{M}_2^{(\ell)}$) has zeros. This is because, as noted above, $\mathcal{R}^{(u,u)}$ is defined in the expression for $\mathcal{M}_{\mathrm{df},3}$ with factors of $\mathcal{M}_2^{(\ell)}$ pulled out on both sides [as can be seen from Eq. (5.23)]. Thus the effects of a vanishing $\mathcal{M}_2^{(\ell)}$ are already included. Assuming so, then Eq. (5.34) shows that $\mathcal{K}_{\mathrm{df},3}^{\prime(u,u)}$ vanishes at such positions—specifically, $\mathcal{K}_{\mathrm{df},3}^{\prime(u,u)}(\mathbf{k},\mathbf{p})_{\ell m;\ell' m'} = 0$ if $\mathcal{K}_2(\mathbf{k})_{\ell m} = 0$ or $\mathcal{K}_2(\mathbf{p})_{\ell' m'} = 0$. This implies that the divergences in $\overline{\mathcal{K}}_2^{-1}$ occurring in the expression for $X^{(u,u)}$ are canceled by the behavior of $\mathcal{K}_{\mathrm{df},3}^{\prime(u,u)}$. Thus we conclude that Eq. (5.43) is a legitimate form of the quantization condition.

We can repeat the arguments just given using the quantization condition written in terms of $\widetilde{\mathcal{K}}_{\mathrm{df},3}^{(u,u)}$, Eq. (5.7), and the relation between $\widetilde{\mathcal{K}}_{\mathrm{df},3}^{(u,u)}$ and a different choice for $\mathcal{R}^{(u,u)}$ given in Eq. (5.36). The result is that the quantization condition can be written in exactly the form of Eq. (5.43), except with the new choice of $\mathcal{R}^{(u,u)}$. One disadvantage of this choice of $\mathcal{R}^{(u,u)}$ is that it is not Lorentz invariant. This follows because it is defined in terms of the TOPT asymmetric amplitude $\widetilde{\mathcal{M}}_3^{(u,u)}$, which depends on the choice of frame used to define

the time axis. By contrast, the form of $\mathcal{R}^{(u,u)}$ obtained by equating $\mathcal{M}_{\mathrm{df},3}^{\mathcal{R},(u,u)}$ to $\mathcal{M}_{\mathrm{df},3}^{(u,u)}$ is Lorentz invariant, as long as the relativistic form of $\widetilde{G}$ is used.

5.5 *Summary and outlook*

The main result of this work is the demonstration that the three-particle quantization condition for scalar particles with a $\mathbb{Z}_2$ symmetry obtained in the RFT approach in Ref. [28] (and extended in BS1) can be rewritten in terms of the R matrix of Refs. [78, 79] in the simple form

$$\det\left[\overline{\mathcal{K}}_{2,L}^{-1} + \widetilde{F} + \widetilde{G} - (2\omega L^3)^{-1}\mathcal{R}^{(u,u)}(2\omega L^3)^{-1}\right] = 0\,. \tag{5.45}$$

This provides the generalization of the s-wave FVU result of Refs. [32, 41], Eq. (5.8), to all angular momenta of the dimer, and shows the equivalence of the RFT and FVU approaches in general.[12] We stress that the derivation of Eq. (5.45) requires the use of a smooth cutoff function (as opposed to a hard cutoff) as well as the presence of the "barrier factors" in the definition of $\widetilde{G}$ [see discussion below Eq. (C.10)]. We note that, while the two-particle interaction enters with a factor of $1/L^3$ (contained in $\overline{\mathcal{K}}_{2,L}$), the three-particle interaction term comes with a $1/L^6$. This is as expected based on the overlap amplitudes of particles with wavefunctions distributed throughout the volume, and is consistent with the results of the threshold expansion [65, 66, 68]. We expect that by taking the nonrelativistic limit of this form of the quantization condition, one will obtain the generalization of the NREFT quantization condition of Refs. [30, 31] to all dimer angular momenta.

We have also found that the R matrix is not unique, but rather that Eq. (5.45) holds for two different choices of $\mathcal{R}^{(u,u)}$, which are in turn related to the two different asymmetric forms of the three-particle K matrix that we have discussed, namely $\mathcal{K}_{\mathrm{df},3}^{\prime(u,u)}$ and $\widetilde{\mathcal{K}}_{\mathrm{df},3}^{(u,u)}$. We have

[12] As noted earlier, Eq. (5.8) is obtained from the original result for the FVU quantization condition, given in Refs. [32, 41], only after some algebraic manipulations [74]. Presumably, our generalized result could be rewritten in a form similar to that of the original works, but we have not attempted this.

argued that the lack of uniqueness of $\mathcal{R}^{(u,u)}$ is an example of the general result that asymmetric forms of amplitudes are intrinsically ambiguous, since the process of symmetrization is not invertible. This is most obviously seen in the fact that one can consider two different asymmetric forms of the three-particle scattering amplitude, $\mathcal{M}_3^{(u,u)}$ and $\widetilde{\mathcal{M}}_3^{(u,u)}$, whose definitions differ by whether the asymmetry is defined with respect to a Feynman-diagram-based skeleton expansion [29] or an expansion in terms of time-ordered perturbation theory (see BS1).

Looking forward, an important question is how the new, asymmetric form of the quantization condition, Eq. (5.45), compares in practice with the original, symmetric form of Eq. (5.1). The advantages of the new form include its simplicity and the fact that $\mathcal{R}^{(u,u)}$ is independent of the choice of PV prescription. It is also closely connected to phenomenological analyses of scattering amplitudes, through which intuition and experience concerning appropriate parametrizations of $\mathcal{R}^{(u,u)}$ have been developed. The disadvantage of the new form is that $\mathcal{R}^{(u,u)}$ is an asymmetric amplitude, whose general description requires additional parameters in comparison to the symmetric K matrix $\mathcal{K}_{\mathrm{df},3}$ that enters Eq. (5.1). This is clear, for example, in the threshold expansion worked out in Ref. [76], where a significant reduction in parameters occurs because of the symmetry of $\mathcal{K}_{\mathrm{df},3}$.[13]

[13] One can also see this in the result for $\mathcal{K}_{\mathrm{df},3}^{(u,u)}$ one obtains in leading-order chiral perturbation theory, by extending the calculations described in Ref. [51].

Part III

PRACTICAL IMPLEMENTATION

In the following three chapters, we present three different numerical implementations of quantization conditions for three identical scalars. Each chapter and its corresponding appendix is taken from a different research publication: Chapter 6 and Appendix D are from Ref. [76]; Chapter 7 and Appendix E are from Ref. [36]; and Chapter 8 and Appendix F are from Ref. [51].

Chapter 6

IMPLEMENTING THE THREE-PARTICLE QUANTIZATION CONDITION INCLUDING HIGHER PARTIAL WAVES[1]

6.1 Introduction

There has been considerable recent progress developing the formalism necessary to extract the properties of resonances coupling to three-particle channels from simulations of lattice QCD, with three different approaches being followed [28–32, 34, 35]. For a recent review, see Ref. [74]. The outputs of this work are quantization conditions, which relate the finite-volume spectrum with given quantum numbers to the infinite-volume two- and three-particle interactions. This development is timely since simulations now have extensive results for the finite-volume spectrum above the three-particle threshold; see, e.g., Refs. [55, 94, 95] and the recent review in Ref. [26]. Turning the formalism into a practical tool remains, however, a significant challenge. To date, this has been done only for the simplest case, in which all particles are spinless and identical, the total momentum vanishes, the two-particle interaction is purely s-wave, and three particles interact only via a momentum-independent contact interaction [31, 32, 39–41].[2] This is the analog in the three-particle system of the initial implementations of the two-particle quantization condition of Lüscher [24, 25], which assumed only s-wave interactions and vanishing total momentum.

In the two-particle case, such an approximation makes sense for levels close to the two-particle threshold, since higher partial waves are suppressed by powers of the relative mo-

[1] This chapter and Appendix D are taken directly from Ref. [76].

[2] There is also an induced three-particle interaction due to the exchange of a virtual particle between a pair of two-particle interactions. This is included in all approaches.

mentum. In the meson sector it begins to fail for energies around 1 GeV. Indeed, recent applications of the two-particle quantization condition use multiple partial waves (see, e.g., Refs. [96, 97]). Similar considerations apply for three particles, and we expect that for many resonances of interest one will need to include higher partial waves.

The aim of this paper is to take the first step in this direction by including the first higher partial wave that enters in the case of identical, spinless particles, namely the d wave.[3] In the language of Refs. [30–32], we include dimers (two-particle channels) with both $\ell = 0$ and $\ell = 2$. At the same time, for consistency, we make a corresponding extension of the three-particle interaction beyond its local (pure s-wave) form. We will explain how to implement the formalism in this generalized setting, and show examples for which the higher-order terms have a significant impact on the finite-volume spectrum.

Three-particle quantization conditions have been developed with three different approaches. These use, respectively, generic relativistic effective field theory analyzed diagrammatically to all orders in perturbation theory (the RFT approach) [28, 34, 35], non-relativistic effective field theory (NREFT) [30, 31], and unitarity constraints on the two- and three-particle S-matrix elements applied to finite-volume amplitudes (the finite-volume unitarity or FVU approach) [32]. To date, only in the RFT approach has the formalism been worked out explicitly with no limitations on the two-particle partial waves, whereas in the other two approaches the quantization condition has been written down only for s-wave dimers.[4] Therefore we adopt the RFT approach in this work. Specifically, we use the formalism of Ref. [28], which applies to identical, spinless particles, with a G-parity-like $\mathbb{Z}_2$ symmetry that forbids $2 \leftrightarrow 3$ transitions. Another important feature of this approach is that it can be made relativistic [34], which turns out to simplify the expansion about threshold. Although we use the RFT approach, we expect that many of the technical considerations and general conclusions

[3] The p wave is absent due to Bose symmetry.

[4] It is expected, however, that there is no barrier to extending to higher waves.

will apply to all three approaches to the quantization condition.

The formalism of Ref. [28] is restricted to two-particle interactions that do not lead to poles in $\mathcal{K}_2$, the two-particle K matrix. If there are such poles, then one should use the generalized, and more complicated, formalism derived in Ref. [35]. For simplicity, we consider here only examples in which there are no K-matrix poles.

Since our main goal is to show how the formalism works when including higher waves, our numerical examples are mainly chosen for illustrative purposes and do not represent physical systems. However, there is one case in nature for which our simplified setting applies, namely the $3\pi^+$ system. Thus, in one of our examples, we set the two-particle scattering parameters to those measured experimentally for two charged pions, and illustrate the dependence of the resulting three-pion spectrum on the three-particle scattering parameters. This is similar to the study made in Ref. [41] using the FVU approach, except here we include d-wave dimers.

All three-particle quantization conditions involve an intermediate three-particle scattering quantity that is not physical, but that can be related, in a second step, to the infinite-volume scattering amplitude by solving integral equations. In the RFT formalism this quantity is called $\mathcal{K}_{\mathrm{df},3}$, and the second step is explained in Ref. [29]. We do not discuss the implementation of this second step in the present work. Clearly, it will be important to do so in the future, but the methods required are quite different from those needed for the quantization condition.

This paper develops the ideas already sketched in Sec. 4 of Ref. [98]. It is organized as follows. In the next section we recall the quantization condition of Ref. [28], and explain how one can consistently expand $\mathcal{K}_{\mathrm{df},3}$ about the three-particle threshold, with d-wave interactions entering at quadratic order. In Sec. 6.3 we describe the implementation of the quantization condition including d-wave interactions, focusing on how to make use of the factorization into different irreducible representations (irreps) of the cubic group. Subsequently, in Sec. 6.4 we show results illustrating the effect of d-wave interactions on the three-particle spectrum,

including in Sec. 6.4.3 the case of the $3\pi^+$ system with realistic interactions, which is a target for a potential lattice QCD study. In addition, in Sec. 6.4.4, we address the issue of characterizing unphysical solutions to the quantization condition. We summarize and close the discussion in Sec. 8.6.

We also include seven appendices describing technical details. Appendix D.1 is a collection of relevant definitions, whereas Appendices D.2 and D.3 provide further details concerning the topics of Sec. 6.3. Appendix D.4 describes the calculation of the leading contribution of d-wave scattering to the threshold expansion. Finally, the remaining appendices relate to the free solutions discussed in Sec. 6.4.4: Appendix D.5 motivates the presence of these solutions in excited states, Appendix D.6 explains why they are absent in the isotropic approximation of Refs. [28, 39], and Appendix D.7 explains in an example why removing the free solutions requires higher orders in the threshold expansion of $\mathcal{K}_{\text{df},3}$.

6.2 Threshold expansion of the three-particle quantization condition

As noted above, we consider a theory of identical, scalar particles, with interactions constrained only by the imposition of a $\mathbb{Z}_2$ global symmetry that prevents odd-legged vertices. In such a theory, the spectrum of odd-particle-number states in a cubic box of length L, with periodic boundary conditions, is determined by solutions to the quantization condition [28]

$$\det\left[F_3(E,L)^{-1} + \mathcal{K}_{\text{df},3}(E)\right] = 0\,. \tag{6.1}$$

This holds up to finite-volume corrections that are exponentially suppressed, i.e., which fall as $\exp(-mL)$ up to powers of L, where m is the mass of the particle. In Eq. (6.1), F_3 and $\mathcal{K}_{\text{df},3}$ are matrices with index space $\{\mathbf{k},\ell,m\}$, where $\mathbf{k} \in (2\pi/L)\mathbb{Z}^3$ is the finite-volume momentum assigned to one of the particles (the "spectator"), while ℓ and m specify the angular momentum of the other two (the "dimer").[5] This matrix space will be truncated, as

[5]Context determines which meaning of m is intended.

explained in Sec. 6.3 below, so that the quantization condition (6.1) becomes tractable. The matrix F_3 is a complicated object given in Eq. (6.28) below; all we need to know for now is that it depends on the two-particle K matrix, $\mathcal{K}_2$. Thus the infinite-volume quantities that enter into the quantization condition are $\mathcal{K}_2$ and the three-particle quasilocal interaction $\mathcal{K}_{\mathrm{df},3}$.[6]

The quantization condition (6.1) is valid only when the CM (center of momentum) energy lies in the range $m < E^* < 5m$, within which the only odd-particle-number states that can go on shell involve three particles (rather than one, five, seven, etc.). Here $E^* = \sqrt{E^2 - \mathbf{P}^2}$, with $(E, \mathbf{P})$ the total four-momentum of the state. As in the previous numerical studies [30, 32, 39, 40], we further restrict our considerations to the overall rest frame, with $\mathbf{P} = 0$, implying $E^* = E$ henceforth. We also recall that Eq. (6.1) assumes that there are no poles in $\mathcal{K}_2$ in the kinematic regime of interest. We discuss the constraints that this places on the two-particle scattering parameters in Sec. 6.3.

The aim of this section is to develop a systematic expansion of $\mathcal{K}_{\mathrm{df},3}$ about the three-particle threshold at $E = 3m$. To that end, we make use of the fact that, unlike the matrix F_3, $\mathcal{K}_{\mathrm{df},3}$ is an infinite-volume quantity, and so is defined for arbitrary choices of the three incoming and three outgoing on-shell momenta in the scattering process, and not just for finite-volume momenta. It is also important that it can be chosen to be relativistically invariant, if an appropriate choice of the kinematic function $\widetilde{G}$ entering F_3 is made [34] [see Eq. (D.3)].

In the remainder of this section, we first recall the threshold expansion of $\mathcal{K}_2$ and its relation to the partial wave decomposition, and then describe the generalization of the threshold expansion to $\mathcal{K}_{\mathrm{df},3}$, extending an analysis given in Ref. [39]. Finally, we show how the terms in this expansion are decomposed into the matrix form needed for Eq. (6.1).

---

[6] The subscript "df" stands for "divergence-free", indicating that a long distance one-particle exchange contribution that can diverge has been removed. For further details, see Ref. [28].

6.2.1 Warm up: expanding $\mathcal{K}_2$ about threshold

To illustrate the method that we employ for $\mathcal{K}_{\mathrm{df},3}$, we first consider the simpler, and well-understood, case of the two-particle K matrix, $\mathcal{K}_2$. Since $\mathcal{K}_2$ is relativistically invariant, it depends only on the standard Mandelstam variables s_2, t_2 and $u_2 = 4m^2 - s_2 - t_2$. It is convenient to use dimensionless variables that vanish at threshold,

$$\widetilde{\Delta}_2 = \frac{s_2 - 4m^2}{4m^2} = \frac{q_2^{*2}}{m^2}\,, \quad \widetilde{t}_2 = \frac{t_2}{4m^2} = -\frac{q_2^{*2}}{2m^2}(1-c_\theta)\,, \quad \widetilde{u}_2 = \frac{u_2}{4m^2} = -\frac{q_2^{*2}}{2m^2}(1+c_\theta)\,, \tag{6.2}$$

where q_2^* is the magnitude of the momentum of each particle in the CM frame, and c_θ is the cosine of the scattering angle. For physical scattering, $\widetilde{\Delta}_2$, $-\widetilde{t}_2$ and $-\widetilde{u}_2$ are all non-negative, and satisfy

$$\widetilde{\Delta}_2 = -\widetilde{t}_2 - \widetilde{u}_2\,, \tag{6.3}$$

implying that $-\widetilde{t}_2$ and $-\widetilde{u}_2$ are both bounded by $\widetilde{\Delta}_2$.

Since $\mathcal{K}_2$ is known to be analytic near threshold, we can expand it in powers of $\widetilde{\Delta}_2$, $\widetilde{t}_2$ and $\widetilde{u}_2$. The previous considerations imply that, for generic kinematics (i.e., $\theta \neq 0$ or π), all three quantities are of the same order. Bose symmetry implies that the expression must be symmetric under $\widetilde{t}_2 \leftrightarrow \widetilde{u}_2$. Thus, through quadratic order we have

$$\mathcal{K}_2 = \widetilde{c}_0 + \widetilde{c}_1\widetilde{\Delta}_2 + \widetilde{c}_2\widetilde{\Delta}_2^2 + \widetilde{c}_3\left(\widetilde{t}_2^{\,2} + \widetilde{u}_2^{\,2}\right) + \mathcal{O}(\widetilde{\Delta}_2^3)\,, \tag{6.4}$$

where the $\widetilde{c}_i$ are constants (which are real since $\mathcal{K}_2$ is real), and we have used the constraint (6.3) to reduce the number of independent terms. We now decompose this result into partial waves, using

$$\mathcal{K}_2 = \sum_{\ell=0}^{\infty}(2\ell+1)\mathcal{K}_2^{(\ell)}(\widetilde{\Delta}_2)P_\ell(\cos\theta)\,. \tag{6.5}$$

All odd partial waves vanish by Bose symmetry, while Eq. (6.4) leads to

$$\mathcal{K}_2^{(0)} = \widetilde{c}_0 + \widetilde{c}_1\widetilde{\Delta}_2 + (\widetilde{c}_2 + \tfrac{2}{3}\widetilde{c}_3)\widetilde{\Delta}_2^2 + \mathcal{O}(\widetilde{\Delta}_2^3)\,, \tag{6.6}$$

$$\mathcal{K}_2^{(2)} = \tfrac{1}{15}\widetilde{c}_3\widetilde{\Delta}_2^2 + \mathcal{O}(\widetilde{\Delta}_2^3)\,. \tag{6.7}$$

The first equation gives the first three terms in the effective range expansion for $\mathcal{K}_2$, while from the second equation we recover the well-known result that $\mathcal{K}_2^{(2)} \propto q_2^{*4}$ near threshold. By extending this analysis, one can show that $\mathcal{K}_2^{(\ell)}$ only enters when we include terms of $\mathcal{O}(\widetilde{\Delta}_2^\ell)$ in the threshold expansion [39].

The threshold expansion has a finite radius of convergence. In particular, we know that $\mathcal{K}_2$ has a left-hand cut at $\widetilde{\Delta}_2 = -1$, so that the radius of convergence cannot be greater than $|\widetilde{\Delta}_2| = 1$. In practice, we truncate the expansion at the order shown in Eqs. (6.6) and (6.7) (and set $\mathcal{K}_2^{(\ell)} = 0$ for $\ell \geq 3$), use a cutoff function such that $\widetilde{\Delta}_2 > -1$, and restrict $E < 5m$ implying that $\widetilde{\Delta}_2 < 3$. We are thus assuming that the deviations from the truncated threshold expansion are small over this kinematic range.

6.2.2 Invariants for three-particle scattering

To extend the analysis to the three-particle amplitude $\mathcal{K}_{\text{df},3}$, we begin by listing the generalized Mandelstam variables,

$$s \equiv E^2\,, \quad s_{ij} \equiv (p_i + p_j)^2 = s_{ji}, \quad s'_{ij} \equiv (p'_i + p'_j)^2 = s'_{ji}\,, \quad t_{ij} \equiv (p_i - p'_j)^2\,, \tag{6.8}$$

where p_i (p'_i), $i = 1 - 3$, are the incoming (outgoing) momenta. As in the two-particle case, it is convenient to use dimensionless quantities that vanish at threshold,

$$\Delta \equiv \frac{s - 9m^2}{9m^2}\,, \quad \Delta_i \equiv \frac{s_{jk} - 4m^2}{9m^2}\,, \qquad \Delta'_i \equiv \frac{s'_{jk} - 4m^2}{9m^2}\,, \quad \widetilde{t}_{ij} \equiv \frac{t_{ij}}{9m^2}\,, \tag{6.9}$$

where in the definitions of Δ_i and Δ'_i, (i,j,k) form a cylic permutation of $(1,2,3)$. These sixteen quantities are constrained by the following eight independent relations,

$$\sum_{i=1}^{3} \Delta_i = \sum_{i=1}^{3} \Delta'_i = \Delta \tag{6.10}$$

$$\sum_{j=1}^{3} \widetilde{t}_{ij} = \Delta_i - \Delta, \quad \sum_{j=1}^{3} \widetilde{t}_{ji} = \Delta'_i - \Delta. \qquad [i = 1,2,3]\,. \tag{6.11}$$

Thus only eight are independent: the overall CM energy (parametrized here by Δ) and seven "angular" degrees of freedom.[7] This counting is as expected: six on-shell momenta with total incoming and outgoing 4-momentum fixed have $3 \cdot 6 - 4 \cdot 2 = 10$ degrees of freedom, which is reduced to 7 by overall rotation invariance.

For physical scattering, it is straightforward to show that Δ_i, Δ'_i, $-\widetilde{t}_{ij}$ are all non-negative, and the constraint equations then lead to the inequality

$$0 \leq \Delta_i, \Delta'_i, -\widetilde{t}_{ij} \leq \Delta\,. \tag{6.12}$$

Thus all the variables $\{\Delta, \Delta_i, \Delta'_i, \widetilde{t}_{ij}\}$ can be treated as being of the same order in an expansion about threshold.

6.2.3 Expanding $\mathcal{K}_{df,3}$ about threshold

By construction, $\mathcal{K}_{\rm df,3}$ is a smooth function for some region around threshold.[8] Thus it can be expanded in a Taylor series in the variables $\{\Delta, \Delta_i, \Delta'_i, \widetilde{t}_{ij}\}$, which are all treated as being of $\mathcal{O}(\Delta)$. Since $\mathcal{K}_{\rm df,3}$ is real, the coefficients in this expansion must also be real. The expansion must also respect the symmetries of $\mathcal{K}_{\rm df,3}$, which is invariant under [34]:[9]

---

[7] We call these variables angular since they span a compact space.

[8] More precisely, what is shown in Ref. [28] is that $\mathcal{K}_{\rm df,3}$ has no kinematic singularities at threshold, a result that is checked by the explicit perturbative calculations of Refs. [81, 82]. There can be dynamical singularities due to a three-particle resonance, but, generically, this will lie away from threshold.

[9] The first two symmetries hold because we are considering identical bosons. They would not hold in the more general case of nonidentical particles, allowing additional terms to be present in $\mathcal{K}_{\rm df,3}$.

- Interchange of any two incoming particles: $p_i \leftrightarrow p_j \Rightarrow \Delta_i \leftrightarrow \Delta_j$ and $\widetilde{t}_{ik} \leftrightarrow \widetilde{t}_{jk}$
- Interchange of any two outgoing particles: $p'_i \leftrightarrow p'_j \Rightarrow \Delta'_i \leftrightarrow \Delta'_j$ and $\widetilde{t}_{ki} \leftrightarrow \widetilde{t}_{kj}$
- Time reversal: $p_i \leftrightarrow p'_i \;\; (\forall i) \;\; \Rightarrow \;\; \Delta_i \leftrightarrow \Delta'_i$ and $\widetilde{t}_{ij} \leftrightarrow \widetilde{t}_{ji} \;\; (\forall ij)$

It is then a tedious but straightforward exercise to write down the allowed terms at each order in Δ, and simplify them using the constraints (6.10)–(6.11). Through quadratic order we find

$$m^2 \mathcal{K}_{\mathrm{df},3} = \mathcal{K}^{\mathrm{iso}} + \mathcal{K}_{\mathrm{df},3}^{(2,A)} \Delta_A^{(2)} + \mathcal{K}_{\mathrm{df},3}^{(2,B)} \Delta_B^{(2)} + \mathcal{O}(\Delta^3)\,, \tag{6.13}$$

$$\mathcal{K}^{\mathrm{iso}} = \mathcal{K}_{\mathrm{df},3}^{\mathrm{iso}} + \mathcal{K}_{\mathrm{df},3}^{\mathrm{iso},1} \Delta + \mathcal{K}_{\mathrm{df},3}^{\mathrm{iso},2} \Delta^2 \tag{6.14}$$

$$\Delta_A^{(2)} = \sum_{i=1}^{3} (\Delta_i^2 + \Delta_i'^2) - \Delta^2, \tag{6.15}$$

$$\Delta_B^{(2)} = \sum_{i,j=1}^{3} \widetilde{t}_{ij}^{\,2} - \Delta^2\,, \tag{6.16}$$

where $\mathcal{K}_{\mathrm{df},3}^{\mathrm{iso}}$, $\mathcal{K}_{\mathrm{df},3}^{\mathrm{iso},1}$, $\mathcal{K}_{\mathrm{df},3}^{\mathrm{iso},2}$, $\mathcal{K}_{\mathrm{df},3}^{(2,A)}$ and $\mathcal{K}_{\mathrm{df},3}^{(2,B)}$ are real, dimensionless constants. We thus see that there is a single term both at leading (zeroth) order and at first order, while there are three independent terms at quadratic order. The particular linear combinations of the quadratic terms that appear in Eqs. (6.15) and (6.16) (and in particular the subtraction of Δ^2 in $\Delta_A^{(2)}$ and $\Delta_B^{(2)}$) are chosen based on our numerical experiments described below in order to ensure that their contributions to the finite-volume spectrum are distinct.

As noted in Ref. [39], the leading order contribution to $\mathcal{K}_{\mathrm{df},3}$ in Eq. (6.13) is independent of momenta p_i and p'_j. This shows that the isotropic approximation to $\mathcal{K}_{\mathrm{df},3}$, defined as independence of the seven angular variables, arises naturally in the same way as the s-wave approximation to $\mathcal{K}_2$. What we add here is the result that $\mathcal{K}_{\mathrm{df},3}$ remains isotropic at $\mathcal{O}(\Delta)$, having only an overall linear dependence on s. Furthermore, at quadratic order, we find only two terms that depend on angular variables ($\Delta_A^{(2)}$ and $\Delta_B^{(2)}$), compared to the seven angular variables that are needed to fully characterize three-particle scattering. Thus, if it is a good

approximation to truncate the threshold expansion at $\mathcal{O}(\Delta^2)$, the number of parameters needed to describe $\mathcal{K}_{\rm df,3}$ is smaller than one might naively have expected.

For most of our numerical investigations, we have restricted ourselves to quadratic order in the expansion of $\mathcal{K}_{\rm df,3}$. It is interesting, however, to push the classification to higher order for at least three reasons. First, in order to know how rapidly the number of parameters grows; second, to see which dimer partial waves enter; and, third, to investigate the issue of solutions to the quantization condition with energies given by those of three noninteracting particles (see Sec. 6.4.4). Thus we have classified all terms of cubic order. We find eight independent terms: three that are just Δ times each of the terms of quadratic order, plus five new angular terms,

$$\Delta_A^{(3)} = \sum_i \left(\Delta_i^3 + \Delta_i'^3\right), \qquad \Delta_B^{(3)} = \sum_{i,j} \widetilde{t}_{ij}^{\,3} \tag{6.17}$$

$$\Delta_C^{(3)} = \sum_{i,j} \Delta_i \widetilde{t}_{ij} \Delta_j', \qquad \Delta_D^{(3)} = \sum_{i,j} \widetilde{t}_{ij}^{\,2} \left(\Delta_i + \Delta_j'\right) \tag{6.18}$$

$$\Delta_E^{(3)} = \sum_{\sigma \in S_3} \widetilde{t}_{1\sigma(1)} \widetilde{t}_{2\sigma(2)} \widetilde{t}_{3\sigma(3)}, \tag{6.19}$$

where $\sigma \in S_3$ is a permutation of the indices $(1, 2, 3)$. Thus the number of terms is growing fairly rapidly with order.[10]

6.2.4 Decomposing $\mathcal{K}_{df,3}$

In order to use $\mathcal{K}_{\rm df,3}$ in the quantization condition, we need to decompose it into the variables used in its matrix form. This is the analog of the partial wave decomposition of $\mathcal{K}_2$, described in Sec. 6.2.1 above.

The steps in this decomposition were presented in Ref. [28] and we recall them here. The

[10] We do not think that there is any significance to the fact that the number of terms depending on angular variables through cubic order, i.e. $2 + 5 = 7$, equals the number of independent angles in three-particle scattering. The dependence on these angles can be arbitrarily complicated, so there is not a one-to-one correspondence between variables and functions.

total four-momentum P^μ is fixed, in our case to $(E, \mathbf{0})$. One each of the initial and final particles is designated as the spectator, with three-momenta denoted $\mathbf{k}$ and $\mathbf{p}$, respectively. Since $\mathcal{K}_{\mathrm{df},3}$ is symmetric separately under initial and final particle interchange, it does not matter which particles are chosen as the spectators, and we take $\mathbf{k} = \mathbf{p}_3$ and $\mathbf{p} = \mathbf{p}_3{}'$. The remaining two particles form the (initial and final) dimers. The total momenta of both dimers are fixed, e.g. to $P - p_3$ in the initial state. For each dimer, we can boost to its CM frame, and the only remaining degree of freedom is the direction of one of the particles in the dimer in this frame. We take this particle to be p_1 in the initial state, and denote its direction in the dimer CM frame by $\hat{a}^*$. Similarly, the direction of p_1' in the final-state-dimer CM frame is called $\hat{a}'^*$. Using these variables we can write[11]

$$\mathcal{K}_{\mathrm{df},3} = \mathcal{K}_{\mathrm{df},3}(\mathbf{p}, \hat{a}'^*; \mathbf{k}, \hat{a}^*) \,. \tag{6.20}$$

The next step is to set each spectator momentum to one of the allowed finite-volume values, e.g. $\mathbf{k} = \mathbf{n}(2\pi/L)$, with $\mathbf{n}$ a vector of integers. The final step is then to decompose the dependence on $\hat{a}^*$ and $\hat{a}'^*$ into spherical harmonics

$$\mathcal{K}_{\mathrm{df},3}(\mathbf{p}, \hat{a}'^*; \mathbf{k}, \hat{a}^*) = 4\pi Y^*_{\ell' m'}(\hat{a}'^*) \mathcal{K}_{\mathrm{df},3;p\ell' m';k\ell m} Y_{\ell m}(\hat{a}^*) \,, \tag{6.21}$$

where there is an implicit sum over all angular-momentum indices. This defines the entries in the matrix form of $\mathcal{K}_{\mathrm{df},3}$.[12] In practice, we use the real version of spherical harmonics, so the complex conjugation in Eq. (6.21) has no impact.

The simplest example of this decomposition is for the isotropic terms in $\mathcal{K}_{\mathrm{df},3}$, namely $\mathcal{K}^{\mathrm{iso}}$ in Eq. (6.14). Recalling that E, and thus Δ, is fixed, $\mathcal{K}^{\mathrm{iso}}$ is simply a constant. This

[11] As above, the $2\cdot(3+2) = 10$ momentum components are reduced to seven independent angular variables by rotation invariance.

[12] Note that we follow Ref. [28] and drop the vector symbol on the momenta in the matrix indices, in order not to overly clutter the notation.

implies that the matrix form of $\mathcal{K}^{\rm iso}$ vanishes unless $\ell' = \ell = 0$, and is independent of $\mathbf{p}, \mathbf{k}$:

$$\mathcal{K}^{\rm iso}_{{\rm df},3;p\ell' m';k\ell m} = \mathcal{K}^{\rm iso}\delta_{\ell' 0}\delta_{m' 0}\delta_{\ell 0}\delta_{m 0}\,. \tag{6.22}$$

The approximation $\mathcal{K}_{{\rm df},3} = \mathcal{K}^{\rm iso}$ is studied in Ref. [39].

We next work out the decomposition of $\Delta_A^{(2)}$, Eq. (6.15), which is conveniently written as

$$\Delta_A^{(2)} = \left[\Delta_3^2 + \Delta_3'^2 - \Delta^2\right] + \left[\Delta_1^2 + \Delta_2^2\right] + \left[\Delta_1'^2 + \Delta_2'^2\right]\,. \tag{6.23}$$

The first term depends on $\mathbf{k}^2$ and $\mathbf{p}^2$, but not on $\hat{a}^*$ or $\hat{a}'^*$. This can be seen from

$$9m^2\Delta_3 = (P - p_3)^2 - 4m^2 = E^2 - 2E\omega_k - 3m^2\,, \tag{6.24}$$

with $\omega_k = \sqrt{\mathbf{k}^2 + m^2}$, and the corresponding result for Δ_3'. Thus the first term in Eq. (6.23) leads to a purely s-wave ($\ell' = \ell = 0$) contribution to $\mathcal{K}_{{\rm df},3}$, although now with nontrivial dependence on $\mathbf{k}$ and $\mathbf{p}$, so this differs from an isotropic contribution.

The second term in Eq. (6.23) can be rewritten using

$$\frac{9m^2}{2}\left[\Delta_1^2 + \Delta_2^2\right] = (p_+ \cdot p_3 - 2m^2)^2 + (p_- \cdot p_3)^2 = (E\omega_k - 3m^2)^2 + \frac{4E^2}{E_{2,k}^{*2}}(\mathbf{a}^* \cdot \mathbf{k})^2\,, \tag{6.25}$$

where $p_\pm = p_1 \pm p_2$, and $E_{2,k}^{*2} = (P - p_3)^2$. To obtain the second form one must explicitly boost to the dimer CM frame, in which $\mathbf{p}_-$ equals $2\mathbf{a}^*$, with $a^{*2} = 9m^2\Delta_3/4$. The first term on the right-hand side of Eq. (6.25) is independent of $\hat{a}^*$, and thus again contributes only an s-wave component. The second term, however, depends quadratically on $\hat{a}^*$, and thus, through the addition theorem for spherical harmonics,[13]

$$(\hat{a} \cdot \hat{k})^2 = \frac{1}{3} + \frac{8\pi}{15}\sum_m Y_{2m}^*(\hat{a})Y_{2m}(\hat{k})\,, \tag{6.26}$$

leads to both s- and d-wave contributions. In other words, both $\mathcal{K}_{{\rm df},3;p00;k00}$ and $\mathcal{K}_{{\rm df},3;p00;k2m}$ are nonvanishing. These contributions are straightforward to work out from the above equations, and we do not display them explicitly.

[13] Again, in practice, we use real spherical harmonics, so the complex conjugation is not needed.

The final term in Eq. (6.23) differs from the second term only by changing unprimed quantities to their primed correspondents. Thus one finds contributions both to $\mathcal{K}_{\mathrm{df},3;p00;k00}$ and $\mathcal{K}_{\mathrm{df},3;p2m';k00}$. Overall, we conclude that the angular dependence in $\Delta_A^{(2)}$ leads to both s- and d-wave dimer interactions, although there are no terms with both $\ell = 2$ and $\ell' = 2$. The latter result arises from the fact that there are no terms in $\Delta_A^{(2)}$ that depend on both incoming and outgoing momenta.

Finally, we consider $\Delta_B^{(2)}$, given in Eq. (6.16). This is more complicated to decompose because $\widetilde{t}_{ij}$ contains both incoming and outgoing momenta, but this same property leads to contributions with $\ell = \ell' = 2$. We provide only a sketch of the decomposition, as the details are tedious, lengthy, and straightforward to automate. Expanding $\Delta_B^{(2)}$, one finds terms that are similar to those dealt with in $\Delta_A^{(2)}$, which lead to additional contributions to $\mathcal{K}_{\mathrm{df},3;p00;k00}$, $\mathcal{K}_{\mathrm{df},3;p00,k2m}$, and $\mathcal{K}_{\mathrm{df},3;p2m';k00}$, and a term proportional to

$$(p_- \cdot p'_-)^2 = a_i^* a_j^* S_{ij,rs} a_r'^* a_s'^* \,, \tag{6.27}$$

where $p'_\pm = p'_1 \pm p'_2$, i, j, r, and s are now spatial vector indices, and S is a tensor that depends on $\mathbf{k}$ and $\mathbf{p}$ and is symmetric separately under $i \leftrightarrow j$ and $r \leftrightarrow s$. By decomposing S into the spherical tensor basis one finds contributions to the $\ell = \ell' = 2$ part of $\mathcal{K}_{\mathrm{df},3}$, $\mathcal{K}_{\mathrm{df},3;p2m';k2m}$, as well as to the other three components.

In summary, because the terms of $\mathcal{O}(\Delta^2)$ in $\mathcal{K}_{\mathrm{df},3}$ are at most quadratic in $\mathbf{a}^*$ and/or $\mathbf{a}'^*$, they give rise to dimer interactions that are either s- or d-wave. This is the analog of the result derived in Sec. 6.2.1 that, at the same order, only $\mathcal{K}_2^{(0)}$ and $\mathcal{K}_2^{(2)}$ are present.

The generalization to higher order is straightforward. Terms of $\mathcal{O}(\Delta^3)$, can, in principle be cubic in $\mathbf{a}^*$ and/or $\mathbf{a}'^*$, but Bose symmetry forbids odd powers. Thus $\mathcal{O}(\Delta^3)$ terms lead only to s- and d-wave contributions to $\mathcal{K}_{\mathrm{df},3}$, as we have checked explicitly. In order to obtain contributions with $\ell = 4$ or $\ell' = 4$ one must work at $\mathcal{O}(\Delta^4)$ in the threshold expansion. The pattern continues similarly at higher order.

6.3 Implementing the quantization condition

In this section we describe how we numerically implement the quantization condition, Eq. (6.1), when working to quadratic order in the threshold expansion. The expression for F_3 is[14]

$$F_3 = \frac{1}{L^3}\left[\frac{\widetilde{F}}{3} - \widetilde{F}H^{-1}\widetilde{F}\right], \tag{6.28}$$

$$H = \frac{1}{2\omega\mathcal{K}_2} + \widetilde{F} + \widetilde{G}, \tag{6.29}$$

where all quantities are matrices with indices $\{k, \ell, m\}$. $\mathcal{K}_2$ is a diagonal matrix

$$\left[\frac{1}{2\omega\mathcal{K}_2}\right]_{p\ell' m';k\ell m} = \delta_{pk}\delta_{\ell'\ell}\delta_{m'm}\frac{1}{2\omega_k\mathcal{K}_{2;k}^{(\ell)}}, \tag{6.30}$$

where the only nonzero elements are the s- and d-wave terms

$$\frac{1}{\mathcal{K}_{2;k}^{(0)}} = \frac{1}{16\pi E_{2,k}^*}\left\{-\frac{1}{a_0} + r_0\frac{q_{2,k}^{*2}}{2} + P_0(r_0)^3 q_{2,k}^{*4} + |q_{2,k}^*|[1 - H(\mathbf{k})]\right\}, \tag{6.31}$$

$$\frac{1}{\mathcal{K}_{2;k}^{(2)}} = \frac{1}{16\pi E_{2,k}^*}\frac{1}{q_{2,k}^{*4}}\left\{-\frac{1}{a_2^5} + |q_{2,k}^{*5}|[1 - H(\mathbf{k})]\right\}. \tag{6.32}$$

Here $E_{2,k}^{*2} = (P-k)^2$ is the invariant mass of the dimer, while $q_k^* = \sqrt{E_{2,k}^{*2}/4 - m^2}$ is the momentum of each particle composing the dimer in its CM frame.[15] The expression (6.31) is the standard form for the effective range expansion through quadratic order, with a_0 the s-wave scattering length, r_0 the effective range, and P_0 the shape parameter. Expanding the overall factor of $E_{2,k}^*$ about threshold, and for now ignoring the $1 - H(\mathbf{k})$ term, one recovers the form given in Eq. (6.6). Similarly, aside from the $1 - H$ term, the expression for $\mathcal{K}_{2;k}^{(2)}$, Eq. (6.32), is equivalent to the earlier result, Eq. (6.7). Here the leading order term is

[14] This is the form given in Appendix C of Ref. [28], with $\widetilde{F} = F/(2\omega)$ and $\widetilde{G} = G/(2\omega)$. The matrix H should not be confused with the cutoff function $H(\mathbf{k})$, which is always shown with an argument.

[15] These quantities were denoted s_2 and q_2^*, respectively, in Sec. 6.2.1, but here we need to make explicit that they depend on $\mathbf{k}$. The notation here is the same as in Ref. [28].

parametrized in terms of the d-wave scattering length a_2.[16]

The $1 - H$ terms in the expressions (6.31) and (6.32) arise from the need to introduce a smooth cutoff function $H(\mathbf{k})$ that vanishes for $E^{*2}_{2,k} \leq 0$. We refer the reader to Refs. [28, 68] for further explanation of both the need for this cutoff and the manner in which it enters these expressions. It is sufficient to note here that the $1 - H$ term turns on smoothly only well below the dimer threshold at $E^*_{2,k} = 2m$. The explicit form of $H(\mathbf{k})$ that we use is given in Appendix D.1.

As noted above, the quantization condition holds only if there are no poles in $\mathcal{K}_2$ in the kinematic regime under study. The kinematic range of $q^*_{2,k}$ is given by $-m^2 < q^{*2}_{2,k} < 3m^2$ (corresponding to $0 < E^{*2}_{2,k} < 16m^2$). The parameters in Eqs. (6.31) and (6.32) are thus constrained so that neither right-hand side vanishes for this range of $q^{*2}_{2,k}$. In our numerical investigations, we always use values of the scattering parameters that satisfy these constraints. For a_2 the constraint is that $ma_2 < 1$, with arbitrarily negative values allowed.

The other two quantities appearing in F_3 are the finite-volume kinematic functions $\widetilde{F}$ and $\widetilde{G}$. The former is essentially a two-particle quantity, and thus is diagonal in spectator momenta, though not in the angular-momentum indices:[17]

$$\widetilde{F}_{p\ell' m';k\ell m} \equiv \delta_{pk} H(\mathbf{k}) \widetilde{F}_{\ell' m';\ell m}(\mathbf{k}) \,. \tag{6.33}$$

$\widetilde{G}$ is a kinematic function that arises from one-particle exchange between dimers, and is thus a quantity that involves all three particles. In particular, it is not diagonal in any of the indices. We give the explicit forms of $\widetilde{F}$ and $\widetilde{G}$ in Appendix D.1, and provide some details of their numerical evaluation of $\widetilde{F}$ in Appendix D.2.

An important property is that $\widetilde{G}_{p\ell' m';k\ell m}$ is proportional to $H(\mathbf{p})H(\mathbf{k})$, and is thus trun-

[16] This expansion is often written with a different definition of a_2, in which a_2^5 is replaced by a_2. We prefer the present form since then a_2 has dimensions of length.

[17] We are abusing notation here, but the two versions of $\widetilde{F}$ will always be distinguishable by the presence or absence of the argument $\mathbf{k}$.

cated to the finite number of values of spectator momenta for which $H(\mathbf{k}) \neq 0$. We call this number $N_{\text{spect}}(E, L)$. The same truncation applies to $\widetilde{F}$, due to the factor of $H(\mathbf{k})$ in Eq. (C.9). Both matrices are, however, infinite-dimensional in angular-momentum space. This is to be contrasted to $\mathcal{K}_2$ and $\mathcal{K}_{\text{df},3}$, which are (by approximation) truncated in angular momenta but not in spectator-momentum space. In angular momentum space the dimension is $1 + 5 = 6$ when keeping both s and d waves.

Nevertheless, it turns out that these two truncations are sufficient to reduce the quantization condition, Eq. (6.1), to a determinant of a $6N_{\text{spect}}$-dimensional matrix. To show this, we first write the quantization condition as

$$\det\left[F_3^{-1}\right] \det\left[1 + F_3 \mathcal{K}_{\text{df},3}\right] = 0\,. \tag{6.34}$$

It appears from this rewriting that there will be solutions to the quantization condition when $\det[F_3] \to \infty$, i.e., when F_3 has a diverging eigenvalue. However, in that case, the second determinant will, for a general $\mathcal{K}_{\text{df},3}$, also diverge, leading to a finite product. Thus we expect that the only solutions of the quantization condition (6.1) for general $\mathcal{K}_{\text{df},3}$ will be those that also satisfy

$$\det[1 + F_3 \mathcal{K}_{\text{df},3}] = 0\,. \tag{6.35}$$

This also makes sense intuitively, since we expect all finite-volume energies to depend upon the three-particle interaction. The advantage of the form (6.35) is that it has been shown in Ref. [28] that it effectively truncates all matrices that appear (i.e., $\widetilde{F}$, $\widetilde{G}$, $\mathcal{K}_2$ and $\mathcal{K}_{\text{df},3}$) to N_{spect} entries in spectator-momentum space and to s and d waves in angular-momentum space. By "effectively" we mean that elements of the matrices that lie outside the truncated space do not contribute to the determinant.

In the following, we also consider at times the further truncation to only s-wave dimer interactions. This is effected by setting to zero all entries in the matrices having $\ell = 2$, so that their dimension becomes N_{spect}.

We have now explained how all the matrices contained in the quantization condition Eq. (6.1) are constructed, for given values of E and L. We combine these matrices to form $F_3^{-1}+\mathcal{K}_{\mathrm{df},3}$, and calculate its eigenvalues. For a given choice of L, the finite-volume spectrum is then given by those values of E for which an eigenvalue vanishes.

The practical calculation of this spectrum is facilitated by decomposing into irreducible representations (irreps) of the symmetry group of finite-volume scattering. For a cubic box with $\mathbf{P} = 0$, this is the cubic group, O_h. For the case of pure s-wave dimers, this decomposition has been worked out for the NREFT and FVU quantization conditions in Ref. [40]. It has also been used implicitly in the numerical study of the isotropic approximation to the RFT quantization condition in Ref. [39], since the isotropic approximation automatically involves a projection onto the trivial (A_1^+) irrep.[18] The new result that we now present is the generalization of the decomposition to the case in which one has both s- and d-wave dimers.

6.3.1 Projecting onto cubic group irreps

We begin by recalling some useful properties of the cubic group, O_h. It has dimension $[O_h] = 48$, and ten irreps. Its character table can be found, e.g. in Ref. [99]. The labels for, and dimensions of, the irreps can be seen in Table 6.1 below. Each finite-volume momentum, $\mathbf{k} = (2\pi/L)\mathbf{n}_k$, lies in a "shell" (also known as an orbit) composed of all momenta related to $\mathbf{k}$ by cubic group transformations. We refer to this shell as o_k. There are seven types of shell, differing by the symmetry properties of the individual elements. We label these by the form of $\mathbf{n}_k$: (000), (00a), (aa0), (aaa), (ab0), (aab) and (abc), where a, b and c are all different, nonzero components. They have dimensions $N_o = 1$, 6, 12, 8, 24, 24 and 48, respectively. For example, $\mathbf{n}_k = \hat{x}$ lies in the (001) shell of type (00a), and $\mathbf{n}_k = \hat{x} + 2\hat{z}$ lies in the (120) shell of type (ab0). Each element in a shell is invariant under rotations in a subgroup of O_h, called its little group, L_k. The little groups for all elements in a shell are isomorphic, with

[18] For a more detailed discussion of the isotropic approximation, see Appendix D.6.

dimension $[L_k] = [O_h]/N_o$.

The four matrices that enter the quantization condition Eq. (6.1), namely $2\omega\mathcal{K}_2$, $\mathcal{K}_{\mathrm{df},3}$, $\widetilde{F}$ and $\widetilde{G}$, are all invariant under a set of orthogonal transformations $U(R)$, where $R \in O_h$. Specifically, if M is one of these matrices, then

$$M = U(R) M U(R)^T\,, \qquad U(R)U(R)^T = \mathbf{1}\,, \tag{6.36}$$

$$U(R) = S(R) \otimes \mathcal{D}(R)^T, \tag{6.37}$$

$$U(R)_{p\ell' m';k\ell m} = \delta_{o_p o_k} S^{(o_p)}_{pk}(R)\delta_{\ell'\ell}\mathcal{D}^{(\ell)}_{mm'}(R). \tag{6.38}$$

Here the Wigner D-matrix is defined in Eq. (D.7), while $S(R)$ permutes the spectator momenta within shells:

$$S(R)_{pk} = \delta_{o_p o_k} S^{(o_p)}_{pk}(R) = \delta_{p_R k} \equiv \begin{cases} 1, & R\mathbf{p} = \mathbf{k} \\ 0, & \text{otherwise}\,. \end{cases} \tag{6.39}$$

For $2\omega\mathcal{K}_2$ and $\mathcal{K}_{\mathrm{df},3}$ this result follows because they are invariant under rotations, while for $\widetilde{F}$ and $\widetilde{G}$ it follows from the fact that they are form-invariant under cubic-group rotations if the quantization axis that defines the spherical harmonics is rotated along with the spectator momenta.

The matrices $\{U(R)^T\}_{R\in O_h}$ furnish a representation of O_h:

$$U(R_2R_1)^T = U(R_2)^T U(R_1)^T\,, \quad \forall R_1, R_2 \in O_h\,, \quad \text{and} \quad U(\mathbf{1}_3)^T = \mathbf{1}_{k\ell m}\,. \tag{6.40}$$

One may decompose this reducible representation into irreps I of the cubic group using projection matrices (see, e.g., Ref. [100])

$$P_I = \frac{d_I}{[O_h]} \sum_{R\in O_h} \chi_I(R) U(R)^T\,, \tag{6.41}$$

where d_I is the dimension of I and $\chi_I(R)$ its character.[19] An important simplifying property

[19]Normally one would write $\chi_I(R)^*$ in Eq. (6.41), but since O_h only involves real orthogonal transformations, all characters are real and the conjugation is trivial.

of $U(R)$, which carries over to P_I, is that it is block-diagonal. For the spectator-momentum indices, this follows because

$$U(R)^T_{pk} = S(R)_{kp} \otimes \mathcal{D}(R) = \delta_{k_R\, p}\mathcal{D}(R) = \begin{cases} \mathcal{D}(R), & R\mathbf{k} = \mathbf{p} \\ 0, & \text{otherwise}\,, \end{cases} \tag{6.42}$$

which implies that each $U(R)$ is block diagonal in shells, o. We label the resulting "shell blocks" of P_I as $P_{I,o}$. These shell blocks inherit from $\mathcal{D}(R)$ the property of being block diagonal in ℓ, and we label the corresponding sub-blocks as $P_{I,o(\ell)}$, with $\ell = 0$ or 2. The result is that we can write P_I in the form

$$P_I = \text{diag}(P_{I,o_1},\ P_{I,o_2}, \ldots)\,, \qquad P_{I,o} = \text{diag}(P_{I,o(0)},\ P_{I,o(2)})\,. \tag{6.43}$$

This simplified structure allows for more efficient computation of the P_I matrices, as explained in Appendix D.3.1.

Using these projectors, we can decompose the quantization condition into separate conditions for each irrep. From Eq. (6.36) we know that $[P_I, M] = 0$, for each of the four matrices M, from which it follows that

$$[P_I, F_3^{-1} + \mathcal{K}_{\text{df},3}] = 0 \qquad (\forall I)\,. \tag{6.44}$$

Using $\sum_I P_I = \mathbf{1}$, and the orthogonality of the projectors onto different irreps, one can then show that the determinant factorizes into that for each irrep

$$\det[F_3^{-1} + \mathcal{K}_{\text{df},3}] = \prod_I \det_{\text{sub},I}[P_I(F_3^{-1} + \mathcal{K}_{\text{df},3})P_I]\,, \tag{6.45}$$

where the subscript indicates that the determinant is taken only over the subspace onto which P_I projects. Thus the quantization condition for irrep I becomes

$$\det_{\text{sub},I}[P_I(F_3^{-1} + \mathcal{K}_{\text{df},3})P_I] = 0\,, \tag{6.46}$$

If desired, one can also apply the projectors to all the matrices contained in F_3, Eq. (6.28),

Table 6.1: Dimension of irrep projection sub-blocks for each shell-type and angular momentum, $(d(P_{I,o(0)}), d(P_{I,o(2)}))$. Each row corresponds to an irrep of the cubic group O_h, whose dimension is also listed for completeness.

		shell types						
irrep	dim	(000)	$(00a)$	$(aa0)$	(aaa)	$(ab0)$	(aab)	(abc)
A_1^+	1	$(1,0)$	$(1,1)$	$(1,2)$	$(1,1)$	$(1,3)$	$(1,3)$	$(1,5)$
A_2^+	1	$(0,0)$	$(0,1)$	$(0,1)$	$(0,0)$	$(1,3)$	$(0,2)$	$(1,5)$
E^+	2	$(0,2)$	$(2,4)$	$(2,6)$	$(0,4)$	$(4,12)$	$(2,10)$	$(4,20)$
T_1^+	3	$(0,0)$	$(0,3)$	$(0,9)$	$(0,6)$	$(3,21)$	$(3,21)$	$(9,45)$
T_2^+	3	$(0,3)$	$(0,6)$	$(3,12)$	$(3,9)$	$(3,21)$	$(6,24)$	$(9,45)$
A_1^-	1	$(0,0)$	$(0,0)$	$(0,1)$	$(0,0)$	$(0,2)$	$(0,2)$	$(1,5)$
A_2^-	1	$(0,0)$	$(0,1)$	$(0,1)$	$(1,1)$	$(0,2)$	$(1,3)$	$(1,5)$
E^-	2	$(0,0)$	$(0,2)$	$(0,4)$	$(0,4)$	$(0,8)$	$(2,10)$	$(4,20)$
T_1^-	3	$(0,0)$	$(3,6)$	$(3,12)$	$(3,9)$	$(6,24)$	$(6,24)$	$(9,45)$
T_2^-	3	$(0,0)$	$(0,6)$	$(3,12)$	$(0,6)$	$(6,24)$	$(3,21)$	$(9,45)$

so that the entire evaluation of the quantization condition involves matrices of reduced dimensionality.

The number of eigenvalues in a given irrep is given by the dimension of the projected subspaces, $d(P_I)$. This is obtained by summing the dimensions of the sub-blocks,

$$d(P_I) = \sum_o \sum_{\ell=0,2} d(P_{I,o(\ell)}) \,, \tag{6.47}$$

where the sum over o runs over all shells that are "active", i.e., that lie below the cutoff. We explain how the $d(P_{I,o(\ell)})$ are calculated in Appendix D.3.2, and list the results in Table 6.1. From this we learn, for example, that the $\mathbf{k} = \mathbf{0}$ shell contains one A_1^+ irrep for $\ell = 0$, and one each of the E^+ and T_2^+ irreps for $\ell = 2$. Note that shells can contain multiple versions of a given irrep, e.g., the $(00a)$ shell-type with $\ell = 2$ contains two versions each of the E^+, T_2^+, T_1^- and T_2^- irreps.

At this stage it is useful to give an example of how shells become active as E and L are increased. With our cutoff, described in Appendix D.1, the maximum value of $|\mathbf{n}_k|$, $n_{k,\max}$,

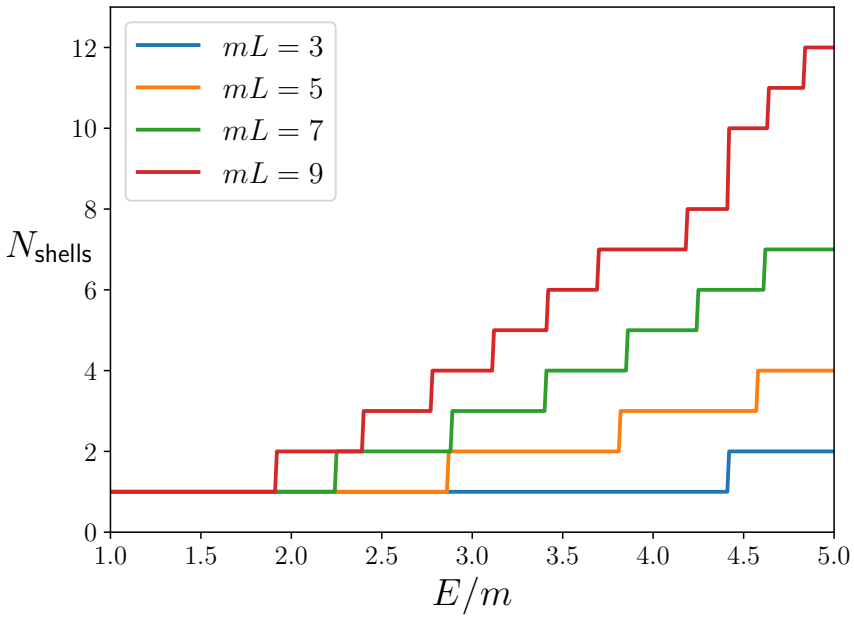

Figure 6.1: Number of active momentum shells for fixed mL as a function of E.

is determined by the vanishing of $E_{2,k}^{*2}$:

$$E_{2,k}^{*2} = 0 \quad \Rightarrow \quad n_{k,\max} = \frac{L}{2\pi}\left(\frac{E^2 - m^2}{2E}\right) . \tag{6.48}$$

This can be easily converted into the number of active shells, an example being shown in Fig. 6.1. The first fifteen shells are (000), (001), (110), (111), (002), (120), (112), (220), (221), (003), (130), (113), (222), (230) and (123), at which point examples of all seven types have appeared.

Although each P_I is block diagonal in o and ℓ, $F_3^{-1} + \mathcal{K}_{\text{df},3}$ is generally not. Thus even though each eigenvector of $F_3^{-1} + \mathcal{K}_{\text{df},3}$ lies in a single irrep, it will generally be a nontrivial linear combination of vectors lying in the subspaces projected onto by $P_{I,o(\ell)}$. However, we can still use Table 6.1 to determine how many eigenvalues will be present in a given irrep for a given choice of E and L. For example, suppose we have both s- and d-wave interactions

turned on and we are in the E, L regime where only the first two momentum shells, (000) and (001), are active, so that $N_{\text{spect}} = 1 + 6 = 7$. Then the table tells us that $F_3^{-1} + \mathcal{K}_{\text{df},3}$ has 3 eigenvalues in A_1^+ since

$$\begin{aligned} d(P_{A_1^+}) &= d(P_{A_1^+,000(0)}) + d(P_{A_1^+,000(2)}) + d(P_{A_1^+,001(0)}) + d(P_{A_1^+,001(2)}) \\ &= 1 + 0 + 1 + 1 = 3\,. \end{aligned} \tag{6.49}$$

Looking at the other irreps, we see that in this regime there is 1 eigenvalue in A_2^+, 8 in E^+, 3 in T_1^+, 9 in T_2^+, 0 in A_1^-, 1 in A_2^-, 2 in E^-, 9 in T_1^-, and 6 in T_2^- giving the correct total of $6N_{\text{spect}} = 42$ eigenvalues. We stress that eigenvalues lying in a given irrep always come in degenerate multiplets corresponding to the dimension of the irrep. Thus, for example, the eight eigenvalues in the E^+ irrep in the two-shell regime consist of four two-fold-degenerate pairs.

A point that may lead to confusion when we present results in the following section is that the number of eigenvalues of $F_3^{-1} + \mathcal{K}_{\text{df},3}$ bears no direct relation to the number of solutions to the quantization condition. For there to be a solution, an eigenvalue must vanish, and this occurs only for a subset of the eigenvalues in the energy range of interest. This point can be seen explicitly if the interactions $\mathcal{K}_2$ and $\mathcal{K}_{\text{df},3}$ are weak, for then we expect the number of states to be the same as for noninteracting particles. We quote in Table 6.2 the irreps that appear in the first few three-particle levels for noninteracting particles. These states have energies

$$E^{\text{free}}(\mathbf{n}_1, \mathbf{n}_2) = \sum_{i=1}^{3} \sqrt{m^2 + (2\pi/L)^2 \mathbf{n}_i^2}\,, \qquad \mathbf{n}_3 = -\mathbf{n}_1 - \mathbf{n}_2\,, \tag{6.50}$$

where $\mathbf{n}_i$ are integer vectors. As an example of the difference between the dimensions of $F_3^{-1} + \mathcal{K}_{\text{df},3}$ and the number of solutions, we consider $mL = 5$ and the A_1^+ irrep, and focus on the energy range $E/m = 3 - 5$. From Fig. 6.1 we see that the number of active momentum shells begins at 2 for $E = 3m$, increases to 3 at some point, and then reaches 4 below $E = 5m$.

Table 6.2: Irreps appearing in the lowest energy levels of three identical noninteracting particles. The first column gives the level number (for values of $mL \sim 5$), starting at zero. The states are labeled by the squares of the three vectors $\mathbf{n}_i$ that determine the momenta of the particles—see Eq. (6.50)—and these are given in the second column. The third column gives the degeneracy, and the final column the irreps that appear.

level	$(\mathbf{n}_1^2, \mathbf{n}_2^2, \mathbf{n}_3^3)$	degen.	irreps
0	$(0,0,0)$	1	A_1^+
1	$(1,1,0)$	3	$A_1^+ + E^+$
2	$(2,2,0)$	6	$A_1^+ + E^+ + T_2^+$
3	$(2,1,1)$	12	$A_1^+ + E^+ + T_2^+ + T_1^- + T_2^-$
4	$(3,3,0)$	4	$A_1^+ + T_2^+$

From Table 6.1 we deduce that the corresponding number of eigenvectors in the A_1^+ irrep are 3, 6 and 8. By contrast, the free levels in this irrep occur at $E = 3m$, $E = 4.21m$, $E = 5.08m$, ... For weak interactions, we expect solutions to the quantization condition only near these three values, and thus we find that, in all cases, the number of eigenvalues of $F_3^{-1} + \mathcal{K}_{\text{df},3}$ significantly exceeds the number of solutions at, or below, the given energy.

We close this section by noting that the components of $\mathcal{K}_{\text{df},3}$, given in Eq. (6.13), can themselves be decomposed into different irreps. While it is clear that $\mathcal{K}_{\text{df},3}^{\text{iso}}$, Eq. (6.14), lies purely in the A_1^+ irrep, we also find that the same is true for the $\mathcal{K}_{\text{df},3}^{(2,A)}$ term. The $\mathcal{K}_{\text{df},3}^{(2,B)}$ term, however, has components that lie in the A_1^+, E^+, T_2^+ and T_1^- irreps. For components lying in the remaining irreps one must go to cubic or higher order in the threshold expansion.

6.4 Results

The goal of this section is to illustrate the impact of including d-wave interactions in the quantization condition. In particular, we aim to determine which energy levels and which irreps are particularly sensitive to such interactions. We begin, however, with a case where the impact of d-wave interactions is small, namely the ground state energy with a weak

two-particle interaction. This allows us to test of our implementation of the quantization condition in a regime where we can make an analytic prediction. We then consider the impact of a strong d-wave interaction, $m|a_2| \sim 1$, comparing its effect on the ground and excited states, and for different irreps. Next we study the sensitivity of the finite-volume spectrum of the physical $3\pi^+$ state, with $\mathcal{K}_2$ taken from experiment, to the various terms in $\mathcal{K}_{\text{df},3}$. And, finally, we discuss the different types of unphysical solutions to the quantization condition that appear.

6.4.1 Threshold expansion including a_2

In this section we consider the energy of the lightest two- and three-particle states in the case of weak two-particle interactions, and with the three-particle interaction $\mathcal{K}_{\text{df},3}$ set to zero. The energy of these states (called $E_2^{(0)}$ and $E_3^{(0)}$, respectively) lie close to their noninteracting values, and we define the differences as

$$\Delta E_n = E_n^{(0)} - n \times m \,. \tag{6.51}$$

These can be expanded in powers of $1/L$ (up to logarithms), the results being called the threshold expansions. These expansions have been worked out in a relativistic theory to $\mathcal{O}(L^{-6})$ in Refs. [24, 68, 81]:[20]

$$\Delta E_2 = \frac{4\pi a_0}{mL^3}\left\{1 + c_1\left(\frac{a_0}{\pi L}\right) + c_2\left(\frac{a_0}{\pi L}\right)^2 + c_3\left(\frac{a_0}{\pi L}\right)^3 + \frac{2\pi r_0 (a_0)^2}{L^3} - \frac{\pi a_0}{m^2 L^3}\right\} + \mathcal{O}(L^{-7})\,, \tag{6.52}$$

$$\begin{aligned}\Delta E_3 =& \frac{12\pi a_0}{mL^3}\left\{1 + d_1\left(\frac{a_0}{\pi L}\right) + d_2\left(\frac{a_0}{\pi L}\right)^2 + \frac{64\pi^2 (a_0)^2 \mathcal{C}_3}{mL^3} + \frac{3\pi a_0}{m^2 L^3} + \frac{6\pi r_0 (a_0)^2}{L^3}\right. \\ &\left. + \left(\frac{a_0}{\pi L}\right)^3 \left(d_3 + c_L \log\frac{mL}{2\pi}\right)\right\} - \frac{\mathcal{M}_{3,\text{thr}}}{48 m^3 L^6} + \mathcal{O}(L^{-7})\,.\end{aligned} \tag{6.53}$$

[20] The terms up to $\mathcal{O}(L^{-5})$ agree with those obtained previously using nonrelativistic QM [65, 66].

Here c_L, $\mathcal{C}_3$, and the c_i and d_i, are numerical constant available in the aforementioned references, and $\mathcal{M}_{3,\text{thr}}$ is a subtracted three-particle threshold scattering amplitude, whose definition will be discussed in Appendix D.4.

What we observe from these results is that they depend, through $\mathcal{O}(L^{-5})$, only on the s-wave scattering length, a_0, with the effective range r_0 first entering at $\mathcal{O}(L^{-6})$. There is no explicit dependence on the d-wave scattering amplitude at this order. We can understand this pattern qualitatively as follows.[21] The typical relative momentum, q, satisfies $\Delta E \sim q^2/m$, and thus, since $\Delta E \sim a_0/L^3$, we learn that $q^2 \sim a_0/L^3$. Using the effective range expansion, Eq. (6.31), we then expect that the relative contribution from the r_0 term will be $r_0 a_0 q^2 \sim r_0 a_0^2/L^3$, and this is indeed what is seen in Eqs. (6.52) and (6.53). By the same argument, we expect the q^4 terms proportional to both P_0 and a_2^5 to appear first at relative order $\mathcal{O}(L^{-6})$, and thus contribute to ΔE_n at $\mathcal{O}(L^{-9})$. If this were the case, it would be very challenging to see the dependence of the threshold energies on a_2.

However, it turns out that there is an additional contribution of $\mathcal{O}(L^{-6})$ to ΔE_3 that depends on a_2, and indeed on all higher partial waves, hidden in $\mathcal{M}_{3,\text{thr}}$. In Appendix D.4 we calculate the leading dependence on a_2 in a perturbative expansion in the scattering amplitudes, finding

$$m^2 \mathcal{M}_{3,\text{thr}} \supset d_{\text{thr}} (m a_0)^2 (m a_2)^5 \left[1 + \mathcal{O}(a_0) + \mathcal{O}(a_2^5)\right] , \quad d_{\text{thr}} = -14110 \,. \tag{6.54}$$

The appearance of a_2^5, rather than a_2, follows from our parametrization of the d-wave K matrix, Eq. (6.32). In order to isolate the a_2 dependence of ΔE_3, we consider the difference

$$\delta E^d(L, a_0, a_2) = \Delta E_3(L, a_0, a_2) - \Delta E_3(L, a_0, a_2 = 0) \,. \tag{6.55}$$

Substituting Eq. (6.54) into the expression for ΔE_3, Eq. (6.53), we obtain the theoretical

[21] See also Appendix C in Ref. [101].

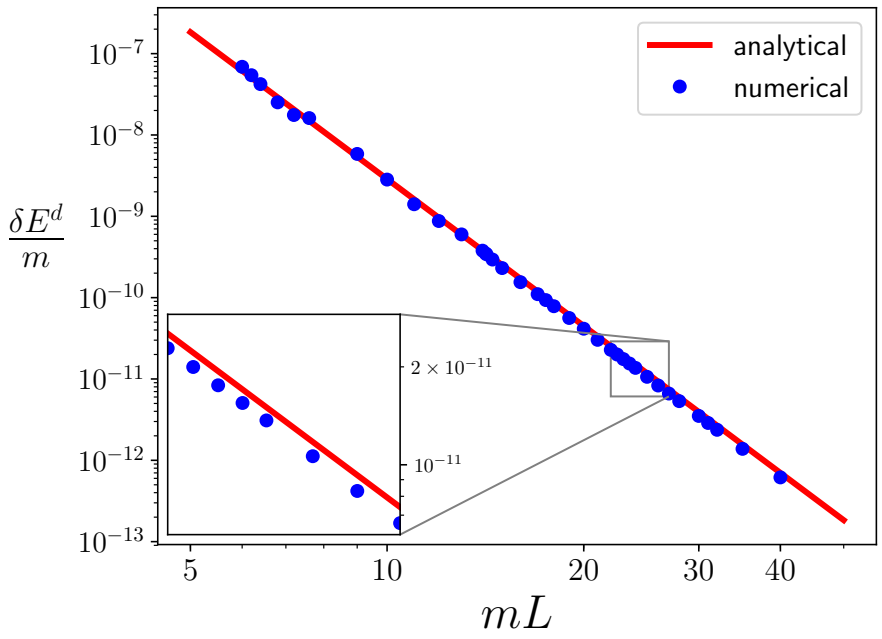

Figure 6.2: Comparison of the analytical prediction (which is absolutely normalized) with the results from a numerical solution of the quantization condition. The parameters are $ma_0 = 0.1$, $ma_2 = 0.25$, and $r_0 = P_0 = \mathcal{K}_{\mathrm{df},3} = 0$. The lack of linearity for smaller values of mL is related to the opening up of new momentum shells.

prediction

$$\frac{\delta E^d}{m} = -\frac{d_{\mathrm{thr}}}{48}\frac{(ma_0)^2\,(ma_2)^5}{(mL)^6}\left[1 + \mathcal{O}(a_0) + \mathcal{O}(a_2^5)\right] + \mathcal{O}\left(L^{-7}\right)\,. \tag{6.56}$$

We have checked that the results from numerically solving the quantization condition are consistent with Eq. (6.56). In particular, we have verified that the leading dependence on a_0, a_2 and $1/L$ is as predicted. An example of the comparison, showing the L dependence, is given in Fig. 6.2. Agreement at the 10% level holds over many orders of magnitude. Based on our tests, we find that the major source of this small discrepancy arises from terms of higher order in a_0.

This comparison provides a strong cross-check of our numerical implementation. However,

for weakly interacting system, such as mesons in QCD, one cannot achieve, using lattice calculations, results for the spectrum with the precision shown in the figure, nor can one work at such large values of mL. We now turn to situations in which a_2 has a numerically more significant effect.

6.4.2 Effects of a_2 on the three-particle spectrum

We begin by studying the strongly interacting regime, where $m|a_2| \sim 1$. This regime, although hardly conceivable in particle physics, represents an interesting academic problem that is relevant in the physics of cold atoms [102, 103].

In Fig. 6.3, we show the three particle spectrum for $E < 4m$ in two irreps, A_1^+ and E^+, as a function of negative ma_2. Here we have fixed the volume to $mL = 8.1$, and chosen a weakly attractive s-wave interaction, $ma_0 = -0.1$, with other scattering parameters set to zero. We choose negative values for ma_2 in order to avoid the possibility of a pole in $\mathcal{K}_2^{(2)}$, Eq. (6.32), for which our formalism breaks down. Note that negative a_2 corresponds, at least for small magnitudes, to an attractive interaction, as seen from the result for δE^d, Eq. (6.56). Since we use a small value of $m|a_0|$, the energy levels at the right-hand edges of both plots (where $a_2 = 0$) lie close to the energies of three noninteracting particles (which are $E/m = 3$, 3.53, 3.97, 4.02, ... for $mL = 8.1$). As $m|a_2|$ increases, the energies are almost flat, until at a value $m|a_2| \sim 1$, the levels shift rapidly downwards. This shift begins at smaller values of $m|a_2|$ for excited states. As the magnitude of a_2 increases, the excited states approach lower-lying states until an avoided level crossing occurs. We also observe that states in the E^+ irrep are more sensitive to d-wave interactions, which seems to be a general feature, as will be seen in the following section.

Another interesting observation from Fig. 6.3 is the presence of a deep subthreshold state for $m|a_2| > 1$. This resembles the Efimov effect, which describes a three-particle bound state arising from an attractive two-particle interaction $m|a_0| \gg 1$ [104]. The Efimov bound

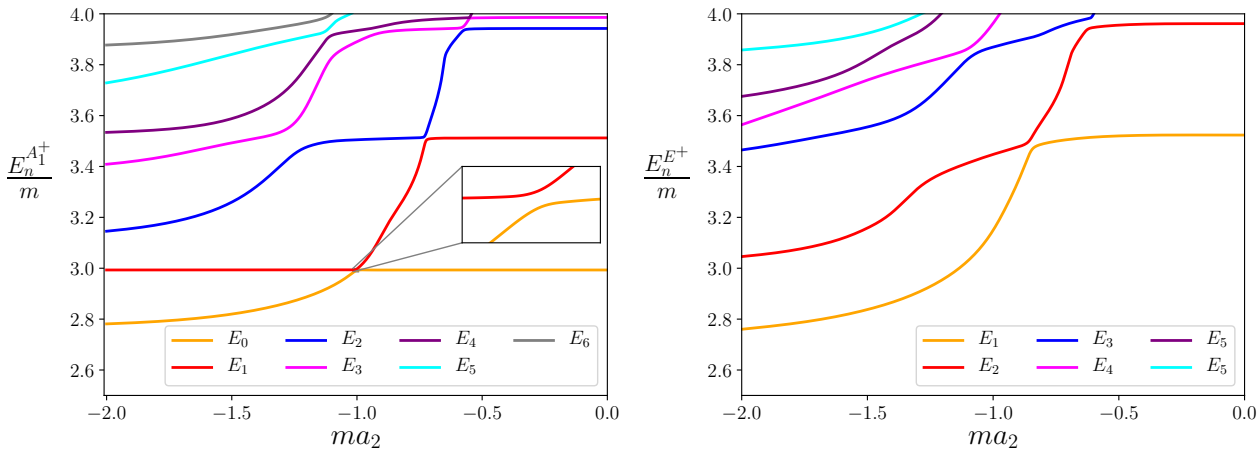

(a) A_1^+ irrep (b) E^+ irrep

Figure 6.3: Energy levels as a function of ma_2 in the region $E < 4m$ with $mL = 8.1$ and $ma_0 = -0.1$, $r_0 = P_0 = \mathcal{K}_{\text{df},3} = 0$ in the A_1^+ irrep (left) and the E^+ irrep (right).

state has been reproduced numerically with only s-wave interactions present, both in the NREFT approach [31, 40] and in the isotropic approximation of the RFT formalism [39]. Moreover, there is some theoretical work regarding the existence of this generalized Efimov scenario in the presence of d-wave interactions [103], although there is no result concerning the asymptotic volume dependence, unlike in the s-wave case [105]. We have been able to solve the quantization condition numerically up to $mL = 37.5$ and the bound state energy barely changes, which strongly suggests that it is indeed an infinite volume bound state. Results for $ma_2 = -1.3$ are shown in Fig. 6.4. The volume dependence of the energy is dominated by effects of the UV cut-off, which manifest themselves as small oscillations when a new shells become active. These are similar to oscillations observed in several quantities in Ref. [39].

We close by commenting on the impact of using a relativistic formalism, as opposed to a NR approach, on the results of this section. We expect that the qualitative features of the results will be unchanged, but that the quantitative energy levels will be changed

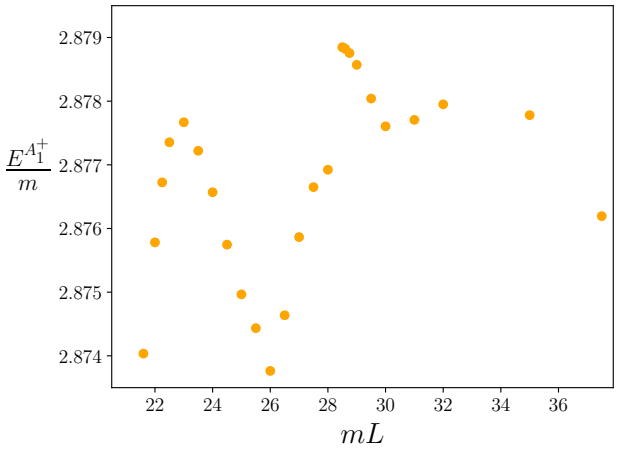

Figure 6.4: Energy of the subthreshold state in the A_1^+ irrep as a function of mL. The parameters are $ma_0 = -0.1$, $ma_2 = -1.3$ and $r_0 = P_0 = \mathcal{K}_{\mathrm{df},3} = 0$. Note the highly compressed vertical scale.

once they differ significantly from $3m$. Thus, for example, we expect that the energy of the subthreshold state will be only slightly changed, since it lies at the border of the NR regime.

6.4.3 Application: spectrum of $3\pi^+$ on the lattice

The simplest application in QCD for the three-particle quantization condition is the $3\pi^+$ system, not only from the theoretical point of view—no resonant subchannels—but also from the technical side—no quark-disconnected diagrams and a good signal/noise ratio. Here we use our formalism to predict the $3\pi^+$ spectrum, using values for the two-body scattering parameters determined from experiment, and a range of choices for the parameters in $\mathcal{K}_{\mathrm{df},3}$.[22] Our focus will be on how to differentiate effects arising from the different components of $\mathcal{K}_{\mathrm{df},3}$, listed in Eq. (6.13).

An important point in the following is that that there is no natural size for the parameters

[22] We ignore QED effects, which are numerically small, and, in any case, cannot be incorporated into the present formalism.

in $\mathcal{K}_{\mathrm{df},3}$: the magnitudes of the dimensionless coefficients $\mathcal{K}^{\mathrm{iso}}_{\mathrm{df},3}$, $\mathcal{K}^{\mathrm{iso},1}_{\mathrm{df},3}$, $\mathcal{K}^{\mathrm{iso},2}_{\mathrm{df},3}$, $\mathcal{K}^{(2,A)}_{\mathrm{df},3}$, and $\mathcal{K}^{(2,B)}_{\mathrm{df},3}$ are not constrained. Strictly speaking, we know this only for $\mathcal{K}^{\mathrm{iso}}_{\mathrm{df},3}$, because, in the nonrelativistic limit, it is related to the three-particle contact interaction in NREFT (a relation given explicitly in Ref. [74]), and it is well known that the latter interaction varies in a log-periodic manner from $-\infty$ to ∞ as the cutoff varies [106]. But we see no reason why this should not also apply to the other coefficients. In particular, we note that the physical three-particle scattering amplitude, $\mathcal{M}_3$, does not diverge when $\mathcal{K}_{\mathrm{df},3}$ does [29, 39].

We take the parameters describing isospin-2 $\pi\pi$ scattering from Ref. [107]:

$$m_\pi a_0 = 0.0422, \quad m_\pi r_0 = 56.21, \quad P_0 = -3.08 \cdot 10^{-4}, \quad m_\pi a_2 = -0.1867\,. \tag{6.57}$$

In a lattice simulation, these parameters would be extracted from the two-pion spectrum, using the two-particle quantization condition. Indeed, there is considerable recent work on the $2\pi^+$ system using lattice methods, in some cases incorporating d-wave interactions [95, 108–112]. We emphasize that one must determine these parameters with high precision in order to disentangle the two- and three-body effects in the three-particle spectrum.

For the relatively weak two-particle interactions of Eq. (6.57), the energy levels lie close to the noninteracting energies of Eq. (6.50). For the regime of box sizes available in current lattice simulations, $4 \lesssim m_\pi L \lesssim 6$, there are at most three such levels below the five-particle threshold, $E = 5m_\pi$ (above which the quantization condition breaks down). For these levels, the solutions lie in three irreps: $\Gamma = A_1^+, E^+, T_2^+$ (see Table 6.2). We denote the difference between the actual energy and its noninteracting value as

$$\Delta E_n^\Gamma = E_n^\Gamma - E_n^{\mathrm{free}} \tag{6.58}$$

where $n = 0, 1, \ldots$ labels the levels following the numbering scheme of Table 6.2. It is known that, asymptotically, [77]

$$\Delta E_n^\Gamma \propto \frac{a_0}{mL^3} + \mathcal{O}(L^{-4})\,. \tag{6.59}$$

We stress, however, that the asymptotic result is not numerically accurate for the range of mL that we consider.

Let us start from the ground state, which lies in the A_1^+ irrep. Here our expectations are guided by the threshold expansion, Eq. (6.53). In addition to explicit dependence on a_0 and r_0, and the implicit dependence on a_2 worked out in Sec. 6.4.1, the energy depends on $\mathcal{K}_{\mathrm{df},3}$ through the $\mathcal{M}_{3,\mathrm{thr}}/L^6$ term. Following the arguments given in Sec. 6.4.1, we expect that only $\mathcal{K}_{\mathrm{df},3}^{\mathrm{iso}}$ will enter at this order, with dependence on $\mathcal{K}_{\mathrm{df},3}^{\mathrm{iso},1}$ suppressed by $1/L^3$ and that on $\mathcal{K}_{\mathrm{df},3}^{\mathrm{iso},2}$, $\mathcal{K}_{\mathrm{df},3}^{(2,A)}$ and $\mathcal{K}_{\mathrm{df},3}^{(2,B)}$ by $1/L^6$. This is borne out by our numerical results, shown in Fig. E.2. The left panel compares results with several choices of parameters: (i) those of Eq. (6.57) plus $\mathcal{K}_{\mathrm{df},3} = 0$ (labeled "s- and d-wave"—black, dotted line); (ii) the same as (i) but with $\mathcal{K}_{\mathrm{df},3}^{\mathrm{iso}} = 300$ and all other parameters in $\mathcal{K}_{\mathrm{df},3}$ vanishing (magenta); (iii) the same as (ii) but with $\mathcal{K}_{\mathrm{df},3}^{\mathrm{iso},1}$ also turned on, taking the three values 135 (blue), 270 (cyan) and 810 (grey); and (iv) the isotropic approximation, i.e., with only s-wave interactions, and a_0 the only nonzero scattering parameter (orange). We see that adding d-wave two-particle interactions has a similar impact to adding $\mathcal{K}_{\mathrm{df},3}^{\mathrm{iso}} = 300$, but that adding $\mathcal{K}_{\mathrm{df},3}^{\mathrm{iso},1}$ with a similar magnitude has almost no impact.

The right panel shows the dependence on $\mathcal{K}_{\mathrm{df},3}^{\mathrm{iso}}$, with other parameters fixed at the values in Eq. (6.57). The range we consider is $\mathcal{K}_{\mathrm{df},3}^{\mathrm{iso}} = [-1000, +1000]$. In order to have sensitivity to $\mathcal{K}_{\mathrm{df},3}^{\mathrm{iso}}$ in this range, a determination of $\Delta E_0/m$ with an error of ≈ 0.01 is needed. Such an error can be achieved with present methods. Thus, as noted in Ref. [39], if one has a sufficiently accurate knowledge of the two-particle scattering parameters, one can use the ground state energy to determine the leading three-particle parameter $\mathcal{K}_{\mathrm{df},3}^{\mathrm{iso}}$. Indeed, this approach has been carried out successfully in Refs. [47, 55].

In Fig. 6.6, we investigate the sensitivity of the energy of the first excited state to the various two-particle scattering parameters, comparing the two irreps that are present. The magnitude of the energy shifts are comparable to those for the ground state, but the de-

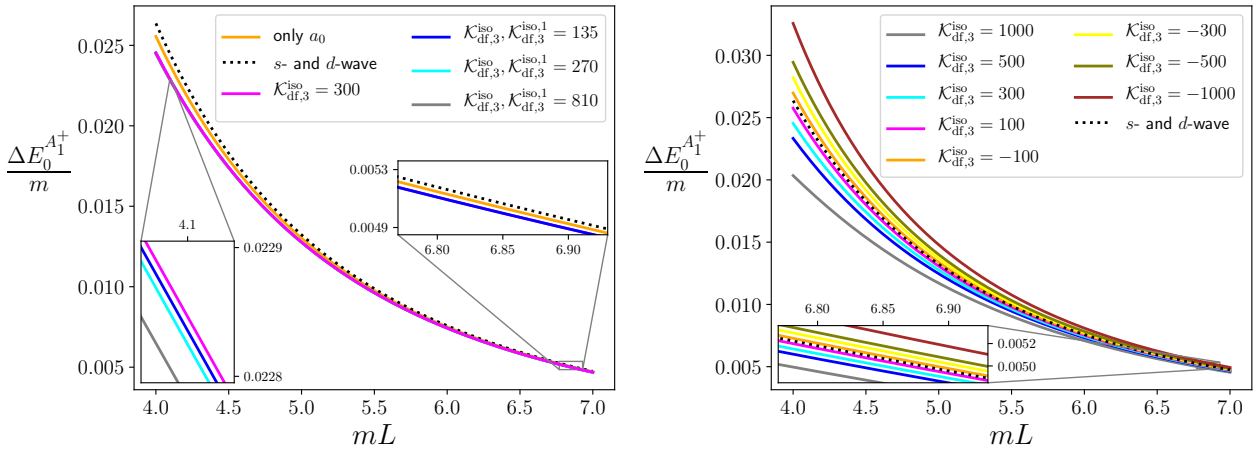

Figure 6.5: Energy shift for the ground state in the A_1^+ irrep, for which $E_0^{\mathrm{free}} = 3m$. The two-particle scattering parameters are those in Eq. (6.57), aside from the orange curve in the left panel, where only a_0 is nonzero. The three particle scattering parameters are as indicated in the legend, and explained further in the text. We use the convention that a parameter value not given explicitly is set to the value given earlier. For example, the blue line in the left panel has the parameters set to $\mathcal{K}_{\mathrm{df},3}^{\mathrm{iso}} = 300$ and $\mathcal{K}_{\mathrm{df},3}^{\mathrm{iso},1} = 135$, while $\mathcal{K}_{\mathrm{df},3}^{\mathrm{iso},2} = \mathcal{K}_{\mathrm{df},3}^{(2,A)} = \mathcal{K}_{\mathrm{df},3}^{(2,B)} = 0$.

pendence on the scattering parameters differs markedly. This can be understood because the relative momenta between the particles is nonvanishing for the excited state. Denoting generically the relative momenta by q, this satisfies $q/m \approx 2\pi/(mL) \sim \mathcal{O}(1)$. Because of this we expect that the higher-order terms in the effective range expansion, i.e. r_0 and P_0, should play a much more significant role. This is borne out by the results in the figure, particularly for the A_1^+ irrep. We observe that the effect of these additional terms is opposite in the two irreps, which is consistent with the prediction of the threshold expansion generalized to excited states [77]. We also see that adding d-wave dimers has almost no impact on the A_1^+ irrep (indeed, the effect is smaller than for the ground state) while the impact is comparable to that of r_0 and P_0 for the E^+ irrep. Qualitatively, this is as expected, since the averaging over orientations in the A_1^+ irrep suppresses the overlap with d-wave dimers.

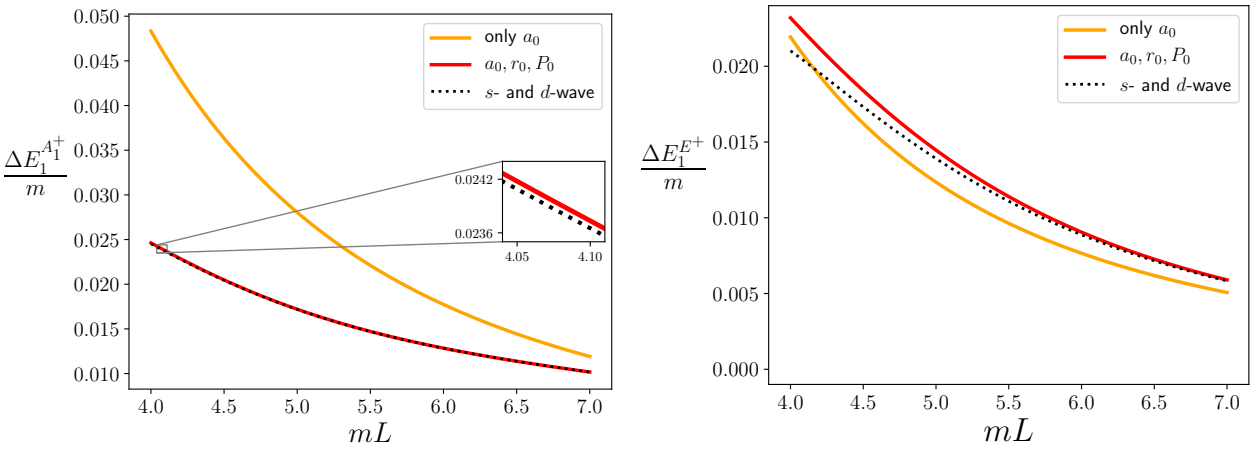

Figure 6.6: Energy shift of the first excited state in the A_1^+ irrep (left) and E^+ irrep (right). In the range of mL shown, $E_1^{\text{free}}/m = 4.7 - 3.9$. The quantization condition is solved with only two-particle scattering parameters being nonzero, while $\mathcal{K}_{\text{df},3} = 0$. When a parameter is nonzero, its value is given by Eq. (6.57). The solid orange and red curves include only s-wave dimers, the former having only a_0 turned on ("only a_0"), with the latter having all three s-wave parameters in $\mathcal{K}_2$ nonzero ("a_0, r_0, P_0"). The dotted black line shows the impact of adding d-wave dimers, with a_2 nonzero ("s- and d-wave").

In Fig. 6.7 we illustrate the dependence of the same two excited states on the five parameters in $\mathcal{K}_{\text{df},3}$, Eq. (6.13). Because $q/m \sim \mathcal{O}(1)$ we expect that, unlike for the ground state, the energy should be sensitive to all five parameters, and not just to $\mathcal{K}_{\text{df},3}^{\text{iso}}$. This is borne out for the A_1^+ irrep, where there is strong sensitivity to all three isotropic parameters, and a somewhat weaker dependence on $\mathcal{K}_{\text{df},3}^{(2,A)}$ and $\mathcal{K}_{\text{df},3}^{(2,B)}$. As noted above, only $\mathcal{K}_{\text{df},3}^{(2,B)}$ affects the E^+ irrep, and Fig. 6.7 illustrates this dependence.

The energy shift for the second excited states are shown in Fig. 6.8. We show results only for those volumes for which the states lie below the five-particle threshold, which requires $mL \gtrsim 5.2$. The A_1^+ energy-shift depends on all parameters in $\mathcal{K}_{\text{df},3}$, while the E^+ and T_2^+ irreps depend only on $\mathcal{K}_{\text{df},3}^{(2,B)}$. The results show a similar dependence on parameters as for the first excited states. We also find that the E^+ and T_2^+ irreps show the greatest sensitivity

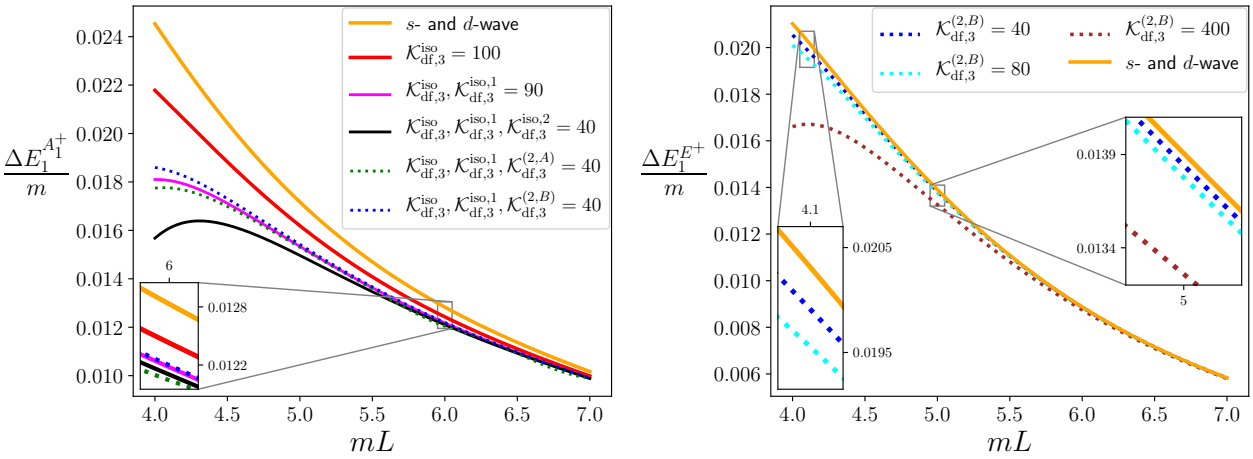

Figure 6.7: Energy shift of the first excited state in the A_1^+ irrep (left) and E^+ irrep (right) with various choices of the parameters in $\mathcal{K}_{\mathrm{df},3}$. The two-particle scattering parameters are given by Eq. (6.57) for all curves. The choices of $\mathcal{K}_{\mathrm{df},3}$ parameters is explained by the legend, with the convention that a parameter value not given explicitly is set to the value given earlier. For example, the black line has the parameters set to $\mathcal{K}_{\mathrm{df},3}^{\mathrm{iso}} = 100$, $\mathcal{K}_{\mathrm{df},3}^{\mathrm{iso},1} = 90$, and $\mathcal{K}_{\mathrm{df},3}^{\mathrm{iso},2} = 40$, while $\mathcal{K}_{\mathrm{df},3}^{(2,A)} = \mathcal{K}_{\mathrm{df},3}^{(2,B)} = 0$.

to a_2 of all the states considered.

To sum up, a possible program for determining the coefficients in $\mathcal{K}_{\mathrm{df},3}$ up to quadratic order in the threshold expansion is as follows:

1. Determine a_0, r_0, P_0, and a_2 from the two-body sector using standard two-particle methods.

2. Extract $\mathcal{K}_{\mathrm{df},3}^{\mathrm{iso}}$ from the threshold state.

3. Use states in the E^+ and T_2^+ irreps to calculate $\mathcal{K}_{\mathrm{df},3}^{(2,B)}$.

4. Use the excited states in the A_1^+ irrep to obtain the rest of the parameters. The most difficult parameter to determine would be $\mathcal{K}_{\mathrm{df},3}^{(2,A)}$, because its contribution to the energy is smaller.

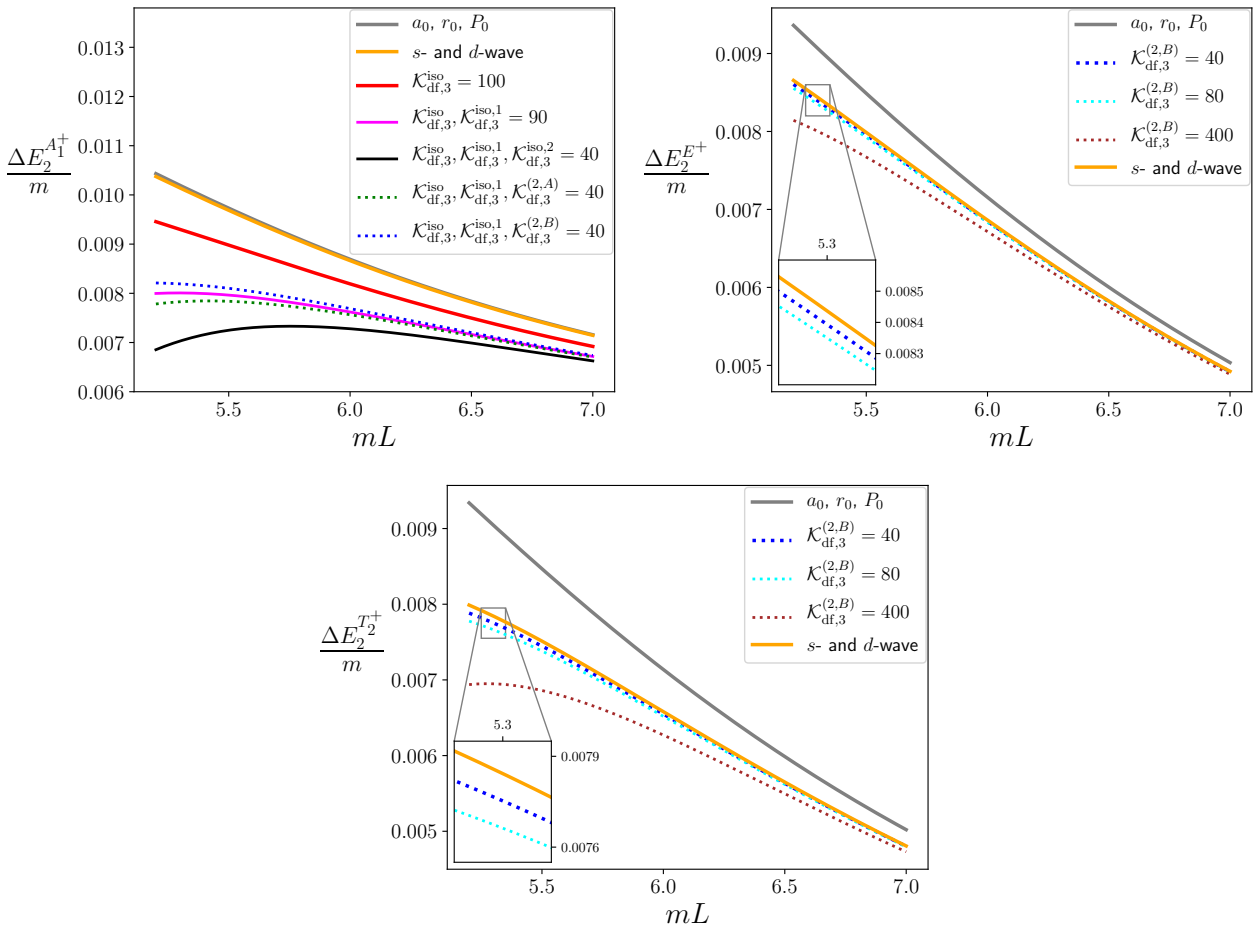

Figure 6.8: Energy shift of the second excited states in the A_1^+ irrep (top left), the E^+ irrep (top right) and T_2^+ irrep (bottom). The meaning of the legend is as in previous figures.

Further information could be obtained using moving frames, as has been done very successfully in the two-particle case. The formalism of Ref. [28] is still valid, but the detailed implementation along the lines of this paper has yet to be worked out.

We close by commenting on the importance of using a relativistic formalism for the results that we have presented in this section. We note that the excited states whose energies we consider lie in the relativistic regime. For example, at $mL = 5.5$, the relativistic noninteract-

ing energy of the second excited state is $E_2^{\text{free}} = 4.80m$, to be compared to the nonrelativistic energy $3m + 2m(2\pi/(mL))^2 = 5.61m$. Nevertheless, it may be that the energy splittings ΔE_n^Γ are much less sensitive to relativistic effects, and it would be interesting to implement the NREFT approach including d waves in order to study this. We do expect, however, that the parametrization of the three-particle interaction will require additional terms once the constraints of relativistic invariance are removed.

6.4.4 Unphysical solutions

In this section we describe solutions to the quantization condition that are, for various reasons, unphysical. These fall roughly into two classes (although there is some overlap): solutions that occur at the energies of three noninteracting particles (which we refer to as "free solutions", occurring at "free energies"), and solutions that correspond to poles in the finite-volume correlator that have the wrong sign of the residue. The latter were first observed in Ref. [39] within the isotropic approximation. In the following, we begin with a general discussion of the properties of physical solutions, and then discuss the two classes of unphysical solutions in turn.

General properties of physical solutions

We recall here the properties that physical solutions to the quantization condition, Eq. (6.1), must obey. This extends the analysis presented in Ref. [39] for the isotropic approximation.

The key quantity is the two-point correlation function in Euclidean time,

$$\widetilde{C}_L(\tau) = \langle 0|\mathcal{O}(\tau)\mathcal{O}^\dagger(0)|0\rangle\,, \tag{6.60}$$

where the operator $\mathcal{O}^\dagger$ has the correct quantum numbers to create three particles (and here also has $\mathbf{P} = 0$). We stress that its hermitian conjugate is used to destroy the states. Inserting a complete set of finite-volume states with appropriate quantum numbers, we find

the standard result

$$\widetilde{C}_L(\tau) = \sum_j \frac{c_j}{2E_j} \exp(-E_j|\tau|)\,, \tag{6.61}$$

where $E_j > 0$ are the energies relative to the vacuum, and the c_j are real and positive. Fourier transforming to Euclidean energy and Wick rotating yields

$$C_L(E) = \sum_j c_j \frac{i}{E^2 - E_j^2} = \sum_j \frac{ic_j}{(E+E_j)(E-E_j)}\,, \tag{6.62}$$

where E is the Minkowski energy that appears in the quantization condition. Thus $C_L(E)$ is composed of single poles whose residues, for $E > 0$, are given by i times real, positive coefficients.

Next we recall from the analysis of Ref. [28] that the correlator can also be written as

$$C_L(E) = A^\dagger \frac{i}{F_3^{-1} + \mathcal{K}_{\mathrm{df},3}} A = \sum_j |A^\dagger \cdot v_j(E)|^2 \frac{i}{\lambda_j(E)}\,, \tag{6.63}$$

where A is a column vector, and to obtain the second form we have decomposed $F_3^{-1} + \mathcal{K}_{\mathrm{df},3}$ in terms of its eigenvalues $\lambda_j(E)$ and eigenvectors $v_j(E)$.[23] Since $F_3^{-1} + \mathcal{K}_{\mathrm{df},3}$ is real and symmetric, the eigenvalues are real.

It follows from comparing Eqs. (6.62) and (6.63) that

(a) $\lambda_j(E)$ cannot have double zeros. This is because, in the vicinity of a double zero at E_j, $C_L(E)$ would have a double pole, $C_L(E) \propto 1/(E-E_j)^2$. The same prohibition applies to higher-order zeros.

(b) Eigenvalues of $F_3^{-1} + \mathcal{K}_{\mathrm{df},3}$ that pass through zero (and thus lead to solutions to the quantization condition) must do so from below as E increases. To understand this, note that, if $\lambda_j(E)$ has a single zero at $E = E_j$, then

$$C_L(E) = |A^\dagger \cdot v_j(E_j)|^2 \frac{i}{\lambda_j'(E_j)(E-E_j)} + \text{non-pole}\,. \tag{6.64}$$

[23] For the sake of brevity, we do not show explicitly that the quantities also depend on L.

Comparing to Eq. (6.62) we learn that

$$\lambda_j'(E_j) \equiv \left.\frac{d\lambda_j(E)}{dE}\right|_{E=E_j} > 0\,. \tag{6.65}$$

This is the generalization of a condition found in Ref. [39] for the isotropic approximation (where there is only a single relevant eigenvalue).

Any solutions to the quantization condition that do not satisfy both of these conditions we refer to as unphysical.

We are aware of only three possible sources for unphysical solutions. First, they can arise from the truncation of the quantization condition to a finite-number of partial waves. Second, they could be the result of an unphysical parametrization of $\mathcal{K}_2$ and $\mathcal{K}_{\text{df},3}$; for example, the truncation of the threshold expansion for $\mathcal{K}_{\text{df},3}$ could be unphysical. And, finally, the exponentially-suppressed terms that we have dropped could be large in some regions of parameter space, particularly for small mL. We now present examples of unphysical solutions that we have found in our numerical investigation.

Solutions with the wrong residue

In this section we give examples of unphysical solutions to the quantization condition that do not satisfy Eq. (6.65), i.e. which lead to single poles whose residues have the wrong sign. These were observed in the isotropic approximation in Ref. [39], where it was found that they occurred only when $|\mathcal{K}_{\text{df},3}^{\text{iso}}|$ was very large. Here we investigate how this result generalizes in the presence of d-wave dimers.

We first investigate whether unphysical solutions can be induced by adding d-wave interactions alone, with $\mathcal{K}_{\text{df},3} = 0$. We do not find such solutions for large negative values of ma_2—the results obtained in Sec. 6.4.2 all correspond to zero crossings in the correct direction. However, as ma_2 approaches unity (which, as we saw in Sec. 6.3, is the upper bound allowed for the formalism), we do find examples of unphysical solutions. Since we

have seen in Secs. 6.4.2 and 6.4.3 that the impact of d-wave interactions is greater for irreps other than A_1^+, we focus on the E^+ irrep, and work in the vicinity of the energy of the first noninteracting excited state, E_1^{free}. In Fig. 6.9, we plot the smallest eigenvalue in magnitude of $F_3^{-1} + \mathcal{K}_{\text{df},3} = F_3^{-1}$ in the E^+ irrep as a function of energy, for two different values of mL and a range of positive values of ma_2 approaching unity. The only other nonvanishing scattering parameter is $ma_0 = -0.1$. Consider first the left panel, with $mL = 8.1$. When $a_2 = 0$, there is a solution at $E \approx E_1^{\text{free}} = 3.53m$, as shown by the lowest level in Fig. 6.3(b). As a_2 is increased, the energy shifts upwards, as expected since positive a_2 corresponds to a repulsive interaction. When $ma_2 = 0.9$, the level is at $E_1 \approx 3.6m$, and moves to yet higher energies as ma_2 increases. These solutions are physical, as shown in the bottom-left inset. For $ma_2 = 0.9$ and 0.91, however, there is also a single unphysical solution near $E = 3.85m$, which displays the additional unphysical behavior of having a decreasing energy with increasingly repulsive a_2. Furthermore, for $ma_2 = 0.92$, there is a triplet of solutions—two unphysical and one physical. Since they are clearly related, we consider all three to be unphysical. For even larger ma_2, there are no solutions in the energy range shown.

The right panel, Fig. 6.9(b), displays a similar pattern, with an additional twist. Here $mL = 10$, so that $E_1^{\text{free}} = 3.36m$. The energy of the physical solution lies above this, and increases with increasing ma_2. There is also an unphysical solution at higher energy, whose energy decreases with increasing ma_2. The new feature is the presence of a double zero at E_1^{free}. As discussed above, this is manifestly unphysical since it leads to a double pole in $C_L(E)$. It is also unexpected, as its energy lies at that of noninteracting particles. We discuss such solutions in detail in the following section.

Another example of unphysical solutions in shown in Fig. 6.10, this time induced by a large, negative value of $\mathcal{K}_{\text{df},3}^{(2,B)}$. Recall that, out of the parameters in $\mathcal{K}_{\text{df},3}$, the E^+ irrep is only sensitive to $\mathcal{K}_{\text{df},3}^{(2,B)}$. Again, there are physical solutions that have the expected behavior of increasing energy with increasingly negative $\mathcal{K}_{\text{df},3}^{(2,B)}$ (which corresponds to a repulsive in-

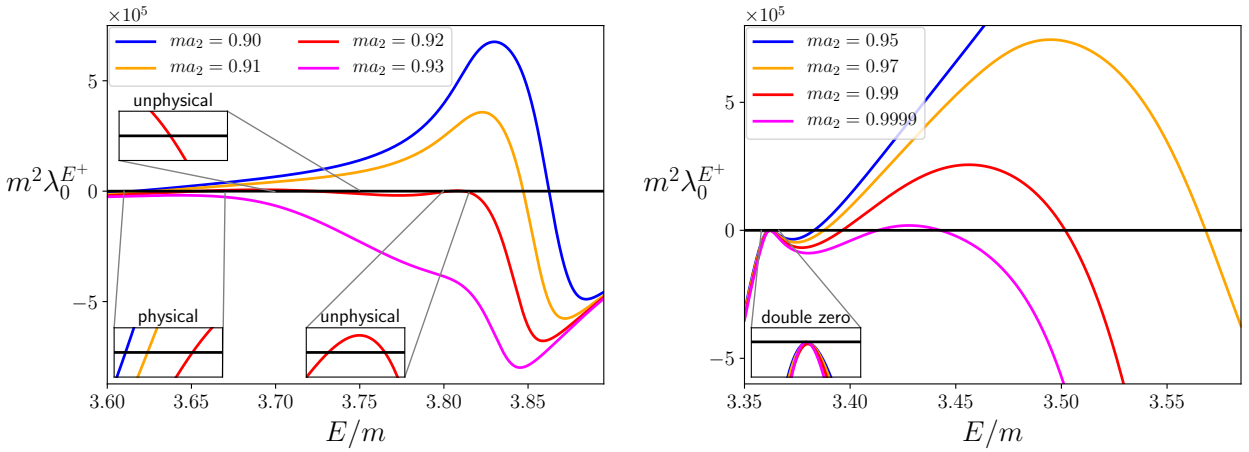

(a) $mL = 8.1$ (b) $mL = 10$

Figure 6.9: Smallest eigenvalue in magnitude of F_3^{-1} in the E^+ irrep as a function of the energy for two different values of mL. The parameters are $ma_0 = -0.1$ and $r_0 = P_0 = \mathcal{K}_{\mathrm{df},3} = 0$. Physical and unphysical solutions as well as a double pole at the free energy (to be discussed in Sec. 6.4.4) are indicated.

teraction), but there are also unphysical solutions at higher energy with opposite dependence on $\mathcal{K}_{\mathrm{df},3}^{(2,B)}$. Eventually, for large enough $|\mathcal{K}_{\mathrm{df},3}^{(2,B)}|$ both solutions disappear.

We do not yet understand the source of these unphysical solutions, i.e. which of the three possible sources mentioned at the end of the previous section are most important. This is a topic for future study. Our attitude is that, if a physical solution is well separated from an unphysical one, and its behavior as interactions are made more attractive or repulsive is reasonable, then we accept the physical solution and reject the unphysical one. The examples we have shown occur when the interactions are strong and repulsive, in which limit the two solutions come close together, and at some point become unreliable. For attractive interactions, the two solutions are far apart, often with the unphysical one lying outside the range in which the quantization condition is valid. In this regime, which includes that discussed in Sec. 6.4.2, we trust the physical solutions.

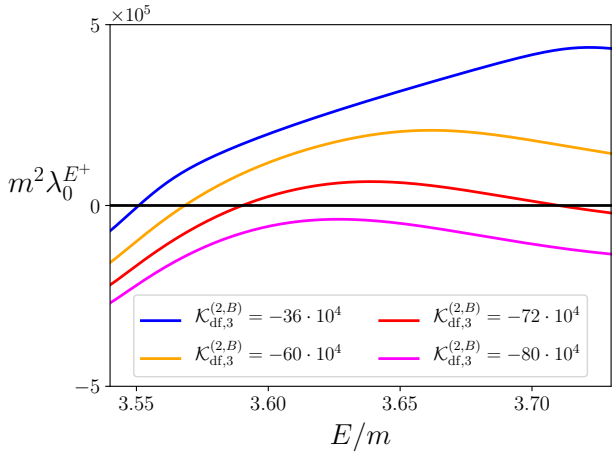

Figure 6.10: Eigenvalue of $F_3^{-1} + \mathcal{K}_{\mathrm{df},3}$ with smallest magnitude in the E^+ irrep as a function of the energy. The parameters are $mL = 8.1$, $ma_0 = ma_2 = 0.1$, $r_0 = P_0 = 0$, and $\mathcal{K}_{\mathrm{df},3} = 0$ for all terms except $\mathcal{K}_{\mathrm{df},3}^{(2,B)}$.

We conclude by stressing that, in the case of three pions in QCD, the interactions are relatively weak, and we do not expect unphysical solutions to be relevant.

Solutions at free particle energies

This section concerns "free solutions": solutions to the quantization condition that, even in the presence of interactions, lie at one of the energies given in Eq. (6.50). We expect that, in general, there will be no such solutions. Exceptions can occur only if the symmetry of the finite-volume three-particle state is such that the chosen interactions do not couple to it. An example in the two-particle sector is that, if $\mathbf{P} = 0$, a finite-volume state lying in the E^+ irrep would not be shifted from its noninteracting value if only s- and p-wave interactions were included, since the lowest wave contributing to E^+ has $\ell = 2$. One question we address here is where such examples occur in the three-particle sector.

We were prompted to study this issue by finding examples of free solutions in our numerical study. One example has already been seen above, in Fig. 6.9(b), and further examples

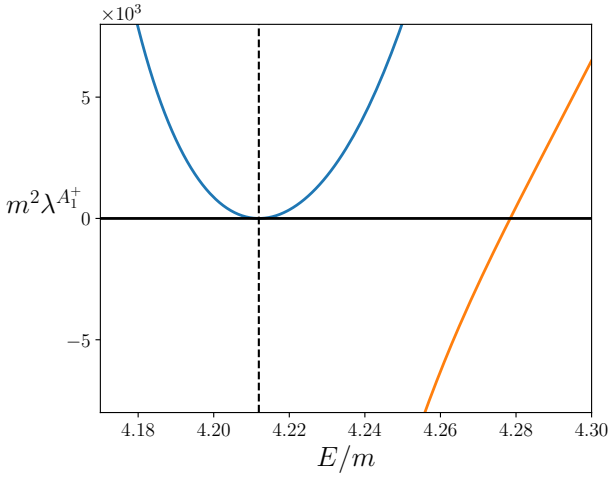

(a) A_1^+ irrep, s wave

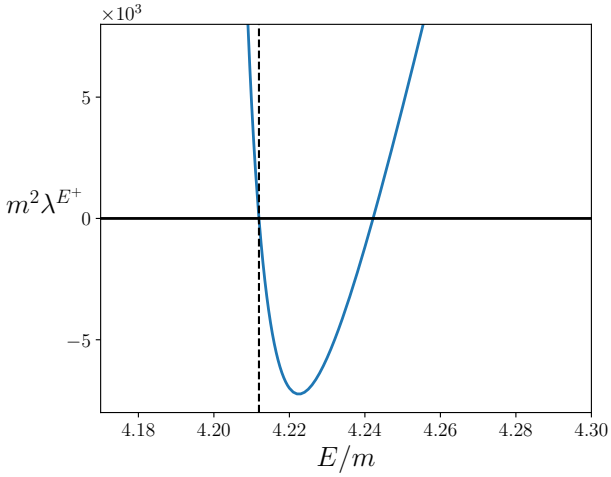

(b) E^+ irrep, s wave

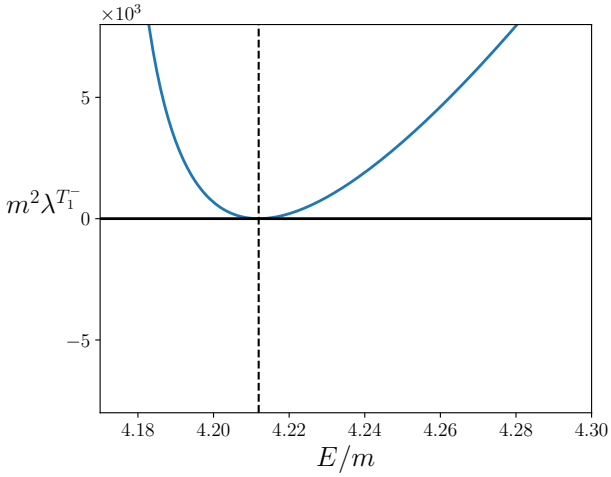

(c) T_1^- irrep, s and d waves

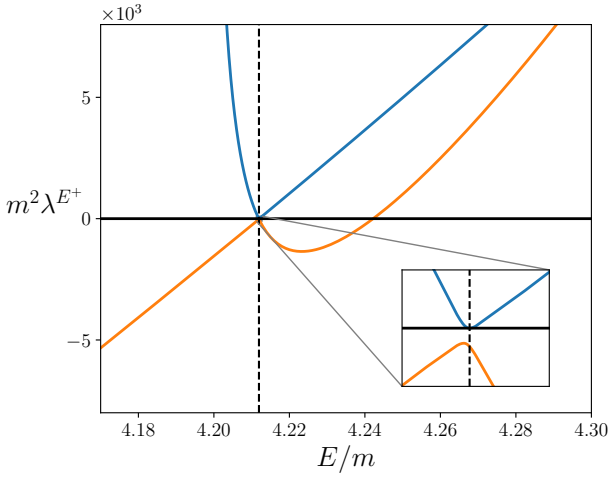

(d) E^+ irrep, s and d waves

Figure 6.11: Examples of solutions to the quantization condition for $\mathcal{K}_{\text{df},3} = 0$ occurring at the free energy E_1^{free} (shown in all plots as the vertical dashed line). Plots show eigenvalues of F_3^{-1} as a function of E/m, with $ma_0 = 0.1$, $r_0 = P_0 = 0$ and $mL = 5$. Solutions to the quantization occur when an eigenvalue crosses zero. (a) A_1^+ irrep with only $\ell = 0$ channels; (b) E^+ irrep, with only $\ell = 0$ channels; (c) T_1^- irrep, with both $\ell = 0$ and 2, and $ma_2 = 0.1$; (d) E^+ irrep, with both $\ell = 0$ and 2, and $ma_2 = 0.1$. For the E^+/T_1^- irreps, all eigenvalues are doubly/triply degenerate. In (d), both apparent crossings are in fact avoided, as illustrated by the inset.

Level	ℓ	Irreps with zeros	Zeros removed by
E_1^{free}	0	A_1^+; T_1^-; $E^+(1)$	($\mathcal{K}_{\text{df},3}^{(2,A)}$ or $\mathcal{K}_{\text{df},3}^{(2,B)}$); $\mathcal{K}_{\text{df},3}^{(2,B)}$; $\mathcal{K}_{\text{df},3}^{(2,B)}$
E_1^{free}	0 & 2	A_1^+; T_1^-; E^+	$\geq$ quartic for each
E_2^{free}	0	A_1^+; T_1^-; T_2^-	($\mathcal{K}_{\text{df},3}^{(2,A)}$ or $\mathcal{K}_{\text{df},3}^{(2,B)}$); $\mathcal{K}_{\text{df},3}^{(2,B)}$; ($\mathcal{K}_{\text{df},3}{}^{(3,B)}$ or $\mathcal{K}_{\text{df},3}{}^{(3,E)}$)
E_2^{free}	0 & 2	A_1^+; E^+; T_2^+; T_1^-; T_2^-	$\geq$ quartic for each

Table 6.3: Irreps in which free zeros appear for the first two excited levels when $\mathcal{K}_{\text{df},3} = 0$. The "(1)" in the first row denotes that the E_1^{free}, $\ell = 0$ free zeros in the E^+ irrep are single roots with unphysical residue; all other free zeros in the table are (unphysical) double roots. Also noted are the lowest-order terms in the threshold expansion of $\mathcal{K}_{\text{df},3}$ that remove the free zeros. The notation "$\geq$ quartic" indicates that a term of at least quartic order is needed. Note that cubic-order terms are needed to remove the E_2^{free}, $\ell = 0$ free zeros in the T_2^- irrep, as neither of the quadratic terms $\mathcal{K}_{\text{df},3}^{(2,A)}$ and $\mathcal{K}_{\text{df},3}^{(2,B)}$ has nonzero eigenvalues in this irrep.

are shown in Fig. 6.11. The first two plots show solutions with only s-wave channels included. In Fig. 6.11(a), which shows results for the A_1^+ irrep, we see a double zero at the first excited free energy, E_1^{free}, as well as a solution shifted to slightly higher energies. The latter is expected, since the repulsive interactions should raise the energy of the free state. In the E^+ irrep, by contrast, there is a single zero at E_1^{free}, with the unphysical sign for the residue, as well as an interacting solution at higher energy. The other two plots show examples of free zeros when s- and d-wave channels are included. Both the T_1^- irrep, shown in Fig. 6.11(c), and the E^+ irrep, shown in Fig. 6.11(d), have a double-zero at E_1^{free}.

We find similar results for higher excited free energy levels, in which case they appear in an increasing number of irreps. We list these irreps for the first two excited free energies in Table 6.3. There are, however, no free solutions for the lowest free energy $E_0^{\text{free}} = 3m$.[24]

In all the examples we have found, the free solutions are also unphysical—they are either double zeros or single zeros with the wrong residue. We do not know if this is a general

[24]Strictly speaking, this is only true when one uses the improved form of the quantization condition given in Eq. (D.13), and described in Appendix D.1, which removes spurious solutions to Eq. (6.1).

result. Also, although the examples shown above are for $\mathcal{K}_{\mathrm{df},3} = 0$, free solutions also occur when some components of $\mathcal{K}_{\mathrm{df},3}$ are turned on. Indeed, one of the questions we address in the following is which components of $\mathcal{K}_{\mathrm{df},3}$ are required to either remove the free solutions or move them away from E_n^{free}. Our first task, however, is to understand in more detail when and why free solutions occur. All such solutions originate from the fact that $\widetilde{F}$ and $\widetilde{G}$ have single poles at all the free energies. These can lead to poles in F_3 and thus zeros in F_3^{-1}. We analyze in detail only the lowest two free energies, i.e. those with level number $n = 0$ and 1 in the notation of Table 6.2, and then draw some general conclusions.

For $E \approx E_0^{\mathrm{free}} = 3m$, the only elements of $\widetilde{F}$ and $\widetilde{G}$ that have poles at E_0^{free} have vanishing spectator momenta and $\ell = 0$,[25] specifically

$$\widetilde{F}_{000;000} \sim \frac{1}{2}\widetilde{G}_{000;000} \sim p_0 \equiv \frac{1}{16m^3L^3(E-3m)} \,. \tag{6.66}$$

Here we are using the symbol $\sim$ to indicate "up to nonpole parts". All other elements of these matrices, and of $\mathcal{K}_2$, either vanish or are of $\mathcal{O}(1)$. From Table 6.1 it now follows that poles in $\widetilde{F}$ and $\widetilde{G}$ only appear in the A_1^+ irrep, and the issue is whether these lead to a pole in F_3.

To address this we consider the simplest case in which the volume is chosen such that only the lowest two momentum shells are active, which is the case for $mL \approx 5$. From Table 6.1 we then see that in the A_1^+ irrep the matrices are three dimensional, with indices

$$([\text{shell } 1, \ell = 0],\ [\text{shell } 2, \ell = 0],\ [\text{shell } 2, \ell = 2]) \,. \tag{6.67}$$

We will use a $1 + 2$ block notation for the matrices, since this conveys all the necessary

[25] Pole contributions with $\ell = 2$ and/or $\ell' = 2$ vanish because, at the pole, $\mathbf{a}^* = \mathbf{a}'^* = 0$.

information. Close to E_0^{free} the matrices have the form[26]

$$\widetilde{F} = \begin{pmatrix} p_0 + \mathcal{O}(1) & 0 \\ 0 & \mathcal{O}(1) \end{pmatrix}, \quad \widetilde{G} = \begin{pmatrix} 2p_0 + \mathcal{O}(1) & \mathcal{O}(1) \\ \mathcal{O}(1) & \mathcal{O}(1) \end{pmatrix}, \tag{6.68}$$

where $\mathcal{O}(1)$ elements are constrained only by the fact that $\widetilde{F}$ and $\widetilde{G}$ are symmetric. $\mathcal{K}_2$ is a diagonal matrix with $\mathcal{O}(1)$ elements. From this it follows that

$$H = \widetilde{F} + \widetilde{G} + (2\omega\mathcal{K}_2)^{-1} = \begin{pmatrix} 3p_0 + \mathcal{O}(1) & \mathcal{O}(1) \\ \mathcal{O}(1) & \mathcal{O}(1) \end{pmatrix} \quad \Rightarrow \quad H^{-1} = \begin{pmatrix} \frac{1}{3p_0} + \mathcal{O}(1/p_0^2) & \mathcal{O}(1/p_0) \\ \mathcal{O}(1/p_0) & \mathcal{O}(1) \end{pmatrix} \tag{6.69}$$

and thus in turn that

$$\widetilde{F}H^{-1}\widetilde{F} = \begin{pmatrix} p_0/3 + \mathcal{O}(1) & \mathcal{O}(1) \\ \mathcal{O}(1) & \mathcal{O}(1) \end{pmatrix} \quad \Rightarrow \quad F_3 = \mathcal{O}(1)\,. \tag{6.70}$$

We thus find that free poles at E_0^{free} cancel in F_3. This argument generalizes to any number of active shells, since there are no additional poles, and the only change is that the second block in the above analysis is enlarged. The result agrees with our numerical finding that there are no free poles at E_0^{free}.

Next we consider poles at the second free energy, E_1^{free}. For $mL \approx 4-6$ there are then three active shells, so the matrices to consider become larger, e.g. six-dimensional in the A_1^+ irrep, and the analysis correspondingly more complicated. We work out the case of the A_1^+ irrep in Appendix D.5, both with $\ell = 0$ channels only and with $\ell = 0$ and 2 channels included. In both cases we find that F_3^{-1} has a double zero at $E = E_1^{\text{free}}$. This lies in a one-dimensional subspace of the full matrix space, and what differs between the two cases is

[26] There are also potential poles in the $\ell = 2$ components arising from the vanishing of $q_{2,k}^*$ and $q_{2,p}^*$ in $\widetilde{G}$ and $\widetilde{F}$, Eqs. (D.3) and (D.9). However, as discussed at the end of Appendix D.1, the quantization condition can be formulated such that these purely kinematical poles are canceled, and it is legitimate to ignore them.

this subspace. For $\ell = 0$ only, the matrix indices are

$$([\text{shell } 1, \ell = 0],\ [\text{shell } 2, \ell = 0],\ [\text{shell } 3, \ell = 0], \dots) \ . \tag{6.71}$$

with the dimension depending on the choice of L. The double zero of F_3^{-1} lies, in this case, in the space spanned by

$$\langle x_1' | = \sqrt{\tfrac{1}{7}} \left(\sqrt{6}, -1, 0, \dots \right) \ . \tag{6.72}$$

For $\ell = 0$ and 2, the matrix indices are

$$([\text{shell } 1, \ell = 0],\ [\text{shell } 2, \ell = 0],\ [\text{shell } 2, \ell = 2], [\text{shell } 3, \ell = 0],\ \dots) \ , \tag{6.73}$$

and the space of the double zero of F_3^{-1} is spanned by

$$\langle x_1 | = \sqrt{\tfrac{1}{12}} \left(\sqrt{6}, -1, -\sqrt{5}, 0, \dots \right) \ . \tag{6.74}$$

The factors in Eqs. (6.72) and (6.74) result from the form of the spherical harmonics and the size of the first two shells. They are thus kinematical.

These analytic results confirm what we find numerically. For example, the double zero at E_1^{free} shown in Fig. 6.11(a) exactly matches that expected from the analysis of Appendix D.5, and we have checked numerically that it lies in the predicted subspace.

We now discuss how the single zeros at free energies arise. There is a particularly simple case in which we can easily understand these analytically: the E^+ irrep when we keep only s-wave channels *and* choose mL such that only the first two shells are active. We must also choose mL such that $E_1^{\text{free}} < 5m$ (so that the formalism applies); one example is $mL = 3.8$, for which $E_1^{\text{free}} = 4.86m$. In fact, as shown in Table 6.1, the first shell has no E^+ component for $\ell = 0$, so this simple case actually involves only the second shell, for which the E^+ irrep appears once. Although the E^+ irrep is two-dimensional, within this space all matrices are proportional to the identity. Thus the matrices are effectively one-dimensional.

The second shell consists of six elements, which we label by the direction of the spectator

momentum $\mathbf{k}$ in the following order

$$\mathbf{k} \in o_{001} = (2\pi/L)\{-\hat{z}, -\hat{y}, -\hat{x}, \hat{x}, \hat{y}, \hat{z}\}\,. \tag{6.75}$$

In this basis, the E^+ eigenvectors can be chosen as

$$\tfrac{1}{2}(1, 0, -1, -1, 0, 1) \quad \text{and} \quad \sqrt{\tfrac{1}{12}}(-1, 2, -1, -1, 2, -1)\,. \tag{6.76}$$

It is then simple to calculate the pole terms to be

$$\widetilde{F} = \mathbf{1}\,[p_1 + \mathcal{O}(1)] \quad \text{and} \quad \widetilde{G} = \mathbf{1}\,[p_1 + \mathcal{O}(1)]\,, \tag{6.77}$$

where

$$p_1 \equiv \frac{1}{8m\omega_1^2 L^3 (E - E_1^{\text{free}})}\,. \tag{6.78}$$

It immediately follows that

$$F_3 = \frac{1}{L^3}\left[\frac{\widetilde{F}}{3} - \widetilde{F} H^{-1} \widetilde{F}\right] = -\frac{p_1}{6L^3}\mathbf{1}\,[1 + \mathcal{O}(1/p_1)]\,. \tag{6.79}$$

Thus F_3 indeed has a single pole at $E = E_1^{\text{free}}$, and F_3^{-1} a single (doubly degenerate) zero. Increasing L so that there are more active shells does not change the pole structure or the presence of the single zero. We also see that the zero in F_3^{-1} has a negative coefficient, implying that it decreases through zero, consistent with the behavior seen in Fig. 6.11(b).

Thus we have understood in a few simple cases why the free zeros listed in Table 6.3 appear. It is interesting to contrast this to the results of Ref. [39], where the quantization condition was studied numerically in the isotropic approximation. In that work no free zeros in F_3^{-1} were found. At first this may seem puzzling, because the isotropic approximation is a subset of our analysis when we restrict to $\ell = 0$ channels. The resolution is that the additional isotropic projection that is used is orthogonal to the subspace in which the zeros live. This is demonstrated in Appendix D.6, along with a derivation of the precise relation between the isotropic approximation and the analysis carried out here.

The final stage of our analysis is to study whether the inclusion of components of $\mathcal{K}_{\text{df},3}$ removes the free zeros. Here by "remove" we mean that there is no longer a solution to the quantization condition at a free energy. This can be accomplished either by removing the solution altogether (which is possible for a double zero, which only touches the axis) or by moving it away from the free energy (the likely solution for a single zero). We expect that if $\mathcal{K}_{\text{df},3}$ were not truncated then there would be no free zeros, since there would be some overlap between the state and the three-particle interaction. This is indeed consistent with what we find. What turns out to be surprising, however, is which components of $\mathcal{K}_{\text{df},3}$ that are needed to remove the free zeros.

We first consider the $\ell = 0$, A_1^+ case. To remove the double zero, it must be that the projection of $\mathcal{K}_{\text{df},3}$ into the space of zeros is nonvanishing:

$$[\mathcal{K}_{\text{df},3}(E_1^{\text{free}})]|x_1'\rangle \neq 0\,, \tag{6.80}$$

where $|x_1'\rangle$ is defined in Eq. (6.72). Here the square brackets indicate the matrix that results when $\mathcal{K}_{\text{df},3}$ is decomposed into the $k\ell m$ basis and projected into an irrep. Note that this equation need only hold for $E = E_1^{\text{free}}$, i.e. at the energy of the free zero.

The isotropic parts of $\mathcal{K}_{\text{df},3}$, Eq. (6.14), do not solve the problem. These terms have the matrix form

$$[\mathcal{K}^{\text{iso}}] \propto |1_K\rangle\langle 1_K|\,, \tag{6.81}$$

where

$$\langle 1_K| = \left(1, \sqrt{6}, \sqrt{12}, \dots\right)\,. \tag{6.82}$$

Since this vector is orthogonal to $|x_1'\rangle$, it follows that, for all energies,

$$[\mathcal{K}^{\text{iso}}]|x_1'\rangle = 0\,, \tag{6.83}$$

so that Eq. (6.80) is not satisfied. The form of $|1_K\rangle$ follows from the fact that $\mathcal{K}^{\text{iso}}$ is

independent of the spectator momentum, so that the A_1^+ projection simply gives factors of the square root of the multiplicity of the shells. We thus expect that the inclusion of *any* dependence on the spectator momentum will lead to a $[\mathcal{K}_{\text{df},3}]$ satisfying Eq. (6.80). This is what we find in practice with both of the quadratic terms, i.e. those with coefficients $\mathcal{K}_{\text{df},3}^{(2,A)}$ and $\mathcal{K}_{\text{df},3}^{(2,B)}$ [see Eqs. (6.15) and (6.16)].

This result is an example of a general pattern: the part of $\mathcal{K}_{\text{df},3}$ that "removes" the free zeros comes from terms that involve higher values of ℓ than those being included in F_3^{-1}. Here, we need quadratic terms, which have both $\ell = 0$ and 2 components, in order to remove the free zeros from the $\ell = 0$ part of F_3^{-1}. To be clear, the $\ell = 2$ components of the quadratic terms play no role; it is simply that by going to higher order one obtains a more complicated form of the $\ell = 0$ parts, and this is sufficient to remove the unwanted free zeros. Further examples of this are shown in the last column of Table 6.3, where we list, for all irreps that enter in a given free momentum shell, the terms in $\mathcal{K}_{\text{df},3}$ that remove the free zero.

The second example we consider is the combined $\ell = 0$ and 2 part of F_3^{-1} in the A_1^+ irrep. In this case, we need

$$[\mathcal{K}_{\text{df},3}(E_1^{\text{free}})]|x_1\rangle \neq 0 \tag{6.84}$$

[with $|x_1\rangle$ given in Eq. (6.74)] in order to remove the free zeros. We find numerically that this equation is not satisfied by any of the quadratic or cubic terms contributing to $\mathcal{K}_{\text{df},3}$, but that quartic terms do satisfy it.[27] This exemplifies the general pattern discussed above: quadratic and cubic terms contain only $\ell = 0$ and 2, while quartic terms include also $\ell = 4$ parts. We were initially surprised by this result, because $\mathcal{K}_{\text{df},3}$ is an infinite-volume quantity, while $|x_1\rangle$ arises from finite-volume considerations. However, we show analytically in Appendix D.7 that orthogonality follows solely from the rotation invariance and particle-interchange symmetry of $\mathcal{K}_{\text{df},3}$, together with the fact that quadratic and cubic terms contain only $\ell = 0$ and 2

[27] In this case it is crucial to set the energy to E_1^{free}; for other energies Eq. (6.84) is satisfied.

parts. Thus it is an example of the phenomenon described at the beginning of this section, in which symmetries make the finite-volume state transparent to certain interactions. It is also clear from the arguments in Appendix D.7 that all that is required for Eq. (6.84) to be satisfied is to use contributions to $\mathcal{K}_{\mathrm{df},3}$ that involve $\ell \geq 4$, i.e. terms of quartic or higher order in the threshold expansion.

Finally, we consider the case of the single zero in the E^+ irrep for $\ell = 0$ channels only, shown in Fig 6.11(b). Here we aim to shift the zero away from the free energy. This is accomplished by including a contribution from $\mathcal{K}_{\mathrm{df},3}$ that lives in the E^+ irrep. As noted in the final paragraph of Sec. 6.3, the lowest-order term in the threshold expansion for which this is the case is the $\mathcal{K}_{\mathrm{df},3}^{(2,B)}$ term. Thus, once again, we have to use a term in $\mathcal{K}_{\mathrm{df},3}$ that contains higher values of ℓ (here $\ell = 2$) than are included in F_3.

These theoretical arguments are supported by our numerical results. We show two examples in Fig. 6.12. These correspond to the two cases shown in Figs. 6.11(a) and 6.11(b), except that we have turned on $\mathcal{K}_{\mathrm{df},3}^{(2,A)}$ and $\mathcal{K}_{\mathrm{df},3}^{(2,B)}$, respectively. We expect the double-zero in the former case (A_1^+ irrep) to removed by the addition of any quadratic term in $\mathcal{K}_{\mathrm{df},3}$, and the figure shows that $\mathcal{K}_{\mathrm{df},3}^{(2,A)}$ does the job. In Fig. 6.12(b), corresponding to the E^+ irrep, we need to use the $\mathcal{K}_{\mathrm{df},3}^{(2,B)}$ term, since $\mathcal{K}_{\mathrm{df},3}^{(2,A)}$ does not contain an E^+ component. Since this is a single zero, it is not removed, but is rather shifted to a non-free energy. Note, however, that it remains unphysical because it decreases through zero. In fact, for higher values of $\mathcal{K}_{\mathrm{df},3}^{(2,B)}$, the zeros coalesce and then disappear.

We close this section with two general comments on the nature of the resolution that we have presented to the problem of unwanted free solutions. The first concerns the result that we need higher-order terms in the threshold expansion of $\mathcal{K}_{\mathrm{df},3}$ in order to remove the free zeros of a given order in F_3^{-1}. On its face, this invalidates the threshold expansion, for we are evaluating distinct terms in the quantization condition at different orders. We do not think this is the case, however, because we know that, above threshold, *all terms* in the expansion

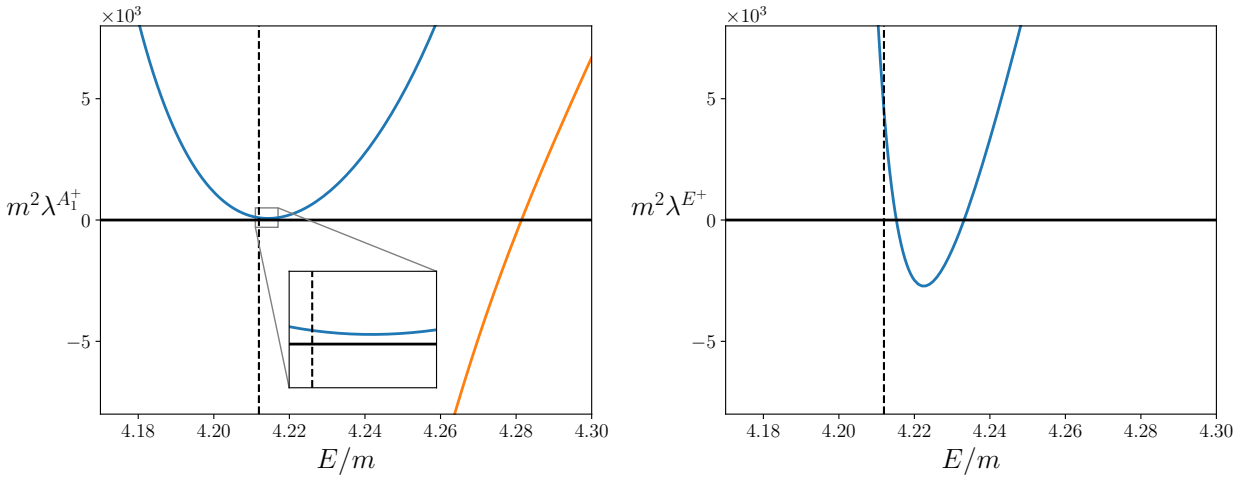

(a) E^+ irrep, s wave

(b) T_1^- irrep, s wave

Figure 6.12: Effect of turning on $\mathcal{K}_{\mathrm{df},3}$ on the free solutions shown in Fig. 6.11(a) and 6.11(b), with all other parameters unchanged. Eigenvalues are now those of $F_3^{-1}+\mathcal{K}_{\mathrm{df},3}$. (a) A_1^+ irrep with $\mathcal{K}_{\mathrm{df},3}^{(2,A)} = 8000$; (b) E^+ irrep with $\mathcal{K}_{\mathrm{df},3}^{(2,B)} = 8000$.

of $\mathcal{K}_{\mathrm{df},3}$ are present at some level, and it only takes an infinitesimal value for the coefficient of the requisite higher-order term to remove the unwanted solution. Thus we conclude that we can proceed, in practice, by truncating the expansion of all quantities at the same order in the threshold expansion, and simply ignore the free solutions.

The second comment concerns the fact that our resolution fails if the coefficient of the required parts of $\mathcal{K}_{\mathrm{df},3}$ vanish. In fact, this would require the simultaneous vanishing of an infinite number of terms in the threshold expansion, since higher-order terms in the correct irrep can remove the free solutions. Thus it would require an enormous fine-tuning, which seems highly implausible, especially because there is no enhancement of the symmetry of $\mathcal{K}_{\mathrm{df},3}$ at the tuned point.

6.5 Conclusions

The work presented in this paper is the first step towards the systematic inclusion of higher partial waves in the three-particle quantization condition. We have used the generic relativistic field theory (RFT) approach, formulated so that the three-particle scattering quantity, $\mathcal{K}_{\mathrm{df},3}$, is Lorentz invariant. This invariance proves very important in simplifying the threshold expansion of $\mathcal{K}_{\mathrm{df},3}$. Indeed, we find that, at quadratic order and for identical particles, only five parameters control the contribution from the three-particle sector, of which only two describe dependence on angular degrees of freedom. This provides a simple starting point for studying the impact of $\mathcal{K}_{\mathrm{df},3}$. Working at quadratic order implies keeping both s- and d-wave two-particle channels (dimers). We have numerically implemented the quantization condition at this order, and obtained several new results that we now highlight.

The first of these is to determine the projection onto irreps of the cubic group including higher partial waves. This has previously been done only for the case of s-wave dimers [40]. The generalization is nontrivial, since both the spectator momentum and the parameters of the dimer transform. While we have worked this out explicitly only for coupled s- and d-wave dimers, the formalism holds for dimers with any angular momentum.

Second, we have understood how the two-particle scattering amplitudes in higher partial waves enter in the $1/L$ expansion of the energy of the three-particle ground state. We find that all even partial waves enter at $\mathcal{O}(1/L^6)$, and have calculated analytically the dependence on the d-wave amplitude in the weak-coupling limit and for $\mathcal{K}_{\mathrm{df},3} = 0$. Although this contribution itself is likely too small to be seen in present simulations of three-particle systems, we have used it as a nontrivial check of our implementation.

Third, we have shown that d-wave interactions, if they are moderately strong, can have a sizable effect on the finite-volume three-particle spectrum. For example, we have presented evidence for a generalized Efimov-like three-particle bound state induced by a strongly attractive d-wave two-particle interaction.

Fourth, we have shown how the five parameters describing $\mathcal{K}_{\mathrm{df},3}$ lead to distinguishable effects on the spectrum of the $3\pi^+$ system, suggesting that they can be separately determined in a dedicated lattice study. Indeed, this is the system within QCD to which our truncated formalism is most applicable.

Finally, we have characterized solutions to the quantization condition that are unphysical. These presumably arise because of the truncation to a small number of partial waves, and the fact that we have dropped terms that are exponentially suppressed in mL. One class of solutions generally appears when either the two- or the three-particle interactions are strong and repulsive. Our approach is to use parameters such that there are no unphysical solutions near to the physical solutions of interest. The second class of solutions are those that occur at the energies of three noninteracting particles. We have presented numerical evidence and analytical arguments that these are removed if sufficiently high-order terms in $\mathcal{K}_{\mathrm{df},3}$ are included. We expect that other approaches to the three-particle quantization condition will face similar issues, for which our observations may be relevant.

There remain many directions for future study. In order to make our implementation more useful, it is important to generalize it to moving frames. The underlying formalism of Ref. [28] applies in all finite-volume frames, but the projectors onto irreps will need to be generalized to account for the reduced symmetry. Another important generalization is to include subchannel resonances, i.e., dynamical poles in $\mathcal{K}_2$. For this one must implement the formalism of Ref. [35], and go beyond the threshold expansion. Finally, we recall that $\mathcal{K}_{\mathrm{df},3}$ is an intermediate quantity, related to the physical three-particle scattering amplitude, $\mathcal{M}_3$, by integral equations. Since it is only by looking for complex poles in $\mathcal{M}_3$ that one can study three-particle resonances, it is crucial to develop methods to solve the necessary integral equations.

To conclude, we would like to restate that, as it is a relativistic approach, our implementation can simultaneously be useful to both the lattice QCD community and the field of cold

atom physics.

Chapter 7

NUMERICAL EXPLORATION OF THREE RELATIVISTIC PARTICLES IN A FINITE VOLUME INCLUDING TWO-PARTICLE RESONANCES AND BOUND STATES[1]

7.1 Introduction

Lattice quantum chromodynamics (LQCD), in which QCD correlators are estimated numerically via Monte Carlo importance sampling of the path integral, has proven to be a powerful tool for determining low-energy properties of hadrons. Currently, one of the major frontiers of numerical LQCD is the calculation of few-hadron observables. In particular, there has been substantial recent progress in the determination of scattering amplitudes, including cases for which multiple channels are open and couple to underlying resonances [96, 97, 112–125].[2] These studies rely on formalism that maps quantities obtained via LQCD, namely finite-volume observables, to infinite-volume amplitudes [24, 25, 27, 56, 57, 60, 61, 63, 126, 127].

Presently, one of the primary limitations on the study of resonances and light nuclei is the absence of a complete formalism that can provide such a mapping for energies above three-particle production thresholds. In fact, finite-volume spectra are already being obtained above three-particle thresholds using a large basis of interpolators including those built from three single-hadron operators, each projected to definite momentum [1, 120, 128].[3] Without a three-particle formalism, the information contained in these spectra is inaccessible. This was recently emphasized in a USQCD whitepaper: "*...the development of a rigorous*

[1]This chapter and Appendix E are taken directly from Ref. [36].

[2]See Ref. [26] for a recent review.

[3]Similar work has also been done in the φ^4 theory [55].

three-body (and higher) formalism is vital to have confidence in the calculations of high-lying resonances" [129].

While a complete formalism is not yet in place, there has been considerable progress in this direction, following three approaches. The first is based on a generic relativistic effective field theory (the relativistic field theory or RFT approach) [28, 29, 34, 35, 39, 76], the second uses non-relativistic effective field theory (the NREFT method) [30, 31, 40], and the third applies unitary constraints in finite volumes (the FVU or finite-volume unitarity approach) [32, 41].[4] For a recent review, including a discussion of the relation between the different formalisms, see Ref. [74]. At present, the only formalism that is both fully relativistic and incorporates partial-wave mixing (both due to the physical three-body dynamics and the reduction of rotational symmetry in a finite volume) is the RFT approach. In this work we focus on this approach and extend its range of applicability.

In the original derivation, given in Ref. [28], it was necessary to assume that a quantity closely related to the two-particle K matrix had no singularities in the kinematic region of interest. This implies that the formalism cannot be used if the two-particle subchannels contain resonances that are narrow enough to induce such singularities, or bound states, which generically give poles in the K-matrix-like quantity. The formalism also breaks down if the K matrix contains poles above threshold that do not correspond to a physical phenomenon, as occurs, for example, when the corresponding phase shift passes through $\pi/2$ from above. These restrictions are a major practical shortcoming of the original RFT approach. They are also surprising, as the problematic poles do not, in general, correspond to physical quantities. All such technical restrictions were lifted by a recent extension of the formalism given in Ref. [35], but at the cost of including an unphysical channel at intermediate stages for each bound state or resonance, making the approach cumbersome in practical implementations.

In prior studies, we have explored the numerical implementation of the original formal-

[4] It is worth emphasizing that efforts to constrain infinite-volume three-particle amplitudes from finite-volume LQCD results has partially motivated several infinite-volume studies [78, 79, 92, 93, 130].

ism of Ref. [28] in simple limits. First, in Ref. [39] we considered the low-energy, isotropic approximation, in which scattering in two-particle subchannels is dominated by the s-wave, and the three-particle scattering quantity, $\mathcal{K}_{\text{df},3}$, is independent of the spectator momentum. Second, in Ref. [76], we considered the case in which d-wave scattering, the dominant subleading partial wave for identical particle systems at low energies, was no longer negligible, with corresponding nonisotropic contributions added to $\mathcal{K}_{\text{df},3}$. The latter investigation demonstrated that higher partial wave systems can indeed be implemented numerically using the RFT approach. However, because of the above-mentioned restrictions, in both studies we were only able to consider dynamics where two-particle subsystems did not have bound states or resonances. Three-particle bound states, for which no issues arise, are considered in Refs. [39, 76, 80].

In this work we describe and implement an alternative modification of the formalism of Ref. [28] that removes the restriction on K matrix poles. This new approach does not require the introduction of unphysical channels, and is thus much simpler than that given in Ref. [35]. Indeed, the numerical implementation of the new approach requires only slight modifications compared to that for the original formalism, so the methods of Refs. [39, 76] can be used with minimal change. We stress that, by allowing for a general two-particle K matrix, our improvement of the original formalism brings it to the same status in this regard as the NREFT and FVU approaches [31, 32, 40, 41], since the latter do not require restrictions on the two-particle K matrix. We also note that, since the RFT formalism is valid for arbitrary partial waves, and has been implemented for combined s- and d-waves, we are able to consider three-particle systems not previously addressed in the literature. Finally we comment that this new method is also of relevance for $2 \to 3$ scattering, already considered in the context of the RFT formalism in Ref. [34]. Further work is required to relate the present ideas to the coupled-channel formalism of Ref. [34].

The main purpose of the present note is to show examples of the results that are obtained

using the modified formalism. In a companion paper [131] we will describe in detail why the modified formalism is valid, as well as the relation to the more complicated approach of Ref. [35].

The finite- to infinite-volume relation consists of two steps. The first uses a three-particle quantization condition to relate the finite-volume spectrum, $E_n(L)$, to an intermediate, scheme-dependent, infinite-volume three-particle scattering quantity, $\mathcal{K}_{\mathrm{df},3}$, while the second requires solving infinite-volume integral equations to relate $\mathcal{K}_{\mathrm{df},3}$ to the physical scattering amplitude, $\mathcal{M}_3$. In Ref. [39], we implemented both steps, although the latter only below and at the three-particle threshold. Here, in the interests of brevity and clarity, we mainly consider the first step, $E_n(L) \leftrightarrow \mathcal{K}_{\mathrm{df},3}$, and only indirectly explore some consequences of the second: $\mathcal{K}_{\mathrm{df},3} \leftrightarrow \mathcal{M}_3$.

As in all work to date, we restrict ourselves to the case of identical scalar particles. Thus, strictly speaking, the formalism applies in QCD only to three identical pions (e.g. $\pi^+\pi^+\pi^+$). We further restrict ourselves to theories with a G-parity-like $\mathbb{Z}_2$ symmetry that conserves particle-number modulo two (as is the case for three pions in the isospin-symmetric limit).[5] This forbids $2 \to 3$ transitions, which, in the energy range we consider, leads effectively to particle-number conservation. Furthermore, since many features of the finite-volume spectrum are determined by kinematics, we expect that the examples we show will shed light on the three-nucleon system. To illustrate this, in Sec. 7.4.3 we choose parameters to mimic the *nnp* or *npp* three-nucleon systems, with a two-particle bound state (called a dimer state) having the same binding energy as the deuteron, and the three-particle bound state (referred to as a trimer state) having the same binding energy as the triton or helium-3. This enables us to study a toy version of nucleon-deuteron scattering and reproduce the well known Phillips line of nuclear effective field theory [132, 133].

---

[5]The presence of a $\mathbb{Z}_2$ symmetry was assumed in the original derivation [28, 29], and has also been assumed in all numerical investigations so far. The formalism for a theory without a $\mathbb{Z}_2$ symmetry has been developed [34], but has not yet been numerically implemented.

This example brings out an important general point. The three-particle quantization condition was developed in order to map finite-volume energies into infinite-volume scattering observables. It turns out, however, that the formalism also predicts the properties of two- and three-particle resonances and bound states, given a description of the microscopic physics as encoded in the two-particle K matrix and $\mathcal{K}_{\text{df},3}$. This aspect is independent of the finite-volume and emerges because the integral equations relating $\mathcal{K}_{\text{df},3}$ to $\mathcal{M}_3$ exactly solve the unitarity constraints on the scattering amplitude [93]. This alternative application of the formalism was already used in Ref. [39], where we extracted the vertex function of a trimer and found good agreement with the Efimov wave-function. Similarly, in Ref. [76], we used the approach to give evidence for a trimer that is bound primarily by attractive d-wave interactions.

The remainder of this paper is organized as follows. We begin, in Sec. 7.2, by providing a brief recap of the essential components of the formalism of Ref. [28]. This is followed in Sec. 7.3 by a description of the modified formalism that allows for the study of three-body states with either resonant or bound subsystems. In Sec. 7.4 we illustrate the power of this formalism by applying it to various examples: First, in Sec. 7.4.1 we determine the finite-volume spectrum for systems with dimers; then, in Sec. 7.4.2, we evaluate the finite-volume spectrum below the three-particle threshold at large volumes, in order to determine the particle-dimer scattering amplitude for a range of two-body scattering lengths; third, in Sec. 7.4.3, we tune $\mathcal{K}_{\text{df},3}^{\text{iso}}$ and the two-body parameters to determine the neutron-deuterium scattering amplitude in a toy model without spin or isospin; next in Sec. 7.4.4 we present the three-particle spectrum in the case of a two-particle resonance; and, finally, in Sec. 7.4.5, we consider the implication of including d-wave dimers. We present concluding remarks in Sec. 9. We also include two appendices. In Appendix E.1 we explore the role that the scheme-dependence of $\mathcal{K}_{\text{df},3}$ plays in determining the finite-volume energy spectrum. In Appendix E.2 we explain how the predictions for the particle-dimer scattering length are

obtained in the NREFT framework.

7.2 Recap of the quantization condition and its approximations

In the presence of a $\mathbb{Z}_2$ symmetry, the finite-volume spectrum is determined by the solutions, $E = E_n(L)$ with $n = 0, 1, 2, \ldots$, to the quantization condition [28][6]

$$\det\left[F_3(E,L)^{-1} + \mathcal{K}_{\mathrm{df},3}(E)\right] = 0\,. \tag{7.1}$$

Here L is the linear extent of the finite cubic spatial volume, effected by applying periodic boundary conditions to the fields defining the theory. Although the formalism holds for arbitrary total three-momentum, $\mathbf{P}$, we consider here only the case in which $\mathbf{P} = 0$, so that the total energy E is also the center-of-mass energy for the three particles. The quantization condition is valid for $E < 5m$, i.e. for energies below the five-particle production threshold.

The second term appearing in the determinant, $\mathcal{K}_{\mathrm{df},3}$, is the aforementioned, scheme-dependent, infinite-volume scattering quantity. It is a smooth, real function of the kinematic variables describing three-to-three scattering and can be understood as the short-distance piece of the three-body interaction.[7] The first term in the determinant, F_3, depends on the physical two-particle scattering amplitude, $\mathcal{M}_2$ (or equivalently, through a straightforward algebraic relation, on the two-particle K matrix, $\mathcal{K}_2$) and on known geometric functions that depend on the box shape and size.

In Eq. (8.1), both F_3 and $\mathcal{K}_{\mathrm{df},3}$ are written as infinite-dimensional matrices acting on the space of three, on-shell particles in finite volume. Each object carries two copies of the index set $\mathbf{k}, \ell, m$, where $\mathbf{k} = 2\pi\mathbf{n}/L$ is a finite-volume momentum, given in terms of a 3-vector

---

[6]The quantization condition holds up to exponentially-suppressed corrections, scaling as e^{-mL}, which are assumed negligible, and ignored, throughout this work.

[7]The label "df" denotes "divergence-free", and indicates that kinematical divergences, present in the three-particle amplitude $\mathcal{M}_3$, are removed in the definition of $\mathcal{K}_{\mathrm{df},3}$. For more details, see Refs. [28, 29]. We note that, just as for the two-body K matrix, $\mathcal{K}_{\mathrm{df},3}$ can have poles induced by the dynamics, although we do not consider this possibility here.

of integers, $\mathbf{n}$, while ℓ and m are angular-momentum indices. The set-up is that $\mathbf{k}$ is the momentum of one of the three on-shell particles, referred to as the spectator, while ℓ and m describe the angular momentum of the other two in their center-of-mass (c.m.) frame. F_3 is intrinsically a finite-volume quantity, and thus comes always in matrix form. By contrast, $\mathcal{K}_{\mathrm{df},3}$ is an infinite-volume quantity depending on continuous momentum coordinates and the matrix version is defined by sampling the function at a discrete set of kinematics, dictated by the volume.[8]

As we describe below, the spectator-momentum index, $\mathbf{k}$, is cut off by a function $H(\mathbf{k})$ that serves as an ultraviolet regulator. Thus the matrices in Eq. (8.1) are infinite only due to their angular-momentum indices. One can expand the two- and three-particle K matrices $\mathcal{K}_2$ and $\mathcal{K}_{\mathrm{df},3}$ about threshold, as explained in Refs. [39, 76]. This leads to a systematic truncation scheme in which $\ell \leq \ell_{\max}$ in all quantities entering the quantization condition, including the kinematic functions [28]. Since both spectator momentum and angular-momentum index sums are truncated, the problem reduces to one involving finite matrices, suitable for numerical implementation. In this work we will present results for both $\ell_{\max} = 0$ (s-wave only) and $\ell_{\max} = 2$ (s- and d-wave mixing).[9]

7.2.1 The s-wave-only approximation: $\ell_{\max} = 0$

The general expression for F_3 is given in Ref. [28]. Here we recall the form only for the simplest case, $\ell_{\max} = 0$, which is the choice we use in most of the numerical explorations described below. In this limit, the index space reduces from $\mathbf{k}, \ell, m$, to the discretized momentum, $\mathbf{k}$. Denoting the s-wave-only version of F_3 by F_3^s, we recall that the latter is

[8] Explicit examples of how to carry out this restriction are given in Ref. [76].

[9] Odd ℓ give vanishing contibutions due to the exchange symmetry of the identical scalar particles.

given by

$$L^3 F_3^s \equiv \frac{\widetilde{F}^s}{3} - \widetilde{F}^s \frac{1}{1/\widetilde{\mathcal{K}}_2^s + \widetilde{F}^s + \widetilde{G}^s} \widetilde{F}^s \,, \tag{7.2}$$

where $\widetilde{F}^s$ and $\widetilde{G}^s$ are geometric matrices in the space of the spectator momentum,

$$[\widetilde{F}^s]_{kp} \equiv \frac{\delta_{kp}}{2} \frac{H(\mathbf{k})}{2\omega_k} \left[\frac{1}{L^3} \sum_{\mathbf{a}} - \mathrm{PV} \int \frac{d^3a}{(2\pi)^3} \right] \frac{H_2(\mathbf{a},\mathbf{b})}{2\omega_a 2\omega_b (E - \omega_k - \omega_a - \omega_b)} \,, \tag{7.3}$$

$$[\widetilde{G}^s]_{kp} \equiv \frac{H(\mathbf{k}) H(\mathbf{p}\,)}{L^3 2\omega_k 2\omega_p (b^2 - m^2)}. \tag{7.4}$$

The sum in Eq. (F.2) runs over all finite-volume momenta, i.e. over all $\mathbf{a} = (2\pi/L)\mathbf{n}_a$ where $\mathbf{n}_a$ is a 3-vector of integers. As we set $\mathbf{P} = 0$, the third particle carries momentum $\mathbf{b} \equiv -\mathbf{a} - \mathbf{k}$. On-shell energies are denoted ω, for example $\omega_k \equiv \sqrt{m^2 + \mathbf{k}^2}$, with m the particle mass. The explicit form of the cutoff function $H(\mathbf{k})$ is given in Refs. [28, 34, 39] and is not repeated here, except to note that we always take $\alpha = -1$ for the parameter in the cutoff function. [See Eq. (A3) of Ref. [34].]

The sum-integral difference in Eq. (F.2) is regulated in the ultraviolet by the function H_2, for which there is considerable freedom. In this work we use the "KSS" form [27], $H_2(\mathbf{a},\mathbf{b}) = \exp[-\alpha_{\mathrm{KSS}}(a^{*2} - q^{*2})]$, explained in detail in Appendix B of Ref. [39].

We note that while $\widetilde{F}^s$ is the same as in Ref. [39], $\widetilde{G}^s$ differs—here we use its relativistic form, since this leads to a Lorentz invariant $\mathcal{K}_{\mathrm{df},3}$. This invariance plays a role when expanding this function about three-particle threshold. Unlike for $\widetilde{G}^s$, it is not necessary that the denominator in $\widetilde{F}^s$ be relativistically invariant. This is because replacing $2\omega_b(E - \omega_k - \omega_a - \omega_b)$ with $(b^2 - m^2)$ leads only to an exponentially suppressed change to $\widetilde{F}^s$.

The final ingredient needed for $\widetilde{F}_3^s$ is the two-particle s-wave K matrix, or, equivalently, the s-wave phase shift δ_s. This appears in the diagonal matrix

$$[1/\widetilde{\mathcal{K}}_2^s]_{kp} \equiv \delta_{kp} \Big(1/\widetilde{\mathcal{K}}_2^s(\mathbf{k}) \Big) \,, \tag{7.5}$$

$$\widetilde{\mathcal{K}}_2^s(\mathbf{k}) \equiv \frac{32\pi\omega_k E_{2,k}^*}{q_{2,k}^* \cot\delta_s(q_{2,k}^*) + |q_{2,k}^*|[1 - H(\mathbf{k})]} \,, \tag{7.6}$$

where

$$E_{2,k}^{*2} = (E - \omega_k)^2 - \mathbf{k}^2 \quad \text{and} \quad q_{2,k}^{*2} = \frac{E_{2,k}^{*2}}{4} - m^2 \tag{7.7}$$

are the total squared energy and particle momentum in the c.m. frame of the nonspectator pair, and δ_s the s-wave phase shift. Were it not for the second term in the denominator of Eq. (F.5), $\widetilde{\mathcal{K}}_2^s$ would simply equal $\mathcal{K}_2/(2\omega_k)$, where

$$\mathcal{K}_2^s(\mathbf{k}) \equiv \frac{16\pi E_{2,k}^*}{q_{2,k}^* \cot \delta_s(q_{2,k}^*)}\,, \tag{7.8}$$

is one standard choice for the definition of the K matrix. Indeed, the equivalence does hold above threshold (i.e. for $E_{2,k}^* > 2m$), where $H(\mathbf{k}) = 1$. The second term is essential, however, for the derivation of Ref. [28], and implies that $\widetilde{\mathcal{K}}_2^s$ is scheme-dependent below threshold.

In what follows, we make use of two parametrizations of the phase shift. The first is a low-energy expansion, commonly referred to as the effective range expansion (ERE), which for the s-wave can be written as

$$q_{2,k}^* \cot \delta_s(q_{2,k}^*) = -\frac{1}{a_0} + \frac{1}{2} r_0 q_{2,k}^{*2} + \mathcal{O}(q_{2,k}^{*4})\,, \tag{7.9}$$

where a_0 and r_0 are the scattering length and the effective range, respectively. In numerical explorations considered below, we will only consider examples with $r_0 = 0$. Our second choice is the Breit-Wigner form, commonly used when a narrow resonance couples to a two-body system. For an s-wave resonance, this can be written

$$\tan \delta_{\text{BW}}(q_{2,k}^*) = \frac{E_{2,k}^* \, \Gamma(E_{2,k}^*)}{m_R^2 - E_{2,k}^{*2}} \qquad \text{with} \qquad \Gamma(E_{2,k}^*) = \frac{g^2}{6\pi} \frac{m_R^2}{E_{2,k}^{*2}} q_{2,k}^*\,, \tag{7.10}$$

where m_R is the resonance mass and g its coupling to the two-particle channel. We describe below one example of the finite-volume three-particle spectrum in the presence of such a resonant two-body interaction. We note that the Breit-Wigner form is similar to the truncated

effective range expansion,

$$q^*_{2,k}\cot\delta_{\rm BW}(q^*_{2,k}) = \frac{m_R^2 - E^{*2}_{2,k}}{E^*_{2,k}}\frac{6\pi}{g^2}\frac{E^{*2}_{2,k}}{m_R^2} = E^*_{2,k}[A + Bq^{*2}_{2,k}]\,, \tag{7.11}$$

with A and B constants. However, in order for there to be a narrow resonance, the A and B terms must cancel, so that one is, in general, outside the range of convergence of the effective range expansion.

We close this subsection by noting that, within the s-wave approximation, $\mathcal{K}_{\rm df,3}$ becomes a function solely of the total energy and the spectator momenta, $\mathcal{K}_{\rm df,3} = \mathcal{K}_{\rm df,3}(E, \mathbf{p}, \mathbf{k})$. This, along with the above-described approximations, leads to a set-up that is analogous to that used to date in the NREFT and FVU approaches [30–32, 40, 41]. However, a careful analysis of the definition of $\mathcal{K}_{\rm df,3}$, which depends implicitly on $\mathcal{K}_2$, reveals that it is not consistent with particle-interchange symmetry to restrict $\mathcal{K}_{\rm df,3}$ to s-waves in the ℓ, m indices, while allowing dependence on the spectator momenta, $\mathbf{k}$ and $\mathbf{p}$. Instead one must apply a consistent truncation across the two- and three-particle sectors. In the case that $\mathcal{K}_2$ is restricted to the s-wave, this implies that $\mathcal{K}_{\rm df,3}$ must be evaluated in the isotropic approximation, to which we now turn.

7.2.2 The isotropic approximation

A systematic method for understanding the implications of particle-interchange and Lorentz symmetry for $\mathcal{K}_{\rm df,3}$ is the threshold expansion [39, 76]. This is a low-energy expansion about the three-particle threshold, and is the analog of the the effective-range expansion described above for $\mathcal{K}_2$ [see Eq. (7.9)]. At leading order in this expansion, corresponding to keeping only the $-1/a_0$ term in (7.9), $\mathcal{K}_{\rm df,3}$ is a constant, which we denote $\mathcal{K}^{\rm iso}_{\rm df,3}$. Here, the superscript "iso" stands for isotropic. Generally we take this to mean that the function is independent of (i.e. constant with respect to) all coordinates besides the total three-particle energy. At the next order in the threshold expansion, corresponding to the $q^{*2}_{2,k}$ term in Eq. (7.9), $\mathcal{K}_{\rm df,3}$

becomes a linear function of E^2 while remaining isotropic. When expressed in terms of the $\mathbf{k}, \ell, m$ indices, this implies that it is pure s-wave, and independent of the initial and final spectator momenta.

An isotropic $\mathcal{K}_{\mathrm{df},3}$, together with the choice $\ell_{\max} = 0$—a combination that we call, following Refs. [28, 39], the isotropic approximation—was shown in Ref. [28] to reduce the $\mathcal{K}_{\mathrm{df},3}$-dependent part of the quantization condition (8.1) to a one-dimensional algebraic equation,

$$F_3^{\mathrm{iso}}(E, L)^{-1} + \mathcal{K}_{\mathrm{df},3}^{\mathrm{iso}}(E) = 0\,. \tag{7.12}$$

Here F_3^{iso} is the isotropic projection of F_3^s,

$$F_3^{\mathrm{iso}} = \langle \mathbf{1} | F_3^s | \mathbf{1} \rangle\,, \tag{7.13}$$

where F_3^s is given in Eq. (F.1), and the vector $|\mathbf{1}\rangle$ has a unit entry for each value of the spectator momentum lying below the cutoff. To reach Eq. (F.8), in addition to the isotropic approximation, one must project onto the trivial finite-volume irrep, denoted $\mathbb{A}_1^+$.[10] In previous work we indicated that (F.8) describes all finite-volume energies that are shifted by interactions. In fact this is not the case; levels that are independent of $\mathcal{K}_{\mathrm{df},3}$, but shifted by $\mathcal{K}_2$, appear in other irreps.

The procedure for solving the quantization condition in the isotropic approximation is simple in principle: given L, $\mathcal{K}_2$ and $\mathcal{K}_{\mathrm{df},3}^{\mathrm{iso}}$, the left-hand side of (F.8) becomes a known function of E and the solutions can be numerically determined with a suitable root-finding algorithm. Details of our numerical implementation are given in Ref. [39] and are unchanged here.

As noted above, if one consistently uses the threshold expansion, then the isotropic approximation requires truncating the effective range expansion (7.9) at second order, and allowing only a linear dependence of $\mathcal{K}_{\mathrm{df},3}^{\mathrm{iso}}$ on E^2. For simplicity, however, in our numerical

[10] The $\mathbb{A}_1^+$ is only the trivial irrep for three scalar particles, while for pseudoscalars it is the $\mathbb{A}_1^-$.

studies we mostly keep only the leading-order terms in the threshold expansion, so that interactions are described in terms of two constants, a and $\mathcal{K}_{\mathrm{df},3}^{\mathrm{iso}}$. We also consider the case of a constant $\mathcal{K}_{\mathrm{df},3}^{\mathrm{iso}}$ and a Breit-Wigner form for the phase shift, Eq. (7.10). Though not consistent with the threshold expansion power counting, we view this as a reasonable starting point for studying the impact of two-particle resonances on the three-particle spectrum.

7.2.3 Including d-wave interactions: $\ell_{\mathrm{max}} = 2$

We also include in our numerical examples a study with $\ell_{\mathrm{max}} = 2$, so that d-wave two-particle interactions are included, as well as three additional terms in $\mathcal{K}_{\mathrm{df},3}$, two of which are not isotropic. A complete description of the set up has been given in Ref. [76], and we do not repeat it here. We note only that the d-wave contribution to $\widetilde{\mathcal{K}}_2$ has the form

$$\widetilde{\mathcal{K}}_2^d(\mathbf{k}) = \frac{32\pi\omega_k E_{2,k}^*}{-1/(a_2^5\, q_{2,k}^{*4}) + |q_{2,k}^*|[1 - H(\mathbf{k})]}\,, \tag{7.14}$$

which should be compared to the s-wave form of Eq. (F.5). Here we are keeping only the leading non-trivial term in the d-wave effective range expansion, which is parametrized by the scattering length a_2. In this truncation, energies in non-trivial irreps are also shifted from their noninteracting values. Nonetheless in this work we restrict attention to the $\mathbb{A}_1^+$ for simplicity. See Ref. [76] for interacting solutions in the two-dimensional $\mathbb{E}^+$ irrep.

7.3 Generalizing the quantization condition

In order for the derivation of the quantization condition, Eq. (8.1), to be valid, it is necessary that all angular-momentum components of the modified K matrix, $\widetilde{\mathcal{K}}_2^{(\ell)}$, have no singularities for all c.m. frame two-particle energies, $E_{2,k}^*$, in the range $0 < E_{2,k}^* < 4m$. As we recall below, this implies that the quantization condition cannot be used for cases in which there are two-particle bound states or resonances, and is a significant restriction on the applicability of the formalism. It turns out, however, that there is a simple way to generalize the formalism

such that, for each value of ℓ, the inverse of $\widetilde{\mathcal{K}}_2^{(\ell)}$ is shifted by an arbitrary real function of $q_{2,k}^{*2}$. This leads to a second version of the modified K matrix in which the problematic singularities have been removed, and this freedom is sufficient to extend the applicability of the formalism to include two-particle bound states and resonances. In this section we explain this generalization and describe its implementation, leaving a detailed derivation to a separate paper [131]. We give three examples of how the approach may be applied. First, in Sec. 7.3.1, we consider s-wave bound states; then, in Sec. 7.3.2, we discuss bound states in the d-wave; and finally, in Sec. 7.3.3, we turn to the case of two-particle resonances.

The modification of the formalism is effected by changing the principal value (PV) prescription used in multiple places in the derivation of Ref. [28]. We recall that the original derivation consists of evaluating a finite-volume two-point correlation function, projected to kinematics for which three-particle states may go on shell. The correlator is expressed in terms of a skeleton expansion in which all three-particle cuts are explicitly displayed, and only the sums over momenta in these types of cuts give power-like L-dependence. One then replaces sums with sum-integral differences plus integrals, which, after extensive analysis, leads to a relation between finite-volume energies, determined by the poles in the correlator, and infinite-volume scattering quantities. The first line of Fig. 7.1 shows the replacement for the simplest diagram contributing to the correlation function.

For those integrals that are singular due to three-particle intermediate states, such as the upper integral in the figure, a pole prescription is required. The PV prescription is used so that the result is a smooth function of the lower (spectator) momentum, $\mathbf{k}$. This allows the second step shown in the figure to be made, in which the lower sum is replaced by an integral (for which a pole prescription is not needed). Thus the PV prescription appears in the sum-integral difference, F, as shown by the example of the s-wave restriction, $\widetilde{F}^s$, given in Eq. (F.2). It also appears in the definition of $\widetilde{\mathcal{K}}_2^{(\ell)}$ and in $\mathcal{K}_{\text{df},3}$. We note that it was found in Ref. [28] that the integrals requiring a PV prescription are all single-loop integrals over a

spatial momentum with the integrand having a pole of the form shown in Eq. (F.2).

In Ref. [131] (*to appear*) we show that the derivation of the quantization condition holds for a large family of pole prescriptions, which we denote collectively by PV′. We first describe these for $\ell_{\max} = 0$, so that only s-wave quantities enter. If the integrand is nonsingular, then no prescription is needed, and the PV′ and PV results are the same. If the integrand has a pole, then the modification is

$$\mathrm{PV}' \int \frac{d^3a}{(2\pi)^3} \frac{H(\mathbf{a})H(\mathbf{b})}{8\omega_a\omega_b(E-\omega_k-\omega_a-\omega_b)} = \mathrm{PV} \int \frac{d^3a}{(2\pi)^3} \frac{H(\mathbf{a})H(\mathbf{b})}{8\omega_a\omega_b(E-\omega_k-\omega_a-\omega_b)} - \frac{I^s_{\mathrm{PV}}(q^{*2}_{2,k})}{32\pi} \,. \quad (7.15)$$

Here I^s_{PV} is any smooth function of $q^{*2}_{2,k}$, while the negative sign and the 32π are for later convenience. The modified prescription is illustrated in the final line of Fig. 7.1. This provides a complete description of the prescription for the purposes of the derivation of the quantization condition.[11] The effect of the change in prescription for $\widetilde{F}^s$ and $\widetilde{\mathcal{K}}^s_2$ is

$$[\widetilde{F}^s]_{kp} \to [\widetilde{F}^s]_{kp} + \delta_{kp} \frac{H(\mathbf{k})}{2\omega_k} \frac{I^s_{\mathrm{PV}}(q^{*2}_{2,k})}{32\pi} \,, \quad (7.16)$$

$$\left[(\widetilde{\mathcal{K}}^s_2)^{-1}\right]_{kp} \to \left[(\widetilde{\mathcal{K}}^s_2)^{-1}\right]_{kp} - \delta_{kp} \frac{H(\mathbf{k})}{2\omega_k} \frac{I^s_{\mathrm{PV}}(q^{*2}_{2,k})}{32\pi} \,. \quad (7.17)$$

The shift in $\widetilde{F}^s$ follows directly from Eq. (7.15), while that in $\widetilde{\mathcal{K}}^s_2$ can be derived by enforcing the prescription-independence of the physical quantity $\mathcal{M}_2$. There is no change in $\widetilde{G}^s$, since it does not contain an integral.

The final quantity affected by changing the PV prescription is $\mathcal{K}_{\mathrm{df},3}$. The change to $\mathcal{K}_{\mathrm{df},3}$ can be determined in principle by studying the infinite-volume integral equations relating $\mathcal{K}_{\mathrm{df},3}$ to $\mathcal{M}_3$. We will describe these changes in Ref. [131], and only note here three important

[11] If the integrand is multiplied by a function of $\mathbf{k}$ and $\mathbf{a}$ having only an s-wave component in the c.m. frame of the non-spectator pair (as must be the case when setting $\ell_{\max} = 0$), then the I^s_{PV} term is multiplied by the on-shell value of this function, obtained in the manner described in Ref. [28]. This result holds because the difference between the on-shell and off-shell values of this function cancels the pole, leading to a nonsingular integral that does not require a pole prescription.

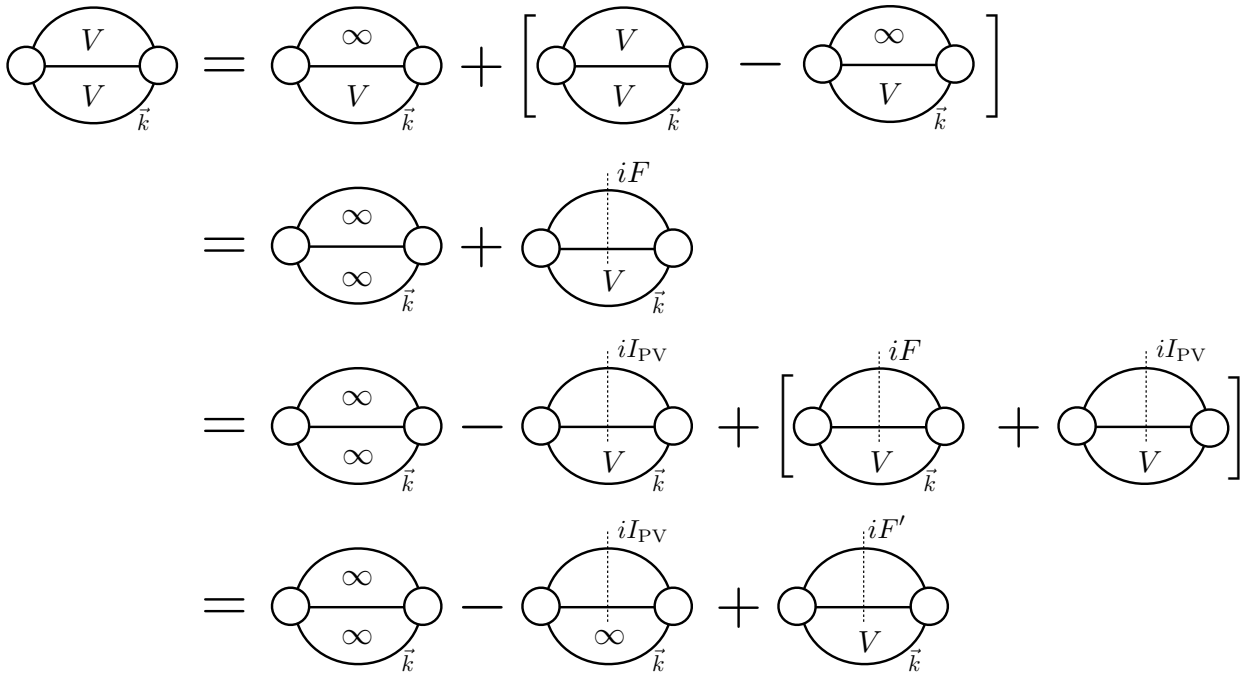

Figure 7.1: Illustration of the previous and modified PV prescriptions used in the analysis of the three-particle correlation function, for the simplest diagram. Loops containing the symbol "∞" are integrated, while those containing a "V" have the spatial components of the momentum summed. All integrals use the PV prescription. In the first line the upper sum is replaced by an integral plus a sum-integral difference. The latter can be replaced by an F cut, as shown in the second line, while the lower loop sum can be replaced by an integral in the first term on this line. In the third line we subtract and add the $I^s_{\rm PV}$ cut. The final line shows that this new cut can be absorbed into the modified F, leaving a modified PV prescription for the upper loop integral.

results: *(i)* if $\mathcal{K}_{\rm df,3}$ vanishes, then it remains zero after the change in prescription; *(ii)* the changes in $\mathcal{K}_{\rm df,3}$ are, in general, energy dependent; *(iii)* an isotropic $\mathcal{K}_{\rm df,3}$ is changed, in general, into a nonisotropic one, containing partial waves beyond s-wave.

We stress that the quantization condition containing the new versions of $\widetilde{F}$, $\widetilde{\mathcal{K}}_2$ and $\mathcal{K}_{\rm df,3}$, must lead to the same relation between the physical scattering amplitudes and the

finite-volume spectrum, for all L, up to exponentially-suppressed effects. All we are doing is reshuffling contributions in the all-orders diagrammatic analysis of the same finite-volume correlator. Nevertheless, once we make an approximation, the spectrum need no longer be independent of $I^s_{\rm PV}$, and the result *(iii)* above shows that, indeed, the spectrum cannot be left strictly invariant if we maintain an isotropic $\mathcal{K}_{\rm df,3}$ while varying $I^s_{\rm PV}$. In other words, we cannot exactly compensate at all values of L for the shifts in $\widetilde{F}^s$ and $\widetilde{\mathcal{K}}_2$ by an (energy-dependent) shift in $\mathcal{K}^{\rm iso}_{\rm df,3}$. Indeed, we can use the residual $I^s_{\rm PV}$ dependence as an estimate of the error due to truncating the quantization condition. This is analogous to the use of scheme-dependence as an estimate of truncation errors in quantities calculated in perturbation theory. We also note that there is no *a priori* theoretical reason to favor any particular choice of $I^s_{\rm PV}$.

We investigate the size of the $I^s_{\rm PV}$ dependence in an example presented in Appendix E.1, finding it to be numerically small. We also note in the appendix that we can use the threshold expansion to estimate the size of any residual $I^s_{\rm PV}$ dependence. In particular, when we enforce the isotropic approximation, residual $I^s_{\rm PV}$ dependence will be suppressed by $\mathcal{O}(\Delta^2)$, where $\Delta = (E^{*2} - 9m^2)/(9m^2)$, since nonisotropic terms in $\mathcal{K}_{\rm df,3}$ enter only at this order in the threshold expansion [76].

The only exception to the above discussion occurs when $\mathcal{K}^{\rm iso}_{\rm df,3}$ vanishes. The result *(i)* implies that no change to $\mathcal{K}^{\rm iso}_{\rm df,3}$ is then needed to maintain the same physical scattering amplitude and spectrum as $I^s_{\rm PV}$ is varied. Indeed, this is seen both in the integral equations relating $\mathcal{K}_{\rm df,3}$ to $\mathcal{M}_3$, to be discussed in Ref. [131], and in the quantization condition, Eq. (F.8), relating $\mathcal{K}_{\rm df,3}$ to $E_n(L)$. In both cases, when $\mathcal{K}^{\rm iso}_{\rm df,3} = 0$ all $I^s_{\rm PV}$ dependence drops out. To see this in detail in the quantization condition note that when $\mathcal{K}^{\rm iso}_{\rm df,3} = 0$, a solution requires that $F^{\rm iso}_3$ diverges. Looking at the form of F^s_3, Eq. (F.1), we see that it only diverges either if $\widetilde{F}^s$ diverges or if the denominator of the second term,

$$H_{FG} = 1/\widetilde{\mathcal{K}}^s_2 + \widetilde{F}^s + \widetilde{G}^s\,, \tag{7.18}$$

has a zero eigenvalue. The former possibility leads to poles at free three-particle energies, which are known from the analysis of Ref. [76] to be absent in the isotropic approximation, cancelling between the two terms defining F_3^s. Thus the only solutions come from zero eigenvalues of H_{FG}. However, as can be seen from Eqs. (7.16) and (7.17), the shifts in $\widetilde{F}^s$ and $1/\widetilde{\mathcal{K}}_2^s$ exactly cancel, so that H_{FG} is independent of I_{PV}^s.

The latter result means, in practice, that we do not need to introduce I_{PV}^s when determining solutions with $\mathcal{K}_{\mathrm{df},3}^{\mathrm{iso}} = 0$, and can use exactly the same numerical method as in Ref. [39]. For nonvanishing $\mathcal{K}_{\mathrm{df},3}^{\mathrm{iso}}$ however, we do need to choose a nonvanishing I_{PV}^s such that the quantization condition is valid for the chosen value of the two-body scattering parameters. In practice, we have found it sufficient to consider only the case of a constant I_{PV}^s. Introducing I_{PV}^s into the numerical analysis is very straightforward, and the methodology of Ref. [39] can be carried over essentially without change.

Before turning to our three specific examples, we close the general discussion with the extension of our new PV′ prescription to higher angular momenta. This is straightforward and the essential feature is that, for each (allowed) choice of ℓ, one has the freedom to introduce a different real, smooth function, $I_{\mathrm{PV}}^{(\ell)}(q_{2,k}^{*2})$. The changes to $\widetilde{F}$ and $\widetilde{\mathcal{K}}_2$, which are now matrices with the full set of indices, are

$$[\widetilde{F}]_{k\ell'm';p\ell m} \to [\widetilde{F}]_{k\ell'm';p\ell m} + \delta_{kp}\delta_{\ell'\ell}\delta_{m'm}\frac{H(\mathbf{k})}{2\omega_k}\frac{I_{\mathrm{PV}}^{(\ell)}(q_{2,k}^{*2})}{32\pi}\,, \tag{7.19}$$

$$\left[(\widetilde{\mathcal{K}}_2)^{-1}\right]_{k\ell'm';p\ell m} \to \left[(\widetilde{\mathcal{K}}_2)^{-1}\right]_{k\ell'm';p\ell m} - \delta_{kp}\delta_{\ell'\ell}\delta_{m'm}\frac{H(\mathbf{k})}{2\omega_k}\frac{I_{\mathrm{PV}}^{(\ell)}(q_{2,k}^{*2})}{32\pi}\,, \tag{7.20}$$

where ℓ and ℓ' are even. As before, if we set $\mathcal{K}_{\mathrm{df},3} = 0$, as we do in some of the numerical examples below, then we can in practice ignore the $I_{\mathrm{PV}}^{(\ell)}$ shift, since it cancels in the quantization condition.

Further details, as well as a discussion of the relationship between the introduction of $I_{\mathrm{PV}}^{(\ell)}$ and the formalism presented in Refs. [34, 35], where the K matrix poles were taken into account explicitly, will be given in Ref. [131].

7.3.1 Using $I^s_{\rm PV}$ to accommodate an s-wave bound state

Here we show that, if we set $I^s_{\rm PV}$ to an appropriate constant, then the quantization condition in the s-wave, isotropic approximation is valid for three-particle systems in which there is a two-particle scalar bound state. Specifically, we consider the case in which we keep only the leading term in the ERE, i.e. the scattering length in Eq. (7.9). This is also one of the examples that we investigate numerically below.

The quantization condition is valid as long as $\widetilde{\mathcal{K}}_2^s$ has no pole in the kinematic range of interest. To study this, we consider the denominator of $\widetilde{\mathcal{K}}_2^s$, which, from Eq. (F.5), together with the modification given in Eq. (7.17), is[12]

$$d_{\rm PV}(q^2) \equiv \frac{32\pi\omega_k E^*_{2,k}}{\widetilde{\mathcal{K}}_2^s}\,, \tag{7.21}$$

$$= -1/(ma_0) + [1 - H(q^2)]|q|/m - I^s_{\rm PV} H(q^2)\sqrt{1+q^2/m^2}\,. \tag{7.22}$$

There is a pole whenever this quantity vanishes. We plot $d_{\rm PV}(q^2)$ for $I^s_{\rm PV} = 0$ and -1 in Fig. 7.2. The cutoff function vanishes when $q^2/m^2 < -1$ so the lower limit in all the plots is set to this value. The upper limit depends on E/m: for $E/m = 3$ it is $q^2/m^2 = 0$, while for $E/m = 5$ (the maximum value for which our quantization condition holds) it is $q^2/m^2 = 3$. In the left-hand figure, where $I^s_{\rm PV} = 0$, the curves are flat for $q^2/m^2 > 0$, and so we do not show the entire range.

[12] Previously we have written H as a function of the spectator momentum, $\mathbf{k}$. The explicit form that we use, given in Ref. [39], is in fact a function of $q^{*2}_{2,k}$ (itself a function of $\mathbf{k}$) and it is more convenient here to make this explicit, at the cost of some abuse of notation.

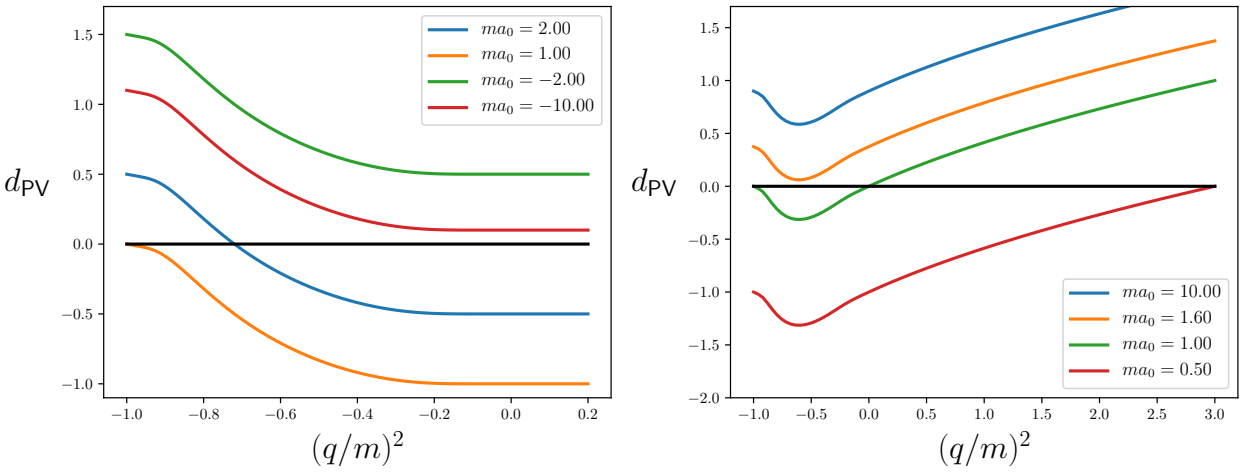

(a) $I^s_{\mathrm{PV}} = 0$ (b) $I^s_{\mathrm{PV}} = -1$

Figure 7.2: Plots of the denominator of $\widetilde{\mathcal{K}}^s_2$, $d_{\mathrm{PV}}(q^2)$, vs. q^2/m^2 for a range of choices of am with $I^s_{\mathrm{PV}} = 0$ (left) and $I^s_{\mathrm{PV}} = -1$ (right). There is a pole in $\widetilde{\mathcal{K}}^s_2$ whenever $d_{\mathrm{PV}}(q^2)$ vanishes. See text for further discussion.

From the left panel we see that, for $I^s_{\mathrm{PV}} = 0$, $d_{\mathrm{PV}}(q^2)$ has a zero-crossing when $ma_0 > 1$, a result that is simple to verify analytically. We stress that the pole that appears lies far below threshold. For example, as $ma_0 \to 1^+$ the pole position approaches $q^2/m^2 = -1$. The pole is not related to a physical quantity, as is made clear by the fact that its position depends on the cutoff function $H(\mathbf{k})$. Nevertheless, it presents a barrier to the derivation of the quantization condition.

The restriction to $ma_0 \leq 1$ implies that the formalism cannot accommodate a two-particle bound state when using $I^s_{\mathrm{PV}} = 0$. To understand this, recall that a bound state occurs when $\mathcal{M}_2$ has a pole for $q^2 < 0$, i.e. when $q \cot \delta_s(q) + |q| = 0$. In our approximation, this becomes $q^2 = -1/a_0^2$. Since our cutoff function leads to the restriction $q^2 > -m^2$, the bound state is present only for $ma_0 > 1$.

The right panel, Fig. 7.2(b), shows that, using the PV′ prescription with $I^s_{\mathrm{PV}} = -1$, the

quantization condition is now valid for $ma_0 < 0.5$ and $ma_0 \gtrsim 1.6$. This shift in the range of validity continues as $I^s_{\rm PV}$ is lowered further. For $I^s_{\rm PV} = -2$ the range becomes $ma_0 < 0.25$ and $ma_0 \gtrsim 1.15$. This raises the question of whether, for any choice of $ma_0 > 1$, there is a value, or range of values, of $I^s_{\rm PV}$ for which the quantization condition is valid. We find numerically that the answer is affirmative—for a given choice of $ma_0 > 1$, as long as $I^s_{\rm PV}$ is sufficiently negative, the quantization condition holds. The minimum value of $I^s_{\rm PV}$ that is needed grows rapidly as ma_0 approaches unity. Nevertheless, the key point is that we can use the quantization condition to study all values of the scattering length by choosing $I^s_{\rm PV}$ to lie in an appropriate range that depends on the value of ma_0.

7.3.2 Using $I^d_{\rm PV}(q^2)$ to accommodate a d-wave bound state

We now turn to the case that a pole appears in the $\ell = 2$ component of our K-matrix-like quantity. In this case, the denominator of $\widetilde{\mathcal{K}}^d_2$, Eq. (7.14), is modified by Eq. (7.20) to

$$d^d_{\rm PV}(q^2) \equiv \frac{32\pi\omega_k E^*_{2,k}}{\widetilde{\mathcal{K}}^d_2}\,, \tag{7.23}$$

$$= -1/(a_2^5 q^4 m) + [1 - H(q^2)]|q|/m - I^d_{\rm PV}(q^2) H(q^2)\sqrt{1 + q^2/m^2}\,. \tag{7.24}$$

This differs from $d^s_{\rm PV}(q^2)$, Eq. (7.22), only by the presence of the $1/q^4$ factor in the first term on the right-hand side. The quantization condition is valid as long as $d^d_{\rm PV}(q^2)$ does not vanish for q^2 in the allowed kinematical range, $-1 < q^2/m^2 < 3$. It is straightforward to show that, for $I^d_{\rm PV} = 0$, such a zero crossing only occurs when the d-wave scattering length satisfies $ma_2 > 1$. This is also the condition for a d-wave bound state to be present:

$$-\frac{1}{a_2^5 q^4} + |q| = 0 \quad \Rightarrow \quad |q| = \frac{1}{a_2}\,, \tag{7.25}$$

which, since $|q| < m$, implies that one must have $ma_2 > 1$. Thus previous numerical investigation of the quantization condition including d-waves was restricted to values of the scattering length such that there were no d-wave dimers.

This restriction can be lifted using the PV′ prescription. A simple choice is to set $I^d_{\rm PV}(q^2) = c/q^4$, with c a constant. Then, by multiplying $d^d_{\rm PV}(q^2)$ by q^4, the analysis becomes very similar to that for $d^s_{\rm PV}(q^2)$, and one finds that, for any value of ma_2, there is a range of values of c for which $d^d_{\rm PV}(q^2)$ has no zero crossing. We use this freedom in the numerical investigations described in Sec. 7.4.5.

7.3.3 Using $I^s_{\rm PV}$ to accommodate an s-wave resonance

Our final example of using the PV′ prescription is for an s-wave resonance with the phase shift given in Eq. (7.10). Here we find it more convenient to show plots of $1/\widetilde{\mathcal{K}}^s_2$ vs. $|\mathbf{k}|$, and these are shown in Fig. 7.3 for the choice of resonance parameters used in our numerical investigations below. Figure 7.3(a) shows the result with the original PV prescription, showing the zero associated with the resonance, and its dependence on E. The right panel, Fig. 7.3(b), shows that by choosing the constant value $I^s_{\rm PV} = -100$, the zero can be removed for the kinematic range of interest.

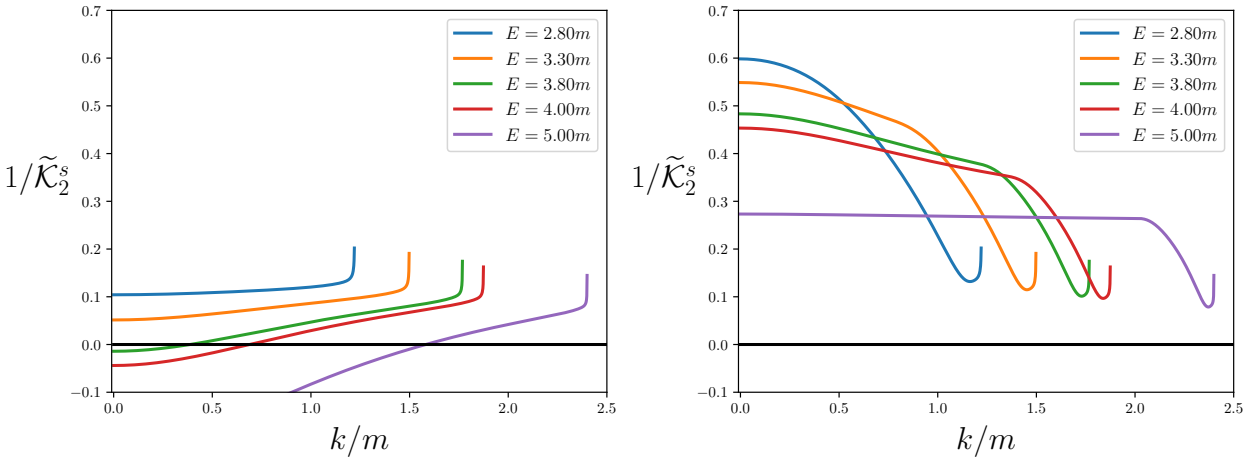

(a) $I^s_{PV} = 0$ (b) $I_{PV} = -100$

Figure 7.3: $1/\widetilde{\mathcal{K}}_2^s$ vs. $|\mathbf{k}|/m$, with $\mathbf{k}$ the spectator momentum for the Breit-Wigner form of the phase shift given in Eq. (7.10), with the resonance parameters set to $g = 1$ and $m_R = 2.7m$. Thus the resonance only leads to a zero crossing for $E > 3.7m$. Results are shown for (a) $I^s_{\mathrm{PV}} = 0$ and (b) $I^s_{\mathrm{PV}} = -100$.

7.4 Numerical results

In this section we present numerical results from the quantization condition using the PV′ prescription, which allows us to consider choices for $\mathcal{K}_2$ that were inaccessible to our previous numerical explorations [39, 76]. Our approach is to assume forms for $\mathcal{K}_2$ and $\mathcal{K}_{\mathrm{df},3}$ and determine the resulting finite-volume spectrum. In a practical application, using LQCD finite-volume energies, one will ultimately identify a broad set of $\mathcal{K}_2$ and $\mathcal{K}_{\mathrm{df},3}$ parametrizations and fit these to the numerically-determined spectrum, ideally for various values of L and various total spatial momenta. This idea, proposed in Ref. [134] and now standard in the analysis of two particle channels, allows one to identify the subset of parametrizations that can describe the physical system under consideration. In addition, the spread in the functional forms $\mathcal{K}_2$ and $\mathcal{K}_{\mathrm{df},3}$ that give a good description provides a systematic uncertainty,

indicating how well the input finite-volume information can constrain these infinite-volume objects. Here, instead, we aim to illustrate the types of behavior that can be expected in the spectrum for different fixed choices of the two- and three-particle interactions.

We begin in Sec. 7.4.1 by working in the isotropic approximation, presenting a global view of the spectrum for values of the s-wave scattering length, $ma_0 > 1$, such that there are two-particle bound states (called dimers). We consider a range of choices of a_0, including those in which the dimer is deeply bound, requiring a relativistic formalism such as ours, as well as those for which the bound state is shallow, allowing comparison with results from the NREFT three-particle formalism [40]. A feature of most of these spectra is the appearance of one or more three-particle bound states (called trimers).

Next, in Sec. 7.4.2, we focus on the region of the spectrum below the three-particle threshold, where finite-volume states are dominantly composed of a dimer together with a particle. Here, by going to large volumes, we are able to use our formalism as a tool for determining the properties of dimer-particle scattering in infinite-volume. This leads us, in Sec. 7.4.3, to adjust the parameters a_0 and $\mathcal{K}_{\mathrm{df},3}$ so that we can model the three-nucleon system with deuteron and triton bound states, albeit without including spin. This is the only example in which we consider nonvanishing $\mathcal{K}_{\mathrm{df},3}$.

Still working in the isotropic approximation, in Sec. 7.4.4 we determine the form of the three-particle spectrum in the presence of a narrow s-wave resonance. To our knowledge, this is the first example of such a study. Finally, in Sec. 7.4.5, we turn on d-wave interactions, leading to the possibility of both s- and d-wave dimers, as well as trimers.

7.4.1 Spectrum with $ma_0 > 1$

In this subsection we work in the isotropic approximation, described in Sec. 7.2.2, and keep only the leading term in the effective range expansion, so that

$$q \cot \delta_0 = -1/a_0 \,. \tag{7.26}$$

As explained above, the key change introduced by working with $ma_0 > 1$ is the presence of a two-particle bound state. The infinite-volume mass of this dimer is given exactly by

$$M_d = 2m\sqrt{1 - 1/(ma_0)^2}\,, \tag{7.27}$$

which varies in the range $0 < M_d < 2m$ as ma_0 changes from 1 to infinity. At the lower end of this range, the dimer is very deeply bound and thus the internal degrees of freedom are relativistic. As ma_0 increases, the binding energy decreases and the bound state dynamics becomes increasingly nonrelativistic (NR). We expect the crossover point to be around $|q^2|/m^2 = 1/(ma_0)^2 \approx 0.1$, which occurs when $ma_0 \approx 3.2$, $M_d \approx 1.9m$. In the NR regime, the dimer wavefunction falls exponentially with a distance scale given by a_0. Thus to avoid large finite-volume effects in the dimer mass we need to use volumes such that $a_0/L = (ma_0)/(mL) \gg 1$; in practice we require $a_0/L \gtrsim 5$. We stress that this constraint is only relevant if we wish to suppress the dimer's volume-dependence and that the quantization condition itself is valid for all choices of a_0/L provided that mL is large enough to safely ignore the the neglected e^{-mL} scaling.

For some range of parameters we also expect there to be one or more three-particle bound states. In particular, we know that when $|ma_0| \gg 1$ so that we are close to the unitary limit, Efimov trimers will form. In fact, we find trimers as soon as ma_0 exceeds ≈ 1.4. All calculations in this subsection are for $\mathcal{K}_{\mathrm{df},3}^{\mathrm{iso}} = 0$ so that the value of I_{PV}^{s} is irrelevant, as explained above.

We first determine the spectra for $1 < ma_0 \leq 2$ for moderate values of mL, aiming for an overview of the phenomena that can occur. Four examples are shown in Fig. F.3. To interpret the resulting spectra (shown by the colored lines in the plot) it is useful to compare to two types of noninteracting energies. First, there are the energies of three noninteracting particles of mass m, which we refer to as $1 + 1 + 1$ levels. These are the same for all four plots. The lowest such level, at $E/m = 3$, is independent of L, while higher levels have

L-dependence and asymptote to $E/m = 3$ as $L \to \infty$. The $1+1+1$ levels are shown as solid grey lines. The second class of noninteracting energies, shown by dashed grey lines, are dimer + particle states, whose energies are given by

$$E_{\mathbf{n}} = \sqrt{M_d^2 + (2\pi/L)^2 \mathbf{n}^2} + \sqrt{m^2 + (2\pi/L)^2 \mathbf{n}^2}\,, \tag{7.28}$$

with $\mathbf{n}$ an integer vector. We refer to these as $2+1$ states for brevity. The lowest such state has $E = M_d + m$, and all the others asymptote to this energy as $L \to \infty$. We note that, when we project onto the $\mathbb{A}_1^+$ irrep of the cubic group then each noninteracting level, both the 1+1+1 and 2+1 types, has one corresponding solution in the quantization condition. We also stress that the dimer is a relativistic bound state for all four values of ma_0 shown in the figure.

The interpretation of the spectrum is simplest for $ma_0 = 1.3$. The lowest two levels correspond to $2+1$ states with energies shifted down slightly by the dimer-particle interactions. By contrast, the third level changes its nature for $mL \sim 8$: above this it is a (shifted) $2+1$ state, while below it is a (shifted) $1+1+1$ state. This shifted state also appears in the second orange-colored level for $8 \lesssim mL \lesssim 10$, and in the third blue level for $10 \lesssim mL$. A similar pattern occurs for higher levels.

Although the spectrum looks superficially similar for the other (larger) values of ma_0, there is, in fact, a qualitative difference. This is because, for $ma_0 \gtrsim 1.4$, a trimer appears. The lowest (blue) level asymptotes to an energy below $M_d + m$. This is not apparent from Fig. F.3, but can be seen for $ma_0 = 2$ by the spectrum at larger L shown in Fig. 7.5. Thus the interpretation of the levels for $ma_0 = 1.6$, 1.8 and 2.0 is as follows: the lowest (blue) level is a trimer or 3 state; the next level (orange) is the lowest $2+1$ state with energy raised by residual interactions. The third level begins at small mL as a shifted $1+1+1$ state, but, for a value of mL that depends on ma_0, it changes its dominant nature to an excited $2+1$ state.

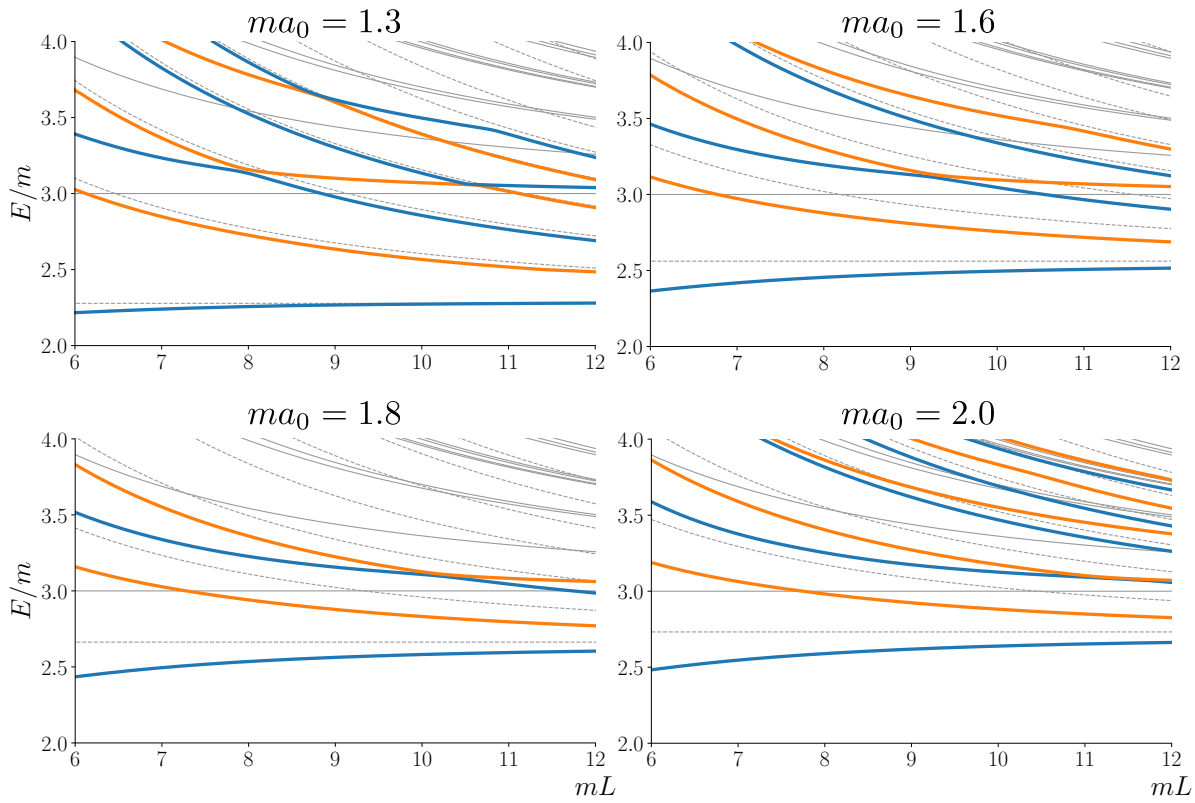

Figure 7.4: The spectrum for four values of ma_0 and $\mathcal{K}_{\mathrm{df},3}^{\mathrm{iso}} = 0$ as a function of mL. All four values lead to relativistic two-particle bound states. Solid grey lines show the energies of three noninteracting particles (1+1+1 states), while dashed grey lines give the energies of noninteracting dimer + particle states (2+1 states). The interacting energy levels are shown in alternating colors to emphasize the avoided level crossings. Although it is not apparent from these plots, by going to larger values of mL we find that the lowest state for $ma_0 = 1.6$, 1.8, and 2.0 is a trimer, while that for $ma_0 = 1.3$ asymptotes to the dimer + particle energy as $mL \to \infty$. See the text for further discussion.

Having summarized the content of Fig. F.3, it is instructive to consider Fig. 7.5 in more detail. Here we restrict attention to a small energy range around the dimer + particle threshold. There are nevertheless several levels, since we work at large mL. All except the trimer asymptote to $E_d + m$ as $L \to \infty$, and in the regime shown, where they lie well below the $1 + 1 + 1$ threshold, all can be considered as dominantly $2 + 1$ levels, with a repulsive

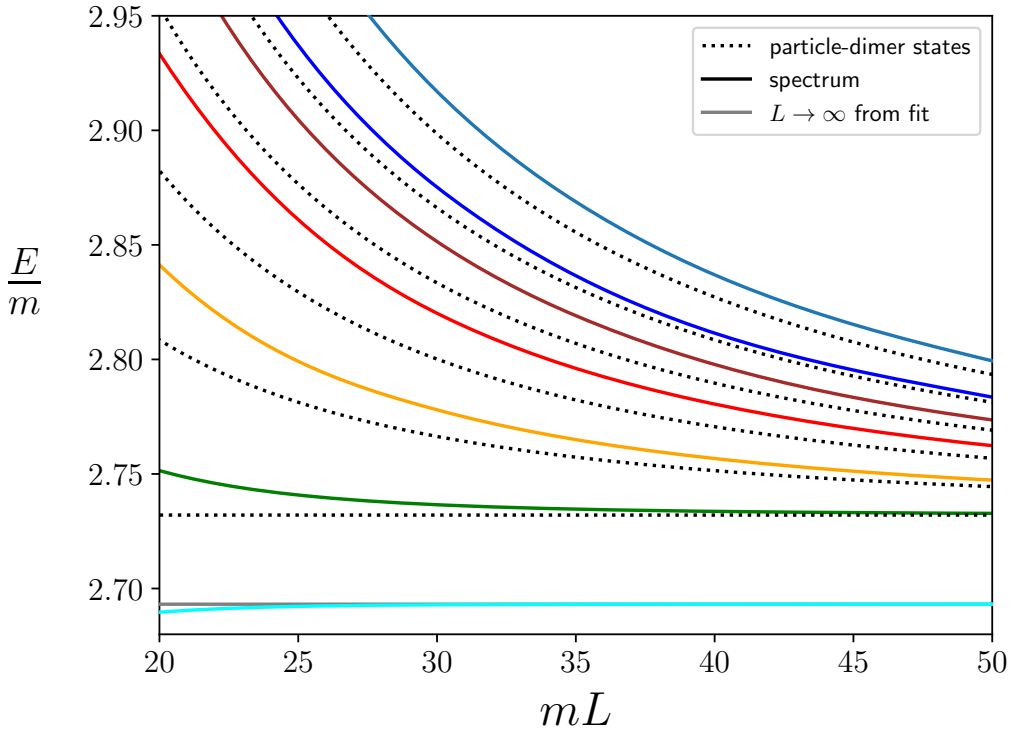

Figure 7.5: Low-lying spectrum for $ma_0 = 2$ and $\mathcal{K}_{\mathrm{df},3}^{\mathrm{iso}} = 0$ for larger mL. This is the continuation to larger volumes of the spectrum shown in the bottom right-hand panel of Fig. F.3. Note the highly compressed vertical scale. The horizontal line for the lowest level gives the $L \to \infty$ asymptote for the trimer energy, using a fit described in the text.

interaction pushing the energies up from their noninteracting values. In the next subsection we will do a quantitative analysis of these energy shifts, which encode information about the dimer-particle phase shift. For now we focus on the volume-dependence of the trimer energy, $E_t(L)$. We fit for $mL > 25$ to the following form:

$$\frac{E_t(L)}{m} = \frac{E_0}{m} - \frac{|C|}{(mL)^{3/2}} e^{-2\kappa L/\sqrt{3}}, \tag{7.29}$$

where $\kappa^2/m^2 = 3 - E_0/m$ with $E_0 = E_t(\infty)$, and $|C|$ a fit parameter. The fit determines the asymptote to be $E_0 \approx 2.6931m$. Equation (7.29) is the result for the asymptotic volume-dependence derived in Ref. [105] for a nonrelativistic bound state in the unitary (large $|ma_0|$)

limit. While it does not obviously apply here (since $ma_0 = 2$ is not in the unitary regime), we find that it gives a very good description of our results. However, as for the higher levels, a more rigorous approach is available for analyzing $E_t(\infty)$, as we discuss in the next subsection.

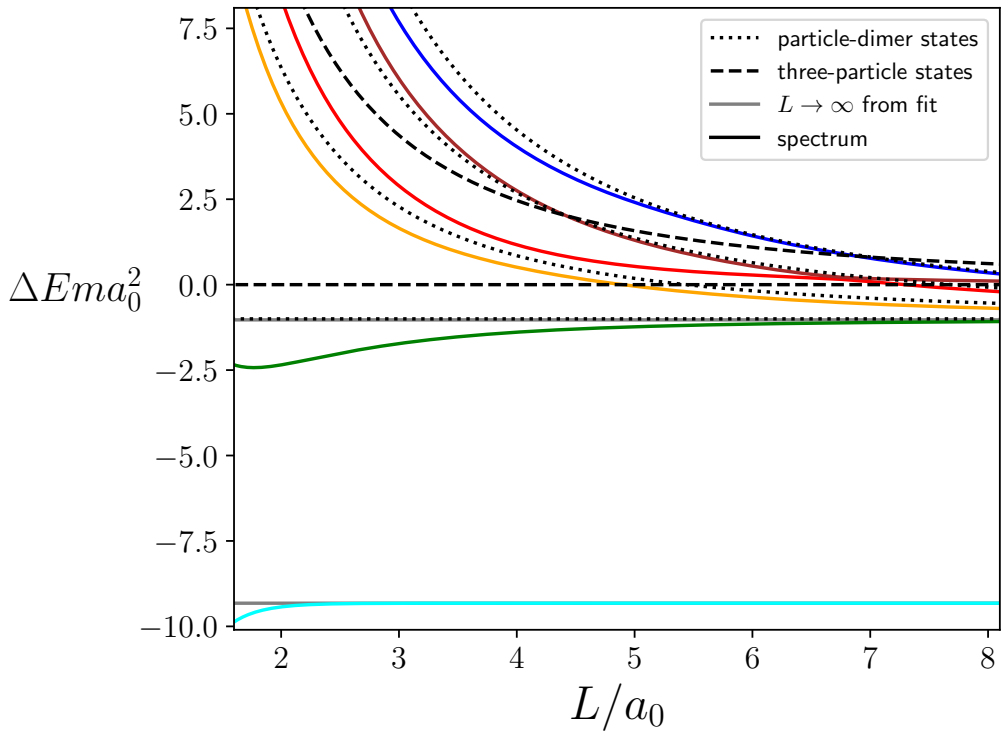

Figure 7.6: Spectrum as a function of the box size for $ma_0 = 16$ and $\mathcal{K}_{\mathrm{df},3}^{\mathrm{iso}} = 0$, with $\Delta E = E - 3m$ the nonrelativistic energy. In order to facilitate comparison with Ref. [40], the quantities plotted are made dimensionless using appropriate factors of a_0, and thus differ from those in Figs. F.3 and 7.5.

We conclude our overview by studying the spectrum for $ma_0 = 16$. For this value of the

scattering length the dimer mass lies well in the NR regime,

$$\frac{M_d}{m} = 1.9961 \approx 2 - \frac{1}{(ma_0)^2}\,, \tag{7.30}$$

so that our results can be compared to those obtained from the NREFT quantization condition, as studied in Ref. [40]. We thus display the spectrum in Fig. 7.6 using the variables adopted in Ref. [40]. This should be compared to Figs. 3 and 6 of that work, from which the strong similarities are evident. In particular, there are two trimers in both cases, dubbed the deep and shallow bound states in Ref. [40]. In that work, these two trimers have energies $\Delta E m a_0^2 = (E - 3m) m a_0^2 = -10$ and -1.016, respectively. We are not aiming to reproduce these numbers precisely, which would require tuning $\mathcal{K}_{\mathrm{df},3}$ to nonzero values, but rather to obtain semiquantitative agreement.

To obtain the trimer energies from our results, we fit the lowest two spectral levels to their asymptotic forms. For the deep (lowest) level we use Eq. (7.29), obtaining $\Delta E_t m a_0^2 = -9.3218$ (corresponding in relativistic units to $E/m = 2.9636$). For the shallow trimer, we treat the state as a bound state of the particle plus dimer, an interpretation that is justified in the following subsection. Thus, following Ref. [40], we can use Lüscher's two-particle quantization condition to predict its asymptotic volume-dependence [135]:

$$\frac{E_t(L)}{m} = \frac{E_0}{m} - \frac{|D|}{mL} e^{-\kappa' L}\,, \quad \kappa' = \sqrt{2\mu(3m - E)}\,, \tag{7.31}$$

with the reduced mass given by $1/\mu = 1/m + 1/M_d \approx 3/(2m)$. This fit yields $\Delta E m a_0^2 = -1.0301$ (corresponding to $E = 2.99598m$). This lies below the particle-dimer threshold, given by

$$\Delta E_d \equiv 3m - (m + M_d) = 2m - M_d \approx \frac{1}{m a_0^2}\,, \tag{7.32}$$

which corresponds to $\Delta E m a_0^2 = -1$ (or, strictly speaking, $\Delta E m a_0^2 = -1.001$ if one includes relativistic effects). The asymptotic energies are shown by the solid grey horizontal lines in Fig. 7.6, and the presence of the shallow dimer is indicated by the small offset between the

horizontal dashed and solid grey lines near $\Delta E m a_0^2 = -1$.

A final noteworthy point of similarity between the results in Fig. 7.6 and those in Ref. [40] concerns the third level (in orange) for $L/a_0 \gtrsim 5$ (so that $\Delta E < 0$). This $2+1$ state lies close to the first excited noninteracting particle-dimer energy, and far from the lowest such energy at $\Delta E m a_0^2 = -1$. Thus it appears that the latter state is missing in the spectrum. This point was observed in Ref. [40], where it was argued that the missing state transmutes in finite volume into the shallow dimer. We give further evidence for this interpretation in the following section.

7.4.2 Dimer-particle scattering

As seen in the previous subsection, states that lie below the three-particle threshold at $E = 3m$ can be interpreted as dimer + particle states, abbreviated as $2+1$ states. In this section, we focus on this energy regime and extend our calculations to very large mL, so as to learn about *infinite-volume* dimer-particle scattering. In particular, we choose $L \gg a_0$, so as to avoid large finite-volume effects in the dimer, which we know from the two-particle quantization condition fall as $\exp(-\kappa L) = \exp(-L/a_0)$. Then, to the extent that the finite-volume states can be described as purely dimer+particle states, we can use the nondegenerate, nonidentical form of the two-particle quantization condition, truncated to the s-wave, to determine the dimer-particle scattering phase shift. In effect, we are using the three-particle quantization condition as a tool both to solve the relativistic two-particle bound state equation and to determine the structure of the resulting dimer by probing it with a third particle. We carry out this calculation in detail for three choices of the two-particle scattering length, $ma_0 = 2$, 6, and 16, again using the isotropic approximation with $\mathcal{K}_{\mathrm{df},3}^{\mathrm{iso}} = 0$. This study extends the idea presented in Ref. [77] in the nonrelativistic limit, where the scattering length of the particle+dimer system was related to the three-body scattering amplitude. The two-particle quantization condition for non-identical scalar

particles, truncated to the s-wave, is [24, 136]

$$k \cot \delta_0(k) = \frac{1}{\pi L} \mathcal{Z}\left(\frac{Lk}{2\pi}\right), \qquad \mathcal{Z}(\eta) = \sum_{\mathbf{j}}^{\mathrm{UV}} \frac{1}{|\mathbf{j}|^2 - \eta^2}, \tag{7.33}$$

where UV indicates a suitable UV regulator, and k is defined through

$$E = \sqrt{m^2 + k^2} + \sqrt{M_d^2 + k^2}, \tag{7.34}$$

with M_d the dimer mass and E the energy of the finite-volume state. Using Eq. (7.33) we obtain the usual one-to-one relation between the spectral levels and the phase shift. It is important to note that this equation holds for all levels in the spectrum that lie in the $2+1$ regime, and not only for the lowest state.

Once we have determined $\delta_0(k)$, we use two forms to parametrize it. The first is the standard effective range expansion (ERE),

$$k \cot \delta_0(k) = -\frac{1}{b_0} + \frac{1}{2} r k^2 + P r^3 k^4 + O(k^6), \tag{7.35}$$

where b_0 is the dimer-particle scattering length. The radius of convergence is typically determined by the branch-point of the t-channel cut, or else a nearby pole in $k \cot \delta_0(k)$, corresponding to a nearby zero in the K matrix. In the case of the latter it is helpful to use an alternative parametrization, taken from infinite-volume studies of nucleon-deuteron scattering [137, 138],

$$k \cot \delta_0(k) = \frac{-\frac{1}{b_0} + \frac{1}{2} r k^2 + P r^3 k^4}{1 - \frac{k^2}{\kappa^2}} + O(k^6). \tag{7.36}$$

We expect that the inclusion of the pole will increase the range over which this form provides a good description of the phase shift.

In many cases we encounter bound states of the dimer-particle system, which occur whenever $k \cot \delta_0(k) = -|k|$. For these, it is important to keep in mind the following consistency

check that holds for physical bound states [139],

$$\frac{d}{dk^2}\left[k\cot\delta_0(k) - \left(-\sqrt{-k^2}\right)\right] < 0\,. \tag{7.37}$$

In words this says that $k\cot\delta_0(k)$ must cross the $-|k|$ line from below as k^2 becomes more negative, equivalently that the slope of $-|k|$ should exceed that of $k\cot\delta_0(k)$ at the crossing. This guarantees that the residue of the corresponding pole in the physical scattering amplitude, $\mathcal{M}_2$, has the proper sign, as dictated by inserting the bound state part of the identity, $\mathbb{I} = |E_B\rangle\langle E_B| + \cdots$, into its definition. One corollary is that, if there are two bound states, $k\cot\delta_0(k)$ must diverge between them [139]. We will see cases of this.

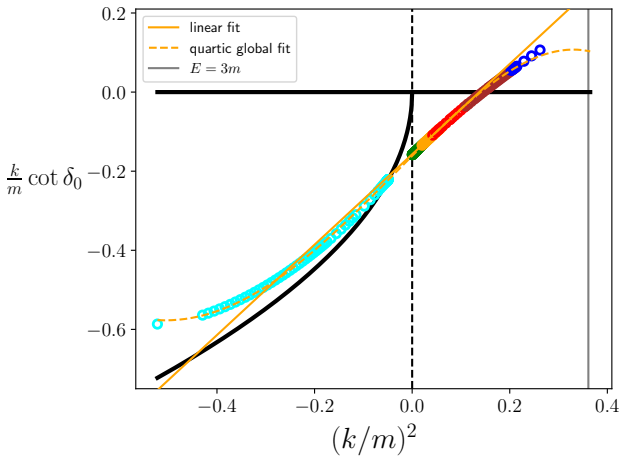

(a) $ma_0 = 2$

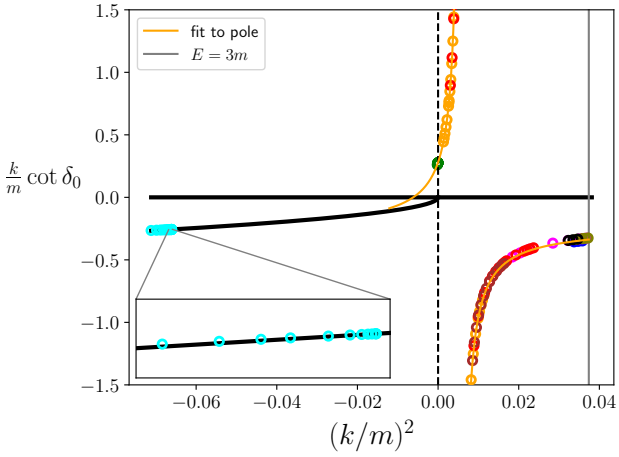

(b) $ma_0 = 6$

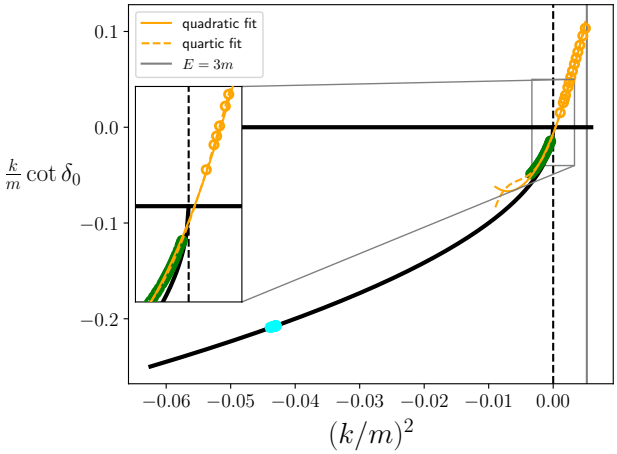

(c) $ma_0 = 16$

Figure 7.7: $k \cot \delta_0(k)$ for particle-dimer scattering as a function of the relative center-of-mass momentum k, as determined from the three-particle finite-volume spectrum in the $2+1$ regime using Eq. (7.33). We set $\mathcal{K}_{\text{df},3}^{\text{iso}} = 0$ throughout, and consider three different choices of ma_0. Different colors represent data points coming from different states in the spectrum, and there is considerable overlap of points for $k^2 > 0$. The solid vertical line near the right-hand edge of each plot shows the value of $(k/m)^2$ corresponding to the three-particle threshold, i.e. $E = 3m$. The curved solid line for negative k^2 shows $-|k| = -\sqrt{-k^2}$. A bound state is present whenever $k \cot \delta_0(k)$ passes through this line. The fits and other aspects of the plots are described in the text.

We begin with the case of $ma_0 = 2$, with a relativistic dimer lying well below the three particle threshold, as discussed in Sec. 7.4.1. The results for $k \cot \delta_0(k)$ obtained using Eq. (7.33), are shown in Fig. 7.7(a). The color coding matches that of the levels in Fig. 7.5: the cyan points lying at $k^2 < 0$ come from the trimer state, while the other points come from the levels lying above the $2+1$ threshold at $E/m = 1+\sqrt{3}$. We use volumes $mL = 4-50$ for the lowest state, and $mL = 20-70$ for the rest, so that all the states lie below $E = 3m$ and satisfy $L/a_0 \gg 1$. We observe several important features: *(i)* The results for $k \cot \delta_0(k)$ from different levels overlap, and are consistent.[13] *(ii)* The results from the trimer and the $2+1$ states can be well described by a quartic order ERE curve, shown in the figure by the dashed line. We also show a linear fit (i.e. including b_0 and r) to the orange points to give an idea of the rate of convergence of the ERE. *(iii)* The bound state that occurs where the ERE crosses $-|k|$ line is the trimer seen in Fig. F.3 above. The crossing occurs in the physical direction required by Eq. (7.37). *(iv)* The inclusion of higher order terms in the ERE is essential to describe our results. Thus, although the underlying two-particle interaction is described exactly by the leading order term in its ERE (by construction), the resulting dimer-particle ERE shows more structure. It is the result of solving the field-theoretic problem of particle scattering from a relativistic bound state. In particular, the value of the dimer-particle scattering length $mb_0 \approx 6$ is not close to that for the underlying particles, $ma_0 = 2$. *(v)* Finally, we note that, were we to truncate the ERE as shown by the solid line, then there would be a second bound-state crossing at $(k/m)^2 \approx -0.4$, but the direction of crossing the $-|k/m|$ curve would be unphysical. This is avoided by the results themselves and shows again the necessity of higher terms in the ERE.

We deduce from this first example that the energy levels for $E < 3m$ are well described by a dimer + particle effective theory, and that the trimer at this value of ma_0 should be

[13] We do not expect perfect consistency, since there are exponentially suppressed corrections to the quantization condition that are not included. Indeed, if we zoom in on the plots, we find that the overlap is not perfect.

understood as a dimer-particle bound state. A somewhat similar, nearly-physical situation is $\pi\sigma$ or $\pi\rho$ scattering for quark masses at which the σ or ρ is stable. The latter case has been as studied in Ref. [97]. The current quantization condition cannot, however, directly address either of these cases, due to the restriction to identical particles.

The second example we study is that with $ma_0 = 6$. The results for this case are shown in Fig. 7.7(b). The corresponding dimer lies much closer to threshold, $M_d = 1.97m$, as can be seen from the smaller range of $(k/m)^2$ available below the three-particle threshold. Nevertheless, by going to large volumes, with $mL = 60 - 170$, we are able to determine $k \cot \delta_0(k)$ from seven levels and fill out the curve for $k^2 > 0$. If we use smaller values of L, then the results begin to depart from the universal curve, due to large finite-volume effects on the dimer itself.[14]

The result for $k \cot \delta_0(k)$ is significantly changed from that with $ma_0 = 2$. For one thing, the dimer-particle scattering length has changed sign to $mb_0 \approx -3.6$, corresponding to a moderate attraction and no bound state (trimer) near threshold. For another, there is a pole that limits the range of applicability of the standard ERE to a tiny region around threshold. The presence of such a pole indicates only that the phase shift is passing through 0 mod π; it is similar to that seen in physical nucleon-deuteron scattering, as discussed in Sec. 7.4.3 below. We find that using the modified ERE of Eq. (7.36), we obtain an excellent description of the results around and above threshold. This is shown in the figure by the orange curve, which is a fit only to the orange points (the third energy-level in the spectrum), so as to emphasize the consistency with the results from the other levels. The exception to this consistency are the results from the trimer, shown again in cyan. Although difficult to see from the figure, these points do pass through the $-|k/m|$ line in the physical direction. In order to avoid an unphysical crossing, these points can be connected to the orange curve

[14] These can be partially removed by using the quantization condition with k determined using the volume-dependent dimer mass, $M_d(L)$, but we have not pursued this approach as we are able to work directly for values of L for which $M_d(L) - M_d$ is extremely small.

only if there is an intervening pole. Thus, while the trimer will appear as a pole in the dimer-particle scattering amplitude, the behavior of the phase shift is not given by a simple function, unlike in the previous case.

The last example studied in detail is that for $ma_0 = 16$, with results shown in Fig. 7.7(c). The dimer is now very shallow, $M_d = 1.996$, so the energy regime described by dimer + particle states is much reduced. Because of this, and the need to have $L \gg a_0$, we have results for only one level above threshold (which itself requires $mL > 80$). As we saw in Sec. 7.4.1, there are now two trimers, one shallow (the green points) and the other deeper (those in cyan). A quadratic fit to the orange points, shown by the solid line, correctly determines the bound state energy, with $mb_0 \approx 100$. But, as for $ma_0 = 6$, the ERE has a small radius of convergence and cannot describe all the results. Our interpretation is that the form of $k \cot \delta_0(k)$ is qualitatively similar to that for $ma_0 = 6$, but with the pole moved to the right so that b_0 changes sign.[15] Again the deeply bound trimer cannot be viewed as a simple dimer-particle bound state.

To conclude this subsection, we show in Fig. 7.8 the dependence of the particle-dimer scattering length, b_0, on the underlying two-particle scattering length, a_0. This allows us to understand the results for $ma_0 = 2$, 6, and 16 in a broader context. For $ma_0 < 1.4$ (the left-most two points in the plot) there is only a moderate attraction between particle and dimer (corresponding to $b_0 < 0$) and no trimer. As ma_0 increases, b_0 has a pole and changes sign. For $mb_0 \gg 1$, we expect there to be a shallow trimer that can be interpreted as a $2+1$ bound state, and the results for $ma_0 = 2$ show an example of this. As ma_0 increases further,

[15] Comparing Figs. 7.7(b) and 7.7(c) allows us to understand in more detail the issue of the missing level discussed at the end of the previous subsection. The quantization condition (7.33) is satisfied whenever $k \cot \delta_0(k)$ equals the (appropriately rescaled) Lüscher zeta function. Far below threshold, the right-hand side of the quantization condition asymptotes to the line $-|k|$, while it approaches $+\infty$ as $k^2 \to 0$. Thus, at fixed mL, as one lowers the $k \cot \delta_0(k)$ curve (moving, say, from the shape seen in Fig. 7.7(b) to that of Fig. 7.7(c)) the lowest solution to the quantization condition will vary continuously from a $2+1$ scattering state (with $b_0 < 0$) to a shallow bound state (with $b_0 > 0$). No additional finite-volume state appears as b_0 crosses zero.

mb_0 decreases, and the trimer becomes increasingly bound, as exemplified by the results at $ma_0 = 6$. Continuing further, there is another pole in mb_0, above which a second shallow bound state appears, as we have seen at $ma_0 = 16$.

For large ma_0, the dimer is nonrelativistic, and thus we expect that NREFT can be used to study the $2 + 1$ system analytically. We describe in Appendix E.2 how this can be done in the isotropic low-energy approximation, with only one free parameter corresponding to the three-particle contact interaction, or, equivalently, the cutoff Λ. The solid curve in Fig. 7.8 shows the result after tuning the cutoff so that the curve matches the results from the quantization condition at large ma_0. It describes our results well down to $ma_0 \approx 2$, where we expect relativistic effects to become important. This comparison provides another crosscheck of our formalism, while also showing where relativistic effects are important.

The properties of the trimers are well studied and understood in NREFT. In particular, as we approach unitarity ($ma_0 \to \infty$) a sequence of Efimov bound states will appear. Thus we known that the curve in Fig. 7.8 will have an infinite sequence of poles, separated asymptotically by a factor of ≈ 22 in ma_0 [104, 133]. Turning this around, we can interpret the appearance of the second trimer seen at $ma_0 = 16$ as the second state in the Efimov sequence. We note however that the separation of the first and second trimer in ma_0 is smaller than the NREFT prediction due to relativistic effects—with the ratio given by ≈ 9, rather than ≈ 22.

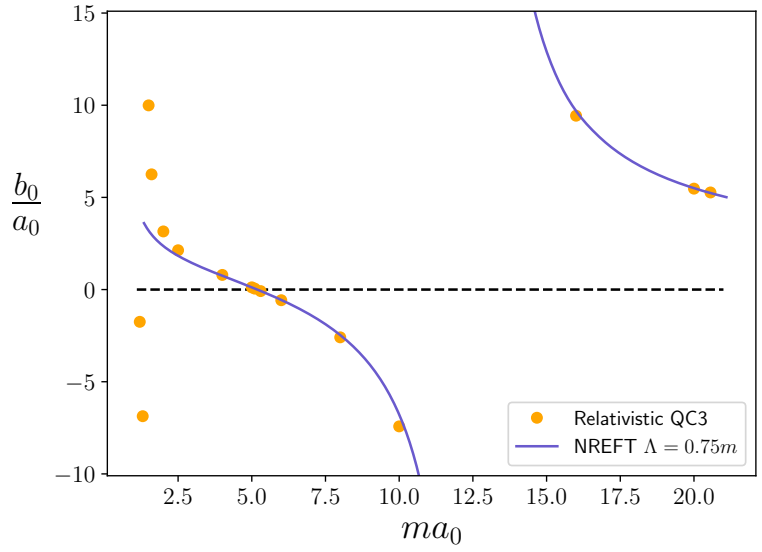

Figure 7.8: Ratio of particle-dimer scattering length, b_0, to the fundamental scattering length, a_0, as a function of ma_0. Orange points give the results obtained from the analysis described in this subsection applied to the output of the three-particle quantization condition (QC3). The solid (blue) line is the result from (infinite-volume) NREFT, discussed in more detail in Appendix E.2. The rapid variation of points on the left-side of the plot correspond to a narrow pole in the relation between b_0 and a_0 that only arises in the relativistic theory.

7.4.3 Tuning toward a physical system: a model of neutron-deuterium scattering

So far we have only considered the effects of two-particle interactions on the finite-volume spectrum. In this section we go beyond this restriction by studying how non-vanishing values of $\mathcal{K}_{\text{df},3}^{\text{iso}}$ affect the finite-volume spectrum in the isotropic approximation, and in particular how these impact the particle-dimer phase shift. To explore this, we consider a toy model that mimics three-nucleon interactions. Specifically, we assume isospin symmetry, so that proton-neutron and neutron-neutron interactions are identical, and ignore spin-dependent interactions. In this way, we arrive at a system for which the current form of the three-body

quantization condition is applicable. We then tune the parameters a_0 and $\mathcal{K}^{\text{iso}}_{\text{df},3}$ to match the physical system as closely as possible. Since this requires nonvanishing $\mathcal{K}^{\text{iso}}_{\text{df},3}$, we must use the modificed PV$'$ pole prescription with nonzero I^s_{PV}. Following the discussion of Sec. 7.3.1, we set $I^s_{\text{PV}} = -1$.

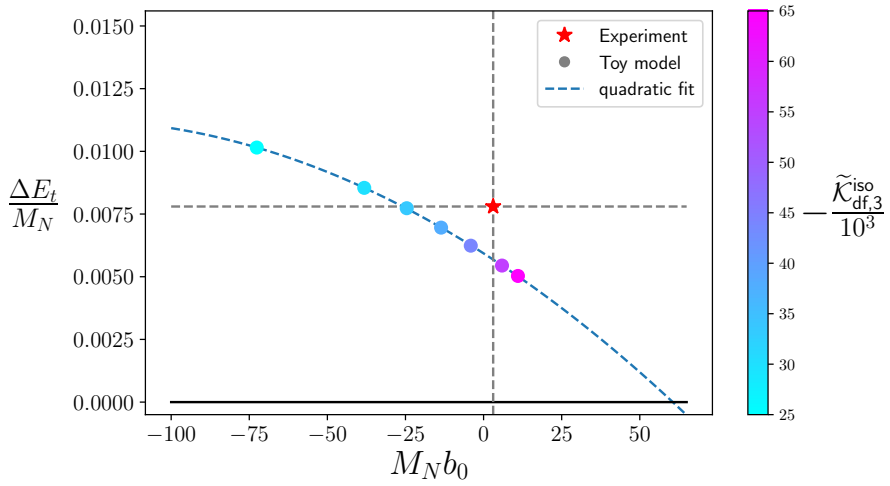

Figure 7.9: Correlation between the triton (trimer) binding energy and the particle-dimer (nucleon-deuteron) scattering length. This is usually referred to as the Phillips line. The value of $\widetilde{\mathcal{K}}^{\text{iso}}_{\text{df},3} = M_N^2 \mathcal{K}^{\text{iso}}_{\text{df},3}$ used for each point can be determined from the color gradient at right. For further discussion see the text.

We choose the value of the scattering length to reproduce the physical deuterium to nucleon mass ratio,

$$\frac{M_d}{M_N} \simeq 1.99763 \;\Rightarrow\; M_N a_0 = 20.56, \tag{7.38}$$

where we set $m = M_N$, with M_N the average of the proton and neutron masses. As we can see from Fig. 7.8, with $\mathcal{K}^{\text{iso}}_{\text{df},3} = 0$ this value of a_0 leads to two trimers. To obtain a single trimer with mass close to that of the triton, M_t, it turns out that we need large, negative values of $\mathcal{K}^{\text{iso}}_{\text{df},3}$. Figure 7.9 shows the resulting tritium binding energy, $\Delta E_t = 3M_N - M_t$, using a

continuous color gradient to identify the value of $\mathcal{K}^{\text{iso}}_{\text{df},3}$. For each choice of this parameter, we also determine the particle-dimer scattering length using the methods of the previous subsection. This allows us to plot ΔE_t vs. b_0 (in dimensionless units), as shown in the figure. These two quantities have been observed to be highly correlated in different potential models, following an approximate linear behavior known as the Phillips line [132].[16] We also include an experimental point, obtained with the physical values of M_t and the neutron-deuteron scattering in the doublet (spin 1/2) channel, the latter taken from Ref. [141]:

$$\frac{M_t}{M_N} \simeq 2.9922\,, \quad M_N b_0 \simeq 3.1. \tag{7.39}$$

We observe that, even though our toy model cannot reproduce both experimental values simultaneously, the nearly linear dependence is qualitatively similar to the Phillips line shown in Ref. [140]. It suggests that a sizeable three-particle interaction term is needed to understand the triton.

We now study the phase shift of our toy nucleon-deuteron system in more detail. We choose to fix the tritium mass to its physical value, which will not reproduce the experimental scattering length, as already discussed. With $M_N^2 \mathcal{K}^{\text{iso}}_{\text{df},3} = -33500$ we find $M_t = 2.99227 M_N$ which is close enough for the purposes of this work. In Fig. 7.10 we show the resulting nucleon-deuteron phase shift, obtained using the method of the previous subsection. It is instructive to compare this plot to those shown in Fig. 7.7, which are obtained with $\mathcal{K}^{\text{iso}}_{\text{df},3} = 0$. Qualitatively, the present results are most similar to those at $ma_0 = 6$, Fig. 7.7(b), despite the present value of $ma_0 = 20.56$ lying closer to $ma_0 = 16$. This can be understood as follows: as one increases a_0 while keeping $\mathcal{K}^{\text{iso}}_{\text{df},3} = 0$, the pole moves to higher energies and a second bound state emerges. Turning on a negative (and thus repulsive) $\mathcal{K}^{\text{iso}}_{\text{df},3}$, the pole is moved to lower values of k^2 and the shallow bound state smoothly turns into a scattering

[16] See Fig. 13 of Ref. [140] and surrounding discussion. The fact that potential models lead to results in the Phillips plot that lie in an almost one-dimensional subspace was subsequently understood as being due to the fact that only one three-particle parameter is necessary at leading order in NREFT [133]. The same explanation holds within our toy model, with its single three-particle parameter.

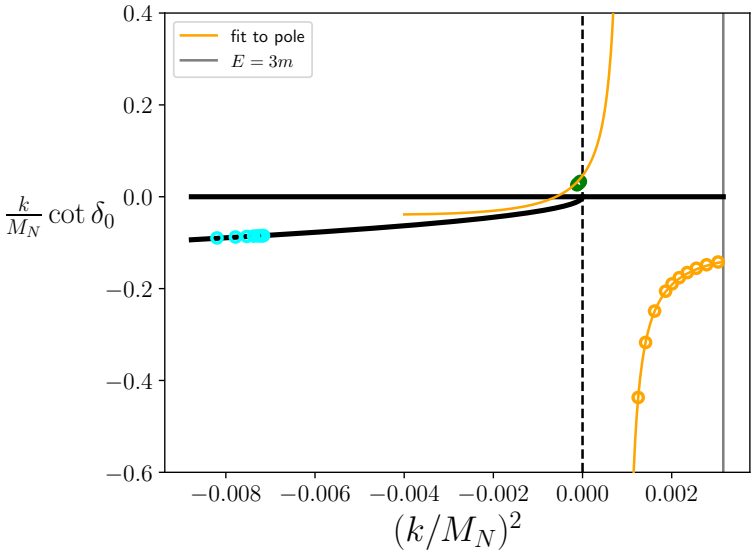

Figure 7.10: s-wave phase shift as a function of the center-of-mass frame momentum for the simplified toy model describing nucleon-deuteron scattering. Parameters are $M_N a_0 = 20.56$ and $M_N^2 \mathcal{K}_{\mathrm{df},3}^{\mathrm{iso}} = -33500$. Notation as in Fig. 7.7. The fit is discussed in the text.

state. We thus see that the differences from the $ma_0 = 16$ results of Fig. 7.7(c) are mainly due to the three-particle interaction.

Fitting the orange points in Fig. 7.10 to the modified ERE of Eq. (7.36), we find that it provides an excellent description, including the green points from the level close to threshold. It is interesting to compare this to experimental results for $N-D$ scattering. There is indeed evidence of a pole $k \cot \delta_0(k)$ close to threshold in both $n-D$ and $p-D$ scattering, although in the former it lies below threshold, while in the latter its position is not settled [137, 138, 142]. In fact, in our model the position of the pole can be inferred from Fig. 7.9: the point for which $mb_0 = 0$ is when the pole in $k \cot \delta_0(k)$ is at threshold. We speculate that we could further tune our model by adding an energy dependence to $\mathcal{K}_{\mathrm{df},3}^{\mathrm{iso}}$ in such a way that the pole shifts to lower energies, while keeping M_t constant. However, this is beyond the scope of our already simplified example.

In summary, a simplified model with two parameters is able to reproduce qualitative features of the nucleon-deuterium phase shift, such as the presence of only one bound state and a pole in $k \cot \delta_0(k)$. Furthermore, it suggests that a repulsive three-body force is necessary to explain the dynamics of the system. It is thus a good example of how one could use the quantization condition to solve the infinite-volume dynamics of a realistic three-particle system. Of course, in the present instance the dynamics is nonrelativistic, and NREFT calculations are much more advanced and realistic than our toy model. The advantage of our approach, however, is that it works also in the relativistic domain.

We conclude this section with a comment. Current lattice simulations with physical quark masses have volumes satisfying $M_N L \lesssim 30$. For such volumes the finite-L effects on the deuteron are significant and thus, to study nucleon-deuteron scattering using such lattices, one cannot employ the effective two-body description used above. Instead, one will require the full form of the three-body quantization condition to analyze lattice results even in the region $E < 3M_N$.

7.4.4 Three-particle spectrum with resonances

The previous subsections focused on cases in which the two-particle channel had bound states. However, as explained in Section 7.3.3, the modified PV$'$ prescription also allows the study of systems in which two-particle subchannels are resonant. In this subsection we give an example of the three-particle spectrum in such a situation.

Specifically, we use the parametrization of $\mathcal{K}_2$ given in Eq. (7.10), with $g = 1$ and $m_R = 2.7m$, and, for simplicity of implementation, set $\mathcal{K}_{\mathrm{df},3} = 0$. The resulting spectrum is shown in Fig. 7.11. The first thing to notice is that there are additional states compared to those expected for three almost free particles. These extra states can be interpreted as resonance + particle states. As in previous examples, there are avoided level crossings that occur when two states interchange their interpretation—a clear case occurring for the second and third

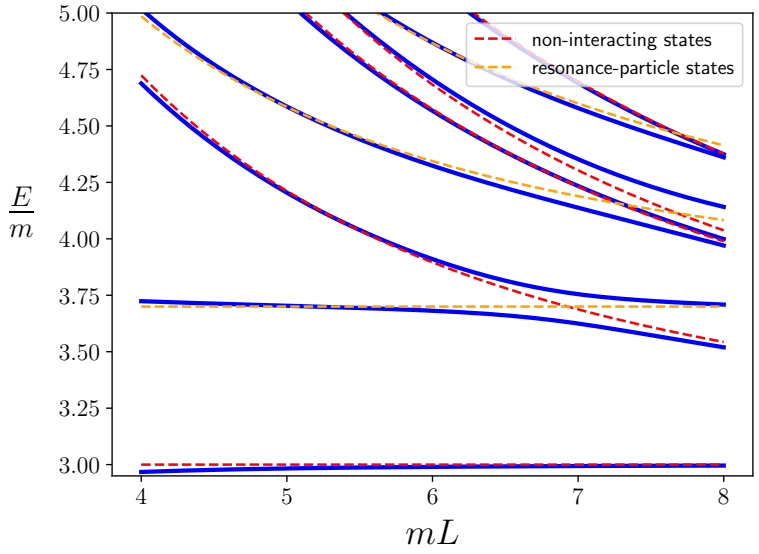

Figure 7.11: Three-particle spectrum (solid blue lines) in the isotropic approximation in the presence of a two-particle resonance with $g = 1$, $m_R = 2.7m$ and $\mathcal{K}_{\mathrm{df},3} = 0$. Noninteracting three-particle states (red dashed lines) and noninteracting particle + resonance states (orange dashed lines) are shown for comparison.

levels around $mL = 7$. Thus we find that, for a narrow resonance, a simple interpretation of the low-lying levels is possible. As in the two-particle case, however, for a broad resonance we expect that a simple interpretation of levels will not be possible, and the only way to interpret the spectrum is simply to use the full quantization condition and fit the parameters contained in $\mathcal{K}_2$ and $\mathcal{K}_{\mathrm{df},3}$.

7.4.5 Including d-wave dimers

In our final numerical example we move beyond the isotropic approximation and include both s- and d-wave two-particle channels. This setup has been studied previously in Ref. [76], but only for parameters such that there are no dimers and no subchannel resonances. Our aim is to investigate the spectrum in a situation that is more akin to those that arise in nature,

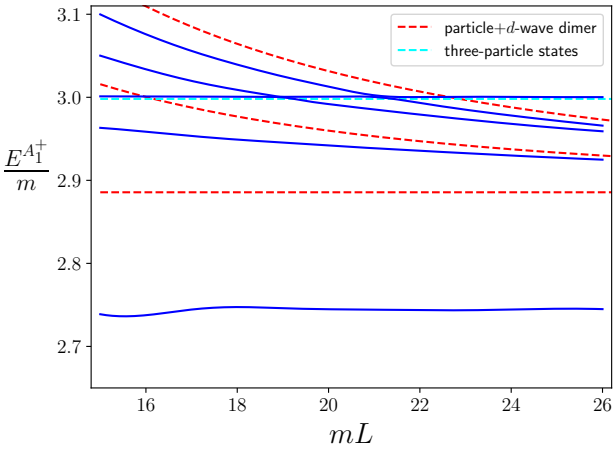

(a) $ma_0 = 0.1$, $ma_2 = 3.0$ and $\mathcal{K}_{\text{df},3} = 0$.

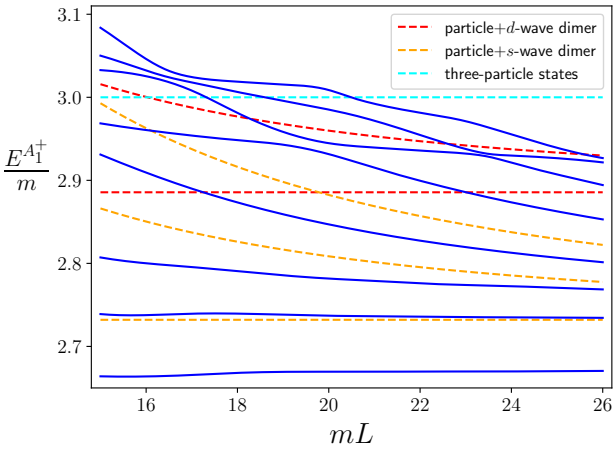

(b) $ma_0 = 2.0$, $ma_2 = 3.0$ and $\mathcal{K}_{\text{df},3} = 0$.

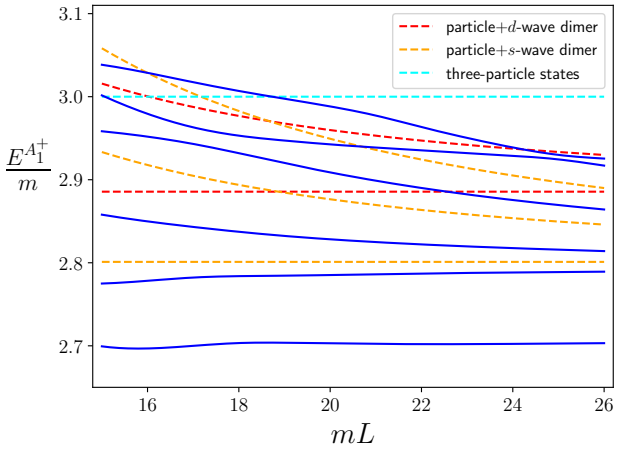

(c) $ma_0 = 2.3$, $ma_2 = 3.0$ and $\mathcal{K}_{\text{df},3} = 0$.

Figure 7.12: Finite-volume spectra (solid blue lines) of the three-particle systems in the A_1^+ irrep with both s- and d-wave two-particle interactions. Noninteracting three-particle levels, as well as those involving particle + dimer, are also shown. (In the upper right panel, the cyan dashed line at $E = 3m$ has been shifted slightly downward to make it visible.) See text for further discussion.

i.e. with multiple two-particle channels in which there are bound states. As explained in Sec. 7.3.2, the PV′ prescription allows us to study such systems using the quantization condition of Ref. [28], by introducing a different $I_{\text{PV}}^{(\ell)}$ for each partial wave. Including $I_{\text{PV}}^{(\ell)}$ in

the implementation of Ref. [76] is straightforward. In fact, we will consider here only the choice $\mathcal{K}_{\mathrm{df},3} = 0$, for which we can use the original implementation without change.

We consider only the simplest nontrivial extension of the examples in previous sections, in which both s- and d-wave scattering are described by the lowest terms in their respective threshold expansions, Eqs. (7.9) and (7.14). Since we also set $\mathcal{K}_{\mathrm{df},3} = 0$, there are only two parameters: the scattering lengths a_0 and a_2. We focus on values of the latter such that $ma_2 > 1$, implying that there is an infinite-volume tensor bound state at

$$M_d^{\ell=2} = 2m\sqrt{1 - 1/(ma_2)^2}\,. \tag{7.40}$$

For the sake of brevity, we consider only three-particle states lying in the $\mathbb{A}_1^+$ irrep, although we stress that our implementation allows one to study all available irreps, as shown in Ref. [76]. It is important to keep in mind in the following that, due to the possibility of switching the spectator particle, the contributions of s- and d-wave subchannels are coupled, even in infinite volume.[17]

The first case we analyze is $ma_0 = 0.1$ and $ma_2 = 3.0$, leading to the spectrum shown in Fig. 7.12(a). For these parameters there is a d-wave dimer with $M_d^{\ell=2} \approx 1.886m$ but no s-wave dimer. Although such a situation may be unphysical (since in NRQM a potential with a d-wave bound state would also have at least one s-wave bound state), it is a simple starting point for studying the finite-volume spectrum. The spectrum shows a deeply bound trimer, similar to that observed in Ref. [76] for $ma_2 \approx -2$. In addition, there are several states that can be interpreted as particle + d-wave dimer scattering states, and which behave similarly to those in the pure s-wave case discussed earlier. We see also several strikingly-narrow avoided level crossings for $E \approx 3m$ (whose nature as avoided crossings can only be seen on a magnified version of the plot). This narrowness is due to the very weak s-wave scattering

[17] For example, if the total angular momentum is $J = 0$ (which is the dominant contribution in the $\mathbb{A}_1^+$ irrep in the case of $\mathbf{P} = 0$), this can be produced both by an s-wave dimer with orbital angular-momentum $\bar{\ell} = 0$ relative to the spectator, or by a d-wave dimer with $\bar{\ell} = 2$.

length, so that, away from the crossings, the level at $E \approx 3m$ is nearly a noninteracting state of three particles at rest. We observe that the trimer energy has small oscillations, which are similar to those seen in Ref. [76], and are likely indicative of unphysical effects arising from the truncation of the quantization condition or the enhancement of exponentially-suppressed effects. These deserve further investigation, but this is beyond the scope of this paper.

A more physical situation is when there are both s- and d-wave dimers, with the former being more deeply bound. With this in mind, we explore the effect of increasing ma_0 while holding ma_2 fixed, plotting the spectrum for $ma_0 = 2$ and $ma_2 = 3$ in Fig. 7.12(b), and for $ma_0 = 2.3$ and $ma_2 = 3$ in Fig. 7.12(c). We take these two different choices of a_0 in order to help clarify the interpretation of the spectrum. In Fig. 7.12(c) we clearly see two trimers. We interpret the lower one as s-wave dominated (and thus similar to the trimers seen in earlier subsections) since it becomes more deeply bound for $ma_0 = 2$. As for the upper trimer in Fig. 7.12(c), we conjecture that it is primarily caused by the d-wave attraction. This is based on the observation that it smoothly transforms into the d-wave trimer of Fig. 7.12(a) as ma_0 is decreased.

To make these characterizations rigorous it would be instructive to study the pole positions of these two trimers in the scattering amplitudes of the (scalar dimer + particle) $\leftrightarrow$ (tensor dimer + particle) coupled-channel system. In particular the set of two channels leads to the appearance of four Riemann sheets, conveniently labeled by the sign of the imaginary part of momentum carried by each element of the back-to-back particle-dimer pair. For example the second sheet is defined by $\mathrm{Im}k_{M_0+m} < 0$ and $\mathrm{Im}k_{M_2+m} > 0$ and poles on the lower half of this sheet are close to physical scattering energies and are often interpreted as bound states (or molecules) built from the constituents of the heavy channel—in this case a $M_d^{\ell=2}+m$ molecule. The interpretation follows from noting that, if the lighter channel were turned off, the pole would move to the real axis of the physical sheet and thus become a physical bound state pole. This behavior was observed for the f_0-like state in the scalar-

isoscalar LQCD calculation presented in Ref. [143]. Performing a coupled channel analysis here to extract the upper trimer pole position goes beyond the scope of this work, but would be an interesting future application of these results.

The higher levels in Fig. 7.12 appear to be predominantly particle + s-wave dimer states, but there are some clear avoided crossings which we interpret as levels changing their nature to particle + d-wave dimer states. The situation becomes even more complicated for $E > 3m$, where three-particle components become relevant.

We conclude by noting that, while the examples considered here are not directly relevant to hadronic physics, they may be of relevance to the physics of cold atoms.

7.5 Conclusions

In this work we have presented an extension of the formalism of Ref. [28] that allows the study of three-body systems in the presence of two-body resonances or bound states. This removes a major shortcoming of the original formalism, which had previously only been resolved by a more complicated approach requiring the introduction of a fictitious two-body channel for each resonance [35]. In addition, our extension may provide an alternative for the $2 \to 3$ scattering formalism derived in Ref. [34]. We provide here only an intuitive explanation of the new extension; a derivation will be presented in Ref. [131], along with a discussion of the relation to the work of Refs. [34, 35]. We stress that, with this extension, the formalism for s-wave dimers with general two-particle interactions is now of similar complexity to implement as that obtained from the other approaches (NREFT and FVU), while being the only one worked out explicitly for higher partial waves.

The extended formalism can be implemented numerically with only minor changes to the methods developed for the original formalism in Refs. [39, 76]. This has allowed us to present several examples of the influence of two-particle bound states and resonances on the finite-volume three-particle spectrum, including a case in which both s- and d-wave interactions

are included.

We have also presented several examples where the three-particle quantization condition can be used to study infinite-volume physics, despite being originally formulated with finite-volume applications in mind. The simplest example is the determination of the presence and binding energies of trimers. We reproduce the expected Efimov-like trimers as the unitary limit of two-particle scattering is approached, and can extend the results into the relativistic domain. We also find a complex pattern of trimers induced by a combination of s- and d-wave two-particle attraction. What is most novel here, however, is that the quantization condition can be used to determine the dimer-particle scattering amplitude for essentially all energies below the breakup threshold, reproducing expectations in the nonrelativistic regime and obtaining new results for relativistically-bound dimers. As an application, we study a toy model of the nucleon-deuteron-triton system, without spin or isospin, which we find requires the use of a nonvanishing value for the three-particle quasilocal interaction $\mathcal{K}_{\text{df},3}$.

With the extension presented here, we now have a relativistic formalism that is straightforward to implement and can be used for any system of identical scalar particles, with any (finite) number of two-particle partial waves. In QCD, however, the only such system is three pions with $I = 3$, for which all subchannels, having $I = 2$, are neither resonant nor have bound states. The next step in the development of a generally applicable formalism is to include nonidentical but degenerate scalars, which would allow the application to a general three-pion system in the isosymmetric limit, and thus to the ω, a_1, a_2 and other mesonic resonances. This generalization is now one of our main priorities going forward.

One topic not directly addressed here is the use of the integral equations connecting $\mathcal{K}_{\text{df},3}$ to $\mathcal{M}_3$. We note, however, that the methods introduced in Ref. [39] to solve these equations below or at threshold for the case without subchannel resonances or dimers should apply as well in the presence of such resonances and dimers. They would allow us, for example, to study the wavefunction of the triton in our toy model. We save such calculations until we

can address a more physical example, rather than toy models.

Finally, an important issue that we have not addressed here is the presence of unphysical solutions to the quantization condition for certain choices of parameters, as observed in Refs. [39, 76]. We are presently investigating whether these are removed by increasing the cutoff used to truncate the sum over the spectator momentum. Resolving this is another major priority in order to provide a fully general tool for studying all possible three-particle systems.

Chapter 8

$I = 3$ PION SCATTERING AMPLITUDE FROM LQCD[1]

8.1 Introduction

Lattice QCD (LQCD) provides a powerful (if indirect) tool for *ab initio* calculations of strong-interaction scattering amplitudes. The formalism for determining two-particle amplitudes is well understood [24, 25, 27, 56, 57, 60–63, 101, 126, 127], and there has been enormous progress in its implementation in recent years [58, 96, 97, 112–125, 144–146] (see Ref. [26] for a review). The present frontier is the determination of three-particle scattering amplitudes and related decay amplitudes. LQCD calculations promise access to three-particle scattering processes that are difficult or impossible to access experimentally. Examples of important applications are understanding properties of resonances with significant three-particle branching ratios (including the Roper resonance [147], and many of the X, Y and Z resonances [148]), determining the three-nucleon interaction (important for large nuclei and neutron star properties), predicting weak decays to three particles (e.g. $K \to 3\pi$), and calculating the 3π contribution to the hadronic-vacuum polarization that enters into the prediction of muonic $g-2$ [149].

Three-particle amplitudes are determined using LQCD by calculating the energies of two- and three-particle states in a finite volume [64, 150]. The challenges to carrying this out are twofold. On the one hand, the calculation of spectral levels becomes more challenging as the number of particles increases. On the other, one must develop a theoretical formalism relating the spectrum to scattering amplitudes. Significant progress has recently

[1]This chapter and Appendix F are taken directly from Ref. [51].

been achieved in both directions, with energies well above the three-particle threshold being successfully measured, and a formalism for three identical (pseudo)scalar particles available. The formalism has been developed and implemented following three approaches: generic relativistic effective field theory (RFT) [28, 29, 34–36, 39, 76], nonrelativistic effective field theory (NREFT) [30, 31, 40, 77], and (relativistic) finite volume unitarity (FVU) [32, 41] (see also Refs. [71, 72] and Ref. [74] for a review). To date, only the RFT formalism has been explicitly worked out including higher partial waves. The application to LQCD results has so far been restricted to the energy of the three-particle ground state, either using the threshold expansion [47, 55, 66], or, more recently, the FVU approach for $3\pi^+$ [41].

Recently, precise results were presented for the spectrum of $2\pi^+$ and $3\pi^+$ states in $O(a)$-improved isosymmetric QCD with pions having close to physical mass, $M \approx 200$ MeV [1]. These were obtained in a cubic box of length L with $ML \approx 4.2$, for several values of the total momentum $\mathbf{P} = (2\pi/L)\mathbf{d}$ with $\mathbf{d} \in \mathbb{Z}^3$, and for several irreducible representations (irreps) of the corresponding symmetry groups. Isospin symmetry ensures that G parity is exactly conserved and thus that the $2\pi^+$ and $3\pi^+$ sectors are decoupled. In total, sixteen $2\pi^+$ levels and eleven $3\pi^+$ levels were obtained below the respective inelastic thresholds at $E_2^* = 4M$ and $E^* = 5M$, Here E_2^* and $E^* = \sqrt{E^2 - \mathbf{P}^2}$ are the corresponding center-of-mass energies, with E the total three-particle energy.

The purpose of this Letter is to perform a global analysis of the spectra of Ref. [1] using the RFT formalism and determine the underlying $3\pi^+$ interaction. This breaks new ground for an analysis of the three-particle spectrum in several ways: we use multiple excited states, in both trivial and nontrivial irreps, including results from moving frames. This analysis therefore serves as a testing ground for the utility of the three-particle formalism in an almost physical example. An additional appealing feature is that the size of the $3\pi^+$ interaction can be calculated using chiral perturbation theory (χPT). We present the leading order (LO) prediction here.

After this paper was made public, an independent study of the results of Ref. [1], using the FVU approach, appeared [52].

8.2 Formalism and Implementation

All approaches to determining three-particle scattering amplitudes using LQCD proceed in two steps, which we outline here. In the first step, one uses a quantization condition (QC), which predicts the finite-volume spectrum in terms of an intermediate infinite-volume three-particle scattering quantity. In the RFT approach, the QC for identical, spinless particles with a G-parity-like Z_2 symmetry takes the form (up to corrections of $\mathcal{O}(1\%)$ that are exponentially-suppressed in ML) [28]

$$\det\left[F_3(E,\mathbf{P},L)^{-1}+\mathcal{K}_{\mathrm{df},3}(E^*)\right]=0\,. \tag{8.1}$$

Here F_3 and $\mathcal{K}_{\mathrm{df},3}$ are matrices in a space describing three on-shell particles in finite volume. They have indices of angular momentum of the interacting pair, ℓ, m, and finite-volume momentum of the spectator particle, k. F_3 depends on the two-particle scattering amplitude and on known geometric functions, while $\mathcal{K}_{\mathrm{df},3}$ is the three-particle scattering quantity referred to above. It is quasilocal, real, and free of singularities related to three-particle thresholds, thus playing a similar role to the two-particle K matrix $\mathcal{K}_2$ in two-particle scattering. It is, however, unphysical, as it depends on an ultraviolet (UV) cutoff. Given prior knowledge of $\mathcal{K}_2$, and a parametrization of $\mathcal{K}_{\mathrm{df},3}$, the energies of finite-volume states are determined by the vanishing of the determinant in Eq. (8.1). The parameters in $\mathcal{K}_{\mathrm{df},3}$ are then adjusted to fit to the numerically-determined spectrum. Examples on how to numerically solve Eq. (8.1) have been presented in Refs. [36, 39, 76].

The second step requires solving infinite-volume integral equations in order to relate $\mathcal{K}_{\mathrm{df},3}$ to the three-particle scattering amplitude $\mathcal{M}_3$. In fact, as explained below, it is a divergence-free version of the latter, denoted $\mathcal{M}_{\mathrm{df},3}$, that is most useful. The equations relating $\mathcal{K}_{\mathrm{df},3}$ to

$\mathcal{M}_{\text{df},3}$ were derived in Ref. [29], and solved in Ref. [39].

The parametrizations we use for $\mathcal{K}_2$ and $\mathcal{K}_{\text{df},3}$ are based on an expansion about two- and three-particle thresholds. For $\mathcal{K}_2$ this leads to the standard effective range expansion (ERE), recalled below. At linear order in this expansion only s-wave interactions are nonvanishing, with d-wave interactions first entering at quadratic order (p-wave interactions are forbidden by Bose symmetry). For $\mathcal{K}_{\text{df},3}$, the expansion is in powers of $\Delta = (E^{*2} - 9M^2)/(9M^2)$, and was developed in Refs. [39, 76] based on the Lorentz and particle-interchange invariance of $\mathcal{K}_{\text{df},3}$. Through linear order in Δ, $\mathcal{K}_{\text{df},3}$ is given by

$$\mathcal{K}_{\text{df},3} = \mathcal{K}_{\text{df},3}^{\text{iso}} = \mathcal{K}_{\text{df},3}^{\text{iso},0} + \mathcal{K}_{\text{df},3}^{\text{iso},1}\Delta\,, \tag{8.2}$$

where $\mathcal{K}_{\text{df},3}^{\text{iso},0}$ and $\mathcal{K}_{\text{df},3}^{\text{iso},1}$ are constants. There is no dependence on the momenta of the three particles at this order; this corresponds to a contact interaction, and leads to the designation "isotropic". Momentum dependence first enters at $\mathcal{O}(\Delta^2)$.

In our main analysis we keep only the s-wave two-particle interaction and the isotropic terms in Eq. (8.2). With these approximations, the QC of Eq. (8.1) reduces to a finite matrix equation that can be solved by straightforward numerical methods. Previous implementations have considered only the three-particle rest frame, $\mathbf{P} = 0$ [36, 39, 76] (see also Ref. [40, 41]). Here we have extended the implementation to moving frames, so that we can use all the results obtained by Ref. [1]. The details of the implementation, including projections onto irreps of the appropriate little groups, are described in Appendix F.1.

8.3 χPT prediction for $\mathcal{K}_{\mathrm{df},3}$ and $\mathcal{M}_{\mathrm{df},3}$

$\mathcal{M}_{\mathrm{df},3}$ and $\mathcal{K}_{\mathrm{df},3}$ have not previously been calculated in χPT , so here we present the leading order (LO) result. The LO Lagrangian in the isosymmetric two-flavor theory is [18, 151]

$$\begin{aligned} \mathcal{L}_\chi &= \frac{F^2}{4}\mathrm{tr}\,\left(\partial_\mu U \partial^\mu U^\dagger\right) + \frac{M^2F^2}{4}\mathrm{tr}\,\left(U+U^\dagger\right)\,, \\ &\text{with } U = e^{i\phi/F}\,, \quad \phi = \begin{pmatrix} \pi^0 & \sqrt{2}\pi^+ \\ \sqrt{2}\pi^- & -\pi^0 \end{pmatrix}\,. \end{aligned} \tag{8.3}$$

Here F is the decay constant in the chiral limit, normalized such that $F_\pi = 92.4$ MeV. We note that at this order, $F = F_\pi$. Expanding in powers of the pion fields, $\mathcal{L} = \mathcal{L}_{2\pi}+\mathcal{L}_{4\pi}+\mathcal{L}_{6\pi}+\cdots$, we need only the 4π and 6π vertices.

From $\mathcal{L}_{4\pi}$ we obtain the standard LO result for the $2\pi^+$ scattering amplitude [152],

$$\mathcal{M}_2 = \frac{2M^2 - E_2^{*2}}{F^2}\,, \tag{8.4}$$

which displays the well-known Adler zero below threshold at $E_2^{*2} = 2M^2$ [153]. Given the ERE parametrization of the s-wave phase shift,

$$q\cot\delta_0(q) = -\frac{1}{a_0} + \frac{rq^2}{2} + Pr^3q^4 + \cdots\,, \tag{8.5}$$

where $q^2 = E_2^{*2}/4 - M^2$, one can infer from Eq. (8.4) the LO results for the scattering length and effective range:

$$Ma_0 = \frac{M^2}{16\pi F^2} \quad \text{and} \quad M^2 r a_0 = 3\,. \tag{8.6}$$

The $3\pi^+$ amplitude $\mathcal{M}_3$ is given at LO by the diagrams of Fig. 8.1. As is well known, $\mathcal{M}_3$ diverges for certain external momenta, as the propagator in Fig. 8.1(a) can go on shell.

This motivated the introduction of a divergence-free amplitude in Ref. [28]:

$$\mathcal{M}_{\mathrm{df},3} \equiv \mathcal{M}_3 - \mathcal{D}\,, \tag{8.7}$$

$$\mathcal{D} = \mathcal{S}\Big\{ -\mathcal{M}_2(s_{12})\frac{1}{b^2 - M^2}\mathcal{M}_2(s'_{12})\Big\} + O\left(\mathcal{M}_2^3\right)\,, \tag{8.8}$$

where $s_{12} = (p_1 + p_2)^2$, $s'_{12} = (k_1 + k_2)^2$, $b = p_1 + p_2 - k_3$, and $\mathcal{S}$ indicates symmetrization over momentum assignments. $\mathcal{D}$ is defined to have the same divergences as $\mathcal{M}_3$, so that their difference is finite. At LO in χPT , only the LO term in $\mathcal{D}$ contributes and we find

$$M^2\mathcal{M}_{\mathrm{df},3} = \frac{M^4}{F^4}(18 + 27\Delta) = (16\pi M a_0)^2(18 + 27\Delta)\,, \tag{8.9}$$

a result that is real and isotropic. As a side result, we have also calculated the related threshold amplitude that enters into the $1/L$ expansion of the three-particle energy [68], finding $\mathcal{M}_{3,\mathrm{th}} = 27M^2/F^4$.

The last step is to relate $\mathcal{M}_{\mathrm{df},3}$ to $\mathcal{K}_{\mathrm{df},3}$. As discussed in Appendix F.2, we find these quantities to be equal at LO

$$\mathcal{K}_{\mathrm{df},3} = \mathcal{M}_{\mathrm{df},3}\left[1 + \mathcal{O}(M^2/F^2)\right]\,, \tag{8.10}$$

so that $\mathcal{K}_{\mathrm{df},3}$ is also given by Eq. (8.9). This implies that $\mathcal{K}_{\mathrm{df},3}$ is scheme-independent at LO in χPT . In Appendix F.2 we also quantify the expected size of the corrections, finding them to range between $10 - 50\%$, with the larger error applying to the term linear in Δ.

8.4 Fitting the two-particle spectrum

Determining the two-particle phase shift is an essential step, as it enters into the three-particle QC. In particular, we need a parametrization valid below threshold, as the two-particle momentum in the three-particle QC takes values in the range $q^2/M^2 \in [-1, 3]$. We extract information on the s-wave phase shift using a form of the two-particle QC that holds in all frames for those irreps that couple to $J = 0$. Details are given in Appendix F.3. We use the bootstrap samples provided in Ref. [1] to determine statistical errors, so that correlations

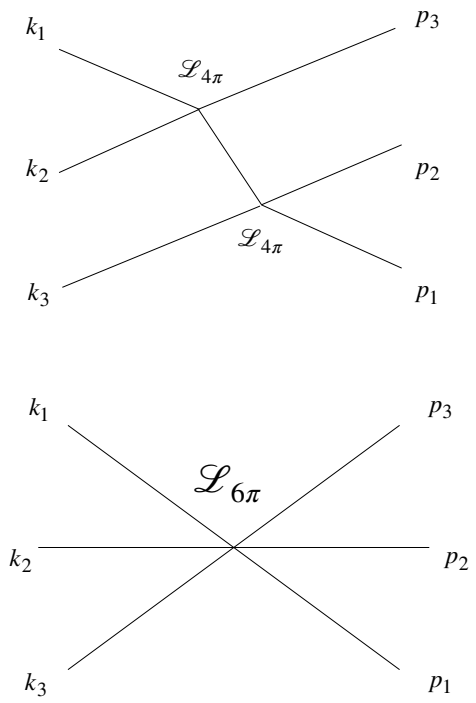

Figure 8.1: LO contributions to the three-particle scattering amplitude $\mathcal{M}_3$. Momentum assignments must be symmetrized.

are accounted for properly.

We use a parametrization of the phase shift (adapted from that of Ref. [107]; see also Ref. [154]) that includes the Adler zero predicted by χPT , as well as the kinematical factor E_2^*:

$$\frac{q}{M}\cot\delta_0(q) = \frac{E_2^* M}{E_2^{*2} - 2z_2^2}\left(B_0 + B_1\frac{q^2}{M^2} + B_2\frac{q^4}{M^4} + \cdots\right). \tag{8.11}$$

We either set $z_2^2 = M^2$, the LO value, or leave it as a free parameter. B_0 and B_1 are related in a simple way to a_0 and r [see Eqs. (F.37) and (F.38) in Appendix F.3]. Previous lattice studies have used the ERE, Eq. (8.5) (see, e.g. Refs. [95, 108, 109]), but this has the disadvantage, due to the Adler zero, of having a radius of convergence of $|q^2| = |M^2 - z_2^2/2| \approx$

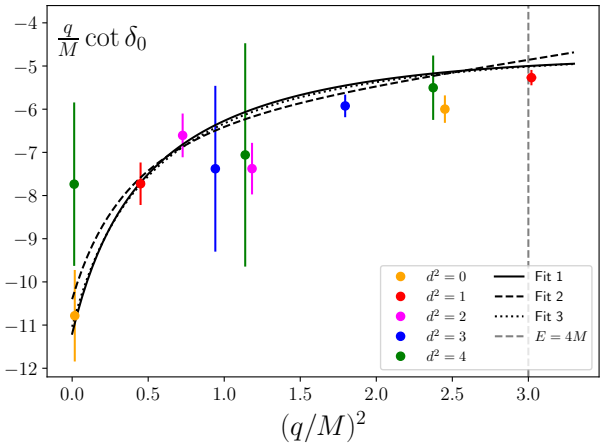

Figure 8.2: Values of $q\cot\delta_0$ obtained from the two-particle spectrum of Ref. [1] using the two-particle QC, together with various fits.

Fit	B_0	B_1	B_2	z_2^2/M^2	χ^2/dof	Ma_0	M^2ra_0
1	-11.2(7)	-2.1(3)	—	1 (fixed)	12.13/(11-2)	0.089(6)	2.63(8)
2	-10.4(9)	-3.7(1.0)	0.5(3)	1 (fixed)	9.75/(11-3)	0.096(8)	2.3(3)
3	-11.7(1.8)	-2.0(4)	—	0.94(22)	12.06/(11-3)	0.091(9)	2.4(9)

Table 8.1: Fits of the two-particle spectrum to the Adler-zero form of $q\cot\delta_0$, Eq. (8.11).

$M^2/2$. In particular, the ERE gives results for $-1 < q^2/M^2 < 0$ that are substantially different from the Adler-zero form. This is related to the fact that in (8.11), B_1 and B_2 are both of next-to-leading order (NLO) in χPT , in contrast to the ERE form where r and P are both nonzero at LO, as can be seen from the explicit χPT expressions given in Ref. [108]. The formal radius of convergence of our expression (8.11) is $|q^2| = M^2$, due to the left-hand cut, but following common practice we ignore this and use it up to $q^2/M^2 = 3$. In Appendix F.3 we show that fitting with the restriction $|q^2|/M^2 < 1$ has only a small impact on the resulting parameters We also have checked that fits using the ERE form provide a worse description of the data.

The results of several fits are listed in Table 8.1 and shown in Fig. 8.2. All fits give

reasonable values of χ^2/d.o.f., and yield values for $M^2 r a_0$ close to the predicted LO value of 3. Using the value of F obtained from the same lattice configurations in Ref. [155, 156], the LO chiral prediction from Eq. (8.6) is $Ma_0 = 0.0938(12)$, and this is also in good agreement with the results of the fits. Overall, we conclude that the spectrum from Ref. [1] confirms the expectations from χPT . We choose the minimal fit 1 as our standard choice since B_2 is poorly determined (fit 2) and the Adler-zero position is consistent with the LO result if allowed to float (fit 3). We have performed a similar fit to the five energy levels from Ref. [1] which are sensitive only to the d-wave amplitude. Details are in Appendix F.3. Despite very small shifts from the free energies, we find a 3σ signal for the d-wave scattering length, $(Ma_2)^5 = 0.0006(2)$, where a_2 is defined in Eq. (F.40) of Appendix F.3. The smallness of this result is qualitatively consistent with the fact that this is a NLO effect in χPT , and justifies our neglect of d-waves in the three-particle analysis.

8.5 Fitting the three-particle spectrum

We now use the three-particle spectrum to determine $\mathcal{K}^{\text{iso}}_{\text{df},3}$. Eight levels are sensitive to $\mathcal{K}^{\text{iso}}_{\text{df},3}$, while three are in irreps only sensitive to two-particle interactions. Since all levels are correlated, a global fit to two- and three-particle spectra is needed to properly estimate errors. Further details on the fits described in this section can be found in Appendix F.3.

Before presenting the global fits, however, we use an approach ("method 1") that allows a separate determination of $\mathcal{K}^{\text{iso}}_{\text{df},3}$ for each of the eight levels sensitive to this parameter. Within each bootstrap sample, we fit the two-particle levels to the fit 1 Adler-zero form described above, and then adjust $\mathcal{K}^{\text{iso}}_{\text{df},3}$ so that the three-particle QC reproduces the energy of the level under consideration. The results are shown in Fig. 8.3. The values of $\mathcal{K}^{\text{iso}}_{\text{df},3}$ are all positive, and a constant fit yields $M^2\mathcal{K}^{\text{iso}}_{\text{df},3} = 560(270)$ with χ^2/d.o.f. $= 8.5/7$. The LO χPT result (given by $M^2\mathcal{K}^{\text{iso}}_{\text{df},3} = 360 + 540\Delta$, taking Ma_0 from fit 1) is reasonably consistent with the linear fit, as shown. This indicates that a significant result for $\mathcal{K}^{\text{iso}}_{\text{df},3}$ of the expected size

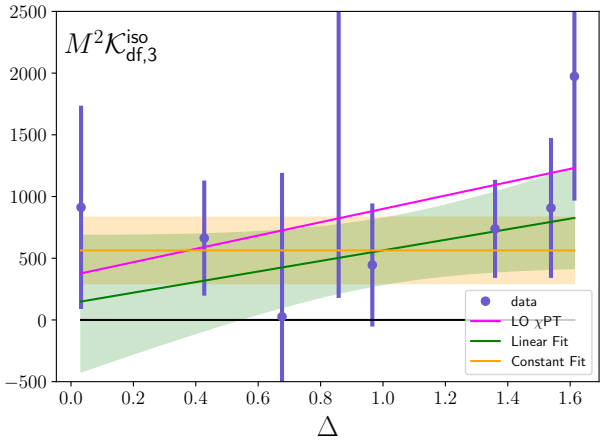

Figure 8.3: Results for $M^2\mathcal{K}_{\mathrm{df},3}^{\mathrm{iso}}$ from individual three-particle levels, using method 1, together with constant and linear fits, and the LO prediction of χPT .

Fit	B_0	B_1	z_2^2/M^2	$M^2\mathcal{K}_{\mathrm{df},3}^{\mathrm{iso},0}$	$M^2\mathcal{K}_{\mathrm{df},3}^{\mathrm{iso},1}$	χ^2/dof	Ma_0	M^2ra_0
4	-11.1(7)	-2.3(3)	1 (fixed)	270(160)	—	27.06/(22-3)	0.090(6)	2.59(8)
5	-11.1(7)	-2.4(3)	1 (fixed)	550(330)	-280(290)	26.04/(22-4)	0.090(5)	2.57(8)

Table 8.2: Global fits to the two- and three-particle spectrum using the two- and three-particle QCs.

may be obtainable.

This fit does not include three-particle energy levels in irreps sensitive only to δ_0. These, however, can be used as a consistency check. As shown in Appendix F.3, we find good agreement between the data and the energies predicted by the QC.

To establish the true significance of the results for $\mathcal{K}_{\mathrm{df},3}^{\mathrm{iso}}$ we perform global fits to the eleven two-particle and eleven three-particle levels that depend on δ_0 and/or $\mathcal{K}_{\mathrm{df},3}^{\mathrm{iso}}$. We do so both for constant and linear $\mathcal{K}_{\mathrm{df},3}^{\mathrm{iso}}$. The results are collected in Table 8.2. Fit 4 finds a value for $\mathcal{K}_{\mathrm{df},3}^{\mathrm{iso}}$ that has around 1.8σ statistical significance, and also gives values for B_0 and B_1 that are consistent with those from fits 1-3 above and with the LO χPT predictions. The p-value of the fit is $p = 0.103$.

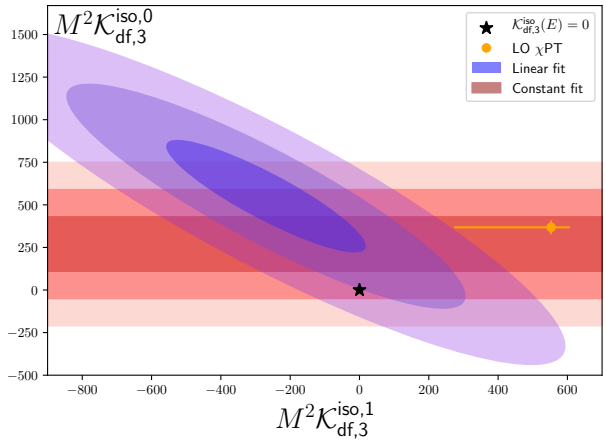

Figure 8.4: One, two, and three-sigma confidence intervals for $M^2\mathcal{K}^{\text{iso}}_{\text{df},3}$ for the two different global fits (4 and 5).

In fit 5, we try a linear ansatz for $\mathcal{K}^{\text{iso}}_{\text{df},3}$, and find that the current dataset of Ref. [1] is insufficient for a separate extraction of both constant and linear terms. We note, however, that, even in this fit, the scenario $\mathcal{K}^{\text{iso}}_{\text{df},3} = 0$ is excluded at $\sim 2\sigma$. We also provide a comparison between the data and the predicted spectrum from this fit in Fig. F.3 of Appendix F.3.

In Fig. 8.4 we present a summary of the errors resulting from the global fits. We also include the value from LO χPT , along with an estimate of the NLO corrections obtained in Appendix F.2, and quoted in Eq. (F.35). As can be seen, the constant term agrees well with the prediction, whereas the larger disagreement for the linear term is only of marginal significance given the large uncertainty in the χPT prediction.

One concern with our global fits is that we are using the forms for $\mathcal{K}_2$ and $\mathcal{K}^{\text{iso}}_{\text{df},3}$ beyond their radii of convergence. For $\mathcal{K}^{\text{iso}}_{\text{df},3}$ we do not know the radius of convergence, but a reasonable estimate is that one should use levels only with $|\Delta| < 1$. To check the importance of this issue, we have repeated the global fits imposing $q^2/M^2 < 1$ and $\Delta < 1$, so that the fit includes only five $2\pi^+$ and five $3\pi^+$ levels. We find fit parameters that are consistent with those in Table 8.2, but with much larger errors. For example, the result from the equivalent

of fit 4 gives $M^2\mathcal{K}_{\mathrm{df},3}^{\mathrm{iso},0} = 610(350)$.

We close by commenting on sources of systematic errors. The results of Ref. [1] are subject to discretization errors, but these are of $O(a^2)$, and likely small compared to the statistical errors from [1]. The quantization condition itself neglects exponentially-suppressed corrections, but these are numerically small ($e^{-ML} \sim 1\%$) compared to our final statistical error. Errors from truncation of the threshold expansion for $\mathcal{K}_2$ and $\mathcal{K}_{\mathrm{df},3}$ are also present, but harder to estimate.

8.6 Conclusions

We have presented statistical evidence for a nonzero $3\pi^+$ contact interaction, obtained by analyzing the spectrum of three pion states in isosymmetric QCD with $M \approx 200$ MeV obtained in Ref. [1]. This illustrates the utility of the three-particle quantization condition. It also emphasizes the need for a relativistic formalism, since most of the spectral levels used here are in the relativistic regime. It gives an example where lattice methods can provide results for scattering quantities that are not directly accessible to experiment.

We expect that forthcoming generalizations to the formalism (to incorporate nondegenerate particles with spin, etc.), combined with advances in the methods of lattice QCD (to allow the accurate determination of the spectrum in an increasing array of systems), will allow generalization of the present results to resonant three-particle systems in the next few years.

Chapter 9

CONCLUSIONS

In this thesis, we have presented several theoretical and practical advances to three-particle quantization conditions. We have provided an alternative derivation of the QC3 for identical scalars (e.g. $\pi^+\pi^+\pi^+$ or $K^+K^+K^+$) that utilizes time-ordered perturbation theory to simplify the diagrammatic expansion of the finite-volume correlator, organizing the infinite sum of diagrams into a simple closed-form expression. We have shown that the resulting QC3 is equivalent to that of the original RFT derivation (Refs. [28, 29]), as well as that of the FVU approach (Refs. [32, 41]), proving the equivalence of the two different relativistic formalisms. We have also used the TOPT strategy to derive a QC3 for three nondegenerate scalars (e.g. $D_s^+D^0\pi^-$ or $D_s^+D^0D^+$), establishing the generalizing power of the new method.

In addition to these theoretical advances, we have presented results from multiple practical implementations of the QC3 for identical scalars. We have detailed the first implementation that included d-wave dimer interactions and energy levels in all irreps, as well as a numerical exploration of two-particle bound states and resonances. We have also shown results from the first ever extraction of the $3\pi^+$ scattering amplitude from LQCD data, serving as a proof-of-principle that LQCD and QC3 formalism are now at a stage where a first-principles analysis of three-hadron scattering is feasible and worth pursuing.

Since starting work on this thesis, we have put out preprints for two additional projects. In Ref. [157], we use the TOPT strategy to derive a QC3 in the case of two identical scalars plus a third nondegenerate scalar, which is applicable to systems such as $\pi^+\pi^+K^+$ and $K^+K^+\pi^+$. In Ref. [158], we present results from implementing QCs to fit $3K^+$ and $3\pi^+$ scattering amplitudes to FV spectra computed with LQCD, using many more levels than we did in Chapter 8.

In the future, we hope to continue generalizing the QC3 formalism and to increase the scope of QC3 implementations. Two short-term goals are to generalize the QC3 to allow for particles with nonzero spin (e.g. nucleons) and for multiple three-particle channels. The latter

would immediately allow several new scattering processes to be studied (e.g. $\pi^+\pi^-\pi^0 \leftrightarrow 3\pi^0$, $D_s^+ D^0\pi^- \leftrightarrow D^0 D^0 K^0$), while combining the former with methods from Refs. [34, 36] would allow a first-principles study of the Roper resonance $N(1440) \to N\pi\pi, N\pi$. A more ambitious goal is to derive a quantization condition for 4→4 scattering; this was a major motivation for trying to simplify the complicated QC3 derivation of Ref. [28], as with the TOPT formalism developed in Chapter 3, deriving a four-particle QC seems much less daunting.

We also anticipate that many of these generalized quantization conditions will be implemented in the near future, both for numerical exploration and for fitting FV spectra of new systems, as the computational abilities of LQCD continue to improve. The next generalization to be implemented will likely be the QC3 for 2+1 systems that we recently derived in Ref. [157], as we expect the next available lattice data to be for $\pi^+\pi^+K^+$ and $K^+K^+\pi^+$. However, it is only a matter of time before other generalizations such as the QC3 for three-pion states of different isospins (Ref. [37]) and the QC3 for nondegenerate scalars (Chapter 4) become necessary to implement; the field of extracting three-particle scattering amplitudes from LQCD is still in its infancy, and we only expect it to grow.

BIBLIOGRAPHY

[1] B. Hörz and A. Hanlon, "Two- and three-pion finite-volume spectra at maximal isospin from lattice QCD," Phys. Rev. Lett. **123**, 142002 (2019), arXiv:1905.04277 [hep-lat] .

[2] D. Griffiths, *Introduction to elementary particles* (2008).

[3] M. Thomson, *Modern Particle Physics* (Cambridge University Press, 2013).

[4] B. Odom, D. Hanneke, B. D'Urso, and G. Gabrielse, "New measurement of the electron magnetic moment using a one-electron quantum cyclotron," Phys. Rev. Lett. **97**, 030801 (2006).

[5] F. Wilson, "Fermi's theory of beta decay," American Journal of Physics **36**, 1150 (1968).

[6] S. L. Glashow, "Partial Symmetries of Weak Interactions," Nucl. Phys. **22**, 579–588 (1961).

[7] S. Weinberg, "A model of leptons," Phys. Rev. Lett. **19**, 1264–1266 (1967).

[8] A. Salam, "Proceedings of the 8th nobel symposium," Almquist & Wiskell, Stockholm (1968).

[9] L. Di Lella and C. Rubbia, "The discovery of the w and z particles," in *60 Years of CERN Experiments and Discoveries* (World Scientific, 2015) pp. 137–163.

[10] G. ROCHESTERD and C. BUTLERD, "Evidence for the existence of new unstable elementary particles," Nature **160**, 855–857 (1947).

[11] M. Gell-Mann, *A Schematic Model of Baryons and Mesons 1* (CRC Press, 2018).

[12] G. Zweig, *An SU(3) model for strong interaction symmetry and its breaking*, Tech. Rep. (CM-P00042884, 1964).

[13] F. Tkachov, "A contribution to the history of quarks: Boris struminsky's 1965 jinr publication," arXiv preprint arXiv:0904.0343 (2009).

[14] H. B. Nielsen and M. Ninomiya, "The adler-bell-jackiw anomaly and weyl fermions in a crystal," Physics Letters B **130**, 389–396 (1983).

[15] C. Michael, "Adjoint sources in lattice gauge theory," Nuclear Physics B **259**, 58–76 (1985).

[16] A. collaboration, B. Blossier, M. D. Morte, G. v. Hippel, T. Mendes, and R. Sommer, "On the generalized eigenvalue method for energies and matrix elements in lattice field theory," Journal of High Energy Physics **2009**, 094–094 (2009).

[17] M. Mahbub, A. O. Cais, W. Kamleh, B. Lasscock, D. B. Leinweber, A. G. Williams, C. Collaboration, *et al.*, "Isolating excited states of the nucleon in lattice qcd," Physical Review D **80**, 054507 (2009).

[18] S. Weinberg, "Phenomenological Lagrangians," *Proceedings, Symposium Honoring Julian Schwinger on the Occasion of his 60th Birthday: Los Angeles, California, February 18-19, 1978*, Physica **A96**, 327–340 (1979).

[19] R. Jaffe, "Multiquark hadrons. i. phenomenology of q 2 q 2 mesons," Physical Review D **15**, 267 (1977).

[20] R. Aaij, B. Adeva, M. Adinolfi, Z. Ajaltouni, S. Akar, J. Albrecht, F. Alessio, M. Alexander, S. Ali, G. Alkhazov, *et al.*, "Observation of the ξb-$\rightarrow$ j/$\psi\lambda$k- decay," Physics Letters B **772**, 265–273 (2017).

[21] M. Karliner, J. L. Rosner, and T. Skwarnicki, "Multiquark states," Annual Review of Nuclear and Particle Science **68**, 17–44 (2018).

[22] S. Borsanyi, S. Durr, Z. Fodor, C. Hoelbling, S. Katz, S. Krieg, L. Lellouch, T. Lippert, A. Portelli, K. Szabo, *et al.*, "Ab initio calculation of the neutron-proton mass difference," Science **347**, 1452–1455 (2015).

[23] Z. Fodor and C. Hoelbling, "Light hadron masses from lattice qcd," Reviews of Modern Physics **84**, 449–495 (2012).

[24] M. Lüscher, "Volume Dependence of the Energy Spectrum in Massive Quantum Field Theories. 2. Scattering States," Commun.Math.Phys. **105**, 153–188 (1986).

[25] M. Lüscher, "Two particle states on a torus and their relation to the scattering matrix," Nucl.Phys. **B354**, 531–578 (1991).

[26] R. A. Briceño, J. J. Dudek, and R. D. Young, "Scattering processes and resonances from lattice QCD," Rev. Mod. Phys. **90**, 025001 (2018), arXiv:1706.06223 [hep-lat] .

[27] C. h. Kim, C. T. Sachrajda, and S. R. Sharpe, "Finite-volume effects for two-hadron states in moving frames," Nucl. Phys. **B727**, 218–243 (2005), arXiv:hep-lat/0507006 [hep-lat] .

[28] M. T. Hansen and S. R. Sharpe, "Relativistic, model-independent, three-particle quantization condition," Phys. Rev. **D90**, 116003 (2014), arXiv:1408.5933 [hep-lat] .

[29] M. T. Hansen and S. R. Sharpe, "Expressing the three-particle finite-volume spectrum in terms of the three-to-three scattering amplitude," Phys. Rev. **D92**, 114509 (2015), arXiv:1504.04248 [hep-lat] .

[30] H.-W. Hammer, J.-Y. Pang, and A. Rusetsky, "Three-particle quantization condition in a finite volume: 1. The role of the three-particle force," JHEP **09**, 109 (2017), arXiv:1706.07700 [hep-lat] .

[31] H. W. Hammer, J. Y. Pang, and A. Rusetsky, "Three particle quantization condition in a finite volume: 2. general formalism and the analysis of data," JHEP **10**, 115 (2017), arXiv:1707.02176 [hep-lat] .

[32] M. Mai and M. Döring, "Three-body Unitarity in the Finite Volume," Eur. Phys. J. **A53**, 240 (2017), arXiv:1709.08222 [hep-lat] .

[33] S. Aoki, T. Doi, T. Hatsuda, Y. Ikeda, T. Inoue, N. Ishii, K. Murano, H. Nemura, and K. Sasaki (HAL QCD), "Lattice QCD approach to Nuclear Physics," PTEP **2012**, 01A105 (2012), arXiv:1206.5088 [hep-lat] .

[34] R. A. Briceño, M. T. Hansen, and S. R. Sharpe, "Relating the finite-volume spectrum and the two-and-three-particle S matrix for relativistic systems of identical scalar particles," Phys. Rev. **D95**, 074510 (2017), arXiv:1701.07465 [hep-lat] .

[35] R. A. Briceño, M. T. Hansen, and S. R. Sharpe, "Three-particle systems with resonant subprocesses in a finite volume," Phys. Rev. **D99**, 014516 (2019), arXiv:1810.01429 [hep-lat] .

[36] F. Romero-López, S. R. Sharpe, T. D. Blanton, R. A. Briceño, and M. T. Hansen, "Numerical exploration of three relativistic particles in a finite volume including two-particle resonances and bound states," JHEP **10**, 007 (2019), arXiv:1908.02411 [hep-lat] .

[37] M. T. Hansen, F. Romero-López, and S. R. Sharpe, "Generalizing the relativistic quantization condition to include all three-pion isospin channels," JHEP **07**, 047 (2020), arXiv:2003.10974 [hep-lat] .

[38] M. T. Hansen, F. Romero-López, and S. R. Sharpe, "Decay amplitudes to three hadrons from finite-volume matrix elements," (2021), arXiv:2101.10246 [hep-lat] .

[39] R. A. Briceño, M. T. Hansen, and S. R. Sharpe, "Numerical study of the relativistic three-body quantization condition in the isotropic approximation," Phys. Rev. **D98**, 014506 (2018), arXiv:1803.04169 [hep-lat] .

[40] M. Döring, H. W. Hammer, M. Mai, J. Y. Pang, A. Rusetsky, and J. Wu, "Three-body spectrum in a finite volume: the role of cubic symmetry," Phys. Rev. **D97**, 114508 (2018), arXiv:1802.03362 [hep-lat] .

[41] M. Mai and M. Döring, "Finite-Volume Spectrum of $\pi^+\pi^+$ and $\pi^+\pi^+\pi^+$ Systems," Phys. Rev. Lett. **122**, 062503 (2019), arXiv:1807.04746 [hep-lat] .

[42] M. Mai, M. Döring, and A. Rusetsky, "Multi-particle systems on the lattice and chiral extrapolations: a brief review," (2021), arXiv:2103.00577 [hep-lat] .

[43] T. D. Blanton and S. R. Sharpe, "Equivalence of relativistic three-particle quantization conditions," Phys. Rev. D **102**, 054515 (2020), arXiv:2007.16190 [hep-lat] .

[44] T. D. Blanton and S. R. Sharpe, "Relativistic three-particle quantization condition for nondegenerate scalars," (2020), arXiv:2011.05520 [hep-lat] .

[45] T. D. Blanton and S. R. Sharpe, "Alternative derivation of the relativistic three-particle quantization condition," Phys. Rev. D **102**, 054520 (2020), arXiv:2007.16188 [hep-lat] .

[46] S. R. Beane, W. Detmold, T. C. Luu, K. Orginos, M. J. Savage, and A. Torok, "Multi-Pion Systems in Lattice QCD and the Three-Pion Interaction," Phys. Rev. Lett. **100**, 082004 (2008), arXiv:0710.1827 [hep-lat] .

[47] W. Detmold, M. J. Savage, A. Torok, S. R. Beane, T. C. Luu, K. Orginos, and A. Parreno, "Multi-Pion States in Lattice QCD and the Charged-Pion Condensate," Phys. Rev. **D78**, 014507 (2008), arXiv:0803.2728 [hep-lat] .

[48] W. Detmold and B. Smigielski, "Lattice QCD study of mixed systems of pions and kaons," Phys. Rev. D **84**, 014508 (2011), arXiv:1103.4362 [hep-lat] .

[49] W. Detmold, "Multi-hadron systems in lattice QCD," Eur. Phys. J. A **49**, 83 (2013).

[50] W. Detmold and A. N. Nicholson, "Baryon masses at nonzero isospin/kaon density," Phys. Rev. D **88**, 074501 (2013), arXiv:1308.5186 [hep-lat] .

[51] T. D. Blanton, F. Romero-López, and S. R. Sharpe, "$I = 3$ three-pion scattering amplitude from lattice QCD," Phys. Rev. Lett. **124**, 032001 (2020), arXiv:1909.02973 [hep-lat] .

[52] M. Mai, M. Döring, C. Culver, and A. Alexandru, "Three-body unitarity versus finite-volume $\pi^+\pi^+\pi^+$ spectrum from lattice QCD," Phys. Rev. D **101**, 054510 (2020), arXiv:1909.05749 [hep-lat] .

[53] C. Culver, M. Mai, R. Brett, A. Alexandru, and M. Döring, "Three body spectrum from lattice QCD," Phys. Rev. D **101**, 114507 (2020), arXiv:1911.09047 [hep-lat] .

[54] S. Beane *et al.*, "Charged multi-hadron systems in lattice QCD+QED," (2020), arXiv:2003.12130 [hep-lat] .

[55] F. Romero-López, A. Rusetsky, and C. Urbach, "Two- and three-body interactions in φ^4 theory from lattice simulations," Eur. Phys. J. **C78**, 846 (2018), arXiv:1806.02367 [hep-lat] .

[56] K. Rummukainen and S. A. Gottlieb, "Resonance scattering phase shifts on a nonrest frame lattice," Nucl. Phys. **B450**, 397–436 (1995), arXiv:hep-lat/9503028 [hep-lat] .

[57] S. He, X. Feng, and C. Liu, "Two particle states and the S-matrix elements in multi-channel scattering," JHEP **07**, 011 (2005), arXiv:hep-lat/0504019 [hep-lat] .

[58] M. Lage, U.-G. Meißner, and A. Rusetsky, "A Method to measure the antikaon-nucleon scattering length in lattice QCD," Phys.Lett. **B681**, 439–443 (2009), arXiv:0905.0069 [hep-lat] .

[59] Z. Fu, "Rummukainen-Gottlieb's formula on two-particle system with different mass," Phys.Rev. **D85**, 014506 (2012), arXiv:1110.0319 [hep-lat] .

[60] M. T. Hansen and S. R. Sharpe, "Multiple-channel generalization of Lellouch-Lüscher formula," Phys.Rev. **D86**, 016007 (2012), arXiv:1204.0826 [hep-lat] .

[61] R. A. Briceño and Z. Davoudi, "Moving multichannel systems in a finite volume with application to proton-proton fusion," Phys. Rev. **D88**, 094507 (2013), arXiv:1204.1110 [hep-lat] .

[62] M. Göckeler, R. Horsley, M. Lage, U. G. Meißner, P. E. L. Rakow, A. Rusetsky, G. Schierholz, and J. M. Zanotti, "Scattering phases for meson and baryon resonances on general moving-frame lattices," Phys. Rev. D **86**, 094513 (2012), arXiv:1206.4141 [hep-lat] .

[63] R. A. Briceño, "Two-particle multichannel systems in a finite volume with arbitrary spin," Phys. Rev. **D89**, 074507 (2014), arXiv:1401.3312 [hep-lat] .

[64] K. Polejaeva and A. Rusetsky, "Three particles in a finite volume," Eur. Phys. J. A **48**, 67 (2012), arXiv:1203.1241 [hep-lat] .

[65] S. Tan, "Three-boson problem at low energy and implications for dilute Bose-Einstein condensates," Phys. Rev. A **78**, 013636 (2008), arXiv:0709.2530 [cond-mat.stat-mech] .

[66] S. R. Beane, W. Detmold, and M. J. Savage, "n-Boson Energies at Finite Volume and Three-Boson Interactions," Phys. Rev. **D76**, 074507 (2007), arXiv:0707.1670 [hep-lat] .

[67] W. Detmold and M. J. Savage, "The Energy of n Identical Bosons in a Finite Volume at O(L**-7)," Phys. Rev. **D77**, 057502 (2008), arXiv:0801.0763 [hep-lat] .

[68] M. T. Hansen and S. R. Sharpe, "Threshold expansion of the three-particle quantization condition," Phys. Rev. **D93**, 096006 (2016), [Erratum: Phys. Rev.D96,no.3,039901(2017)], arXiv:1602.00324 [hep-lat] .

[69] W. Detmold and M. Flynn, "Finite-volume matrix elements in multiboson states," Phys. Rev. D **91**, 074509 (2015), arXiv:1412.3895 [hep-lat] .

[70] R. A. Briceño and Z. Davoudi, "Three-particle scattering amplitudes from a finite volume formalism," Phys. Rev. **D87**, 094507 (2013), arXiv:1212.3398 [hep-lat] .

[71] P. Guo and V. Gasparian, "A solvable three-body model in finite volume," Phys. Lett. **B774**, 441–445 (2017), arXiv:1701.00438 [hep-lat] .

[72] P. Klos, S. König, H. W. Hammer, J. E. Lynn, and A. Schwenk, "Signatures of few-body resonances in finite volume," Phys. Rev. **C98**, 034004 (2018), arXiv:1805.02029 [nucl-th] .

[73] P. Guo, M. Döring, and A. P. Szczepaniak, "Variational approach to N-body interactions in finite volume," Phys. Rev. **D98**, 094502 (2018), arXiv:1810.01261 [hep-lat] .

[74] M. T. Hansen and S. R. Sharpe, "Lattice QCD and Three-particle Decays of Resonances," Ann. Rev. Nucl. Part. Sci. **69**, 65–107 (2019), arXiv:1901.00483 [hep-lat] .

[75] A. Rusetsky, "Three particles on the lattice," in *37th International Symposium on Lattice Field Theory* (2019) arXiv:1911.01253 [hep-lat] .

[76] T. D. Blanton, F. Romero-López, and S. R. Sharpe, "Implementing the three-particle quantization condition including higher partial waves," JHEP **03**, 106 (2019), arXiv:1901.07095 [hep-lat] .

[77] J.-Y. Pang, J.-J. Wu, H.-W. Hammer, U.-G. Meißner, and A. Rusetsky, "Energy shift of the three-particle system in a finite volume," Phys. Rev. **D99**, 074513 (2019), arXiv:1902.01111 [hep-lat] .

[78] M. Mai, B. Hu, M. Döring, A. Pilloni, and A. Szczepaniak, "Three-body Unitarity with Isobars Revisited," Eur. Phys. J. **A53**, 177 (2017), arXiv:1706.06118 [nucl-th] .

[79] A. Jackura, C. Fernández-Ramírez, V. Mathieu, M. Mikhasenko, J. Nys, A. Pilloni, K. Saldaña, N. Sherrill, and A. P. Szczepaniak (JPAC), "Phenomenology of Relativistic $\mathbf{3} \to \mathbf{3}$ Reaction Amplitudes within the Isobar Approximation," Eur. Phys. J. **C79**, 56 (2019), arXiv:1809.10523 [hep-ph] .

[80] M. T. Hansen and S. R. Sharpe, "Applying the relativistic quantization condition to a three-particle bound state in a periodic box," Phys. Rev. **D95**, 034501 (2017), arXiv:1609.04317 [hep-lat] .

[81] M. T. Hansen and S. R. Sharpe, "Perturbative results for two and three particle threshold energies in finite volume," Phys. Rev. **D93**, 014506 (2016), arXiv:1509.07929 [hep-lat] .

[82] S. R. Sharpe, "Testing the threshold expansion for three-particle energies at fourth order in ϕ^4 theory," Phys. Rev. **D96**, 054515 (2017), [Erratum: Phys. Rev.D98,no.9,099901(2018)], arXiv:1707.04279 [hep-lat] .

[83] G. F. Sterman, *An Introduction to quantum field theory* (Cambridge University Press, 1993).

[84] Y. Li, J.-J. Wu, R. D. Young, and T.-S. H. Lee, "The General Formalism of Momentum Transformations in a Moving Finite Volume," in preparation (2020).

[85] M. Fischer, B. Kostrzewa, L. Liu, F. Romero-López, M. Ueding, and C. Urbach, "Scattering of two and three physical pions at maximal isospin from lattice QCD," (2020), arXiv:2008.03035 [hep-lat] .

[86] M. T. Hansen, R. A. Briceño, R. G. Edwards, C. E. Thomas, and D. J. Wilson, "The energy-dependent $\pi^+\pi^+\pi^+$ scattering amplitude from QCD," Phys. Rev. Lett. **126**, 012001 (2021), arXiv:2009.04931 [hep-lat] .

[87] A. Alexandru, R. Brett, C. Culver, M. Döring, D. Guo, F. X. Lee, and M. Mai, "Finite-volume energy spectrum of the $K^-K^-K^-$ system," Phys. Rev. D **102**, 114523 (2020), arXiv:2009.12358 [hep-lat] .

[88] F. Romero-López, A. Rusetsky, N. Schlage, and C. Urbach, "Relativistic N-particle energy shift in finite volume," (2020), arXiv:2010.11715 [hep-lat] .

[89] P. Guo and B. Long, "Multi- π^+ systems in a finite volume," Phys. Rev. D **101**, 094510 (2020), arXiv:2002.09266 [hep-lat] .

[90] P. Guo, "Modeling few-body resonances in finite volume," Phys. Rev. D **102**, 054514 (2020), arXiv:2007.12790 [hep-lat] .

[91] J.-Y. Pang, J.-J. Wu, and L.-S. Geng, "DDK system in finite volume," Phys. Rev. D **102**, 114515 (2020), arXiv:2008.13014 [hep-lat] .

[92] A. W. Jackura, S. M. Dawid, C. Fernández-Ramírez, V. Mathieu, M. Mikhasenko, A. Pilloni, S. R. Sharpe, and A. P. Szczepaniak, "Equivalence of three-particle scattering formalisms," Phys. Rev. **D100**, 034508 (2019), arXiv:1905.12007 [hep-ph] .

[93] R. A. Briceño, M. T. Hansen, S. R. Sharpe, and A. P. Szczepaniak, "Unitarity of the infinite-volume three-particle scattering amplitude arising from a finite-volume formalism," Phys. Rev. **D100**, 054508 (2019), arXiv:1905.11188 [hep-lat] .

[94] J. J. Dudek, R. G. Edwards, P. Guo, and C. E. Thomas (Hadron Spectrum), "Toward the excited isoscalar meson spectrum from lattice QCD," Phys. Rev. **D88**, 094505 (2013), arXiv:1309.2608 [hep-lat] .

[95] J. Bulava, B. Fahy, B. Hörz, K. J. Juge, C. Morningstar, and C. H. Wong, "$I = 1$ and $I = 2$ $\pi - \pi$ scattering phase shifts from $N_{\rm f} = 2 + 1$ lattice QCD," Nucl. Phys. **B910**, 842–867 (2016), arXiv:1604.05593 [hep-lat] .

[96] C. W. Andersen, J. Bulava, B. Hörz, and C. Morningstar, "Elastic $I = 3/2p$-wave nucleon-pion scattering amplitude and the $\Delta(1232)$ resonance from N_f=2+1 lattice QCD," Phys. Rev. **D97**, 014506 (2018), arXiv:1710.01557 [hep-lat] .

[97] A. J. Woss, C. E. Thomas, J. J. Dudek, R. G. Edwards, and D. J. Wilson, "Dynamically-coupled partial-waves in $\rho\pi$ isospin-2 scattering from lattice QCD," JHEP **07**, 043 (2018), arXiv:1802.05580 [hep-lat] .

[98] T. D. Blanton, R. A. Briceño, M. T. Hansen, F. Romero-López, and S. R. Sharpe, "Progress report on the relativistic three-particle quantization condition," in *36th International Symposium on Lattice Field Theory (Lattice 2018) East Lansing, MI, United States, July 22-28, 2018* (2018) arXiv:1810.06634 [hep-lat] .

[99] P. W. Atkins, M. S. Child, and C. S. G. Phillips, *Tables for group theory*, Vol. 6 (Oxford University Press Oxford, 1970).

[100] H. Georgi, "Lie Algebras In Particle Physics. From Isospin To Unified Theories," Front. Phys. **54**, 1–255 (1982).

[101] T. Luu and M. J. Savage, "Extracting Scattering Phase-Shifts in Higher Partial-Waves from Lattice QCD Calculations," Phys. Rev. **D83**, 114508 (2011), arXiv:1101.3347 [hep-lat] .

[102] P. M. A. Mestrom, J. Wang, C. H. Greene, and J. P. D'Incao, "Efimov–van der waals universality for ultracold atoms with positive scattering lengths," Phys. Rev. A **95**, 032707 (2017).

[103] J. Wang, J. P. D'Incao, Y. Wang, and C. H. Greene, "Universal three-body recombination via resonant d-wave interactions," Phys. Rev. A **86**, 062511 (2012).

[104] V. Efimov, "Energy levels arising from resonant two-body forces in a three-body system," Physics Letters B **33**, 563 – 564 (1970).

[105] U.-G. Mei„ner, G. Ríos, and A. Rusetsky, "Spectrum of three-body bound states in a finite volume," Phys. Rev. Lett. **114**, 091602 (2015), [Erratum: Phys. Rev. Lett.117,no.6,069902(2016)], arXiv:1412.4969 [hep-lat] .

[106] P. F. Bedaque, H. W. Hammer, and U. van Kolck, "Renormalization of the three-body system with short range interactions," Phys. Rev. Lett. **82**, 463–467 (1999), arXiv:nucl-th/9809025 [nucl-th] .

[107] F. J. Yndurain, "Low-energy pion physics," (2002), arXiv:hep-ph/0212282 [hep-ph] .

[108] S. R. Beane, E. Chang, W. Detmold, H. W. Lin, T. C. Luu, K. Orginos, A. Parreno, M. J. Savage, A. Torok, and A. Walker-Loud (NPLQCD), "The I=2 pipi S-wave Scattering Phase Shift from Lattice QCD," Phys. Rev. **D85**, 034505 (2012), arXiv:1107.5023 [hep-lat] .

[109] J. J. Dudek, R. G. Edwards, and C. E. Thomas, "S and D-wave phase shifts in isospin-2 pi pi scattering from lattice QCD," Phys. Rev. **D86**, 034031 (2012), arXiv:1203.6041 [hep-ph] .

[110] Z. Fu, "Lattice QCD study of the s-wave $\pi\pi$ scattering lengths in the I=0 and 2 channels," Phys. Rev. **D87**, 074501 (2013), arXiv:1303.0517 [hep-lat] .

[111] T. Kurth, N. Ishii, T. Doi, S. Aoki, and T. Hatsuda, "Phase shifts in $I = 2$ $\pi\pi$-scattering from two lattice approaches," JHEP **12**, 015 (2013), arXiv:1305.4462 [hep-lat] .

[112] C. Helmes, C. Jost, B. Knippschild, C. Liu, J. Liu, L. Liu, C. Urbach, M. Ueding, Z. Wang, and M. Werner (ETM), "Hadron-hadron interactions from $N_f = 2 + 1 + 1$ lattice QCD: isospin-2 $\pi\pi$ scattering length," JHEP **09**, 109 (2015), arXiv:1506.00408 [hep-lat] .

[113] D. J. Wilson, R. A. Briceño, J. J. Dudek, R. G. Edwards, and C. E. Thomas, "Coupled $\pi\pi, K\bar{K}$ scattering in P-wave and the ρ resonance from lattice QCD," Phys. Rev. **D92**, 094502 (2015), arXiv:1507.02599 [hep-ph] .

[114] R. A. Briceño, J. J. Dudek, R. G. Edwards, and D. J. Wilson, "Isoscalar $\pi\pi$ scattering and the σ meson resonance from QCD," Phys. Rev. Lett. **118**, 022002 (2017), arXiv:1607.05900 [hep-ph] .

[115] R. Brett, J. Bulava, J. Fallica, A. Hanlon, B. Hörz, and C. Morningstar, "Determination of s- and p-wave $I = 1/2$ $K\pi$ scattering amplitudes in $N_{\rm f} = 2 + 1$ lattice QCD," Nucl. Phys. **B932**, 29–51 (2018), arXiv:1802.03100 [hep-lat] .

[116] D. Guo, A. Alexandru, R. Molina, M. Mai, and M. Döring, "Extraction of isoscalar $\pi\pi$ phase-shifts from lattice QCD," Phys. Rev. **D98**, 014507 (2018), arXiv:1803.02897 [hep-lat] .

[117] C. Andersen, J. Bulava, B. Hörz, and C. Morningstar, "The $I = 1$ pion-pion scattering amplitude and timelike pion form factor from $N_{\rm f} = 2 + 1$ lattice QCD," Nucl. Phys. **B939**, 145–173 (2019), arXiv:1808.05007 [hep-lat] .

[118] J. J. Dudek, R. G. Edwards, C. E. Thomas, and D. J. Wilson (Hadron Spectrum), "Resonances in coupled $\pi K - \eta K$ scattering from quantum chromodynamics," Phys. Rev. Lett. **113**, 182001 (2014), arXiv:1406.4158 [hep-ph] .

[119] J. J. Dudek, R. G. Edwards, and D. J. Wilson (Hadron Spectrum), "An a_0 resonance in strongly coupled $\pi\eta$, $K\overline{K}$ scattering from lattice QCD," Phys. Rev. **D93**, 094506 (2016), arXiv:1602.05122 [hep-ph] .

[120] A. J. Woss, C. E. Thomas, J. J. Dudek, R. G. Edwards, and D. J. Wilson, "The b_1 resonance in coupled $\pi\omega$, $\pi\phi$ scattering from lattice QCD," (2019), arXiv:1904.04136 [hep-lat] .

[121] C. Helmes, C. Jost, B. Knippschild, B. Kostrzewa, L. Liu, F. Pittler, C. Urbach, and M. Werner (ETM), "Hadron-Hadron Interactions from $N_f = 2 + 1 + 1$ Lattice QCD: $I = 3/2$ πK Scattering Length," Phys. Rev. **D98**, 114511 (2018), arXiv:1809.08886 [hep-lat] .

[122] L. Liu *et al.*, "Isospin-0 $\pi\pi$ s-wave scattering length from twisted mass lattice QCD," Phys. Rev. **D96**, 054516 (2017), arXiv:1612.02061 [hep-lat] .

[123] C. Helmes, C. Jost, B. Knippschild, B. Kostrzewa, L. Liu, C. Urbach, and M. Werner, "Hadron-Hadron Interactions from $N_f = 2+1+1$ lattice QCD: Isospin-1 KK scattering length," Phys. Rev. **D96**, 034510 (2017), arXiv:1703.04737 [hep-lat] .

[124] M. Werner *et al.*, "Hadron-Hadron Interactions from $N_f = 2+1+1$ Lattice QCD: The ρ-resonance," Eur. Phys. J. **A56**, 61 (2020), arXiv:1907.01237 [hep-lat] .

[125] C. Culver, M. Mai, A. Alexandru, M. Döring, and F. X. Lee, "Pion scattering in the isospin $I = 2$ channel from elongated lattices," Phys. Rev. **D100**, 034509 (2019), arXiv:1905.10202 [hep-lat] .

[126] V. Bernard, M. Lage, U.-G. Mei„ner, and A. Rusetsky, JHEP **1101**, 019 (2011), arXiv:1010.6018 [hep-lat] .

[127] F. Romero-López, A. Rusetsky, and C. Urbach, "Vector particle scattering on the lattice," Phys. Rev. **D98**, 014503 (2018), arXiv:1802.03458 [hep-lat] .

[128] G. K. C. Cheung, C. E. Thomas, J. J. Dudek, and R. G. Edwards (Hadron Spectrum), "Tetraquark operators in lattice QCD and exotic flavour states in the charm sector," JHEP **11**, 033 (2017), arXiv:1709.01417 [hep-lat] .

[129] W. Detmold, R. G. Edwards, J. J. Dudek, M. Engelhardt, H.-W. Lin, S. Meinel, K. Orginos, and P. Shanahan, "Hadrons and Nuclei," (2019), arXiv:1904.09512 [hep-lat] .

[130] M. Mikhasenko, Y. Wunderlich, A. Jackura, V. Mathieu, A. Pilloni, B. Ketzer, and A. P. Szczepaniak, "Three-body scattering: Ladders and Resonances," (2019), arXiv:1904.11894 [hep-ph] .

[131] T. D. Blanton, R. A. Briceño, M. T. Hansen, F. Romero-López, and S. R. Sharpe (2019) in progress .

[132] A. C. Phillips, "Consistency of the low-energy three-nucleon observables and the separable interaction model," Nucl. Phys. **A107**, 209–216 (1968).

[133] P. F. Bedaque, H. W. Hammer, and U. van Kolck, "Effective theory of the triton," Nucl. Phys. **A676**, 357–370 (2000), arXiv:nucl-th/9906032 [nucl-th] .

[134] P. Guo, J. Dudek, R. Edwards, and A. P. Szczepaniak, "Coupled-channel scattering on a torus," Phys. Rev. **D88**, 014501 (2013), arXiv:1211.0929 [hep-lat] .

[135] M. Lüscher, "Volume Dependence of the Energy Spectrum in Massive Quantum Field Theories. 1. Stable Particle States," Commun.Math.Phys. **104**, 177 (1986).

[136] S. R. Beane, P. F. Bedaque, A. Parreno, and M. J. Savage, "Exploring hyperons and hypernuclei with lattice QCD," Nucl. Phys. **A747**, 55–74 (2005), arXiv:nucl-th/0311027 [nucl-th] .

[137] T. Black, H. Karwowski, E. Ludwig, A. Kievsky, S. Rosati, and M. Viviani, "Determination of proton-deuteron scattering lengths," Physics Letters B **471**, 103 – 107 (1999).

[138] Y. V. Orlov and Y. P. Orevkov, "Doublet coulomb-nuclear scattering length and other parameters of the effective-range function for proton-deuteron scattering from an analysis of present-day data," Physics of Atomic Nuclei **69**, 828–840 (2006).

[139] T. Iritani, S. Aoki, T. Doi, T. Hatsuda, Y. Ikeda, T. Inoue, N. Ishii, H. Nemura, and K. Sasaki, "Are two nucleons bound in lattice QCD for heavy quark masses? Consistency check with Lushcer finite volume formula," Phys. Rev. **D96**, 034521 (2017), arXiv:1703.07210 [hep-lat] .

[140] H. W. Hammer, S. König, and U. van Kolck, "Nuclear effective field theory: status and perspectives," (2019), arXiv:1906.12122 [nucl-th] .

[141] W. Dilg, L. Koester, and W. Nistler, "The neutron-deuteron scattering lengths," Phys. Lett. **36B**, 208–210 (1971).

[142] V. A. Babenko and N. M. Petrov, "Analysis of experimental data on doublet neutron-deuteron scattering at energies below the deuteron-breakup threshold on the basis of

the pole approximation of the effective-range function," Physics of Atomic Nuclei **71**, 50–57 (2008).

[143] R. A. Briceño, J. J. Dudek, R. G. Edwards, and D. J. Wilson, "Isoscalar $\pi\pi, K\overline{K}, \eta\eta$ scattering and the σ, f_0, f_2 mesons from QCD," Phys. Rev. **D97**, 054513 (2018), arXiv:1708.06667 [hep-lat] .

[144] X. Feng, K. Jansen, and D. B. Renner, "The pi+ pi+ scattering length from maximally twisted mass lattice QCD," Phys. Lett. **B684**, 268–274 (2010), arXiv:0909.3255 [hep-lat] .

[145] M. Mai, C. Culver, A. Alexandru, M. Döring, and F. X. Lee, "Cross-channel study of pion scattering from lattice qcd," Phys.Rev.D **100**, 114514 (2019), arXiv:1908.01847 [hep-lat] .

[146] M. Doring, U. G. Mei„ner, E. Oset, and A. Rusetsky, "Scalar mesons moving in a finite volume and the role of partial wave mixing," Eur. Phys. J. **A48**, 114 (2012), arXiv:1205.4838 [hep-lat] .

[147] L. D. Roper, "Evidence for a P_{11} pion-nucleon resonance at 556 mev," Phys. Rev. Lett. **12**, 340–342 (1964).

[148] R. F. Lebed, R. E. Mitchell, and E. S. Swanson, "Heavy-Quark QCD Exotica," Prog. Part. Nucl. Phys. **93**, 143–194 (2017), arXiv:1610.04528 [hep-ph] .

[149] M. Hoferichter, B.-L. Hoid, and B. Kubis, "Three-pion contribution to hadronic vacuum polarization," JHEP **08**, 137 (2019), arXiv:1907.01556 [hep-ph] .

[150] S. Kreuzer and H. W. Grießhammer, "Three particles in a finite volume: The breakdown of spherical symmetry," Eur. Phys. J. **A48**, 93 (2012), arXiv:1205.0277 [nucl-th] .

[151] J. Gasser and H. Leutwyler, "Chiral Perturbation Theory to One Loop," Annals Phys. **158**, 142 (1984).

[152] S. Weinberg, "Pion scattering lengths," Phys. Rev. Lett. **17**, 616–621 (1966).

[153] S. L. Adler, "Consistency conditions on the strong interactions implied by a partially conserved axial vector current," Phys. Rev. **137**, B1022–B1033 (1965), [,140(1964)].

[154] J. R. Pelaez, A. Rodas, and J. Ruiz de Elvira, "Global parameterization of $\pi\pi$ scattering up to 2 gev," (2019), arXiv:1907.13162 [hep-ph] .

[155] M. Bruno, T. Korzec, and S. Schaefer, "Setting the scale for the CLS $2 + 1$ flavor ensembles," Phys. Rev. **D95**, 074504 (2017), arXiv:1608.08900 [hep-lat] .

[156] M. Bruno *et al.*, "Simulation of QCD with $N_f = 2 + 1$ flavors of non-perturbatively improved Wilson fermions," JHEP **02**, 043 (2015), arXiv:1411.3982 [hep-lat] .

[157] T. D. Blanton and S. R. Sharpe, "Three-particle finite-volume formalism for $\pi^+\pi^+K^+$ and related systems," (2021), arXiv:2105.12094 [hep-lat] .

[158] T. D. Blanton, A. D. Hanlon, B. Hörz, C. Morningstar, F. Romero-López, and S. R. Sharpe, "Interactions of two and three mesons including higher partial waves from lattice QCD," (2021), arXiv:2106.05590 [hep-lat] .

[159] P. F. Bedaque, H. W. Hammer, and U. van Kolck, "The Three boson system with short range interactions," Nucl. Phys. **A646**, 444–466 (1999), arXiv:nucl-th/9811046 [nucl-th] .

Appendix A

APPENDIX TO CHAPTER 3

A.1 Technical comments on time-ordered perturbation theory

In this appendix we address two technical issues concerning the application of TOPT described in the main text. These are, first, the use of the physical, renormalized mass in energy denominators—and more generally, our apparent neglect of self-energy diagrams—and, second, the presence of an additional class of diagrams with relevant (three-particle) cuts. Both issues have been partially addressed previously in Ref. [34], and our discussion here leans heavily on the analysis in that work.

We begin with the first issue, which we first restate in more detail. In the discussion in the main text, the kinematic factor associated with each cut involves the physical mass m rather than the bare mass. In particular, the factors of ω_k that appear in both energy denominators and propagator factors are given by $\omega_k = \sqrt{m^2 + \mathbf{k}^2}$. This appears to ignore the fact that the full propagator in any RFT has a more complicated analytic form than a simple pole, due to the usual iteration of self-energy diagrams. In fact, we are not ignoring self-energy diagrams, but instead dealing with them first in the context of a Feynman diagram decomposition, and then converting to TOPT to give the rules described in Sec. 3.2.1.

To explain our approach, we begin by writing the quantity under consideration, i.e. $C_{3,L}$ or $\widetilde{\mathcal{M}}_{3,L}^{(u,u)}$, in terms of the Feynman diagrams that follow from the Lagrangian of our generic relativistic effective field theory. Following HS1, we organize these diagrams into a skeleton expansion in terms of Bethe-Salpeter kernels and appropriately defined dressed propagators. The only subtlety here is that for diagrams in which all of the momentum is carried by a single propagator, the self-energy diagrams that dress this propagator must be 3PIs, instead

of the usual 1PIs. This allows all possible contributions with three-particle intermediate states to be made explicit. This is explained in the text surrounding Eq. (49) of HS1, and the distinction between 1PIs and 3PIs self-energies is illustrated (in the context of a theory without the $\mathbb{Z}_2$ symmetry) in Fig. 4 of Ref. [34].

At this stage HS1 use TOPT in a qualitative way to explain why all the self-energy diagrams in both types of dressed propagators (1PIs- and 3PIs-dressed) can be evaluated in infinite volume [see footnote 18 of HS1]. We now follow Ref. [34] and use a diagram-by-diagram regularization, in which each Feynman diagram is accompanied by counterterms chosen such that it satisfies the renormalization conditions given in Eq. (14) of Ref. [34]. In words, these conditions ensure that all self-energy diagrams, and their first derivatives with respect to p^2, vanish on shell (when evaluated in infinite volume). Each self-energy diagram thus behaves as $(p^2 - m^2)^2$ close to the on-shell point, where we are using the result that Feynman diagrams yield Lorentz-invariant expressions. It then follows that, in the usual geometric series that builds up the fully dressed propagator, only the leading term—a single, undressed propagator—has a pole, and this is of unit residue and at the position of the physical mass. All other contributions to the dressed propagator are either momentum-independent constants or vanish as powers of $p^2 - m^2$. For example, a sequence with an undressed propagator followed by a self-energy and another undressed propagator has the leading behavior $(p^2 - m^2)^{-1}(p^2 - m^2)^2(p^2 - m^2)^{-1}$, i.e. a constant. Such contributions correspond in position space to delta functions or derivatives thereof, and thus can be collapsed to pointlike interactions. (Examples of this collapse, albeit in a slightly different context, are given in Appendix B.2 of Ref. [34].) Any tadpole loops that result (propagators beginning or ending at the same vertex) can also be collapsed, since, as discussed in Appendix B.1 of Ref. [34], they have nonsingular summands that cannot enter into a cut. The end result of these manipulations is that we are left to evaluate the subset of diagrams in which there are no self-energy contributions or tadpole loops, except for self-energy diagrams involving

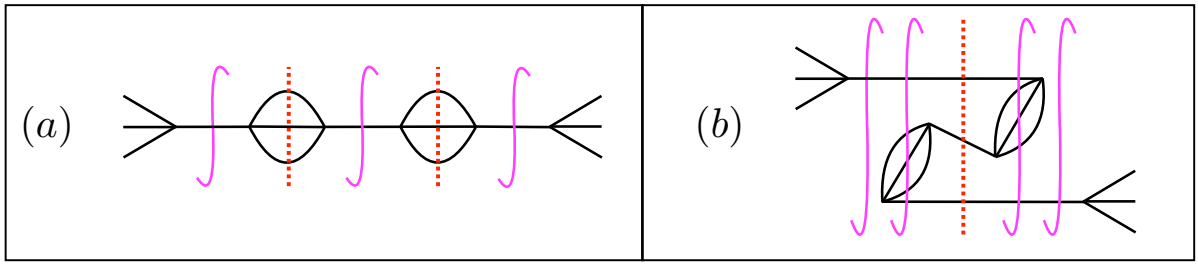

Figure A.1: Examples of TOPT diagrams for $\widetilde{\mathcal{M}}_{3,L}^{(u,u)}$ in which all the momentum flows through a single propagator. Notation as in Fig. 3.1. The two panels show different time orderings of the same Feynman diagram, and involve self-energy insertions containing three propagators. The time-ordering shown in (a) has two genuine three-particle cuts, lying between which is a contribution to $\mathcal{B}_3$. Time-ordering (b) has a fake three-particle cut that cancels when all time orderings are included. If the propagators carrying all the momentum are collapsed to point-like vertices, which is valid for $p^2 \gg m^2$ as discussed in the text, then diagrams of type (a) remain, while those with the Z-type time ordering shown in (b) are removed, since such a time ordering is no longer possible.

three-particle cuts if they are on a single propagator that carries all the momentum. [An example of such a diagram is Fig. A.1(a), viewed as a Feynman diagram.] When evaluating this reduced class of diagrams we must use modified vertices, due to the collapse of propagators and tadpole loops, but the key point is that all propagators that remain have their free form in terms of the physical mass.

At this stage we can break each Feynman diagram into its constituent time orderings, following the method explained, for example, in Ref. [83]. This leads to the rules described in Sec. 3.2.1, with all factors of ω containing the physical mass. The only subtlety is the need to break up counterterms for vertex diagrams into Lorentz noncovariant parts so that each TOPT diagram is finite. This does not present problems, as discussed in Appendix B.5 of Ref. [34]. Thus we have resolved the first issue.

We now turn to the second issue, which concerns a class of diagrams that leads to "fake" three-particle cuts. By fake, we mean that they will be canceled when all time orderings are added. Diagrams in this class all have the momentum carried by a single propagator,

and involve the self-energy diagrams that allow three-particle cuts. These are the self-energy diagrams that were not part of collapsed dressed propagators in the analysis above. In TOPT, such diagrams can have genuine three-particle cuts, as shown for example in Fig. A.1(a), as well "Z-type" configurations that have fake cuts, as in Fig. A.1(b). We know the latter cuts must cancel, because if we sum over all time orderings, we will end up with a result having singularities (higher-order poles) only at $p^2 = m^2$.

The simplest way of dealing with this issue is to restrict E^* to lie far above m, so that we do not approach the single-particle pole. For example, we could consider $E^* > E_0^* = 2m$, so that $p^2 > E_0^{*2} = 4m^2$ and $p^2 - m^2 > 3m^2$. In that case, the single propagator can be Taylor-expanded about $p^2 = E_0^{*2}$, and thus collapsed to a series of momentum-dependent vertices. This completely removes the Z-type time-orderings, while retaining those that lead to genuine relevant cuts.

A.2 Relating $\overline{\mathcal{K}}_{2,L}$ to $\mathcal{K}_2$

In this appendix we derive Eqs. (3.65)-(C.3) in the main text, i.e. we show that the two-particle matrix contained in $\overline{\mathcal{K}}_{2,L}$ is indeed (a variant of) the K matrix. A secondary purpose is to explain the definition of the generalized PV pole prescription.

Our approach is to consider the two-particle finite-volume amplitude $\mathcal{M}_{2,L}$, which is given by the sum of all amputated $2 \to 2$ diagrams. Since our notation is set up for three-particle correlators, we package $\mathcal{M}_{2,L}$ in an analogous manner to that used for $\overline{\mathcal{B}}_{2,L}$ [Eq. (3.11)],

$$\left[\overline{\mathcal{M}}_{2,L}\right]_{ka;pr} \equiv \delta_{kp} 2\omega_k L^3 \mathcal{M}_{2,L}(E_{2,k}, \mathbf{P}_{2,k}; \mathbf{a}; \mathbf{r}) \,, \quad E_{2,k} \equiv E - \omega_k \,, \quad \mathbf{P}_{2,k} \equiv \mathbf{P} - \mathbf{k} \,. \tag{A.1}$$

This amplitude is off shell in general. It is given in TOPT by

$$i\overline{\mathcal{M}}_{2,L} = i\overline{\mathcal{B}}_{2,L} \frac{1}{1 - iD_F i\overline{\mathcal{B}}_{2,L}} \,, \tag{A.2}$$

which, using the on-shell projection result Eq. (3.57), as well as the definition of $\overline{\mathcal{K}}_{2,L}$,

Eq. (3.65), can be rewritten as

$$i\overline{\mathcal{M}}_{2,L} = i\overline{\mathcal{K}}_{2,L}\frac{1}{1 - i\widetilde{F}i\overline{\mathcal{K}}_{2,L}}\,. \tag{A.3}$$

If we project external indices on shell, so that all matrices are square, we can invert this result to obtain

$$\left(\overline{\mathcal{M}}^{\text{on}}_{2,L}\right)^{-1} = \left(\overline{\mathcal{K}}^{\text{on}}_{2,L}\right)^{-1} + \widetilde{F}\,, \tag{A.4}$$

where the "on" labels indicate that both amplitudes must be completely on shell for the equation to hold.

The next step is to take the infinite-volume limit in such a way that the left-hand side goes over to the (inverse of the) on-shell infinite-volume scattering amplitude. To obtain this limit, we first remove extraneous common factors (introduced by carrying along the spectator) by multiplying Eq. (A.4) by the matrix $2\omega L^3$ [defined in Eq. (C.4)] and dropping the δ_{kp} that is common to all three terms. We then take the $L \to \infty$ limit holding $E_{2,k}$ and $\mathbf{P}_{2,k}$ fixed, which ensures that in the CMF of the scattering pair, the momentum of each particle in the pair is held fixed at $q^*_{2,k}$. Following the prescription used in HS2, we make this limit well defined by reintroducing the factors of $i\epsilon$ into the energy denominators contained in the factors of D_F in Eq. (A.2), and only then turning sums into integrals. The result is

$$\delta_{\ell\ell'}\delta_{mm'}\left[\mathcal{M}_2^{(\ell)}(q^*_{2,k})\right]^{-1} = \delta_{\ell\ell'}\delta_{mm'}\left[\mathcal{K}_2^{(\ell)}(q^*_{2,k})\right]^{-1} + \delta_{\ell\ell'}\delta_{mm'}\widetilde{\rho}^{(\ell)}_{\text{PV}}(q^{*2}_{2,k})\,, \tag{A.5}$$

where $\mathcal{M}_2^{(\ell)}$ is the ℓth partial wave of $\mathcal{M}_2$,

$$\widetilde{\rho}^{(\ell)}_{\text{PV}}(q^{*2}_{2,k}) \equiv H(\mathbf{k})\left[\widetilde{\rho}(q^{*2}_{2,k}) + \frac{1}{32\pi^2}I^{(\ell)}_{\text{PV}}(q^{*2}_{2,k})\right]\,, \tag{A.6}$$

with the phase space factor given by

$$\widetilde{\rho}(q^{*2}_{2,k}) \equiv \frac{1}{16\pi E^*_{2,k}}\begin{cases} -i|q^*_{2,k}| & q^{*2}_{2,k} > 0 \\ \;\;|q^*_{2,k}| & q^{*2}_{2,k} \le 0 \end{cases}\,, \tag{A.7}$$

and $I_{\rm PV}^{(\ell)}$ is an arbitrary real, smooth function. Here we have assumed that $H(\mathbf{k})$ is, in fact, a function of $q_{2,k}^{*2}$, as is the case in all numerical work to date [36, 39, 51, 76]. The second term on the right-hand side of Eq. (A.5) is obtained using Eqs. (22)-(26) of HS1 (where the standard PV prescription is defined in the context of $\widetilde{F}$), together with Eq. (3.5) of Ref. [36] (where the generalized PV prescription is defined), which together lead to

$$2\omega_k L^3 \widetilde{F}_{k\ell m;p\ell' m'} = \delta_{kp}\left[F^{i\epsilon}_{\ell m;\ell' m'}(\mathbf{k}) + \delta_{\ell\ell'}\delta_{mm'}\widetilde{\rho}^{(\ell)}_{\rm PV}(q^{*2}_{2,k})\right] , \tag{A.8}$$

where

$$F^{i\epsilon}_{\ell m;\ell' m'}(\mathbf{k}) \equiv \frac{H(\mathbf{k})}{2!}\left[\frac{1}{L^3}\sum_{\mathbf{a}}^{\rm UV} - \int_{\mathbf{a}}^{\rm UV}\right]\frac{1}{2\omega_a}\frac{\mathcal{Y}_{\ell m}(\mathbf{a}^*_k)}{q^{*\ell}_{2,k}}\frac{1}{2\omega_b(E-\omega_k-\omega_a-\omega_b+i\epsilon)}\frac{\mathcal{Y}_{\ell' m'}(\mathbf{a}^*_k)}{q^{*\ell'}_{2,k}} \tag{A.9}$$

is the quantity defined in Eq. (24) of HS1. Note that $F^{i\epsilon} \to 0$ in the "$i\epsilon$" $L \to \infty$ limit.

A.3 Algebraic matrix manipulations

In the main text, we encounter several times [see for example, Eqs. (3.60) and (3.85)] matrix expressions of the form

$$m_2 + m_3 = (c_2 + c_3)\frac{1}{1-(f+g)(c_2+c_3)} , \tag{A.10}$$

$$= \frac{1}{1-(c_2+c_3)(f+g)}(c_2+c_3) , \tag{A.11}$$

$$m_2 = c_2\frac{1}{1-fc_2} \quad \Rightarrow \quad m_2^{-1} = c_2^{-1} - f , \tag{A.12}$$

from which we wish to determine an expression for m_3. For the sake of clarity and completeness, we collect here the algebraic steps that lead to the form used in the main text. We stress that these and similar steps have been repeatedly used in previous RFT papers, i.e. in HS1, HS2, and Refs. [34–37].

As a first step, we define d_{23} as $m_2 + m_3$ evaluated when $c_3 \to 0$:

$$d_{23} \equiv c_2 \frac{1}{1-(f+g)c_2} \,. \tag{A.13}$$

This can be rewritten as

$$d_{23}^{-1} = c_2^{-1} - f - g = m_2^{-1} - g \quad \Rightarrow \quad d_{23} = m_2 \frac{1}{1-gm_2} = m_2 + d_3 \,, \quad d_3 \equiv m_2 g m_2 \frac{1}{1-gm_2} \,. \tag{A.14}$$

In words, m_2 is obtained by summing all the c_2 terms joining by factors of f, and d_{23} is then obtained by putting in factors of g in all possible ways.

Our aim is to pull out the c_3 dependence of m_3 from Eq. (A.10). The steps are

$$\begin{aligned}
m_2 + m_3 - d_{23} &= (1 + c_3 c_2^{-1}) \frac{1}{c_2^{-1} - (f+g)(1+c_3 c_2^{-1})} - d_{23} && \text{(A.15)} \\
&= (1 + c_3 c_2^{-1}) \frac{1}{d_{23}^{-1} - (f+g) c_3 c_2^{-1}} - d_{23} && \text{(A.16)} \\
&= (1 + c_3 c_2^{-1}) \frac{1}{1 - d_{23}(f+g) c_3 c_2^{-1}} d_{23} - d_{23} && \text{(A.17)} \\
&= c_3 c_2^{-1} \frac{1}{1 - d_{23}(f+g) c_3 c_2^{-1}} d_{23} + d_{23}(f+g) c_3 c_2^{-1} \frac{1}{1 - d_{23}(f+g) c_3 c_2^{-1}} d_{23} && \text{(A.18)} \\
&= [1 + d_{23}(f+g)] c_3 c_2^{-1} \frac{1}{1 - d_{23}(f+g) c_3 c_2^{-1}} d_{23} && \text{(A.19)} \\
&= \frac{1}{1 - c_2(f+g)} c_3 \frac{1}{1 - c_2^{-1} d_{23}(f+g) c_3} c_2^{-1} d_{23} \,. && \text{(A.20)}
\end{aligned}$$

This can be further simplified using

$$c_2^{-1} d_{23} = \frac{1}{1-(f+g)c_2} = 1 + (f+g) d_{23} \,. \tag{A.21}$$

A useful way of rewriting the final result is

$$m_3 = d_3 + [1 + d_{23}(f+g)] c_3 \frac{1}{1 - [1 + (f+g)d_{23}](f+g)c_3} [1 + (f+g) d_{23}] \,, \tag{A.22}$$

which is used to obtain, for example, Eqs. (3.72) and (3.86).

Clearly this derivation relies on the existence of the various inverse matrices that appear, and thus, in particular, it assumes that the matrices are square.

A.4 Asymmetrization identities

In this appendix we derive the identities needed in Sec. 3.4.2 to asymmetrize the HS2 amplitude $\mathcal{M}_{3,L}^{(u,u)}$. These results are extensions of the symmetrization identities derived in HS1 [see Eqs. (163) and (198) of that work and surrounding discussions].

A.4.1 General asymmetric kernels

Here we review the notation developed in HS1 to describe general asymmetric kernels, e.g. $\mathcal{K}_{\text{df},3}^{(u,u)}$, as well as collecting some of their key properties. To lighten the notation we denote a generic asymmetric kernel as $Z^{(u)}$, where we only make explicit the symmetry status of one "side" of the kernel. The meaning of the superscripts (u) and (u,u) have been explained in the main text, with the key point being that, in the $\{k\ell m\}$ index space describing three on-shell particles, the momentum label k is always associated with the spectator.

We only consider amplitudes that are fully on shell, denoting the four-momenta of the three particles as k (spectator), p, and $b = P - k - p$ (the interacting pair). The discussion in Sec. 3.2.3 explains the procedure for on-shell projection that defines $Z_{k\ell m}^{(u)}$ (where again we show only one set of indices). Using Eq. (3.31), the full momentum dependence of $Z^{(u)}$ is given by

$$Z^{(u)}(\mathbf{k}, \widehat{\mathbf{p}}_k^*) = Z_{k\ell m}^{(u)} \sqrt{4\pi} Y_{\ell m}(\widehat{\mathbf{p}}_k^*)\,, \tag{A.23}$$

where $\mathbf{p}_k^*$ is obtained by the boost of Eqs. (B.15) and (B.16) (which is equivalent to the boost of HS1 since the particles are on shell). Since the kernel is on shell, it depends only on the direction of $\mathbf{p}_k^*$ and not its magnitude (for given $\mathbf{k}$). Because we are considering identical particles, $Z^{(u)}$ is invariant under $p \leftrightarrow b$ interchange. Since this interchange is effected in our

variables by changing the sign of $\widehat{\mathbf{p}}_k^*$, $Z^{(u)}$ satisfies

$$Z^{(u)}(\mathbf{k},\widehat{\mathbf{p}}_k^*) = Z^{(u)}(\mathbf{k},\widehat{\mathbf{b}}_k^*) = Z^{(u)}(\mathbf{k},-\widehat{\mathbf{p}}_k^*) \quad \Leftrightarrow \quad Z^{(u)}_{k\ell m} = 0 \text{ if } \ell \text{ is odd}\,. \tag{A.24}$$

We next define asymmetric kernels with superscript (s). Here the momentum k is assigned to one of the interacting pair, while p is assigned to the spectator:

$$Z^{(s)}(\mathbf{k},\widehat{\mathbf{p}}_k^*) = Z^{(s)}_{k\ell' m'}\sqrt{4\pi}Y_{\ell' m'}(\widehat{\mathbf{p}}_k^*) \equiv Z^{(u)}(\mathbf{p},\widehat{\mathbf{k}}_p^*)\,. \tag{A.25}$$

We stress that there is a one-to-one relation between $\{\mathbf{k},\widehat{\mathbf{p}}_k^*\}$ and $\{\mathbf{p},\widehat{\mathbf{k}}_p^*\}$, i.e. one set of variables uniquely determines the other.

In the third option, both k and p are assigned to the interacting pair. Since this configuration is obtained from the $Z^{(s)}$ assignment by interchanging p and b, we have

$$Z^{(\tilde{s})}(\mathbf{k},\widehat{\mathbf{p}}_k^*) = Z^{(\tilde{s})}_{k\ell' m'}\sqrt{4\pi}Y_{\ell' m'}(\widehat{\mathbf{p}}_k^*) \equiv Z^{(s)}(\mathbf{k},-\widehat{\mathbf{p}}_k^*) \quad \Rightarrow \quad Z^{(\tilde{s})}_{k\ell m} = (-1)^\ell Z^{(s)}_{k\ell m}\,. \tag{A.26}$$

In addition, using the one-to-one relation between $\{\mathbf{k},\widehat{\mathbf{p}}_k^*\}$ and $\{\mathbf{b},\widehat{\mathbf{p}}_b^*\}$, and the symmetry of $Z^{(u)}$ under $p \leftrightarrow b$, we have

$$Z^{(\tilde{s})}(\mathbf{k},\widehat{\mathbf{p}}_k^*) = Z^{(u)}(\mathbf{b},\widehat{\mathbf{p}}_b^*)\,. \tag{A.27}$$

We will also need the result from HS1 that $\widetilde{F}$ vanishes if $\ell' + \ell$ is odd:

$$(-1)^{\ell'}\widetilde{F}_{k'\ell' m';k\ell m}(-1)^{\ell} = \widetilde{F}_{k'\ell' m';k\ell m}\,. \tag{A.28}$$

This holds for all boosts that agree on shell, and thus for the Wu boost we use in this work. Together with the results in Eqs. (A.24) and (A.26), this implies the following useful set of equalities,

$$X^{(u)}\widetilde{F}Z^{(\tilde{s})} = X^{(u)}\widetilde{F}Z^{(s)}\,,\;\; X^{(\tilde{s})}\widetilde{F}Z^{(u)} = X^{(s)}\widetilde{F}Z^{(u)}\,,\;\; X^{(s)}\widetilde{F}Z^{(s)} = X^{(\tilde{s})}\widetilde{F}Z^{(\tilde{s})}\,,\;\; X^{(\tilde{s})}\widetilde{F}Z^{(s)} = X^{(s)}\widetilde{F}Z^{(\tilde{s})}\,, \tag{A.29}$$

where X is another kernel.

The symmetric on-shell amplitude is obtained by adding all three attachments

$$Z \equiv Z^{(u+s+\tilde{s})} = Z^{(u)} + Z^{(s)} + Z^{(\tilde{s})}, \tag{A.30}$$

where we are using the convention that adding superscripts corresponds to adding the underlying amplitudes. Equation (A.30) is the on-shell version of the off-shell symmetrization definition given in Eq. (3.84).

A.4.2 Deriving Eqs. (3.102) and (3.103)

The first two asymmetrization identities of Sec. 3.4.2 have essentially been derived in Eq. (163)-(165) of HS1. Here we need a slightly more explicit form, so we repeat the essential steps.

We begin with Eq. (3.102). For concreteness, we act the identity on the vector of amplitudes $\left(Z^{(u)}, Z^{(s+\tilde{s})}\right)$. Then the identity to be demonstrated can be rewritten as

$$\overrightarrow{\Delta} \equiv X^{(u)}[\tilde{F}Z^{(s)} + \tilde{F}Z^{(\tilde{s})} - \tilde{G}Z^{(u)}] = -X^{(u)}\overrightarrow{\mathcal{I}}_G Z^{(u)}\,, \tag{A.31}$$

where $\overrightarrow{\Delta}$ is simply a shorthand for the left-hand side of this equation, with the arrow pointing in the direction of the amplitudes that are being asymmetrized. Using results from Eq. (A.29), this can be written as

$$\overrightarrow{\Delta} = X^{(u)}(2\tilde{F}Z^{(s)} - \tilde{G}Z^{(u)}) = X^{(u)}(2\widetilde{\Sigma}_F Z^{(s)} - 2\widetilde{I}_F Z^{(s)} - \tilde{G}Z^{(u)})\,, \tag{A.32}$$

where the second form is obtained by splitting $\widetilde{F}$, Eq. (C.9), into its sum and integral part, $\widetilde{F} = \widetilde{\Sigma}_F - \widetilde{I}_F$. The explicit form for $\widetilde{\Sigma}_F$ is given in Eq. (A.82). Note that the integral $\widetilde{I}_F$ differs from the integral *operator* $\widetilde{\mathcal{I}}_F$ of Eq. (3.56), the latter being denoted by a calligraphic symbol. We regulate the UV by inserting a factor of $H(\mathbf{p})$, and choose the relativistic form of the pole term, both choices that only change $\widetilde{F}$ by exponentially suppressed terms. Then,

using the definition of $\widetilde{G}$, Eq. (C.10), we find

$$X^{(u)}\left[2\widetilde{\Sigma}_F Z^{(s)} - \widetilde{G} Z^{(u)}\right] = \sum_{\mathbf{k}} \frac{1}{2\omega_k L^3} \sum_{\mathbf{p}} \frac{1}{2\omega_p L^3} \sum_{\ell m} X^{(u)}_{k\ell m} \frac{\mathcal{Y}_{\ell m}(\mathbf{p}_k^*)}{q_{2,k}^{*\ell}} \frac{H(\mathbf{k})H(\mathbf{p})}{b^2 - m^2}$$
$$\times \left\{ \sum_{\ell' m'} \left(\frac{p_k^*}{q_{2,k}^*}\right)^{\ell'} \sqrt{4\pi} Y_{\ell' m'}(\widehat{\mathbf{p}}_k^*) Z^{(s)}_{k\ell' m'} - \sum_{\ell' m'} \left(\frac{k_p^*}{q_{2,p}^*}\right)^{\ell'} \sqrt{4\pi} Y_{\ell' m'}(\widehat{\mathbf{k}}_p^*) Z^{(u)}_{p\ell' m'} \right\} . \quad \text{(A.33)}$$

The key observation is now that the expression in curly braces vanishes when $b^2 = m^2$, i.e. when all three particles are on shell. For then $p_k^* = q_{2,k}^*$ and $k_p^* = q_{2,p}^*$, so the sums over ℓ' and m' can be done, leading to $Z^{(s)}(\mathbf{k}, \widehat{\mathbf{p}}_k^*) - Z^{(u)}(\mathbf{p}, \widehat{\mathbf{k}}_p^*)$, which vanishes because of Eq. (A.25). Because of this cancellation, the sum over $\mathbf{p}$ can be replaced by an integral. This integral requires no pole prescription, but if we wish to separate the two terms in curly braces, then we must choose a prescription, and we use the generalized PV prescription. Then the first term in curly braces gives $2\widetilde{I}_F$, which cancels the $-2\widetilde{I}_F$ term in Eq. (A.32). What remains is

$$\overrightarrow{\Delta} = -\sum_{\mathbf{k}} \frac{1}{2\omega_k L^3} \mathrm{PV} \int_{\mathbf{p}} \frac{1}{2\omega_p} X^{(u)}_{k\ell m} G^b_{k\ell m; p\ell' m'} Z^{(u)}_{p\ell' m'} , \quad \text{(A.34)}$$

where G^b is defined in Eq. (3.44). What happens to the sum over $\mathbf{k}$ depends on the form of $X^{(u)}$. If $X^{(u)} = \overline{\mathcal{M}}_{2,L}$, which contains a Kronecker delta, $\mathbf{k}$ is set equal to the external spectator momentum. If $X^{(u)}$ is a three-particle amplitude such as $\mathcal{D}_L^{(u,u)}$, then $\mathbf{k}$ is an internal index and the sum over it can be converted to an integral, since the PV integration over $\mathbf{p}$ leads to a smooth function. In either case, $X^{(u)}$ and $Z^{(u)}$ are sewed together by an integral operator. We define $\overrightarrow{\mathcal{I}}_G$ to be this integral operator, leading to the right-hand side of the identity Eq. (A.31). It is similar to the operator $\widetilde{\mathcal{I}}_F$, and thus we use a similar name.

To summarize, in the difference $\overrightarrow{\Delta}$, the terms cancel exactly on shell, allowing the sums to be replaced by (PV-regulated) integrals. Once this is done, $\widetilde{F}$ vanishes, since it is a sum-integral difference. Thus one simply ends up with an integral over the $-\widetilde{G}$ contribution. We note that the argument holds for both choices of boost to the CMF of the scattered pair

considered in the main text, i.e. the Wu boost and the boost used in HS1. One needs only to use the same boost in $\widetilde{G}$ and $\overrightarrow{\mathcal{I}}_G$.

The argument for the second identity, Eq. (3.103), is essentially the horizontal reflection of that for Eq. (3.102), and we do not repeat the steps. The only change is that the directionality is reversed, leading to the integral operator $\overleftarrow{\mathcal{I}}_G$, which asymmetrizes to the left.

A.4.3 Derivation of Eq. (3.104)

To derive Eq. (3.104), we make it concrete by applying $(X^{(u)}, X^{(s+\tilde{s})})$ on the left and $(Z^{(u)}, Z^{(s+\tilde{s})})$ on the right. Since X and Z are stand-ins for $\mathcal{K}_{\text{df},3}$, they are three-particle amplitudes for which the spectator momentum labels are summed, and not constrained by a Kronecker delta. We denote the difference between the left-hand side of Eq. (3.104) and the $\widetilde{F} + \widetilde{G}$ term on the right-hand side by $\overleftrightarrow{\Delta}$. Our aim is to show that this is an integral operator. We begin by breaking it into four parts

$$3\overleftrightarrow{\Delta} \equiv X^{(u+s+\tilde{s})}\widetilde{F}Z^{(u+s+\tilde{s})} - 3X^{(u)}(\widetilde{F}+\widetilde{G})Z^{(u)} \tag{A.35}$$

$$= \overleftrightarrow{\Delta}_1 + \overleftrightarrow{\Delta}_2 + \overleftrightarrow{\Delta}_3 + \overleftrightarrow{\Delta}_4\,, \tag{A.36}$$

where

$$\overleftrightarrow{\Delta}_1 = X^{(u)}\widetilde{F}Z^{(s+\tilde{s})} - X^{(u)}\widetilde{G}Z^{(u)}\,, \tag{A.37}$$

$$\overleftrightarrow{\Delta}_2 = X^{(s+\tilde{s})}\widetilde{F}Z^{(u)} - X^{(u)}\widetilde{G}Z^{(u)}\,, \tag{A.38}$$

$$\overleftrightarrow{\Delta}_3 = X^{(s)}\widetilde{F}Z^{(s)} + X^{(\tilde{s})}\widetilde{F}Z^{(\tilde{s})} - 2X^{(u)}\widetilde{F}Z^{(u)}\,, \tag{A.39}$$

$$\overleftrightarrow{\Delta}_4 = X^{(\tilde{s})}\widetilde{F}Z^{(s)} + X^{(s)}\widetilde{F}Z^{(\tilde{s})} - X^{(u)}\widetilde{G}Z^{(u)}\,. \tag{A.40}$$

The first two parts can be evaluated using the identities Eq. (3.102) and (3.103), leading to

$$\overleftrightarrow{\Delta}_1 = -X^{(u)}\overrightarrow{\mathcal{I}}_G Z^{(u)} \quad \text{and} \quad \overleftrightarrow{\Delta}_2 = -X^{(u)}\overleftarrow{\mathcal{I}}_G Z^{(u)}\,. \tag{A.41}$$

For the remaining two parts a new analysis is needed.

For $\overleftrightarrow{\Delta}_3$, using the third result in Eq. (A.29), we obtain

$$\overleftrightarrow{\Delta}_3 = 2X^{(s)}\widetilde{F}Z^{(s)} - 2X^{(u)}\widetilde{F}Z^{(u)}\,. \tag{A.42}$$

Separating the $\widetilde{F}$'s into sum and integral parts, we have

$$\overleftrightarrow{\Delta}_3 \equiv \overleftrightarrow{\Delta}_{3\Sigma} - \overleftrightarrow{\Delta}_{3I}\,, \tag{A.43}$$

$$\overleftrightarrow{\Delta}_{3\Sigma} = 2X^{(s)}\widetilde{\Sigma}_F Z^{(s)} - 2X^{(u)}\widetilde{\Sigma}_F Z^{(u)}\,, \tag{A.44}$$

$$\overleftrightarrow{\Delta}_{3I} = 2X^{(s)}\widetilde{I}_F Z^{(s)} - 2X^{(u)}\widetilde{I}_F Z^{(u)}\,. \tag{A.45}$$

The integral part can be converted into a double integral because of the smoothness of the first PV-regulated integral,

$$\overleftrightarrow{\Delta}_{3I} = \int_{\mathbf{k}} \mathrm{PV}\int_{\mathbf{p}} \left\{ X^{(s)}_{k\ell' m'} F^b_{\ell' m';\ell m}(\mathbf{k},\mathbf{p}) Z^{(s)}_{k\ell m} - X^{(u)}_{k\ell' m'} F^b_{\ell' m';\ell m}(\mathbf{k},\mathbf{p}) Z^{(u)}_{k\ell m} \right\}\,, \tag{A.46}$$

where (again regulating the $\mathbf{p}$ integral in the UV with $H(\mathbf{p})$, but here keeping the original form of the pole)

$$F^b_{\ell' m';\ell m}(\mathbf{k},\mathbf{p}) = \frac{\mathcal{Y}_{\ell' m'}(\mathbf{p}^*_k)}{q^{*\ell'}_{2,k}} \frac{H(\mathbf{k})H(\mathbf{p})}{2\omega_k 2\omega_p 2\omega_b (E-\omega_k-\omega_p-\omega_b)} \frac{\mathcal{Y}_{\ell m}(\mathbf{p}^*_k)}{q^{*\ell}_{2,k}}\,. \tag{A.47}$$

The sum part $\overleftrightarrow{\Delta}_{3\Sigma}$ has the same form as (A.46) except that both integrals are replaced by sums. Naively we might expect the two terms to cancel, since the difference between (s) and (u) quantities is just a $\mathbf{k} \leftrightarrow \mathbf{p}$ relabeling. To investigate this we interchange the dummy variables $\mathbf{k}$ and $\mathbf{p}$ for the second term in the sum, resulting in[1]

$$\overleftrightarrow{\Delta}_{3\Sigma} = \frac{1}{L^6}\sum_{\mathbf{k},\mathbf{p}} \left\{ X^{(s)}_{k\ell' m'} F^b_{\ell' m';\ell m}(\mathbf{k},\mathbf{p}) Z^{(s)}_{k\ell m} - X^{(u)}_{p\ell' m'} F^b_{\ell' m';\ell m}(\mathbf{p},\mathbf{k}) Z^{(u)}_{p\ell m} \right\}\,. \tag{A.48}$$

[1] An alternative approach, used, for example, in the analysis around Eq. (196) of HS1, is to use the sum-integral identity in reverse to write the original expression for $\overleftrightarrow{\Delta}_3$ in terms of *off-shell* amplitudes, which are more easily manipulated. We do not follow this approach, however, since it requires accounting for the difference between off-shell amplitudes calculated using Feynman diagrams and TOPT. Instead, we work entirely with on-shell amplitudes.

The summand has a pole at each of the free three-particle energies, with residue

$$\frac{1}{8\omega_k\omega_p\omega_b}\left[X^{(s)}(\mathbf{k},\widehat{\mathbf{p}}_k^*)Z^{(s)}(\mathbf{k},\widehat{\mathbf{p}}_k^*)-X^{(u)}(\mathbf{p},\widehat{\mathbf{k}}_p^*)Z^{(u)}(\mathbf{p},\widehat{\mathbf{k}}_p^*)\right]\Bigg|_{\text{on shell}}, \tag{A.49}$$

which vanishes due to Eq. (A.25). Thus the sum can be converted into an integral. We choose to do the $\mathbf{p}$ integral first using the generalized PV prescription, leading to

$$\overleftrightarrow{\Delta}_{3\Sigma}=\int_{\mathbf{k}}\mathrm{PV}\int_{\mathbf{p}}\left\{X^{(s)}_{k\ell'm'}F^b_{\ell'm';\ell m}(\mathbf{k},\mathbf{p})Z^{(s)}_{k\ell m}-X^{(u)}_{p\ell'm'}F^b_{\ell'm';\ell m}(\mathbf{p},\mathbf{k})Z^{(u)}_{p\ell m}\right\}. \tag{A.50}$$

As far as we can see, this difference does not vanish. What we have achieved, however, is to convert the sum part of $\overleftrightarrow{\Delta}_3$ into an integral. Subtracting from this the result from Eq. (A.46), the terms involving (s) quantities cancel, leading to

$$\overleftrightarrow{\Delta}_3=\int_{\mathbf{k}}\mathrm{PV}\int_{\mathbf{p}}\left\{X^{(u)}_{k\ell'm'}F^b_{\ell'm';\ell m}(\mathbf{k},\mathbf{p})Z^{(u)}_{k\ell m}-X^{(u)}_{p\ell'm'}F^b_{\ell'm';\ell m}(\mathbf{p},\mathbf{k})Z^{(u)}_{p\ell m}\right\} \tag{A.51}$$

$$\equiv X^{(u)}\overleftrightarrow{\mathcal{I}}_F Z^{(u)}. \tag{A.52}$$

We have not found a useful way to simplify this further, but this result is sufficient for our purposes. The key point is that it involves an integral operator that acts on the (u) components of the amplitudes.

Finally, we consider $\overleftrightarrow{\Delta}_4$, Eq. (A.40), which can be analyzed using a combination of the methods used above. We only give an outline of the calculation. First, using Eq. (A.29), we see that the first two terms are the same, so that

$$\overleftrightarrow{\Delta}_4=X^{(\tilde{s})}2\widetilde{F}Z^{(s)}-X^{(u)}\widetilde{G}Z^{(u)}=X^{(\tilde{s})}2\widetilde{\Sigma}_F Z^{(s)}-X^{(u)}\widetilde{G}Z^{(u)}-X^{(\tilde{s})}2\widetilde{I}_F Z^{(s)}. \tag{A.53}$$

The first two terms involve double sums over $\mathbf{k}$ and $\mathbf{p}$. For the $\widetilde{G}$ term we replace the sum over $\mathbf{k}$ with that over $\mathbf{b}$, which is simply a change of variables, and then rename $\mathbf{k}$ as $\mathbf{b}$ and vice versa. Then the residue of the pole in E is

$$\frac{1}{8\omega_k\omega_p\omega_b}\left[X^{(\tilde{s})}(\mathbf{k},\widehat{\mathbf{p}}_k^*)Z^{(s)}(\mathbf{k},\widehat{\mathbf{p}}_k^*)-X^{(u)}(\mathbf{b},\widehat{\mathbf{p}}_b^*)Z^{(u)}(\mathbf{p},\widehat{\mathbf{b}}_p^*)\right]\Bigg|_{\text{on shell}}. \tag{A.54}$$

The identities Eqs. (A.24) and (A.27) imply that this vanishes. Thus, once again, we can replace the sums by (PV-regulated) integrals. This sends $\widetilde{\Sigma}_F \to \widetilde{I}_F$, canceling the existing $\widetilde{I}_F$ term (which, as above, can be converted to a double integral) and leaving only the integral over the $\widetilde{G}$ term.

In this way we find

$$\overleftrightarrow{\Delta}_4 = -X^{(u)} \int_{\mathbf{k}} \mathrm{PV} \int_{\mathbf{p}} Z^{(u)}_{b\ell' m'} G^b_{b\ell' m; p\ell m} Z^{(u)}_{p\ell m} \equiv X^{(u)} \overleftrightarrow{\mathcal{I}}_G Z^{(u)} \,. \tag{A.55}$$

We use a bidirectional arrow since the order of integrals here is irrelevant (as long as the first one is done using the PV prescription). This can be shown by starting from the form involving $X^{(s)} \widetilde{F} Z^{(\bar{s})}$.

Pulling together the results for the four components, given in Eqs. (A.41), (A.52), and (A.55), we have

$$\overleftrightarrow{\Delta} = -\frac{1}{3} X^{(u)} \left(\overrightarrow{\mathcal{I}}_G + \overleftarrow{\mathcal{I}}_G - \overleftrightarrow{\mathcal{I}}_F + \overleftrightarrow{\mathcal{I}}_G \right) Z^{(u)} \tag{A.56}$$

$$\equiv X^{(u)} \otimes_G Z^{(u)} \,, \tag{A.57}$$

where in the second line we have introduced a compact notation. All that matters for the argument in the main text is that this is a known integral joining operator acting on the asymmetric (u) kernels. As before, this result holds independent of the choice of boost.

A.5 Relating $\widetilde{\mathcal{K}}^{(u,u)}_{\mathrm{df},3}$ to $\mathcal{M}_3$

The aim in this appendix is to take an appropriate infinite-volume limit of Eq. (3.86) and obtain integral equations relating $\mathcal{M}_3$ to $\widetilde{\mathcal{K}}^{(u,u)}_{\mathrm{df},3}$. All quantities in this subsection will be on shell, so that our $\mathcal{M}_{3,L}$, $\mathcal{M}_{2,L}$, and $\mathcal{D}^{(u,u)}_L$ are strictly the same as those in HS2. Since our result for $\widetilde{\mathcal{M}}^{(u,u)}_{3,L}$ is similar to that for the corresponding quantity $\mathcal{M}^{(u,u)}_{3,L}$ in HS2 [see Eq. (68) of that work], we can take over much of the analysis essentially without change.

The infinite-volume limit that is required has been described in Appendix A.2. It sends

$$[\mathcal{M}_{3,L}]_{k\ell m;p\ell' m'} \to \mathcal{M}_3(\mathbf{k},\mathbf{p})_{\ell m;\ell' m'}\,, \tag{A.58}$$

where now $\mathbf{k}$ and $\mathbf{p}$ are continuous variables. Analogous limits hold for $\widetilde{\mathcal{M}}_{3,L}^{(u,u)}$, $\mathcal{D}_L^{(u,u)}$, and $\widetilde{\mathcal{T}}_L^{(u,u)}$. As noted earlier, $\widetilde{\mathcal{K}}_{\mathrm{df},3}^{(u,u)}$ is already an infinite-volume quantity, so the only change is to replace discrete with continuous momenta. For the other quantities, we have

$$\lim_{L\to\infty}[\overline{\mathcal{M}}_{2,L}]_{k\ell m;p\ell' m'} = \overline{\delta}(\mathbf{k}-\mathbf{p})\mathcal{M}_2(\mathbf{k})_{\ell m;\ell' m'}\,, \tag{A.59}$$

$$\overline{\delta}(\mathbf{k}-\mathbf{p}) \equiv 2\omega_k(2\pi)^3\delta^3(\mathbf{k}-\mathbf{p}) \tag{A.60}$$

$$\mathcal{M}_2(\mathbf{k})_{\ell m;\ell' m'} = \delta_{\ell\ell'}\delta_{mm'}\mathcal{M}_2^{(\ell)}(q_{2,k}^*)\,, \tag{A.61}$$

where $\mathcal{M}_2^{(\ell)}$ is the ℓth partial wave of $\mathcal{M}_2$, while from Eq. (A.8) we read off that

$$\lim_{L\to\infty} 2\omega_k L^3 \widetilde{F}_{k\ell m;p\ell' m'} 2\omega_p L^3 = \overline{\delta}(\mathbf{k}-\mathbf{p})\widetilde{\rho}_{\mathrm{PV}}(\mathbf{k})_{\ell m;\ell' m'}\,, \tag{A.62}$$

$$\widetilde{\rho}_{\mathrm{PV}}(\mathbf{k})_{\ell m;\ell' m'} = \delta_{\ell\ell'}\delta_{mm'}\widetilde{\rho}_{\mathrm{PV}}^{(\ell)}(q_{2,k}^{*2})\,, \tag{A.63}$$

where $\widetilde{\rho}_{\mathrm{PV}}^{(\ell)}$, given in Eq. (C.7), is a smooth function, and, finally,

$$\lim_{L\to\infty} 2\omega_k L^3\, \widetilde{G}_{k\ell m;p\ell' m'} 2\omega_p L^3 \equiv G^{\infty}_{\ell m;\ell' m'}(\mathbf{k},\mathbf{p}) = \frac{\mathcal{Y}_{\ell m}(\mathbf{p}_k^*)}{q_{2,k}^{*\ell}} \frac{H(\mathbf{k})H(\mathbf{p})}{b^2-m^2+i\epsilon} \frac{\mathcal{Y}_{\ell' m'}(\mathbf{k}_p^*)}{q_{2,p}^{*\ell'}}\,. \tag{A.64}$$

The latter function, taken from HS2, is simply G^b, Eq. (3.44), but with the $i\epsilon$ added back, and the discrete momentum indices converted to continuous arguments.

When the $L\to\infty$ limit is taken in this way, it is straightforward to see that the factors of $(2\omega L^3)^{-1}$ coming with $\widetilde{F}$ and $\widetilde{G}$ convert all momentum sums into integrals with Lorentz-invariant measure

$$\sum_{\mathbf{k}} \frac{1}{2\omega_k L^3} \xrightarrow{L\to\infty} \int \frac{d^3k}{2\omega_k(2\pi)^3} \equiv \int_{\mathbf{k}} \frac{1}{2\omega_k}\,. \tag{A.65}$$

Matrix equations involving geometric series then become integral equations. In particular,

Eq. (5.11) becomes

$$i\mathcal{D}^{(u,u)}(\mathbf{k},\mathbf{p}) = i\mathcal{M}_2(\mathbf{k})\int_s \frac{1}{2\omega_s} iG^{\infty}(\mathbf{k},\mathbf{s})\left[\overline{\delta}(\mathbf{s}-\mathbf{p})i\mathcal{M}_2(\mathbf{p}) + i\mathcal{D}^{(u,u)}(\mathbf{s},\mathbf{p})\right], \tag{A.66}$$

where angular-momentum indices are implicit. This is identical to Eq. (85) of HS2. The core geometric series in Eq. (3.86) becomes an integral equation for $\widetilde{\mathcal{T}}^{(u,u)}$,

$$\begin{aligned} i\widetilde{\mathcal{T}}^{(u,u)}(\mathbf{k},\mathbf{p}) = i\widetilde{\mathcal{K}}^{(u,u)}_{\mathrm{df},3}(\mathbf{k},\mathbf{p}) + \int_{\mathbf{r},\mathbf{s},\mathbf{t}} \frac{1}{2\omega_r 2\omega_s 2\omega_t}\left[\overline{\delta}(\mathbf{k}-\mathbf{r})i\widetilde{\rho}_{\mathrm{PV}}(\mathbf{k}) + iG^{\infty}(\mathbf{k},\mathbf{r})\right] \\ \times\left[\overline{\delta}(\mathbf{r}-\mathbf{s})i\mathcal{M}_2(\mathbf{r}) + i\mathcal{D}^{(u,u)}(\mathbf{r},\mathbf{s})\right]\left[\overline{\delta}(\mathbf{s}-\mathbf{t})i\widetilde{\rho}_{\mathrm{PV}}(\mathbf{s}) + iG^{\infty}(\mathbf{s},\mathbf{t})\right] i\widetilde{\mathcal{T}}^{(u,u)}(\mathbf{t},\mathbf{p})\,. \end{aligned} \tag{A.67}$$

This differs from the corresponding equation in HS2 [Eq. (91) of that work] due to the asymmetry of our $\widetilde{\mathcal{K}}^{(u,u)}_{\mathrm{df},3}$, and the presence here of factors of $\widetilde{F}+\widetilde{G}$ in place of $\widetilde{F}$. Finally, the factors on either side of $\widetilde{\mathcal{T}}^{(u,u)}_L$ in Eq. (3.86) become integral operators. That on the left becomes

$$\widetilde{\mathcal{L}}^{(u,u)}(\mathbf{k},\mathbf{s}) = \overline{\delta}(\mathbf{k}-\mathbf{s}) + \int_{\mathbf{r}} \frac{1}{2\omega_r}\left[\overline{\delta}(\mathbf{k}-\mathbf{r})i\mathcal{M}_2(\mathbf{k}) + i\mathcal{D}^{(u,u)}(\mathbf{k},\mathbf{r})\right]\left[\overline{\delta}(\mathbf{r}-\mathbf{s})i\widetilde{\rho}_{\mathrm{PV}}(\mathbf{r}) + iG^{\infty}(\mathbf{r},\mathbf{s})\right], \tag{A.68}$$

while that on the right, $\widetilde{\mathcal{R}}^{(u,u)}$, is given by the horizontal reflection. These also differ from their analogs in HS2 ($\mathcal{L}^{(u,u)}$ and $\mathcal{R}^{(u,u)}$) by the presence here of contributions resulting from $\widetilde{F}+\widetilde{G}$ in place of $\widetilde{F}$.

Putting these pieces together, we obtain the final expression for $\widetilde{\mathcal{M}}^{(u,u)}_3$,

$$i\widetilde{\mathcal{M}}^{(u,u)}_3(\mathbf{k},\mathbf{p}) = i\mathcal{D}^{(u,u)}(\mathbf{k},\mathbf{p}) + \int_{\mathbf{r},\mathbf{s}} \frac{1}{2\omega_r 2\omega_s} i\widetilde{\mathcal{L}}^{(u,u)}(\mathbf{k},\mathbf{r})i\widetilde{\mathcal{T}}^{(u,u)}(\mathbf{r},\mathbf{s})i\widetilde{\mathcal{R}}^{(u,u)}(\mathbf{s},\mathbf{p})\,. \tag{A.69}$$

This is then symmetrized to obtain $\mathcal{M}_3(\mathbf{k},\mathbf{p})$. The symmetrization of on-shell quantities is given by the on-shell limit of Eq. (3.84), and has been discussed extensively in HS2 [see discussion around Eqs. (35)-(37) of that work].

One property of this result is that, despite the apparently Lorentz invariant form of the relations derived in this appendix, $\widetilde{\mathcal{K}}^{(u,u)}_{\mathrm{df},3}$ is not Lorentz invariant. Here by $\widetilde{\mathcal{K}}^{(u,u)}_{\mathrm{df},3}$ we refer to the form obtained after multiplying $\widetilde{\mathcal{K}}^{(u,u)}_{\mathrm{df},3}(\mathbf{k},\mathbf{p})_{\ell' m';\ell m}$ by spherical harmonics and

summing over angular momentum indices, i.e. the quantity that depends only on the external momenta. It cannot be Lorentz invariant because $\widetilde{\mathcal{M}}_3^{(u,u)}$ is not invariant, as its asymmetry is defined in terms of TOPT kernels, and these are frame dependent.

In summary, the relation between our asymmetric kernel $\widetilde{\mathcal{K}}_{\mathrm{df},3}^{(u,u)}$ and $\mathcal{M}_3$ is of a similar form to that between $\mathcal{K}_{\mathrm{df},3}$ and $\mathcal{M}_3$ obtained in HS2. The main point is that such a relation exists, so that our new quantization condition has the same logical status as that of HS1. We expect that solving the integral equations numerically (usually done by going back to the matrix form) will be of similar difficulty.

A.6 Deriving Eqs. (3.108) and (3.109)

In this appendix we provide some details of the derivation of Eqs. (3.108) and (3.109). We make extensive use of the following identities:

$$i\mathcal{D}_{23,L}^{(u,u)} = \frac{1}{1 - i\overline{\mathcal{K}}_2 i(\widetilde{F} + \widetilde{G})} i\overline{\mathcal{K}}_2 \tag{A.70}$$

$$= \left[1 + \frac{1}{1 - i\overline{\mathcal{K}}_2 i(\widetilde{F} + \widetilde{G})} i\overline{\mathcal{K}}_2 i(\widetilde{F} + \widetilde{G})\right] i\overline{\mathcal{K}}_2 \,, \tag{A.71}$$

$$i(\widetilde{F} + \widetilde{G})\left[1 + i\mathcal{D}_{23,L}^{(u,u)} i(\widetilde{F} + \widetilde{G})\right] = i(\widetilde{F} + \widetilde{G}) \frac{1}{1 - i\overline{\mathcal{K}}_2 i(\widetilde{F} + \widetilde{G})} = \frac{1}{1 - i(\widetilde{F} + \widetilde{G}) i\overline{\mathcal{K}}_2} i(\widetilde{F} + \widetilde{G}) \,, \tag{A.72}$$

where $\mathcal{D}_{23,L}^{(u,u)}$ is defined in Eq. (3.90).

We start from Eqs. (3.106) and (3.107). Using the identities (A.71) and (A.70) in turn, we find

$$i\mathcal{D}_{23,L}^{(u,u)}(-i\overrightarrow{\mathcal{I}}_G) i\mathcal{K}_{\mathrm{df},3}^{\prime(u,u)} = \left[1 + \frac{1}{1 - i\overline{\mathcal{K}}_2 i(\widetilde{F} + \widetilde{G})} i\overline{\mathcal{K}}_2 i(\widetilde{F} + \widetilde{G})\right] i\overline{\mathcal{K}}_2 (-i\overrightarrow{\mathcal{I}}_G) i\mathcal{K}_{\mathrm{df},3}^{\prime(u,u)} \tag{A.73}$$

$$= \left[1 + i\mathcal{D}_{23,L}^{(u,u)} i(\widetilde{F} + \widetilde{G})\right] i\overline{\mathcal{K}}_2 (-i\overrightarrow{\mathcal{I}}_G) i\mathcal{K}_{\mathrm{df},3}^{\prime(u,u)} \,, \tag{A.74}$$

so that the factor on the left-hand end of Eq. (3.106) can be written (when acting to the

right on $\mathcal{K}'^{(u,u)}_{\mathrm{df},3}$)

$$\left[1+i\mathcal{D}^{(u,u)}_{23,L}i(\widetilde{F}+\widetilde{G}-\overrightarrow{\mathcal{I}}_G)\right]=\left[1+i\mathcal{D}^{(u,u)}_{23,L}i(\widetilde{F}+\widetilde{G})\right]\left(1-i\overline{\mathcal{K}}_2i\overrightarrow{\mathcal{I}}_G\right)\,. \tag{A.75}$$

The factor on the right-hand end of Eq. (3.106) gives the horizontal reflection of this expression.

To simplify $\mathcal{T}^{(u,u)}_L$, Eq. (3.107), we first use (A.71) to obtain

$$i\overleftarrow{\mathcal{I}}_G i\mathcal{D}^{(u,u)}_{23,L}i\overrightarrow{\mathcal{I}}_G=i\overleftarrow{\mathcal{I}}_G\overline{\mathcal{K}}_2i\overrightarrow{\mathcal{I}}_G+i\overleftarrow{\mathcal{I}}_G\overline{\mathcal{K}}_2\frac{1}{1-i(\widetilde{F}+\widetilde{G})i\overline{\mathcal{K}}_2}i(\widetilde{F}+\widetilde{G})i\overline{\mathcal{K}}_2i\overrightarrow{\mathcal{I}}_G\,, \tag{A.76}$$

and then expand out the term that lies between factors of $\mathcal{K}^{(u,u)}_{\mathrm{df},3}$ using (A.72)

$$i(\widetilde{F}+\widetilde{G}+\otimes_G)+i(\widetilde{F}+\widetilde{G}-\overleftarrow{\mathcal{I}}_G)i\mathcal{D}^{(u,u)}_{23,L}i(\widetilde{F}+\widetilde{G}-\overrightarrow{\mathcal{I}}_G) \tag{A.77}$$

$$\begin{aligned}
&=i\otimes_G+i(\widetilde{F}+\widetilde{G})\frac{1}{1-i\overline{\mathcal{K}}_2i(\widetilde{F}+\widetilde{G})}\\
&\quad-i(\widetilde{F}+\widetilde{G})\frac{1}{1-i\overline{\mathcal{K}}_2i(\widetilde{F}+\widetilde{G})}i\overline{\mathcal{K}}_2i\overrightarrow{\mathcal{I}}_G\\
&\quad-i\overleftarrow{\mathcal{I}}_Gi\overline{\mathcal{K}}_2\frac{1}{1-i(\widetilde{F}+\widetilde{G})i\overline{\mathcal{K}}_2}i(\widetilde{F}+\widetilde{G})\\
&\quad+i\overleftarrow{\mathcal{I}}_G\overline{\mathcal{K}}_2i\overrightarrow{\mathcal{I}}_G+i\overleftarrow{\mathcal{I}}_G\overline{\mathcal{K}}_2\frac{1}{1-i(\widetilde{F}+\widetilde{G})i\overline{\mathcal{K}}_2}i(\widetilde{F}+\widetilde{G})i\overline{\mathcal{K}}_2i\overrightarrow{\mathcal{I}}_G
\end{aligned} \tag{A.78}$$

$$\begin{aligned}
&=i\otimes_2+i\overleftarrow{\mathcal{I}}_G\overline{\mathcal{K}}_2i\overrightarrow{\mathcal{I}}_G\\
&\quad+\left(1-i\overleftarrow{\mathcal{I}}_Gi\overline{\mathcal{K}}_2\right)\left[1+i(\widetilde{F}+\widetilde{G})i\mathcal{D}^{(u,u)}_{23,L}\right]i(\widetilde{F}+\widetilde{G})\left(1-i\overline{\mathcal{K}}_2i\overrightarrow{\mathcal{I}}_G\right)\,.
\end{aligned} \tag{A.79}$$

Inserting Eq. (A.75), its reflection, and Eq. (A.79) into Eqs. (3.106) and (3.107) and reorganizing leads to Eqs. (3.108) and (3.109).

A.7 $\widetilde{\Sigma}_F$ *approach*

In Sec. 3.2.3, we chose to deal with off-shell F cuts using the "$\widetilde{F}$ approach," which is essentially the standard strategy used in HS1 and subsequent RFT works. In this appendix we sketch an alternative method, which we refer to as the $\widetilde{\Sigma}_F$ approach.

The $\widetilde{\Sigma}_F$ and $\widetilde{F}$ approaches share the same goal, namely to rewrite quantities of the form

$$[X' D_F X]_{p'r';pr} = [X']_{p'r';k'a'} [D_F]_{k'a';ka} [X]_{ka;pr} \,, \qquad X' \in \{\widehat{A}', \overline{\mathcal{B}}_{2,L}, \mathcal{B}_3\} \,, \quad X \in \{\widehat{A}, \overline{\mathcal{B}}_{2,L}, \mathcal{B}_3\} \tag{A.80}$$

in terms of a part in which the "middle" indices are projected on-shell and a remainder. In the $\widetilde{\Sigma}_F$ approach, we use exactly the same strategy that we used to deal with G cuts in Sec. 3.2.3. The end result is an F-cut analog of Eq. (3.52):

$$X' D_F X = X' \left(\widetilde{\Sigma}_F + \delta \widetilde{F} \right) X \,. \tag{A.81}$$

Here

$$\left[\widetilde{\Sigma}_F \right]_{k'\ell'm';k\ell m} \equiv \frac{\delta_{k'k}}{2!} H(\mathbf{k}) \sum_{\mathbf{a}}^{\text{UV}} \frac{\mathcal{Y}_{\ell' m'}(\mathbf{a}_k^*)}{q_{2,k}^{*\ell'}} \frac{1}{2\omega_k L^3} \frac{1}{b_{ka}^2 - m^2} \frac{1}{2\omega_a L^3} \frac{\mathcal{Y}_{\ell m}(\mathbf{a}_k^*)}{q_{2,k}^{*\ell}} \tag{A.82}$$

is the analog of $\widetilde{G}$,[2] while $\delta \widetilde{F}$ plays the analogous role to $\delta \widetilde{G}$. In particular, $\delta \widetilde{F}$ accounts for all nonsingular off-shell contributions (with its exact definition depending on the choice of X' and X), and we can therefore treat it as an infinite-volume quantity by replacing all internal sums in $X' \delta \widetilde{F} X$ with integrals.

Two important differences between the $\widetilde{F}$ and $\widetilde{\Sigma}_F$ approaches are now clear. The first concerns the UV cutoff: $\widetilde{\Sigma}_F$ depends on the cutoff, while $\widetilde{F}$ does not (up to exponentially-suppressed terms). We stress, however, that $\widetilde{\Sigma}_F$ is well defined for all choices of cutoff function, due to our use of the Wu boost.

The second difference is that the integrals in $\delta \widetilde{F}$ do not require a pole prescription, since the integrand is smooth. This is in contrast to the integral in $\widetilde{F}$ (denoted $\widetilde{\mathcal{I}}_F$ above), which requires a PV prescription. This difference is the main advantage of the $\widetilde{\Sigma}_F$ approach.

---

[2] Following the G-cut procedure exactly actually gives two factors of $H(\mathbf{k})$ in $\widetilde{\Sigma}_F$ (one from each endcap), but this is overkill since the spectator is shared by both endcaps. Using $H(\mathbf{k})$ instead of $[H(\mathbf{k})]^2$ in $\widetilde{\Sigma}_F$ (and consequently the $\delta \widetilde{F}$ term) is simply a matter of preference.

A.7.1 Quantization condition

Inserting Eqs. (A.81) and (3.52) into Eq. (3.24), we find

$$C_{3,L} - C_{3,\infty}^{(0)} = \widehat{A}'\, i\Big(\widetilde{\Sigma}_F + \widetilde{G} + \delta\widetilde{F} + \delta\widetilde{G}\Big)\frac{1}{1 - i\Big(\overline{\mathcal{B}}_{2,L} + \mathcal{B}_3\Big)i\Big(\widetilde{\Sigma}_F + \widetilde{G} + \delta\widetilde{F} + \delta\widetilde{G}\Big)}\widehat{A} \tag{A.83}$$

$$= \delta C_{3,\infty}^{\Sigma_F} + A'^{\Sigma_F,(u)} i\Big(\widetilde{\Sigma}_F + \widetilde{G}\Big)\frac{1}{1 - i\mathcal{K}_{\mathrm{df},23,L}^{\Sigma_F,(u,u)} i\Big(\widetilde{\Sigma}_F + \widetilde{G}\Big)} A^{\Sigma_F,(u)}\,, \tag{A.84}$$

where all quantities in the last term are evaluated on shell, with

$$i\mathcal{K}_{\mathrm{df},23,L}^{\Sigma_F,(u,u)} \equiv \frac{1}{1 - i\Big(\overline{\mathcal{B}}_{2,L} + \mathcal{B}_3\Big)i\Big(\delta\widetilde{F} + \delta\widetilde{G}\Big)} i\Big(\overline{\mathcal{B}}_{2,L} + \mathcal{B}_3\Big) \tag{A.85}$$

$$A'^{\Sigma_F,(u)} \equiv \widehat{A}'\frac{1}{1 - i\Big(\delta\widetilde{F} + \delta\widetilde{G}\Big)i\Big(\overline{\mathcal{B}}_{2,L} + \mathcal{B}_3\Big)} \tag{A.86}$$

$$A^{\Sigma_F,(u)} \equiv \frac{1}{1 - i\Big(\overline{\mathcal{B}}_{2,L} + \mathcal{B}_3\Big)i\Big(\delta\widetilde{F} + \delta\widetilde{G}\Big)}\widehat{A} \tag{A.87}$$

$$\delta C_{3,\infty}^{\Sigma_F} \equiv \widehat{A}' i\Big(\delta\widetilde{F} + \delta\widetilde{G}\Big)\frac{1}{1 - i(\overline{\mathcal{B}}_{2,L} + \mathcal{B}_3)i\Big(\delta\widetilde{F} + \delta\widetilde{G}\Big)}\widehat{A}\,. \tag{A.88}$$

We note that $\mathcal{K}_{\mathrm{df},23,L}^{\Sigma_F,(u,u)}$ can be split up as

$$\mathcal{K}_{\mathrm{df},23,L}^{\Sigma_F,(u,u)} = \overline{\mathcal{K}}_{2,L}^{\Sigma_F} + \mathcal{K}_{\mathrm{df},3}^{\Sigma_F,(u,u)}\,, \tag{A.89}$$

where

$$i\overline{\mathcal{K}}_{2,L}^{\Sigma_F} \equiv \frac{1}{1 - i\overline{\mathcal{B}}_{2,L} i\delta\widetilde{F}} i\overline{\mathcal{B}}_{2,L} = 2\omega L^3 i\mathcal{K}_2^{\Sigma_F}\,, \tag{A.90}$$

$$\Big[\mathcal{K}_2^{\Sigma_F}\Big]_{k'\ell'm';k\ell m} \equiv \delta_{k'k}\Big[\mathcal{K}_2^{\Sigma_F}(\mathbf{k})\Big]_{\ell'm';\ell m}\,. \tag{A.91}$$

Here $\mathcal{K}_2^{\Sigma_F}$ and $\mathcal{K}_{\mathrm{df},3}^{\Sigma_F,(u,u)}$ are the respective $\widetilde{\Sigma}_F$-approach analogs of the K matrices $\mathcal{K}_2$ and $\widetilde{\mathcal{K}}_{\mathrm{df},3}^{(u,u)}$ in the $\widetilde{F}$ approach, with their definitions only differing by using $\delta\widetilde{F}$ in place of $\widetilde{\mathcal{I}}_F$.

From Eq. (A.84), we obtain the quantization condition in the $\widetilde{\Sigma}_F$ approach:

$$\det\Big[1 + \Big(2\omega L^3\mathcal{K}_2^{\Sigma_F} + \mathcal{K}_{\mathrm{df},3}^{\Sigma_F,(u,u)}\Big)\Big(\widetilde{\Sigma}_F + \widetilde{G}\Big)\Big] = 0\,. \tag{A.92}$$

For this to be useful, we need to relate the infinite-volume quantities $\mathcal{K}_2^{\Sigma_F}$ and $\mathcal{K}_{\mathrm{df},3}^{\Sigma_F,(u,u)}$ to scattering amplitudes, and we do so in the next two subsections.

A.7.2 Relating $\mathcal{K}_2^{\Sigma_F}$ to $\mathcal{M}_2$

From Appendix A.2 and the equations above, we have

$$i\overline{\mathcal{M}}_{2,L} = i\overline{\mathcal{B}}_{2,L}\frac{1}{1 - iD_F i\overline{\mathcal{B}}_{2,L}} \tag{A.93}$$

$$= i\overline{\mathcal{K}}_{2,L}^{\Sigma_F}\frac{1}{1 - i\widetilde{\Sigma}_F i\overline{\mathcal{K}}_{2,L}^{\Sigma_F}}\,, \tag{A.94}$$

which gives a simple inverse relation between the on-shell FV amplitudes:

$$\left(\overline{\mathcal{M}}_{2,L}^{\mathrm{on}}\right)^{-1} = \left(\overline{\mathcal{K}}_{2,L}^{\Sigma_F,\mathrm{on}}\right)^{-1} + \widetilde{\Sigma}_F\,, \tag{A.95}$$

where again the "on" labels indicate that the amplitudes must be completely on shell for the equation to hold. To obtain the corresponding infinite-volume relation between $\mathcal{M}_2$ and $\mathcal{K}_2^{\widetilde{\Sigma}_F}$, we follow the same steps as we did in Appendix A.2: eliminate the common spectator term by multiplying by $2\omega L^3$ and dropping the $\delta_{k'k}$, take the $L \to \infty$ limit holding $E_{2,k}$ and $\mathbf{P}_{2,k}$ (and therefore $q_{2,k}^*$) fixed by reintroducing the $i\epsilon$ term in D_F, and convert all sums to integrals. The result is

$$\delta_{\ell'\ell}\delta_{m'm}\left[\mathcal{M}_2^{(\ell)}(q_{2,k}^*)\right]^{-1} = \left\{\left[\mathcal{K}_2^{\Sigma_F}(\mathbf{k})\right]^{-1}\right\}_{\ell'm';\ell m} + \left[I_F^{i\epsilon}(\mathbf{k})\right]_{\ell'm';\ell m}\,, \tag{A.96}$$

where

$$\left[I_F^{i\epsilon}(\mathbf{k})\right]_{\ell'm';\ell m} \equiv \frac{H(\mathbf{k})}{2!}\int_{\mathbf{a}}^{\mathrm{UV}}\frac{1}{2\omega_a}\frac{\mathcal{Y}_{\ell'm'}(\mathbf{a}_k^*)}{q_{2,k}^{*\ell'}}\frac{1}{b_{ka}^2 - m^2 + i\epsilon}\frac{\mathcal{Y}_{\ell m}(\mathbf{a}_k^*)}{q_{2,k}^{*\ell}}\,. \tag{A.97}$$

A new feature that arises here is that $I_F^{i\epsilon}$ is not diagonal in ℓ and m. This is because, when using the Wu boost, the transformation to the pair CMF does not lead to an integrand that, aside from the harmonic polynomials, is a rotational scalar. It follows from Eq. (A.96) that $\mathcal{K}_2^{\Sigma_F}$ must also have off-diagonal terms. This is not a problem in principle, but is a

cumbersome feature of this approach.

A.7.3 Relating $\mathcal{K}_{\rm df,3}^{\Sigma_F,(u,u)}$ to $\mathcal{M}_3$

We provide only a sketch of the derivation of this relation, since the analysis follows closely that given in Appendix A.5. We start from Eq. (3.83) and substitute Eqs. (A.81) and (3.52) to obtain

$$i\left(\overline{\mathcal{M}}_{2,L}+\widetilde{\mathcal{M}}_{3,L}^{(u,u)}\right)=i\mathcal{K}_{\rm df,23,L}^{\Sigma_F,(u,u)}\frac{1}{1-i(\widetilde{\Sigma}_F+\widetilde{G})\,i\mathcal{K}_{\rm df,23,L}^{\Sigma_F,(u,u)}}\,. \tag{A.98}$$

Following the steps in the main text, we can extract from this a result for $\widetilde{\mathcal{M}}_{3,L}^{(u,u)}$ identical to Eqs. (3.86)-(3.90) except for the substitutions $\widetilde{\mathcal{K}}_{\rm df,3}^{(u,u)}\to\mathcal{K}_{\rm df,3}^{\Sigma_F,(u,u)}$ and $\widetilde{F}\to\widetilde{\Sigma}_F$. We then take the infinite-volume limit as in Appendix A.5 and obtain the same set of equations with $\widetilde{\mathcal{K}}_{\rm df,3}^{(u,u)}\to\mathcal{K}_{\rm df,3}^{\Sigma_F,(u,u)}$ and $\widetilde{\rho}_{\rm PV}(\mathbf{k})\to I_F^{i\epsilon}(\mathbf{k})$.

Appendix B

APPENDIX TO CHAPTER 4

B.1 Technical details

In this appendix we collect some technical details relevant for the discussion of the main text.

First we discuss the smooth cutoff functions $H^{(i)}(\mathbf{p}_i)$ that enter into $\widetilde{G}^{(ij)}$. Aside from one feature, these are straightforward generalizations of the cutoff introduced in Ref. [28] and used in all subsequent RFT works. These functions smoothly cut off the sums or integrals over the spectator momentum $\mathbf{p}_i$ once the flavor $j+k$ pair lies far below its threshold. To implement this, we use the quantity $\sigma_i = (P - p_i)^2$, which equals $(m_j + m_k)^2$ at the pair threshold, and decreases as one drops below this threshold. For identical particles, σ_i is the same as the quantity $E^{*2}_{2,k}$ used in the definition of the cutoff function in Ref. [28]. If we use the same boost as in that work, which is discussed below, then we are restricted to the range $\sigma_i > 0$, since the boost becomes singular when $\sigma_i = 0$. Another constraint, described in BS1, is that the cutoff function should equal unity for some range below the pair threshold. This ensures that all terms which are dropped in the derivation are exponentially suppressed. Finally, we also need the function to be Lorentz invariant. One choice that satisfies these

requirements is

$$H^{(i)}(\mathbf{p}_i) = J(z_i)\,, \quad z_i = (1+\epsilon_H)\frac{\sigma_i}{(m_j+m_k)^2}\,, \tag{B.1}$$

$$J(z) = \begin{cases} 0, & z \leq 0 \\ \exp\left(-\frac{1}{z}\exp\left[-\frac{1}{1-z}\right]\right), & 0 < z < 1 \\ 1, & 1 \leq z\,. \end{cases} \tag{B.2}$$

Here choosing $\epsilon_H > 0$ ensures that the cutoff function reaches unity below threshold, at the point where $\sigma_i = (m_j+m_k)^2/(1+\epsilon_H)$. We expect that, in practice, a value $\epsilon_H \sim 0.1$ should be sufficiently large. We stress that the choice of cutoff functions is not unique, and the choice above is simply an example, albeit one that is close to those that have been used in previous numerical implementations [36, 39, 51, 76].

We next give some details concerning the two boosts that have been mentioned in the main text. These enter into both the on-shell projections of kernels and amplitudes, and in the definitions of $\widetilde{F}^{(i)}$ and $\widetilde{G}^{(ij)}$. To explain the boosts, we use the example of the quantity $\mathbf{p}_j^{*(p_i)}$ that enters in $\widetilde{F}^{(i)}$, Eq. (C.9). The setup is that the four-momenta $p_i = (\omega_{p_i}, \mathbf{p}_i)$ and $p_j = (\omega_{p_j}, \mathbf{p}_j)$ are on shell. The former is the spectator momentum, and the latter is the pair momentum relative to which the decomposition into spherical harmonics is defined (after boosting to the pair CMF). We note that, in situations where we use the boosts, these two particles are always on shell, either because (in the TOPT approach) all intermediate particles are on shell, or (in the Feynman-diagram approach) we have set them on shell in preparation for full on-shell projection, as discussed in Appendix B.2. For the boost of Ref. [28], referred to subsequently as the "HS boost", we obtain $\mathbf{p}_j^{*(p_i)}$ by boosting p_j using boost velocity

$$\boldsymbol{\beta}_{\rm HS} = -\frac{\mathbf{P}-\mathbf{p}_i}{E-\omega_{p_i}}\,. \tag{B.3}$$

The transformation is

$$p_j \longrightarrow p_j^* = \Lambda(\boldsymbol{\beta}_{\rm HS}) p_j \equiv \left(\omega_{p_j}^{*(p_i)}, \mathbf{p}_j^{*(p_i)}\right) , \tag{B.4}$$

where Λ is the corresponding Lorentz transformation matrix. By construction, this transforms the pair four-momentum $P - p_i$ to its CMF,

$$\Lambda(\boldsymbol{\beta}_{\rm HS})(P - p_i) = (\sqrt{\sigma_i}, \mathbf{0}) , \qquad \sigma_i = (P - p_i)^2 . \tag{B.5}$$

For the Wu boost, the setup is the same, but the boost velocity is changed to

$$\boldsymbol{\beta}_{\rm Wu} = -\frac{\mathbf{P} - \mathbf{p}_i}{\omega_{p_j} + \omega_{p_k}} , \tag{B.6}$$

where $\mathbf{p}_k = \mathbf{P} - \mathbf{p}_i - \mathbf{p}_j$ is the momentum of the third particle. Thus the result for $\mathbf{p}_j^{*(p_i)}$ is in general different. The exception is if all three particles are on shell *and* total four-momentum is conserved, for then $E - \omega_{p_i} = \omega_{p_j} + \omega_{p_k}$, and the boost velocities are the same. Because of this, it does not matter which boost we use when defining on-shell projected quantities such as the elements of $\widehat{\mathcal{K}}_{\rm df,3}$, $\widehat{\mathcal{M}}_3$, etc.

When using TOPT, as in Secs 4.4 and 4.5, one should initially use the Wu boost, as explained in BS1. This is because the boost is designed to apply for three on-shell particles. However, once one has obtained results in terms of on-shell projected quantities, e.g. $C_{3,L}$ in Eq. (4.32), one can change to the HS boost in the definitions of the elements of $\widehat{F}_G$. For $\widetilde{F}^{(i)}$ the change is exponentially suppressed, while for $\widetilde{G}^{(ij)}$ the change is nonsingular (since the boosts agree at the pole) and can be absorbed into a shift in $\delta\widetilde{G}^{(ij)}$. In this way, one finds that the same form for $C_{3,L}$ holds, but with redefined quantities $\widehat{\mathcal{K}}_{\rm df,3}$, $\widehat{A}_F$, and $\widehat{A}'_F$. The only caveat is that the cutoff functions $H^{(i)}$ must be chosen such that the HS boost is well defined, which requires $\sigma_i > 0$, as discussed above. By contrast, for the Wu boost there is no such constraint on σ_i. The conclusion, already noted in BS1 for identical particles, is that the TOPT forms of the quantization condition and the relation of $\mathcal{M}_3$ to $\widehat{\mathcal{K}}_{\rm df,3}$ are valid with both boosts, although $\widehat{\mathcal{K}}_{\rm df,3}$ will, of course, depend on the choice.

The situation is reversed in the Feynman-diagram approach. In the initial derivation, the third particle is off shell, and so the natural choice is the HS boost. Once we obtain the result for, say, $\widehat{\mathcal{M}}'_{3,L}$, however, we could switch to using the Wu boost. We could also raise the cutoff in the functions $H^{(i)}$ to allow $\sigma_i < 0$, since that only changes the elements of $\widehat{F}_G$ away from the pole. However, there is a clear reason not to use the Wu boost, which is that only with the HS boost can one obtain a Lorentz-invariant $\widehat{\mathcal{K}}'_{\text{df},3}$, i.e. one that is Lorentz invariant when combined with spherical harmonics as in Eq. (4.93). We close this section by explaining this result.

The context for the discussion is the infinite-volume relation between $\mathcal{M}_3$ and $\widehat{\mathcal{K}}'_{\text{df},3}$ derived in Sec. 4.7. As described in that section, the only nontrivial part of the demonstration of Lorentz invariance concerns the transformation properties of $[\widehat{G}^\infty]_{ij}$, Eq. (4.87). If we Lorentz transform the momentum arguments $p_i = (\omega_{p_i}, \mathbf{p}_i)$ and $k_j = (\omega_{k_j}, \mathbf{k}_j)$, then the arguments of the spherical harmonics, $\mathbf{k}_j^{*(p_i)}$ and $\mathbf{p}_i^{*(k_j)}$, should only be rotated.

To show that this is the case with the HS boost, we focus on $\mathbf{k}_j^{*(p_i)}$. This is defined by

$$k_j^* = \Lambda(\boldsymbol{\beta}_{\text{HS}}) k_j \equiv \left(\omega_{k_j}^{*(p_i)}, \mathbf{k}_j^{*(p_i)}\right) . \tag{B.7}$$

Now we apply an arbitrary global transformation Λ_0 to all momenta, so that

$$p_j \to p'_i = \Lambda_0 p_i \,, \quad k_j \to k'_j = \Lambda_0 k_j \,, \quad P \to P' = \Lambda_0 P \,, \quad \text{etc.} \,, \tag{B.8}$$

and then boost to the pair CMF, which now requires the boost velocity

$$\boldsymbol{\beta}'_{\text{HS}} = -\frac{\mathbf{P}' - \mathbf{p}'_i}{E' - \omega_{p'_i}} \,. \tag{B.9}$$

Thus we find a new value of $\mathbf{k}_j^{*(p_i)}$, given by the spatial part of

$$k_j'^* = \Lambda(\boldsymbol{\beta}'_{\text{HS}}) k'_j = \Lambda(\boldsymbol{\beta}'_{\text{HS}}) \Lambda_0 k_j \,. \tag{B.10}$$

To proceed, we note that, by definition, the boosts satisfy the following relations:

$$\Lambda(\boldsymbol{\beta}_{\rm HS})(P-p_i) = (\sqrt{\sigma_1},\mathbf{0}) = \Lambda(\boldsymbol{\beta}'_{\rm HS})(P'-p'_i) = \Lambda(\boldsymbol{\beta}'_{\rm HS})\Lambda_0(P-p_i)\,, \tag{B.11}$$

from which follows the standard result that

$$\Lambda(\boldsymbol{\beta}'_{\rm HS})\Lambda_0 = \Lambda({\rm rot})\Lambda(\boldsymbol{\beta}_{\rm HS})\,, \tag{B.12}$$

where $\Lambda({\rm rot})$ implements a rotation. The precise form of the rotation can, of course, be determined, but is not needed here. Inserting this into Eq. (B.10) we find

$$k'^{*}_j = \Lambda({\rm rot})\Lambda(\boldsymbol{\beta}_{\rm HS})k_j = \Lambda({\rm rot})k'_j\,, \tag{B.13}$$

which yields the claimed result that $\mathbf{k}_j^{*(p_i)}$ and $\mathbf{k}_j'^{*(p_i)}$ are related by a rotation. A completely analogous argument holds for $\mathbf{p}_i^{*(k_j)}$.

Now we show why this argument fails for the Wu boost. The definitions of k^*_j and k'^*_j take the same form as above, except that $\boldsymbol{\beta}_{\rm HS}$ in Eq. (B.7) and $\boldsymbol{\beta}'_{\rm HS}$ in Eq. (B.10), are replaced, respectively, by

$$\boldsymbol{\beta}_{\rm Wu} = -\frac{\mathbf{P}-\mathbf{p}_i}{\omega_b+\omega_{k_j}}\,, \quad \boldsymbol{\beta}'_{\rm Wu} = -\frac{\mathbf{P}'-\mathbf{p}'_i}{\omega_{b'}+\omega_{k'_j}}\,, \tag{B.14}$$

where $\mathbf{b} = \mathbf{P}-\mathbf{p}_i-\mathbf{k}_j$ and $\mathbf{b}' = \mathbf{P}'-\mathbf{p}'_i-\mathbf{k}'_j$. These boosts are defined by the properties

$$\Lambda(\boldsymbol{\beta}_{\rm Wu})(k_j+b) = \left(\sqrt{(\omega_b+\omega_{k_j})^2-|\mathbf{P}-\mathbf{p}_i|^2},\mathbf{0}\right)\,, \tag{B.15}$$

$$\Lambda(\boldsymbol{\beta}'_{\rm Wu})(k'_j+b') = \left(\sqrt{(\omega_{b'}+\omega_{k'_j})^2-|\mathbf{P}'-\mathbf{p}'_i|^2},\mathbf{0}\right)\,, \tag{B.16}$$

where $b = (\omega_b,\mathbf{b})$ and $b' = (\omega_{b'},\mathbf{b}')$. This brings up the obstruction to continuing the argument as for the HS boost, namely that

$$b' \neq \Lambda_0 b\,. \tag{B.17}$$

The quantities that do transform in this manner are $b_{\rm off} = P-p_i-k_j$ and $b'_{\rm off} = P'-p'_i-k'_j$, but, in general, $b \neq b_{\rm off}$ and $b' \neq b'_{\rm off}$. A related obstruction to the argument is that the

right-hand sides of Eqs. (B.15) and (B.16) are not, in general, equal. Because of these issues, the analog of Eq. (B.12) for Wu boosts is not valid, and $\mathbf{k}_j^{*(p_i)}$ and $\mathbf{k}_j'^{*(p_i)}$ are not, in general, related by a rotation. Thus the arguments of Sec. 4.7 concerning Lorentz invariance do not hold.

B.2 Details of derivation using Feynman diagrams

In this appendix we explain how Eqs. (4.63)-(4.68) are obtained from the initial skeleton expansion by doing the energy integrals over independent momenta.

As discussed in Ref. [28], when doing an integral over the energy component of a four-momentum associated with a propagator, we can close the contour in the complex plane so as to pick up the contribution from the particle pole, and exclude the antiparticle pole contribution. The integral will also contain contributions from other poles (e.g. corresponding to a three-particle cut across the dressed propagator, or the antiparticle pole contributions from another propagator), but these can never lead to an on-shell cut of the entire diagram. Thus we can separate the contributions from each such integral into that from the particle pole, which we refer to as the "on-shell" contribution, and the remainder, denoted "off-shell." If any of the contributions from the three propagators in a given cut (of which only two are integrated, due to overall momentum conservation) are off shell, then we know that the cut is nonsingular, and momentum sums can be replaced by integrals. The contributions from off-shell propagators can then be absorbed into shifts in the Bethe-Salpeter kernels, leading to a reshuffled skeleton expansion in which all independent momenta are now on shell. Important features of this reshuffling are that it maintains Lorentz invariance of the kernels, and that it does not mix up the elements of $\widehat{\mathcal{M}}_{3,L}'^{\text{off}}$.

To explain this in more detail, as well as to highlight some technical features, we work through three examples. We begin with one involving only B_2 kernels, shown in Fig. B.1. A detailed explanation of the steps is given in the caption, and we comment here on how the

procedure is generalized to all such diagrams. The first step is to integrate over the energies of all internal spectator momenta. In the example shown, there is one such momentum (the upper, orange line). In general there are multiple spectator momenta, in different loops. We find that the order of integration of their energies does not matter, since all lead to the same final decomposition in terms of shifted kernels. The result of these first integrals are on- and off-shell terms, one of each in the example. For the off-shell terms, all spatial momenta associated with the spectator can now be integrated, including any involving the interacting pair. Thus, in the example, the lower (black) propagator between the middle $B_2^{(3)}$s can also be fully integrated when the off-shell part of the upper (orange, spectator) propagator is taken. This results in an infinite-volume quantity that can be absorbed by a shift in the (11) element of B_3, as shown by the first term of the second and third lines of the figure.

In the second step, the energies of all remaining independent momenta are integrated. These lie in what we call F-type cuts, i.e. those which, in the TOPT analysis described in the previous section, would lead to factors of $\widetilde{F}$. Here we must choose which of the interacting pair to integrate, and, as in the TOPT analysis, we pick that whose flavor follows cyclically from the flavor of the spectator. In our example the spectator has flavor 3, so we integrate the energy of the flavor 1 propagator in the lower pair. The integrations over all F-type cuts in such diagrams can be done independently, with each leading to on- and an off-shell contributions, as shown in the second line in the figure. We then absorb any sequences of interacting pairs connected by off-shell propagators into shifts in the corresponding B_2 kernels, since the loops within them can be fully integrated. The final result is a set of diagrams containing (possibly shifted) kernels in which all propagators with independent momenta are on shell, and with only one propagator per cut whose momentum can be off shell.

At this stage we can already understand most of the factors present in Eqs. (4.63)-(4.68), in particular those involving $B_2^{(i)}$ and $\delta B_2^{(i)}$. Each cut is associated with two on-shell and

one off-shell propagator, and with two loop sums, leading to the kinematical factors in $D'^{(i)}$, Eq. (4.68). The on-shell projectors that enter the diagonal elements of $\widehat{D'}$ correspond to F-type cuts and are determined by the cyclical flavor rule. For example, if the spectator has flavor 3, as in Fig. B.1, then the on-shell flavors are 3 and 1, requiring on-shell projectors $\overleftarrow{O}^{(2)}$ and $\overrightarrow{O}^{(2)}$. Thus the 33 element of $\widehat{D'}$ is $D'^{(2)}$. The off-diagonal elements of $\widehat{D'}$ correspond to G-type cuts in which the spectator is switched, in which case the two on-shell flavors are simply those of the spectators on either side. Thus, for example, the 12 element of $\widehat{D'}$ is $D'^{(3)}$, which places flavors 1 and 2 on shell. The geometric series in Eq. (4.63) then produces all possible orderings of F-type and G-type cuts.

Another feature to be explained is the presence of factors of $2\omega L^3$ in the projected $\overline{B}^{(i)}_{2,L}$, Eqs. (4.70)-(4.73). These are needed because, in general, a spectator propagator spans multiple F-type cuts, but should only appear once in the final expression. Each F-type cut comes with a factor of $1/(2\omega L^3)$—contained in the corresponding $D'^{(i)}$—and all but one are canceled by the factors of $2\omega L^3$ in the numerators of the $\overline{B}^{(i)}_{2,L}$s. This structure, which follows exactly the pattern of the TOPT result, yields the correct propagator factors, and factors of L^3, for each diagram.

We next consider diagrams involving only B_3 kernels, the simplest nontrivial example of which is analyzed in Fig. B.2. Since we are considering a contribution to one of the nine elements of the matrix, $[\widehat{\mathcal{M}}'^{\text{off}}_{3,L}]_{31}$, there is an overall factor of 1/9, which we partition equally between the two external B_3 kernels in the initial expression. We now have to choose for which two of the propagators we do the energy integrals. The choice needed to match the form of Eqs. (4.63)-(4.68) is to pick equal weights for all three pairs, which leads to the last three terms in the equation in the figure. This matches the result obtained by expanding out Eqs. (4.63)-(4.68) and evaluating the term corresponding to that in the figure,

$$\left(|1\rangle\,\frac{B_3}{9}\,\langle 1|\right)\widehat{D'}\left(|1\rangle\,\frac{B_3}{9}\,\langle 1|\right) = |1\rangle\,\frac{B_3}{9}\mathbb{1}_{\mathbf{p},\mathbf{k}}(3D'^{(1)}+3D'^{(2)}+3D'^{(3)})\frac{B_3}{9}\,\langle 1|\,, \tag{B.18}$$

where $\mathbb{1}^{\mathbf{P}}$ is defined in Eq. (4.8). All contributions containing an off-shell propagator, which are not shown explicitly in the figure, are included in the shift to the three-particle kernel. The extension of this analysis to multiple adjacent B_3 kernels is straightforward.

Our final example, shown in Fig. B.3, is of a case with both B_3 and B_2 kernels. The factors of $1/3$ contained in the B_3 kernels in the original expression appear for the same reason as in the previous example. The ordering of energy integrals is as in the first example: spectators first (here the top, flavor 3, orange line), and then those lying between B_3 and B_2 kernels. For the latter we again have a choice, and we pick two-thirds of the contribution to have the lower, flavor 1, black line to be integrated, with the remaining one-third having the middle, flavor 2, green line integrated. Subsuming cuts with off-shell propagators into shifts in the kernels leads to the result shown in the figure. The resulting factors match those that arise from the desired equations; for example,

$$\left(|1\rangle\,\frac{B_3}{9}\,\langle 1|\right)\widehat{D}'\widehat{B}\Big|_{B_2^{(3)}\ \text{part}}\widehat{D}'\left(|1\rangle\,\frac{B_3}{9}\,\langle 1|\right) = |1\rangle\,\frac{B_3}{9}\mathbb{1}_{\mathbf{p},\mathbf{k}}(D'^{(1)}+2D'^{(2)})\overline{B}^{(3)}_{2,L}\mathbb{1}_{\mathbf{p},\mathbf{k}}(D'^{(1)}+2D'^{(2)})\frac{B_3}{9}\,\langle 1| \tag{B.19}$$

agrees with the factors in the final two lines in the figure.

Diagrams with multiple B_2 kernels, including switches, between B_3s are analyzed by a combination of the above-described methods. First all spectator energies are integrated, then those in the F-type cuts (choosing which flavor to integrate as in the first example), and finally those between B_3s and adjacent B_2s (with flavor choices as in our third example). This results in a unique decomposition into diagrams in which all independent internal propagators on shell. To obtain a simple final expression, we add in the disconnected contributions with a single spectator line (of, say, flavor i) and one or more $B_2^{(i)}$s, which build up the quantity $\widehat{\mathcal{M}}'^{\text{off}}_{2,L}$ discussed in the main text. The combination is then given by Eq. (4.63).

A final technical issue is whether the same total shifts to the kernels, i.e. $\delta B_3^{(ij)}$ and $\overline{\delta B}_2^{(i)}$, appear in all resulting diagrams. To demonstrate this we note that every diagram that results from the energy integrations is of the same form as one of the unintegrated diagrams,

except with some propagators on shell and some kernels replaced by their shifts. No new topologies arise. Now we consider one topology, and insert every possible choice for the shift in each of the kernels. Each of the diagrams that results can be uniquely traced back to an allowed original unintegrated diagram. Thus every energy-integrated diagram that should appear does appear.

B.3 Derivation of symmetrization identities

In this appendix we derive the identities (4.100)-(4.102). We lean heavily on the derivation of the analogous identities for identical particles given in Appendix D of BS1, although we have made some improvements to the argument.

The first identity replaces the $\widehat{G}$ elements of $\widehat{F}_G$ with factors of $\widehat{F}\overrightarrow{\mathcal{S}}$ plus integral operators. We demonstrate this result by considering a representative example,

$$X_1(\{\mathbf{p}\})_{p_1\ell'm'}\widetilde{G}^{(12)}_{p_1\ell'm';k_2\ell m}(-1)^\ell Z_2(\{\mathbf{k}\})_{k_2\ell m} - X_1(\{\mathbf{p}\})_{p_1\ell'm'}\widetilde{F}^{(1)}_{p_1\ell'm';k_1\ell m}Z_2(\{\mathbf{k}\})_{k_1\ell m}$$
$$= X_1(\{\mathbf{p}\})_{p_1\ell'm'}\left[\widehat{\overrightarrow{\mathcal{I}}}_{G,12}\right]_{p_1\ell'm';k_2\ell m}Z_2(\{\mathbf{k}\})_{k_2\ell m}\,, \quad \text{(B.20)}$$

where there is an implicit sum over repeated indices (including over ℓ which appears thrice in one term). Here we are using the notation of Sec. 4.8.1, and stress in particular the difference between $Z_2(\{\mathbf{k}\})_{k_2\ell m}$ and $Z_2(\{\mathbf{k}\})_{k_1\ell m}$. Both involve the same underlying infinite-volume on-shell quantity Z_2, but the former is expressed in the coordinates in which the spectator has flavor 2 (with momentum $\mathbf{k}_2$), and the spherical harmonics are defined relative to the flavor 3 particle, while the latter quantity is expressed in coordinates in which the flavor 1 particle is the spectator (with momentum $\mathbf{k}_1$), and the harmonics are defined relative to the particle of flavor 2. The precise definition of the decompositions into spherical harmonics is given in Eq. (4.23).

Using the definitions of $\widetilde{G}^{(ij)}$ and $\widetilde{F}^{(i)}$, Eqs. (C.10) and (C.9), the left-hand side of

Eq. (B.20) can be written as

$$\sum_{\mathbf{p}_1\ell'm'}\sum_{\mathbf{k}_2} X_1(\{\mathbf{p}\})_{p_1\ell'm'}\frac{H^{(1)}(\mathbf{p}_1)}{2\omega_{p_1}L^3}\frac{\mathcal{Y}_{\ell'm'}(\mathbf{k}_2^{*(p_1)})}{q_{2,p_1}^{*\ell'}}\frac{H^{(2)}(\mathbf{k}_2)}{b_{12}^2-m_3^2}\frac{1}{2\omega_{k_2}L^3}$$
$$\times\left\{\sum_{\ell m}\left[\frac{\mathcal{Y}_{\ell m}(\mathbf{p}_1^{*(k_2)})}{q_{2,k_2}^{*\ell}}(-1)^\ell Z_2(\{\mathbf{k}\})_{k_2\ell m}-\frac{\mathcal{Y}_{\ell m}(\mathbf{k}_2^{*(p_1)})}{q_{2,p_1}^{*\ell}}Z_2(\{\mathbf{k}\})_{p_1\ell m}\right]\right\}+\text{integral term from }\widetilde{F}^{(1)}\,. \tag{B.21}$$

Here we have made several emendations to $\widetilde{F}^{(1)}$: used $H^{(2)}(\mathbf{k}_2)$ as the UV regulator, converted to the relativistic form of the denominator, labeled the dummy variable in the sum as $\mathbf{k}_2$, and used the Kronecker delta to set $\mathbf{k}_1=\mathbf{p}_1$. We have also made the sums explicit. The key observation is that, if $\mathbf{p}_1$ and $\mathbf{k}_2$ are chosen such that $b_{12}=P-p_1^{\text{on}}-k_2^{\text{on}}$ is on shell, i.e. $b_{12}^2=m_3^2$, then the term in curly braces vanishes. This is because both contributions to this term become equal to $Z_2(\{\mathbf{p}_1,\mathbf{k}_2,\mathbf{k}_3\})$, where $\mathbf{k}_3=\mathbf{P}-\mathbf{p}_1-\mathbf{k}_2$. This in turn is because, at the on-shell point, we have

$$|\mathbf{p}_1^{*(k_2)}|=q_{2,k_2}^*\quad\text{and}\quad|\mathbf{k}_2^{*(p_1)}|=q_{2,p_1}^*\,, \tag{B.22}$$

so that the ratios involving harmonic polynomials reduce to spherical harmonics, e.g.

$$\frac{\mathcal{Y}_{\ell m}(\mathbf{k}_2^{*(p_1)})}{q_{2,p_1}^{*\ell}}\longrightarrow\sqrt{4\pi}Y_{\ell m}(\hat{k}_2^{*(p_1)})\,. \tag{B.23}$$

The sums over ℓ and m can then be done. The only remaining subtlety is in the first term in curly braces, where the $(-1)^\ell$ is needed to convert the spherical harmonics from being defined with respect to flavor 1 to being defined relative to flavor 3, so as to match the convention used in $Z_2(\{\mathbf{k}\})_{k_2\ell m}$.

Since the term in curly braces vanishes on shell, it cancels the pole at $b_{13}^2=m^2$, so that the sum over $\mathbf{k}_2$ can be replaced by an integral, up to exponentially suppressed contributions. If we introduce a PV pole prescription, then this integral can be split into two terms, one for each of the terms in curly braces. The second of these simply cancels the integral term

from $\widetilde{F}^{(1)}$, leaving an integral over the first term in curly braces, i.e. the term that originated from $\widetilde{G}^{(12)}$. For this remaining term the sum over $\mathbf{p}_1$ can also be converted into an integral, due to the PV pole prescription used for the integral over $\mathbf{k}_2$. Thus the left-hand side of Eq. (B.20) becomes

$$\int_{\mathbf{p}_1} \sum_{\ell' m'} \mathrm{PV} \int_{\mathbf{k}_2} \sum_{\ell m} X_1(\{\mathbf{p}\})_{p_1 \ell' m'} \frac{\mathcal{Y}_{\ell' m'}(\mathbf{k}_2^{*(p_1)})}{q_{2,p_1}^{*\ell'}} \frac{H^{(1)}(\mathbf{k}_1) H^{(2)}(\mathbf{k}_2)}{b_{12}^2 - m_3^2} \frac{\mathcal{Y}_{\ell m}(\mathbf{p}_1^{*(k_2)})}{q_{2,k_2}^{*\ell}} (-1)^\ell Z_2(\{\mathbf{k}\})_{k_2 \ell m} \,, \tag{B.24}$$

which defines the integral operator on the right-hand side of Eq. (B.20). Here we are using the Lorentz-invariant measure for the momentum integrals, defined in Eq. (4.80).

We now introduce a compact notation for the result Eq. (B.20),

$$[X_1]_1 [\widehat{G}]_{12} [Z_2]_2 - [X_1]_1 [\widehat{F}]_{11} [Z_2]_1 = [X_1]_1 [\widehat{\overrightarrow{\mathcal{I}}}_G]_{12} [Z_2]_2 \,. \tag{B.25}$$

By essentially the same argument, we can extend this result to all nonvanishing elements of $\widehat{G}$, obtaining

$$[X_i]_i [\widehat{G}]_{ij} [Z_j]_j - [X_i]_i [\widehat{F}]_{ii} [Z_j]_i = [X_i]_i [\widehat{\overrightarrow{\mathcal{I}}}_G]_{ij} [Z_j]_j \,, \qquad i \neq j \text{ (no sum)} \,. \tag{B.26}$$

This fills out the off-diagonal matrix of integral operators $\widehat{\overrightarrow{\mathcal{I}}}_G$, and completes the derivation of the first symmetrization identity.

Using the same arguments, but with the roles of X and Z interchanged, we obtain

$$[X_i]_i [\widehat{G}]_{ij} [Z_j]_j - [X_i]_j [\widehat{F}]_{jj} [Z_j]_j = [X_i]_i [\widehat{\overleftarrow{\mathcal{I}}}_G]_{ij} [Z_j]_j \,, \qquad i \neq j \text{ (no sum)} \,, \tag{B.27}$$

where in the new integral operator the order of integrals is interchanged compared to that in Eq. (B.24). This result leads immediately to the second symmetrization identity, Eq. (4.101).

We now turn to the third identity, Eq. (4.102). In our new notation this is equivalent to

$$\Delta \equiv 3 \sum_{i,j} [X_i]_i [\widehat{F}_G]_{ij} [Z_j]_j - \sum_i [X_1 + X_2 + X_3]_i [\widehat{F}]_{ii} [Z_1 + Z_2 + Z_3]_i = 3 \sum_{i,j} [X_i]_i [\widehat{\mathcal{I}}_{FG}]_{ij} [Z_j]_j \,. \tag{B.28}$$

To demonstrate this (and define the integral operator $\widehat{\mathcal{I}}_{FG}$) we break the left-hand side into

four parts

$$\Delta = \Delta_1 + \Delta_2 + \Delta_3 + \Delta_4 \,, \tag{B.29}$$

$$\Delta_1 = \sum_{i\neq j} \left([X_i]_i [\widehat{F}_G]_{ij} [Z_j]_j - [X_i]_i [\widehat{F}]_{ii} [Z_j]_i \right) \,, \tag{B.30}$$

$$\Delta_2 = \sum_{i\neq j} \left([X_i]_i [\widehat{F}_G]_{ij} [Z_j]_j - [X_i]_j [\widehat{F}]_{jj} [Z_j]_j \right) \,, \tag{B.31}$$

$$\Delta_3 = \sum_{i\neq j} \left([X_j]_j [\widehat{F}]_{jj} [Z_j]_j - [X_j]_i [\widehat{F}]_{ii} [Z_j]_i \right) \,, \tag{B.32}$$

$$\Delta_4 = \sum_{i\neq j} \left([X_i]_i [\widehat{F}_G]_{ij} [Z_j]_j - [X_i]_k [\widehat{F}]_{kk} [Z_j]_k \right) \,, \tag{B.33}$$

where in the final equation k is the third flavor index, i.e. $k \neq i$ and $k \neq j$. The first two parts can be evaluated using Eqs. (B.26) and (B.27), respectively. For the remaining two, we need additional work.

Δ_3 involves the difference between choosing two different spectator flavors for an F cut. To evaluate this difference we focus on the case where $i = 1$ and $j = 2$, and also replace X_j and Z_j with X and Z, respectively, since the flavor of these quantities plays no role in the argument. Thus we consider

$$\Delta_3^{(21)} = [X]_2 [\widehat{F}]_{22} [Z]_2 - [X]_1 [\widehat{F}]_{11} [Z]_1 \,. \tag{B.34}$$

Considering first the sum parts of the $\widetilde{F}^{(i)}$s, we have

$$\begin{aligned} \Delta_{3\Sigma}^{(21)} = {} & \frac{1}{L^6} \sum_{\mathbf{k}_2 \ell' m'} H^{(2)}(\mathbf{k}_2) \sum_{\mathbf{k}_3 \ell m} X_{k_2 \ell' m'} \frac{\mathcal{Y}_{\ell' m'}(\mathbf{k}_3^{*(k_2)})}{q_{2,k_2}^{*\ell'}} H^{(1)}(\mathbf{k}_1) D_{123} \frac{\mathcal{Y}_{\ell m}(\mathbf{k}_3^{*(k_2)})}{q_{2,k_2}^{*\ell}} Z_{k_2 \ell m} \\ & - \frac{1}{L^6} \sum_{\mathbf{k}_1 \ell' m'} H^{(1)}(\mathbf{k}_1) \sum_{\mathbf{k}_2 \ell m} X_{k_1 \ell' m'} \frac{\mathcal{Y}_{\ell' m'}(\mathbf{k}_2^{*(k_1)})}{q_{2,k_1}^{*\ell'}} H^{(2)}(\mathbf{k}_2) D_{123} \frac{\mathcal{Y}_{\ell m}(\mathbf{k}_2^{*(k_1)})}{q_{2,k_1}^{*\ell}} Z_{k_1 \ell m} \,, \end{aligned} \tag{B.35}$$

where we have chosen the nonrelativistic form for the denominator (which is the same for both terms), i.e.

$$D_{123} \equiv \frac{1}{8\omega_{k_1}\omega_{k_2}\omega_{k_3}(E - \omega_{k_1} - \omega_{k_2} - \omega_{k_3})} \,, \tag{B.36}$$

and regulated the UV in the $\mathbf{k}_3$ sum in the first term with $H^{(1)}(\mathbf{k}_1)$, where $\mathbf{k}_1 = \mathbf{P} - \mathbf{k}_2 - \mathbf{k}_3$, and in the $\mathbf{k}_2$ sum in the second term with $H^{(2)}(\mathbf{k}_2)$. If we now change the summation variable in the second term from $\mathbf{k}_1$ to $\mathbf{k}_3$, we obtain

$$\Delta_{3\Sigma}^{(21)} = \frac{1}{L^6} \sum_{\mathbf{k}_2\mathbf{k}_3} H^{(1)}(\mathbf{k}_1) H^{(2)}(\mathbf{k}_2) D_{123} \Bigg\{ \sum_{\ell' m' \ell m} \Bigg[X_{k_2 \ell' m'} \frac{\mathcal{Y}_{\ell' m'}(\mathbf{k}_3^{*(k_2)})}{q_{2,k_2}^{*\ell'}} \frac{\mathcal{Y}_{\ell m}(\mathbf{k}_3^{*(k_2)})}{q_{2,k_2}^{*\ell}} Z_{k_2 \ell m} - X_{k_1 \ell' m'} \frac{\mathcal{Y}_{\ell' m'}(\mathbf{k}_2^{*(k_1)})}{q_{2,k_1}^{*\ell'}} \frac{\mathcal{Y}_{\ell m}(\mathbf{k}_2^{*(k_1)})}{q_{2,k_1}^{*\ell}} Z_{k_1 \ell m} \Bigg] \Bigg\}, \quad \text{(B.37)}$$

where the order of summations is immaterial. Again the term in curly braces vanishes on shell, although here this requires summing over both sets of spherical harmonic indices. Thus we can replace the double momentum sum by a double integral. Combining this with the integral parts from the $\widetilde{F}^{(i)}$s in $\Delta_3^{(12)}$ the result can be brought into the form

$$\Delta_3^{(21)} = \Big[\int_{\mathbf{k}_2} \mathrm{PV} \int_{\mathbf{k}_3} - \int_{\mathbf{k}_3} \mathrm{PV} \int_{\mathbf{k}_2} \Big] \sum_{\ell' m' \ell m} X_{k_2 \ell' m'} \frac{\mathcal{Y}_{\ell' m'}(\mathbf{k}_3^{*(k_2)})}{q_{2,k_2}^{*\ell'}} \frac{H^{(1)}(\mathbf{k}_1) H^{(2)}(\mathbf{k}_2)}{2\omega_{k_1}(E - \omega_{k_1} - \omega_{k_2} - \omega_{k_3})} \frac{\mathcal{Y}_{\ell m}(\mathbf{k}_3^{*(k_2)})}{q_{2,k_2}^{*\ell}} Z_{k_2 \ell m} \,. \quad \text{(B.38)}$$

By a similar argument, one can show that $\Delta_3^{(23)}$ is given by the same expression. This shows that the integral operator can be written such that it only depends on the flavor 2. Thus we use the following notation for the final result

$$\Delta_3^{(21)} = \Delta_3^{(23)} \equiv [X]_2 [\widehat{\mathcal{I}}_F]_{22} [Z]_2 \,, \quad \text{(B.39)}$$

where $\widehat{\mathcal{I}}_F$ is a diagonal matrix of integral operators.

Finally we consider Δ_4, where we only sketch the argument. The sum part of $\widetilde{F}^{(k)}$ cancels with the summand of $[\widehat{F}_G]_{ij}$ at the on-shell point, so that, for this combination, the sums can be replaced by integrals. The pole prescription can be chosen so that the integral over the $\widetilde{F}^{(k)}$ summand cancels the integral part of this quantity, leaving an integral over the $\widetilde{G}$ term. The end result is that

$$\Delta_4 = \sum_{i \neq j} [X_i]_i [\widehat{\mathcal{I}}_G]_{ij} [Z_j]_j \,, \quad \text{(B.40)}$$

where the integral operator is given, for example, by

$$[X_1]_1[\widehat{\mathcal{I}}_G]_{12}[Z_2]_2 = \int_{\mathbf{k}_1} \mathrm{PV} \int_{\mathbf{k}_2} \sum_{\ell' m' \ell m} X_{k_1 \ell' m'} \frac{\mathcal{Y}_{\ell' m'}(\mathbf{k}_2^{*(k_1)})}{q_{2,k_1}^{*\ell'}} \frac{H^{(1)}(\mathbf{k}_1) H^{(2)}(\mathbf{k}_2)}{2\omega_{k_3}(E - \omega_{k_1} - \omega_{k_2} - \omega_{k_3})} \frac{\mathcal{Y}_{\ell m}(\mathbf{k}_1^{*(k_2)})}{q_{2,k_2}^{*\ell}} (-1)^\ell Z_{k_2 \ell m} \,. \tag{B.41}$$

We define the diagonal elements of $\widehat{\mathcal{I}}_G$ to vanish.

Combining these results we obtain

$$\Delta = \mathbf{X} \left(\overrightarrow{\widehat{\mathcal{I}}}_G + \overleftarrow{\widehat{\mathcal{I}}}_G + 2\widehat{\mathcal{I}}_F + \widehat{\mathcal{I}}_G \right) \mathbf{Z} \equiv \mathbf{X} 3 \widehat{\mathcal{I}}_{FG} \mathbf{Z} \,, \tag{B.42}$$

which completes the demonstration of Eq. (B.28).

B.4 Derivation of Eqs. (4.105) and (4.106)

In this appendix we show that the two forms of $\widehat{\mathcal{M}}'_{\mathrm{df},3,L}$, Eqs. (4.79) and (4.105), are equivalent. We find it easiest to start from the latter relation and work back to the former.

We will need the following results for $\widehat{\mathcal{D}}_{23,L}$,

$$i\widehat{\mathcal{D}}_{23,L} = \frac{1}{1 - i\widehat{\overleftrightarrow{\mathcal{K}}}_{2,L} i\widehat{F}_G} i\widehat{\overleftrightarrow{\mathcal{K}}}_{2,L} \,, \tag{B.43}$$

$$= (1 + i\widehat{\mathcal{D}}_{23,L} i\widehat{F}_G) i\widehat{\overleftrightarrow{\mathcal{K}}}_{2,L} \,, \tag{B.44}$$

$$= i\widehat{\overleftrightarrow{\mathcal{K}}}_{2,L} + i\widehat{\overleftrightarrow{\mathcal{K}}}_{2,L} (1 + i\widehat{F}_G i\widehat{\mathcal{D}}_{23,L}) i\widehat{F}_G i\widehat{\overleftrightarrow{\mathcal{K}}}_{2,L} \,, \tag{B.45}$$

which follow from Eqs. (4.55) and (4.50).

We first note that, using Eq. (B.44),

$$\left[1 + i\widehat{\mathcal{D}}_{23,L} i(\widehat{F}_G - \overrightarrow{\widehat{\mathcal{I}}}_G) \right] = \left[1 + i\widehat{\mathcal{D}}_{23,L} i\widehat{F}_G \right] \widehat{L}_G \,, \tag{B.46}$$

$$\widehat{L}_G \equiv \left[1 - i\widehat{\overleftrightarrow{\mathcal{K}}}_{2,L} i\overrightarrow{\widehat{\mathcal{I}}}_G \right] \,, \tag{B.47}$$

and, similarly,

$$\left[1 + i(\widehat{F}_G - \overleftarrow{\widehat{\mathcal{I}}}_G) i\widehat{\mathcal{D}}_{23,L})\right] = \widehat{R}_G \left[1 + i\widehat{F}_G i\widehat{\mathcal{D}}_{23,L}\right] , \tag{B.48}$$

$$\widehat{R}_G \equiv \left[1 - i\overleftarrow{\widehat{\mathcal{I}}}_G i\widehat{\overline{\mathcal{K}}}_{2,L}\right] . \tag{B.49}$$

Given these results, Eq. (4.105) can be rewritten

$$\widehat{\mathcal{M}}'_{\mathrm{df},3,L} = \left[1 + i\widehat{\mathcal{D}}_{23,L} i\widehat{F}_G\right] \widehat{L}_G \widehat{\mathcal{T}}_L \widehat{R}_G \left[1 + i\widehat{F}_G i\widehat{\mathcal{D}}_{23,L}\right] . \tag{B.50}$$

Comparing to Eq. (4.79), this implies that what we need to show is that

$$\widehat{L}_G i\widehat{\mathcal{T}}_L \widehat{R}_G = i\widehat{\mathcal{K}}'_{\mathrm{df},3} \frac{1}{1 - [1 + i\widehat{F}_G i\widehat{\mathcal{D}}_{23,L}] i\widehat{F}_G i\widehat{\mathcal{K}}'_{\mathrm{df},3}} . \tag{B.51}$$

To proceed, we rewrite the definition of $\widehat{\mathcal{T}}_L$, Eq. (4.106), as

$$[i\widehat{\mathcal{T}}_L]^{-1} = [i\widehat{\mathcal{K}}''_{\mathrm{df},3}]^{-1} - i(\widehat{F}_G - \widehat{\mathcal{I}}_{FG}) - i(\widehat{F}_G - \overleftarrow{\widehat{\mathcal{I}}}_G) i\widehat{\mathcal{D}}_{23,L} i(\widehat{F}_G - \overrightarrow{\widehat{\mathcal{I}}}_G) \tag{B.52}$$

$$= [i\widehat{\mathcal{K}}''_{\mathrm{df},3}]^{-1} + i\widehat{\mathcal{I}}_{FG} - i\overleftarrow{\widehat{\mathcal{I}}}_G i\widehat{\overline{\mathcal{K}}}_{2,L} i\overrightarrow{\widehat{\mathcal{I}}}_G - \widehat{R}_G(1 + i\widehat{F}_G i\widehat{\mathcal{D}}_{23,L}) i\widehat{F}_G \widehat{L}_G , \tag{B.53}$$

$$= [i\widehat{Z}]^{-1} - \widehat{R}_G(1 + i\widehat{F}_G i\widehat{\mathcal{D}}_{23,L}) i\widehat{F}_G \widehat{L}_G , \tag{B.54}$$

where to obtain the second line we have used Eqs. (B.44) and (B.45), and to obtain the third line we have used Eq. (4.103). Thus

$$\widehat{L}_G i\widehat{\mathcal{T}}_L \widehat{R}_G = \widehat{L}_G i\widehat{Z} \frac{1}{1 - \widehat{R}_G(1 + i\widehat{F}_G i\widehat{\mathcal{D}}_{23,L}) i\widehat{F}_G \widehat{L}_G i\widehat{Z}} \widehat{R}_G \tag{B.55}$$

$$= \widehat{L}_G i\widehat{Z}\widehat{R}_G \frac{1}{1 - (1 + i\widehat{F}_G i\widehat{\mathcal{D}}_{23,L}) i\widehat{F}_G \widehat{L}_G i\widehat{Z}\widehat{R}_G} , \tag{B.56}$$

which gives the desired result (B.51) since we can rewrite Eq. (4.104) as $\widehat{L}_G \widehat{Z} \widehat{R}_G = \widehat{\mathcal{K}}'_{\mathrm{df},3}$.

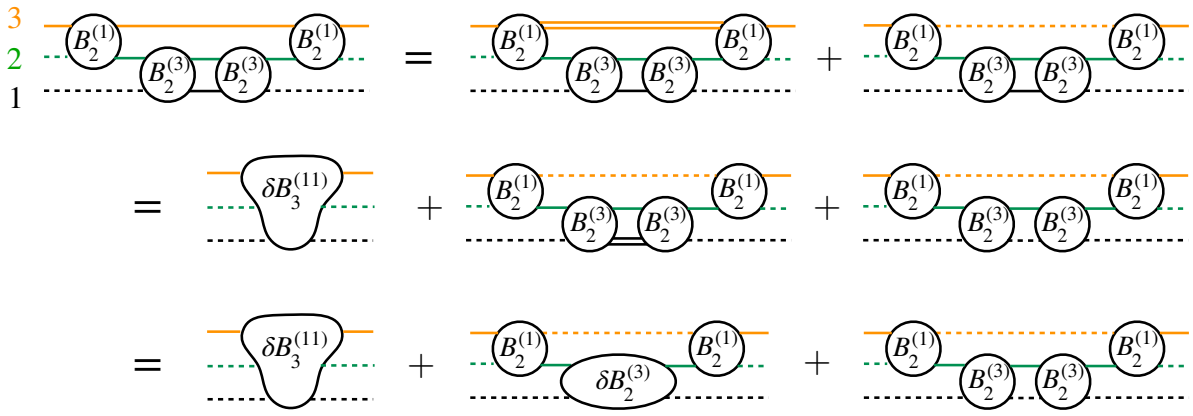

Figure B.1: An example of the first step in the analysis for a contribution to $[\widehat{\mathcal{M}}'^{\text{off}}_{3,L}]_{11}$ containing only B_2 kernels. Colors and labels indicate flavors as in earlier figures. Solid lines indicate fully dressed propagators, prior to integration over energy, except for the external lines, where a solid propagator indicates only that it is has an off-shell momentum. Dashed lines indicate on-shell propagators, which come with a factor of $1/(2\omega)$ when internal (due to the energy integration picking up the particle pole), or are amputated when external. Double solid line propagators indicate that only the off-shell contributions from the energy integral are kept, as described in the text. These cannot lead to a three-particle on-shell cut. In the first step, the energy of the flavor 3 (upper, orange) spectator propagator is integrated, leading to the off- and on-shell terms as shown. The former can be absorbed into a shift in the appropriate element of the three-particle Bethe-Salpeter kernel, as shown by the first term on the second line, and is not manipulated further. In the second step, the flavor 1 (lower, black) propagator is integrated over its energy, again leading to on- and off-shell contributions for both diagrams. In the final step, the two $B_2^{(3)}$ kernels connected by an off-shell (double-line) propagator (which can now be integrated) are absorbed into a shift in that kernel. This leads to the three diagrams shown on the bottom line, in which all independent internal propagators are on shell. The remaining propagators (which in this case are the middle, green, flavor 2 lines) have four-momenta that are determined by the momenta flowing through the other lines and in general are off shell.

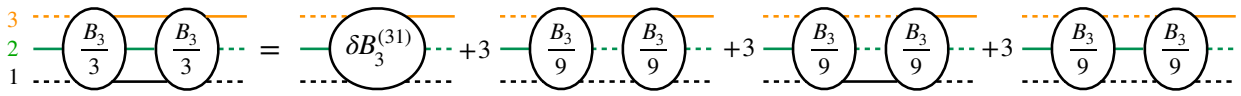

Figure B.2: Example of the first step in the analysis for a diagram that contributes to $[\widehat{\mathcal{M}}'^{\text{off}}_{3,L}]_{31}$ and contains two B_3 kernels. Notation as in Fig. B.1. Only the final result is shown. See text for further discussion.

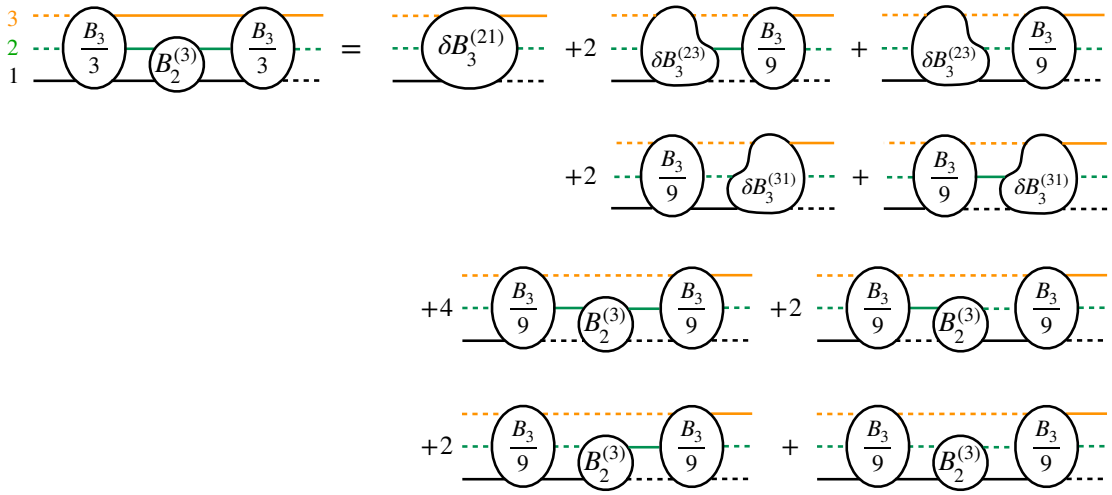

Figure B.3: Example of the first step in the analysis for a diagram that contributes to $[\widehat{\mathcal{M}}'^{\text{off}}_{3,L}]_{21}$ and contains both B_3 and B_2 kernels. Notation as in Fig. B.1. Only the final result is shown. See text for further discussion.

Appendix C

APPENDIX TO CHAPTER 5

C.1 Summary of notation and definitions

We collect here the definitions of quantities used in the main text, and explain the notation that is used. These results are drawn from Refs. [28, 29] and [43], and we use the notation of the latter work (referred to as BS1 in the main text). We present a bare-bones description here—see these references for further details.

Configurations of three on-shell particles are described by denoting one of the particles as the spectator and the other two as the interacting pair, or "dimer" for short. These designations are intrinsically asymmetric, and this is used when defining the asymmetric kernels such as $\mathcal{R}^{(u,u)}$ and $\mathcal{K}_{\text{df},3}^{\prime(u,u)}$, where any initial two-particle interaction is always chosen to involve the dimer, although subsequently all three particles interact. For symmetric quantities such as $\mathcal{K}_{\text{df},3}$, the choice of which momentum is denoted the spectator is irrelevant.

In more detail, for a given total 4-momentum $P^\mu = (E, \mathbf{P})$, the momentum dependence of quantities is specified by giving the momentum of the spectator, call it $\mathbf{k}$, and then boosting to the center-of-mass frame (CMF) of the dimer and decomposing the momentum dependence of one particle in the dimer into spherical harmonics. Thus the variables are $\{\mathbf{k}, \ell, m\}$. A similar set of variables is used for both initial and final momenta, so that, for example, the on-shell scattering amplitude can be written $\mathcal{M}_3(\mathbf{k}, \mathbf{p})_{\ell m;\ell' m'}$. In infinite volume, $\mathbf{k}$ and $\mathbf{p}$ are continuous variables.

In the quantization conditions, the spectator momenta are constrained by the boundary conditions, here chosen to be periodic in the box size L. Then $\mathbf{k} = \frac{2\pi}{L}\mathbf{n}$, with $\mathbf{n} \in \mathbb{Z}^3$. Thus all of the variables become discrete, and we denote the full set by $\{k\ell m\}$, with k a shorthand

for the discrete choices of $\mathbf{k}$. All quantities in the quantization condition are then matrices in which each of the indices runs over the set $\{k\ell m\}$. For quantities that are initially defined in infinite volume, the restriction to the finite-volume matrix versions is exemplified by

$$\mathcal{R}^{(u,u)}_{k\ell m;p\ell' m'} = \mathcal{R}^{(u,u)}(\mathbf{k},\mathbf{p})_{\ell m;\ell' m'}\,, \qquad \{\mathbf{k},\mathbf{p}\} \in \frac{2\pi}{L}\mathbb{Z}^3\,. \tag{C.1}$$

Two-particle quantities that enter the quantization condition naturally come with associated factors of $2\omega_k L^3$, where $\omega_k = \sqrt{\mathbf{k}^2 + m^2}$, with m the particle mass. These quantities are overlined, to distinguish them from the infinite-volume two-particle amplitude that they contain, and given a subscript "L" to emphasize their volume dependence. For example,

$$\left[\overline{\mathcal{K}}_{2,L}\right]_{k\ell m;p\ell' m'} = \left[(2\omega L^3)\mathcal{K}_2\right]_{k\ell m;p\ell' m'}\,, \tag{C.2}$$

$$\left[\mathcal{K}_2\right]_{k\ell m;p\ell' m'} = \delta_{kp}\delta_{\ell\ell'}\delta_{mm'}\mathcal{K}_2^{(\ell)}(q^*_{2,k})\,, \tag{C.3}$$

$$\left[2\omega L^3\right]_{k\ell m;p\ell' m'} = \delta_{kp}\delta_{\ell\ell'}\delta_{mm'}2\omega_k L^3\,, \tag{C.4}$$

where $\mathcal{K}_2^{(\ell)}$ is the ℓth partial wave of the infinite-volume two-particle K matrix, which depends on the dimer CMF relative momentum,

$$q^*_{2,k} = \sqrt{E^{*2}_{2,k}/4 - m^2}\,, \qquad E^{*2}_{2,k} = (E-\omega_k)^2 - (\mathbf{P}-\mathbf{k})^2\,. \tag{C.5}$$

Following Refs. [28, 36], we define $\mathcal{K}_2$ using a generalized principal value (PV) pole prescription, such that its relation to the physical two-particle scattering amplitude $\mathcal{M}_2$ is

$$\left[\mathcal{K}_2^{(\ell)}(q^*_{2,k})\right]^{-1} = \left[\mathcal{M}_2^{(\ell)}(q^*_{2,k})\right]^{-1} - \widetilde{\rho}^{(\ell)}_{\mathrm{PV}}(q^{*2}_{2,k})\,, \tag{C.6}$$

where

$$\widetilde{\rho}^{(\ell)}_{\mathrm{PV}}(q^{*2}_{2,k}) = H(\mathbf{k})\left[\widetilde{\rho}(q^{*2}_{2,k}) + \frac{1}{32\pi^2} I^{(\ell)}_{\mathrm{PV}}(q^{*2}_{2,k})\right]\,, \tag{C.7}$$

with the phase space factor given by

$$\widetilde{\rho}(q_{2,k}^{*2}) = \frac{1}{16\pi E_{2,k}^*} \begin{cases} -i|q_{2,k}^*| & q_{2,k}^{*2} > 0 \\ |q_{2,k}^*| & q_{2,k}^{*2} \leq 0 \end{cases} . \tag{C.8}$$

$I_{\mathrm{PV}}^{(\ell)}$ is an arbitrary real, smooth function, which is used to move poles in $\mathcal{K}_2$ out of the kinematic range of interest. $H(\mathbf{k})$ is a smooth cutoff function, which cuts off the sum over $\mathbf{k}$ for $|\mathbf{k}| \sim m$. Examples are given in Refs. [28, 34].

The kinematic functions $\widetilde{F}$ and $\widetilde{G}$ are

$$\widetilde{F}_{k\ell m;p\ell' m'} = \delta_{kp} \frac{H(\mathbf{k})}{2\omega_k L^3} \left[\frac{1}{L^3} \sum_{\mathbf{a}}^{\mathrm{UV}} - \mathrm{PV} \int^{\mathrm{UV}} \frac{d^3a}{(2\pi)^3} \right] \frac{\mathcal{Y}_{\ell m}(\mathbf{a}_k^*)}{q_{2,k}^{*\ell}} \frac{1}{2!2\omega_a(b_{ka}^2 - m^2)} \frac{\mathcal{Y}_{\ell' m'}(\mathbf{a}_k^*)}{q_{2,k}^{*\ell'}} , \tag{C.9}$$

$$\widetilde{G}_{k\ell m;p\ell' m'} = \frac{1}{2\omega_k L^3} \frac{\mathcal{Y}_{\ell m}(\mathbf{p}_k^*)}{q_{2,k}^{*\ell}} \frac{H(\mathbf{k})H(\mathbf{p})}{b_{pk}^2 - m^2} \frac{\mathcal{Y}_{\ell' m'}(\mathbf{k}_p^*)}{q_{2,p}^{*\ell'}} \frac{1}{2\omega_p L^3} . \tag{C.10}$$

Here $b_{ka}^\mu \equiv P^\mu - k^\mu - a^\mu$ is a four vector, with $k^\mu = (\omega_k, \mathbf{k})$ and $a^\mu = (\omega_a, \mathbf{a})$, and b_{kp} is defined analogously. The sum over $\mathbf{a}$ in $\widetilde{F}$ runs over the finite-volume set. Momenta with an asterisk, e.g. $\mathbf{a}_k^*$ and $\mathbf{p}_k^*$, are boosted from the original frame (with total momentum $\mathbf{P}$) into the CMF of the dimer. There is some flexibility in the choice of boost, with two examples being given in Refs. [28] and BS1. The former leads to a relativistically covariant $\widetilde{G}$, in the sense that the vectors $\mathbf{p}_k^*$ and $\mathbf{k}_p^*$ are unchanged (up to global rotations) when the initial frame is given an arbitrary boost. We refer to this form of $\widetilde{G}$ as the "relativistic form" in the main text. The harmonic polynomials are defined by

$$\mathcal{Y}_{\ell m}(\mathbf{a}) = \sqrt{4\pi} Y_{\ell m}(\widehat{\mathbf{a}}) |\mathbf{a}|^\ell , \tag{C.11}$$

with the spherical harmonics chosen to be in the real basis. The factors of $|\mathbf{p}_k^*|^\ell / q_{2,k}^{*\ell}$ in $\widetilde{G}$ are called "barrier factors" in the main text, and are needed to assure the smoothness of $\widetilde{G}$ when $|\mathbf{p}_k^*| \to 0$. The superscript UV on the sum and integral in $\widetilde{F}$ indicate an ultraviolet regularization, the nature of which affects $\widetilde{F}$ only at the level of exponentially suppressed terms. Finally, the integral in $\widetilde{F}$ is defined by the generalized pole prescription mentioned

above [36].

With these definitions, the finite-volume two-particle scattering amplitude (defined in Ref. [29]) is given by

$$\left[\overline{\mathcal{M}}_{2,L}\right]^{-1} = \left[\overline{\mathcal{K}}_{2,L}\right]^{-1} + \widetilde{F}\,, \tag{C.12}$$

which in the appropriate $L \to \infty$ limit goes over to Eq. (C.6).

C.2 Infinite-volume limits

In this appendix we provide further details of the infinite-volume limit needed to obtain Eq. (5.12) from Eq. (5.10), and discuss the properties of the inverses that appear in Secs. 5.3.4 and 5.4.

To obtain Eq. (5.12) we need to show that

$$\lim_{L\to\infty} X_L(\widetilde{F}+\widetilde{G})Z_L = \lim_{L\to\infty} X_L \frac{1}{(2\omega L^3)}(2\omega L^3)(\widetilde{F}+\widetilde{G})(2\omega L^3)\frac{1}{(2\omega L^3)}Z_L \tag{C.13}$$

$$= X_\infty(\widetilde{\rho}_{\rm PV} + G^\infty)Z_\infty\,, \tag{C.14}$$

with $X_L, Z_L \in \{\mathcal{K}'^{(u,u)}_{{\rm df},3}, \overline{\mathcal{K}}_{2,L}\}$ being finite-volume matrices, and X_∞, Z_∞ their corresponding infinite volume limits, given in Eqs. (5.15) and (5.16). The factors of $1/(2\omega L^3)$ convert the sums over intermediate momenta into the Lorentz-invariant integrals that are implicit in the infinite-volume form, Eq. (C.14). The remainder of the result can be obtained using

$$\lim_{L\to\infty} 2\omega_k L^3 \widetilde{F}_{k\ell m;p\ell' m'} 2\omega_p L^3 = \widetilde{\rho}_{\rm PV}(\mathbf{k},\mathbf{p})_{\ell m;\ell' m'} \tag{C.15}$$

$$\lim_{L\to\infty} 2\omega_k L^3 \widetilde{G}_{k\ell m;p\ell' m'} 2\omega_p L^3 = G^\infty(\mathbf{k},\mathbf{p})_{\ell m;\ell' m'}\,. \tag{C.16}$$

The first line follows from the results in Appendix B of BS1, while the second follows from the definitions of $\widetilde{G}$, Eq. (C.10), and G^∞, Eq. (F.23).

We now turn to the definition of inverses of infinite-volume quantities, beginning with

$\overline{\mathcal{K}}_2^{-1}$. Given our integration measure, this should satisfy

$$\sum_{\ell''m''} \int_{\mathbf{r}} \overline{\mathcal{K}}_2{}^{-1}(\mathbf{k},\mathbf{r})_{\ell m;\ell''m''} \overline{\mathcal{K}}_2(\mathbf{r},\mathbf{p})_{\ell' m'';\ell' m'} = \overline{\delta}(\mathbf{k}-\mathbf{p})\delta_{\ell\ell'}\delta_{mm'}\,, \tag{C.17}$$

from which it follows that

$$\overline{\mathcal{K}}_2^{-1}(\mathbf{k},\mathbf{p})_{\ell m;\ell' m'} \equiv \overline{\delta}(\mathbf{k}-\mathbf{p})\delta_{\ell\ell'}\delta_{mm'} \left[\mathcal{K}_2^{(\ell)}(q_{2,k}^*)\right]^{-1}. \tag{C.18}$$

A drawback of our notation is that, although the infinite-volume limit of $\overline{\mathcal{K}}_{2,L}$, given in Eq. (5.16), looks natural, the same is not true of the inverse

$$\lim_{L\to\infty} (2\omega L^3)\left[\overline{\mathcal{K}}_{2,L}\right]^{-1}(2\omega L^3) = \overline{\mathcal{K}}_2^{-1}\,. \tag{C.19}$$

The extra factors of $(2\omega L^3)$ are, however, needed so that the limit of matrix products is as expected. For example, we have

$$\lim_{L\to\infty}\left[\mathcal{K}_{\mathrm{df},3}'^{(u,u)}\overline{\mathcal{K}}_{2,L}^{-1}\mathcal{K}_{\mathrm{df},3}'^{(u,u)}\right]_{k\ell m;p\ell' m'} = \left[\mathcal{K}_{\mathrm{df},3}'^{(u,u)}\overline{\mathcal{K}}_2^{-1}\mathcal{K}_{\mathrm{df},3}'^{(u,u)}\right](\mathbf{k},\mathbf{p})_{\ell m;\ell' m'}\,, \tag{C.20}$$

with the matrix multiplications converted to Lorentz-invariant integrals by the induced factors of $(2\omega L^3)^{-1}$. The only places where these extra factors are not absorbed are on the ends of expressions, such as in Eq. (5.41).

The inverses of $\mathcal{K}_{\mathrm{df},3}'^{(u,u)}$ and $\mathcal{R}^{(u,u)}$ appearing in Sec. 5.4 are defined as in Eq. (C.17), e.g.

$$\sum_{\ell''m''} \int_{\mathbf{r}} [\mathcal{R}^{(u,u)}]^{-1}(\mathbf{k},\mathbf{r})_{\ell m;\ell''m''} \mathcal{R}^{(u,u)}(\mathbf{r},\mathbf{p})_{\ell' m'';\ell' m'} = \overline{\delta}(\mathbf{k}-\mathbf{p})\delta_{\ell\ell'}\delta_{mm'}\,, \tag{C.21}$$

The relation of these inverses to the inverses of their finite-volume versions display similar peculiarities to that seen in Eq. (C.19), but these relations are not needed in the arguments of the main text.

Appendix D

APPENDIX TO CHAPTER 6

D.1 Definitions

Here we collect definitions of quantities appearing in F_3, Eq. (6.28), that are not given in the main text.

We begin with the cutoff function:

$$H(\mathbf{k}) = J(z)\,, \qquad z = \frac{E_{2,k}^{*2} - (1+\alpha_H)m^2}{(3-\alpha_H)m^2}\,, \tag{D.1}$$

$$J(z) = \begin{cases} 0, & z \le 0 \\ \exp\left(-\frac{1}{z}\exp\left[-\frac{1}{1-z}\right]\right), & 0 < z < 1 \\ 1, & 1 \le z \end{cases} \tag{D.2}$$

with $\alpha_H \in [-1, 3)$ a constant. We choose $\alpha_H = -1$, corresponding to the highest cutoff, in all our numerical investigations.

For $\widetilde{G}$ we use the relativistic form suggested in Ref. [34],

$$\widetilde{G}_{p\ell' m';k\ell m} \equiv \frac{1}{L^3}\frac{1}{2\omega_p}\frac{H(\mathbf{p})H(\mathbf{k})}{b^2-m^2}\frac{4\pi\mathcal{Y}_{\ell' m'}(\mathbf{k}^*)\mathcal{Y}_{\ell m}(\mathbf{p}^*)}{q_{2,p}^{*\ell'}\, q_{2,k}^{*\ell}}\frac{1}{2\omega_k}\,, \tag{D.3}$$

where $b = P - p - k$ is the momentum of the exchanged particle, $\mathbf{p}^*$ is the result of boosting p to the CM frame of the dimer for which k is the spectator momentum, and *vice versa*. Explicitly, we have

$$\mathbf{p}^* = (\gamma_k - 1)(\hat{p}\cdot\hat{k})\hat{k} + \omega_p\gamma_k\beta_k\hat{k} + \mathbf{p}, \quad \beta_k = \frac{|\mathbf{k}\,|}{E-\omega_k}, \quad \gamma_k = (1-\beta_k^2)^{-1/2}\,, \tag{D.4}$$

with $\mathbf{k}^*$ given by $\mathbf{p} \leftrightarrow \mathbf{k}$. Finally, $\mathcal{Y}_{\ell m}(\mathbf{k})$ are harmonic polynomials,

$$\mathcal{Y}_{\ell m}(\mathbf{k}) \equiv k^\ell Y_{\ell m}(\hat{k})\,, \tag{D.5}$$

where $Y_{\ell m}$ are the *real* spherical harmonics. The elements of $\widetilde{G}$ are clearly straightforward to evaluate numerically.

For completeness, we quote the real d-wave harmonic polynomials

$$\begin{aligned}
\sqrt{4\pi}\mathcal{Y}_{2-2}(\mathbf{k}) &= \sqrt{15}k_1k_2\,,\\
\sqrt{4\pi}\mathcal{Y}_{2-1}(\mathbf{k}) &= \sqrt{15}k_2k_3\,,\\
\sqrt{4\pi}\mathcal{Y}_{20}(\mathbf{k}) &= \sqrt{5}(2k_3^2 - k_1^2 - k_2^2)/2\,,\\
\sqrt{4\pi}\mathcal{Y}_{21}(\mathbf{k}) &= \sqrt{15}k_1k_3\,,\\
\sqrt{4\pi}\mathcal{Y}_{22}(\mathbf{k}) &= \sqrt{15}(k_1^2 - k_2^2)/2\,.
\end{aligned} \tag{D.6}$$

The associated Wigner D-matrices are

$$\mathcal{D}_{\ell' m',\ell m}(R) = \int d\Omega_{\hat{r}} Y_{\ell' m'}(R\hat{r}) Y_{\ell m}(\hat{r}) = \delta_{\ell\ell'}\mathcal{D}^{(\ell)}_{m'm}(R)\,, \tag{D.7}$$

where R is a rotation matrix. They are orthogonal matrices, and implement rotations of the spherical harmonics:

$$Y_{\ell m}(R\hat{r}) = \sum_{m'=-\ell}^{\ell} \mathcal{D}^{(\ell)}_{mm'}(R) Y_{\ell m'}(\hat{r})\,. \tag{D.8}$$

Finally, $\widetilde{F}(\mathbf{k})$ is a sum-integral difference that is proportional to the zeta functions that appear in the two-particle quantization condition [24, 25]. It requires ultraviolet (UV) regularization, and can be written in various forms that are equivalent up to exponentially-suppressed corrections. The form that follows from that presented in Ref. [28] is

$$\widetilde{F}(\mathbf{k})_{\ell' m';\ell m} = \left[\frac{1}{L^3}\sum_{\mathbf{a}} - \mathrm{PV}\int \frac{d^3a}{(2\pi)^3}\right] \frac{1}{(q^*_{2,k})^{\ell'+\ell}} \frac{H(\mathbf{a})H(\mathbf{b})4\pi\mathcal{Y}_{\ell' m'}(\mathbf{a}^*)\mathcal{Y}_{\ell m}(\mathbf{a}^*)}{16\omega_k\omega_a\omega_b(E-\omega_k-\omega_a-\omega_b)}\,, \tag{D.9}$$

where $b = P - k - a$ here, and $\mathbf{a}^*$ is the result of boosting a to the dimer rest frame, with k the spectator. Here the UV regularization is provided by the product of H functions, and the

integral over the pole is defined by the principle value prescription (leading to a real result). Instead, we use a different form that is simpler to evaluate numerically. Following the steps similar to those used in Ref. [27], we change variables and introduce a new regularization, finding that, up to exponentially-suppressed corrections, $\widetilde{F}$ can be rewritten as

$$\widetilde{F}(\mathbf{k})_{\ell' m';\ell m} = \frac{1}{32\pi^2 L\omega_k(E-\omega_k)} \left[\sum_{\mathbf{n}_a} -\mathrm{PV}\int d^3 n_a\right] \frac{e^{\alpha(x^2-r^2)}}{x^2-r^2} \frac{4\pi \mathcal{Y}_{\ell' m'}(\mathbf{r})\mathcal{Y}_{\ell m}(\mathbf{r})}{x^{\ell'+\ell}}\,, \tag{D.10}$$

where $\mathbf{a} = \mathbf{n}_a(2\pi/L)$, $x = q^*_{2,k}L/(2\pi)$, and

$$\mathbf{r}(\mathbf{n}_k, \mathbf{n}_a) = \mathbf{n}_a + \mathbf{n}_k \left[\frac{\mathbf{n}_a \cdot \mathbf{n}_k}{n_k^2}\left(\frac{1}{\gamma_k} - 1\right) + \frac{1}{2\gamma_k}\right]\,, \tag{D.11}$$

with $\mathbf{k} = \mathbf{n}_k(2\pi/L)$. The UV regularization is now provided by the exponential in the integrand, and is parametrized by $\alpha > 0$. What is shown in Ref. [27] is that the α dependence is exponentially suppressed in L, and that, in practice, one should choose a value that is small enough that the dependence on α lies below the accuracy required. We find that $\alpha \approx 0.5$ is usually small enough.

An important technical point is that, as seen from Eq. (C.9), in the full matrix form $\widetilde{F}_{p\ell' m';k\ell m}$, $\widetilde{F}(\mathbf{k})$ is always multiplied by $H(\mathbf{k})$, from which it follows that γ_k is always finite and real whenever $\widetilde{F}_{p\ell' m';k\ell m}$ is nonvanishing.

We close this appendix by commenting on the factors of q^* (which we use generically for $q^*_{2,k}$ or $q^*_{2,p}$) in the denominators of $\widetilde{G}$ and $\widetilde{F}$. These lead to poles for particular kinematic configurations, which in turn can lead to solutions to the quantization condition. These solutions appear to be similar to free solutions discussed in Sec. 6.4.4, but are in fact spurious. To understand this we need an argument given in Appendix A of Ref. [28], which shows that the factors of q^* in the denominators are always canceled by corresponding factors in the numerators of $\mathcal{K}_2$, $\mathcal{K}_{\mathrm{df},3}$, and the end cap factors $A^\dagger$ and A in the finite-volume correlation function $C_L(E)$ [see Eq. (6.63)]. The presence of the necessary factors of q^* in $\mathcal{K}_2$ can be seen from Eq. (6.32), while those in $\mathcal{K}_{\mathrm{df},3}$ arise from the quadratic dependence on $\mathbf{a}^*$ and

$\mathbf{a}'^*$ described in Sec. 6.3.1. Indeed, one can derive a version of the quantization condition in which all such factors are absent. To do so, we define the matrix

$$Q_{p\ell' m';k\ell m} = \delta_{pk}\delta_{\ell'\ell}\delta_{m'm} q_{2,k}^{*\ell} \,. \tag{D.12}$$

Then, from the arguments of Ref. [28] we know that we can write the end caps as $A = Q\widetilde{A}$ and $A^\dagger = \widetilde{A}^\dagger Q$, with $\widetilde{A}$ and $\widetilde{A}^\dagger$ nonsingular. Thus an alternative, improved form of the quantization condition is

$$\det[(QF_3Q)^{-1} + Q^{-1}\mathcal{K}_{\mathrm{df},3}Q^{-1}] = 0 \,. \tag{D.13}$$

Now we observe that, by simple algebraic manipulations, we can rewrite this form of the quantization condition in terms of $Q\widetilde{F}Q$, $Q\widetilde{G}Q$, $Q^{-1}\mathcal{K}_2Q^{-1}$ and $Q^{-1}\mathcal{K}_{\mathrm{df},3}Q^{-1}$, in all of which the factors of q^* cancel. Since the difference between the two quantization conditions is a factor of $\det(Q^2)$, it follows that the solutions to the new form, Eq. (D.13), are the same as those to Eq. (6.1), except that spurious solutions to the latter, arising from the factors of q^*, are removed. In conclusion, we can use the original form of the quantization condition, Eq. (6.1), as long as we ignore the spurious solutions.

D.2 Numerical evaluation of $\widetilde{F}$

In this appendix we describe some technical details concerning the evaluation of $\widetilde{F}(\mathbf{k})$.

D.2.1 Evaluating the integrals

An advantage of the form Eq. (D.10) is that the integrals can be evaluated analytically. Dropping overall factors, the integral that is needed is

$$I^F_{\ell' m';\ell m} = \mathrm{PV}\int d^3n_a \frac{e^{\alpha(x^2-r^2)}}{x^2-r^2} 4\pi \mathcal{Y}_{\ell' m'}(\mathbf{r})\mathcal{Y}_{\ell m}(\mathbf{r}) \,. \tag{D.14}$$

Changing variables to $\mathbf{r}$, we find

$$I^F_{\ell' m';\ell m} = \gamma \mathrm{PV} \int d^3 r \frac{e^{\alpha(x^2-r^2)}}{x^2-r^2} 4\pi \mathcal{Y}_{\ell' m'}(\mathbf{r}) \mathcal{Y}_{\ell m}(\mathbf{r}) = \delta_{\ell' \ell} \delta_{m' m} I^F_\ell \,, \tag{D.15}$$

$$I^F_\ell = 4\pi\gamma \mathrm{PV} \int r^2 dr \frac{e^{\alpha(x^2-r^2)}}{x^2-r^2} r^{2\ell} \,. \tag{D.16}$$

The remaining integral can be evaluated analytically for all ℓ. The explicit result for $\ell = 0$ was worked out in Ref. [39], and we have extended this to the $\ell = 2$ case. For convenience, we quote both results

$$I^F_0 = 4\pi\gamma \left[-\sqrt{\frac{\pi}{\alpha}} \frac{1}{2} e^{\alpha x^2} + \frac{\pi x}{2} \mathrm{Erfi}\left(\sqrt{\alpha x^2}\right) \right] \tag{D.17}$$

$$I^F_2 = 4\pi\gamma \left[-\sqrt{\frac{\pi}{\alpha^5}} \frac{3 + 2\alpha x^2 + 4\alpha^2 x^4}{8} e^{\alpha x^2} + \frac{\pi x^5}{2} \mathrm{Erfi}\left(\sqrt{\alpha x^2}\right) \right] . \tag{D.18}$$

D.2.2 Cutting off the sum

The sum in Eq. (D.10) is convergent, but in practice we must introduce a cutoff in order to evaluate it numerically. We use a spherical cutoff, $|\mathbf{n}_a| < n_{\max}$, and in this section explain how we choose $n_{\max}$.

The basic idea is to split the sum S as

$$S = S_< + S_> \,, \tag{D.19}$$

where $S_<$ is the contribution from below the cutoff, and $S_>$ the remainder. Assuming that the pole in the summand lies well below the cutoff, then $S_>$ can be well-approximated by a remainder integral, $R_>$. We evaluate this integral, and then choose $n_{\max}$ such that $R_>$ lies below our desired accuracy. The resulting $n_{\max}$ depends on E, L and the orbit of $\mathbf{k}$.

Dropping overall factors, and changing the overall sign, the sum of interest from Eq. (D.10) is

$$S = H(\mathbf{k}) \sum_{\mathbf{n}_a} \frac{e^{\alpha(x^2-r^2)}}{r^2-x^2} r^{\ell'+\ell} 4\pi Y_{\ell' m'}(\hat{r}) Y_{\ell m}(\hat{r}) \,. \tag{D.20}$$

Here we have included the cutoff function $H(\mathbf{k})$ that enters in the expression for $\widetilde{F}_{p\ell' m';k\ell m}$, Eq. (C.9). Although this is an overall factor, it will play an important role in the determination of $n_{\max}$.

The integral $R_>$ that results when replacing the sum over $\mathbf{n}_a$ with an integral is more easily evaluated by changing variables to $\mathbf{r}$. The relation between $\mathbf{n}_a$ and $\mathbf{r}$, Eq. (D.11), can be rewritten as

$$\gamma_k r_\parallel = n_{a,\parallel} - \frac{n_k}{2}\,, \qquad r_\perp = n_{a,\perp}\,, \tag{D.21}$$

with $\parallel$ and $\perp$ defined relative to $\mathbf{k}$. The cutoff is chosen such that $n_{\max} \gg n_k$, implying that the $n_k/2$ term in the expression for $r_\parallel$ is subleading. Dropping this term, we find that a spherical cutoff on $\mathbf{n}_a$ corresponds to an ellipsoidal cutoff on $\mathbf{r}$. This makes the integral difficult to evaluate, so we replace this with a spherical cutoff, $|\mathbf{r}| < \Lambda$, choosing $\Lambda = n_{\max}/\gamma_k$. We call the resulting integral R_Λ. The resulting spherical region is a superset of the original ellipsiodal region, so that we overestimate the remainder, $R_\Lambda > R_>$, since the integrand is positive.

To evaluate R_Λ we make two further approximations. First, we drop the x^2 term in the denominator, which is subleading since $r^2 \gg x^2$ within the region of integration. Second, we make the replacement $4\pi Y_{\ell' m'}(\hat{r}) Y_{\ell m}(\hat{r}) \to 1$, which leads to an overestimate of the integral. Then we find

$$R_\Lambda \approx \overline{R}_\lambda \equiv \gamma_k H(\mathbf{k}) 4\pi \int_\Lambda^\infty dr\; e^{\alpha(x^2-r^2)} r^{\ell'+\ell} \tag{D.22}$$

$$= \begin{cases} \gamma_k H(\mathbf{k}) e^{\alpha x^2} 2\pi \sqrt{\frac{\pi}{\alpha}} \mathrm{Erfc}\left[\sqrt{\alpha}\Lambda\right], & \ell' = \ell = 0 \\ \gamma_k H(\mathbf{k}) e^{\alpha x^2} \frac{\pi}{\alpha} \{2\Lambda e^{-\alpha\Lambda^2} + \sqrt{\frac{\pi}{\alpha}} \mathrm{Erfc}\left[\sqrt{\alpha}\Lambda\right]\}, & \ell' + \ell = 2 \\ \gamma_k H(\mathbf{k}) e^{\alpha x^2} \frac{\pi}{\alpha^2} \{(3\Lambda + 2\alpha\Lambda^3) e^{-\alpha\Lambda^2} + \frac{3}{2}\sqrt{\frac{\pi}{\alpha}} \mathrm{Erfc}\left[\sqrt{\alpha}\Lambda\right]\}, & \ell' + \ell = 4. \end{cases} \tag{D.23}$$

The overall factor of γ_k is the Jacobian from changing the integration variable from $\mathbf{n}_a$ to $\mathbf{r}$. We choose the Λ by specifying a tolerance ϵ (we use $\epsilon = 10^{-9}$) and numerically solving

$\overline{R}_\Lambda = \epsilon$.[1] Given Λ, we then obtain the cutoff for the sum using $n_{\max} = \gamma_k \Lambda$.

We can now explain why we include the factor of $H(\mathbf{k})$ in S. As $|\mathbf{k}|$ approaches the value where $H(\mathbf{k})$ vanishes, γ_k diverges. This leads to an increase in $n_{\max}$, both from the factor of γ_k in $\overline{R}_\Lambda$, and because $n_{\max}/\Lambda = \gamma_k$. However, this increase is more than compensated by the very rapid drop in $H(\mathbf{k})$ near the end point, so that $n_{\max}$ is always finite.

D.2.3 Using cubic symmetries

Symmetries can be exploited to optimize the computation of $\widetilde{F}$. It follows from Eq. (C.9) that $\widetilde{F}(R\mathbf{k})$ can be obtained from $\widetilde{F}(\mathbf{k})$ via an orthogonal transformation for any cubic-group transformation $R \in O_h$,

$$\widetilde{F}(R\mathbf{k}) = \mathcal{D}(R)\widetilde{F}(\mathbf{k})\mathcal{D}(R)^T . \tag{D.24}$$

Here $\mathcal{D}(R)$ is the Wigner D-matrix defined in Eq. (D.7). Thus once one has computed $\widetilde{F}(\mathbf{k})$ for some finite-volume momentum $\mathbf{k}$, one can use Eq. (D.24) to obtain $\widetilde{F}(\mathbf{k}')$ for all $\mathbf{k}'$ in the same momentum shell. Furthermore, for each initial $\widetilde{F}(\mathbf{k})$ that one computes directly, any symmetries of $\mathbf{k}$ can be used to simplify the construction of $\widetilde{F}(\mathbf{k})$. In particular, if R is in the little group of $\mathbf{k}$ (so that $R\mathbf{k} = \mathbf{k}$), then Eq. (D.24) says that $\widetilde{F}(\mathbf{k})$ is invariant under the transformation. This often leads to linear relationships between several matrix elements $\widetilde{F}_{\ell' m', \ell m}(\mathbf{k})$, in which case one need only compute the linearly-independent elements in order to construct the full matrix.

D.3 Further details of the projection onto cubic group irreps

We collect here some results that we have found useful in the computation of the projection matrices and the determination of their properties.

---

[1] In practice we use the $\ell' = \ell = 0$ result for $\overline{R}_\Lambda$ in all cases, which is a further approximation, but one that we find makes a small numerical impact.

D.3.1 Computing P_I efficiently

The projector P_I is defined in Eq. (6.41). As explained in the main text, it is block diagonal in momentum shells and in angular momentum, with blocks $P_{I,o(\ell)}$. Here we explain how to simplify the computation of $P_{I,o(\ell)}$ by reducing the sum in Eq. (6.41), which runs over all 48 elements of O_h, to a sum over the elements of the little group of an element of the shell under consideration.

Let $\mathbf{k}'$ and $\mathbf{k}''$ be two elements of the orbit. Then, from Eqs. (6.41) and (6.42), we have

$$\left[P_{I,o(\ell)}\right]_{k''k'} = \frac{d_I}{[O_h]} \sum_{R\in O_h} \chi_I(R)\delta_{k'_R k''}\mathcal{D}^{(\ell)}(R)\,, \tag{D.25}$$

where $\delta_{k'_R k''}$ is unity if $R\mathbf{k}' = \mathbf{k}''$ and zero otherwise. Thus the sum is restricted to those elements of O_h that rotate $\mathbf{k}'$ into $\mathbf{k}''$. A convenient representation of these elements makes use of an (arbitrarily chosen) canonical element of the orbit, denoted $\mathbf{k}$. Let R_{L_k} be an element of the little group L_k of $\mathbf{k}$. Then all the elements of O_h that rotate $\mathbf{k}'$ to $\mathbf{k}''$ can be written as $R_{k''k}R_{L_k}R_{kk'}$, where $R_{kk'}$ is any choice of transformation from $\mathbf{k}'$ to $\mathbf{k}$, and $R_{k''k}$ is any choice of transformation from $\mathbf{k}$ to $\mathbf{k}''$. Thus the number of elements contributing to the sum in Eq. (D.25) is $[L_k]$, the dimension of L_k. This allows us to rewrite the projector as

$$\left[P_{I,o(\ell)}\right]_{k''k'} = \frac{d_I}{[O_h]} \sum_{R\in L_k} \chi_I(R_{k''k}RR_{kk'})\mathcal{D}^{(\ell)}(R_{k''k}RR_{kk'}) \tag{D.26}$$

$$= \frac{d_I}{N_o}\mathcal{D}^{(\ell)}(R_{k''k}) \left[\frac{1}{[L_k]} \sum_{R\in L_k} \chi_I(R_{k''k}RR_{kk'})\mathcal{D}^{(\ell)}(R)\right] \mathcal{D}^{(\ell)}(R_{kk'})\,, \tag{D.27}$$

where $N_o = [O_h]/[L_k]$ is the number of elements in the orbit.

Once we have constructed the block projectors, we combine them into P_I using Eq. (6.43). In practice, we want to reduce our original matrices ($M = \widetilde{F}$ etc.) down to the part that lives in the projected subspace, which has dimension $d(P_I)$. To do so, we evaluate the eigenvalues and eigenvectors of P_I. Since P_I is a projector, its eigenvalues λ_i are either zero or unity.

We keep only the eigenvectors with unit eigenvalues, for these span the projection subspace. We orthonormalize the eigenvectors, and label them $\{\mathbf{v}_i\}_{i=1}^{d(P_I)}$. The reduced matrix is then given by

$$M_{ij}^{\text{red}} = \mathbf{v}_i^{\text{Tr}} \cdot M \cdot \mathbf{v}_j \qquad (i, j \in 1 - d(P_I)) \,. \tag{D.28}$$

D.3.2 Dimensions of irrep projection subspaces

As explained in the main text, in order to determine the number of eigenvalues of M that fall into a given irrep we need to compute the dimensions of the sub-block projectors,

$$d(P_{I,o(\ell)}) = \text{Tr } P_{I,o(\ell)} \,. \tag{D.29}$$

Using the result for the projector, Eq. (D.27), we find

$$d(P_{I,o(\ell)}) = \sum_{\mathbf{k}' \in o} \text{Tr} \left[P_{I,o(\ell)} \right]_{k'k'} \,, \tag{D.30}$$

$$= \frac{d_I}{[L_k]} \sum_{R \in L_k} \chi_I(R) \text{ Tr } \mathcal{D}^{(\ell)}(R) \,, \tag{D.31}$$

where the trace is only over the angular momentum indices, m, and to obtain the second line we have used the cyclicity of the trace, the fact that $R_{k'k} = R_{kk'}^{-1}$, and the standard group-theoretic result $\chi(R'RR'^{-1}) = \chi(R)$. The resulting dimensions are collected in Table 6.1.

D.4 a_2 dependence of $\mathcal{M}_{3,\text{thr}}$

In Sec. 6.2, we show that to determine the a_2 dependence of the three-particle threshold energy, we need to calculate the corresponding dependence of $\mathcal{M}_{3,\text{thr}}$. The calculation is described in this appendix.

We begin by recalling from Ref. [68] that $\mathcal{M}_{3,\text{thr}}$ is defined by doing the minimal subtrac-

tions necessary to have a finite quantity at threshold,

$$\mathcal{M}_{3,\text{thr}} = \lim_{\delta\to 0}\Big[\mathcal{M}_3(0,\hat{a}'^*;0,\hat{a}^*) \\ - I_{0,\delta}(0,\hat{a}'^*;0,\hat{a}^*) - \int_\delta \frac{d^3k_1}{(2\pi)^3}\Xi_1(\mathbf{k}_1) - \int_\delta \frac{d^3k_1}{(2\pi)^3}\frac{d^3k_2}{(2\pi)^3}\Xi_2(\mathbf{k}_1,\mathbf{k}_2)\Big]\,. \tag{D.32}$$

Here $\mathcal{M}_3$ is the three-particle scattering amplitude, expressed in terms of the same variables used for $\mathcal{K}_{\text{df},3}$ in Eq. (6.20). The infrared (IR) divergence of $\mathcal{M}_3$ at threshold is regularized using the δ-scheme of Ref. [68], and three subtractions are needed in order to obtain a finite result. The explicit expressions for I_0, Ξ_1 and Ξ_2 are given in Sec. D of Ref. [68], but will not be needed. All we need to know here is that the subtractions depend on a_0, but not on a_2. Thus dependence on a_2 can only enter through $\mathcal{M}_3$ itself.

To determine this dependence it is useful to recall the definition of the divergence-free scattering amplitude from Ref. [29],

$$\mathcal{M}_{\text{df},3}(\mathbf{p},\hat{a}'^*;\mathbf{k},\hat{a}^*) = \mathcal{M}_3(\mathbf{p},\hat{a}'^*;\mathbf{k},\hat{a}^*) - \mathcal{D}(\mathbf{p},\hat{a}'^*;\mathbf{k},\hat{a}^*)\,. \tag{D.33}$$

Here $\mathcal{D}$ is a quantity that depends only on the two-particle scattering amplitude $\mathcal{M}_2$, whose expression will be given below. It is chosen so as to subtract IR divergences from $\mathcal{M}_3$ not only at threshold, but also above. Reordering Eq. (D.33) as $\mathcal{M}_3 = \mathcal{M}_{\text{df},3} + \mathcal{D}$, we note that, in general, both contributions to $\mathcal{M}_3$ depend on a_2. However, we also know from Ref. [29] that $\mathcal{M}_{\text{df},3}$ vanishes when $\mathcal{K}_{\text{df},3} = 0$. So, in this limit, which is the case we consider numerically, $\mathcal{M}_3 = \mathcal{D}$. This allows us to calculate the a_2 dependence of $\mathcal{M}_3$. We know that this dependence is finite at threshold because no a_2-dependent subtraction was needed in Eq. (D.32).

Before calculating the a_2 dependence of $\mathcal{M}_3$, it is instructive to relate the two subtracted versions of $\mathcal{M}_3$,

$$\mathcal{M}_{3,\text{thr}} = \mathcal{M}_{\text{df},3}(0,\hat{a}'^*;0,\hat{a}^*)\Big|_{E=3m} + \text{IR finite terms}\,. \tag{D.34}$$

Since, as already noted, $\mathcal{M}_{\text{df},3}$ vanishes when $\mathcal{K}_{\text{df},3} = 0$, we see that it is the IR finite terms

that must contain the contribution to $\mathcal{M}_{3,\text{thr}}$ from higher partial waves.

What we have learned so far is that, for $\mathcal{K}_{\text{df},3} = 0$, the a_2 dependence of $\mathcal{M}_{3,\text{thr}}$ is given by that of $\mathcal{D}$ evaluated at threshold. Here we are interested in determining the leading dependence, which, as discussed in the main text, is proportional to a_2^5. This is given by

$$\mathcal{M}_{3,\text{thr}} \supset a_2^5 \frac{d\mathcal{D}_{\text{thr}}}{d(a_2^5)}\bigg|_{a_2=0} . \tag{D.35}$$

Here $\mathcal{D}_{\text{thr}}$ is $\mathcal{D}(\mathbf{p}, \hat{a}'^*; \mathbf{k}, \hat{a}^*)$ evaluated at $E = 3m$ and $\mathbf{p} = \mathbf{k} = 0$, so that there is no dependence on $\hat{a}^*$ and $\hat{a}'^*$. In fact, $\mathcal{D}$ itself diverges in this limit, but the derivative in Eq. (D.35) does not.

To proceed, we need the explicit expression for $\mathcal{D}$, given in Ref. [29]. It is obtained by symmetrizing over initial and final momenta the quantity $\mathcal{D}^{(u,u)}$, which is given by

$$\mathcal{D}^{(u,u)}(\mathbf{p},\mathbf{k}) = -\mathcal{M}_2(\mathbf{p})G^\infty(\mathbf{p},\mathbf{k})\mathcal{M}_2(\mathbf{p}) + \int_s \frac{1}{2\omega_s}\mathcal{M}_2(\mathbf{p})G^\infty(\mathbf{p},\mathbf{s})\mathcal{M}_2(\mathbf{s})G^\infty(\mathbf{s},\mathbf{k})\mathcal{M}_2(\mathbf{k}) + \dots . \tag{D.36}$$

Here $\int_s \equiv \int d^3s/(2\pi)^3$, and the $\hat{a}^*$ and $\hat{a}'^*$ dependence has been decomposed into partial waves, so that all quantities are implicitly matrices in angular momentum space. The spectator-momentum dependence is, however, kept explicit. $\mathcal{M}_2(\mathbf{p})$ is the two-particle scattering amplitude for the dimer when the spectator-momentum is $\mathbf{p}$. As for $\mathcal{K}_2$ [see Eq. (6.30)], it is diagonal in angular momentum

$$\mathcal{M}_2(\mathbf{p})_{\ell' m';\ell m} = \delta_{\ell'\ell}\delta_{m'm}\mathcal{M}_2^{(\ell)} . \tag{D.37}$$

It contains all (even) partial waves, including, in particular, the d-wave amplitude. Finally, G^∞ is given by

$$G^\infty_{\ell' m';\ell m}(\mathbf{p},\mathbf{k}) \equiv \frac{H(\mathbf{p})H(\mathbf{k})}{b^2 - m^2}\frac{4\pi \mathcal{Y}_{\ell' m'}(\mathbf{k}^*)\mathcal{Y}_{\ell m}(\mathbf{p}^*)}{q_{2,p}^{*\ell'}\, q_{2,k}^{*\ell}} , \tag{D.38}$$

where the kinematic quantities are the same as those appearing in Eq. (D.3). Equation (D.38) is the relativistically-invariant version of the definition given in Eq. (81) of Ref. [29].

At threshold, only the s-wave part of $\mathcal{D}^{(u,u)}$ is nonzero, and symmetrization simply leads to an overall factor of 9:

$$\left.\frac{d\mathcal{D}_{\text{thr}}}{d(a_2^5)}\right|_{a_2=0} = 9\left.\frac{d\mathcal{D}^{(u,u)}_{00;00}(\mathbf{0},\mathbf{0})}{d(a_2^5)}\right|_{a_2=0} . \tag{D.39}$$

Looking at Eq. (D.36), we see that the s-wave projection implies that the factors of $\mathcal{M}_2$ on both ends are pure s-wave, so the first appearance of d-wave scattering occurs in the second term. This gives the leading a_2-dependent part of $\mathcal{D}^{(u,u)}$:

$$\mathcal{D}^{(u,u)}_{00;00}(\mathbf{0},\mathbf{0}) \supset I_d = \int_s \sum_{m=-2}^{2} \frac{1}{2\omega_s} \mathcal{M}_2^{(0)}(\mathbf{0}) G^{\infty}_{00;2m}(\mathbf{0},\mathbf{s}\,) \mathcal{M}_2^{(2)}(\mathbf{s}\,) G^{\infty}_{2m;00}(\mathbf{s},\mathbf{0}) \mathcal{M}_2^{(0)}(\mathbf{0}) . \tag{D.40}$$

At leading order in perturbation theory in a_0 and a_2, $\mathcal{M}_2^{(\ell)} = \mathcal{K}_2^{(\ell)}$, with $\mathcal{K}_2^{(\ell)}$ given by the leading terms in Eqs. (6.31) and (6.32). Inserting these results, we find that I_d is IR and UV convergent, so we do not need to actually take the derivative in Eq. (D.39). By numerical evaluation we find

$$\mathcal{M}_{3,\text{thr}} \supset 9I_d = -\frac{14109.6}{m^2} \times (ma_0)^2 (ma_2)^5 [1 + \mathcal{O}(a_0) + \mathcal{O}(a_2^5)] . \tag{D.41}$$

This gives the leading term in the result (6.54) quoted in the main text. The corrections in (D.41) arise from the subleading terms in the expressions for $\mathcal{K}_2^{(\ell)}$.

We close with two further observations. First, a similar calculation with $\mathcal{M}_2^{(2)}$ in I_d replaced by any (even) higher-order amplitude leads to a nonzero contribution to $\mathcal{M}_{3,\text{thr}}$. Thus all higher partial waves contribute to ΔE_3 at $\mathcal{O}(L^{-6})$. Second, higher-order terms in $\mathcal{D}^{(u,u)}$ will also contribute to $\mathcal{M}_{3,\text{thr}}$, although suppressed by powers of a_ℓ. For example, the first term not shown in Eq. (D.36), which has four factors of $\mathcal{M}_2$, leads to contributions to ΔE_3 proportional to $a_0^3 a_2^5/L^6$ and $a_0^2 a_2^{10}/L^6$. These are of the same order as the corrections in Eq. (D.41).

D.5 Free solutions at the first excited energy

In this appendix we analyze free solutions to the quantization condition in the A_1^+ irrep at the energy of the first excited noninteracting state, $E_1^{\text{free}} = m + 2\omega_1$ (with $\omega_1 = \sqrt{m^2 + k_L^2}$ and $k_L = 2\pi/L$). Our aim is to understand when F_3^{-1} has zeros at this energy, and to determine their properties. We work with box lengths $4 \lesssim mL \lesssim 6$ such that there are three active shells, although the final result generalizes straightforwardly to any number of shells.

D.5.1 A_1^+ irrep with s and d waves

We first consider the case in which both $\ell = 0$ and $\ell = 2$ channels are included. The matrices that enter into the quantization condition are then six dimensional: the first three indices as in Eq. (6.67), and the remaining three from the third shell (one with $\ell = 0$, and two with $\ell = 2$; see Table 6.1). The free poles enter only in the first two shells, and are proportional to

$$p = \frac{3}{8L^3 m\omega_1^2 \left(E - E_1^{\text{free}}\right)} \,. \tag{D.42}$$

It will be useful to introduce the vectors

$$\langle v_1| = (1,0,0,0,0,0)\,, \quad \langle v_2| = \left(0, \sqrt{\frac{1}{6}}, \sqrt{\frac{5}{6}}, 0, 0, 0\right)\,, \tag{D.43}$$

in terms of which the pole parts are given by [using Eqs. (D.9) and (D.3)]

$$\widetilde{F} = p\left(|v_1\rangle\langle v_1| + 2|v_2\rangle\langle v_2|\right) + \mathcal{O}(1)\,, \tag{D.44}$$

$$\widetilde{G} = 2p\left(|v_1\rangle\langle v_2| + |v_2\rangle\langle v_1| + |v_2\rangle\langle v_2|\right) + \mathcal{O}(1)\,. \tag{D.45}$$

As in the example discussed in Sec. 6.4.4, all we need to know about the $\mathcal{O}(1)$ contributions are that they are real and symmetric. The relative factor of $\sqrt{5}$ between the two terms in

$\langle v_2|$ arises from $Y_{20}(\hat{z}) = \sqrt{5}Y_{00}(\hat{z})$. Combining the results for $\widetilde{F}$ and $\widetilde{G}$ we find

$$H = 5p|w_1\rangle\langle w_1| + \mathcal{O}(1)\,, \quad |w_1\rangle = \sqrt{\tfrac{1}{5}}\left(|v_1\rangle + 2|v_2\rangle\right)\,. \tag{D.46}$$

Thus, while the pole parts of $\widetilde{F}$ and $\widetilde{G}$ are both of rank 2, that of H is of rank 1, due to a partial cancelation.

In the following, we determine the pole structure of F_3, aiming to find a basis in which this structure is simple. We begin by changing to a more convenient basis, namely $|w_1\rangle$ combined with

$$|w_2\rangle = \sqrt{\tfrac{1}{5}}\left(2|v_1\rangle - |v_2\rangle\right)\,, \tag{D.47}$$

and any choice of four other vectors filling out the orthonormal set. We use a $1+1+4$ block notation, in which

$$H = p\begin{pmatrix} 5 & 0 & 0 \\ 0 & 0 & 0 \\ 0 & 0 & 0 \end{pmatrix} + \mathcal{O}(1) \quad \text{and} \quad \widetilde{F} = p\begin{pmatrix} 9/5 & -2/5 & 0 \\ -2/5 & 6/5 & 0 \\ 0 & 0 & 0 \end{pmatrix} + \mathcal{O}(1)\,. \tag{D.48}$$

The inverse of H has the form

$$H^{-1} = \begin{pmatrix} 1/(5p) + \mathcal{O}(1/p^2) & \alpha_{12}/p + \mathcal{O}(1/p^2) & \alpha_{13}/p + \mathcal{O}(1/p^2) \\ \alpha_{12}/p + \mathcal{O}(1/p^2) & \alpha_{22} + \beta_{22}/p + \mathcal{O}(1/p^2) & \alpha_{23} + \mathcal{O}(1/p) \\ \alpha_{13}^{\mathrm{Tr}}/p + \mathcal{O}(1/p^2) & \alpha_{23}^{\mathrm{Tr}} + \mathcal{O}(1/p) & \overset{\leftrightarrow}{\alpha}_{33} + \mathcal{O}(1/p) \end{pmatrix}\,, \tag{D.49}$$

where the quantities α_{12}, α_{22}, β_{22} etc. are given in terms of the $\mathcal{O}(1)$ parts of H in a way that is not pertinent. At this stage we can see that $\widetilde{F}H^{-1}\widetilde{F}$ will contain a double pole proportional to α_{22} that will have the form of an outer product, as well as a complicated single-pole term. Performing the algebra we find

$$L^3F_3 = p^2\frac{4\alpha_{22}}{25}\begin{pmatrix} -1 & 3 & 0 \\ 3 & -9 & 0 \\ 0 & 0 & 0 \end{pmatrix} + p\begin{pmatrix} a & b & -\mathbf{z} \\ b & -9a-6b & 3\mathbf{z} \\ -\mathbf{z}^{\mathrm{Tr}} & 3\mathbf{z}^{\mathrm{Tr}} & 0 \end{pmatrix} + \mathcal{O}(1)\,, \tag{D.50}$$

where a, b and $\mathbf{z}$ are given in terms of the α_{ij} and β_{22}.

Thus we have learned that F_3 contains a free double pole that can be written

$$-p^2\frac{8\alpha_{22}}{5L^3}|x_1\rangle\langle x_1|\,, \qquad \langle x_1| = \sqrt{\tfrac{1}{10}}\,(-1,3,0) = \sqrt{\tfrac{1}{2}}\,(\langle v_1| - \langle v_2|)\ . \tag{D.51}$$

The form of $|x_1\rangle$ is determined entirely by the pole structure of $\widetilde{F}$ and H, although the overall coefficient is determined by the $\mathcal{O}(1)$ parts. Qualitatively we can say that although F contains two independent poles in this irrep, the H^{-1} factor cancels one of them, leading to a left-over double pole.

We conclude by discussing the impact of the single pole contribution to F_3. First we note that the coefficient of p can be written as

$$-(8a+6b)|x_1\rangle\langle x_1| - \frac{1}{\sqrt{10}N_2}\left(|x_1\rangle\langle x_2| + |x_2\rangle\langle x_1|\right) \tag{D.52}$$

where the new normalized basis vector is

$$\langle x_2| = N_2\,(9a+3b, 3a+b, -10\mathbf{z})\ . \tag{D.53}$$

Thus in the basis consisting of $|x_1\rangle$, $|x_2\rangle$ and four other orthonormal vectors, F_3 has the $1+1+4$ block form

$$F_3 = \begin{pmatrix} fp^2+gp & hp & 0 \\ hp & 0 & 0 \\ 0 & 0 & 0 \end{pmatrix} + \mathcal{O}(1)\,, \tag{D.54}$$

where f, g and h are known constants. This matrix can be diagonalized using a final, fourth basis. All we need to know here is that, close to the pole, when $|p| \gg 1$, the shift in the eigenvalues due to the off-diagonal hp term is $\pm(hp)^2/(fp^2+gp) \sim \mathcal{O}(1)$. Thus in the final basis we have

$$F_3 = \mathrm{diag}\left[fp^2+gp+\mathcal{O}(1), \mathcal{O}(1), \mathcal{O}(1), \mathcal{O}(1), \mathcal{O}(1), \mathcal{O}(1)\right]\ , \tag{D.55}$$

and thus

$$F_3^{-1} = \text{diag}\left[1/(fp^2) + \mathcal{O}(1/p^3), \mathcal{O}(1), \mathcal{O}(1), \mathcal{O}(1), \mathcal{O}(1), \mathcal{O}(1)\right] . \tag{D.56}$$

Note that the size of the change to this final basis is proportional to $1/p$, and thus vanishes at the zero of F_3^{-1}, so that the double zero lies in the subspace spanned by $|x_1\rangle$.

In summary, we find that the single pole in F_3 is hidden beneath the double pole, such that in the inverse there is simply a double zero. As L is increased, there are more active shells, but the only change to the result of this section is that the number of vanishing components of $|x_1\rangle$ increases [see Eq. (D.51)]. The nonvanishing components are unchanged.

D.5.2 A_1^+ irrep with only s waves

We have repeated the previous analysis for the case of only $\ell = 0$ contributions and three active shells.[2] The matrices are now three dimensional, with one entry per shell. We do not present the details, except to note that we follow the same steps as in the previous subsection, and find very similar conclusions aside from some changes in factors. In particular, F_3^{-1} still has a double zero, but this now lives in the space spanned by the vector

$$\langle x_1'| = \left(\sqrt{\tfrac{6}{7}}, -\sqrt{\tfrac{1}{7}}, 0\right) , \tag{D.57}$$

where entries are ordered as in Eq. (6.71).

D.6 Properties of the isotropic approximation

This appendix recalls the definition of the isotropic approximation, describes its relation to the work of this paper, and explains why the free solutions discussed in Sec. 6.4.4 are absent in this approximation.

The isotropic approximation was introduced in Ref. [28] and used in the numerical in-

[2] This builds upon, and corrects, the analysis given in Appendix C of Ref. [28].

vestigation of Ref. [39]. It involves three components: (1) Only $\ell = 0$ dimer channels are included in $\widetilde{F}$, $\widetilde{G}$, $\mathcal{K}_2$ and $\mathcal{K}_{\text{df},3}$; (2) The resulting $\mathcal{K}_{\text{df},3}$ is taken to be independent of the spectator momentum, although dependence on the total energy E is allowed; (3) F_3 is projected onto the isotropic vector $|1_K\rangle$, which has a unit entry for every available choice of spectator momentum. Note that the third step automatically picks out solutions in the A_1^+ irrep.

The isotropic approximation is thus a subset of an approach we use several times in this paper, namely restricting dimers to $\ell = 0$, keeping only the isotropic part of $\mathcal{K}_{\text{df},3}$ in the expansion about threshold, and projecting onto the A_1^+ irrep. We refer to this as the "low-energy A_1^+ approximation". The major difference is the absence of the third step—we do not project onto $|1_K\rangle$. A minor difference is that, for $\mathcal{K}_{\text{df},3}$ to be purely isotropic, we must work only at linear order in the threshold expansion. Thus we can have at most a linear dependence of $\mathcal{K}_{\text{df},3}$ on E^2, as opposed to the arbitrary dependence allowed in the isotropic approximation.

To explain the relationship between the two approximations, we begin in the low-energy A_1^+ approximation. All matrices, including F_3, are labeled by an index denoting the shell of the spectator momentum, as shown in Eq. (6.71). All matrices have the same finite dimension given by the number of shells lying below our cutoff. Since $\mathcal{K}_{\text{df},3}$ is isotropic, the quantization condition is[3]

$$\det\left([F_3]^{-1} + |1_K\rangle \mathcal{K}^{\text{iso}} \langle 1_K|\right) = 0\,, \tag{D.58}$$

where the square braces indicate the A_1^+, $\ell = 0$ matrix, and

$$\langle 1_K| = \left(1, \sqrt{6}, \sqrt{12}, \dots\right) \tag{D.59}$$

in this basis. The entries here are the square roots of the sizes of the shells. We can rewrite

[3]Note that $[F_3]^{-1} = [F_3^{-1}]$ because of the cubic symmetry of the components of F_3.

the determinant in the quantization condition as

$$\det\left([F_3]^{-1}\right)\det\left(1+[F_3]|1_K\rangle\mathcal{K}^{\rm iso}\langle 1_K|\right)=\frac{1+\langle 1_K|[F_3]|1_K\rangle\mathcal{K}^{\rm iso}}{\det[F_3]}\,, \tag{D.60}$$

where we have used $\det(1+M)=\exp\mathrm{tr}\,\ln(1+M)$, expanded in M, used the cyclicity of the trace, and resummed. The isotropic approximation consists of keeping only the solutions arising from the numerator on the right-hand side of Eq. (D.60), i.e. those satisfying

$$F_3^{\rm iso}\equiv\langle 1_K|[F_3]|1_K\rangle=-1/\mathcal{K}^{\rm iso}\,. \tag{D.61}$$

It follows from Eq. (D.60) that any solution in the isotropic approximation is also a solution in the low-energy A_1^+ approximation, barring an accidental, and unexpected, juxtaposition with a zero of $\det([F_3])$.[4] Thus, aside from this caveat, which appears to be irrelevant in practice, all solutions to the low-energy A_1^+ approximation that require a nonzero $\mathcal{K}^{\rm iso}$ are also obtained in the isotropic approximation.

What are lost in the isotropic approximation are solutions to the quantization condition (D.58) that arise when an eigenvector of F_3 diverges (so that $\det([F_3])\to\infty$) while $F_3^{\rm iso}$ remains finite. This requires that the corresponding eigenvector of F_3 is orthogonal to $|1_K\rangle$. In our experience, this only happens for solutions that occur at free energies (which, we recall, means one of the energies of three noninteracting particles in the given volume), although we do not know of a fundamental reason why this should be so. Furthermore, it was found numerically in Ref. [39] that there are no free solutions in the isotropic approximation. Taken together, these observations suggest that the isotropic approximation picks out all the non-free solutions to the quantization condition obtained in the low-energy A_1^+ approximation.

In the remainder of this appendix we explain analytically the result found numerically in Ref. [39], namely that there are no free solutions in the isotropic approximation. As discussed in Sec. 6.4.4, such solutions occur first at $E=E_1^{\rm free}$, and there yield a double pole in $\det(F_3)$

[4] This holds also when $\mathcal{K}^{\rm iso}\to 0$, for then a solution to Eq. (F.8) implies that $[F_3]$ has a diverging eigenvalue, and thus that $\det([F_3^{-1}])\to 0$.

lying in the space spanned by $|x_1'\rangle$, Eq. (6.72). This pole is, however, absent in the isotropic approximation because $\langle 1_K|x_1'\rangle = 0$, so the pole is removed from $F_3^{\rm iso}$.

Our aim is to generalize this argument to any excited free energy. We will do so for $\mathbf{P} = 0$, and for an excited state in which the three momenta, labeled $\mathbf{k}$, $\mathbf{p}$ and $\mathbf{b} = -\mathbf{k} - \mathbf{a}$, lie in different shells, e.g. $\mathbf{k} = k_L(0,0,1)$, $\mathbf{p} = k_L(1,1,0)$ and $\mathbf{b} = k_L(-1,-1,-1)$, with $k_L = 2\pi/L$. We denote the degeneracies of these shells by N_1, N_2, and N_3, respectively (6, 12 and 8 in our example). For each choice of $\mathbf{k}$ from shell 1, we define N_{12} as the number of choices of $\mathbf{p}$ from shell 2 that can lead to a free solution, and define N_{13} analogously. By cubic symmetry N_{12} and N_{13} do not depend on the choice of $\mathbf{k}$ from shell 1. Clearly we have $N_{12} = N_{13}$, since each solution contains both a $\mathbf{p}$ and $\mathbf{b}$. We define $N_{23} = N_{21}$ and $N_{31} = N_{32}$ analogously. The total degeneracy of free-particle solutions is then

$$N_{\rm sol} = N_1 N_{12} = N_2 N_{23} = N_3 N_{31}\,. \tag{D.62}$$

As above, we denote the $\ell = 0$, A_1^+ parts of $\widetilde{F}$ and $\widetilde{G}$ by $[\widetilde{F}]$ and $[\widetilde{G}]$, which are indexed by the shell number. The poles in these matrices occur only when both indices lie in one of the three shells discussed above, and thus we can focus on this three-dimensional subspace. The matrices in this subspace have the form

$$[\widetilde{F}] = p\begin{pmatrix} N_{12} & 0 & 0 \\ 0 & N_{23} & 0 \\ 0 & 0 & N_{31} \end{pmatrix} + \mathcal{O}(1) \quad \text{and} \quad [\widetilde{G}] = p\begin{pmatrix} 0 & \sqrt{N_{12}N_{23}} & \sqrt{N_{12}N_{31}} \\ \sqrt{N_{23}N_{12}} & 0 & \sqrt{N_{23}N_{31}} \\ \sqrt{N_{31}N_{12}} & \sqrt{N_{31}N_{23}} & 0 \end{pmatrix} + \mathcal{O}(1)\,, \tag{D.63}$$

where

$$p = \frac{1}{8L^3\omega_k\omega_p\omega_b(E - \omega_k - \omega_p - \omega_b)}\,. \tag{D.64}$$

The coefficients in $[\widetilde{F}]$ count the number of choices of $\mathbf{a}$ in Eq. (D.9) that lead to the pole. For example, for the $(1,1)$ element, there are $N_{12} + N_{13} = 2N_{12}$ choices, which combines

with the overall factor of $1/2$ in $\widetilde{F}$ to give the quoted result N_{12}. To understand the form of $[\widetilde{G}]$ consider the $(1,2)$ element of the pole part. This arises from each of the $N_{\rm sol}$ solutions, multiplied by the normalization factors for the A_1^+ projections, $1/\sqrt{N_1 N_2}$. Then we use

$$\frac{N_{\rm sol}}{\sqrt{N_1 N_2}} = \sqrt{\frac{N_1 N_{12} N_2 N_{23}}{N_1 N_2}} = \sqrt{N_{12} N_{23}} \tag{D.65}$$

to obtain the quoted result.

Combining, we find that the pole part of H lives in a one-dimensional subspace,

$$[H] = [\widetilde{F}] + [\widetilde{G}] + [1/(2\omega\mathcal{K}_2)] = |W_1\rangle \lambda p \langle W_1| + \mathcal{O}(1)\,, \tag{D.66}$$

$$\langle W_1| = \left(\sqrt{\frac{N_{12}}{\lambda}}, \sqrt{\frac{N_{23}}{\lambda}}, \sqrt{\frac{N_{31}}{\lambda}}\right)\,, \quad \lambda = N_{12}+N_{23}+N_{31}\,. \tag{D.67}$$

Here we are assuming that $\mathcal{K}_2$ does not have a zero at $E = E_1^{\rm free}$. It follows from Eq. (D.66) that $[H]^{-1}$ has the form (see, e.g., Eq. (C14) of Ref. [28]):

$$[H]^{-1} = |W_1\rangle \frac{1+\mathcal{O}(1/p)}{\lambda p} \langle W_1| + \mathcal{O}(1/p) \sum_{i\neq 1} (|W_1\rangle\langle W_i| + |W_i\rangle\langle W_1|) + \sum_{i,j\neq 1} |W_i\rangle \mathcal{O}(1) \langle W_j|\,. \tag{D.68}$$

Here $|W_2\rangle$ and $|W_3\rangle$ are any choice for the other two members of an orthonormal basis of which $|W_1\rangle$ is a member. Note that only the coefficient of the first term is known; for all other terms only the power of p is known.

We can now calculate the pole part of $F_3^{\rm iso}$, which requires projection with $\langle 1_K|$. Within our subspace

$$\langle 1_K| \longrightarrow \left(\sqrt{N_1}, \sqrt{N_2}, \sqrt{N_3}\right)\,, \tag{D.69}$$

from which it follows that

$$\langle 1_K|[\widetilde{F}] = p\sqrt{\lambda N_{\rm sol}}\langle W_1| + \mathcal{O}(1)\,, \tag{D.70}$$

$$\langle 1_K|[\widetilde{F}]|1_K\rangle = 3pN_{sol} + \mathcal{O}(1)\,, \tag{D.71}$$

$$\langle 1_K|[\widetilde{F}][H]^{-1}[\widetilde{F}]|1_K\rangle = pN_{\rm sol} + \mathcal{O}(1)\,, \tag{D.72}$$

and thus that

$$F_3^{\rm iso} = \frac{1}{L^3}\langle 1_K|\left(\frac{[\widetilde{F}]}{3} - [\widetilde{F}][H]^{-1}[\widetilde{F}]\right)|1_K\rangle = \mathcal{O}(1)\,. \tag{D.73}$$

As claimed, all poles have canceled from $F_3^{\rm iso}$.

It is straightforward to generalize this result to the case that two or more shells are the same, and also to moving frames, i.e. $\mathbf{P} \neq 0$, although we do not present the details here.

D.7 Failure of Eq. (6.84) for quadratic and cubic terms in the threshold expansion

As noted in the main text, we find numerically that the following results hold,

$$[\mathcal{K}_{\rm df,3}{}^{(2)}(E_1^{\rm free})]|x_1\rangle = [\mathcal{K}_{\rm df,3}{}^{(3)}(E_1^{\rm free})]|x_1\rangle = 0\,, \tag{D.74}$$

where the superscript on $\mathcal{K}_{\rm df,3}$ indicates the order in the threshold expansion of $\mathcal{K}_{\rm df,3}$. The vector $|x_1\rangle$ is given in Eq. (6.74), and the square brackets indicate the A_1^+ projection of $\mathcal{K}_{\rm df,3}$ expressed in the $k\ell m$ basis. Our aim here is to give an analytic explanation for these results.

We can rewrite Eq. (D.74), using the symmetry of $\mathcal{K}_{\rm df,3}$ and the form of $|x_1\rangle$, as

$$[\mathcal{K}_{\rm df,3}{}^{(2,3)}]_{1i} = \sqrt{\tfrac{1}{6}}[\mathcal{K}_{\rm df,3}{}^{(2,3)}]_{2i} + \sqrt{\tfrac{5}{6}}[\mathcal{K}_{\rm df,3}{}^{(2,3)}]_{3i} \quad \text{at} \quad E = E_1^{\rm free}\,, \quad \forall i\,. \tag{D.75}$$

The ordering of the indices is given in Eq. (6.73). We recall that the $\sqrt{6}$ here arises because the first shell has 6 elements, while the $\sqrt{5}$ arises because $Y_{20}(\hat{z}) = \sqrt{5}Y_{00}$. The superscript on $\mathcal{K}_{\rm df,3}$ indicates that the equation should hold for both the quadratic and cubic terms in the threshold expansion.

We wish to demonstrate Eq. (D.75) for any choice of i. To do so we first change notation, recalling from Sec. 6.2.4 that the $\mathbf{k}, \ell, m$ indices can be replaced by dependence on $\mathbf{k}, \hat{a}^*$. Here we are also replacing the spectator-momentum index k with $\mathbf{k}$, both in order to be more explicit, and because $\mathcal{K}_{\text{df},3}$ is an infinite-volume quantity that is defined for all $\mathbf{k}$. At first, we make this change only for the initial-state indices, leading to the hybrid notation $\mathcal{K}_{\text{df},3}(E; \mathbf{p}, \ell', m'; \mathbf{k}, \hat{a}^*)$.[5] In terms of this new quantity, we claim that Eq. (D.75) holds for any choice of the index i if

$$\mathcal{K}_{\text{df},3}{}^{(2,3)}(E_1^{\text{free}}; \mathbf{0}, 0, 0; \mathbf{k}, \hat{a}^*) + c\,\mathcal{K}_{\text{df},3}{}^{(2,3)}(E_1^{\text{free}}; \mathbf{0}, 2, 0; \mathbf{k}, \hat{a}^*) = \\ \mathcal{K}_{\text{df},3}{}^{(2,3)}(E_1^{\text{free}}; k_L\hat{z}, 0, 0; \mathbf{k}, \hat{a}^*) + \sqrt{5}\mathcal{K}_{\text{df},3}{}^{(2,3)}(E_1^{\text{free}}; k_L\hat{z}, 2, 0; \mathbf{k}, \hat{a}^*)\,, \quad \text{(D.76)}$$

is valid for all $\mathbf{k}$ and $\hat{a}^*$, and for one choice of c. To understand this, first note that (D.76) applies for an arbitrary initial state, and this subsumes all possible values of the finite-volume index i. As for the final state, to obtain Eq. (D.75) we need to project onto the A_1^+ irrep. Doing so, the second term on the left-hand side of Eq. (D.76) vanishes, as can be seen from the absence of an $\ell = 2$ entry in the A_1^+ row of the (000) shell column in Table 6.1. This is why it is sufficient if Eq. (D.76) holds for one value of c. The A_1^+ projections of the remaining three terms in Eq. (D.76) leads to the three terms in Eq. (D.75). The averaging over the first shell leads to the factors of $\sqrt{6}$ in the latter result. Note that to perform this averaging one must also use the rotation invariance of $\mathcal{K}_{\text{df},3}$. It is also important that $m' = 0$ in the last term in Eq. (D.76), since this is the component that lives in the A_1^+ irrep when the spectator momentum lies in the $\hat{z}$ direction.

In the following, we demonstrate that Eq. (D.76) holds if $c = \sqrt{5}$. There are three inputs needed for this demonstration. The first is the observation that the same configuration of final-state particles can contribute to both sides of Eq. (D.76). To explain this we need

[5] We are abusing notation by using the same name, $\mathcal{K}_{\text{df},3}$, for the function expressed in terms of different variables, but the number of indices uniquely determines which choice of basis we are using.

to write both initial and final states in the form used prior to their decomposition into harmonics, so that we have $\mathcal{K}_{\mathrm{df},3}(E;\mathbf{p},\hat{a}'^*;\mathbf{k},\hat{a}^*)$. Then one can show, using permutation symmetry alone, that

$$\mathcal{K}_{\mathrm{df},3}(E_1^{\mathrm{free}};\mathbf{0},\hat{z};\mathbf{k},\hat{a}^*) = \mathcal{K}_{\mathrm{df},3}(E_1^{\mathrm{free}};k_L\hat{z},\hat{z};\mathbf{k},\hat{a}^*)\,. \tag{D.77}$$

This result holds for any term in the threshold expansion of $\mathcal{K}_{\mathrm{df},3}$ (or, indeed, for the entire quantity), and thus we do not include a superscript. To understand Eq. (D.77), note that the three particles in the final state have momenta $\mathbf{0}$, $k_L\hat{z}$ and $-k_L\hat{z}$. Calling $\mathbf{0}$ the spectator momentum yields the left-hand side of Eq. (D.77), while calling $k_L\hat{z}$ the spectator yields the right-hand side. Since both choices describe the same momentum configuration, they must be equivalent due to the permutation symmetry of $\mathcal{K}_{\mathrm{df},3}$.

The second input is that ${\mathcal{K}_{\mathrm{df},3}}^{(2,3)}$ is either independent of, or quadratic in, $\hat{a}'^*$. This is explained in Sec. 6.2.4, and is in one-to-one correspondence with the fact that only s- and d-waves contribute.

The final key input concerns angular averaging of a quadratic form:

$$(\hat{n}_i\hat{n}_jV_{ij})\,\big|_{\ell=0} + \sqrt{5}\,(\hat{n}_i\hat{n}_jV_{ij})\,\big|_{\ell=2,m=0} = \tfrac{1}{3}V_{ii} + \tfrac{1}{3}\,(2V_{33}-V_{11}-V_{22}) = V_{33}\,, \tag{D.78}$$

where V_{ij} is an arbitrary tensor. In other words, the combination appearing on the left-hand side can be evaluated by setting $\hat{n}=\hat{z}$. The same is trivially true for a quantity that is independent of $\hat{n}$.

Combining the second and third key inputs, we deduce that

$${\mathcal{K}_{\mathrm{df},3}}^{(2,3)}(E;\mathbf{p},0,0;\mathbf{k},\hat{a}^*) + \sqrt{5}{\mathcal{K}_{\mathrm{df},3}}^{(2,3)}(E;\mathbf{p},2,0;\mathbf{k},\hat{a}^*) = {\mathcal{K}_{\mathrm{df},3}}^{(2,3)}(E;\mathbf{p},\hat{a}'^*=\hat{z};\mathbf{k},\hat{a}^*) \tag{D.79}$$

holds for any choice of E and $\mathbf{p}$. Applying this to both sides of Eq. (D.76), with $E=E_1^{\mathrm{free}}$, and $\mathbf{p}=\mathbf{0}$ for the left-hand side and $\mathbf{p}=k_1\hat{z}$ for the right-hand side, we find that Eq. (D.76) with $c=\sqrt{5}$ is equivalent to the first key identity Eq. (D.77). This establishes the desired

result.

This derivation will fail for terms of quartic and higher order in $\mathcal{K}_{\mathrm{df},3}$, since the combination of $\ell' = 0$ and 2 parts that appears in Eq. (D.79) will no longer allow the replacement of $\hat{a}'^*$ with $\hat{z}$, implying that Eq. (D.77) cannot be used. For example, considering one of the terms that arises in quartic terms, we find

$$(\hat{a}'^* \cdot \hat{n})^4\Big|_{\ell'=0} + \sqrt{5}(\hat{a}'^* \cdot \hat{n})^4\Big|_{\ell'=2,m'=0} \neq \hat{n}_z^4 \,. \tag{D.80}$$

We have checked this numerically by decomposing the simplest of the quartic terms and finding that Eq. (D.74) does not hold.

Appendix E

APPENDIX TO CHAPTER 7

E.1 I_{PV}*-dependence of* $\mathcal{K}_{\mathrm{df},3}$ *and the spectrum*

As explained in Sec. 7.3, when we modify the PV prescription according to Eqs. (7.19) and (7.20), the spectrum is formally unchanged for all volumes, provided we make a suitable change to $\mathcal{K}_{\mathrm{df},3}$.[1] In practice, however, this statement breaks down once we approximate the quantization condition by truncating the sum over ℓ. We also note that the required change to $\mathcal{K}_{\mathrm{df},3}$ is not known *a priori*, and must be determined numerically. It is the purpose of this appendix to study, within the context of a concrete example, the size of the required changes to $\mathcal{K}_{\mathrm{df},3}$ and of the residual volume-dependence in the spectrum.

In our example we follow the numerical investigations of Sec. 7.4.1 and use the isotropic approximation with $\ell_{\mathrm{max}} = 0$, so that the infinite-volume amplitudes are parameterized by a_0 and $\mathcal{K}^{\mathrm{iso}}_{\mathrm{df},3}$. We set $ma_0 = 0.1$ and consider two PV schemes: the original one with $I^s_{\mathrm{PV}} = 0$ and the modified one with $I^s_{\mathrm{PV}} = -1$. The derivation of the quantization condition is valid for both choices (see Sec. 7.3.1). We choose a large volume ($mL = 30$) at which to match the spectrum by tuning the values of $\mathcal{K}^{\mathrm{iso}}_{\mathrm{df},3}(I^s_{\mathrm{PV}}; E)$, and then study the volume-dependence of the difference between spectral lines at other volumes.

To show how this works we first consider the lowest energy level, $E_0(L)$. In Fig. E.1, we show the energy dependence of the dimensionless quantity m^2/F_3^{iso} just above threshold for

[1] As usual, this statement holds up to exponentially-suppressed corrections.

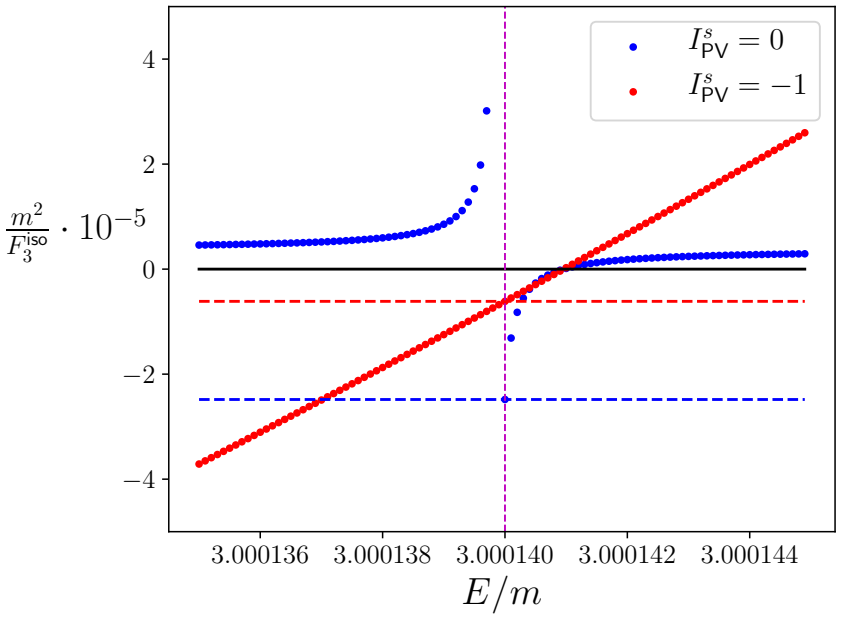

Figure E.1: Determining the I^s_{PV}-dependence of $\mathcal{K}_{\mathrm{df},3}$ in the isotropic approximation using the ground-state energy, E_0, for $ma_0 = 0.1$ and $mL = 30$. Blue and red points show m^2/F_3^{iso} for, $I^s_{\mathrm{PV}} = 0$ and -1, respectively. The vertical purple dashed line shows our chosen tuning energy, while the horizontal dashed curves show the resulting values of $-\mathcal{K}^{\mathrm{iso}}_{\mathrm{df},3}$.

the two choices of $I^s_{\rm PV}$. The quantization condition in the isotropic approximation is

$$m^2\mathcal{K}^{\rm iso}_{{\rm df},3}(I^s_{\rm PV};E) = -\frac{m^2}{F_3^{\rm iso}(I^s_{\rm PV};E,L)}\,, \tag{E.1}$$

where we have made the scheme parameter explicit. As discussed in Sec. 7.3, we know that the solution to the quantization condition is independent of $I^s_{\rm PV}$ if $\mathcal{K}_{{\rm df},3} = 0$. This is seen in the figure by the fact that the two $m^2/F_3^{\rm iso}$ curves cross when they both vanish. We are interested here, however, in cases where $\mathcal{K}_{{\rm df},3} \neq 0$, and so choose an energy away from the crossing ($E_0 = 3.00014m$, shown by the vertical line in the plot) and determine the values of $\mathcal{K}^{\rm iso}_{{\rm df},3}$ so as to attain this energy. We find

$$\begin{aligned} m^2\mathcal{K}^{\rm iso}_{{\rm df},3}(I^s_{\rm PV}=0;E_0) &= 24.828\cdot 10^4\,,\\ m^2\mathcal{K}^{\rm iso}_{{\rm df},3}(I^s_{\rm PV}=-1;E_0) &= 6.1365\cdot 10^4\,. \end{aligned} \tag{E.2}$$

We now determine the ground-state energies for other choices of L, keeping $\mathcal{K}^{\rm iso}_{{\rm df},3}$ fixed at the values given in Eq. (E.2). We then evaluate the difference

$$\delta E_0(L) \equiv E_0(I^s_{\rm PV}=0;L) - E_0(I^s_{\rm PV}=-1;L)\,, \tag{E.3}$$

which is a measure of the residual $I^s_{\rm PV}$ dependence of the spectrum due to approximating the quantization condition. The result is shown in Fig. E.2. It oscillates about zero with an amplitude that decays rapidly with increasing L.

We can understand why the residual $I^s_{\rm PV}$ dependence is so small for the ground state by using the threshold expansion developed in Ref. [76]. Close to threshold, the approximation of $\mathcal{K}_{{\rm df},3}$ by an energy-dependent constant is valid up to corrections of $\mathcal{O}(\Delta)$, where

$$\Delta \equiv \frac{E^2-9m^2}{9m^2}\,. \tag{E.4}$$

Numerically, this is of $\mathcal{O}(0.1\%)$ for the energies we are considering (choosing $mL \approx 10$). Furthermore, what matters for δE_0 is the difference between the contributions of the linear terms for the two choices of $I^s_{\rm PV}$, and the end result is the tiny effect shown in Fig. E.2.

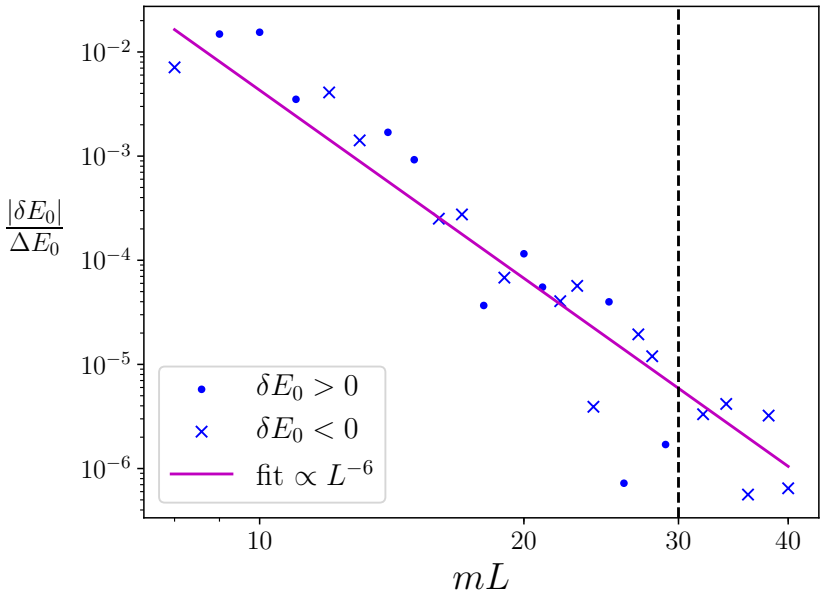

Figure E.2: I_{PV}-dependence of the ground-state energy $E_0(L)$, with δE_0 defined in Eq. (E.3). We plot the ratio to $\Delta E_0 = E_0 - 3m$ in order to give a sense of the relative size of the shift. The vertical line at $mL = 30$ indicates the point at which matching is performed, so that δE_0 vanishes.

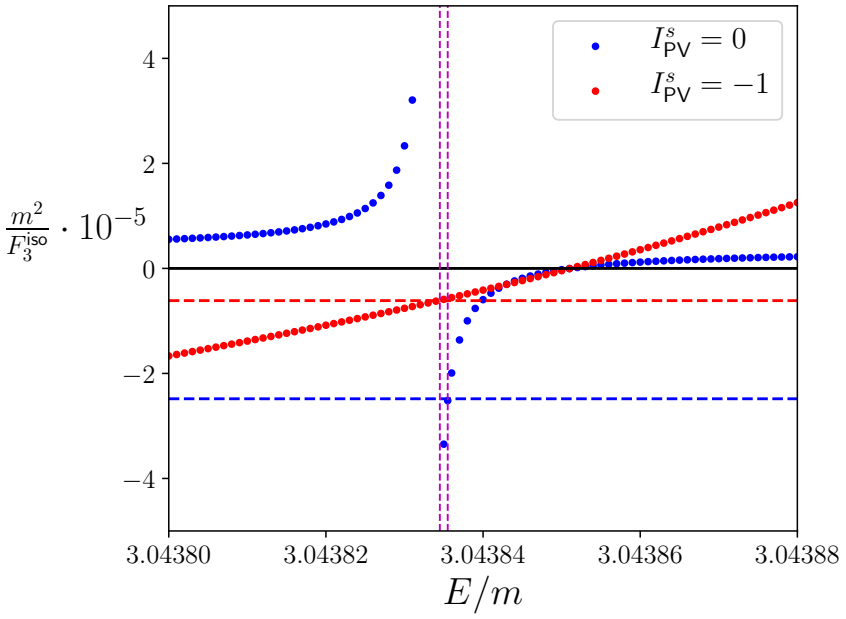

Figure E.3: As for Fig. E.1 but for the first excited state. The dashed magenta lines correspond to the values of $E_1(I_{\mathrm{PV}} = 0; mL = 30)$ and $E_1(I_{\mathrm{PV}} = -1; mL = 30)$ obtained from the constant approximations $m^2\mathcal{K}^{\mathrm{iso}}_{\mathrm{df},3}(I_{\mathrm{PV}} = 0) = 2.4828 \cdot 10^5$ and $m^2\mathcal{K}^{\mathrm{iso}}_{\mathrm{df},3}(I_{\mathrm{PV}} = -1) = 6.1365 \cdot 10^4$. The discrepancy between the two magenta lines is due to our neglect of the higher-order terms in the threshold expansion of $\mathcal{K}_{\mathrm{df},3}$.

We next extend our example to include the first excited state $E_1(L)$. If we continue to assume energy-independent values of $\mathcal{K}_{\mathrm{df},3}^{\mathrm{iso}}$, then the first excited levels at $mL = 30$ disagree by

$$\delta E_1(mL = 30) \equiv E_1(I_{\mathrm{PV}}^s = 0; mL = 30) - E_1(I_{\mathrm{PV}}^s = -1; mL = 30) \approx 10^{-6} m\,, \tag{E.5}$$

as shown in Fig. E.3. Thus, *even at the same value of* L, the spectrum is dependent on I_{PV}^s. We interpret this as being due to our omission of the $\mathcal{O}(\Delta)$ terms in the threshold expansion, which are significantly larger for the first excited state than for the ground state. As shown in Ref. [76], these still lead to an isotropic $\mathcal{K}_{\mathrm{df},3}$, but now with linear energy dependence,

$$\mathcal{K}_{\mathrm{df},3}(I_{\mathrm{PV}}^s; E) \approx \mathcal{K}_{\mathrm{df},3}^{\mathrm{iso},0}(I_{\mathrm{PV}}^s) + \mathcal{K}_{\mathrm{df},3}^{\mathrm{iso},1}(I_{\mathrm{PV}}^s)\Delta\,. \tag{E.6}$$

If we set $\mathcal{K}_{\mathrm{df},3}^{\mathrm{iso},1} = 0$ then we expect $\delta E_1(mL) \sim \Delta$. In fact, we can make a more detailed estimate of δE_1 using the threshold expansion for the excited state developed in Ref. [77]. The three-particle interaction enters the expression for E_1 first at $\mathcal{O}(L^{-6})$. If this is mistuned by $\Delta \sim 1/L^2$ then we expect that $\delta E_1 \propto L^{-8}$. This dependence is indeed what we find, as shown in Fig. E.4,

If we include the linear term in $\mathcal{K}_{\mathrm{df},3}^{\mathrm{iso}}$, Eq. (E.6), then truncation errors are of $\mathcal{O}(\Delta^2)$, so we expect this to perform considerably better. We set $\mathcal{K}_{\mathrm{df},3}^{\mathrm{iso},1}(I_{\mathrm{PV}}^s) = 0$, and then tune $\mathcal{K}_{\mathrm{df},3}^{\mathrm{iso},0}(I_{\mathrm{PV}}^s)$ and $\mathcal{K}_{\mathrm{df},3}^{\mathrm{iso},1}(I_{\mathrm{PV}}^s)$ so as to set $\delta E_1(mL = 30) = 0$. We find that this requires $\mathcal{K}_{\mathrm{df},3}^{\mathrm{iso},1}(I_{\mathrm{PV}}^s = -1) = 4.123 \cdot 10^3$.[2] The resulting δE_1 is shown by the lower (red) points in Fig. E.4. Here we would expect the fall off to be as L^{-10}, since there are two extra powers of momentum. We indeed find a fall off faster than L^{-8}, but with some oscillations that preclude detailed fitting. The detailed behavior and source of this dependence deserves a dedicated study that goes beyond the scope of this work. In such a future investigation we also intend to disentangle two possible sources for the residual I_{PV}^s dependence: *(i)* The isotropic nature

[2] In practice we have left $\mathcal{K}_{\mathrm{df},3}^{\mathrm{iso},0}(I_{\mathrm{PV}}^s)$ unchanged and only tuned $\mathcal{K}_{\mathrm{df},3}^{\mathrm{iso},1}$. This means that δE_0 is slightly mistuned, but by an amount that is small on the scale of most of the values shown in Fig. E.2.

of $\mathcal{K}_{\mathrm{df},3}^{\mathrm{iso}}$ is insufficient to keep the low-energy physics constant under variation of I_{PV}^{s}; and *(ii)* The quantization condition only holds up to neglected e^{-mL} corrections and the exact form of these (and their imprint on the finite-volume solutions) varies with I_{PV}^{s}.

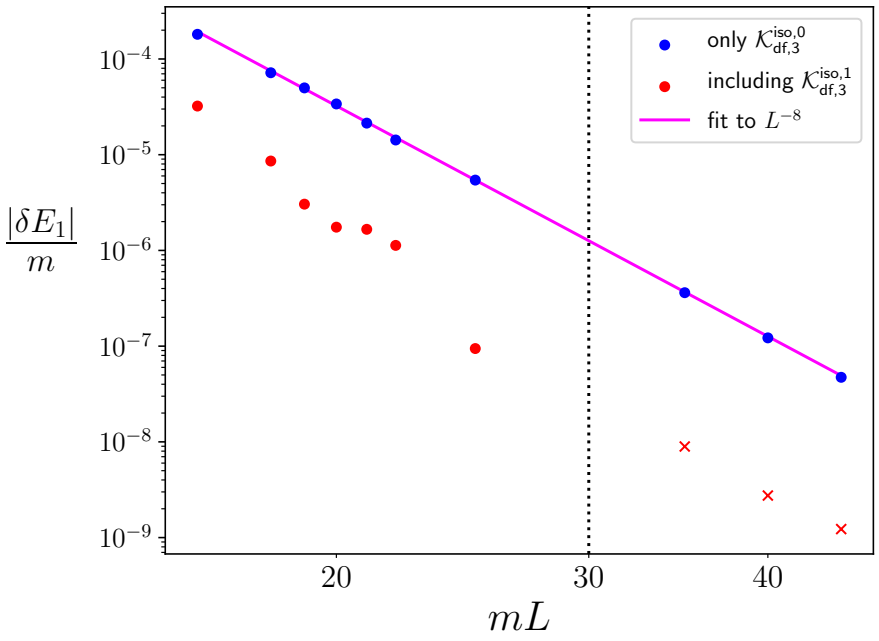

Figure E.4: $|\delta E_1|$ as a function of mL when tuning with only a constant $\mathcal{K}_{\mathrm{df},3}^{\mathrm{iso}}$ (filled blue circles) or with the linear dependence on Δ given in Eq. (E.6) (filled red circles and crosses). The solid (magenta) line shows a fit to the blue points assuming an L^{-8}-dependence. The vertical line indicates the value of mL at which the tuning is done. Thus the corresponding red point vanishes at this value and is not shown. δE_1 is positive for the red circles and negative for the red crosses.

As a first step towards understanding *(i)* we note that, in general, $\mathcal{K}_{\mathrm{df},3}$ includes also non-isotropic terms that enter at $\mathcal{O}(\Delta^2)$ (see Ref. [76]). To summarize, in the main text we explained that modifying I_{PV}^{s} changes an isotropic $\mathcal{K}_{\mathrm{df},3}$ into a nonisotropic one, and in this appendix we have shown that this must be understood as an effect of $\mathcal{O}(\Delta^2)$. It follows that

the shift should be neglected if working at a leading or next-to-leading order:

$$\mathcal{K}_{\mathrm{df},3}(I^s_{\mathrm{PV}}) = \mathcal{K}^{\mathrm{iso}}_{\mathrm{df},3}(I^s_{\mathrm{PV}}) \longrightarrow \mathcal{K}_{\mathrm{df},3}(I'^s_{\mathrm{PV}}) = \mathcal{K}^{\mathrm{iso}}_{\mathrm{df},3}(I'^s_{\mathrm{PV}}) + \mathcal{O}(\Delta^2). \tag{E.7}$$

More generally, it follows that effects of I^s_{PV} may be absorbed in a redefinition of $\mathcal{K}_{\mathrm{df},3}$ up to systematic errors at $\mathcal{O}(\Delta^{k+1})$, where k is the order at which we are truncating the expansion. As stressed in the main text, the estimation of the truncation error by the residual I^s_{PV} dependence is analogous to using scheme-dependence as an estimate of the truncation error in perturbation theory.

E.2 NREFT prediction for the particle-dimer scattering length

In this appendix we explain how we obtain the nonrelativistic effective field theory (NREFT) prediction shown in Fig. 7.8.

At lowest order in NREFT, the dimer-particle scattering amplitude is determined by an integral equation, and is given in terms of the two-particle scattering length, a_0, and the three-body coupling, $H_0(\Lambda)$. Here Λ is a hard cutoff introduced as an ultraviolet regularization. The integral equation is given, for example, in Eq. (6) of Ref. [159]. We are interested specifically in the dimer-particle scattering length, b_0, which is proportional to the scattering amplitude. Thus we use the version of the integral equation given in Eq. (12) of Ref. [159], which is written for a quantity $a(k,p)$ that satisfies $a(0,0) = -b_0$. We further rewrite this equation in terms of $b(p) = -a(0,p)$, and make variables dimensionless using a_0[3], leading to

$$\frac{b(p)}{a_0} = -K(p,0) + \frac{2}{\pi}\int_0^\Lambda dq K(p,q)\frac{b(q)}{a_0}\,, \tag{E.8}$$

$$K(p,k) = \frac{4}{3}\left(1+\sqrt{\frac{3p^2}{4}+1}\right)\left[\frac{1}{pq}\log\left(\frac{q^2+qp+p^2+1}{q^2-qp+p^2+1}\right)+\frac{2H_0}{\Lambda^2}\right], \tag{E.9}$$

with the desired scattering length given by $b_0 = b(0)$. Here we have used the fact that,

[3]In the following equations, q, m, and H_0 actually denote qa_0, ma_0 and $H_0a_0^2$ respectively

at the particle-dimer threshold, and in the NR limit,

$$-mE_{\rm NR} \equiv m(3m - E) = m\left(2m - 2m\sqrt{1 - 1/m^2}\right) \approx 1\,. \tag{E.10}$$

Given a choice of H_0 and Λ, Eq. (E.8) can be solved by discretizing the momentum,

$$\int dq \to \Delta q \sum\,, \tag{E.11}$$

with $\Delta q = \Lambda/N_{\rm steps}$, and solving the resulting matrix equation,

$$b_p = -a_0(1 - \frac{2}{\pi}\Delta q K)^{-1}_{p,k} K_{k,0}\,. \tag{E.12}$$

The result for b_0 converges sufficiently for $N_{\rm steps} \approx 10^4$.

In order to complete the prediction we need to know the appropriate value of $H_0(\Lambda)$ to use. This issue was addressed in Ref. [74], where the relationship between the relativistic quantization condition used here and the NREFT version of Ref. [31] was discussed. In particular, Eq. (94) of Ref. [74] shows that $H_0(\Lambda)$ vanishes if $\mathcal{K}^{\rm iso}_{{\rm df},3} = 0$ (as is the case here) for a choice of Λ that is of $\mathcal{O}(m)$ but is not precisely specified. This uncertainty in Λ is due to the difference between the smooth cutoff needed in the relativistic quantization condition and the hard cutoff used in the NREFT approach. The upshot is that, for one choice of a_0, we need to tune the value of Λ at which H_0 vanishes so that the NREFT result for b_0 matches that obtained from the relativistic quantization condition.[4] Restoring factors of a_0, we do this tuning for the largest value of ma_0 in Fig. 7.8, which is the most nonrelativistic case, finding $\Lambda = 0.75m$. The results for b_0 at all other values of ma_0 are then predictions.

We expect the NREFT prediction to work well for $ma_0 \gg 1$, and this is what we find, as shown in Fig. 7.8. Indeed, this agreement provides an important cross check of the quantization condition itself and of our numerical implementation. The failure of the NREFT prediction that we observe for $ma_0 \lesssim 1$ is also expected, and shows the importance of including relativistic effects.

[4] This is equivalent to fixing $\Lambda = m$ and then tuning H_0.

Appendix F

APPENDIX TO CHAPTER 8

F.1 Implementation of the QC in moving frames

Here we explain the essential features of the implementation of the RFT form of the quantization condition, Eq. (8.1). This has previously been carried out in the rest frame ($\mathbf{P} = 0$), both keeping only s-wave two-particle interactions and an isotropic $\mathcal{K}_{\text{df},3}$ [39], and including d-wave two-particle interactions and the leading nonisotropic terms in $\mathcal{K}_{\text{df},3}$ [76]. The generalization required here is to extend the s-wave plus isotropic $\mathcal{K}_{\text{df},3}$ approximation to moving frames.

F.1.1 s-wave approximation

The matrices in Eq. (8.1) have indices k, ℓ, m. Here k is shorthand for a finite-volume momentum, $\mathbf{k} = (2\pi/L)\mathbf{n}_k$, which is labeled by an integer-valued vector $\mathbf{n}_k$. This is the momentum of one of the three on-shell particles (denoted the spectator). The other indices ℓ, m are the angular momentum quantum numbers of the remaining pair (called the interacting pair) in their center-of-mass frame. The UV cutoff described below automatically cuts off $\mathbf{k}$, while formally ℓ runs over all possible values. To obtain matrices of finite dimension we assume that $\mathcal{K}_2$ is only nonzero in the s-wave and that $\mathcal{K}_{\text{df},3}$ vanishes for $\ell > 0$. It can then be shown that all solutions to Eq. (8.1) that are sensitive to interactions are obtained by truncating all matrices to have $\ell = m = 0$. In particular, $F_{3;p\ell'm',k\ell m}$ reduces to $F^s_{3;pk}$, where we include the superscript as a reminder of restriction to s waves.

The explicit form of F_3^s is [39]

$$L^3 F_3^s \equiv \frac{\widetilde{F}^s}{3} - \widetilde{F}^s \frac{1}{1/\widetilde{\mathcal{K}}_2^s + \widetilde{F}^s + \widetilde{G}^s} \widetilde{F}^s \,, \tag{F.1}$$

where $\widetilde{F}^s$ and $\widetilde{G}^s$ are geometric matrices

$$[\widetilde{F}^s]_{kp} \equiv \frac{\delta_{kp}}{2} \frac{H(\mathbf{k})}{2\omega_k} \left[\frac{1}{L^3} \sum_{\mathbf{a}} - \mathrm{PV} \int \frac{d^3a}{(2\pi)^3} \right] \frac{H_2(\mathbf{a},\mathbf{b})}{2\omega_a 2\omega_b (E - \omega_k - \omega_a - \omega_b)} \,, \tag{F.2}$$

$$[\widetilde{G}^s]_{kp} \equiv \frac{H(\mathbf{k}) H(\mathbf{p}\,)}{L^3 2\omega_k 2\omega_p (b^2 - m^2)}, \qquad b^\mu = P^\mu - k^\mu - p^\mu \tag{F.3}$$

and $\widetilde{\mathcal{K}}_2^s$ is given in terms of the s-wave phase shift by

$$[1/\widetilde{\mathcal{K}}_2^s]_{kp} \equiv \delta_{kp} \Big(1/\widetilde{\mathcal{K}}_2^s(\mathbf{k}) \Big) \,, \tag{F.4}$$

$$\widetilde{\mathcal{K}}_2^s(\mathbf{k}) \equiv \frac{32\pi\omega_k E_{2,k}^*}{q_{2,k}^* \cot\delta_s(q_{2,k}^{*2}) + |q_{2,k}^*|[1 - H(\mathbf{k})]} \,, \tag{F.5}$$

where

$$E_{2,k}^{*2} = (E - \omega_k)^2 - (\mathbf{P} - \mathbf{k})^2 \quad \text{and} \quad q_{2,k}^{*2} = \frac{E_{2,k}^{*2}}{4} - m^2 \,. \tag{F.6}$$

Other quantities appearing in these definitions are the on-shell energies, exemplified by $\omega_k \equiv \sqrt{\mathbf{k}^2 + m^2}$, the corresponding four-momenta, e.g. $k^\mu = (\omega_k, \mathbf{k})$, and the total four-momentum, $P^\mu = (E, \mathbf{P})$. Finally, the functions $H(\mathbf{k})$ and $H_2(\mathbf{a},\mathbf{b})$ are UV cutoffs. $H(\mathbf{k})$ is a smooth function, cutting off the sum over $\mathbf{k}$ when $E_{2,k}^{*2}$ drops below zero, and equaling unity for values of $\mathbf{k}$ such that the interacting pair lies above threshold. We use the explicit form given in Refs. [28, 34, 39, 76], setting the cutoff parameter to the value $\alpha_H = -1$.[1] For the cutoff function H_2 in $\widetilde{F}^s$ we use the "KSS form" given explicitly in Refs. [39, 76].

We observe that the only places where nonzero $\mathbf{P}$ enters above are into the definitions of $E_{2,k}^*$, $q_{2,k}^*$, and b^μ. Thus the numerical construction of the elements of the matrices is just

[1]The lower limit $E_{2,k}^{*2} = 0$ (corresponding to $q_{2,k}^{*2}/m^2 = -1$) is not a fundamental limit, but is related to the specific choice of boost used for below-threshold kinematics in Refs. [28, 34, 39, 76]. It is possible to choose a different form of boost and allow $E_{2,k}^{*2}$ to become negative, and this option is currently under investigation.

as easy for moving frames as for rest frames. The only complication arises when we project onto irreps, as discussed below.

Two-particle interactions enter through the K-matrix-like quantity $\widetilde{\mathcal{K}}_2^s$, which we approximate by inserting the chosen parametrization of the phase shift, either Eq. (8.5) or (8.11), into Eq. (F.5). We note that, above threshold, where $H(\mathbf{k}) = 1$, $2\omega_k \widetilde{\mathcal{K}}_2^s(\mathbf{k})$ is simply the standard two-particle K matrix.

To complete the quantization condition, we need the form of $\mathcal{K}_{\mathrm{df},3}$ in the s-wave approximation. At this stage, $\mathcal{K}_{\mathrm{df},3}$ still depends on the spectator momenta $\mathbf{k}$ and $\mathbf{p}$. However, there is the additional constraint that the matrix form of $\mathcal{K}_{\mathrm{df},3}$ is the restriction to finite-volume momenta of an infinite-volume amplitude that is invariant both under Lorentz transformations and the exchange of both initial- and final-state particles. We intuitively expect that such a symmetric amplitude that is purely s-wave for any two-particle pair cannot depend on the spectator momentum. One way to see that this is indeed the case is to use the threshold expansion developed in Ref. [76]. At any order in the expansion parameter Δ, one can show that the only terms that are purely s-wave are those that are isotropic. Since nonisotropic terms first occur at $\mathcal{O}(\Delta^2)$, we work only at linear order in Δ in order to enforce $\ell_{\max} = 0$ within the context of the threshold expansion. Thus we use

$$\mathcal{K}_{\mathrm{df},3} = \mathcal{K}_{\mathrm{df},3}^{\mathrm{iso}}(\Delta) = \mathcal{K}_{\mathrm{df},3}^{\mathrm{iso},0} + \Delta\, \mathcal{K}_{\mathrm{df},3}^{\mathrm{iso},1} \,. \tag{F.7}$$

This implies that, in matrix form, $\mathcal{K}_{\mathrm{df},3}$ has the same entry in every element, and is thus of rank 1.

As a result of these approximations, the QC reduces to

$$\det\left[F_3^s(E, \mathbf{P}, L)^{-1} + \mathcal{K}_{\mathrm{df},3}^{\mathrm{iso}}(\Delta)\right] = 0 \,, \tag{F.8}$$

where the dimension of the matrices is given by the number of finite-volume momenta for which $H(\mathbf{k}) \neq 0$ for the given choice of E, $\mathbf{P}$, and L. The numerical problem is thus to find the eigenvalues of the matrix in Eq. (F.8) and determine the energies at which they cross

zero for the given choice of the parameters in the s-wave phase shift and $\mathcal{K}_{\mathrm{df},3}^{\mathrm{iso}}$. This problem is greatly simplified in practice by block-diagonalizing the matrix, as we now explain.

F.1.2 Block-diagonalization of the quantization condition

The energy levels of the finite-volume system fall into irreps of the relevant finite-volume symmetry groups for various values of the total three-particle momentum $\mathbf{P}$. For $\mathbf{P} = \mathbf{0}$, the symmetry group is the 48-dimensional cubic group O_h (no double cover is needed since we are dealing with mesons). The procedure for decomposing the QC in this case was first presented in Ref. [76], but the generalization to arbitrary $\mathbf{P}$ is new to this work and deserves explanation. Unlike in Ref. [76] where both $\ell_{\max} \in \{0, 2\}$ were considered, here we focus only on the relevant case of $\ell_{\max} = 0$.

For general $\mathbf{P}$, the finite-volume symmetry group is reduced to the little group $\mathrm{LG}(\mathbf{P})$ of cubic group transformations $R \in O_h$ that leave $\mathbf{P}$ invariant:

$$\mathrm{LG}(\mathbf{P}) \equiv \{R \in O_h | R\mathbf{P} = \mathbf{P}\}. \tag{F.9}$$

We therefore seek to decompose the QC into irreps of $\mathrm{LG}(\mathbf{P})$ instead of O_h, but otherwise the recipe used in Ref. [76] is unchanged. The list of relevant little groups is shown in Table F.1.

For fixed $(E, \mathbf{P}, L)$, each matrix $M \in \{\widetilde{\mathcal{K}}_2^s, \mathcal{K}_{\mathrm{df},3}, \widetilde{F}^s, \widetilde{G}^s, F_3^s\}$ appearing in the QC is invariant under a common set of real unitary (i.e. orthogonal) transformations $\{U(R)\}_{R \in \mathrm{LG}(\mathbf{P})}$:

$$U(R)^T M U(R) = M \quad \forall R \in \mathrm{LG}(\mathbf{P}), \tag{F.10}$$

$$U(R)_{pk} = \begin{cases} (-1)^{\Pi(R)}, & \mathbf{p} = R\mathbf{k} \\ 0, & \text{otherwise.} \end{cases} \tag{F.11}$$

Here $\Pi(R)$ is the parity of the transformation R, which is $+1$ if R is a pure rotation and -1 otherwise. This factor occurs because pions are pseudoscalars and leads to a simple relabeling

$\mathbf{d}$	LG($\mathbf{P}$)	2-pt. irreps	3-pt. irreps
$(0,0,0)$	O_h	A_{1g}^+, E_g^+	A_{1u}^-, E_u^-
$(0,0,1)$	C_{4v}	A_1^+, B_1^+	A_2^-, B_2^{-*}
$(1,1,0)$	C_{2v}	A_1^{+*}, B_1^+	A_2^-
$(1,1,1)$	C_{3v}	A_1^+, E^+	A_2^-, E^-
$(0,0,2)$	C_{4v}	A_1^+, B_1^+	none

Table F.1: Little group LG($\mathbf{P}$) for each total momentum $\mathbf{P} = (2\pi/L)\mathbf{d}$ used in our fits, along with all irreps containing energy levels with $E_2^* \lesssim 4M$ or $E^* \lesssim 5M$. We use the notation of Ref. [1] for irreps. The asterisk indicates cases where the interacting energy lies slightly above the inelastic threshold, although the free energy lies below.

of irreps compared to those of scalars. We note that the definition of $U(R)$ in Eq. (F.11) differs from that in Ref. [76] in three ways: it is sensitive to parity, it only includes $\ell = 0$, and it has momentum indices transposed for notational convenience.

The transformation matrices $\{U(R)\}_{R\in \mathrm{LG}(\mathbf{P})}$ furnish a (reducible) representation of LG($\mathbf{P}$):

$$U(R_1 R_2) = U(R_1)U(R_2) \quad \forall R_1, R_2 \in \mathrm{LG}(\mathbf{P}), \tag{F.12}$$

$$U(\mathbf{1_3}) = \mathbf{1}_k. \tag{F.13}$$

This reducible representation can be decomposed into irreps I of the little group LG($\mathbf{P}$) through the use of projection matrices P_I:

$$P_I = \frac{d_I}{[\mathrm{LG}(\mathbf{P})]} \sum_{R\in \mathrm{LG}(\mathbf{P})} \chi_I(R) U(R)\,, \tag{F.14}$$

where $[\mathrm{LG}(\mathbf{P})]$ is the dimension of the little group, d_I is the dimension of I, and $\chi_I(R)$ is its character. Lastly, we collect the eigenvectors of P_I with nonzero (unit) eigenvalues into $P_{I,\mathrm{sub}}$ to project QC matrices M onto the lower-dimensional irrep subspace:

$$M_{I,\mathrm{sub}} = (P_{I,\mathrm{sub}})^T M P_{I,\mathrm{sub}}. \tag{F.15}$$

These projections partition the eigenvalues of M into the various irreps of LG($\mathbf{P}$), so that

we can study solutions to the QC irrep by irrep.

The isotropic nature of $\mathcal{K}_{\mathrm{df},3}^{\mathrm{iso}}$ implies that it contributes only to the most symmetric irreps, modulo the presence of parity. In particular, for $\mathbf{d} = 0$ it contributes only to the A_{1u}^{-} irrep, while for $\mathbf{d}^2 = \{1, 2, 3\}$ it contributes only to the A_2^{-} irrep of the respective little groups (see Table F.1). For these irreps, one can use the arguments presented in Refs. [28] and extended in Ref. [76] to reduce the QC to a one-dimensional algebraic relation, referred to as the isotropic approximation to the QC. This is not necessary, however, as one can instead simply project onto these irreps as described above. In practice we have used both methods and checked that they agree.

For all other irreps that arise in the elastic portion of the three-particle spectrum, $\mathcal{K}_{\mathrm{df},3}^{\mathrm{iso}}$ does not contribute. This does not mean, however, that there is no shift of the energies from their noninteracting values, as the two-particle interactions do indeed lead to energy shifts. This point was not appreciated in previous work, where it was claimed that there would be no energy shifts in such irreps [76]. The presence of a shift can be understood intuitively in the case of the E_u^{-} irrep for $\mathbf{P} = 0$. Here the lowest total angular momentum contained is $J = 2$. Thus the interacting pair can be in an s-wave, and thus affected by the s-wave two-particle interaction, with the total $J = 2$ being obtained by having the spectator in a d-wave relative to the pair. These irreps (of which there turn out to be three — see Table F.6) provide an additional constraint on the two-particle amplitude.

The generalization of these considerations to include d-waves in moving frames is straightforward, but beyond the scope of this work.

F.2 Non-leading effects in $\mathcal{K}_{\mathrm{df},3}$

We now provide further justification for the results

$$M^2\mathcal{K}_{\mathrm{df},3} = M^2\mathcal{M}_{\mathrm{df},3}(1+\cdots) \tag{F.16}$$

$$= \frac{M^4}{F^4}(18+27\Delta+\cdots) \tag{F.17}$$

discussed in the main text [see Eqs. (8.9) and (F.18)], and estimate the size of the NLO corrections indicated by the ellipses.

F.2.1 Derivation of Eq. (F.16)

We first discuss the derivation of, and corrections to, Eq. (F.16). This result provides the second step in the two-part relation between the three-particle spectrum and the physical three-particle scattering amplitude. The equations governing this step were derived in Ref. [29]. In the case that only s-wave two-particle channels interact, and $\mathcal{K}_{\mathrm{df},3}$ is isotropic, $\mathcal{M}_{\mathrm{df},3}$ is also restricted to the s-wave, but is not, in general, isotropic. Specifically, it is given by [29, 39]

$$\mathcal{M}_{\mathrm{df},3}(p,k) = \mathcal{S}\left\{\frac{\mathcal{L}(k)\mathcal{L}(p)}{1/\mathcal{K}_{\mathrm{df},3}^{\mathrm{iso}} + F_3^{\infty}}\right\}, \tag{F.18}$$

where $\mathcal{S}$ denotes symmetrization over momentum assignments. The other quantities in Eq. (F.18) are

$$\mathcal{L}(k) = \frac{1}{3} - 2\omega(k)\mathcal{M}_2^s(k)\widetilde{\rho}(k) - \int_{\mathbf{s}} \mathcal{D}^{(u,u)}(k,s)\widetilde{\rho}(s)\,, \tag{F.19}$$

$$\widetilde{\rho}(k) = \frac{H(k)}{2\omega(k)}\rho(k)\,, \qquad \rho(k) = \frac{|q_{2,k}^*|}{16\pi E_{2,k}^*}\,, \tag{F.20}$$

where we have given only the subthreshold form of ρ. In the previous equations, all integrals are three-dimensional

$$\int_{\mathbf{s}} = \int \frac{d^3s}{(2\pi)^3}\,, \tag{F.21}$$

despite the fact that the integrands depend only on the magnitudes of the momenta.

Thus to determine $\mathcal{L}(k)$, we need $\mathcal{D}^{(u,u)}$, the asymmetric form of $\mathcal{D}$ in Eq. (8.8) of the main text, which is given by solving

$$\mathcal{D}^{(u,u)}(k,p) = -\mathcal{M}_2^s(k)G^\infty(k,p)\mathcal{M}_2^s(p) - \int_{\mathbf{s}} \frac{1}{2\omega(s)}\mathcal{M}_2^s(k)G^\infty(k,s)\mathcal{D}^{(u,u)}(s,p)\,, \tag{F.22}$$

where we use the relativistic form of G^∞ [34]

$$G^\infty(k,p) = \frac{H(k)H(p)}{(P-k-p)^2 - m^2 + i\epsilon}\,. \tag{F.23}$$

Finally, F_3^∞ is given by

$$F_3^\infty = \int_{\mathbf{k}} \widetilde{\rho}(k)\mathcal{L}(k)\,. \tag{F.24}$$

The above equations depend on the physical two-particle s-wave scattering amplitude, $\mathcal{M}_2^s$, which is related to $\mathcal{K}_2^s$ by

$$\frac{1}{\mathcal{M}_2^s(k)} = \frac{1}{\mathcal{K}_2^s(k)} + \rho(k)\,, \tag{F.25}$$

with $\mathcal{K}_2^s$ given by

$$\frac{1}{\mathcal{K}_2^s(k)} = \frac{1}{16\pi E_{2,k}^*} q_{2,k}^* \cot\delta(q_{2,k}^*)\,. \tag{F.26}$$

The phase shift is given in turn by the parametrization of Eq. 8.11.

We can now explain in detail why $\mathcal{M}_{\mathrm{df},3} = \mathcal{K}_{\mathrm{df},3}$ at LO in χPT , i.e. why Eq. (F.16) is valid. The power-counting parameter is $\epsilon \sim M^2/F^2 \sim k^2/F^2$, in terms of which $\mathcal{M}_2^s \sim \epsilon$, $\tilde{\rho} \sim 1$, and $G^\infty \sim 1/\epsilon$, implying that that $\mathcal{D}^{(u,u)} \sim \epsilon$. It follows that $\mathcal{L} = 1/3 + \mathcal{O}(\epsilon)$, with the determination of the $\mathcal{O}(\epsilon)$ terms requiring the full solution to the integral equation for $\mathcal{D}^{(u,u)}$. In addition, we see that $F_3^\infty \sim \epsilon^0$. Since we know from Eq. (8.9) that $\mathcal{M}_{\mathrm{df},3} \sim \epsilon^2$, it then follows from Eq. (F.18) that also $\mathcal{K}_{\mathrm{df},3}^{\mathrm{iso}} \sim \epsilon^2$, as this is the only way to match powers of ϵ on the two sides. Thus the F_3^∞ term in the denominator is actually of NNLO relative to the dominant $1/\mathcal{K}_{\mathrm{df},3}^{\mathrm{iso}} \sim 1/\epsilon^2$ contribution. In summary, at LO we can set $\mathcal{L} \to 1/3$ and drop

F_3^∞. Symmetrization leads to a factor of 9 that cancels the $(1/3)^2$, leading to $\mathcal{M}_{\mathrm{df},3} = \mathcal{K}_{\mathrm{df},3}^{\mathrm{iso}}$.

To complete the discussion, we note that the restriction to the s-wave, isotropic approximation is also consistent with χPT . In particular, the d-wave amplitude and the nonisotropic part of $\mathcal{K}_{\mathrm{df},3}$ appear first at NLO, since both require an additional factor of k^2 relative to the corresponding LO amplitudes. Thus, at LO, $\mathcal{M}_2 = \mathcal{M}_2^s$ and $\mathcal{K}_{\mathrm{df},3} = \mathcal{K}_{\mathrm{df},3}^{\mathrm{iso}}$. Therfore the result just derived, $\mathcal{M}_{\mathrm{df},3} = \mathcal{K}_{\mathrm{df},3}^{\mathrm{iso}}$ at LO, is equivalent to $\mathcal{M}_{\mathrm{df},3} = \mathcal{K}_{\mathrm{df},3}$. A further check on this is provided by the fact that the LO result for $\mathcal{M}_{\mathrm{df},3}$ calculated explicitly in the main text is isotropic.

F.2.2 Higher order corrections in relation between $\mathcal{M}_{\mathrm{df},3}$ and $\mathcal{K}_{\mathrm{df},3}$

We now turn to an estimate of higher-order corrections to Eq. (F.16). This is provided by solving the equations above and determining the quantities $3\mathcal{L}(k) - 1$, which is of NLO, and $\mathcal{K}_{\mathrm{df},3}^{\mathrm{iso}} F_3^\infty$, which is of NNLO. This is not a complete calculation of higher-order corrections, since, as already noted, d-wave amplitudes and nonisotropic contributions to $\mathcal{K}_{\mathrm{df},3}$ also appear at NLO. A further approximation is that we solve the equations only below the three-particle threshold, so that the pole prescription in G^∞ is not needed. This is sufficient to determine the order of magnitude of the corrections. Methods for solving the equations above threshold have not yet been developed. For convenience, we set $\mathbf{P} = 0$, although this makes no difference to the final result, which is relativistically invariant. This choice implies that, in this subsection and the next, E and E^* are equal, and we use the former for brevity.

Following Ref. [39], the equations are solved by discretizing the momenta as though the system was in a periodic box of size L, leading to $\mathbf{k} = (2\pi/L)\mathbf{n}$ with $\mathbf{n} \in \mathbb{Z}^3$. One then has to invert large matrix equations, which is straightforward. This also allows us to reuse much of the setup needed for the QC itself, since the equations above are obtained by taking the $L \to \infty$ limit of various objects that appear in the QC. We stress, however, that here we are using the finite-volume simply as a device for solving the integral equations and that L here

is not related to the volume in which actual lattice QCD simulations are done.

The function $\mathcal{L}(k)$ is given by Eq. (A14) of Ref. [39]:

$$\mathcal{L}(k) = \lim_{L\to\infty} \mathcal{L}(k;L) = \lim_{L\to\infty} \left\{ \frac{1}{3} - \sum_{\mathbf{p}} \left[\frac{1}{1/(2\omega\mathcal{M}_2^s) + \widetilde{G}^s}\, \widetilde{\rho} \right]_{kp} \right\}, \tag{F.27}$$

where the indices k and p are drawn from the finite-volume set, ω, $\mathcal{M}_2^s$ and $\widetilde{\rho}$ are simply diagonal matrices containing entries of the corresponding infinite-volume quantities evaluated at finite-volume momenta, and the matrix $\widetilde{G}^s$ is

$$\left[\widetilde{G}^s\right]_{kp} = \frac{1}{L^3}\frac{1}{2\omega_k} G^\infty(k,p) \frac{1}{2\omega_p}\,. \tag{F.28}$$

F_3^∞ is given by the discretized form of Eq. (F.24),

$$F_3^\infty = \lim_{L\to\infty} \frac{1}{L^3} \sum_{\mathbf{k}} \widetilde{\rho}(k)\mathcal{L}(k,L)\,. \tag{F.29}$$

We find that the convergence in L is quite rapid, with $ML \gtrsim 30$ enough to obtain the form of the solution to sufficient accuracy.

In order to display results, we choose fit 1 from Table 8.1 for the phase shift that determines $\mathcal{M}_2^s$. The results are little changed when using other fits. In Fig. F.1, we plot the NLO quantity $3\mathcal{L}(k) - 1$ as a function of k^2/M^2 for $2.9 \le E/M < 3.0$. This quantity necessarily vanishes at the maximum value of k, set by the value in which the cutoff function vanishes, $H(k) = 0$. We observe that the correction has a maximum at about 0.25 when $(k/M)^2 \approx 0.75$, but is much smaller for k near zero. Indeed, extrapolating to $E = 3M$, we find $3\mathcal{L}(0) - 1 \approx -0.01$ at threshold. The NNLO quantity $\mathcal{K}_{\mathrm{df},3}^{\mathrm{iso}} F_3^\infty$ is shown in Fig. F.2, using $M^2\mathcal{K}_{\mathrm{df},3}^{\mathrm{iso}} = 550$, the value obtained in the first global fit in Table 8.2. The small result, at the percent level, is consistent with this being a higher-order effect.

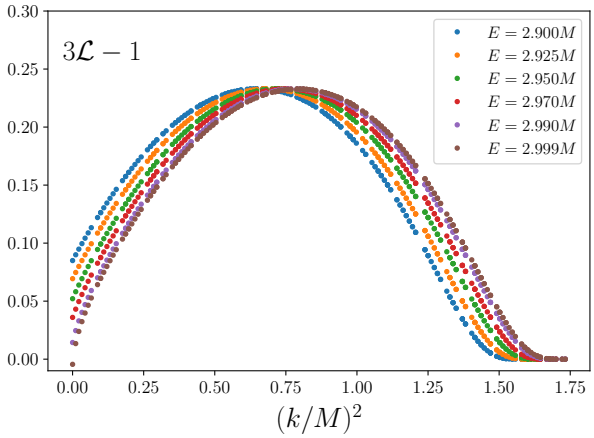

Figure F.1: Dependence of $3\mathcal{L}(k) - 1$ on $(k/M)^2$ for $ML = 60$ and different values of the rest-frame energy, E/M. This quantity indicates the size of the NLO corrections in the relationship between $\mathcal{K}_{\mathrm{df},3}$ and $\mathcal{M}_{\mathrm{df},3}$.

F.2.3 Estimating higher order corrections to $\mathcal{K}_{\mathrm{df},3}$

Here we estimate the corrections in Eq. (F.17) that are indicated by the ellipses. First we consider the value of $\mathcal{K}_{\mathrm{df},3}$ at threshold, where $\Delta = 0$. Corrections arise both in the relation between $\mathcal{K}_{\mathrm{df},3}$ and $\mathcal{M}_{\mathrm{df},3}$, and in the χPT result for $\mathcal{M}_{\mathrm{df},3}$ itself. The results just obtained for $3\mathcal{L}(0) - 1$ and $\mathcal{K}^{\mathrm{iso}}_{\mathrm{df},3}F_3^\infty$ at threshold imply few percent relative corrections in the $\mathcal{K}_{\mathrm{df},3}$ to $\mathcal{M}_{\mathrm{df},3}$ relation. Higher order corrections in the result for $\mathcal{M}_{\mathrm{df},3}$ are expected to be of generic relative size $M^2/(4\pi F)^2 \approx Ma_0/\pi \approx 0.03$. Assuming constants of ~ 3 multiplying these generic corrections, we estimate them conservatively to be no larger than 10%. These generic corrections thus dominate the error estimate at threshold.

Next we consider the corrections to the linear term in Δ in Eq. (F.17). We expect the generic corrections to be of similar relative magnitude as at threshold, i.e. $\lesssim 10\%$. The corrections to the $\mathcal{K}_{\mathrm{df},3}$ to $\mathcal{M}_{\mathrm{df},3}$ relation can, however, be larger. We focus on the dominant contribution, that from $\mathcal{L}(k)\mathcal{L}(p)$ in Eq. (F.18). The momentum dependence of $\mathcal{L}(k)$ near threshold implies that a constant $\mathcal{K}^{\mathrm{iso}}_{\mathrm{df},3}$ will lead to a Δ dependence in $\mathcal{M}_{\mathrm{df},3}$, and *vice versa*.

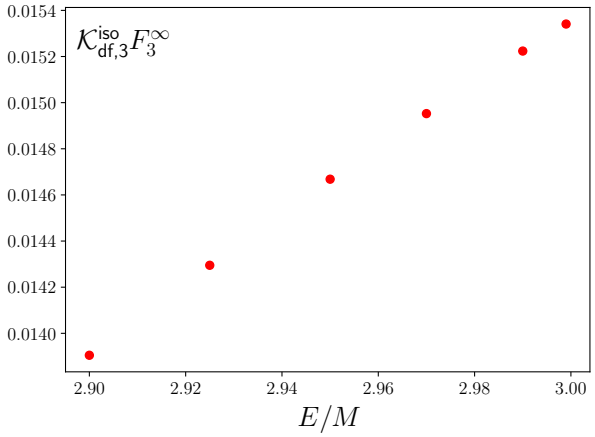

Figure F.2: $\mathcal{K}^{\text{iso}}_{\text{df},3}F_3^\infty$ as a function of the energy, E/M. We set $M^2\mathcal{K}^{\text{iso}}_{\text{df},3} = 550$. This quantity indicates the size of NNLO corrections in the relationship between $\mathcal{K}_{\text{df},3}$ and $\mathcal{M}_{\text{df},3}$.

In particular, if we fix $\mathcal{K}^{\text{iso}}_{\text{df},3}$ to a constant, and calculate the derivative

$$c = \frac{1}{\mathcal{K}^{\text{iso}}_{\text{df},3}} \frac{d\mathcal{M}_{\text{df},3}}{d\Delta}\bigg|_{\mathcal{K}^{\text{iso}}_{\text{df},3},\Delta=0}, \tag{F.30}$$

then we have, for small Δ, and ignoring the generic χPT corrections,

$$M^2\mathcal{K}_{\text{df},3} = \frac{M^4}{F^4}\left[18 + (27 - 18c)\Delta + \mathcal{O}(\Delta^2)\right]. \tag{F.31}$$

In words, the constant feeds down a correction to the linear term.

To estimate c, we use the results of Fig. F.1. These are calculated for $E < 3M$, corresponding to $\Delta < 0$. Recalling that $\mathcal{M}_{\text{df},3}$ and $\mathcal{K}_{\text{df},3}$ are on-shell amplitudes, we observe that to obtain $\Delta < 0$ we require $k^2 < 0$. For example, a configuration $p_1^\mu = (M, \mathbf{0})$, $p_2^\mu = (0, iM, 0, 0)$ and $p_3^\mu = (0, -iM, 0, 0)$ has all particles on shell, $E^2 = M^2$, and thus $\Delta = -8/9$. Taking each of the particles in turn as the spectator, the values of k^2/M^2 are 0, -1 and -1, respectively (remembering that $k^2 \equiv \mathbf{k}^2$). Averaging over the choices of spectator, we find $\langle k^2/M^2\rangle = -2/3$ for $\Delta = -8/9$. In principle, one should do an average over all allowed momentum configurations, but our simple example gives a rough relation between Δ and k^2,

namely

$$\left.\frac{d\Delta}{d(k^2/M^2)}\right|_{k^2=0} \approx 4/3\,. \tag{F.32}$$

The final step is to use Fig. F.1 to estimate

$$\left.\frac{d\,3\mathcal{L}(k)}{d(k^2/M^2)}\right|_{k^2\approx 0, E\approx 3M} \approx \frac{1}{2}\,. \tag{F.33}$$

This is a crude estimate, given that the slope depends on E. Nevertheless, using these results, and the fact that there are two factors of $\mathcal{L}$ in Eq. (F.18), we arrive at the estimate

$$c \approx 2\frac{\left.\frac{d\,3\mathcal{L}(k)}{d(k^2/M^2)}\right|_{k^2\approx 0, E\approx 3M}}{\left.\frac{d\Delta}{d(k^2/M^2)}\right|_{k^2=0}} \approx 0.75\,. \tag{F.34}$$

Inserting this into Eq. (F.31) we find that the term linear in Δ is reduced by about 50% by this correction. We treat this as an asymmetric error, since the sign of the effect is unambiguous. We do not shift the central value, as the error estimate is itself uncertain.

In summary the χPT prediction for $\mathcal{K}_{\mathrm{df},3}$ becomes

$$\begin{aligned} M^2\mathcal{K}^{\mathrm{iso},0}_{\mathrm{df},3} &= \frac{M^4}{F^4}18(1\pm 10\%) = 360\pm 36\,, \\ M^2\mathcal{K}^{\mathrm{iso},1}_{\mathrm{df},3} &= \frac{M^4}{F^4}27(1^{+10\%}_{-51\%}) = 540\,^{+54}_{-275}\,, \end{aligned} \tag{F.35}$$

where numerical values are obtained using $Ma_0 = 0.089$ from fit 1.

F.3 Further details on fits

In this section we provide a more detailed explanation of our fitting procedures, and further details of the results of the fits.

F.3.1 General fitting procedure

We determine $\mathcal{K}_2$ and $\mathcal{K}_{\text{df},3}$ by fitting solutions to the two- and three-particle QCs to the energy levels provided in Ref. [1], which were computed on the CLS D200 $N_f = 2+1$ ensemble, which has pion mass $M \sim 200$ MeV, lattice size $64^3 \times 128$ and inverse lattice spacing $1/a \approx 3.1$ GeV [155, 156]. These parameters imply that $ML \approx 4.2$, which is large enough that we expect neglected exponentially-small corrections are at the percent level.

The three-particle QC, Eq. (8.1), has been discussed above. The two-particle QC for states that couple to $J = 0$ can be written as

$$q \cot \delta_0(q) = \frac{2}{\gamma L \sqrt{\pi}} Z_{00}(q^2, \mathbf{d}), \tag{F.36}$$

where Z_{00} is the standard Lüscher Zeta function, $\mathbf{P} = (2\pi/L)\mathbf{d}$ is the total two-particle momentum, γ is the boost factor to the center-of-mass frame, and $q^2 = E_2^{*2}/4 - M^2$. As discussed in the main text, we consider two parametrization schemes for δ_0: the standard ERE of Eq. (8.5) and the Adler-zero form of Eq. (8.11). The parameters in the two schemes can be related by expanding the Adler-zero form about threshold:

$$Ma_0 = -\frac{1}{B_0}\frac{2M^2 - z_2^2}{M^2} \xrightarrow{z_2 \to M} -\frac{1}{B_0}\,, \tag{F.37}$$

$$M^2 r a_0 = -\frac{2B_1}{B_0} + \frac{2M^2 + z_2^2}{2M^2 - z_2^2} \xrightarrow{z_2 \to M} -\frac{2B_1}{B_0} + 3\,. \tag{F.38}$$

Once we choose a parametrization scheme for $\mathcal{K}_2$ (and $\mathcal{K}_{\text{df},3}$ for three-particle energies), we fit the parameters by minimizing the following χ^2 function [109]:

$$\chi^2 = \sum_{i,j} \left(E_i^* - (E_i^*)^{sol}\right) C_{ij}^{-1} \left(E_j^* - (E_j^*)^{sol}\right), \tag{F.39}$$

where $\{E_i^*\}$ are the center-of-mass energy levels of Ref. [1] with covariance matrix C, and $\{(E_i^*)^{sol}\}$ are the solutions to the appropriate QC(s) for a particular set of parameters. To estimate the statistical uncertainties of our fit parameters, we use the individual bootstrap samples provided by Ref. [1] to perform multiple fits for each scheme. We note that the

Fit	B_0	B_1	B_2	z_2^2/M^2	χ^2/dof	Ma_0	M^2ra_0
6	-10.9(1.0)	-2.5(2.3)	—	1 (fixed)	2.89/(5-2)	0.092(8)	2.5(4)
7	-11.0(1.1)	-2(5)	-1(6)	1 (fixed)	2.86/(5-3)	0.091(9)	2.7(9)
8	-11(8)	-3(7)	—	1.0(8)	2.89/(5-3)	0.091(9)	2.6(1.9)

Table F.2: Fits of the two-particle spectrum to the Adler-zero form of $q\cot\delta_0$, Eq. (8.11), considering only levels for which $q^2/M^2 < 1$.

correlation matrix C is taken to be the same for all bootstrap samples.

F.3.2 Results of additional fits to $\mathcal{K}_2$

We have fit the Adler zero form (8.11) to the restricted data set of the five two-particle levels that lie inside the formal radius of convergence of the expansion, $|q^2|/M^2 < 1$. The results are given in Table F.2, which should be compared to Table 8.1. The main conclusion is that the fits yield compatible parameters, providing a consistency check on the results obtained in the main text. The errors here are larger, as expected, and, indeed, very large in fits 7 and 8, where there are insufficient data points to determine the three parameters.

We have also repeated the Adler-zero fits to all levels in the elastic region using the ERE form, Eq. (8.5). Although this is not justified theoretically (since the radius of convergence is $|q^2|/M^2 \lesssim 1/2$), it provides a comparison with a standard form that has been used in previous lattice calculations of the $I = 2$ two-pion amplitude. The results are shown in Table F.3. The quality of the fits is poor, and the results for M^2ra_0 are in strong disagreement with the LO χPT prediction of 3. This provides additional support to the theoretical arguments favoring the use of the Adler-zero fit form.

F.3.3 Determining the d-wave scattering length

To study two-particle d-wave interactions, we analyze the energy levels of Ref. [1] that lie in irreps that do not couple to s-wave interactions. For each such level, Table F.4 shows the

Fit	Ma_0	Mr	P	χ^2/dof	M^2ra_0
9	0.114(6)	2.15(29)	—	29.81/(11-2)	0.25(3)
10	0.106(8)	5.1(1.3)	-0.0030(14)	23.54/(11-3)	0.54(11)

Table F.3: Fits of the two-particle spectrum to the ERE form of $q \cot \delta_0$, Eq. (8.5). All levels up to (and slightly beyond) the elastic threshold at $q^2/M^2 = 3$ are used, as in fits 1-3 in Table 8.1.

comparison of the determined energy to the corresponding free energy. All energy shifts are small and positive, suggesting a very mildly repulsive d-wave interaction. To quantify this interaction, we use the ERE:

$$q \cot \delta_2(q) = \frac{1}{q^4} \left[\frac{1}{(a_2)^5} + \mathcal{O}(q^2) \right] . \tag{F.40}$$

We then extract the d-wave scattering length a_2 using the d-wave form of the two-particle QC (see, e.g., Refs. [62, 101]), yielding

$$(Ma_2)^5 = 0.0006(2) , \qquad \chi^2/\text{dof} = 3.3/(5-1) = 0.83 . \tag{F.41}$$

This result is nonzero with 3σ significance. It is, however, numerically small, suggesting that we can neglect it in our fits to the three-particle levels.

irrep	E_2^*/M(free)	E_2^*/M(interacting) [1]	difference
$E_2^-(0)$	3.621(13)	3.624(13)	0.003(3)
$B_1^-(1)$	3.885(14)	3.889(15)	0.004(4)
$B_1^-(2)$	4.086(17)	4.091(16)	0.005(2)
$E^-(3)$	3.246(10)	3.246(10)	0.000(2)
$B_1^-(4)$	3.621(13)	3.628(13)	0.006(2)

Table F.4: Comparison of free and interacting spectra (the latter from Ref. [1]) for two-particle states in irreps that do not couple to $\ell = 0$. The number in parentheses for each of the irreps gives $\mathbf{d}^2$ and thus specifies the frame.

To study this further, we examine the systematic error induced in the three-particle

spectrum by neglecting the d-wave scattering length. For this we study the effect of a_2 on the three-particle energy levels in the rest frame, where we have previously implemented the three-particle QC including both s- and d-wave effects [76]. Taking $\mathcal{K}_2$ from the first fit of Table 8.1, and a_2 from Eq. (F.41), we find the results shown in Table F.5. We see that d-wave effects are completely negligible in the A_1^- irrep, and less than a third of the statistical error in the E^- irrep. We therefore expect that, for current precision, d-wave effects can safely be ignored.

irrep	E^*/M [1]	$\delta E^*(a_2)/M$
$A_1^-(0)$	4.780(17)	0.0004(2)
$E^-(0)$	4.691(15)	0.005(2)

Table F.5: Effect of d-wave interactions on the three-particle energy levels in the rest-frame. Here E^* is the center-of-mass energy of the level, while $\delta E^*(a_2) = E^*(a_2) - E^*(0)$ is the shift in this energy upon inclusion of the nonzero a_2 given in Eq. (F.41). We have fixed $M^2\mathcal{K}_{\text{df},3}^{\text{iso}} = 500$, but the results are insensitive to this value. Other notation as in Table F.4.

F.3.4 Fitting $\mathcal{K}_{\text{df},3}^{\text{iso}}$ using method 1

Here we provide more details regarding our fits to determine $\mathcal{K}_{\text{df},3}^{\text{iso}}$ using method 1, which was described briefly in the main text.

Within each bootstrap sample, we (a) fit the simplest Adler-zero form for $\mathcal{K}_2^s$ (fit 1—see Table 8.1), to the eleven two-particle levels that are sensitive to s-wave interactions and lie below (or slightly above) the inelastic threshold at $E_2^* = 4M$; and (b) determine the values of $\mathcal{K}_{\text{df},3}^{\text{iso}}$ that, when inserted in the QC, give the energies of each of the eight three-particle energy levels which are sensitive to $\mathcal{K}_{\text{df},3}^{\text{iso}}$ and lie below (or slightly above) the inelastic threshold at $E^* = 5M$. Averaging over bootstrap samples in the standard way, we obtain the average values for each of the eight $\mathcal{K}_{\text{df},3}^{\text{iso}}$ values, as well as the correlation matrix between them.

Using this correlation matrix, we then do a standard fit to the results for these eight levels, either using a constant or a linear form in Δ.

Fitting to a constant yields

$$M^2\mathcal{K}_{\mathrm{df},3}^{\mathrm{iso}} = 560(270)\,, \qquad \chi^2/\mathrm{dof} \;= 8.5/(8-1) = 1.21\,, \tag{F.42}$$

while a linear parametrization gives

$$M^2\mathcal{K}_{\mathrm{df},3}^{\mathrm{iso}} = 140(430) + 570(500)\Delta\,, \qquad \chi^2/\mathrm{dof} \;= 7.7/(8-2) = 1.28\,. \tag{F.43}$$

The constant fit points towards a 2σ significance on $\mathcal{K}_{\mathrm{df},3}^{\mathrm{iso}}$. For the linear fit we note that the errors highly correlated, and thus even though each parameter is compatible with zero, the point where both vanish and $\mathcal{K}_{\mathrm{df},3}(E) = 0$ is also excluded by 2σ. These results are shown in Fig. 8.3 of the main text.

Finally, as a consistency check, we use the QC to predict the energies for those irreps that are not affected by $\mathcal{K}_{\mathrm{df},3}^{\mathrm{iso}}$, with results shown in Table F.6. We find that the predicted values lie very close to the measured values. This indicates that our restriction to s-waves, and our parametrization of $\mathcal{K}_2^s$, are sufficient given present precision. We therefore include these energy levels in our global fits.

irrep	E^*/M [1]	prediction
$E^-(0)$	4.691(15)	4.685(14)
$B_2^-(1)$	5.008(17)	5.007(16)
$E^-(3)$	4.528(14)	4.529(13)

Table F.6: Prediction for the three-particle energy levels in irreps that are insensitive to $\mathcal{K}_{\mathrm{df},3}^{\mathrm{iso}}$. Notation as in Table F.4.

F.3.5 Correlation matrix for global fits

Here we collect the covariance matrices for the global fits in Table 8.2. We write these as $C = DRD$, with D the diagonal matrix containing the standard errors in the parameters. Our results are

$$\text{Fit 4:} \quad D = \text{diag}\,(0.7, 0.3, 160)\ , \qquad R = \begin{pmatrix} 1 & -0.67 & 0.23 \\ -0.67 & 1 & 0.24 \\ 0.23 & 0.24 & 1 \end{pmatrix}\ , \tag{F.44}$$

$$\text{Fit 5:} \quad D = \text{diag}\,(0.7, 0.3, 330, 290)\ , \qquad R = \begin{pmatrix} 1 & -0.63 & 0.22 & -0.10 \\ -0.63 & 1 & -0.11 & 0.25 \\ 0.22 & -0.11 & 1 & -0.89 \\ -0.10 & 0.25 & -0.89 & 1 \end{pmatrix}\ , \tag{F.45}$$

where the matrix indices are ordered as $(B_0, B_1, M^2\mathcal{K}_{\text{df},3}^{\text{iso},0})$ and $(B_0, B_1, M^2\mathcal{K}_{\text{df},3}^{\text{iso},0}, M^2\mathcal{K}_{\text{df},3}^{\text{iso},1})$, respectively. As can be seen, the correlation is large within the two- and three-particle sector, and smaller between the two different sectors.

F.3.6 Two- and three-pion spectrum

To conclude, we provide a comparison of the data to the predicted two- and three-pion spectra from the quantization conditions. For this, we use the best parameters from fit 5 described in the main text (see Table 8.2). The results are displayed in Fig. F.3. We also include the predictions from the QC above the inelastic thresholds— $E_{CM} = 4M$ and $E_{CM} = 5M$ for the two- and three-particle QC, respectively. As can be seen, our predictions lie on top of the data points within errorbars, even in the inelastic region. This is not surprising, as inelastic channels open up slowly above kinematic thresholds.

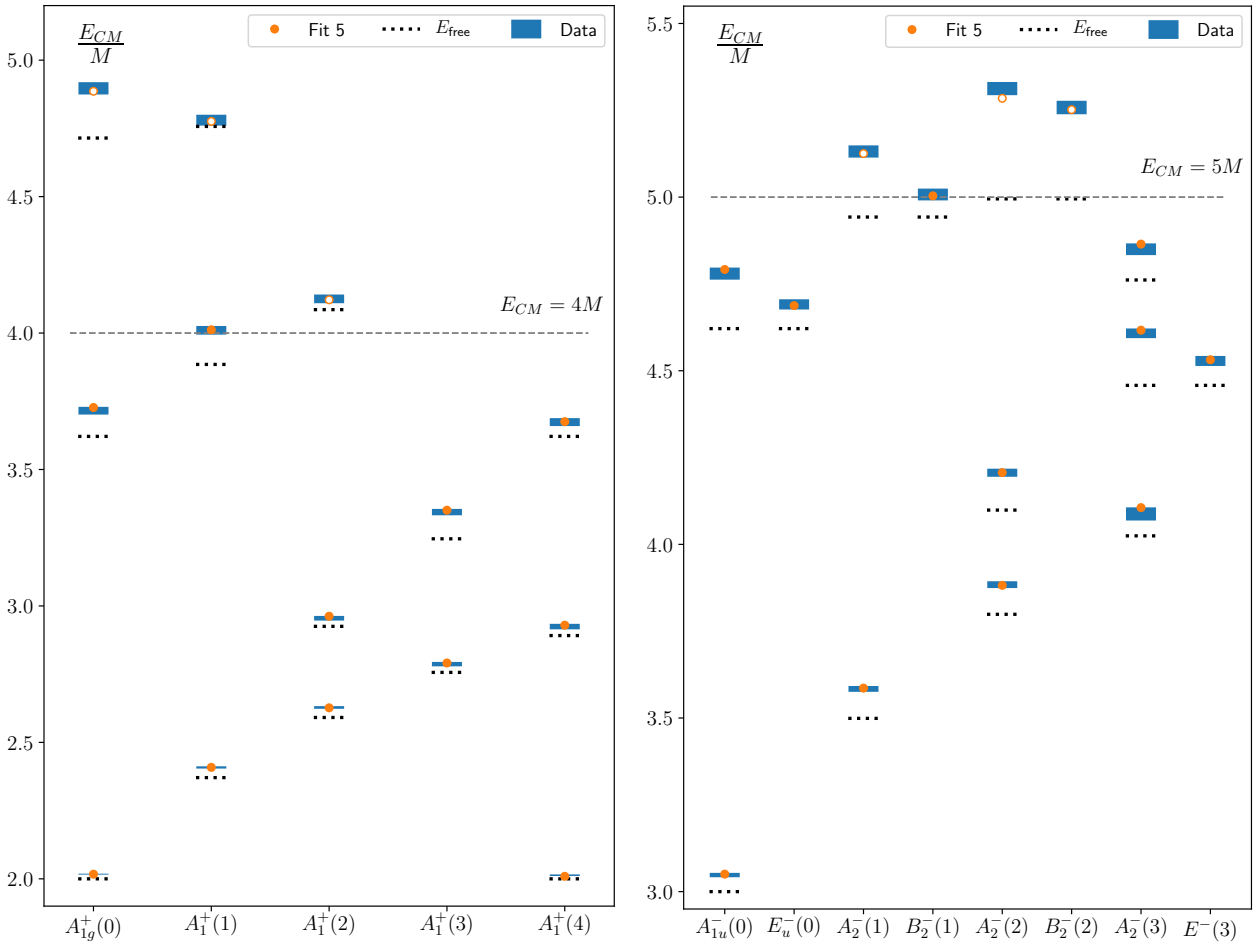

(a) $2\pi^+$ spectrum.

(b) $3\pi^+$ spectrum.

Figure F.3: Two- and three-pion spectra from Ref. [1] (blue) compared to the predictions from the global fit 5 (orange). Hollow orange points above the inelastic thresholds have not been included in the fit, but are shown for comparison. Dashed lines show the non-interacting energy levels.

VITA

Tyler Blanton grew up in Rocky Mount, NC with his younger brother Jason and their loving parents Lee and Laurel Blanton. He performed his undergraduate studies at the University of North Carolina at Chapel Hill, graduating in 2016 with bachelor degrees in physics and applied mathematics. He welcomes your questions at `blanton1@uw.edu`.